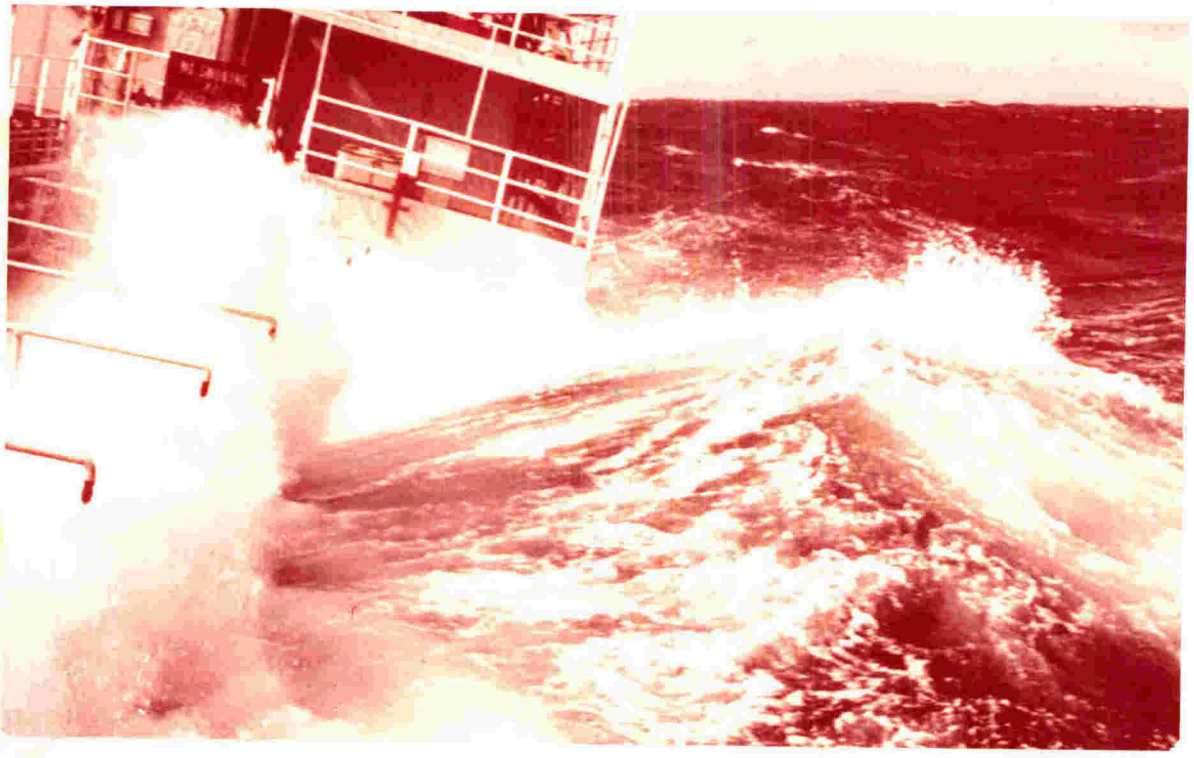

THE SOUTHWEST PACIFIC

# GEOPHYSICAL STUDIES IN THE SOUTHWEST PACIFIC:

## PRIMARILY STUDIES OF CRUSTAL STRUCTURE BETWEEN NEW ZEALAND AND ANTARCTICA

VOLUME 1

ROBIN KEITH HALCRO FALCONER

Submitted for the degree of
Doctor of Philosophy in Physics

Victoria University of Wellington
New Zealand

February 1974

# ABSTRACT

Geophysical data - primarily magnetic field measurements, bathymetry, and seismicity data - are presented for the area between New Zealand and Antarctica from approximately 145°W to 155°E. The data are used to determine the structure of the Pacific-Antarctic boundary, the oceanic part of the Pacific plate and the area of intersection of the Indian, Pacific and Antarctic plates.

In the southwest Pacific basin the magnetic anomalies are very clear and an extensive pattern of anomaly lineations with some offsets is mapped. The magnetic anomalies show that the uniform Pacific basin area formed between about 83 and 63 mybp. The Pacific-Antarctic boundary is shown to differ either side of about 175°W. To the east it is a relatively uniform aseismic spreading ridge, offset by some transform faults. West of 175°W, to 161°E, the boundary consists of a seismically active zone of disturbed bathymetry and magnetic anomalies striking about N70°W. The zone, the Pacific-Antarctic fracture zone, probably consists of several fractures striking about N45°W. The area between the Pacific-Antarctic boundary and the southwest Pacific basin represents the interval 10 to 55 mybp, and only in the east are anomaly lineations clear. The Indian-Antarctic-Pacific triple junction is near 61.5°S, 161°E and is a stable ridge-fault-fault junction; the Indian-Antarctic boundary being the ridge.

Plate tectonics is applied to the area and the structure is shown to fit, and be explained by a different rotation pole for each of the major intervals indicated by the structure, i.e. 0-10 mybp, 10-63 mybp and 63-80 mybp. The poles, with rotation rates deduced from the magnetic anomalies, are used to reconstruct the position of New Zealand relative to Antarctica at 80 mybp. The two continents probably started to separate at close to 83 mybp. The times of the major changes of structure and plate movement in the area are shown to coincide with major plate movement changes in the southwest Pacific area and in the rest of the world.

A new method for determining poles of rotation, based only on epicentre locations, is presented. The method is applied to independently determine the Indian-Pacific, Pacific-Antarctic and Indian-Antarctic poles. The poles should form a consistent set and they do. The method yields effectively instantaneous poles, is quantitative, and is applicable to most plate boundaries.

Earthquake magnitude-frequency relationship b values for the plate boundaries in the area are determined. Comparisons with results from elsewhere indicate an association of high b with high temperature and conversely. Several factors which have previously been suggested as determining b value are shown to not be determinants.

A revised and extended magnetic reversal time scale based on model studies of the southwest Pacific basin anomalies is presented. Other model studies indicate that a magnetized layer thickness of at least 2 km is probable. Variations of anomaly amplitudes are studied.

A detailed study of the application of numerical correlation techniques to magnetic anomalies is presented. It is concluded that horizontal scale variations and discontinuities in profiles can be critical. Methods for overcoming some of the problems, and for determining quantitative error estimates, are given. The methods, and conclusions, are applicable to any correlation problem.

# CONTENTS

## VOLUME 1

# PREFACE

## SCOPE OF THE THESIS WORK

Geomagnetic studies of the seafloor between New Zealand and Antarctica have been carried out by various New Zealand groups since 1958. Christoffel (1961a, b) was the first to present magnetic anomaly profiles and as more data were collected they were analysed by Adams and Christoffel (1962) and Christoffel and Ross (1965). Ross (1966) completed a preliminary analysis of all the data available up to and including 1965. Most of the data were between 165°E and 180°. The amount of magnetic data in that area has more than trebled since 1965; mainly through a research programme of the Physics Department of Victoria University of Wellington, operating from the New Zealand Navy Antarctic resupply vessel HMNZS Endeavour. This thesis is a part of that research programme. Data from several other sources are included and the study extends over a large area of the southwest Pacific.

The primary data are magnetic field measurements, but bathymetry and seismicity data are also used extensively. The data are used to investigate the crustal structure and tectonic history of the oceanic area between New Zealand and Antarctica, between approximately 145°W and 155°E. (See Fig. 0.1 in Vol. 2). The major results are presented in a magnetic anomaly map for the area 45° to 70°S, 145°W to 155°E. With the work of Herron (1971) east of 150°W, and Weissel and Hayes (1972) west of 165°E, the map presented here completes preliminary magnetic coverage of the southern oceans from 70°W to 100°E.

The initial intention was to concentrate on the southwest Pacific basin between 165°E and 180°. The work of Christoffel, Adams, and Ross in part of that area had shown that there was a pattern of lineated magnetic anomalies. Additional data were available, and more could be obtained as the area was accessible from HMNZS Endeavour. It was of interest to study the area in detail, especially as Vine (1966) had pointed out that the magnetic anomaly pattern was similar to that off the west coast of the U.S.A. The data of Pitman et al. (1968) subsequently indicated that the lineations west of 180° were part of an extensive pattern, which east of 180° extended from the New Zealand continent to the Pacific-Antarctic ridge. Their data, and additional unpublished data, were made available by Lamont-Doherty Geological Observatory and the analysis was extended to all of the southwest Pacific basin south of the Chatham Rise and west of 150°W. The extension to 150°W compliments the work of Herron (1971) which covers the area east of 150°W.

The increasing success of plate tectonics as a unifying and predictive theory indicated that broadening of the study beyond the southwest Pacific basin would be useful. The Pacific-Antarctic ridge system is the boundary of the Pacific and Antarctic plates (see Fig. 0.2, Vol. 2) and to understand the southwest Pacific it was necessary to consider data at least to the Pacific-Antarctic boundary in some detail. Magnetic and bathymetric data for the boundary from 145°W to 160°E are analysed. A preliminary examination of data south of the boundary has also been carried out. To investigate the western end of the Pacific-Antarctic boundary a special study was made of the area near 60°S, 160°E where the Indian, Antarctic and Pacific plate intersect. This study is complemented by the work of Weissel and Hayes (1972), Christoffel and R.F. Falconer (1973), and others, in which large extents of the Indian-Antarctic and Indian-Pacific boundaries are examined.

In the course of the study of the area several specific studies which have more general applications have been carried out. These specific studies, which are described below, are a significant part of the whole study.

The primary data for the whole study are magnetic anomalies, and the analysis of these data is very dependent on correlation of anomaly profiles. Recognition of the difficulties of visual correlation led to a study of numerical correlation methods. The methods were applied to the southwest Pacific basin anomalies but the conclusions of the study are relevant to any correlation problem.

The magnetic anomalies in the southwest Pacific basin were also used in a study of the origin of the magnetic anomalies. The results obtained are relevant to other oceanic areas.

The seismicity data for the area were compiled to supplement the magnetic and bathymetric data. This led to two special studies which utilise the seismicity of the Macquarie ridge complex portion of the Indian-Pacific boundary and all of the Pacific-Antarctic and Indian-Antarctic boundaries. One study is an analysis of earthquake magnitude-frequency relationships for the plate boundaries in the area and comparison of the results with other oceanic plate boundaries. The other study presents a new method for determining poles of rotation, with applications of the method to the Indian-Antarctic, Pacific-Antarctic and Indian-Pacific poles. The method is applicable to other plate boundaries.

## THESIS FORMAT

There are ten chapters. Chapter 1 presents background material assumed in subsequent chapters. Chapter 2 is a review of previous work in the area. Chapter 3 describes the sources, reliability and methods of reduction of the

basic data. Chapter 4 presents the data, and from it a detailed description of the structure of the area. Chapter 5 is a study of the application of numerical correlation techniques to magnetic anomaly profiles. Chapter 6 presents magnetic anomaly model studies. Chapter 7 is a study of earthquake magnitude-frequency relationships. Chapter 8 presents a description and applications of a new method of determining poles of rotation from epicentres. Chapter 9 draws on the previous chapters to present a discussion of the tectonic development of the southwest Pacific area. Chapter 10 is a very brief review with comments on possible future work. The material in chapters 5, 6 and 7 is not central to the description of the structure of the area, and could be omitted at a first reading.

Preliminary accounts of some of the work have been presented in Falconer (1972, 1973a, b) and Christoffel and R.K.H. Falconer (1972, 1973). All the material in those papers is presented more fully here, with some revisions where additional data have led to reinterpretation of preliminary conclusions. The papers will therefore not be referred to repeatedly. Copies of them are contained in the pocket at the rear of Vol. 2.

A significant amount of the information is presented in diagram form. For the reader's convenience all the diagrams are in Vol. 2, while all the text is in Vol. 1. The diagrams are numbered with respect to the chapter in which they are first referred to, e.g. Fig. 5.3 is the third figure of Chapter 5. Three large diagrams are contained in the pocket in the back of Vol. 2, but reduced copies of them are in with the other diagrams.

Appendices are at the end of Vol. 1, numbered and lettered with respect to the chapter to which they apply, e.g. Appendix 6B is the second appendix for Chapter 6. Figures for the appendices are at the end of Vol. 2.

ACKNOWLEDGEMENTS

Many people and organizations have contributed to this study. It is not possible to acknowledge everyone individually but I wish to say to everyone - thank you.

I would like to specially thank the following people. Professor D.A. Christoffel for advice, valuable discussions, and encouragement throughout the whole project. Professor Walker for his interest and support. The academic and technical staff, and students, of the Physics Department for assistance and stimulus; especially W. Brown, B.E.G. Coodger and E. Broughton, for construction and maintenance of the equipment, and numerous research assistants for help on HMNZS Endeavour. I would also like to thank staff and students of other departments in the University for their interest and help, especially

D. Vere-Jones for advice on statistical matters. J.W. Brodie and D.E. Hurley of the N.Z. Oceanographic Institute for discussions on bathymetric data. R.D. Adams and S. Gibowicz of Geophysics Division, D.S.I.R., for advice on seismicity. Discussions in person and by mail with D.C. Krause, University of Rhode Island, and R. Houtz and D.E. Hayes, Lamont-Doherty Geological Observatory have been very useful. I am grateful to D.I. Ross for introducing me to the sea on HMNZS Endeavour. The officers and men of the New Zealand Navy have always been most helpful and hospitable to me, and other Victoria University people during our numerous trips on HMNZS Endeavour.

The U.S. National Science Foundation and Lamont-Doherty Geological Observatory provided the opportunity for me to participate in Eltanin cruises 27, 28 and 37. The Applied Mathematics Division, D.S.I.R., provided the facilities for most of the computing. Funds for employing research assistants for work on HMNZS Endeavour, and some data reduction, were provided by the Internal Research Committee of the University.

A considerable amount of the data used are either unpublished or were provided prior to publication. Without these data, and in the detailed form provided, much of this study would not have been possible. I am grateful to the following people and organizations for providing data. N.Z. Oceanographic Institute, through J.W. Brodie and D.E. Hurley, for Endeavour bathymetric data. Geophysics Division, D.S.I.R., through T. Hatherton, for some magnetic profiles. Scripps Institution of Oceanography, through S.M. Smith, for Aries data. U.S. Naval Oceanographic Office, through H.P. Stockard, for Project Magnet data. Lamont-Doherty Geological Observatory, through J.R. Heirtzler, W.C. Pitman, D.E. Hayes and D.A. Christoffel, for Operation Deep Freeze, Vema, Conrad, and Eltanin data.

Rosalie Ellis patiently and expertly typed the draft and final editions of the text. Feriel Falconer also helped with typing and drawings.

Special thanks go to my mother for the upbringing and support that has made my university work possible.

Most of all I would like to thank my wife Feriel for her patience and encouragement throughout all the work. Her contributions, both personal and professional, have been considerable.

# CHAPTER 1

## THE SEAFLOOR : OBSERVATIONS AND THEORIES

This chapter presents background material that is assumed in subsequent chapters. An introduction (1.1) is followed by descriptions of the major morphologic features and crustal structure of the oceanic areas (1.2). Then major theories concerning the evolution of the crust (1.3) and some extensions of these theories (1.4) are discussed. A footnote follows (1.5).

### 1.1 INTRODUCTION

In the last two decades there has been a tremendous increase in the knowledge of the oceanic areas of the earth. Probably the most important conclusion from the new knowledge is that there is a great unity in the structure of the seafloor. Magnetic anomaly patterns in the South Atlantic are virtually identical to those south of Australia (Heirtzler et al., 1968). Paleomagnetic reversal sequences in deep sea cores from the Scotia Sea are the same as those from the North Pacific (Opdyke, 1972). Earthquake first motion patterns from the North Atlantic are just like those from the Indian Ocean (Sykes, 1968). Gravity anomalies across the Japan Trench are very similar to those off Chile (Hayes and Ewing, 1971). Many other examples could be given. There is also much diversity in the oceanic areas and it is probable that this diversity contains many clues to a better understanding of the development of the earth's structure. It is therefore useful to know as much as possible about different areas of the earth.

This study is a contribution on one area, the southwest Pacific. The area cannot be fully understood in isolation from the rest of the earth and throughout this study facts and theories concerning other areas have consciously, and unconsciously, been used to a large extent. It is therefore necessary to briefly discuss some of the knowledge and theories of the structure of the earth. The discussion that follows concentrates on aspects which are most important to this study. Consequently most of it concerns oceanic areas, and even then concentrates on particular topics. The literature on all these topics is now extensive and the references given are frequently to the more recent papers which refer also to earlier work.

## 1.2 MORPHOLOGY AND CRUSTAL STRUCTURE OF THE SEAFLOOR

### 1.2.1 General

The most obvious classification of the earth is into areas of land and areas of ocean. The latter cover 71% of the earth's surface (Wyllie, 1971). However many of the land masses are surrounded by shallow shelves which structurally are more properly considered part of the land area. This reduces the oceanic areas of the earth to 63% of the total area (Menard and Smith, 1966). There is a basic difference in elevation and crustal structure between the continental (land) areas and oceanic areas; and the transition between the two areas is relatively abrupt. Seismic refraction results (Raitt, 1963; James and Steinhart, 1966) and earthquake surface wave studies (Oliver and Dorman, 1963) show that the thickness of the crust is 30-40 km in continental areas but only 6-7 km in oceanic areas (Fig. 1.1).

The oceanic crust is not a single layer but consists of several layers which are defined primarily from compressional wave velocities (Fig. 1.1). Not all the layers are always present but the crustal structure of undisturbed oceanic basins is remarkably uniform and can be considered as "average" oceanic crust (Ludwig et al., 1971). It has the following structure. Firstly one or more layers of sediment, whose thickness is controlled by many factors but ranges from several kilometers to virtually zero. Then a basement layer (Layer 2) of velocity averaging 5 km/sec. The range of Layer 2 thicknesses is 1-6 km but most results are between 0.8 km and 2 km (Shor et al., 1971a). In some areas two or more component layers are observed in Layer 2 (Den et al., 1969; Talwani et al., 1971). Beneath Layer 2 is Layer 3 which has an average velocity of 6.8 ± 0.3 km/sec and an average thickness in the basins of about 5 km. Layer 3 is termed the oceanic layer and Menard (1967a) considers that the essential characteristic of oceanic crust is that it contains this layer. The crust/mantle boundary is defined by the Mohorovicic discontinuity (Moho) below which compressional wave velocities are greater than 7.8 km/sec. The Moho lies at depths between 10 and 13 km below sealevel in ocean basins.

A knowledge of the morphology and crustal structure of the major features of the seafloor has been central to all theories on the evolution of oceanic areas. Heezen and Menard (1963), reviewing the topography of the seafloor, considered that there are three main morphologic divisions: continental margin, ocean-basin floor, and mid-oceanic ridge. Each division is subdivisible and there is a certain amount of overlap. There are also features which do not readily fit into the main divisions. Details of the major features are discussed in following subsections, but first a comment on geophysical techniques.

### 1.2.2 Geophysical techniques

The techniques used for investigating the structure of the oceanic areas will not be reviewed here. They have been fully discussed in many publications, in particular in Volumes three and four of The Sea (Hill, 1963; Maxwell, 1971). An important new development not discussed there is the deep sea drilling project which provides the ability to drill and sample all of the sedimentary layer and at least the upper part of the basement layer of the seafloor.

Deep sea drilling has yielded several important results relevant to the interpretation of results from the primary techniques of investigating oceanic sedimentary deposits i.e. seismic reflection profiling (Hersey, 1963) and sonobuoys (Houtz et al., 1968; Le Pichon et al., 1968). Seismic reflections show only interfaces across which the acoustic impedance changes and they provide no direct evidence of sediment age. Deep sea drilling has shown that (1) Prominant continuous reflectors may not be isochron surfaces as previously thought (Fischer et al., 1970; Ewing et al., 1970; JOIDES 1971a). (2) There may be substantial changes in lithology and major time discontinuities which are undetected by seismic profiling (Kennett et al., 1972; JOIDES, 1973a,b). (3) Sediment at the seafloor may be more than 50 million years old (JOIDES, 1973d), which is dramatic confirmation of the previously recognized importance of bottom water currents as an erosional process (Ewing et al., 1969; Le Pichon et al., 1971b; Watkins and Kennett, 1972). These results have to be kept in mind when seismic reflection records are discussed.

### 1.2.3 Continental Margin

The continental margin consists of the areas associated with the transition from continent to ocean floor. There are two general types of margin. (1) the Atlantic type; consisting of continental shelf, continental slope and continental rise which merges into the oceanbasin; and (2) the Pacific type; that typically has a narrow continental shelf, then a continental slope which goes into a trench, beyond which is the ocean basin (Heezen and Menard, 1963).

The continental shelf varies in width from 0 to 1500 km, averaging 78 km. Gradients on the shelf average 1:1000 and the outer edge is usually delineated by a sharp increase in gradient to the continental slope. The depth of the shelf break averages 133 m but ranges from 20 to 550 m (Menard and Smith, 1966). Where geophysical and direct sampling data coverage is good the continental shelves are found to be similar to their adjacent land

mass (Ludwig et al., 1971). The majority of continental shelves are of Guilcher's (1963) "constructional subsiding" type, which is characterised by a subsiding shelf capped with thick continental sediments (Ludwig et al., 1971).

In some places there are shelf-like features at depths greater than the continental shelf and separated from the regular shelf by a scarp or low continental slope. Heezen et al., (1959) have termed these features marginal plateaus but some examples are referred to as terraces (Hayes and Conolly, 1972). Notable examples are the Malvinas (Falkland) Plateau (Lonardi and Ewing, 1971) and the Blake Plateau (Pratt and Heezen, 1964). The marginal plateaus usually have crustal structure similar to the adjacent continental shelf (Ludwig et al., 1971). They are generally only associated with Atlantic type continental margins.

There are several independent shelves separate from the continents and the large (continental) islands such as Madagascar. These independent shelves are not large and range in depth from shallow, e.g. Rockall Bank (Jones et al., 1972) and the Seychelles (Davies and Francis, 1964) to more than 1000 m, e.g. Agulhas Plateau (Laughton et al., 1971) and South Tasman Rise (Hayes and Conolly, 1972). Geophysical and direct sampling data (e.g. Davies and Francis, 1964; Jones et al., 1972; JOIDES, 1973c) indicate that they are continental.

The continental slope is effectively the outer edge of the continental block (Worzel, 1965). Gradients on the slope range from near vertical to 1:40, and the steepness makes it difficult to determine the crustal structure of the slope. Recent geophysical results (e.g. Luyendyk and Phillips, 1970; Hayes and Ewing, 1970; Talwani and Eldholm, 1972, 1973; Scrutton and du Plessis, 1973) indicate that the structure is more complex than previously thought (e.g. Worzel, 1965). There may be subsided continental crust under the slope, and the continental-oceanic crust boundary may be marked by buried or partly exposed ridges with deeper basement landward.

The continental rise of an Atlantic type margin is a transition area between the steep continental slope and the flat ocean basin. The rise area is discussed further later, as from its crustal structure it is more appropriate to consider it part of the basin.

The trenches which characterise the Pacific type margins reach depths of more than 10 km and are mostly less than 100 km wide. Gradients on the landward walls range from 1:10 to near vertical. The seaward walls are usually not so steep and often exhibit benches indicative of faulting (Fisher and Hess, 1963; Hayes and Ewing, 1971). The floors of some of the trenches are

flat due to the presence of undisturbed turbidite deposits (Scholl et al., 1970; Hayes and Ewing, 1971). The nature or even existence of sediments landward of the trenches is difficult to determine. Small amounts of ponded sediment are not infrequent (Hayes and Ewing, 1971) but substantial sediment deposits have been detected only off Japan (Ludwig et al., 1966) and the Aleutians (JOIDES, 1971c; Holmes et al., 1972; von Huene, 1972). Highly disturbed incoherent sediment would be hard to detect with present techniques.

### 1.2.4 Mid-ocean Ridge

The most prominent feature of the oceanic areas is the mid-ocean ridge system, which covers 33% of the deep ocean floor (Menard and Smith, 1966). The existence of a continuous world-encircling ridge was postulated in the late 1950's on the basis of sparse bathymetric and earthquake epicentre data (Heezen et al., 1959). Subsequent work has verified its existence and Heezen (1969) pointed out that not a single gap has been proven throughout its more than 50,000 km length. The Australian-Antarctic discordance (Hayes and Conolly, 1972) may now be an exception to Heezen's (1969) statement that no fundamental local or regional variations have been found in the essential characteristics of the ridge.

Earthquake epicentres are associated with the axis of the ridge system and the general continuity of the ridge through the Arctic, Atlantic, Indian and Pacific oceans is readily seen from epicentre maps (e.g. Fig. 0.2). Topographically the ridge is approximately triangular in crossection. The depth of the axis varies between 1000 m and 3300 m but is usually between 2300 and 2800 m (Sclater et al., 1971; Anderson et al., 1973). In some areas, particularly the Atlantic and southwest Indian oceans, the axis is marked by a rift up to 2000 m deep, and the ridge flanks have relief up to 1500 m. Elsewhere the triangular crossection is remarkably uniform with relief less than a few hundred meters (Heezen and Ewing, 1963; Heezen, 1969).

At the axis of the mid-ocean ridge sediment thickness is virtually zero (Ewing and Ewing, 1967, 1971). It increases outward from the axis with most of the sediment on the flanks being of pelagic origin. Ponding in hollows and current scour produces some smoothing of the flanks (Ewing et al., 1969; Keen and Manchester, 1970) but flat topography is not generally found until the distal margins of the abyssal plains.

The upper surface of Layer 2, the basement layer, is exposed at the sediment free areas of the ridge. The thickness at the axis of the basement layer is roughly inversely proportional to the spreading rate of the ridge (see later), and there does not appear to be much change in thickness away

from the axis (Menard, 1967b; Shor et al., 1971a). The thickness at the axis of the oceanic layer, Layer 3, ranges from zero on slow spreading ridges (e.g. North Atlantic) to 4-5 km on fast ridges (e.g. East Pacific Rise). Away from the axis the oceanic layer everywhere thickens to an average of about 5 km (Le Pichon et al., 1965; Shor et al, 1971a).

Seismic activity clearly delineates several branches from the main mid-oceanic ridge system (Fig. 0.2). Of these branches the Chile ridge (Herron and Hayes, 1969), Galapagos ridge (Raff, 1968; Herron and Heirtzler, 1968) and probably the Southwest Atlantic ridge (Morgan and Johnson, 1970) are similar to the main ridge system in structure and tectonic nature. The Macquarie ridge (Hayes and Talwani, 1972) and the Azores-Gibralter ridge (Krause and Watkins, 1970; Laughton et al., 1972) are also seismicly active branches but their morphology is complex and they are not tectonically part of the mid-oceanic ridge system (see later).

### 1.2.5 Ocean basins

The deep ocean basins occupy approximately 40% of the oceanic area (Menard and Smith, 1966) but it may be misleading to specify an area because there is a continuous transition from the mid-ocean ridge to the deep basins which flank the ridge. The transition to the continental margin is usually more marked.

In areas accessible to sediments from the continents there are usually flat abyssal plains with gradients less than 1:1000; the flatness being due to the horizontal nature of turbidity current deposits (Hamilton, 1967a). Elsewhere the basins consist of abyssal hills which have relief ranging from a few meters to 500 m (Heezen and Menard 1963); and the only cover over the basement is pelagic sediment usually less than 300 m thick (Ewing and Ewing, 1971). In areas where detailed surveys have been done the abyssal hills are found to be elongate parallel to the ridges they flank (Moore and Heath, 1967; Menard and Mammerickx, 1967; Naugler and Rea, 1970).

The major accumulations of sediment in oceanic areas are in continental rises and basins adjacent to Atlantic type margins (Ewing and Ewing, 1971; Ewing et al., 1973). The continental rises are essentially sedimentary aprons consisting of highly stratified sections, occasional slump structures, and a general pattern of layers thickening landward. Sediment thicknesses up to 5 km are observed at some margins (Houtz and Markl, 1972). The increase in sediment thickness toward the margin is partly due to increasing depth to the top of the basement. The basement often has a similar outline to the trenches of the Pacific type margins which has led Worzel (1965),

Ludwig et al., (1971), and others to suggest that the continental rise is a sediment-filled trench, and that the Atlantic and Pacific type margins are basically similar. However there are Atlantic type margins with thick sediment at which there is no depression of the basement (Houtz and Markl, 1972; Houtz and Davey, 1973).

The upper surface of the basement layer is usually just as rough under the sediment cover of the basins as it is where it is exposed on the ridges (Ewing and Ewing, 1971). Where the deepest reflector observed is relatively smooth it may represent very low viscosity basalt flows (Vogt and Johnson, 1973) but more probably it represents not smooth basement but highly reflective layers of chert or ash interbedded with sediment (Houtz et al., 1970; Vogt and Johnson, 1973).

### 1.2.6 Island arcs and marginal basins

The term island arc as now used generally implies a morphologic feature consisting of both a trench not associated with a continental margin and an arc structure. The latter consisting of one or more ridges made up of active or inactive volcanoes (Karig, 1970). Some island arcs are arcuate but others are linear and the term arc does not imply any specific shape. The island arc trenches are similar to those associated with Pacific type continental margins (Hayes and Ewing, 1971). On the opposite side of the arc from the trench there is a basin. These basins, termed marginal basins (Menard, 1967a; Karig, 1971) have depths equal to or less than typical ocean basins. Most of them are of oceanic crustal structure in that they have the oceanic Layer 3, although they often have irregular Layer 2 structure (Menard, 1967a; Shor et al, 1971a,b).

### 1.2.7 Islands and Seamounts

A seamount may be defined as a more or less isolated elevation of the seafloor of circular or elliptical plan with at least 1 km of relief and comparatively steep slopes (Menard and Ladd, 1963). All are considered to be of volcanic origin (Heezen and Menard, 1963). Evidence of current volcanic activity has been detected for some seamounts (Kibblewhite, 1966; Johnson, 1970), but the majority are relicts of previous activity. If the islands associated with island arcs and microcontinents (e.g. Seychelles) are excluded, oceanic islands may be considered special cases of seamounts.

Some islands are associated with the mid-oceanic ridge, e.g. Azores, Ascension, Prince Edward and St. Paul; but most rise from the ocean basins. Seamounts (and islands), unlike abyssal hills, are not randomly distributed.

Many of them occur in approximately linear chains. The most notable examples are the Hawaiian Islands and the Emperor seamount chain but numerous other examples can be seen on charts. In some cases the chains rise from a low rise, which presumably is a result of piling up of material from the volcanoes (Menard and Ladd, 1963). Other chains consist of relatively isolated seamounts rising directly from the ocean floor.

### 1.2.8 Fracture Zones

Fracture zones are long, narrow zones of irregular topography. Their topography can consist of elongate troughs, large steep ridges, scarps, seamount lineations, and combinations of all of these (Menard and Chase, 1971; Van Andel, 1971). Different regional depths are often characteristic of the two sides of a fracture zone (Menard, 1964). Where they intersect the mid-oceanic ridge they usually mark offsets in the axis, and deep troughs with depths as great as those in the deep basins may occur (Heezen et al., 1964a,b; Heezen and Nafe, 1964; Matthews et al., 1967). Away from the mid-ocean ridge fracture zones are most commonly indicated by narrow ridges up to 3 km high (Menard and Chase, 1971; Herron, 1971; Rea and Naugler, 1971). but troughs also occur (Erickson et al., 1970; Collette and Rutten, 1972).

## 1.3 MAJOR THEORIES

The major theories which are central to present understanding of the evolution of the earth's crust are continental drift, seafloor spreading and plate tectonics. A fourth newer concept, plumes, is likely to become a major theory but it is probably fair (if conservative) to say that it has not yet achieved the status of the other theories. All the theories are interrelated but it is easiest to describe them in historic sequence.

### 1.3.1 Continental drift

The term continental drift is used to describe the concept that the continents may formerly have been in different positions relative to their present positions. Serious scientific debate about the concept dates from the early twentieth century. Wegener (e.g. 1929) was the first major advocate and he received strong support from Taylor (1910), du Toit (1927; 1937) and others. The main lines of evidence were paleoclimatology, paleontology, the geometrical fit of the continents, and the match of stratigraphy and truncated structures across the oceans. Much of that type of data was and still can be (Meyerhoff and Meyerhoff, 1972a) considered equivocal. However the main objection concerned the mechanism of drift. Jeffreys (1924, 1959)

showed that the rigidity of the crust was such that the continents could not, as had been suggested, "sail through the oceans". He, and others, considered that lack of a suitable mechanism for continental drift was a fundamental objection, and the concept did not achieve widespread support until after interest in the debate revived in the late 1950's with the advent of paleomagnetic studies (Takeuchi, et al., 1970).

The essence of paleomagnetic methods is that the direction of remanent magnetization in suitable rock samples can be used to estimate the position of the magnetic pole at the time the rock formed (Runcorn, 1962). Two assumptions are inherent. (1) The mean geomagnetic field has always been dipolar. (2) The rocks used acquired a magnetization which was closely parallel to the direction of the field at the time of their formation and which has been retained unchanged since.

A wide variety of experimental results indicate that provided suitable precautions are taken the assumption of stable magnetisation is valid (Creer, 1970). The dipole field assumption is more difficult to verify (Stehli 1968, 1970). The magnetic field is not axially symmetric or completely dipolar today (Vestine, 1967). However it appears that when averaged over a few thousand years the field during at least the last 20 million years (hereafter my) has been approximately that of an axial dipole (Irving, 1964; Opdyke and Henry, 1969) although not necessarily a geocentric dipole (Wilson, 1971; McElhinny, 1973b). For earlier periods the evidence is more indirect: (1) There are theoretical reasons for believing that the field would always be closely axially symmetric (Bullard and Gellman, 1954; Lilley, 1970). (2) Internal consistency of paleomagnetic results argues strongly for a dipole field (Runcorn, 1962; Irving, 1964; Creer, 1970). (3) A recent spherical harmonic analysis of paleomagnetic data (Benkova et al., 1973) indicates that the field has been dipolar since the Mesozoic.

The specific contribution of paleomagnetism to the continental drift debate is data for the position of the magnetic pole with respect to different continents at various times. For any one continent the pole positions delineate a regular path with time. If this is interpreted as movement of only the pole the paths for different continents would be the same (Runcorn, 1956). The paths are similar but they diverge from each other going back in time. The logical conclusion is that the continents have moved relative to each other (Runcorn, 1962). Furthermore the movements suggested are compatible with the continental drift suggested from other data (Runcorn, 1962; Irving, 1964; McElhinny, 1973b).

There are now reasonably good polar wander curves for most continents (Runcorn, 1965; Creer, 1970; McElhinny, 1973b) and with care it is possible

to reconstruct the former positions of the continents at various times entirely from paleomagnetic data (Francheteau and Sclater, 1969; McElhinny and Luck, 1970). Fine detail in the movements of the continents is not usually determinable but broad constraints can be placed on their positions at major intervals, e.g. Permian, Jurassic, Cretaceous. Unfortunately there is virtually no data for the movements during Tertiary times (McElhinny, 1973b).

Despite some opposition (Beloussov 1968a,b, 1970; Meyerhoff and Meyerhoff 1972a, b) continental drift is now widely considered to be a proven fact, but in the early 1960's there was much less certainty, mainly because of the difficulties of a suitable mechanism (Jacobs et al., 1959). Convection in various forms had been suggested (e.g. Holmes, 1931; Griggs, 1939) but it was the seafloor spreading concept which provided the first wide acceptance of the plausibility of continental drift.

### 1.3.2 Seafloor spreading

The concept of seafloor spreading formulated by Hess (1962) and Dietz (1961) arose through attempts to explain the known structure of the seafloor. The basic principles of the concept as expressed by Hess (1962) are as follows. (1) The mantle is convecting. (2) The convecting cells have rising limbs under the mid-ocean ridge and mantle material comes to the surface on these ridges. (3) The continents are carried passively on the mantle with convection and do not plow through oceanic crust, but their leading edges are deformed when they impinge upon downward moving limbs of convecting mantle. (4) The cover of sediments on the seafloor "ride down into the jaw crusher of the descending limb are metamorphosed and eventually probably welded onto continents". (5) The ocean basins are impermanent features, and the continents are permanent, although they may be torn apart or welded together and their margins deformed. Even if an ocean basin is assumed to be old the seafloor itself may be much younger as the older seafloor can have descended back into the mantle at a downwelling site - usually assumed to be a trench.

It is not now considered that the oceanic crust is directly part of the convecting system or that the convecting cells are tied to ridge axes (see later), but otherwise the basic principles stated above are still assumed.

Many facts of oceanic crustal structure are explained by the concept. (1) Hot mantle material upwelling at the ridge axes readily explains the high heat flow near the mid ocean ridge (approximately eight times that of the basins (Langseth and von Herzen 1971)). (2) The uniform thickness of Layer 3 is explicable if its base represents a present or past isotherm at which a temperature and pressure reaction occurred. Any of the suggested reactions for the production of Layer 3 would take place in the high temperature regions

of the mid-ocean ridge (Hess 1962, 1965; Cann, 1968, 1970; Vine and Moores, 1972) and as seafloor spreading carries the crust away the reaction boundary is frozen in. (3) The lack of the very thick sediment that would have been expected in permanent ocean basins is explained by the impermanent nature of the basins. (4) The now well known pattern of sediment thickness being zero at the ridge axis and increasing outward is just what would be expected with seafloor spreading from the axis.

Deep sea drilling results have provided widespread confirmation that as predicted by seafloor spreading the maximum age of the sediment increases away from the ridge axis (Fischer et al., 1970; Maxwell et al, 1970; Van Andel, 1972). This is convincing support for the concept of seafloor spreading but even prior to deep sea drilling very convincing support had come from the study of oceanic magnetic anomalies. That Hess should formulate his hypothesis without any reference to them may today seem surprising but in the early 1960's there was only a small amount of magnetic data available (Heezen et al., 1953; Mason, 1958) and no ready explanations for it (Bullard and Mason, 1963).

It was Vine and Matthews (1963) who first clearly stated the hypothesis which has become fundamental to the interpretation of marine magnetic anomaly data. Details of the hypothesis will be discussed more fully in subsequent sections and chapters but briefly the principles are as follows. New crustal material forms at the axis of the mid-ocean ridge and becomes magnetized in the direction of the earth's field at the time at which it cools through the Curie temperature. Seafloor spreading moves the cool material laterally away from the ridge axis and new material upwells. If the earth's magnetic field periodically reverses as spreading continues successive strips of crust paralleling the ridge will be alternately normally and reversely magnetized. Provided remanent magnetization is more important than induced magnetization the alternately magnetized blocks produce an increase or decrease in the ambient field, thus producing linear anomalies.

At the time Vine and Matthews stated their hypothesis seafloor spreading was a relatively new concept and there was no proof of its validity, the importance of remanent magnetization was not widely appreciated, and the existence of reversals had only just been recognized (Wilson, 1962). The acceptance and proof of the Vine and Matthews hypothesis has been a gradual process so it is probably not surprising that three important corollaries of the hypothesis appear to have come into widespread use without a single clear statement of their existence (See Appendix 1A for a bibliographic note). These corollaries are as follows:

(1) Identical anomaly profiles at different places imply that the seafloor at those places is of the same age.

(2) If the reversal dates are known the seafloor can be dated from magnetic anomalies.

(3) If the seafloor age is known reversal dates can be determined from magnetic anomalies.

The first one: identical anomalies imply identical ages follows from the fact that reversals are a world wide phenomena hence all the seafloor formed at any one time has the same polarity. As the seafloor spreads it records the field reversals in taperecorder fashion and all seafloor formed during the same time interval irrespective of where it is on the earth contains the same taperecording. Consequently the anomalies observed in different areas will be the same if the areas formed at the same time. The age of the areas does not need to be known for it to be possible to say that they are of the same age, all that is required is the same anomalies. Of course the reversal sequence, hence magnetic anomaly sequence, has to be sufficiently unique so that it can be assumed that it would not have occurred more than once in time.

The second corollary: reversal dates known, seafloor age determinable, also relies on a unique sequence of anomalies. If the dates of all the reversals in a particular time interval are known it is possible to calculate the magnetic anomaly profile that would be observed over seafloor that had formed by seafloor spreading at a chosen rate during the time interval. If an observed anomaly profile matches the calculated profile it is legitimate to say that the seafloor beneath the observed profile formed during that time interval. Then the age of the seafloor at a point of the profile can be determined. The use of a time interval is important as without several reversals it is not possible to have a sequence which can be matched with a reasonable degree of uniqueness.

The third corollary: seafloor age known, reversal dates determinable, depends on the assumption that the anomalies observed over a section of seafloor are produced by a sequence of normally and reversely magnetized blocks. Not all anomalies need originate this way, especially if there are contrasts of topography or crustal structure, but the assumption is useful in relatively uniform areas. The positions of the boundaries between the normal and reverse blocks are chosen such that a model profile calculated from the blocks fits the observed profile. The age of the seafloor at the block boundaries then defines the date of the field reversals.

In practice all the corollaries are often used in an intertwined fashion. The literature contains many examples of their use but some more important ones are as follows. Vine and Wilson (1965) used reversal dates determined by Cox et al. (1963) from continental lavas to show that the magnetic

anomaly pattern either side of the Juan de Fuca ridge was what would be expected. This was the first confirmation of the Vine and Matthews hypothesis. Vine (1966) and Pitman and Heirtzler (1966) identified the same anomaly pattern over other ridges and used known reversals during the last 3.5 million years before present (hereafter mybp) to determine spreading rates across several ridges. Pitman and Heirtzler (1966) assumed uniform spreading at the East Pacific rise and from the anomalies deduced reversal dates for the last 10 mybp. Vine (1966) went further and calibrated an anomaly sequence in the northeast Pacific back to 80 mybp. He also observed that similar anomalies, hence similar age seafloor could be seen south of New Zealand and in the northeast Pacific. Heirtzler et al. (1968) and many others have identified similar anomaly patterns throughout most of the oceans. Heirtzler et al. (1968) have tabulated the dates of reversals for the last 75 mybp which will simulate the observed anomalies. Minor revisions to these dates have been given by Talwani et al. (1971) and others. Deep sea drilling results (Maxwell et al. 1970; Van Andel 1972) have provided general confirmation of the Heirtzler et al. reversal scale, which was based on a twenty fold extrapolation. Larson and Pitman (1972) have correlated magnetic anomaly lineations in several areas in the northwest Pacific with the north Atlantic and used deep sea drilling dates to date the lineations as 110 to 150 mybp. These are the oldest anomalies to which dates have been assigned. As yet undated anomaly lineations exist in the southeast Pacific (Herron, 1971).

Many more examples could be given. The impact of magnetic anomaly studies on the seafloor spreading concept has been very significant, and coupled with deep sea drilling results has provided virtual proof of seafloor spreading. There are some difficulties with the original concept as expressed by Hess and Dietz if the mantle convection is assumed to take place right up to the seafloor. However the new concept of plate tectonics avoids the difficulties inherent in simple seafloor spreading and provides an even more complete understanding of the structure and evolution of the earth's crust.

### 1.3.3 Plate Tectonics

The concept of plate tectonics is an extension of the ideas of continental drift and seafloor spreading. The key elements were set out by McKenzie and Parker (1967) but Morgan (1968) formalized the concept. The basic assumption is that the earth's surface can be considered to be a mosaic of rigid plates, the boundaries of which are determined by present-day tectonic activity. Fig. 0.2 shows that large areas of the earth are aseismic; these areas are the rigid plates. Most of the seismicity is concentrated in narrow belts,

which mark some of the boundaries between the plates. There are three types of boundary (Fig. 1.2)

(1) Extensional, where plates move apart and new crustal material emerges.

(2) Compressional, where plates move towards each other and material is either absorbed or compressed.

(3) Pure slip, where plates slide parallel to each other and surface material is neither created nor destroyed .

The assumption of rigid plates permits the use of a geometrical framework for describing the motion of the plates. A rigid plate on a sphere can be moved to any other orientation by a single rotation about a properly chosen axis through the centre of the sphere. This means that the relative motion between any two plates can be described by an angular velocity vector. The direction of the vector is specified by the point at which the axis of rotation cuts the surface of the earth. The point is referred to as the rotation pole. The magnitude is specified by the angular speed, referred to as the rotation rate. Details of the methods for determining the rotation vectors are given later but briefly they are as follows.

The position of the rotation pole for two plates can be determined from a knowledge of the direction of motion at two or more points on the boundary between the plates. The rotation rate can be determined from the rate of motion at one or more points. It is also possible to determine the angular velocity vector for two plates without any data from their boundary. This is possible because the angular velocity vectors describing plate motions add vectorially. If the rotation vector $\omega(a,b)$ is known for plates A and B, and $\omega(b,c)$ is known for B and C then the vector for A and C, $\omega(a,c)$, is given by vector addition.

$$\omega(a,b) + \omega(b,c) + \omega(c,a) = 0 \qquad \ldots.1.1$$

and

$$\omega(a,c) = - \omega(c,a)$$

Any number of terms can be included in equation 1.1 so it is possible to use circuits involving more than three plates. Morgan (1968) and Le Pichon (1968) illustrate examples with up to five terms.

The power of plate tectonics is that it is a theory which is able to make predictions. If the pole of rotation for two plates is known it is possible to predict the direction of motion at any point on their boundary. If in addition the rotation rate is known the rate of motion at any point can be determined. The vectors of relative velocity between two plates must lie along small circles about the rotation pole. If the boundary between two

plates is along a small circle only pure slipping motion will occur and the boundary will be a strike-slip fault. If the boundary crosses a small circle either compression or extension will occur, which one depending on the sense of rotation (Fig. 1.2). Thus in principle it is possible to use data from one area of the world to predict quantitatively what is happening in another area.

Le Pichon (1968) was the first to exploit the predictive nature of plate tectonics. He subdivided the earth into only six plates so that with the available data from five plate boundaries he could determine all possible interactions. He was then able to calculate relative velocities at boundaries for which he had no data. Isacks et al. (1968) discussed global seismicity data in terms of plate tectonics. In particular they showed that directions of motion given by slip vectors deduced from the earthquake focal mechanism studies of Sykes (1967) and others agreed with the directions predicted by Le Pichon. Boundaries where pure slip was predicted had strike-slip focal mechanisms and were generally areas of known strike-slip faults. Boundaries where extension was predicted were mid-ocean ridge axes where seafloor spreading was occurring. Boundaries at which compression was predicted were either fold mountains or trenches. The fold mountains were where continental crust was compressed against continental crust. The trenches were where oceanic crust was involved: the island arc trenches where the compression was oceanic-oceanic, the Pacific type continental margin trenches where it was oceanic-continental compression (Fig. 1.3).

The plates are defined by the tectonic activity that defines their boundaries, not from the distribution of continental or oceanic crust. Many plates contain both continental and oceanic areas (Fig. 0.2). However the two types of crust do behave differently. Intermediate (70-300 km) and deep (300-700 km) earthquakes at trenches indicate that the oceanic parts of a plate are going down as a rigid slab (Oliver and Isacks, 1967) - the plate is being "subducted". The lower density of the continental crust prevents it being subducted and when it is under compression only intense folding occurs. Thus the permanence of continents in Hess's (1962) seafloor spreading concept is clearly retained in plate tectonics, and his impermanence of oceanic crust arises from removal of the crust in subduction zones.

The crust as defined by the Moho is only the upper part of the rigid plate. The plate is considered to consist of all of the rigid outer part of the earth below which is a low strength asthenosphere. Attenuation of seismic waves and travel time residuals at trenches indicate that the down going plate is 75-100 km thick (Oliver and Isacks, 1967; Davies and McKenzie, 1969; Aggarwal et al., 1972). Global velocity studies (Kanamori and Press, 1970;

Press, 1970) indicate that the base of the lithosphere is at 70-80 km in oceanic areas and up to 150 km in continental areas. It is the whole of the lithospheric layer which is considered to move as a rigid plate. Although the plate thickness of 70-100 km is substantial some plates are up to 10,000 km long so they are really very thin.

A major difficulty in the original seafloor spreading concept was that the seafloor at the mid-ocean ridge was assumed to be the upper surface of a convection cell. The ridge axis is frequently offset to form short sections of spreading ridge and it is very difficult to suggest a plausible pattern of convection currents which will fit the ridge configuration (Heirtzler, 1968). Plate tectonics alleviates the problem as any convection is assumed to take place below the rigid plate and no correspondence between ridge axis and convection cell is required. The question of whether material upwells passively at ridges because plates are pulled apart or whether it forces them apart is an open question (Morgan, 1972b), but the addition of new material at the mid-ocean ridge is regarded as a plastering onto the vertical side of a sideways moving slab (Sclater and Francheteau, 1970; McKenzie, 1972a) rather than the earlier idea of the rolling over of a rising limb of a mantle convection cell.

Plate tectonics incorporates all the ideas of seafloor spreading except the details of convection, and it provides a much greater understanding of global tectonics. However it provides only a kinematic description of the plate movements. It does not answer the question of what drives the plates. Various driving mechanisms have been discussed by, for example, Hales (1969), Jacoby (1970), Elsasser (1971) and Nelson and Temple (1972). Convection in the upper mantle has featured in most mechanism discussions but it usually presents some difficulties. A new concept of convection plumes from the lower mantle may permit a dynamical description of plate motions, and the hot spots associated with plumes may also provide information on the absolute movements of the plates. If so the usefulness of the concept of plate tectonics will be even greater than it is now.

### 1.3.4 Mantle plumes and hot-spots

The Hawaiian Islands are a long linear volcanic chain the age of which gets progressively older to the northwest. This is explicable if the Pacific plate is moving north westward over a fixed source of volcanism (Wilson, 1965). Other chains of islands and seamounts, and aseismic ridges, that get older away from presently active volcanic sources also can be explained if the lithospheric plates are moving away from or over fixed volcanic sources (Wilson 1963, 1965; Morgan, 1971). The trajectories of four major volcanic lineations in

the Pacific fit a simple rotation of the Pacific plate about a pole, which indicates that the sources are fixed with respect to each other (Morgan, 1972a). Similar analysis for other volcanic chains indicates that the positions of most of the sources are fixed with respect to each other. These sources are now referred to as mantle hot-spots (Morgan, 1971).

The primary criterion for selecting the locations of the active hot-spots is recent volcanism not associated with island arcs. There are more than 20 hot-spots (Morgan, 1972a) the majority of which are in oceanic areas and near spreading axes. Many of them are associated with positive regional gravity anomalies, which led Morgan (1972a,b) to suggest that the hot-spots are the surface expressions of deep mantle plumes roughly 150 km in diameter extending from the lower mantle. The rising material in a plume spreads out in the asthenosphere producing stress on the base of the lithospheric plates. Order of magnitude estimates show that the stresses could have a significant influence on plate motions.

There is increasing interest in the concept of plumes and hot-spots especially as a means of further explaining some of the changes in earth structure that have been deduced from continental drift, seafloor spreading, and plate tectonics. It is difficult to definitely show that the plumes are stationary with respect to the mantle (McElhinny, 1973a,b) but if they are they provide a valuable reference frame for determining absolute plate motions (Dietz and Holden, 1970; Morgan, 1972a,b). The lifetime of an active plume may be of the order of tens of millions of years and the formation of and decay of plumes could be the cause of major changes of plate motions. The location of plumes with respect to plate boundaries could control the symmetry of seafloor spreading. The initiation of a plume under a continent could provide the forces required to start continental drift.

## 1.4 DETAILS AND EXTENSIONS OF THE MAJOR THEORIES

In this section some particular topics that arise from the major theories described above are discussed.

### 1.4.1 Plate boundaries, triple junctions, and continental margins

The boundaries of the plates assumed in plate tectonics are defined by tectonic activity. The terminology usually used for the three types of boundary is as follows

(1) Pure slip boundaries are referred to as fault boundaries.

(2) Compressional boundaries are referred to as trenches, irrespective of whether they are morphologically trenches or fold belts.

(3) Extensional boundaries are referred to as ridges. The extensional areas which have been postulated in marginal basins (Packham and Flavey, 1971; Karig, 1971) are not included in the ridge definition as unlike ridges they are not narrow sites of extension.

Earthquake activity is associated with virtually all of the plate boundaries, the only significant exception being sections of spreading ridge with half-spreading rates greater than 3 cm/yr (Barazangi and Dorman, 1969).

Three plates may meet at one point, referred to as a triple junction (McKenzie and Morgan, 1969). The intersecting boundaries can be of any type and this leads to the classification of triple junctions in terms of the intersecting boundaries. For example the intersection of a ridge and two transform faults would be a ridge-fault-fault junction. In general the position of the junction moves relative to at least one of the intersecting plates. The movement can produce substantial changes in tectonic activity in an area, especially if one of the plate boundaries is a continental margin (McKenzie and Morgan, 1969; Atwater, 1970).

The two types of continental margin discussed in section 1.2.3 are clearly distinguished in plate tectonics (Fig. 1.3). The Atlantic type margin is a boundary between continental and oceanic crust and there is probably also some change in plate thickness across it, but it is not presently the site of any relative movement - it is not a plate boundary. The Pacific type margin, characterized by a trench, is a plate boundary. It is where an oceanic plate is being subducted under a continent. The similarities of the trenches of island arcs and Pacific type margins are easily understood in plate tectonics as both are subduction zones. The Atlantic type margins are considered to have originally been rift boundaries formed by the break-up of a continental mass (Dewey and Bird, 1970). The deepening of the basement at some Atlantic margins is then not a filled trench but is a consequence of the original rifting (Houtz and Markl, 1972; Sleep 1972). Where there is no basement deepening the initial movement may have had a large component of slip (Le Pichon and Hayes, 1971; Houtz and Markl, 1972).

### 1.4.2 Transform faults

Wilson (1965) recognized the continuity of the active tectonic belts of the earth's surface and he discussed how the three tectonic types: mid-ocean ridges, mountains (and trenches), and major faults with horizontal movement, were transformed from one to another. He introduced the term transform fault for the fault which links ridge and ridge, ridge and trench, or trench and trench. Examples of each type are shown in Fig. 1.2.

Transform faults have a special place in plate tectonics. Usage of the term transform fault is often loose but in this study it is taken to mean a boundary at which the relative velocity vector is parallel to the boundary, i.e. the motion is pure slip with no components of extension or compression. Earthquake focal mechanisms would indicate pure strike-slip motion. As an example Fig. 1.4 shows a plate boundary along which a ridge (AB) is transformed into a trench (DE). The section BC is a transform fault, but the section CD is not because the direction of motion is not parallel to the boundary.

The term transform fault also needs to be clearly distinguished from the term fracture zone. Fracture zone is a morphological term (section 1.2.8) but it is also used for a line across which a feature is offset. Fig. 1.5 shows two ridges linked by a ridge-ridge transform fault (AB). The anomaly lineations produced by the two ridges are offset along A'B' so A'B' defines a fracture zone. Sections AA' and BB' are referred to as inactive fracture zones because there is no relative movement along them. Motion takes place only along AB which is an active fracture zone. The term transform fault implies relative motion and so applies to only the section AB. Earthquake activity would occur only along the ridges and the transform fault.

### 1.4.3 Orthogonality of ridges and fracture zones

The active fracture zones on ridge boundaries can be identified from the offset of the topographic axis of the ridge, the offset of anomaly lineations, and seismicity. Focal mechanism studies of earthquakes on the fracture zones (Sykes, 1967; Tobin and Sykes, 1968; Banghar and Sykes, 1969) almost invariably indicate pure strike-slip motion. The active fracture zones are thus transform faults. It appears to be generally true that wherever a ridge axis is offset the active fracture zone and the ridge axis are orthogonal. Since the direction of spreading is parallel to the relative velocity vector the orthogonality of the axis and the fracture zone implies that the spreading direction is perpendicular to the ridge axis. This is not a necessity within the concept of plate tectonics as there is no geometrical reason why an oblique ridge couldn't exist.

Nature tends to minimise the total dissipation of energy so the prevalence of orthogonal ridges and transform faults indicates that that is a minimum energy configuration. Analysis of the dynamics of the configuration (Lachenbruch and Thompson, 1972) shows that friction per unit length on a transform fault must be less than the tensile resistance per unit length on a ridge. This suggests that boundaries will tend towards a configuration that minimizes the length of ridge axis. If a change in plate motion makes an existing spreading boundary oblique, or a new oblique spreading boundary forms, the boundary will readjust

into a series of short offset ridge sections. If the forces at ridge boundaries exert a significant influence on plate motions the preference for the minimum length of spreading ridge may partly dictate the patterns of plate motion.

### 1.4.4 Symmetry of spreading

It is often stated that all magnetic anomalies are symmetrical about the ridge axis thus indicating that seafloor spreading is symmetrical. However magnetic anomalies south of Australia indicate differences of up to 30% in the spreading rate either side of the ridge (Weissel and Hayes, 1971, 1972), and asymmetry is also evident elsewhere (Herron, 1971; Barker, 1972).

Morgan (1972a) argued that symmetrical spreading indicated that material upwelled passively at the ridge axis due to ridges being pulled apart. However he concluded later (Morgan, 1972b) that "we do not know whether rises are characterised by compressive stresses aiding the plate motion or by tensile stresses acting as a brake to plate motion". He argued (1972b) that the important factor is the temperature distribution. The lithosphere strength is strongly temperature-dependent so the plates always break at the hottest point, which will be where the previous material was injected. If the temperature distribution is symmetrical the seafloor spreading will be symmetrical. Morgan (1972b) suggests that symmetry will be best maintained if the material being added at the surface is drawn from shallow depths. Symmetrical spreading will then occur when one plate is fixed and the other plate and the ridge move (Fig. 1.6a) and when the two plates move apart from a fixed ridge (Fig. 1.6b). However if the rising material is strongly coupled to the lower asthenosphere (a plume?) symmetrical spreading will occur if both plates move (Fig. 1.6d) but not if one plate is fixed (Fig. 1.6c).

The question of asymmetry is important when data are available for only one side of the spreading centre. For example Larson and Chase (1972) have suggested that some Mesozoic anomalies mapped in the central Pacific were formed at the Pacific-Antarctic ridge. On the assumption of symmetrical spreading they then suggest that up to 10,000 km of crust has been underthrust beneath West Antarctica or South America. If so it could have great significance for the structure of those areas. However if asymmetrical spreading occurred no underthrusting need have taken place.

### 1.4.5 Topography and age

Mid-ocean ridges exibit a correlation between age and depth, depth increasing with age. Fig. 1.7 shows that many of the ridges have similar depths for the same age. The depth of the axis varies between 1000 m and 3300 m throughout the

oceans but all ridges spreading faster than 4.0 cm/yr have axial depths greater than 2600 m. Axial depths less than 2000 m occur only on ridges spreading at less than 2.0 cm/yr (Anderson et al., 1973). Irrespective of the depth of the axis the depth at 10 mybp is close to 1000 m below the axial depth. Almost all ocean basins older than 80 mybp have mean depths between 5500 and 6000 m (Sclater et al., 1971; Anderson et al., 1973).

A good match to observed topography can be obtained with models of an isostatically compensated lithospheric slab moving away from the ridge axis. The increasing depth being due to thermal contraction as the slab cools (McKenzie and Sclater, 1969, 1971; Le Pichon and Langseth, 1969; Sclater et al., 1971). The agreement with theory has led to widespread use of an empirical depth-age curve (Sclater et al., 1971) as a means of estimating the age of seafloor from topography alone. Places where the active ridge crest may have jumped to a new location have been identified this way (Sclater et al., 1971; Herron, 1972). Changes in spreading rate or cessation of spreading leading to steps in topography have also been elucidated (McKenzie and Sclater, 1971; Anderson and Sclater, 1972; Kasameyer et al., 1972).

### 1.4.6 Determination of rotation vectors

There are several different methods for determining the rotation pole and the rate of rotation for two plates, but all methods depend on two basic geometrical principles of plate tectonics: (1) The direction of relative movement is along a small circle about the rotation pole; (2) The rate of relative movement varies as the sine of the distance from the pole, i.e.

$$v(\theta) = v_m \cdot \sin(\theta) \qquad \ldots.1.2$$

where $v(\theta)$ is the velocity at arc distance $\theta$ from the pole and $v_m$ is the maximum velocity given by $v_m = \omega \cdot$ radius of the earth; $\omega$ being the angular rotation rate.

In general to determine rotation vectors, rates and directions of relative movement at various points are required. A direction can be determined from the slip vector of an earthquake focal mechanism solution or the strike of a fault or fracture zone. If the latter are used they must be active and pure strike-slip (Harrison, 1972a, 1973). The only rates of motion usually used are rates of spreading determined from magnetic anomalies at ridges. Rates determined from earthquakes (Brune, 1968) are not much better than order of magnitude estimates.

The simplest method for determining the rotation pole uses the fact that the perpendicular to a velocity vector is a line of longitude to the pole.

Knowledge of the slip vector at two or more points enables the pole to be found from the intersection of the longitudes. The first two "plate tectonics papers" (McKenzie and Parker, 1967; Morgan, 1968) used this method. Le Pichon (1968) introduced a more quantitative method which uses the differences between observed directions and directions calculated with an assumed pole position. The pole position is varied and the position which minimizes the differences is taken as the rotation pole.

With any method once the pole position is known the rotation rate $\omega$ can in theory be found using equation 1.2 with data from only one point on the boundary. A best fitting rate from several points is preferable.

The rotation pole and the rotation rate can be found at the same time from data of rates of movement (Le Pichon, 1968). The rate at a known direction at several places is required and the method is similar to that using only directions except that the maximum rate of movement is also a parameter to be varied. The method is very sensitive to the value of the maximum rate.

Pitman and Talwani (1972) have described a method based on rotation an anomaly lineation on one side of a ridge about a trial pole until it is superimposed on the same anomaly on the opposite side of the ridge. Some fracture zones are required for constraints. The rotation rate is determined by the age of the anomaly and the angle of rotation.

McKenzie and Sclater (1971) and Chase (1972) have developed numerical methods in which directions and rates are used at the same time. Chase's method provides a simultaneous solution of the rotation vectors for any n interacting plates. It requires data from at least n-1 boundaries. He has obtained a solution using eight plates. The method yields the optimum set of vectors so it is possible that the vectors found will be such that

$$\omega(a,b) + \omega(b,c) = \omega(a,c) \qquad \ldots.1.3$$

does not hold exactly.

A new method for determining the rotation pole will be given in Chapter 8.

## 1.5 ACKNOWLEDGEMENT OF ASSUMPTIONS

In the following chapters geophysical data from the southwest Pacific area will be presented and discussed. A conscious effort has been made to separate the description of the data from the interpretation of the data but that is not always possible. In this chapter the basic principles of continental drift, seafloor spreading, and plate tectonics have been described. In subsequent chapters these basic principles are assumed to be valid.

# CHAPTER 2

## AN INTRODUCTION TO THE SOUTHWEST PACIFIC AREA

This chapter is an introduction to the area studied, based mainly on previously published results. An introduction (2.1) is followed by details of specific areas: the southeast New Zealand plateau (2.2), Antarctica (2.3), Macquarie ridge complex (2.4), Alpine fault (2.5), Tasman basin (2.6), southeast Indian ocean (2.7), south Pacific east of 150°W (2.8), and the southwest Pacific west of 150°W (2.9).

### 2.1 INTRODUCTION

The interpretations of the structure of the southwest Pacific area presented in this thesis have been influenced by, and are dependent on, previous work both in the area studied and in the surrounding areas. It is therefore appropriate to briefly review published results for the whole southwest Pacific area. The review will serve as an introduction to the primary area of study and will describe current knowledge of the surrounding areas. Recent results are included but it should be borne in mind that not all of the results were available when some of the interpretations presented later were made. For example the seismic reflection profiles in the southwest Pacific basin were not available when the magnetic anomaly data were being interpreted; and the major publications on the southeast Indian ridge were not available when a part of that ridge near the triple junction was studied.

The main features of the whole southwest Pacific area are shown in Fig. 0.1 and the primary area of study in Fig. 2.1. To facilitate the discussion the following gross simplification of the structure of the area is made.

The New Zealand continent extends southeast of subaerial New Zealand in the form of the Campbell plateau and Chatham rise. South and east of the continent is the southwest Pacific basin which is bounded on the south by the Pacific-Antarctic ridge system. A complex ridge and trough system, the Macquarie ridge complex, extends south of New Zealand to about 60°S, 160°E, where it meets the western end of the Pacific-Antarctic ridge system and the eastern end of the southeast Indian ridge system. Oceanic basins separate the Pacific-Antarctic and southeast Indian ridge systems from the Antarctic continent, which includes the Ross Sea area.

In terms of plate tectonics the area consists of parts of the Pacific, Antarctic and Indian plates (Fig. 0.2). They intersect near 60°S, 160°E. The Pacific-Antarctic boundary is the axis of the Pacific-Antarctic ridge system. East of 180° it is a relatively simple active ridge with some ridge-

ridge transforms, but from 65°S, 180°, to the triple junction it is a broad fractured zone - the Pacific-Antarctic fracture zone. The Indian-Pacific boundary from the triple junction to New Zealand is the Macquarie complex and is predominantly a transform fault. The boundary continues through New Zealand, the relative motion becoming pure subduction further north in the Tonga-Kermadec arc. The Indian-Antarctic boundary is the axis of the southeast Indian ridge system. It extends west of the triple junction in a series of active east-west ridge sections offset by north-south transforms.

Details of specific parts of the southwest Pacific area are given in the following sections, but there are fuller discussions of particular data and interpretations at relevant places in subsequent chapters.

## 2.2 THE SOUTHEAST NEW ZEALAND PLATEAU

The New Zealand plateau consists of subaerial New Zealand and the surrounding generally flat areas that are elevated above the abyssal ocean floor (Brodie, 1964). It includes the Lord Howe rise and Norfolk ridge northeast of New Zealand, and the Chatham rise and Campbell plateau to the southeast. The two latter are of most interest here.

The Campbell plateau is an extensive area mostly 500 to 1000 m deep. This is deeper than typical continental shelves and a low continental slope separates the plateau from the <200 m deep shelf adjacent to southeast New Zealand. The area can be considered a marginal plateau. Surface wave dispersion studies (Adams, 1962) indicate a crustal thickness of 17-23 km, which is significantly less than the typical continental thickness, 30-40 km, of New Zealand (Thomson and Evison, 1962). The geology of the islands on the plateau, and numerous dredge samples indicate that the plateau is petrologically continental (Summerhayes, 1969; Fleming, 1969). Seismic reflection profiles (Houtz et al., 1967) reveal relatively undisturbed sediments, up to 1 km thick in the centre but thinning towards the edges.

The plateau is considered to consist of a basement of Permo-Jurassic schists and greywackes similar to those of New Zealand, overlain by upper Cretaceous-Tertiary sediment (Houtz et al., 1967; Summerhayes, 1969). Deep-sea drilling at site 277 (Fig. 2.2) did not reach basement but penetrated 470 m to mid-Paleocene (60 mybp) sediment. There was virtually no sediment younger than 30 mybp, which suggests that an erosion surface which is widespread over the Campbell plateau (Summerhayes, 1969) may reflect a major increase in bottom water velocity over the area in the late Cenozoic (Carter and Landis, 1972; JOIDES, 1973d).

The western margin of the plateau is the steep Auckland slope. Post-depositional faulting of sediments (Houtz et al., 1967, 1971) and some low

level seismic activity (Adams, pers comm 1973) indicates slight tectonic activity. The other margins of the plateau are relatively undisturbed (Houtz et al., 1967). The southeastern margin, here referred to as the Campbell slope, is moderately steep with gradients up to 1:4. Seismic reflection profiles (Fig. 2.3) show that the oceanic basement does not dip down at the margin. JOIDES site 275 on the Campbell slope (Fig. 2.3, profile B) yielded upper Cretaceous sediment within 15 m of the surface. Site 276 at the foot of the slope indicated Eocene or older sediment at the surface. Neither site reached basement. These JOIDES results confirm the important erosional effect of the strong western boundary current that sweeps the eastern side of the Campbell plateau and Chatham rise (Reid et al., 1968; Warren, 1973).

The Bounty trough forms the northern margin of the Campbell plateau. The trough is an unusual seafloor feature in that it is a transition from shoreline to deep ocean basin that extends over a much longer distance than normal (Krause, 1966). In the upper part of the trough there are sediment thicknesses of 1.5 km or more, the deeper parts of the sedimentary column being crumpled (Houtz et al., 1967, 1973). The trough probably acts as a channel for turbidity currents, which have deposited 1 km of turbidite deposits at the seaward end between the Campbell plateau and the Chatham rise (Houtz et al., 1967; Ewing et al., 1969).

The Chatham rise is shallower than the Campbell plateau and has a more ridge-like structure. It consists of a Permo-Jurassic schist and greywacke basement, overlain by Tertiary sediments (Cullen, 1965; Houtz et al., 1967; Austin et al., 1973). The northern slope of the Chatham rise is very linear but the southern slope is more irregular. At the base of the south Chatham slope beyond the Bounty trough, basement pinnacles or ridges are present (Fig. 2.3, profile D). The eastern end of the rise (Fig. 2.3, profile E) is much less steep than any of the other margins of the Campbell plateau or Chatham rise.

There is considerable interest in the relationship of the Campbell plateau, Bounty trough, and Chatham rise to each other, and to New Zealand. The main geological trends within New Zealand form an inverted S-shape (Wellman, 1956; Fleming, 1969), the southern end of which strikes offshore in the southeast of the South Island (Fig. 2.4a). A structural break at the western end of the Chatham rise (Krause, 1966; Houtz et al., 1967) and the intermediate crustal thickness of the Campbell plateau (Adams, 1962) suggests that the plateau and rise are not completely continuous with New Zealand. Cullen (1967a) has postulated a fault just off the east coast of the South Island (Fig. 2.4a) with the Chatham rise being a displaced continuation of the South Island schist axis.

Such large horizontal displacement is not supported by the continuation of the Southland syncline magnetic structures to at least 300 km offshore (McMullen, 1967). Fleming (1969) extends the South Island structure onto the Chatham rise without finite displacement but with pronounced curvature (Fig. 2.4a). Wellman (1973b) prefers to link the Southland syncline with east-west magnetic trends on the northern Campbell plateau (Ross, 1966; McMullen, 1967).

The east-west trend of the offshore structures is generally considered (e.g. Fleming, 1969; Griffiths, 1971; Wellman, 1973b) as having arisen from anticlockwise rotation of the Campbell plateau-Chatham rise area with respect to New Zealand (Fig. 2.4). However Austin et al., (1973) have proposed the opposite rotation, with the Chatham rise formerly against the east coast of the North Island. All models consider the Bounty trough to be an extensional feature formed by relative separation of the Chatham rise and the Campbell plateau.

The major orogenic activity associated with the formation of the Campbell plateau and Chatham rise is believed to have been complete by the end of the Rangitata orogeny in mid-Cretaceous times (Fleming 1969, Suggate 1972). Since then the area has been characterised mainly by slow subsidence and continuing sedimentation (Summerhayes, 1969). Pliocene volcanic activity on Chatham, Campbell and Auckland Islands (N.Z. Geol. Survey, 1972), and Quaternary activity on the Antipodes Islands (Cullen, 1969b) could be related to similar activity in the southeast of the South Island, but it probably does not indicate major tectonic activity. The times of various proposed rotations and/or translations of Campbell plateau and Chatham rise with respect to New Zealand range from pre mid-Cretaceous (Fleming, 1969) to late Cretaceous-early Tertiary (Cullen, 1970; Austin et al., 1973). Most authors consider that the Bounty trough had formed before the end of the Cretaceous, and that no major tectonic activity has taken place within the southeast New Zealand plateau since then.

## 2.3 ANTARCTICA

The Antarctic continent can be considered two separate regions; east Antarctica - mainly in east longitudes, and west Antarctica - mainly in west longitudes. Surface wave dispersion studies, reviewed by Adams (1972a), and seismic and gravity data (Woollard, 1962) indicate that the crustal thickness of east Antarctica is 35-45 km, while that of west Antarctica including the Ross shelf is 25-35 km. Geologically (Adie, 1962; Hamilton, 1967b) east Antarctica is a stable pre-Cambrian shield area bordered on the west by the

Paleozoic orogenic belt of the trans-Antarctic mountains. The western side of these mountains is usually considered to be the boundary between east and west Antarctica. West Antarctica is smaller, younger, and has had a more complex tectonic history than east Antarctica. It may consist of several large, separate blocks.

Relative movement between east and west Antarctica and/or rotation of blocks within west Antarctica has been suggested by, for example, Schopf (1969), van der Linden (1969), Cullen (1970), and Hayes and Ringis (1973). The movements, mostly pre-Tertiary, have been proposed mainly to accommodate continental reconstructions based on geology or seafloor spreading. Paleomagnetic data, reviewed by McElhinny (1973b), provide some support for relative movements. Different paleomagnetic pole positions from various parts of west Antarctica suggest that several separate regions are involved, not necessarily related to east Antarctica. The data are too few to permit reliable determinations of the relative movements, but movements do not appear to have been great since the upper Cretaceous.

There is a complete absence of tectonic earthquakes in Antarctica (Evison, 1967; Adams, 1972b) which suggests, but does not prove, that currently there is no movement between east and west Antarctica, and no plate boundaries in Antarctica. However there is active and recent volcanic activity at several places on the Victoria Land coast (western side of the Ross Sea) and Cenozoic volcanism in Marie Byrd Land, West Antarctica (Hamilton, 1967b). The former could be related to past, or incipient, movements between east and west Antarctica; the latter could be related to former movements within west Antarctica or subduction of material produced at the Pacific-Antarctic ridge. There is no evidence of any recent subduction.

The part of Antarctica that is of most interest to this study is the Ross Sea area, the coast to the east (Marie Byrd Land), and part of the coast to the west (Wilkes Land). Little is known of the continental margin off Marie Byrd Land but the presence of thick, gently dipping turbites in the Pacific-Antarctic basin indicates that the margin has been tectonically inactive for some time (Ewing et al., 1969; Houtz et al., 1973). On the Wilkes Land margin there are no geophysical data for 170°E to 150°E, but further west seismic reflection and sonobuoy data reveal that the oceanic basement of the south Indian basin dips steeply towards the margin (Houtz and Markl, 1972). Sediment thickness in the continental rise reaches 6 km, with the basement at least 9 km below sealevel even at 150 km from the continental margin - the nearest to the slope that its depth is known. On both the Wilkes Land and Marie Byrd Land coasts the depth of the continental shelf break is 200 to 700 m, which is deeper than in most areas of the world.

The Ross shelf, with a mean depth of about 500 m (Houtz and Davey, 1973) is also deeper than many continental shelves, but it is interesting to note that its depth is similar to that of the Campbell plateau. All the available data indicate that the Ross shelf is continental: crustal thickness about 30 km, no appreciable magnetic anomalies (Adams and Christoffel, 1962; Ross, 1966; unpublished data), marble and gneiss basement at deepsea drilling site 270 (Fig. 2.2) (JOIDES, 1973c), basement velocities typical of continental areas (Houtz and Davey, 1973), and gravity anomalies compatible with continental structure (Davey, pers comm 1973). Iselin Bank, which extends northward at 180°, is probably also continental but data are lacking to establish that it is structurally continuous with the Ross shelf proper.

The margin of the Ross shelf can be divided into two parts (Houtz and Davey, 1973). West of Iselin Bank the margin is complex with several basement ridges and the oceanic basement depth not exceeding 4.5 km (Fig. 2.5, profile F). East of Iselin Bank the continental slope and rise are relatively gentle due to a wedge of sediment up to 4 km thick (Fig. 2.5, profile G). Houtz and Davey consider that this profile shows a rift-like structure and major down-fault of the basement. They note that no similar rift is seen off the Campbell plateau, which may once have been adjacent to the eastern Ross shelf, and they suggest that either the faulting occurred after separation or the marginal rift remained at the Ross shelf margin. Interpretation of the tectonic history of the margin is very dependant on the details of any Antarctica-Campbell plateau reconstruction.

## 2.4 MACQUARIE RIDGE COMPLEX

Hayes et al. (1972a) introduced the term Macquarie ridge complex for the complex ridge and trough structure that extends southward from southeast New Zealand to a connection with the Pacific-Antarctic and Indian-Antarctic ridge systems near 61.5°S, 161°E (Fig. 2.1). The complex consists of a narrow discontinuous topographic high, the Macquarie ridge, and several flanking trenches and elongate deeps.

Simplified bathymetry of the area is shown in Fig. 2.6 and some representative bathymetric and magnetic profiles in Fig. 2.7. The two major structural elements of the complex are the ridge and the deeps. The relative positions of these delineate four sections.

(1) A northern section, New Zealand to 51°S, where a prominent trench, the Puysegur trench, lies to the west of the ridge (Fig. 2.7, profile A).

(2) A central section, 51°S-56°S, where the Macquarie trench lies to the east of the ridge (profile B).

(3) A southern section, 56°S to about 60°S, where the arcuate Hjort trench is west of the ridge (profile D). In this section the ridge is less pronounced than further north. It branches eastwards and does not extend as far as 60°S.

(4) South of 60°S to about 61.5°S. This section is not considered in the Macquarie complex by Hayes and Talwani (1972) but it will be shown in later chapters that it is part of the Indian-Pacific boundary and should be included in discussions of the complex. It is characterised by a trough that strikes SSE from near the southern end of the Hjort trench.

The Macquarie ridge area has attracted a lot of attention recently and in only the last six years at least 40 papers have appeared which discuss detail some aspect of the area. Hayes and Talwani (1972) have pointed out that most studies have been confined to limited portions of the area or have treated only one or two geophysical properties. This has led to differing conclusions on the nature of the complex. It has been considered a mid-ocean ridge (e.g. Ewing and Heezen, 1956; Kibblewhite and Denham, 1967), an island arc (e.g. Summerhayes, 1967, 1969; Cullen, 1967b) and a transform fault (e.g. Christoffel, 1971; Houtz et al., 1971).

The concept of plate tectonics has been important to the recent discussions of the area. The complex is seismically active and it delineates the southern part of the Indian-Pacific boundary (Fig. 0.2). There have been several determinations of the Indian-Pacific pole position (see later) all of which put it less than 20° east of the complex. They all predict that the dominant motion on the complex is right lateral strike-slip motion. Focal mechanism studies (Sykes, 1967; Banghar and Sykes, 1969; Johnson and Molnar, 1972) indicate this type of motion, and also some thrust motion of the Pacific plate over the Indian plate.

All the earthquakes on the complex are reported as shallow, but in the southwest of New Zealand (Fiordland) there are earthquakes down to 140 km (Hamilton and Evison, 1967; Smith, 1971). These intermediate earthquakes, the presence of the Puysegur trench, pronounced gravity anomalies off Fiordland (Hayes and Talwani, 1972; Woodward, 1973), and the Quaternary andesite volcanism of Solander Island at the head of the Solander trough, have led to suggestions that the northern part of the complex and Fiordland is a subduction area. The Fiordland seismic zone dips to the southeast which is not in accord with northeastward motion predicted by the Indian-Pacific rotation vector. Christoffel and van der Linden (1972) and Hayes and Talwani (1972) have discussed several solutions to this conflict. Hayes and Talwani prefer to consider that the area is not a subduction zone but merely a boundary where oceanic plate is slipping past continental plate.

The "trenches" and deeps that are a part of the complex are all narrower than typical trenches, and only Macquarie trench east of the central part of the ridge has any sediment in it. Deep troughs are common in active fracture zones and plate tectonics suggests that the complex is primarily a major fracture zone. The "trenches" could all be fracture zone features rather than subduction features.

Christoffel (1971) has used finite rotations about the Indian-Pacific pole to investigate the evolution of the complex during the last 10 my. One of his models predicts crustal extension in the central part of the complex; the part that contains Macquarie Island. Varne et al., (1969) and Varne and Rubenach (1972) have concluded from the geology of the island that it is a section of typical oceanic crust uplifted by about 3 km. The date of the uplift is tentatively mid-Miocene (15 mybp). Extensional tectonics would not be expected to produce the substantial uplift of the island, but major strike-slip motion with some thrusting could. Williamson and Rubenach (1972) have pointed out that oceanic crust of Macquarie Island need not have formed in situ i.e. it doesn't necessarily imply crustal extension in that portion of the complex.

The complex is separated from the Campbell plateau by the Solander trough and the Emerald basin. The Solander trough contains at least 1.5 km, probably more, of well layered sediment, and parts of the Emerald basin contain up to 1 km of sediment (Houtz et al., 1971, 1973; Hayes and Talwani, 1972). The southern part of the Emerald basin is separated from the smooth southwest Pacific basin by a zone of rougher topography that extends from the end of the Auckland slope to the southern end of the Hjort trench (Fig. 2.8). The bathymetry shows the Solander trough-Emerald basin area as an elongate enclosed basin. The basement depth of most of it would be 4.5-5 km so if the depth-age relationship (Fig. 1.7) is valid for the area the age would be at least 30 my. At deepsea drilling site 278 in the Emerald basin (Fig. 2.6) pillow basalt basement was reached at 4.1 km below sealevel and the contact sediment was of mid-Oligocene age (30 mybp). The basement age could be considerably older than this if bottom currents had eroded sediment. At present bottom currents in the area of the complex are substantial and flow patterns are critically dependent on the relatively small gaps in the Macquarie ridge (Gordon, 1972). Even minor changes in the configuration of the ridge could significantly alter sediment deposition and erosion east of the complex.

No magnetic lineations have been detected in the southern Emerald basin, although there are significant anomalies (Christoffel and R.F. Falconer, 1973). Further north between 51° and 53°S Christoffel and R.F. Falconer, and independently Hayes and Talwani (1972), have tentatively identified lineations east

of, and parallel to, the complex. The anomalies do not obviously match any of the Tertiary anomaly sequence, and as they are associated with basement relief Christoffel and Falconer suggested that they may have originated from fracturing accompanying the formation of the complex.

Deepsea drilling site 279 was on the southern end of the northern part of the Macquarie ridge (Fig. 2.6). It reached vesicular basalt basement at 3.6 km below sealevel and the contact sediment was of mid-Miocene age (15 mybp). Again the basement age could be older.

Basement ages, or ages of uplift of the Macquarie complex would not necessarily relate to the age of the seafloor either side of the complex. The seafloor age to the west as determined from magnetic anomalies (Weissel and Hayes, 1972; Christoffel and R.F. Falconer, 1973) ranges from zero at 61.5°S to 35 mybp at 53°S, and probably older further north (see later). The age of the Solander trough-Emerald basin area is not known but the depth suggests 30-50 mybp. The complex itself is a zone of active shear, and for any part an age of uplift, or leaky transform crustal formation (Menard and Atwater, 1968) could range from present day to whenever motion commenced.

The complexity of the area may be largely due to the proximity of the rotation pole for the boundary. Small changes in the pole position and/or the orientation of parts of the boundary with respect to the relative velocity vector could lead to substantial changes in tectonics. The history of the area is likely to have been complex but the dominant motion along the boundary has probably been strike-slip motion.

## 2.5 THE ALPINE FAULT

The zone of seismicity that defines the Indian-Pacific boundary (Fig. 0.2) continues north of the Macquarie ridge complex through New Zealand to the Tonga-Kermadec arc. In addition to shallow seismicity throughout the zone, westward dipping deep and intermediate earthquakes (Isacks et al., 1968; Hamilton and Gale, 1968) indicate that as far south as the northern end of the South Island the Pacific plate is subducting under the Indian plate. Further south all the seismicity is shallow, apart from the localised zone of intermediate depth earthquakes in Fiordland that was referred to in the previous section. The lack of deep or intermediate earthquakes in the South Island does not necessarily indicate lack of compression, and the active uplift of the Southern Alps suggests that there is some compression. However directions of motion calculated from the Indian-Pacific pole (Hayes and Talwani, 1972) indicate primarily strike-slip motion along the South Island seismic belt. The motion is generally considered to be associated with the Alpine fault and its branches.

The Alpine fault is a major fault that extends from Fiordland to at least the northern end of the South Island (Fig. 2.4a) (Wellman, 1956; Suggate, 1963). In the northern part of the South Island several major faults branch from the main trace, and all these faults are often included in the Alpine fault zone. Continuation of the faults into others in the North Island has been suggested (e.g. Suggate, 1963; Wellman, 1972) but definite evidence is lacking. In terms of plate tectonics the Alpine fault zone in the South Island is the shear zone boundary between the Indian and Pacific plates. In the North Island area the relative plate movement is mainly subduction and the surface trace of the plate boundary is probably the Hikurangi trench. The North Island faults therefore do not indicate the plate boundary.

The Alpine fault can be very clearly defined from the offset of major Paleozoic and Mesozoic geological structures. The offset is 450-480 km in a dextral sense (Wellman, 1956; Suggate, 1963; Fleming, 1969). The fault is also morphologically distinct and exhibits recent dextral movement and uplift (Suggate, 1963; Wellman, 1973a). Most authors accept that there has been some very recent strike-slip movement but there are considerable differences of opinion on when most of the 450 km offset occurred. Suggate (1963, 1972) and Fleming (1969) conclude that all the movement took place during the Rangitata orogeny (upper Jurassic-lower Cretaceous). P. Wellman and Cooper (1971) have the majority of the movement during the Rangitata orogeny but 120 km of movement in the last 10 my. Griffiths and Varne (1972) have all the movement between 50 and 10 mybp. Wellman (1973a) has it all since 25 mybp with most of it since 10 mybp. Christoffel (1971) has it all since 10 mybp.

Various plate tectonic models predict rates of movement on the fault of 3 to 6 cm/y during the last 10 my. This would take up all the observed offset in less than 15 my. As Weissel and Hayes (1972) point out, what then would be the nature of the Indian-Pacific boundary prior to 15 mybp? Griffiths and Varne (1972) conclude that the total offset of the New Zealand geosyncline (Fleming, 1969) since mid-Cretaceous is 1200 km. The Alpine fault offset is only a small part of this and the extra offset may represent movement prior to the Alpine fault movement. Griffiths and Varne suggest bending and stretching rather than simple strike-slip motion. A better understanding of the movements in the New Zealand area is required to adequately understand the evolution of the whole southwest Pacific area.

## 2.6 TASMAN BASIN

Many models of the evolution of the southwest Pacific area (e.g. van der Linden, 1969; Cullen, 1970; Griffiths, 1971; Suggate, 1972) start with a much distorted New Zealand plateau adjacent to eastern Australia in the Mesozoic. To understand the evolution to the present configuration a knowledge of the age and mode of formation of the Tasman basin is clearly important. It is only from recently obtained magnetic data (Hayes and Ringis, 1973) that definite conclusions have been possible.

Hayes and Ringis (1973) have mapped throughout most of the central Tasman basin a pattern of magnetic anomaly lineations that trend northwest. The anomalies are symmetrical about an axis that is coincident with a buried basement ridge revealed by seismic profiler data. The anomaly at the axis is number 24 (60 mybp)* and the anomalies either side extend clearly to 32A (74 mybp) and tentatively to 36 (80 mybp). Anomaly 36 lies close to the continental edges of east Australia and the Lord Howe rise and the magnetic pattern occupies all of the basin south to about 45°S. All of the central Tasman basin therefore appears to have formed by conventional seafloor spreading that started at 80 mybp and ceased at 60 mybp. The half spreading rate was about 2.2 cm/y.

There is a distinct morphological boundary between the central Tasman basin and the southern Tasman basin. Magnetic anomaly lineations in the southern basin (see later) are related to the southeast Indian ridge and are almost orthogonal to the central Tasman anomalies. The southern Tasman area is younger than 50 my so the boundary between the areas must have been an area of major shearing from 80 to 60 mybp.

Hayes and Ringis (1973) have used the central Tasman basin anomalies to reconstruct the former position of the Lord Howe rise-western New Zealand area with respect to Australia. They then use the Sproll and Dietz (1969) Australia-Antarctica reconstruction (see later) and 480 km of movement on the Alpine fault, to obtain a fit of Australia, Antarctica, and the New Zealand plateau. The reconstruction produces some overlap of the southern Campbell plateau on Marie Byrd land. Further discussion of New Zealand-Antarctica reconstructions will be given in Chapter 9.

---

*Throughout this study the magnetic anomaly numbering system used is that established by Pitman et al. (1968) and extended by Christoffel and Falconer (1972) and this study. The anomaly dates are from Heirtzler et al. (1968), Talwani et al. (1971) and Falconer (1973b). Details are given later.

## 2.7 SOUTHEAST INDIAN OCEAN

Most of the current knowledge of the southeast Indian ocean between Australia and Antarctica is presented in several papers in Volume 19 of the Antarctic Research Series. For this study the most important papers are those on the morphology (Hayes and Conolly, 1972), the magnetic anomalies (Weissel and Hayes, 1972), and the seismic profiler results (Houtz and Markl, 1972). Their results are summarized in Fig. 2.9. The area further west is less well surveyed and Fig. 2.10, from McKenzie and Sclater (1971), shows the main elements of what is known of that area. Throughout the whole southeast Indian ocean area the interpretations of the bathymetric and magnetic data have been influenced by the seismicity data : epicentres from Barazangi and Dorman (1969), USCGS, and Sykes (1970a); and focal mechanism studies of Sykes (1967) and Banghar and Sykes (1969).

The dominant morphological feature of the area is the southeast Indian ridge. It extends from the Indian-Antarctic-Pacific triple junction near 61.5°S, 161°E, to the Indian-Antarctic-Somali-triple junction in the central Indian ocean near 25°S, 10°E. Eastward of 140°E the ridge "steps" southwards in a series of short ridge sections offset by seismically active fracture zones. The inactive traces of these fracture zones can be traced for large distances away from the ridge axis. From 140°E to 100°E the ridge trends approximately east-west. Further westward it "steps" northward to the central Indian ridge-ridge-ridge triple junction.

Throughout most of the length of the ridge topographic relief on the ridge is minor, the axis is aseismic, and the present spreading rate is 3.3-3.7 cm/y. However at the western end the topography is rougher, there is a median rift, there is seismicity on the axis, and the spreading rate is 3.0 cm/y. This contrast in ridge character is seen elsewhere in the world and the data from this area support the suggestions of Menard (1967b) and Cann (1968) that the cutoff between the two types is at a spreading rate of about 3.0 cm/y.

A major exception to the regularity of the ridge is the Australian-Antarctic discordance between 120°and 128°E. The discordance is unlike anything yet reported in the world oceans. It is a very disrupted area in which the topographic grain trends at right angles to the axis of the ridge. It is deeper than the uniform ridge areas east and west of it, is seismically active, and recent (< 10 mybp) magnetic anomalies have not been identified in it. The zone of disturbed morphology and magnetic patterns extends only 500 km either side of the inferred ridge axis and is bounded by a clearly observed anomaly 6 (20 mybp). This suggests that the discordance is a relatively recent feature. It may be produced by down-welling in the mantle (a negative plume?).

Magnetic anomaly lineations have been mapped in some detail from the Macquarie ridge complex to 100°E by Weissel and Hayes (1972), and in less detail further west by McKenzie and Sclater (1971). Anomalies out to number 21 or 22 (55 mybp) have been identified either side of the ridge between 140°E and 110°E. Older anomalies have not been identified, and off both Australia and Antarctica there are gaps of about 200 km between anomaly 22 and the continental shelf. Magnetic quiet zones occupy most of the gaps. East of 140°, where the ridge axis "steps" southward, magnetic lineations are not well known south of the ridge but to the north they extend to 45 mybp in the southern Tasman basin. Lineations extend right to the Macquarie ridge complex and so provide the age of the seafloor on the western side of the complex. The age ranges from zero at 61.5°S to 35 mybp at 52°S, and possibly older further north (Weissel and Hayes, 1972; Christoffel and R.F. Falconer, 1973).

Seismic reflection and sonobuoy data (Houtz and Markl, 1972) have provided information on the configuration of the oceanic basement throughout much of the area. It was mentioned in section 2.3 that off the Antarctic margin there is a considerable thickness of sediment and the basement dips steeply. At the Australian margin there is less sediment but the shape of the basement is very similar. Houtz and Markl have noted that there are no indications of subduction on either margin so the deepened basement presumably formed at a rifting margin. The margin of the western side of the Tasmanian shelf is more complex and is similar to that west of Iselin bank - where Tasmania is fitted in most reconstructions of the former positions of Australia and Antarctica.

A computerized reconstruction based on the fit of the 1000 fm contour (Sproll and Dietz, 1969) is shown in Fig. 2.11. Smith and Hallam (1970) have obtained a very similar reconstruction using the 500 fm contour. The time for which the reconstruction is appropriate is not accurately known. Paleomagnetic results (McElhinny and Wellman, 1969) and the magnetic anomaly lineations (Weissel and Hayes, 1972) indicate that Australia has been moving northward with respect to Antarctica since 55 mybp. At that time the continents were about 400 km apart so some separation had taken place prior to then. Smith and Hallam (1970), Jones (1971) and others believe that initial rifting began in the mid-Jurassic with the main phase in the Tertiary. However paleomagnetic results (McElhinny, 1973b) indicate that Australia and Antarctica were considerably more than 400 km apart in the Jurassic. McElhinny concludes that the tectonic history of eastern Australia was more complicated than a simple rifting history.

In the reconstruction shown in Fig. 2.11 the south Tasman rise (Fig. 2.9) is not included. The rise is continental (JOIDES, 1973d) and if it had

been retained in its present position with respect to Australia it would have overlapped Iselin bank and part of the Ross shelf. A second "discrepancy" is that the present ridge axes east of 140°E are too far south to accommodate symmetrical spreading (Weissel and Hayes, 1972). The tectonic history of the eastern-most part of the southeast Indian ocean appears to have been complex.

The magnetic data in the southeast Indian ocean are important to understanding that region, but the observation that in one area there was a period of asymmetrical seafloor spreading is of very general importance. Weissel and Hayes (1971, 1972) have shown that from 40 to 15 mybp between 128°and 140°E, material was accreting on the northern side 30-40% faster than on the southern side. In the adjacent area to the west spreading was symmetrical during the same interval. The total rate of opening was the same in both areas so there was no deformation within the separating plates. At the time asymmetry commenced the spreading ridge was not offset between the two areas so the asymmetrical spreading led to an offset which increased with time. Had the ridge initially been offset the offset would have either increased or decreased, depending on the particular configuration. The documentation of asymmetric spreading in this area has important implications for the interpretation of other oceanic areas.

## 2.8 SOUTH PACIFIC EAST OF 150°W

Pitman et al. (1968) have presented magnetic data for the whole south Pacific east of 180°, and have shown that there is an extensive pattern of magnetic anomaly lineations symmetric about the Pacific-Antarctic ridge. A more detailed analysis of the area east of 150°W has been presented by Herron (1971) (Fig. 2.12). Her analysis was based primarily on bathymetric and magnetic profiles and seismicity data, available up to 1968. Vine (1966), Pitman and Heirtzler (1966), and Pitman et al. (1968) had previously discussed some of the magnetic profiles in detail. Sediment distribution in the area has been described by Ewing and Ewing (1967), Ewing et al. (1969), and Houtz et al. (1973). The seismicity has been discussed by Sykes (1963, 1967), Barazangi and Dorman (1969), Northrop et al. (1970), Forsyth (1972) and Northrop (1973); and the bathymetry by Zhivago (1962), Menard (1964), Heezen and Tharp (1972) and others. All these results lead to an adequate preliminary understanding of the area north of 60°S, but the area further south is not adequately known.

The dominant feature of the area (Fig. 2.12) is the Pacific-Antarctic ridge, which is also referred to as the Albatross cordillera. The ridge is a "type" example of a fast (> 3 cm/y) spreading ridge - almost triangular

in cross-section, no rift valley, aseismic, small scale relief no greater than a few hundred meters except where there are fracture zones, virtually no detectable sediment within several hundred kilometers of the axis, and easily identifiable magnetic patterns either side of the ridge. Several fracture zones offset both the axis of the ridge and the anomaly lineations either side. At some of the ridge offsets deep troughs occur, with up to 5 km relief. Away from the ridge axis the fracture zones are often expressed as narrow ridges or steps in the topography. Virtually all the seismicity in the area is associated with the offsets of the ridge axis.

Fig. 2.12 shows Herron's (1971) interpretation of the area. All the magnetic anomalies identified throughout the area are part of the sequence 1 to 32 (0 to 75 mybp), except for some possibly older anomalies in the extreme southeast. The fracture zone identifications were based on topography, magnetic anomaly offsets, and to a lesser extent the earthquake epicentres. Herron pointed out that the trends of some of the fracture zones, especially in the southern part of the Eltanin fracture zone, were not well established from bathymetry, and the fractures were drawn perpendicular to the magnetic lineations.

The magnetic lineations in the area follow two main trends: northeasterly following the Pacific-Antarctic ridge axis, and northwesterly subparallel to the Chile rise axis. West of the Eltanin fracture zone only the northeasterly trends are present: on the north side of the ridge out to at least anomaly 32 (west of 150°W, see later) and on the south side out to anomaly 27 (67 mybp). (Herron's identification of anomaly 32 in the south is dubious.) East of the Eltanin fracture zone the extent of the northeasterly trending anomalies decreases to the north, until at 36°S anomaly 5 (10 mybp) is the oldest northeasterly trending anomaly that can be identified. The boundary with the northwesterly trending Chile ridge anomalies is clear, but the inferred northwesterly trends west of the Pacific-Antarctic ridge are based on anomaly identifications that are at best weak. Northwesterly trending anomalies may be present there, but any anomaly pattern is certainly not as clear as that west of the Eltanin fracture zone.

Morgan (1968) and Le Pichon (1968) used Pitman et al.'s (1968) magnetic data to determine the Pacific-Antarctic pole of rotation. Both obtained poles within 2° of 70°S, 120°E. Le Pichon then used rotations about his pole to reconstruct the relative positions of Antarctica and the New Zealand plateau at 38 and 72 mybp. His conclusions need to be modified in the light of more recent data. Herron (1971) concludes that the more complete data east of 150°W fit a pole near 70°S, 120°E only for the last 10 my. Prior to then a pole near 62°S, 165°E would be more suitable.

Herron also concludes that the uniform anomaly patterns west of the Eltanin fracture zone indicate relatively uniform seafloor spreading there for the last 75 my, while the two different trends east of the Eltanin fracture zone indicate that the present Pacific-Antarctic ridge there, is a comparatively young system that has developed on the western flank of an older northwest trending system. Although the portion of the Eltanin fracture zone within the Pacific plate can be interpreted as the inactive trace of the present Pacific-Antarctic ridge-ridge transform, Herron believes it could have been the major plate boundary between a large plate consisting of most of the Pacific, and a smaller southwest Pacific plate.

## 2.9 SOUTHWEST PACIFIC WEST OF 150°W

The data which will be presented and analysed in this study are primarily from the southwest Pacific basin and the Pacific-Antarctic ridge system, west of about 150°W (Fig. 2.1). A brief description is given here of the major features of the area, and some of the previous work that has been done in the area. The description will serve as an introduction to the more detailed discussions in subsequent chapters.

All the major morphological features of the area are effectively summarized in the bathymetric contours of Figs.0.1 and 2.1, and the bathymetric profiles of Fig. 2.13. Common seafloor features such as mid-oceanic ridge, deep basin, Atlantic type continental margin, continental shelf, and seamounts, are all present; and there is also a very extensive fracture zone.

The major feature of the southwest Pacific area is the vast triangular southwest Pacific basin. In the northeast it extends 5000 km from the Pacific-Antarctic ridge to the Tonga-Kermadec trench, while in the southwest it extends less than 500 km from the Pacific-Antarctic fracture zone to the Campbell plateau. This study is concerned only with the southwestern part. There the basin is bounded on the south by the Pacific-Antarctic ridge system, and on the north by the Campbell plateau and Chatham rise. It is narrowest at the west where there is a marked boundary between it and the Emerald basin (Fig. 2.8). Eastwards it broadens into the south Pacific but for this study the term southwest Pacific basin will refer to only the area west of the Louisville ridge.

Choice of the Louisville ridge as a boundary is somewhat arbitrary as there are no obvious morphological differences in the basin either side of it. However it does appear to be a continuous feature of some sort. Hayes and Ewing (1971) first pointed out its extent, and they state that it is evident as a narrow topographic high on every sounding track across a line from the Eltanin fracture zone to the Tonga-Kermadec trench at 26°S. It is usually

less than 100 km wide and although its depth varies from <500 m to 4000 m its relief with respect to the basin is always 800 m or more. Herron (1971) and Hayes and Ewing (1971) consider that the Louisville ridge may be a relict plate boundary. If it is, the basins either side of it could be structurally different.

Most of the southwest Pacific basin has a depth close to 5 km. It does not have an abyssal plain as there are no flat-lying turbidite deposits, except locally near the mouth of the Bounty trough (Ewing et al., 1969). Sections of the only published seismic reflection profiles in the basin are shown in Fig. 2.14 and it can be seen that there is little sediment. A sediment isopach map of Houtz et al. (1973), compiled from additional unpublished data indicates that sediment thickness is mostly less than 200 m throughout the basin, except near the continental margin. Sediment deposition near the margin is very influenced by bottom currents, which hydrographic data (Reid et al., 1968; Warren, 1973) and direct measurements (Jacobs et al., 1970) indicate are substantial. All the available seismic reflection profiles at the margin are shown in Fig. 2.3. The JOIDES results at profile B, discussed in section 2.2, indicate that the observed sediment does not represent a complete time section. Houtz (Pers comm, 1972) reports that for profile B a sonobuoy gave a 5.6 km/sec refraction precisely tangent to acoustic basement, so the visible basement is undoubtedly the top of Layer 2. None of the profiles across the margin indicate basement dipping towards the margin.

The southwest Pacific basin merges in the south into the northern flanks of the Pacific-Antarctic ridge system. There is a marked contrast in the ridge system within the area and this contrast is well illustrated by the two profiles in Fig. 2.13. East of about 175°W the ridge is aseismic, broad, symmetrical, has only minor relief, the axial depth is 2500-2800 m, and there is no sediment within several hundred kilometers of the axis. From about 175°W to the junction with the Macquarie complex and southeast Indian ridge near 61.5°S, 161°E the ridge system has all the characteristics of a major fracture zone rather than a uniform ridge. Christoffel and Falconer (1972) have suggested the term Pacific-Antarctic fracture zone for this section. It is characterised by seismic activity, extremely rough topography, relief of 4 km or more, depths as shallow as 1 km, marked asymmetry, and some sediment close to the axis (Fig. 2.15).

South of the Pacific-Antarctic boundary there is also a contrast east and west of about 175°W. The area between 180° and 150°W is not well surveyed but the indications are that the Pacific-Antarctic ridge symmetry extends south into the Pacific-Antarctic basin. East of 150°W the basin is known to have at least 1 km of sediment (Houtz et al., 1973), considerably more than in the southwest Pacific basin. The difference is probably due to the availability of sediment from Antarctica and different bottom current patterns.

The Balleny basin south of the Pacific-Antarctic fracture zone could be considered a transition between the Pacific-Antarctic basin east of about 175°W, and the south Indian basin west of about the Balleny Islands. Two features of the Balleny basin are conspicuous.

(1) It is almost 2 km shallower than the southwest Pacific basin and the difference is not all attributable to sediment fill. There is up to 1 km of sediment in the Balleny basin (Figs. 2.15, 2.16) but the asymmetry across the Pacific-Antarctic fracture zone is still evident in the basement.

(2) Seamounts and large banks are numerous. This is a marked contrast to the other basins in the southwest Pacific-southeast Indian area, where seamounts are virtually unknown. Many of the Balleny basin seamounts are associated with large magnetic anomalies and they are presumably volcanic. The Balleny Islands at the west are of volcanic origin (Berninghausen and van Padang, 1960) and consist of olivine basalt (J.W. Cole, pers comm 1973). Scott Island to the east is also of volcanic origin. Ash in deepsea cores indicates that there has been volcanic activity in the Balleny basin area for at least the last 2 my (Lisitzin, 1962; Huang et al., 1972; Goodell, 1973).

The numerous seamounts, the volcanic activity, the very distorted sediments, and the graben-like structure (Fig. 2.16) all suggest a complex tectonic history for the Balleny basin area.

It has usually been assumed that all the area between the New Zealand plateau and Antarctica is of oceanic crustal structure. Surface wave dispersion on paths to Antarctica from earthquakes in the Eltanin fracture zone and further east, indicate a crustal thickness of 5-10 km for the Pacific-Antarctic ridge and the Pacific-Antarctic basin (Evison et al., 1960; Adams, 1964). Adams (pers comm, 1973) has found similar thicknesses for the southwest Pacific basin. There are no seismic refraction data to confirm the surface wave results but a variety of other geophysical data indicate that it is valid to assume that the area is oceanic.

Gravity data on the tracks shown in Fig. 2.17 have been published (Hayes et al., 1972b), and Talwani and Meijer (1972) have briefly discussed them. The data are typical of what could be expected from the morphology of the area. Large free-air anomalies are observed across the disturbed topography of the Pacific-Antarctic fracture zone, but the Balleny and southwest Pacific basins are featureless. Data across the continental margins are in agreement with the seismic profiler evidence that the basement does not dip towards the margins.

Heat flow data in the southwest Pacific area are shown in Fig. 2.17. The data are too few to draw any definite conclusions from but there is nothing unusual in any of the results.

Magnetic data are the primary data for this study, and have been the primary data for most of the previous geophysical work in the area. Christoffel (1961 a,b) from only two magnetic profiles identified correlations in the southwest Pacific basin. Adams and Christoffel (1962), and Christoffel and Ross (1965) extended the correlations with two more tracks. Ross (1966) presented a more detailed analysis of ten tracks, some with bathymetric data also. He later (Ross, 1967b) discussed the Pacific-Antarctic fracture zone in more detail, although not as a fracture zone. He noted the depth asymmetry across the feature and concluded from estimates of depth to magnetic basement that the basement was also asymmetric.

All the work of Christoffel, Adams, and Ross was between 170°E and 180°. They all clearly came up against a loss of correlation between tracks south of the flat part of the southwest Pacific basin, and not surprisingly no symmetrical anomalies were observed. Operation Deepfreeze data across the Pacific-Antarctic ridge between 180° and 150°W which contain symmetrical anomalies were presented in a data report (U.S. Navy Hydrographic Office, 1962) but although reverse magnetization was noted (Appendix 1A) the symmetry was not recognized. It wasn't until 1966 that Vine (1966) and Pitman and Heirtzler (1966) identified symmetrical anomalies on the Pacific-Antarctic ridge east of 150°W. Vine also pointed out that the southwest Pacific basin anomalies described by Christoffel and Ross (1965) were identical to those in the northeast Pacific. The full impact of this was not apparent until 1968 when Pitman et al. (1968) presented more data east of 180° that showed that there was a pattern of lineations, with some offsets, extending from the Pacific-Antarctic ridge to the New Zealand plateau. All or some of the same pattern could also be seen in other areas of the world, and from it Heirtzler et al. (1968) established the magnetic reversal time scale which is now widely used.

It is tempting to speculate on what might have happened if the early tracks of Christoffel, Adams, and Ross had been a bit further east beyond 180°, where the magnetic anomaly patterns are clear right to the symmetrical Pacific-Antarctic ridge. The amount of data between 165°E and 180° has more than trebled since 1965 but the correlations are still not much clearer than those established by Christoffel and Ross (1965). There is however a much better understanding of the relationship of that area to the rest of the southwest Pacific; and a preliminary picture of the tectonic history of the whole southwest Pacific area can be presented. This will be done in subsequent chapters.

# CHAPTER 3

## THE DATA : SOURCES AND REDUCTION

This chapter presents details on the sources, reliability, and methods of analysis of the primary data used in the study. An introduction (3.1) is followed by details of the magnetic and bathymetric data sources (3.2), navigation calculations (3.3), magnetic data reliability and reduction (3.4), bathymetric data (3.5), seismicity data (3.6), map projections (3.7), and computer programs (3.8).

### 3.1 INTRODUCTION

The primary data for this study are magnetic field measurements; bathymetry; and data from earthquakes in the area. Some of the bathymetric and magnetic data have been discussed previously by Christoffel (1961 a,b), Adams and Christoffel (1962), Ross (1966; 1967 a,b), Christoffel and Ross (1965, 1970) and Pitman et al., (1968). The data used by these workers were available in source form for this study. It has been analysed "afresh" with a large amount of new data.

The limitations of the data and the methods of processing it are very relevant to the conclusions drawn from the data. This chapter describes the basic data and the methods used to prepare it for geophysical interpretation. The brevity of the description belies the considerable amount of time and effort expended by many individuals and organizations that have been involved in the collection and reduction of the data.

### 3.2 MAGNETIC AND BATHYMETRIC DATA SOURCES

The tracks for which magnetic data were available are shown in Fig. 3.1. Tracks for south of 70°S, the Macquarie Ridge Complex, the Campbell Plateau and north of 45°S are not shown as those areas were not part of the magnetic anomaly study. The data used came in various forms from several sources. In some cases the reliability of the data is related to the source so the nomenclature used throughout for identifying profiles is indicative of the source. The nomenclature and sources are as follows:

(1) One or two alphabetical letters, e.g. H, AA: Data obtained on New Zealand Navy antarctic resupply trips between New Zealand and McMurdo Sound, Antarctica. Three institutions were involved in collecting the magnetic data. Two profiles, C and F, were obtained in 1958/59 by the Naval Research Laboratory from the "old" wooden hulled HMNZS Endeavour.

All subsequent profiles were obtained from the "new" steel-hulled HMNZS Endeavour; four by the Geophysics Division of DSIR, 19 by the Physics Department, Victoria University of Wellington. Bathymetric data from most of the tracks is held by the New Zealand Oceanographic Institute, DSIR.

(2) ELT plus two digits, e.g. ELT23: Data collected by Lamont-Doherty Geological Observatory from the U.S. National Science Foundation ship USNS Eltanin.

(3) ODF plus one digit, e.g. ODF3: Data obtained by the U.S. Navy on Operation Deep Freeze cruises.

(4) The letter A plus three digits, e.g. A708: U.S. Naval Oceanographic Office, Project Magnetic aeromagnetic flights.

(5) V16: Lamont-Doherty Geological Observatory, cruise 16 of R.V. Vema.

(6) C08: Lamont-Doherty Geological Observatory, cruise 8 of R.V. Conrad.

(7) MN: Scripps Institution of Oceanography, Monsoon Expedition, R.V. Argo.

(8) AR: Scripps Institution of Oceanography, Aries Expedition, R.V. Thomas Washington.

There are 52 separately designated tracks but some, e.g. A408, consist of two or more sections which for convenience are seperately labelled, e.g. A408N and A408S. This gives 67 labelled sections, varying in length from 200 km to more than 2000 km. The data are not continuous on all the sections.

For convenience all the non-New Zealand data are referred to as USA data as it all originated from USA sources.

## 3.3 NAVIGATION

All the magnetic and bathymetric data were obtained from ships or aircraft. The original data were recorded with respect to time and with a knowledge of the position with time the original data were reduced to positional data. Navigation uncertainties are a significant factor in the use of the data.

Navigation calculations for all the shipborne USA data were done at Lamont-Doherty Geological Observatory using the computer system described by Talwani (1969). Navigation calculations for all the New Zealand data were done by "hand" but some of it was also computer reduced at Lamont-Doherty Geological Observatory by D.A. Christoffel. There are no significant differences between the results of the two methods. The basic principles of the hand and computer methods are the same, and are as follows.

The raw navigation data are records of all course and speed changes, fixes obtained, and dead reckoned positions (usually at 0800, 1200 and 2000 hours); as well as pitlog mileage and estimated speed every hour.

With this data the track is reduced to a series of segments over which the course and/or speed is assumed constant. The segments are delineated by navigation points. The only real fixed points are where satellite or astronomical fixes, or coastal sightings, are obtained. The track between fixes is calculated using the logged course and speed changes to give a dead reckoned track from one fix to the time of the next fix. The difference between the second fix and the dead reckoned position is attributed to a constant "current". This "current" is then applied to the navigation points between the two fixes to obtain the adjusted track.

The US Navy satellite navigation system (Guier, 1966) was used on Eltanin cruises 20 onwards, and on the Aries cruise. The system provides fixes at intervals of usually less than three hours and the accuracy of the fixes is normally better than 1 km (Talwani et al., 1966). All other cruises used only celestial navigation for which fixes are unlikely to be accurate to better than ± 4 km, frequently worse. In some cases no reliable fixes were obtained for sections of more than 1000 km. With course and speed changes and varying weather conditions dead reckoning over long distances can be very inaccurate. Some dead reckoned positions were found to be up to 100 km in error when fixes were obtained.

The navigation data for each aeromagnetic track consisted of a list of navigation points, between which the course speed and altitude was assumed constant. The flight altitudes were mostly between 2.5 km and 3.0 km. Navigation accuracy for the aeromagnetic tracks is probably comparable with the non-satellite controlled shipborne tracks.

The accuracy of the satellite controlled tracks is probably better than ± 5 km. The other tracks must be considered much less reliable but from tracks which intersect or are very close it appears that errors are mostly less than 25 km. Apart from a few cases, which will be specifically referred to, none of the tracks has been adjusted on the basis of other tracks. Areas in this study where the track density is good, and detailed surveys elsewhere (e.g. Grim and Erickson, 1969, Chase et al., 1970; Loncarevic and Parker, 1971) show that small irregularities in magnetic anomalies patterns and bathymetry are common. Adjusting tracks on the basis of the features being investigated might obscure valid detail.

It must be noted that IN SOME AREAS NAVIGATION UNCERTAINTIES ARE THE FUNDAMENTAL LIMITATION ON THE USEFULNESS OF THE DATA.

## 3.4 REDUCTION OF MAGNETIC DATA

### 3.4.1 General

The form in which the magnetic data were finally used was mainly anomaly profiles, either plotted linearly against latitude or distance, or plotted on mercator charts perpendicular to the ship's track. Whether processed by hand or computer several steps were required to get the data to that form from the original magnetometer records. The original records were available for all the New Zealand data, but not for the USA data. The latter were provided in some or all of the following forms. (1) Computer listings of data (Fig. 3.2). (2) Computer plotted linear profiles of magnetic anomalies (Fig. 3.3). (3) Anomaly profiles computer plotted on mercator projections (Fig. 3.4). Some of the USA data have been published in reports (listed in Appendix 3A) but the magnetic data as used in this study were more detailed than shown in the reports.

The first step in the process of reducing the data of each track was the digitizing or replotting of the original record. For the New Zealand data the sampling interval was five minutes or less, always ensuring that sampling was sufficient to record all the detail which could reliably be read in the records. In the USA data the sampling interval was variable but it is believed that all significant detail was retained. After the digitizing or replotting the record of field viz. time was combined with the navigation data to produce a record of total field viz. position. From this a record of magnetic anomaly viz. position was prepared. Before describing the last step in more detail the reliability of the total field readings will be discussed.

### 3.4.2 Accuracy of total field readings

All the shipborne magnetic data were obtained with proton precession magnetometers, which give an absolute measurement of the total field. The calibration of the electronic system should be better than ±2nT but as most data were digitized off chart records the final accuracy is unlikely to be better than ±10nT. Noise in the system can lead to errors and in some New Zealand data variations of up to ±50nT occur. The sensing lead is towed behind the ship to minimise the effect of the ship and spinning of the sensor could give errors of ±25nT (Barrett, 1968) but errors as large as that do not appear to be present. The New Zealand systems had preamplifiers in the towed "fish" which contained the sensing coil and it is possible that magnetic parts of the preamplifiers (e.g. relays) could have a slight effect on the field at the sensor. This would not significantly affect the use of the data for crustal studies, but might be significant for studies of the total field.

The aeromagnetic data were obtained with fluxgate magnetometers. They are not absolute instruments but the calibration should be better than ±10nT. Uncertainties in digitizing the microfilm copies of the original analogue records are probably ±20nT.

The field measured at the sensor may contain a component due to the permanent and/or induced magnetization of the ship or aircraft. For aeromagnetic flights special precautions are taken to minimize the effect of the aircraft. For all the USA shipborne data the sensor was at least two ships' lengths astern, which should make the effect of the ship negligible (Bullard and Mason, 1961). For the New Zealand data precise information on the distance astern is not known for most trips, but it is known that for the "new" Endeavour the distance was frequently less than the ship's length (110 m). The effect of the ship is definitely significant for distances less than 80 m (See Appendix 3B) and it must be assumed that at least some of the New Zealand data may have been affected. This is not likely to produce disturbances with wavelengths comparable to those of crustal anomalies, but it could be significant for regional anomalies.

### 3.4.3 Time variations of the field

Repeated measurements of the field at any place would show that the field changes with time. Fluctuations with periods of seconds to a few days are produced by effects external to the earth. Longer periods of tens to hundreds of years, termed secular variation, are produced by changes within the earth's core. Secular variation is not very important for crustal studies but the short period fluctuations can be.

Due to the motion of the ship or aircraft time variations of the field appear as pseudo spatial variations. For aircraft, periods less than 10 minutes produce effects comparable to crustal anomalies. For ships, short periods appear in the records as high frequency "noise", but bay-type disturbances (periods of minutes to several hours (Matsushita, 1967)) would not be distinguishable from crustal anomalies. Duirnal variations would appear as regional anomalies with wavelengths of 250-500 km, depending on the ship speed.

Ionespheric effects are very latitude dependent, being greatest in the auroral zone which lies directly across much of the region (Fig. 3.5). In the auroral zone area short period field variations could be more than 1000nT under severe ionespheric storm conditions. Magnetic recording stations at Amberley, Macquarie Island, and Scott Base (Fig. 3.5) could provide records of magnetic field variations, but it is impractical to use those records to correct aircraft or ship-borne data as there is commonly no direct relation-

ship between the amplitudes or phases of field variations at points even 100 km apart (Sato, 1965; Roberts and Knapp, 1958). All that can be done is to determine when severe disturbances were likely to have occurred. Since ionespheric storms are in general worldwide the planetary magnetic index Kp (Lincoln, 1967) is a convenient indicator of when disturbed conditions occur. The index is based on disturbances recorded at selected stations throughout the world. It is defined for three hour intervals and indicates peak, not average, conditions during the intervals. It may not adequately indicate conditions in auroral zones (Lincoln, 1967) but the general level of likely variations can be obtained from the local K values assigned to given amplitude ranges at a magnetic observatory. Table 3.1 gives the ranges for observatories in the area.

Table 3.1 Magnetic observatory K indices and local field variations.

| Station | Maximum peak to peak amplitudes (in nT) for K values | | | | | | | | | |
|---|---|---|---|---|---|---|---|---|---|---|
| | K = 0 | 1 | 2 | 3 | 4 | 5 | 6 | 7 | 8 | 9 |
| Amberley | 5 | 10 | 20 | 40 | 70 | 120 | 200 | 330 | 500 | > 500 |
| Macquarie | 15 | 30 | 60 | 120 | 210 | 360 | 600 | 990 | 1500 | >1500 |
| Scott | 20 | 40 | 80 | 160 | 280 | 480 | 800 | 1320 | 2000 | >2000 |

The published Kp indexes (e.g. Lincoln 1966) for all the periods during which magnetic data had been obtained were checked. Periods with Kp $\geq$ 5 were noted and the magnetic data examined for those periods. There were four occasions when shipboard personnel had noted that the records were noisy, readings fluctuating by up to 75 nT with periods up to a few minutes. All four occasions were either in, or adjacent to, three hour intervals with Kp $\geq$ 7. Profile P of Fig. 3.6 shows one of these disturbed intervals. During part of the Kp = 7 period fluctuations were severe enough to make the record indecipherable. However as Fig. 3.7 shows "noise" was not apparent throughout all of the period of high Kp. Such differences can be expected because of local variations and because Kp is defined from peak, not average, conditions.

Where the high frequency noise is not too severe it can be averaged out when the records are digitized. However it is not possible to know whether the temporal variations also had longer periods and so produced pseudo crustal anomalies. Some of the short wavelength anomalies in profile P (Fig. 3.6) may be temporal variations, but this section of the profile is over the Pacific-Antarctic Fracture Zone and short wavelength crustal anomalies could

be expected. Profile N (Fig. 3.6) from similar water depths, but obtained in quiet ionespheric conditions, has "real" short wavelength anomalies similar to the possibly pseudo anomalies in profile P. Only an extremely accurately navigated repeat track along profile P would resolve the ambiguity.

In general it is impossible to be certain that a record has not been affected by ionespheric disturbances. The only practical solution is to note when disturbances (say Kp $\geq$ 5) occur and treat the data concerned with reserve. Temporal variations are unlikely to produce features which would be correlated between tracks so the worst effect is a loss of correlation when there may have been some.

### 3.4.4 Removal of regional field

The magnetic field measured at or near the earth's surface contains spatial variations in two general wavelength domains; less than 200 km and greater than 2000 km (Alldredge and van Voorhis, 1961, Alldredge et al., 1963). The long wavelengths originate from the earth's core, the shorter wavelengths from the crust. The crustal variations have amplitudes typically less than 2000 nT, which for the area studied is less than 5% of the total field. Since it is the short wavelength variations which are of interest for this study it is convenient to remove the larger long wavelength regional field. This is done by determining the regional field at each data point and subtracting it from the measured total field, to leave what is referred to as the magnetic anomaly.

First the regional field has to be determined. A practical method is to determine the field from the total field data itself. For a single profile a regional trend can be estimated either visually (Ross, 1966) or numerically (Schlich and Patriat, 1967) on the assumption that the regional wavelength is long. If there are several profiles in an area a local regional field can be determined either by simple averaging (Heirtzler et al., 1966) or by fitting a polynomial in latitude and longitude (Krause, 1966). An alternative method for determining the regional field is to use a field which is based on independent data. Analysis of global data has enabled the earth's field to be expressed in terms of spherical harmonic coefficients up to degree and order 11. Given the coefficients it is possible to calculate the field at any given point for a particular time. Several different sets of coefficients have been published. Some (e.g. Hurwitz et al., 1966) are defined for only one time, but others (e.g. Cain et al., 1967; IAGA, 1969) take into account secular variation and so are applicable over a period of time.

For all the computer reduced data regional field values were calculated from spherical harmonic coefficients. The coefficients used for most of

the data were those for the International Geomagnetic Reference Field (IGRF) (IAGA, 1969), but for a few tracks and for all the data in the Lamont-Doherty data reports the coefficients used were those for the field GSFC 12/66 (Cain et al., 1967). The latter yielded magnetic anomaly profiles with mean values of -200 nT to -400 nT. The IGRF field gave mean values varying from approximately -100 nT to +100 nT. More detailed comparisons between observed and calculated fields are discussed later. It is sufficient to say here that the anomaly profiles produced with the spherical harmonic fields are adequate for the analysis of crustal anomalies.

For the hand reduced New Zealand data regional field values were determined from the data itself. The method used was as follows. After navigation calculations for a track had been done the total field data were plotted in profile form, usually with respect to latitude as most tracks were approximately north-south. Then a smooth regional field was sketched on the profile, based on the assumption that the mean anomaly level is zero. Significant course changes had to be noted as they can change the gradient of the regional field. The magnetic anomaly profile is then obtained by subtracting the regional field value from the total field at each point. When data were available from several tracks a better estimate of the regional field was obtained by plotting regional values estimated from each track and contouring the values. Fig. 3.8 shows an example of the regional field determined this way. Because of the effects of secular variation tracks from only one summer season (Dec-Feb) were used at any one time. The regional field obtained from the map was then applied to the total field profiles to get anomaly profiles. In this way local effects and errors in a single profile were minimized.

The "hand" method yields anomaly profiles which are quite adequate for this study, but the methods based on numerically calculated regional fields are preferable. The latter are better suited to computer data reduction methods, but more importantly (Bullard, 1967) they are objective and it is always possible to know exactly how particular data have been treated.

The primary use of the regional field data is the production of anomaly profiles from the original total field data. However the seperation of the local (crustal) anomalies from the total field also provides information on the regional field. Ross (1966) presented two applications. (1) The use of regional field maps of different epochs to study changes in the regional field. (2) The mapping of regional anomalies with wavelengths of more than 100 km. Both topics are of interest but they are not central to this study of the structure of the crust. They are discussed further in appendices; regional anomalies in Appendix 3C, and changes in the regional field in Appendix 3D.

## 3.5 BATHYMETRIC DATA

The bathymetric data used were mainly echosounding profiles; charts were used to a lesser extent. The profiles were obtained on tracks shown in Fig. 3.1 but bathymetric data were not available for all the tracks. Since the bathymetric profiles were obtained simultaneously with the magnetic data there are no navigation uncertainties when relating magnetics and bathymetry.

For New Zealand profiles the original records were available. They were obtained with an Edo sounder and details less than 100-200 m are not well resolved in water deeper than 800 m. Horizontal resolution is not better than 2 km. Most of the USA profiles were obtained with precision depth recorders. Resolution would be better than 5 m in flat areas but less in rough areas due to side echoes. However most of the USA data were available only from the published reports (See Appendix 3A) in which the resolution is not better than 100 m vertically and 5 km horizontally. Profiles from parts of tracks ELT 27, 32 and 33, ODF5, and Aries were available in a slightly more detailed form. The profiles were not corrected for variations of the velocity of sound in water. The corrections would be of the order of + 150 m in 5000 m of water.

Bathymetric charts which were consulted are listed in Appendix 3E. Being compiled from numerous tracks they suffer the navigation limitations discussed in section 3.3. Even the most recent charts contain only a small number of satellite controlled tracks. The Macquarie Ridge is the only area for which the charts are adequate, and even there the data coverage is insufficient to resolve several important problems. New data have shown that parts of some existing charts are incorrect. Contours shown in various diagrams are based on the latest charts of the relevant areas, adjusted where necessary from the available profiles.

## 3.6 SEISMICITY DATA

### 3.6.1 Introduction

The seismicity data used in this study are the times, epicentre co-ordinates, depths, and magnitudes of earthquakes detected in the area. The ability to detect an earthquake and the accuracy with which it can be located depends on the number, distribution and quality of the seismograph stations observing the earthquake. Prior to the installation of many stations in Antarctica during and after the IGY (1957) reliable detection in the south-west Pacific was probably limited to earthquakes of magnitude greater than 6.0. The installation of the World Wide Standard Network, begun in 1961,

(Oliver and Murphy, 1971) led to further improvement in detection level. It is probable that now most earthquakes of magnitude greater than 4.5 and certainly all greater than 5.5 are detected (Everenden, 1969). The

### 3.6.3 Reliability of data

It is difficult to assess the accuracy of the epicentres because the true position is not known for any of the earthquakes. Everenden's (1969) theoretical analysis of the capabilities of the World Wide Standard Network indicated that errors of 30 km are likely in the Macquarie Ridge area, with even larger errors elsewhere in the region. He considered a minimum configuration of only four stations, whereas the minimum number of stations for any earthquake in the USCGS file is six, and only 13% of the earthquakes were observed by less than 10 stations.

Sykes (1970a) relocated only the better observed earthquakes, and for most earthquakes he used more data than the USCGS. He noted that his locations show less scatter than the USCGS locations for 1961 to 1967 given by Barazangi and Dorman (1969). Sykes considered 66 of the 73 earthquakes which are in the USCGS file for the overlapping period. Differences between the positions given by Sykes and the USCGS for the same earthquake show no strong bias (Fig. 3.11). Only seven differences are greater than 30 km and the standard deviation is 24 km. Breakdown of the results into the three plate boundaries involved indicates no bias on a particular boundary. The seven USCGS earthquakes which were not considered by Sykes were observed by less than 10 stations and may be less accurately determined than the others.

Evernden's results and the Sykes:USCGS comparison suggest that most of the epicentres used in this study are accurate to within 30 km, but errors of 50 km could be present. This estimate of accuracy relates to the precision of the computations involved. In addition there may be systematic errors due to velocity inhomogeneities in the earth. Errors in location of up to 55 km attributable to inhomogeneities have been reported for explosion locations, i.e. accurately known epicentres (Davies and McKenzie, 1969). Systematic errors could be particularly significant in the Macquarie Complex, where velocity inhomogeneities might be expected and various elements of structure "swap sides".

The reported depths of all the earthquakes in the USCGS file are shallower than 44 km. Earthquakes down to 140 km are observed between 44°S and 46°S in Fiordland (Hamilton and Evison 1967; Smith, 1971) but these do not extend offshore. However the distribution of stations is not favourable for determining depths and Adams (pers comm 1972) says that for the northern Macquarie Complex some earthquakes listed as crustal could have been deeper.

### 3.6.4 Time variability

The earthquakes are not uniformly distributed in time; most of them occur in clusters. Each cluster consists of several earthquakes near one place, all occurring within hours or days. Spatially all the earthquakes within a cluster could be at one place as positions vary by less than 40 km. However the spatial scatter could be real as most of the stress would not be released at one point.

The majority of clusters consist of only two or three earthquakes with a range in magnitude of less than 0.3. They are therefore not typical foreshock or aftershock sequences associated with one main earthquake (Mogi, 1963b; Sykes, 1970b). On the northern Macquarie Complex there are three larger clusters of five, seven and ten earthquakes respectively. These clusters are probably aftershock sequences as each began with an earthquake of magnitude greater than 6.0.

In addition to the time clustering there are longer length time trends. The most notable is on the 500 km of the Macquarie complex south of 57°S. There was no activity for three years then in the following three years there were nine separate "events" for a total of 15 earthquakes. Another example is the short, well-defined fracture zone at 55°S, 144°E for which all the activity is from only two years.

It is clear that the addition or omission of a few years data can considerably alter the apparent pattern of seismicity. Currently the spreading ridges are aseismic and most of the activity is on fracture zones. However there are also well defined fracture zones which are aseismic. The guiding principle must be that seismic activity reflects tectonic activity but aseismicity does not necessarily indicate lack of tectonic activity.

## 3.7 MAP PROJECTIONS

Several different map projections have been used as each one has properties most suitable for particular purposes. None is without some distortion - an unavoidable consequence of the spherical nature of the earth. Measurements involving distances and directions have taken into account the particular projection used or were calculated accurately assuming a spherical earth.

All the navigation calculations were done on mercator projections. The magnetic anomaly trends were also compiled and are presented on mercator projections. Two factors influenced this choice of projection for the magnetic data. One, the relationships between tracks are most important and as much of the data were hand plotted tracks were most easily plotted on

mercator projections. Two, the data reduced at Lamont-Doherty Geological Observatory had anomaly profiles drawn along tracks plotted on mercator projections. An additional advantage of using the mercator projection is that the main magnetic anomaly chart which will be presented here is the same projection and scale as the anomaly charts of adjoining areas presented by Herron (1971) and Weissel and Hayes (1972).

The mercator projection does produce large area distortions, especially in polar regions. For small areas it is adequate but for large areas azimuthal projections are better. Several of these have been used, all as polar projections - (1) The equidistant projection: convenient for hand plotting data. (2) The equal area: has obvious advantages for comparing areas. (3) The stereographic: has the very useful property that a circle on the earth projects as a circle on the map, although the geometrical centre of a circle on the map is not necessarily the geographical centre of the circle. Ordinary rectangular grids are used in a few situations.

Most forms of profile presentation involve some distortion as tracks have to be projected on to a line. Anomaly profiles shown in some diagrams are from mercator projections and so do not have a fixed linear scale. All distances, spreading rates, etc. quoted have been accurately measured off charts or calculated assuming a spherical earth.

## 3.8 COMPUTER PROGRAMS

Much of the work has involved use of computers. Where possible available programs were used but several programs had to be developed for specific problems; in particular for the numerical correlation studies of Chapter 5, the epicentral method of Chapter 8, and general map plotting. Brief details of the programs are given in Appendix 3F. The program listings are not given as the programs were developed specifically for this project and are not very general. They were also written specifically for the Elliott 503 computer of the Applied Mathematics Division, DSIR. The programing language is a modified form of ALGOL 60. Some of the programs which may be of interest are being modified to make them suitable for more general use.

## Postscript to section 3.7 : Map Projections

It has been discovered that the Xerox machine that some of the diagrams were copied on produced non-linear distortion. This is an unfortunate addition to the distortion already produced by representing the earths surface on a flat surface.

# CHAPTER 4

## THE STRUCTURE OF THE SOUTHWEST PACIFIC AREA

This chapter presents the available data and describes the structure of the southwest Pacific area. A statement of the approach taken (4.1) is followed by an introduction (4.2). Then specific areas are described: the southwest Pacific basin (4.3), Pacific-Antarctic ridge system (4.4), the transition area between the previous two (4.5), triple junction area (4.6), and the area south of the Pacific-Antarctic ridge system (4.7).

### 4.1 STATEMENT OF PRINCIPLES

In this chapter geophysical data are presented, and used to describe the structure of the southwest Pacific area. The emphasis is on a description of the structure not on interpretation of that structure in terms of tectonic models. Poles of rotation are not discussed, spreading rates are not calculated, detailed magnetic anomaly model studies are not given, and fracture zones are not compared with arcs about rotation poles. Such topics will be discussed, but only in later chapters.

The separate presentation of interpretation and description of the structure reflects the approach that was adopted during the data analysis. Whenever possible data were examined, integrated with other data, and the structure of an area mapped from the data. Then an explanation of the structure was sought, or the structure was compared with what was expected from a hypothesis. A conscious effort was made to avoid examining the data with an "expected structure" in mind.

The main results of this chapter are presented in Fig. 4.1, and most of the chapter will be a detailed explanation of that diagram. The diagram is almost entirely based on magnetic data, but bathymetry and seismicity have played an important subsidiary role. A full understanding of the area certainly requires data other than magnetic data, and in the detailed discussions in subsequent sections all the available geophysical data are considered.

The lineations shown in Fig. 4.1 have been mapped by visually identifying features common to two or more magnetic anomaly profiles. The lineations are numbered according to a system established by Pitman et al. (1968) and extended in this study. The numerical values of the numbers are not significant, as the numbers are only labels used to designate particular characteristic anomalies. The use of the numbering system is however significant, as it implies that the anomaly pattern in the southwest Pacific is part of a sequence of anomalies that has been observed in many areas of the

world. Acceptance of the origin of the anomalies as being due to seafloor spreading implies age similarities with other areas. According to current estimates the seafloor will range in age from 82 my at anomaly 37 to zero at anomaly 1. Recognition that the southwest Pacific area is part of a global pattern, and knowledge of the age of the seafloor in the area, are not strictly necessary for this chapter. The structure of the area could be described in isolation but there is no point in not using nomenclature that is widely used, where it is appropriate.

There are substantial areas in Fig. 4.1 where no anomaly identifications are shown. In some areas there are no data, but in others there are data and there are anomalies. The lack of identifications in the latter areas indicates that no lineations or distinctive anomalies have been identified there; it does not merely mean that there are none within the sequence 1-37. The standards used for accepting either identification of a distinctive anomaly in a single track or correlations between tracks are conservative. The structure of all the area is not simple, the available data tracks are not very numerous, and for many of them navigation uncertainties are significant. There is little point in assuming that every anomaly is produced by seafloor spreading or that data from one track must correlate with other data nearby. Mapping features in an area is important but it has been considered just as important to not map a feature which has not been adequately identified. Areas which are too complex to interpret simply, need to be recognized as such, as their complexity is information that may be as useful as that of the easily understood areas.

## 4.2 INTRODUCTION

Fig. 4.2 shows five bathymetric and magnetic profiles that are representative of the area. They are also representative of the data available, which are not continuous on all the tracks in the area (Fig. 3.1). The profiles illustrate several features, the identification of which simplifies the description of the area.

The ELT25 bathymetric profile shows a relatively smooth symmetrical ridge, which merges into a basin to the north. The northern end of the track goes up the Bounty trough which accounts for the gradual continental slope. The magnetic profile shows a section of high amplitude short wavelength anomalies symmetrical about the ridge axis. Longer wavelength anomalies are clearly seen in the basin but the anomalies on the ridge flank are in general of low amplitude.

The ODF5 magnetic profile is similar to ELT25 in that symmetry is seen about an axis. The sequence of anomalies from 25 to 32 is also clearly seen,

but although the sequence is of similar length to that in ELT25 it is closer to the ridge axis.

The magnetic profile H shows the anomaly group 25-32 with similar length to the previous profiles. No symmetry centre is obvious in either the bathymetric or magnetic profile. The topographic axis is relatively rough and the flat basin south of it is conspicuously shallower than the basin to the north.

Profile B still shows anomalies 25-32 but they are closer to "the ridge". The section of disturbed bathymetry is broader than to the east.

The ELT27b magnetic profile clearly shows symmetry, and the anomaly sequence agrees closely with that of current spreading ridges. The bathymetry is also symmetrical and is subdued.

The representative profiles illustrate: the uniformity and persistence of a sequence of anomalies in the southwest Pacific basin; the progressive decrease from east to west of the distance of this sequence from the topographic axis of the Pacific-Antarctic ridge system; the regular topography and symmetrical anomaly patterns over the actively spreading Pacific-Antarctic ridge; the rough topography and lack of symmetry of the Pacific-Antarctic fracture zone; and only a short distance westward a smooth symmetrical section of actively spreading Indian-Antarctic ridge.

These general observations indicate that it is appropriate to consider the whole area in five sections: (1) the southwest Pacific basin, (2) the Pacific-Antarctic ridge system, (3) the area inbetween those two, (4) south of the ridge system, (5) the Indian-Antarctic ridge area. These five areas are discussed separately in the following sections.

## 4.3 SOUTHWEST PACIFIC BASIN

### 4.3.1 General

Magnetic anomalies in the southwest Pacific basin are particularly clear and it has been possible to map magnetic lineations in detail. The results are contained in Fig. 4.1 but Fig. 4.3 shows them in greater detail. Before further discussing the results the nomenclature used for the anomalies needs to be explained.

It has become customary to assign numbers, or other labels, to anomalies which are distinctive and have been identified at several places. Probably the best known anomaly sequence is that numbered 1 to 32 by Pitman et al. (1968) (Fig. 4.4A). It is observed in many areas of the world and the geomagnetic reversal time scale for the last 75 mybp is based on it (Fig. 4.4B). A collection of representative profiles from the southwest Pacific basin

(Fig. 4.5) show that the oldest part of the sequence is represented in the basin. Fig. 4.5 also shows distinctive anomalies beyond number 32. Their regular occurrence over a wide area justifies labelling them, which has been done as follows.

Christoffel and Falconer (1972) assigned the numbers 34 and 36 to the broad positive anomaly beyond 32. The assignment is unusual in that the numbers refer to the ends of the same anomaly, not to two separate anomalies. Number 35 was used in the early compilation stages but it is not now used as the peak to which it was assigned subsequently appeared to be only a local feature. Number 33 is here used for the small but distinctive positive anomaly in the negative beyond 32. It is not mapped as a separate lineation but it is very important as it contributes to the distinctiveness of anomalies 32 and 34. Anomaly 32 is also made distinctive by the peak prior to it, which has been labelled 32A. A positive anomaly beyond 36 has been numbered 37, but it is more variable in appearance than the other numbered anomalies, and may be produced by basement structure rather than reversals.

There is unfortunately some duplication in the numbering of the anomalies beyond 32, because McKenzie and Sclater (1971) used number 33 for the feature that Christoffel and Falconer (1972) independantly numbered 34-36. Mascle and Phillips (1972) have followed McKenzie and Sclater, but Hayes and Ringis (1973) have followed Christoffel and Falconer; so the confusion is already established in the literature.

The existence of the magnetic lineations in the southwest Pacific basin has been known for some time from the work of Christoffel (1961 a,b), Adams and Christoffel (1962), Christoffel and Ross (1965, 1970), Ross (1966), and Pitman et al. (1968); but the results shown in Fig. 4.3 are more detailed than previously shown. All the data of the previous workers are included in Fig. 4.3, along with almost twice as much new data. New data have led to minor revisions of some of the earlier work, including the preliminary version of Fig. 4.3 presented by Christoffel and Falconer (1972). The general pattern of lineations and offsets is not unexpected and is similar to many such patterns in the world. It is therefore of most interest to discuss some of the unusual features of the area. Before doing this some general points should be noted.

In Fig. 4.3 individual anomaly lineations are mapped but the identification of an individual anomaly is usually dependant on its relationship to adjacent anomalies in the sequence. For example anomaly 30 "requires" anomalies on both sides of it, whereas anomaly 31 "requires" no anomaly on one side of it. Figs 4.6 and 4.7 show most of the profiles on which Fig. 4.3 is based. Whilst some individual anomaly identifications may not be

strong the overall pattern is convincing, especially when working with anomaly profiles plotted along the tracks and with tracing paper available. Minor kinks in the mapped anomaly lineations may be real or they may be due to navigation uncertainties - none of the tracks has been adjusted. The fracture zones are determined only from the offsets of the magnetic anomalies, not from bathymetry. They have been drawn straight, but in most cases they are not tightly determined. They may be wider than the lines imply. For convenience the fracture zones have been named, and Fig. 4.8 shows a simplified version of Fig. 4.3 with the fracture zones labelled.

Details of the structure of the southwest Pacific basin are discussed below. In general the discussion proceeds from east to west in Fig. 4.3.

### 4.3.2 The Louisville ridge

The Louisville ridge strikes through the northeast corner of the area studied (Fig. 4.3). The squares indicate positions of the ridge listed by Hayes and Ewing (1971), and observed on ELT17 and ELT28. Two east-west profiles across the ridge near 161°W are shown in Fig. 4.9. Profile ELT28 is only 45 km north of ELT17 so the difference in the ridge is very marked over only a short distance. Depths for other crossings in the area are equally variable.

The ELT28 seismic reflection profile (Fig. 4.10) across the ridge is interesting because it shows flat "basement" near the ridge. Flat basement, more probably a flat reflector above basement (section 1.2.5), is rare in the south Pacific (Houtz, pers comm 1973). The proximity of the flat layer to the Louisville ridge suggests a causal relationship. If it is ash at least some part of the ridge must have been subaerial to produce the ash. If it is smooth basalt flows, volcanic activity associated with the ridge is still implied. The very variable depth of the ridge suggests a series of volcanic seamounts, rather than a tectonically controlled ridge such as the Macquarie ridge.

Magnetic anomalies are clear west of the ridge; see for example anomalies 32A-36 on profile A409 (Fig. 4.6). East of the ridge there are anomalies, but they are not similar to those to the west; and even with Herron's (1971) data east of 150°W no lineations are apparent.

### 4.3.3 Tairoa fracture zone

The existence of the Tairoa fracture zone (Fig. 4.8) was first noted by Pitman et al. (1968) from only profile ELT23 (Fig. 4.11). Additional data have more clearly established it; see for example the duplication

of anomalies in C08, ELT23 and A408N (Fig. 4.6) shown by splitting the profiles. The offset across the fracture is dextral; approximately 340 km for anomalies 25-31, but less for older anomalies because of a "missing section" between anomalies 31 and 32 west of the fracture. There is some bathymetric relief in this missing section on profile ELT23 (Fig. 4.11). The Tairoa fracture zone as mapped in Fig. 4.3 is not perpendicular to the anomaly lineations.

The ELT23 profile across the fracture (Fig. 4.11) shows an unusual blocklike bathymetric feature. The block is 220 km wide and up to 1200 m higher than the surrounding flat floor. Bathymetric relief greater than a few hundred metres is rare throughout the southwest Pacific basin. Presumably the block is related to the fracture zone but it is mostly on one side of it. It is interesting to note that the western set of anomalies 27-29 are directly over the block but are not in any way irregular.

### 4.3.4 Rangirua-Toarahi area

Between the Tairoa fracture zone and the Rangirua fracture zone (Fig. 4.8) anomalies 25-29 are quite uniform, but there is a disturbance of anomalies 30 and 31. Profiles ELT25, ODF6, A408S and V16 (Fig. 4.6) show a progressive broadening of anomaly 30, until on V16 there is effectively a whole extra anomaly. On ELT25 the section from anomaly 29 to 31 corresponds to a broad 300 m high bathymetric hump.

The irregularities of anomalies 30 and 31 do not appear to be related to the unusual configuration of anomalies 32A and 32 just east of the Bollons seamount (Fig. 4.12). Duplication of anomalies 32A and 32 is very clear on V16 (Fig. 4.6) and less clear but plausible on A408S. The Toarahi fracture zone is based on this duplication, and numerical studies to be discussed later support the interpretation. The existence of the Toarahi fracture zone appears definite but its strike is very uncertain as the navigation control on V16 and A4085 is not good. A slight shift of either track would alter the fracture zone direction considerably. The offset is dextral and about 80 km.

The Rangirua fracture zone is a more substantial feature, evident as a sinistral offset of the whole anomaly sequence (Fig. 4.3). The offset is about 100 km in the south, but 150 or 220 km in the north, depending on whether the offset is measured to the east or west side of the Toarahi fracture zone. The interpretation at the southern end is not completely clear and the navigation control on ODF8 and DD is extremely poor. There is nothing noticeable in the bathymetry on the two DD crossings of the fracture

zone. At the northern end no anomalies beyond 32 are evident in V16 or A408S and the bathymetric and magnetic profiles are featureless to the shelf edge.

### 4.3.5 Bollons seamount

The Bollons seamount is interesting for several reasons. Firstly because it doesn't appear to be where it is shown on most maps. Fig. 4.13 shows one chart of the area, and bathymetric profiles in the area are shown in Fig. 4.14. It is clear that the seamount is not between X and X' on V16 where the chart puts it. A location about 110 km to the southeast, between A and Z, seems more probable; and profiles T and W indicate that it is not a single peak feature. On neither T or W are there any short wavelength magnetic anomalies associated with the peaks, which suggests but obviously does not prove, that Bollons seamount could be continental in structure.

The very flat seafloor at the foot of the continental slope on V16, W, and T (Fig. 4.14) probably reflects turbidite deposits. The channels at the foot of the slope on W and T suggest that the strong western boundary current may sweep between the plateau and Bollons seamount.

### 4.3.6 The Waimori, Matua, and Pahemo fracture zones

From the Rangirua fracture zone to about 178°E the anomaly lineations are in general very uniform. The only minor feature is uncertainty of anomalies 25 and 26 at the western end; see for example profiles L, ODF5 and A706 (Figs 4.6, 4.7). This uncertain area is associated with minor bathymetric roughness.

Between 178°E and 175°E Christoffel and Ross (1970) mapped a fracture zone with sinistral offset tending to zero at 60°S. The addition of more data indicates that the area is more complex and three fracture zones are present: the Waimori, the Matua, and the Pahemo (Fig. 4.8).

The Matua and Pahemo fracture zones are each orthogonal to the lineations, have a sinistral offset of about 50 km, and are not conspicuous in bathymetric profiles that cross them. The ELT32b seismic reflection profile (Fig. 2.14, profile I) crosses the Matua fracture zone between 0 and 45 km, and shows that basement expression of the fracture zone is slight. North of the line of the Matua fracture zone (Fig. 4.3) magnetic anomalies are random, see for example profiles S, F and K (Fig. 4.7), and no lineations have been identified.

The Waimori fracture zone is identified from the offset of anomalies 32A-34, see for example profiles ODF5, ELT27 and H (Figs 4.6, 4.7).

The offset is dextral, about 80 km. The fracture zone is a very local feature as only anomalies 32A-34 are offset, but the distance from anomaly 34 to 36 just east of the fracture is atypical and could be related to the fracture. The interpretation in Fig. 4.3 shows track ELT32b just west of the fracture, not crossing it, but there is a disturbance in the basement just south of anomaly 32 on this track - see Fig. 2.14, profile I, 350 to 400 km. This suggests that the trend of the Waimori fracture zone may be more northeast than shown in Fig. 4.3. Even with the trend shown it is not parallel to the other fracture zones and is not orthogonal to the lineations.

### 4.3.7 West of 175°E

West of about 175°E the anomaly pattern is clear (Fig. 4.3), and a complete sequence of anomalies 25 to 36 is seen either side of the Kohiku fracture zone (Fig. 4.8). The offset across the fracture zone decreases from about 80 km at anomaly 25 to about 45 km at anomaly 34. Bathymetry on profiles C and P is not irregular where they cross the inferred position of the fracture and unfortunately there are no bathymetry data for profile V. The seismic reflection profile A in Fig. 2.3 is from track ELT32a, and the pronounced basement step at 115 km is at 56°S, just east of the fracture zone line drawn in Fig. 4.3. The northern part of the fracture probably trends more northerly than shown, and it could be a broad feature.

The clear anomaly patterns of the southwest Pacific basin do not extend west of about 166°E. Anomalies 30 and 31 are tentatively identified at 165°E on ODF9 and M (Fig. 4.7) but the other anomalies are not seen. Christoffel and R.F. Falconer (1973) have independently examined the magnetic data west of 165°E and they also found no lineations, although there are anomalies. Fig. 4.15 shows that the termination of the anomaly lineations probably coincides with the termination of the flat part of the southwest Pacific basin.

### 4.3.8 Continental margin

It can be seen in Fig. 4.3 that anomaly 36 is close to the Campbell slope, and it may be significant that it is equally close to the Bollons seamount. The fracture zones west of 180° could be interpreted as maintaining the basically ENE trending anomaly lineations at a uniform distance from the irregular shaped continental margin.

East of the Bollons seamount anomaly 36 is not close to the south Chatham slope, i.e. the continental margin. The area between the margin and

anomaly 36 is not a magnetic quiet zone but no lineations are evident. Fig. 4.16 shows some bathymetric profiles across the margin and it is noticeable that in several cases bathymetric, presumably basement, features occur close to anomaly 36. The basement off the south Chatham slope is more complex than off the Campbell slope (Fig. 2.3) but in both areas the uniform basin basement appears to extend to about anomaly 36. It may be that east of the Bollons seamount the true margin of the southwest Pacific basin is not the south Chatham slope but is further offshore.

## 4.4 PACIFIC-ANTARCTIC RIDGE SYSTEM

### 4.4.1 General

The Pacific-Antarctic ridge system cuts across the area studied (Fig. 2.1); the latitude of its axis varying from about 60°S at 150°W, to 65°S at 180°, to 61.5°S at 161°E. The axis could be defined by bathymetric, magnetic or seismicity data, but no one type of data adequately reflects the differing nature of the system throughout the area.

Bathymetry profiles (Fig. 4.2) discussed in section 4.2 illustrate the contrast of the regularity of the Pacific-Antarctic ridge east of 180° with the roughness of the Pacific-Antarctic fracture zone from about 180° to 161°E.

Earthquake epicentres (Fig. 3.9) show the Pacific-Antarctic fracture zone to be seismically active while most of the Pacific-Antarctic ridge is aseismic.

Magnetic anomaly profiles (Fig. 4.17) show at 150°W a symmetrical sequence of anomalies so typical of seafloor spreading during the last 10 mybp that a model profile (Fig. 4.4A) isn't needed to identify the anomalies. An equally clear sequence exists at the opposite side of the area at 158°E (Fig. 4.17). In between, the axis of the Pacific-Antarctic ridge system is mostly characterized by high amplitude, short wavelength anomalies, but only east of about 175°W are anomalies typical of recent spreading readily identifiable.

On the basis of the structure of the area, and the available data coverage (Fig. 3.1) the ridge system (Fig. 2.1) will be discussed in four sections: (1) near 150°W, (2) 155°W to 166°W, (3) 166°W to 180°, (4) west of about 180°.

### 4.4.2 150°W area

The primary area for this study is west of 150°W, but to adequately define the structure of the Pacific-Antarctic ridge near 150°W data further east have been considered. Fig. 4.18 shows the interpretation of

the magnetic data in the area near 150°W, and Fig. 4.19 shows the track coverage.

Pitman et al. (1968) discussed four of the profiles in the area, noting that anomalies typical of current seafloor spreading were easy to recognize. Their profiles were: V16; ODF8 (Fig. 4.17); and ODF6 and ELT19 (Fig. 4.4B). Herron (1971) used also ELT20 and ELT25 in her analysis of the area east of 150°W (Fig. 2.12). The addition here of ELT33 and ELT43 has led to some revisions of Herron's interpretation. It has also led to the identification of a new fracture zone at 150°W (Fig. 4.18), for which the name Hangu fracture zone is here suggested.

The existence of the Hangu fracture zone is very clearly shown by the magnetic profiles in Fig. 4.20. In profile ELT43, which is almost east-west (Fig. 4.19), the duplication of the central anomaly is obvious. Profile ELT25 crosses the fracture close to the offset of the axis and a section of anomalies is missing. Bathymetry was not available for ELT43 but ELT25 bathymetry does not obviously indicate the existence of the fracture zone. There is no seismicity associated with the fracture.

The identification of the Hangu fracture zone is significant because it shows that a fracture zone with a substantial offset (70 km, dextral) may not be reflected in bathymetric and seismic data.

The fracture zone at 56-57°S between 140° and 145°W (Fig. 4.18) is defined almost completely from bathymetric and seismic data, although its existence could be weakly inferred from magnetic data (Fig. 2.12). Bathymetrically the fracture zone appears as extreme ridge and trough topography with up to 4 km relief over distances of less than 10 km. The trend of the fracture is well determined as there are several tracks across it. The epicentres suggest that the ridge offset is about 310 km and magnetic data indicate that it is dextral. It is probably appropriate to refer to the fracture as the Tairoa fracture zone, as it appears (Fig. 4.1) to be continuous with the offset of magnetic lineations in the southwest Pacific basin, that was named the Tairoa fracture zone (section 4.33).

The position of the ridge crest just west of the Tairoa fracture zone (Fig. 4.18) and the orientation of the ridge just east of the Hangu fracture zone, suggest that between 145° and 149°W there could be a dextral offset of the ridge crest of about 75 km. The minor seismic activity could reflect such a fracture zone. However the anomalies near 60°S, 144°W are offset sinistrally and Herron (1971) used this to infer a sinistral ridge offset of 50 km at 149°W (Fig. 2.12). Anomalies 8-12 on the north side of the ridge are not offset either sinistrally or dextrally. It has been shown in section 4.3 that in the southwest Pacific basin there are anomaly offsets

which are only local. It therefore may be unwise to infer offsets or lack of offsets in the ridge axis from anomaly lineations away from the axis.

West of the Hangu fracture zone (Fig. 4.18) another fracture zone is implied by the anomaly positions and "irregularity" of anomalies on the western end of profile ELT43 (Fig. 4.20). The details of the fracture are very uncertain as the navigation on ODF8 (Fig. 4.19) is bad and to reconcile it with ELT43 and ELT25 it has been necessary to shift the anomalies about 40 km northwards "along the track". Shifting the track in other directions could alter the interpretation.

### 4.4.3 155°W to 166°W

For the Pacific-Antarctic ridge system from about 155°W to 166°W there were no bathymetric or magnetic data (Fig. 3.1), and earthquake epicentres provide the only information. Fig. 4.21 shows the area. The active spreading ridge west of 166°W is discussed in the next section. The epicentres near 160°W appear to form a group with a strike similar to the fracture zones to the east (Fig. 4.18), and orthogonal to the spreading ridge. This suggests that these epicentres reflect fracture zone activity. There may be one fracture zone with a dextral (?) offset of 200 km, or two shorter fracture zones.

### 4.4.4 166°W to 180°

The area between about 166°W and 180° cannot be easily interpreted in terms of anomaly lineations and fracture zones (Fig. 4.22) despite the reasonable data coverage (Fig. 4.23). The lack of a simple interpretation probably reflects the complexity of the area, but it is also a product of the very poor navigation control. In this area north-bound tracks are often just emerging from long periods of numerous course and speed changes in pack ice, while south-bound tracks have run hundreds of kilometres in heavy seas. Weather conditions and/or 24 hour sunlight mean that reliable fixes are rare. Position uncertainties on many tracks could exceed 50 km. This makes it difficult to reliably map anomaly lineations, as many of the anomalies have wavelengths of 20 km or less.

There certainly are recognizable anomalies in the area; see for example Fig. 4.17 profiles MNW, MNH and ODF5; and the existence of the anomalies mapped in Fig. 4.22 is adequately established. The strikes of the lineations are probably not reliably determined and no significance can be attached to variations in their strikes. The strikes of the fracture zones are also very uncertain. The tentative central anomaly identifications at 178°W and 180° are based on profiles T and ODF3 respectively (Fig. 4.17). Considering the adjacent profiles: W, L and H; these central anomaly identifications must be considered at best weak.

Anomalies of the recent seafloor spreading sequence are relatively clear at 168°W, but the general pattern becomes more confused westward. The bathymetry (Fig. 4.24) also reflects the trend from uniform ridge in the east to more chaotic structure further westward. In conclusion it can be said that the characteristic bathymetric and magnetic uniformity of the Pacific-Antarctic ridge does not appear to extend west of about 175°W.

### 4.4.5 Pacific-Antarctic fracture zone

The axis of the Pacific-Antarctic ridge system is approximately delineated by the 3 km contour (Figs 0.1, 2.1), and it is noticeable that the contours show a marked change in trend just east of 65°S, 180°. East of there the trend is southwesterly, while to the west it is northwesterly. Ross (1967b) was the first to discuss in detail the western section between 180° and 160°E. From five bathymetric and seven magnetic profiles he showed that the bathymetric contours reflect a broad N65°W trending zone of disturbed bathymetry and magnetics. The data coverage in that area is now extensive (Fig. 3.1) but it will be shown in this section that the main conclusions are still that the area is complex. The bathymetric and magnetic profiles which will be presented are a representative sample of the available data.

Representative bathymetric profiles shown in Fig. 4.25 illustrate the complex topography. The most notable features are: depths less than 2 km; relief greater than 4 km; and the marked asymmetry about the topographic axis. The asymmetry evident in the bathymetry does not reflect symmetrical basement buried on the south side by sediment. There is sediment there (Figs 2.15, 2.16) but the basement is still asymmetrical. East and west of this area the ridges are smooth and symmetrical; the axes are deeper than 2 km; and extreme topography is present only at active fracture zones.

Magnetic anomaly profiles shown in Fig. 4.26 indicate a zone of high amplitude, short wavelength anomalies trending about N65°W. The magnetic zone is coincident with the rough topography, which is approximately enclosed by the 3 km contour. The track coverage in the area is quite good (Fig. 3.1) but no correlations of anomalies between tracks have been established in or adjacent to the zone of disturbed magnetics. Consequently the magnetic data do not indicate whether there are any local trends different from the overall N65°W trend.

It is natural to examine the magnetic profiles for evidence of recent seafloor spreading, particularly as that can be seen at 175°W and 160°E (Fig. 4.17). The profiles in Fig. 4.17 between 175°W and 160°E are aligned approximately on the axis of the rough topography, but more particularly they are aligned on a squarish anomaly - where one is present in a profile.

A squarish anomaly is characteristic of the axis of current spreading (Fig. 4.4A), but to identify recent spreading with any confidence it would be necessary to also have at least a few of the characteristic anomalies on both sides, or even only one side, of the central anomaly. With this criterion current seafloor spreading is not readily apparent anywhere between about 175°W and 160°E (Fig. 4.17).

One profile which has attracted some attention because of its squarish anomaly is profile B, shown in detail in Fig. 4.27. T.M. Geddes (pers comm, 1973) has done extensive model studies for this profile, taking account of the bathymetry. He has used sequences of normally and reversely magnetized blocks defined by the reversal time scale (Fig. 4.4) and finds that a wide range of different spreading rates, centre positions, or magnetized layer configurations will simulate at least parts of the profile. Lack of a simple unique solution is not surprising, considering the complex bathymetry. Model studies for other profiles in the area would also be dominated by the effects of extreme topography.

The magnetic profiles (Fig. 4.17) have also been examined for symmetry of any sort. Limited symmetry could be suggested in several profiles; for example ODF3, B, MNEb, P and N. Profile N (Fig. 4.27) attracted attention because of its large amplitude anomalies. There is some degree of symmetry in its bathymetry, but numerical studies, which will be discussed more fully later, show that it is difficult to justify choosing a unique magnetic symmetry centre. Similar conclusions are reached for other profiles.

A zone of seismic activity is coincident with the zone of disturbed topography and magnetics (Figs 4.26, 4.25). The epicentres are scattered and their locations could be inaccurate by more than 25 km (section 3.6.3), so there is little point in detailed comparisons of individual epicentres with bathymetric features. The gaps in seismicity (Fig. 4.26) are probably not significant as the data cover only nine years, and during that interval events occurred in only six years. It should be noted that east and west of this area the ridge axes are aseismic and all the seismicity is on active fracture zones.

The bathymetric, magnetic, and seismic data all suggest that the prominent feature striking N65°W between about 180° and 160°E is a major fracture zone. The name Pacific-Antarctic fracture zone was suggested for it by Christoffel and Falconer (1972).

The area around 60°S, 160°E will be discussed in section 4.6, and it will be shown that the western end of the Pacific-Antarctic fracture zone can be fairly reliably determined as 61.5°S, 161°E. The eastern limit of the fracture zone is less distinct. The seismicity extends to 180°;

active seafloor spreading is clearly identifiable at 175°W (Fig. 4.22); and the structure inbetween is indefinite. It is reasonable to conclude that the eastern end of the Pacific-Antarctic fracture zone is between 65° and 66°S, and 175°W and 180°. The whole zone is more than 1000 km long which makes it one of the world's major fracture zones.

The bathymetric relief of the Pacific-Antarctic fracture zone is typical of major fracture zones, but the width of the disturbed area is greater than normal. Fig. 4.25 shows that the disturbed zone is 200 km wide. Fracture zones elsewhere are frequently less than 50 km wide. The width suggests that the zone may be several fractures with a more northerly trend. The earthquakes are scattered but could be interpreted as several sections striking N45°W, especially the group near 165°E. If there are several fractures there may be short sections of ridge linking them. If the ridge axes were orthogonal to fractures trending N45°W, they would be less than 50 km long, as the fractures cannot be much displaced. Such short ridge sections would be difficult to detect with the data tracks that are available.

In the Hayes and Conolly (1972) bathymetric map for west of 169°E (Fig. 2.8) the Pacific-Antarctic fracture zone area is interpreted as consisting of orthogonal ridges and fractures with the fractures trending about N30°W. The data coverage in the area is minimal and the contours are clearly idealised. More detailed New Zealand Oceanographic Institute maps in preparation (Hurley and Krause, 1973a, b), also west of 169°E, show features trending N45°W. However the contours are not uniquely determined by the available data, and the interpretation has been partly based on Falconer's (1972) suggestion that fracture zones would trend N45°W. Detailed surveys are needed to determine local structure within the overall structure of the Pacific-Antarctic fracture zone.

## 4.5 BETWEEN ANOMALY 25 AND THE PACIFIC-ANTARCTIC RIDGE SYSTEM

In section 4.3 the southwest Pacific basin was discussed, and it was shown that there is a clear pattern of magnetic anomalies extending south to anomaly 25. In section 4.4 the discussion "jumped" to the axis of the Pacific-Antarctic ridge system. Anomalies out to about number 5 either side of a smooth axis were shown to be clear east of 175°W, while west of there is the disturbed Pacific-Antarctic fracture zone. In this section the area between the basin and the ridge system is discussed. The area can be loosely defined as being between anomaly 25 and either anomaly 5 or the Pacific-Antarctic fracture zone. It can also be considered as the northern flanks of the Pacific-Antarctic ridge system.

Representative bathymetric and magnetic profiles (Fig. 4.2) show that the width of the area decreases from east to west. In the east the distance from anomaly 25 to anomaly 5 is almost 1000 km. In the west the distance at 170°W between anomaly 25 and the axis of the Pacific-Antarctic fracture zone is only 200 km, and further west even anomaly 25 is "lost" in the fracture zone. Fig. 4.1 shows that despite reasonable data coverage only a few magnetic lineations have been identified in the area. The difficulty of identifying anomaly lineations is the main characteristic of the area.

Magnetic anomalies 25-36 in the southwest Pacific basin are distinctive and easy to correlate, but south of anomaly 25 the nature of the anomalies changes markedly. In the east (e.g. profile ELT25, Fig. 4.2) the anomaly amplitudes between numbers 25 and 5 are low, there is a mixture of wavelengths, and the general appearance of the profiles is one of noise rather than of distinctive anomaly sequences. In the west, e.g. profiles B and H, the amplitudes are larger but distinctive anomalies are still not clear.

Some identifications of lineations and individual anomalies have been made in the area (Fig. 4.1); mainly in the eastern part. Fig. 4.28 shows several profiles east of 170°W with the assumed anomaly identifications. These identifications are based heavily on the work of Pitman et al. (1968), who established the correlations shown between profiles ELT23, ELT19, ODF6 and ODF8. The basis of the anomaly numbering system is indicated in Fig. 4.4A, where a model profile based on a north Pacific type profile is shown with profiles ODF6 and ELT19. It is clear that between anomalies 5 and 24 the correlations between the profiles are far less obvious than between anomalies 25 and 32.

Although anomalies 5 to 25 are observed in many areas of the world detailed correlations of peaks in the sequence are rarely possible. Usually great reliance is placed on distinctive features such as: the width of anomaly 5, the short wavelength group beyond it, the width of 6, the prominence of 13 with a gap beside it, the width of 20 and 21 with a gap between them, the uniformity of peaks in 21-24, and the double of 25-26 with gaps either side. When the southwest Pacific profiles in Figs 4.4A and 4.28 are examined legitimate doubts can be raised about some of the assignments of numbers to anomalies: peaks are missing between 23 and 25, the distinctive gap between 20 and 21 is hardly distinctive, and 13 isn't really prominent. There are undoubtedly correlations between tracks, and the lineations shown in the east of Fig. 4.1 are adequately established. However the assignment of the numbers to exact anomalies between 5 and 25 must be considered much less reliable.

In the area north of the Pacific-Antarctic fracture zone (Fig. 4.1) virtually no anomaly assignments have been made, or lineations identified, despite the high track density. Fig. 4.29 shows some of the profiles from this area. The most notable features are the decrease to the west of the distance between anomaly 25 and the axis, and the appreciable amplitudes of many of the anomalies in the area. Correlation is evident between profiles ELT27a and H at their northern end but the two tracks are virtually coincident there. A group of anomalies that could be anomalies 21 to 24 may be present in, for example, D, H, ELT27a and T; and anomaly 24 has been included in Fig. 4.1. The identification is not strong though, as it appears on so few tracks. The identification of anomalies 8 to 12 in ODF5 and T is possibly more acceptable. Correlations between profiles could be suggested in several places but the anomalies are mostly not distinctive which means that the correlations are not unique. When the data are examined in map form with anomaly profiles along the tracks, most correlations are so ambiguous that they would be of little use.

Bathymetric relief can have a substantial influence on magnetic anomalies especially if water depths are not great. The rough topography north of the Pacific-Antarctic fracture zone (Figs 4.2, 4.25) undoubtedly contributes to the difficulty in correlating anomalies there; but the fact that the bathymetry is rough, in itself, suggests that the area is complex and so lack of clear magnetic patterns is not surprising. To the east the northern flanks of the Pacific-Antarctic ridge are relatively uniform, e.g. profile ELT25 Fig. 4.2, and it is there that some correlations have been possible.

A notable relationship between bathymetric and magnetic structure throughout the area is that the southern boundary of the easily identifiable anomalies (usually number 25) is the southern boundary of the relatively flat basin topography. The profiles in Fig. 4.2 illustrate this. On these and many other profiles it is noticeable that rough topography first occurs just south of anomaly 25. Admittedly none of the topography in the east is very rough, but there is usually some significant relief at the magnetic boundary there. The transition from basin to rough topography becomes more abrupt towards the west (Fig. 4.25), and invariably occurs close to the southern limit of the correlatable anomalies.

The lack of identifiable anomaly lineations west of about $165^{o}W$ (Fig. 4.1) means that it is not possible to know if the fracture zones to the north in the southwest Pacific basin extend further south. Further east it appears that the Tairoa fracture zone exists from the basin to the ridge. East of that fracture only anomalies down to number 20 are identifiable

(profiles A408N and ELT23, Fig. 4.28) but to the west the full sequence is identified (e.g. profiles ODF6, ELT25). The offset of anomaly 20 is about 350 km dextral, which is similar to the 340 km offset of anomaly 25, and the 310 km offset of the axis at 56°S. The available tracks are widely spaced near the fracture so the actual position of the fracture is not well determined (Fig. 4.1). However it seems reasonable to infer that it continues from the well determined offset in the basin to the major fracture at the ridge crest.

## 4.6 THE INDIAN-ANTARCTIC-PACIFIC TRIPLE JUNCTION

### 4.6.1 General

In this section the area of intersection of the Pacific-Antarctic and southeast Indian ridge systems and the Macquarie ridge complex (Fig. 2.1) is described. The area is referred to as the triple junction area because it is where the Indian, Antarctic and Pacific plates intersect. Discussion in terms of plate tectonics is deferred until Chapter 9; here only the basic structure is described.

Fig. 4.30 shows the area, with the track control for the magnetic data in the vicinity of the triple junction. The area was included in the southeast Indian ocean morphology and magnetic anomaly studies of Hayes and Conolly (1972) and Weissel and Hayes (1972) (Fig. 2.9). Falconer (1972) quite independently studied the area and as he had more data he described the area in greater detail. The description given here follows Falconer (1972) with some additional seismicity data.* Important data that Weissel and Hayes didn't have are magnetic profiles AA and AR a-e (Fig. 4.30). Two bathymetric charts of the area, in preparation (Hurley and Krause, 1973a, b), provide some bathymetric data that Hayes and Conolly didn't have. There are minor differences of interpretation between the different workers.

There are three major structural features in the area, and they intersect near 61.5°S, 161°E. These features and the boundaries they define as follows. (1) Indian-Antarctic boundary: a section of the southeast Indian ridge striking N55°E. (2) Indian-Pacific boundary: the Macquarie ridge complex striking very approximately north-south. (3) Pacific-Antarctic boundary: the Pacific-Antarctic fracture zone striking about N70°W. It is most convenient to describe these three features separately.

---

*In Falconer (1972) and some other papers the name Indian-Antarctic ridge is used for what is here referred to as the southeast Indian ridge. The usage here follows that of many papers on the area published in Volume 19 of the Antarctic Research Series.

4.6.2 Indian-Antarctic boundary

The anomaly lineations shown in Fig. 4.30 clearly indicate an actively spreading ridge striking N55°E between about 62.5°S, 157.5°E and 61.5°S, 161°E. The magnetic anomaly profiles on which the lineations are based are shown in Fig. 4.31. Even without the model profile it would be easy to see that on many profiles anomalies are symmetrical about the anomaly labelled 1; and it is clear that the sequence of anomalies are those indicative of sea-floor spreading during the last 10mybp (the outer edge of anomaly 5 is approximately 10 mybp).

The Aries tracks (label : AR) and the Eltanin tracks (label : EL) are satellite controlled so the anomaly positions are accurately established. The anomaly lineations (Fig. 8.30), including several unnumbered ones not shown, are closely parallel to the axis. The Aries track ARc in fact consists of four close tracks (two profiles are shown in Fig. 8.31) and correlations show that even over short distances individual anomalies strike N55°E.

Bathymetry also indicates a regular ridge (Fig. 4.32, profile EL27a), the axis of which coincides with the magnetic axis. Hayes and Conolly (1972) have inferred offsets in the ridge axis (Fig. 2.9), but Hurley and Krause's (1973a, b) charts in preparation do not indicate any offsets. Neither are there any offsets in the anomaly lineations either side of the ridge (Fig. 4.30).

The western end of the ridge is terminated by a fracture zone striking N30°W. This feature is clearly identified from epicentres (Fig. 4.30), bathymetry (Fig. 2.8), and offset of magnetic anomalies to the north (Fig. 2.9). The ridge is offset about 320 km in a dextral sense. As a noticeable bathymetric step the fracture zone extends south towards, but not right to, the Balleny Islands. These islands and nearby submarine banks (Dawson, 1970) strike about N35°E. It seems reasonable to infer that they are related to the fracture zone. The fracture zone was named the Balleny fracture zone by both Falconer (1972) and Hayes and Conolly (1972).

The complete lack of epicentres on the southeast Indian ridge section (Fig. 4.30) is in marked contrast to the high activity on the Balleny fracture zone. Active spreading ridge sections identified further west on the southeast Indian ridge are also aseismic, and all the activity is on the fracture zones offsetting them. It is therefore likely that here the eastern end of the ridge is marked by the seismicity close to 61.5°S, 161°E. It is worth noting that Falconer (1972) used only Sykes' (1970a) epicentres, which do not include the epicentres at the end of the ridge axis shown in Fig. 4.30.

Falconer (1972) determined the end of the ridge from the bathymetric and magnetic data. The magnetic anomalies characteristic of recent spreading cannot be recognized on profile AA (Fig. 4.31) closer to the axis than anomaly 2' on the south side of the ridge. Profiles A708 and ARb both show the characteristic anomalies over the southern flank but they are not seen north of the axial anomaly. The bathymetry of profile ARb (Fig. 4.32) south of the axis is typical of the spreading ridge (e.g. profile EL27b), but just north of the axial anomaly there is a marked bathymetric change coincident with the loss of the characteristic anomalies.

The loss of magnetic lineations, the change of bathymetric character, and the earthquake epicentres, all indicate that the ridge terminates just east of the axial anomaly observed on track ARb, and possibly at the axial anomaly on track A708. This position could be given as 61.6°S, 160.7°E but an implied accuracy of 0.1° is probably unwarranted and the position will be taken as 61.5°S, 161°E.

### 4.6.3 Indian-Pacific boundary

The Macquarie ridge complex has been discussed in section 2.4 and it was pointed out there that Hayes and Talwani (1972) did not consider it to extend south of about 60°S; although they did note that the structure south of there was not well defined. Here the Macquarie complex is considered to extend to 61.5°S.

The most prominent feature of the southern part of the complex is the arcuate Hjort trench (Fig. 4.30). Magnetic lineations can be traced from the west right to the trench and the bathymetric transition is very abrupt (Fig. 4.32, profile EL36). East of the trench the topography associated with the Macquarie ridge is much more subdued than further north. No magnetic lineations have been mapped between the trench and the southwest Pacific basin anomalies (section 4.3.7).

As a prominent feature the trench terminates near 59.5°S, 159.5°E. However several tracks south of there show troughs, which are partially reflected in the 3 km contour (Fig. 4.30). These deeps lie on a line striking S25°E from the end of the trench. This line would intersect the southeast Indian ridge near 61.5°S, 161°E. Profile ARb (Fig. 4.32) crosses this line just north of the ridge axis. The profile shows the abrupt transition from the ridge to the southwest Pacific basin.

The seismicity data (Fig. 4.30) are important as they indicate a continuity from the Hjort trench area to the point 61.5°S, 161°E. The epicentres are scattered but they are on or slightly west of the line defined by the bathymetry. In Chapter 8 this seismicity data will be used to show that the the feature defined by the seismicity can be best interpreted as a fracture zone.

The bathymetric data can be interpreted as indicating a fracture zone. Fracture zones are often characterised by deep troughs and marked differences in the depth either side. The Hjort "trench" and the line to the south show these features (Fig. 4.32, profiles EL36 and ARb). Hayes and Conolly map the line south of the Hjort trench, and refer to it as the Hjort fracture zone (Fig. 2.9); but no discussion of the feature is given. They extend it south of the ridge.

### 4.6.4 Pacific-Antarctic boundary

The Pacific-Antarctic fracture zone was described in section 4.4.5 although its western end was not much discussed. The seismicity east of 161°E in Fig. 4.30 is seismicity of the Pacific-Antarctic fracture zone. It is clear that this seismicity intersects the southeast Indian ridge and the southern end of the Macquarie complex near 61.5°S, 161°E.

Profile ARe, Fig. 4.32 is across the Pacific-Antarctic fracture zone, and the bathymetric contrast with profile EL27a across the southeast Indian ridge and profile ARb across the southernmost Macquarie complex, can be described as truly remarkable. The considerable width of the disturbed bathymetric zone makes it hard to bathymetrically define the precise trend of the fracture zone. The overall trend west of 170°E is between 65° and 70° north of west, but as mentioned in section 4.4.5 local trends of N45°W within the zone are possible.

A marked change in depth across the Pacific-Antarctic fracture zone is evident in profile ARe (Fig. 4.32) just as a change is evident across the southern Macquarie complex. The simplicity across the Macquarie line is in marked contrast to the complexity across the Pacific-Antarctic line. Both profiles go into the southwest Pacific basin but obviously the two boundaries are quite different. The Macquarie boundary is probably a simple fracture zone while the complexity of the Pacific-Antarctic boundary is probably due to it being several en echelon fractures.

## 4.7 SOUTH OF THE PACIFIC-ANTARCTIC RIDGE SYSTEM

### 4.7.1 Introduction

In the preface it was explained that the initial intention of this study was to concentrate on a limited area of the southwest Pacific basin, but that when more data became available and the structure of the whole southwest Pacific area became clearer the study was extended to the axial area of the Pacific-Antarctic ridge system. The area south of the ridge system (Fig. 2.1) has also been studied, but in less detail.

East of about 175°W almost no data were available south of the ridge system (Fig. 3.1), but data coverage is better in the Balleny basin area west of 180°. Fig. 4.1 shows that at least from magnetic data little structure has been mapped south of the ridge system. It should be noted that the mercator projection used in Figs 4.1 and 3.1 overemphasises the size of the area south of the ridge system. The equidistant projection of Fig. 2.1 gives a better idea of the relative areas.

The Balleny basin and the Pacific-Antarctic basin will be discussed separately, mainly because of the differing data coverage but also because they are probably structurally different.

### 4.7.2 Balleny basin

The Balleny basin (Figs 0.1, 2.1) is bounded on the north by the Pacific-Antarctic fracture zone and on the south by the Antarctic continent. Its western limit is not clearly defined but can be considered to be the Balleny Islands and the Balleny fracture zone. The eastern limit may be a definite structural boundary just east of 180°.

The bathymetry of the basin is illustrated by profiles in Figs. 4.2 and 4.25. The basin is about 3 km deep in the west, deepening to 3.5-4.0 km in the east. The seafloor is relatively smooth, apparently because of sediment cover. There is up to 1 km of sediment in the basin (Fig. 2.16) and most of it is highly distorted sediment, not flat-lying turbidite deposits. Ross (1967b) determined depths to magnetic basement from magnetic anomalies in the basin and obtained an average value of 3.9 ± 0.3 km, which is in good agreement with the basement depth indicated by seismic profiling.

Moderately flat basement and substantial amounts of sediment extend right to the Pacific-Antarctic fracture zone (Fig. 2.15, and unpublished data (Davey, pers comm 1973)). The lack of any transition between the basin and the fracture is in marked contrast to north of the fracture. At the Antarctic margin the basement is not deeper than 4-4.5 km and there are some basement ridges (section 2.3).

It was mentioned in section 2.9 that the presence of islands and numerous seamounts in the Balleny basin is atypical of the southwest Pacific area. The volcanic Balleny Islands at the west of the basin are at least mildly active, which is interesting since they are about 500 km from the axis of the southeast Indian ridge (Fig. 4.30). They are probably related to the Balleny fracture zone. There are no indications of a feature continuing south of the islands.

Scott Island is at the east of the basin on 180°, and just south of the island is an even more substantial feature (profile L, Fig. 4.25).

The peaks at the south end of that profile are at the western edge of Iselin bank (Fig. 2.1), so the basin is very narrow at 180°. Profile CC in Fig. 4.24 shows that southeast of the Scott Island features there are another three prominent features. All these features combined must form an almost continuous structure from the Pacific-Antarctic fracture zone to Iselin bank; probably marking the eastern end of the Balleny basin.

Seamounts in the basin are common but the graben-like structure shown in Fig. 2.16, profile N, is more unusual. It apparently strikes NNW and is at least 120 km long (Davey, pers comm 1973). It does not continue either to the shelf or to the Balleny Islands. Deepsea drilling site 274 (Fig. 2.2) was on the northern flank of the graben, in 3.3 km of water. It penetrated 415 m to basalt and the overlying sediment age was approximately 40 mybp (JOIDES, 1973c).

Magnetic data are frequently incomplete on profiles in the Balleny basin (e.g. Figs 4.2, 4.17) because pack ice is often encountered there. However the data are sufficient to show that anomaly wavelengths are similar on north-south and east-west tracks. Short wavelength high amplitude anomalies are observed over seamounts, but in general wavelengths are similar or slightly longer than those observed north of the Pacific-Antarctic fracture zone. Lineations related to the southeast Indian ridge are observed in the west to just north of the Balleny Islands (Fig. 4.30), but these have not been traced further south or east. Throughout most of the basin correlations between tracks can be suggested but numerous alternative correlations, and hence trends, are equally plausible. Bad navigation control on many tracks does not help, but even with just satellite controlled tracks correlations are no firmer. Feriel Falconer has independently examined the data and reached similar conclusions.

All the data indicate that the Balleny basin is a complex area.

### 4.7.3 Pacific-Antarctic basin

The Pacific-Antarctic basin (Fig. 2.1) is not well surveyed, especially the western part of it. Bathymetric charts (e.g. Udintsev, 1964; Heezen and Tharp, 1972) show a gentle basin deepening eastward from about 175°W. Most of the basin is 4-4.5 km deep, which is shallower than the southwest Pacific basin. Seismic profiler results east of 140°W indicate up to 1.5 km of undisturbed sediment (Houtz et al., 1973), which suggests that the depth of the basement in the Pacific-Antarctic basin is similar to that in the southwest Pacific basin.

The only track for which magnetic and bathymetric data were available in the Pacific-Antarctic basin area is track ELT33. It crosses the

Pacific-Antarctic ridge near 64°S, 168°W (Fig. 4.23) then heads eastward (Fig. 3.1). From just south of the ridge axis to east of 140°W most of the magnetic anomalies are less than 300 nT and no characteristic anomalies have been identified. Throughout the track there is bathymetric relief of 1 km or more. North of the Pacific-Antarctic ridge such relief is seen only where fracture zones occur. This suggests that there may be several fracture zones south of the ridge between 165°W and 150°W. With so little data extrapolating possible fracture zones from the track to the axis of the ridge is unwarranted.

More data are available south of the ridge east of 150°W (Fig. 2.12), but the coverage is inadequate south of about 62°S. This is unfortunate as it means that throughout the southwest Pacific area the structure on only the northern side of the Pacific-Antarctic ridge system is adequately known. This seriously limits the analysis of the tectonic history of the southwest Pacific area which will be presented later.

# CHAPTER 5

## NUMERICAL CORRELATION STUDIES

This chapter presents the results of a study of the application of numerical correlation techniques to magnetic anomaly profiles. An introduction (5.1) is followed by results from students (5.2), second moment correlation (5.3) and first moment correlation (5.4). Symmetry in profiles is considered in section 5.5, and conclusions on the numerical techniques given in 5.6.

### 5.1 INTRODUCTION

Marine geophysics has been revolutionised in the last decade, primarily through the study of marine magnetic anomalies. Of particular importance has been the identification of almost identical magnetic patterns at widely separated parts of the earth. The identifications are based almost entirely on visual correlation between profiles and the results presented in diagram form. Fisher (1970) has said "Diagrams prove nothing, but bring outstanding features readily to the eye; they are therefore no substitute for such critical tests as may be applied to the data..." Critical tests, in the form of numerical correlation calculations, have been applied to profiles (e.g. Fuller, 1964; Luyendyk et al., 1968; Loncarevic and Parker, 1971, Vogt et al., 1971a, Schouten 1971) but considering the number of publications which present correlations the number which contain critical tests is small.

The human eye and brain is a very efficient and adaptable correlator but it is affected by factors such as the scale at which profiles are plotted, prealignment of profiles, isolated large amplitude peaks, data gaps, preconceived ideas, and the availability of tracing paper. The position that produces maximum agreement is generally taken but that is not necessarily the position of minimum disagreement. Usually only the preferred correlation position is shown, which makes it difficult for a reader to judge whether that is the best alignment position. Even when different people agree on a particular correlation they cannot easily compare their judgements. Numerical correlation should overcome some of the visual limitations and would at least provide a quantitative estimate of correlation.

In an attempt to evaluate the usefulness of numerical correlation techniques a study has been made of correlation between some of the magnetic anomaly profiles discussed in the previous chapter. The intention was <u>not</u> to identify correlations between the profiles. The profiles considered had already been correlated visually and in most places definite opinions were

already held on the correlations. That is why the profiles were chosen. The intention of the study was to apply to the anomaly profiles various numerical correlation methods to see if they support the visual correlations, what are the most important factors and what are the limitations. A brief study has also been made of symmetry in profiles.

## 5.2 STUDENTS' VISUAL CORRELATION

An admittedly biased (but realistic) criterion of the usefulness of any numerical correlation method is that it indicate good correlation for positions at which profiles visually are considered well correlated. This will raise the question of whether the profiles are in fact well correlated. There are many examples in the literature of what are considered well correlated profiles but there are few details on exactly which features of the profiles are considered indicative of the good correlation. In an attempt to assess what features of a profile are used when visually judging correlation some tests were done with groups of university students.

Each group was a first year physics tutorial group consisting of 10-12 students. Virtually all of them had no knowledge of sea floor spreading or magnetic anomalies and so might be considered unbiased. No attempt was made to explain the subject other than to briefly say that the profiles they would be given reflected the structure of the seafloor, were taken along parallel tracks south of New Zealand, and that similar features might appear in some or all of the profiles. To illustrate, two similar profiles, not those they considered, were sketched on the blackboard and several correlated peaks numbered. They were then given the data shown in Fig. 5.1 and asked to number or letter any features which they could recognize in two or more profiles. Fig. 5.2 and the following discussion is an attempt to summarize the results.

Prealignment of the profiles on anomalies 32-34 probably had a dominant effect but the following aspects appear to have also been significant.

Amplitude is not very important; note the identification of anomaly 33 which is very subdued, and the use of the small feature between anomalies 31 and 32A. Anomaly 32A on profile three is quite insignificant but was still frequently associated with the larger feature on profiles one and two.

Horizontal scale may be important. In profiles one, two and three anomalies 31-34 are strongly linked, but anomalies 27-30 of profile three were not picked often. Presumably because the horizontal compression of profile three shifts those anomalies out of alignment with profiles one and two.

The order of the profiles is important. Most of the identifications of anomalies 28-31 on profiles five and six were for those profiles alone, they were not linked to profiles one to three. This may be due to the data gap in profile four. Anomaly 32A on profile four was not associated with profiles one and two, instead it was associated with profile five. Surely it would have been associated with profile two if profile three had not "intervened".

Data gaps are probably crucial. Would anomalies A and B on profile six have been chosen more often if anomaly C had existed? Would anomaly 32A have been picked in profile six if there hadn't been a gap beside it? It may have been if profile six had followed profile two.

A fourth group of students were given the same data as Fig. 5.1 but upside down (Fig. 5.3). They produced similar results to the other groups, correlating only what were for them positive peaks (actual negative anomalies). The anomalies 32-34 were in effect more strongly correlated by this group as everyone matched the 32-34 negative, several drawing a line down the page through it. Small positive peaks appear to be more significant than small negative ones as this group made no attempt to use anomaly 33 and they did use the small positives E and F in anomaly 32 (Fig. 5.3).

## 5.3 SECOND MOMENT CORRELATION

There are many different numerical coefficients that can be used for comparing profiles. The merits of particular coefficients have been discussed by, for example, Gibson (1950), Burnaby (1953), Miller and Khan (1962), and Krumbein and Graybill (1965). For this study the conventional second moment cross-correlation coefficient was chosen, mainly because it is widely used, and its statistical properties are well understood (Bartlett, 1955).

### 5.3.1 The second moment method

Consider two profiles which when digitized at N equidistant points give two series x(i) and y(i). A measure of the similarity of the profiles is the covariance coefficient vr given by

$$vr = \frac{1}{N} \sum_{i=1}^{N} [x(i) - mx].[y(i) - my] \qquad \ldots.5.1$$

where mx and my are the means of series x and y respectively.

The two profiles may be very similar but have different mean amplitudes. It is mainly the shape of the profiles, not the amplitudes, which are to be compared, so it is reasonable to normalise each series to the same amplitude.

This gives the correlation coefficient

$$r = \frac{\frac{1}{N}\sum_{i=1}^{N}[x(i) - mx].[y(i) - my]}{[var(x).var(y)]^{\frac{1}{2}}} \quad ....5.2$$

where var(x), the variance of series x is given by

$$var(x) = \frac{1}{N}\sum_{i=1}^{N}[x(i) - mx]^2 \quad ....5.3$$

Similarly for var(y), the variance of series y.

The correlation coefficient r as defined above has been referred to as the cross correlation coefficient, the Pearson product moment correlation coefficient, and the second moment correlation coefficient. The values of r will vary between +1 for perfect correspondence and -1 for negative correspondence of the series, and r = 0 represents complete non-correlation. For convenience values quoted will be 100 r, i.e. 100 for perfect correspondence.

If one profile, say y, is longer than the other it is possible to calculate the correlation coefficient at several alignment positions of the profiles (Fig. 5.4). This gives

$$r(d) = \frac{\frac{1}{Nx}\sum_{i=1}^{Nx}[x(i) - mx].[y(i+d) - my]}{[var(x).var(y)]^{\frac{1}{2}}} \quad ....5.4$$

where Nx is the number of points in the shorter series x. To preserve the range ±1 for r the mean my, and variance var(y), of series y must be those of section CD, not of the full length AB (Fig. 5.4). Calculation of r as a function r(d) of distance d is equivalent to sweeping profile x along profile y. A maximum in r(d) indicates an alignment position at which correlation is a maximum. In the example of Fig. 5.4 profile x is a portion of profile y. Hence the maximum of r(d) occurs where the short section is aligned with "itself" in the longer profile, and there r(d) = 100. Fig. 5.5 illustrates an example for two different records.

For all the profiles which will be shown the profile label indicates the number of data points in the profile, e.g. R197 has 197 points. Most of the profiles were digitized at intervals of one nautical mile which is sufficient to preserve the details in the profiles and avoid aliasing problems (Jenkins and Watts, 1968).

### 5.3.2 Statistical significance of correlation coefficients

In Fig. 5.5 the alignment position based on the maximum of r(d) appears acceptable but two questions arise. (1) Is the correlation non-zero? (2) If so, are there other positions at which correlation is also non-zero? To answer these quantitatively requires a statistical test.

The standard method is to use the Fisher z-transformation (Dixon and Massey, 1969) to obtain the confidence limits on r. It is then possible to test whether r is statistically different from zero, or to compare different values of r. The z-transformation method assumes that the data are normally distributed and that successive observations are independent. The normality requirement is not critical (Bartlett, 1935) but the independence assumption is very important. The data considered here are profiles which were digitized at close intervals and under these conditions each point is not independent of points adjacent to it. The standard z-transformation can still be applied (Awe, 1964) provided the number of points in the series is taken to be the effective number of independent points, Ne, rather than the total number, N. The problem then is to determine Ne. Three methods have been considered.

The first method is based on sampling theory applied to time series. It can be shown (Jenkins and Watts, 1968) that there are two independent points for each cycle of the highest frequency present in a record. Thus if the shortest wavelength $\lambda$ in a record of N points is known the number of independent points can be found from

$$Ne = \frac{2N}{\lambda} \qquad \ldots.5.5$$

The shortest wavelength $\lambda$ could be estimated from the power spectrum of the profile but this is not likely to be satisfactory. The length of profile used for correlation is generally less than 200 points (see later) which would not give good resolution in the spectrum. Also there is not a definite cutoff in the short wavelength end of the spectrum. A more fundamental objection to the use of the spectrum is that the profiles may not be stationary in frequency. The nature of the process producing the anomalies is such that the existence of a short wavelength anomaly at one place does not necessarily imply that the wavelength is present elsewhere. This is not satisfactory for spectral analysis. An alternative is to visually estimate the shortest wavelength in a profile and then use equation 5.5 to determine Ne. Table 5.1 gives values for profiles shown in Fig. 5.6. The visual method still assumes the continuous presence of the shortest wavelength and so the number of independent points would be overestimated by this method.

Table 5.1 Number of independent points in profiles

| Profile | N | $\lambda$ | L | $Ne = \frac{2N}{\lambda}$ | Ne from maxima | $Ne = \frac{N}{L}$ |
|---|---|---|---|---|---|---|
| N626 | 626 | 4 | 4.8 | 323 | 114 | 130 |
| N280 | 280 | 4 | 6.6 | 70 | 34 | 42 |
| NORM500 | 500 | 2 | 1.0 | 500 | 340 | 500 |
| P480 | 480 | 5 | 7.9 | 192 | 48 | 61 |
| T475 | 475 | 7 | 7.8 | 136 | 52 | 61 |
| B370 | 370 | 7 | 7.1 | 108 | 44 | 52 |
| R197 | 197 | 8 | 7.4 | 49 | 28 | 27 |
| R120 | 120 | 9 | 6.4 | 26 | 16 | 19 |
| R67 | 67 | 5 | 6.6 | 27 | 12 | 10 |

A second method for determining Ne is to assume two independent points for each maxima in the record. For some types of data this assumption can be rigorously justified (Awe, 1964) and it is intuitively reasonable that the number of independent points is related to the number of maxima. It is difficult to standardise the method of counting maxima but since small variations in a record do not contribute much "resolution" to the calculation of r(d) only distinct maxima need be considered. Typical values of Ne found this way (Table 5.1) are, as expected, less than those calculated from the shortest estimated wavelength.

A third method for determining the number of independent points in a record has been given by Awe (1964). It is based on the variance of the autocorrelation function of the record. If series x and y are the same, r(d) calculated with equation 5.4 is a form of autocorrelation. Rearranging Awe's results for digital analysis gives

$$Ne = \frac{N}{L} \qquad \ldots.5.6$$

where

$$L = \Sigma r(d)^2 \qquad \ldots.5.7$$

The summation is carried out only over the central peak of the autocorrelation function and for $r(d) > 0$ (Fig. 5.7). Only half the autocorrelation function is calculated since it is symmetrical. The value L is a measure of the length over which correlation exists between points in the profile and will be referred to as the correlation length. Typical values of Ne determined this way (Table 5.1) are less than those found from the shortest wavelength and are mostly slightly greater than those found from the number of maxima.

The correlation between profiles x and y at any particular alignment position involves only a section of the longer profile y (Fig. 5.4). The number of points of profile y considered at any position will always be equal to the number of points Nx in profile x. The effective number of points in x, Nex, is invariant but the effective number for y, Ney, is that of section CD (Fig. 5.4), and may vary with d. If the nature of profile y does not vary along its length Ney can easily be found from the effective number of points in the full length AB, and the ratio CD:AB. If the nature of profile y does vary along its length Ney would have to be redetermined for various positions. The method based on the number of maxima would be easiest to use in this situation.

In practice it is the number of independent points Ne for the cross-correlation of profiles x and y that is wanted, and this may not be the same as either Nex or Ney. A good approximation for the effective number of independent points can be found from the correlation length method (Awe, 1964) if equation 5.7 is replaced by

$$L = \Sigma rx(d).ry(d) \qquad ....5.8$$

where rx(d) and ry(d) are autocorrelation coefficients of profiles x and y respectively. The summation is carried out only for the central positive values of both rx(d) and ry(d). Table 5.2 lists Ne values found this way for various cross correlations.

Table 5.2 Number of independent points for cross correlation

| x on y | r | L | $Ne = \frac{Nx}{L}$ | From correlation length | | From maxima | |
|---|---|---|---|---|---|---|---|
| | | | | Nex | Ney | Nex | Ney |
| R197 : N626 | 41 | 5.6 | 35 | 27 | 41 | 28 | 28 |
| R197 : N280 | 41 | 7.0 | 28 | 27 | 30 | 28 | 28 |
| R67 : NORM500 | 28 | 1.0 | 67 | 10 | 67 | 16 | 45 |
| R197 : NORM500 | 20 | 1.0 | 197 | 27 | 197 | 28 | 134 |
| R67 : B370 | 83 | 6.8 | 10 | 10 | 9 | 12 | 10 |
| R120 : B370 | 73 | 6.7 | 18 | 19 | 17 | 16 | 14 |
| R197 : B370 | 51 | 7.2 | 27 | 27 | 28 | 28 | 24 |
| R197 : T475 | 36 | 7.6 | 26 | 27 | 25 | 28 | 26 |
| R197 : P480 | 60 | 7.6 | 26 | 27 | 25 | 28 | 24 |

For the correlation of R197 on N626 the position of maximum correlation is in the left hand part of N626 (Fig. 5.6), and for R197 on N280 the position is the same because N280 is the left hand hand end of N626. However the number of independent points Ne (Table 5.2) is different for the two, effectively identical, correlations. The difference arises because the autocorrelation length values used throughout Table 5.2 for Ne (and Ney) were those of the full length of profile y. The right hand part of N626 (Fig. 5.6) contains generally shorter wavelengths than the left hand part and the short wavelengths contribute to the short correlation length, L = 5.6 (Table 5.2). It is only the left hand part of N626 that is relevant for the position of maximum correlation and the correlation length for that part (N280) is L = 7.0 (Table 5.2). Strictly the value of L, hence Ne, should be calculated with only the exact 197 points of N626 or N280 used at the maximum correlation position. If this was done for every step of r(d) the value of Ne could change throughout the correlation sweep.

Once the effective number of independent points is known the standard z-transformation test can be applied. The confidence limits for any value of r can be found or the confidence limits for noncorrelation can be determined. The latter is probably more useful. The noncorrelation level is the maximum value of r which would be expected if the correlation between the profiles was zero. Fig. 5.8 shows how the 95% confidence noncorrelation level varies with the number of independent points. This level will be used subsequently and the value of r for it will be referred to as zr.

To determine zr the value of Ne must be specified. As the discussion above indicates, several alternative methods for estimating Ne are available, and the possibility of variations of Ne throughout a correlation sweep must be recognized. A pragmatic approach would be to use values of either Nex or Ney rather than do a full analysis for every value of d. The simplification is reasonable because if either profile contains obvious changes of wavelength or amplitude structure within its length it should not be considered as a whole for correlation study.

The correlation between two profiles is determined mainly by the most random profile (Bartlett, 1935) so it would probably be sufficient to take the greater of Nex or Ney for the value of Ne. If however Nex and Ney differ considerably caution is required. The data in Fig. 5.9 illustrate it. For R67 correlated with B370 different methods for determining Ne give a range for Ne of 9 to 12 (Table 5.2). This gives a range for zr of 59 to 55 (Fig. 5.9). However for R67 correlated with NORM500 the ranges for Ne and zr are 10-67 and 55-20 respectively. For zr = 20, which is determined from NORM500, 4.5% of the calculated r(d) values are above zr; in good agreement

with the expected 5%. The value zr = 55, determined from R67, would give a misleading impression of the significance of the correlations. This example is admittedly extreme and correlation between profiles such as NORM500 and the others would not normally be attempted. Nevertheless it illustrates the general principle that correlation will be determined by the most random profile.

The method used to determine Nex and Ney is a matter of choice. Values determined from either the number of maxima or the correlation length method are similar (Table 5.1 and 5.2). The shortest wavelength method is probably less useful as it is too dependent on the smallest features (Table 5.1). The correlation length method is quantitative but the visual method based on the number of maxima should be adequate and is easy to apply to only the relevant sections at a given alignment position. It will be used in subsequent applications.

### 5.3.3 Second moment results

The numerical correlation tests were applied to several of the magnetic anomaly profiles of the Southwest Pacific Basin discussed in the previous chapter. A large number of different correlations were calculated but to better illustrate the details of the results examples from only a few different correlations are presented. They are typical of the results obtained.

The correlation between profile R and profile B (Fig. 5.10) illustrates many facets of the numerical method. The maximum value of r(d) for R197 on B370 (Fig. 5.10A) occurs for the alignment position at which the profiles are visually very similar. The maximum correlation, r = 51, is well above the non-correlation level r = 32, and there is only one acceptable alignment position. More specific correlation can be obtained by breaking R197 into smaller pieces and sweeping them along B370. Figs 5.10B,C show that the maximum of r(d) aligns the pieces where they obviously fit. The peak r(d) values are higher than for the longer sweeping piece, but the fluctuations in r(d) are greater. Since the swept piece is short the number of independent points is small and the non-correlation level is higher. The best fitting positions are clearly non-zero but there are also other positions which statistically are correlated. The longer sweeping section R197 gives more unique alignment.

The advantages of short sweeping sections are illustrated by the profiles in Fig. 5.11. The maximum correlation of 69 is well above the non-correlation level 32 but is low considering the appearance of the profiles. If pieces A and B of R197 are swept separately each give r = 100 because

R197 and X207 are identical apart from 10 points artificially added in the middle of X207. Extra sections, or missing sections are common in profiles which cross fracture zones. The only reliable way to detect them is to use short sections.

The numerical correlation is not very sensitive to very small features. For instance in Fig. 5.10 removal of the characteristic but small anomaly 33 from profile R67 changes the peak correlation with B370 by only three. Similar small changes were obtained with other correlations using R67. With longer sections, e.g. R197, the small peak is even less significant. Differentiation of the profiles would amplify small peaks but it complicates the statistical tests for the significance of the calculated correlation (Yule, 1921; Bartlett, 1955).

Fig. 5.12 shows one of the few cases encountered in which the alignment position determined by numerical correlation was not at the preferred visual position. The correlation of 36 is only just above the non-correlation level (32) but it is the only statistically acceptable position. The preferred position (Fig. 5.13) gives r = 25. It is clear that R197 is compressed relative to T475. If R197 is progressively stretched the maximum value of r at the preferred correlation position varies as in Fig. 5.14. The number of maxima in R197 are not altered by the stretching so the effective number of points isn't altered. Hence the rise in correlation from 25 to 76 is very significant with respect to the non-correlation level of 32.

Profiles R197 and B370 (Fig. 5.10) provide further evidence of the importance of horizontal scale. R197 on B370 (Fig. 5.10A) gives r = 51, but a decrease in the length of R197 by only 6% will increase r to 78, which is comparable to the values obtained from the short sections. However the scale variation is not uniformly distributed. For R67 on B370 (Fig. 5.10C) the maximum value of r, 84, is obtained for 2% decrease in the length of R67 whereas for R120 on B370 (Fig. 5.10B) the maximum, r = 81, is with a 5% decrease in R120.

Valuable data can be obtained from only one profile if that profile crosses a fracture zone in a direction which produces duplication of anomalies. Fig. 5.15 shows the previously discussed ELT23 profile across the Tairoa fracture zone. The duplication of anomalies 27-31 is confirmed by sweeping one set of the anomalies along the full profile. The plot of r(d) peaks (r = 76) exactly where the profiles would be visually aligned. The r = 100 peak is where the short section is aligned with itself. Varying the length of the short section indicates that the best fit is obtained with no scale variation.

The ELT23 profile (Fig. 5.15) also illustrates the problem of data gaps. The correlation value of 76 was obtained with the data gap replaced by a straight line between the known values. Replacing the gap with values equal to the mean of the complete profile gives r = 70. Neither method is satisfactory since each effectively inserts an anomaly structure which may not be present. A possible alternative is the omission of any data gap terms from the summations in the calculation of r(d).

It was mentioned earlier that to retain the range ± 100 for r it is necessary to use the mean and variance of only that part of the longer series being compared at any given value of d (Fig. 5.16). When this is done care has to be taken because as Fig. 5.16 shows it is possible to get high values of correlation for positions at which the section CD is not typical of the full length AB. The problem is usually greatest for short sweeping sections against relatively "flat" sections of the longer profile. The properties of the full length AB can be used in place of those of CD to give what will be referred to as a non-normalized correlation coefficient. Several trials have shown that it is generally not satisfactory. The results can be very variable within a sweep (Fig. 5.17) and r is not restricted to ± 1 (Fig. 5.18). The results are most extreme with short sweeping sections.

### 5.3.4 Application to fracture zones

The aim of the numerical correlation study was to study the technique, not to identify correlations. However the numerical results had an influence on the anomaly interpretation of the Toarahi and Rangirua fracture zones (Fig. 5.19). The anomaly identifications had tentatively been made prior to the application of the numerical methods, but the numerical results provided the confidence required to name the fracture zones.

The fracture zones were investigated numerically with sections of profiles A408, V16 and T (Fig. 5.19). Pieces of each of these profiles (Fig. 5.20) were swept along the other profiles but only the peak values of r(d) are discussed. In all cases the lengths of the pieces swept are short so the statistical uncertainties are considerable. The correlation of 65 for section A+B of V16 on A408 supports the anomaly trends between V16 and A408 shown in Fig. 5.19. The duplication of anomalies on V16 is confirmed by the high correlation r = 74, of A on B, and their identification as anomalies 32A-32 is shown by T on A and B respectively. Varying the lengths of the sections will raise all three correlations to 85 or more, clearly above the noncorrelation level of 65. The identification of the southern set of

anomalies on A408 as anomalies 32A-32 is confirmed by T on D and B on D. The visual uncertainty of section C of A408 is also reflected in the numerical results. All the correlations with section C are relatively low and numerically it is not clear whether or not it is anomalies 32A-32.

## 5.4 FIRST MOMENT CORRELATION

If the alignment position for maximum similarity of two profiles is determined numerically the position may depend on the numerical method used. In an attempt to see if the type of coefficient is important another coefficient was selected for detailed comparison with the second moment method. The coefficient chosen was the first moment coefficient described by Gibson (1950). It is referred to as the first moment coefficient because it involves summation of single terms, whereas the second moment method involves summation of products. The first moment method was chosen for the detailed comparison primarily because it also gives correlation values in the range ± 1.

### 5.4.1 The first moment method

The first moment correlation coefficient can be defined as follows.

$$dx = \frac{1}{N} \sum_{i=1}^{N} \text{mod}[x(i) - mx] \qquad \ldots.5.9$$

where mx is the mean of the series. Each term x(i) in the series is adjusted to zero mean and scaled by the mean deviation dx to give a new normalized series

$$xn(i) = \frac{x(i) - mx}{dx} \qquad \ldots.5.10$$

It can be shown that $\sum_{i=1}^{N} xn(i) = 0$ and $\sum_{i=1}^{N} \text{mod}[xn(i)] = 1$. In a similar way series y(i) is converted to series yn(i). Let s(i) measure the similarity between two values xn(i) and yn(i) such that the modulus of s(i) will equal the modulus of the smaller, and such that s(i) will be positive or negative accordingly as nx(i) and ny(i) are the same or opposite sign respectively. This may be written

$$s(i) = 0.5 \quad \text{mod } xn(i) + yn(i) \quad - \text{mod} \quad xn(i) - yn(i) \qquad \ldots.5.11$$

The first moment correlation coefficient rf is defined as

$$rf = \frac{1}{N} \sum_{i=1}^{N} s(i) \qquad \ldots.5.12$$

The coefficient rf, like the second moment coefficient r, varies between ± 1 with + 1 for perfect correlation and zero for noncorrelation. The coefficient can be considered as being made up of two parts: (1) the fit, due to terms when xn(i) and yn(i) are of same sign; and (2) the nonfit, due to terms which differ in sign. This gives

$$rf = fit - nonfit \qquad ....5.13$$

Low correlation arises where the fit and nonfit are similar, high correlation requires both good fit and low nonfit. The coefficient rf can be calculated at different alignment positions of the profiles, giving rf(d), which is analogous to the second moment r(d) described previously.

If series x(i) and y(i) are both normally distributed it can be shown (Gibson 1950) that the first and second moment coefficients are related as follows.

$$(1 - rf^2)^2 = 1 - r^2 \qquad ....5.14$$

Both coefficients would rank normal data similarly, but they may differ with non-normal data, especially if there are very divergent points. The second moment method involves multiplying pairs of terms whereas the first moment always takes the smaller of the two terms. Thus the first moment method should be less affected by large peaks in only one of the profiles.

### 5.4.2 First moment results

Most of the profile correlations studied with the second moment method have also been done with the first moment method. The discussion which follows concentrates on the differences and similarities of the results obtained with the two methods. As before only a limited number of examples are discussed.

An example of the way in which the fit, nonfit and rf vary with alignment position is shown in Fig. 5.21. Positions at which fit is maximum are usually also positions of low nonfit. For perfect correlation (rf = 100) the agreement of the profiles would have to be exact (fit = 100) and the disagreement would have to be zero (nonfit = 0). In practice the amount of disagreement was usually much closer to ideal than was the amount of agreement (Fig. 5.22). Fits of more than 70 were rare and the maximum was only 76. Nonfits less than 30 were common and the positions of maximum correlation, i.e. maximum rf, usually had nonfit less than 10.

The correlation between two profiles varies with position in a similar way with both the first and second moment coefficients (Fig. 5.23).

Equation 5.14 predicts r > rf and this was so for the highest correlation of every pair of profiles compared (Fig. 5.24). For lesser maxima of some pairs r was not always greater than rf (Fig. 5.23) but the correlation at such positions was usually low, probably not nonzero. Throughout the full length of a correlation sweep the relationship between r and rf usually agreed reasonably with that expected theoretically (Fig. 5.25).

For every pair of profiles examined the best alignment position as defined by the maximum numerical correlation was the same for the two methods. However the positions of second best, third best, etc., were not always the same (Fig. 5.26).

Horizontal scale variation has a significant effect with both the first and second moment methods (Fig. 5.27).

The problem of good correlation when the sweeping section is aligned with a portion of the long record that is almost flat is still present in first moment correlation. As with second moment correlation the properties of the full length rather than of just the particular piece of the longer record that is being correlated can be used - giving what has been referred to a non-normal correlation. The non-normal values obtained throughout one correlation sweep can be similar to the regular values but substantial differences can also occur (Fig. 5.28). The variability of the results depends on the particular records being correlated (Fig. 5.29) but the first moment results are much less extreme than the second moment results (Fig. 5.30). The effect of non-normalisation is, as would be expected, more pronounced for short sweeping sections than for long sections, e.g. compare R66 and R197 on T475 (Fig. 5.30).

The advantages of short sweeping sections have been discussed in the section on second moment results. The same disadvantages apply with the first moment and the results are similar. Short sections tend to give higher correlation values, e.g. compare the rf values of R66 and R197 on T475 (Fig. 5.30). However, as with the second moment, more positions of high correlation are found so there is less uniqueness in matching the profiles.

To conclude: All the comparisons of first and second moment results indicate that the two correlation coefficients produce similar results. The first moment is more subdued with irregular data but for both methods the length of the sweeping bit and horizontal scale variations appear to be the critical factors.

## 5.5 SYMMETRY

### 5.5.1 Introduction

A sequence of normally and reversely magnetized blocks symmetrical about a centre need not produce symmetrical magnetic anomalies, but the orientation of most presently active spreading centres is such that symmetrical anomalies are produced (Schouten, 1971). This is fortunate as symmetrical magnetic anomalies have been the keystone of the seafloor spreading concept. Since the first results of Vine and Wilson (1965) at least one new active or extinct spreading centre has been identified from magnetic anomalies every year (e.g. Vine, 1966; Schlich and Patriat, 1967; Dickson et al., 1968; Demenitskaya and Karasik, 1969; Morgan and Johnson, 1970; Bergh, 1971; Ben-Avraham et al., 1972; Hayes and Ringis 1973). In some cases (e.g. Larson et al., 1968; Bergh, 1971) new detailed surveys produced the required data, but in other cases (e.g. Vine, 1966, Pitman et al., 1968) sufficient data had been available for some time.

It is tempting to speculate that the failure to recognize some centres earlier was due to the difficulties of recognizing symmetry in a magnetic anomaly profile. Once a symmetry centre has been marked it is usually easy to identify the matching anomalies, but the first identification of the centre appears to be dependent on pointers such as: a bathymetric ridge, earthquake epicentres, large amplitude short wavelength anomalies, the now well-known central positive anomaly, and predictions from adjacent areas. The essence of the problem is - given a profile, identify in it two identical (similar) sets of anomalies where one set is in inverse order to the other. It is basically a correlation problem similar to those discussed previously and subject to the same limitations, but the required inverse order of one set adds problems. In the literature a common method of presenting symmetry is to show two profiles, one the mirror image of the other, and label the correlated anomalies of the profiles. The method subtly enhances the symmetry because every anomaly is presented twice so twice the number of correlations are shown, i.e. the information is doubled. Strictly the profile should be split about the centre and one half presented, correlated with the other half.

Numerical correlation methods described previously are applicable to the symmetry problem so a brief study has been made to assess their usefulness. Since part of the evaluation of the results is judgement of how the numerical results compare with visual estimates some tests were done with students.

### 5.5.2 Student results

The student tests were similar to those described in section 5.2. Different students were used. They were given the data of either Fig. 5.31A or 5.31B and asked to mark any symmetry centres and number matched anomalies either side of the centre. Two blackboard examples were done, one with a positive anomaly as centre the other with a negative. There was no mention of only one symmetry centre per profile. The results for the two data sets (Fig. 5.32) are quite different and will be discussed separately.

For Fig. 5.32A an average of two centres per profile were picked, but altogether 31 different places were selected in the three profiles. In general, detail was concentrated on and matched anomalies were not extended far either side of the centres - the limits shown in Fig. 5.32A are the maximum. These profiles had been examined previously by several geophysicists but the good centres C1, C3, C5 and C8 had not been noticed, probably because a knowledge of the bathymetric structure was influencing their choice towards the area of centre C9 in profile B, centre C4 in N and centre C10 in EL. This appears to be a good example of the bias of preconceived ideas.

Only 23 students received the data of Fig. 5.31B but the results (Fig. 5.32B) are sufficient to indicate substantial differences from data set A. Fewer centres were picked; only one other than "the centre" in ELT 27 and two in ELT 19. The "success" with ELT 27 is good but the "failure" with ELT 19 is surprising. Informal discussion with the students later indicated that the spikeyness of the profile ELT 19 troubled them. As with data set A, not many anomalies either side of a centre were usually picked, but six students marked the full length of ELT 27. That profile is the same as profile EL of data set A, except for the "errors" in EL at C6 and to the left of C10. It is obvious that such small things, especially the one in the central anomaly, had a crucial effect.

The student correlations in section 5.2 suggested that inexperience lead to lack of success in correlating anomalies between profiles. The results here indicate that inexperience increases perception. Although large scale symmetry such as in profiles ELT 27 and ELT 19 was not well picked smaller scale features were consistently seen. The centres C1, C3, C5 and C8 are certainly as convincing as many in the literature. The ready acceptance of more than one symmetry centre per profile is interesting. Attempts to identify symmetry centres on the flanks of other symmetry centres (ridges) are not numerous in the literature. It is interesting to

consider what the results would be with an unbiased approach concentrating on short sections and detail.

### 5.5.3 Numerical tests for symmetry

Symmetry in a profile can be numerically tested with a modification of the previously described method for correlation between profiles. A section of the profile is selected, inverted and swept along the parent profile. Maxima in the correlation coefficient indicate positions at which there are anomalies similar to but in reverse order to those in the section selected. The sweeping section need not contain the centre of symmetry. The method has been applied to the profiles N, B, and ELT27 of Fig. 5.32. As the primary aim was to assess the usefulness of the numerical method in comparison with visual methods, attention was concentrated on the centres selected by students (Fig. 5.32). The second moment correlation coefficient r was used, and the noncorrelation level zr determined from the autocorrelation length of the sweeping section.

In profile B the students chose three centres (Fig. 5.32A). The centre C3, for example, is tested numerically by selecting just the section of profile over which students marked anomalies either side of the centre, i.e. section A of Fig. 5.33. When this section is inverted and swept along the parent profile the maximum correlation occurs at the symmetry centre. The correlation, r = 54, is well above the zero level zr = 36, but there are two other alignment positions with r = 48 and r = 45 respectively which are also non zero. When just one side of the symmetry centre (Fig. 5.33B) is swept along, the correlation at the symmetry centre is higher (r = 66) and non zero but there is a position elsewhere for which r = 86. The centre C2 (Fig. 5.32A) yields high correlations when either one side (Fig. 5.33D) or both sides (Fig. 5.33D) of it are swept along. However for section D there are three other positions with r > 80, one of r = 90, and for section C there are correlations of 66 and 58 elsewhere. The most popular student centre, C1, (Fig. 5.32A) yields correlation well below the zero level at the chosen centre.

The numerical results for profile N (Fig. 5.34) are similar to those of profile B. For both centres C5 and C4 the maximum correlation is at the symmetry centre but in each case there are two other places with correlations above 55. Other sections of profile N (Fig. 5.35) show that non zero correlation can be achieved in several places even with quite long inverted sections (Fig. 5.35B).

The numerical results with profile ELT27 (Fig. 5.36) are more decisive. For every test section the position of maximum correlation is the "expected" position, and in each case the correlation is well above zero level. For section A, the complete length of one side of the symmetry pattern, there is no alternative position that is non zero. For the other sections there are alternative non zero positions but only for section D are the alternative correlations more than marginally above the zero level. Section C illustrates how symmetrical anomalies can be identified without actually identifying the symmetry centre.

It has been shown previously that horizontal scale variations can have a critical effect on numerical correlations between different profiles. Similar effects can be expected with numerical tests of symmetry. The effects can be employed to determine scale variations either side of a centre. Profile ELT27 (Fig. 5.36) illustrates it well. For section C the correlation rises to 70 for a 4.5% decrease in the length of C. On the other hand, for section D the highest correlation (r = 83) is produced with a 10% increase in length. For section A a decrease of 5% produces the maximum correlation but the change in correlation is only from 56 to 58. Section A contains sections C and D and since they require scale changes in opposite directions the small change in correlation for section A is not surprising.

## 5.6 CONCLUSIONS

It cannot be denied that visual correlation has been very successful in marine geomagnetic research, but it is clear that the numerical correlation methods investigated in this study could usefully supplement visual methods. Particular aspects in which numerical methods can overcome visual difficulties are as follows.

Preconceived ideas: Without doubt a crucial factor in visual correlation. Numerical methods largely overcome the problem. However, with a large amount of data some element of preconception is probably required as it is very time consuming to correlate successive short sections of every profile with the full length of every other profile. In symmetry analysis of a single profile it is more important that complete objectivity is retained by sweeping successive sections of the profile rather than just the parts expected to be symmetrical. Numerical correlation obviates the need for pointers to symmetry such as a bathymetric ridge.

Prealignment of profiles: Student results and the literature indicate that this has a significant influence. Numerical correlation is not influenced by it.

The scale at which profiles are plotted: Important visually, but not numerically. However the actual amplitudes of the anomalies can be important in numerical correlation. With short sweeping sections it is possible to get high correlations with sections of the longer record which do not have what might be considered significant anomalies. Criteria for considering only sections with anomaly amplitudes above certain levels could easily be incorporated in a numerical system.

Data gaps: A problem for both visual and numerical methods. The advantage with a numerical system is that it need not introduce any anomaly structure in the gap, something which visually it is difficult to avoid doing.

There are three aspects in which visual correlation is apparently better than a simple numerical correlation system; (1) small but characteristic anomalies, (2) horizontal scale variations, and (3) missing or extra sections. Visual correlations presented in the literature frequently use small features amid larger ones. Sometimes their smallness is considered diagnostic, sometimes they cause slight splits in major anomalies, other times they make an otherwise regular sequence of anomalies particularly distinctive. The student results indicate that the use of small features is not confined to "the trade". The numerical methods used in this study are not sensitive to very small features. Differentiation of profiles to amplify small peaks has been used in visual correlation (Avery et al., 1968). Since it also amplifies "noise" in the records and complicates statistical tests differentiation is probably of limited use in a simple numerical correlation system. Mathematical methods for inverting an anomaly profile to give a profile of magnetization (Bott, 1967; Emilia and Bodvarsson, 1970; Bott and Hutton, 1970a; Schouten and McCamy, 1972) can be used to amplify small anomalies, but the validity of the technique is a subject of much discussion (e.g. Bott and Hutton, 1970b; Emilia and Bodvarsson, 1970; van den Akker et al., 1970; Blakely and Cox, 1972a; Woodward, 1973). The problem is essentially the same for visual or mathematical methods - does a particular small anomaly reflect regular crustal structure or is it just noise? Consistent appearance on several profiles is (or should be ) the most important criterion. Stacking of profiles (Keen, 1969; Blakely and Cox, 1972a,b) will eliminate noise and enhance consistent anomalies but horizontal scale variations can cause difficulties (Blakely and Cox, 1972a).

Horizontal scale variation is probably the most important factor in a simple numerical correlation method such as that studied here.

Variations in length between two profiles by 20% or more do not appear to significantly affect visual correlation (Vine, 1966), but even a 5% difference can substantially affect numerical correlation. It is not difficult to numerically alter the scale of a profile but if any scale variation changes within a profile it is more difficult. Numerical correlation can however be used to investigate scale variation in profiles. Since correlation effectively uses the full waveform it is probably better than least squares analysis of the spacing of anomaly peaks.

The use of short sweeping sections partially overcomes scale variation; it also helps when there are missing or extra sections in the longer profile. Such sections are common when tracks cross fracture zones. The problem with a short sweeping section is that it increases the likelihood of there being several positions of high correlation. The shorter the section the wider the confidence limits on the correlation coefficient so it is difficult to choose between alternative positions. Visual correlation is also less reliable when only a short section is compared.

Calculation of a numerical value of correlation for any position of profile alignment is relatively simple. Determining the statistical significance of the calculated value is more difficult. The important point is that the significance of any correlation value depends on the nature of the profiles. A correlation of 45 calculated with 200 points may be significant in one case but may not be in another. It is the number of independent points that is important. As discussed in section 5.3.2, a quick estimate can be obtained from the number of maxima in the sections being correlated, and a more quantitative measure can be obtained from the autocorrelation function of the profiles. When the number of independent points is known the standard statistical tests can be used to determine the confidence limits of any calculated correlation value. Some assessment of the confidence limits can, and should accompany any numerical value of correlation. Without it little progress has been made towards objective assessment of the correlation.

This study has concentrated on the first and second moment correlation coefficients. Alternative coefficients have been suggested by, for example, Burnaby (1953), Francheteau et al. (1969) and Harrison (1971). Most forms of coefficient will be substantially affected by horizontal scale variation and it is probable that the exact form of correlation coefficient is not important. The conventional second moment coefficient has the advantage that its statistical properties are well known.

Numerical correlation is useful for comparing profiles expected to be similar, but even with the most ideal data correlation of magnetic anomaly profiles between widely spaced areas can be difficult. This is due to the nature of the process which produces magnetic anomalies. The form of an anomaly profile over a particular structure depends on the inclination of the magnetic field and the orientation of the structure with respect to field; for both the present field and the field at the time at which the structure acquired its magnetization. Consequently the same magnetic reversal sequence at different places on the earth can produce anomalies which vary considerably. Even in a small area the effects of different orientations of the anomaly lineations can be very pronounced (Schouten, 1971). The numerical methods studied here will not overcome such variations, neither will visual methods apart from the experience of the observer. Some of the difficulties are being overcome with mathematical techniques for effectively transforming profiles to a common site, usually the pole (Schouten, 1971; Blakely and Cox, 1972a; Schouten and McCamy, 1972), and inversion to a profile of magnetization is also useful (Bott, 1967; Emilia and Bodvarsson, 1969; Bott and Hutton, 1970a; Schouten and McCamy, 1972). Most of the methods require ideal data, e.g. no data gaps, relatively smooth topography, no diurnal variation errors. They are undoubtedly useful for clarifying any correlations in the original data but the final conclusions of most studies are still being drawn from correlations between profiles of some parameter. When these correlations are done visually all the limitations of visual methods still exist. Numerical correlation could be just as usefully applied to the processed profiles as to the original profiles.

To conclude: Visual methods of correlation are simple, adaptable, and successful, but the fact that they do not provide a quantitative assessment of the quality of any correlation is a major limitation. Numerical correlation methods provide quantitative comparisons that are uninfluenced by personal bias and are amenable to statistical testing. Final interpretation will always be a personal matter but numerical coefficients at least provide a precise means of communication for discussion of the correlations.

Postscript to Chapter 5

After the work in this chapter was completed and typed an unpublished report by Morgan and Loomis (1969) was received. The report describes a numerical correlation method for determining the spreading rate of a magnetic anomaly profile and for detecting gaps or extra sections in the profile. The method is basically as follows. A model profile based on the reversal time scale and a chosen spreading rate is calculated, divided into short sections, and each section is swept along the profile to be investigated. The second moment correlation coefficient is used and the correlation values are presented in an age-offset diagram, from which the spreading rates and/or presence of discontinuities in sections of the profile can be detected. Applications of the technique to one profile are given.

Many of the problems encountered and conclusions reached by Morgan and Loomis are similar to those reached in chapter 5. The numerical technique produced a satisfactory result for the visually estimated interpretation, but also yielded an alternative "unseen" solution which was just as satisfactory. A variation of 10% in the model spreading rate, i.e. a horizontal scale change of 10%, would drastically alter the correlation values obtained. Because of scale variation and discontinuities it was necessary to use very short, sweeping sections. They used sections with only 24 points and the data were such that there would have seldom been more than six or eight independent points. They recognized the significance problem and without any analytical tests adopted r = 75 as the minimum acceptable correlation. Their overall conclusion was that the results obtained were not as definitive as had been hoped, but the advantage of the numerical technique is that it is quantitative and unbiased.

# CHAPTER 6

## MAGNETIC ANOMALY MODEL STUDIES

This chapter presents model studies which provide information on the origin of magnetic anomalies, in particular of the southwest Pacific basin, but in general of the seafloor. After a brief introduction (6.1) the validity of the assumed model is examined (6.2). Then a revised and extended magnetic reversal time scale and its implications are presented (6.3). The possibility of using model profiles to determine the position of formation of the observed anomalies is considered in section 6.4, and the thickness of the source layer of the anomalies is discussed in section 6.5. Variations in the anomaly amplitudes are discussed in section 6.6.

### 6.1 INTRODUCTION

The general characteristics of marine magnetic anomalies are now well known for many areas of the seafloor but the origin of the anomalies is still not adequately understood. Access to the source material is the primary difficulty so most discussions of the cause of anomalies have been based on either a small collection of samples or model studies of observed anomalies. Model studies are important because they can be applied to anomalies of any area and so can provide information on the similarities and differences in the magnetic structure of the seafloor in different areas. It is unlikely that there will ever be adequate direct sampling coverage of the seafloor but model studies will provide the links between detailed knowledge of a few places.

The essence of model studies is the comparison of an observed anomaly profile with a profile calculated from a proposed model of the magnetic structure of the seafloor. A large number of effects may contribute to the anomalies observed at any place but a model cannot easily represent them all. Consequently an understanding of the major factors involved is best obtained by studying anomalies from areas where possible extraneous effects are minimized. The anomalies numbered 25 to 36 in the southwest Pacific basin should be suitable. They are well developed and easily correlated; and the seafloor is 5 km or more deep and relatively undisturbed. The studies in this chapter are confined to these anomalies because the simple structure of the area should mean that simple models have some validity. The models and methods used are less sophisticated than those of, for example, Bott and Ingles (1972), Blakely and Cox (1972a), Schouten (1971), and Schouten and McCamy (1972). Whilst those methods would have made this work easier and enabled more complex models to be used the simple approach has provided valuable information.

The basic model used is as follows. The anomalies are assumed to be due to a series of blocks of alternately normally or reversely magnetized material. The blocks are assumed infinite along the strike of the anomaly lineations. The tops and bottoms of the blocks are flat, and the sides vertical. Only remanent magnetization is considered and the direction of magnetization is based on a geocentric axial dipole field. The computations were carried out with a program based on that described by Heirtzler et al. (1962). I am grateful to T.M. Geddes for providing the program.

## 6.2 THE VALIDITY OF THE MODEL

An example of a calculated model profile is shown in Fig. 6.1. It can be seen that the similarity of the model profile and the observed profiles is reasonable. Nevertheless it would be naive to assume that such a simple model truly reflects the magnetic structure of the seafloor. A discussion of the assumptions of the model follows. The discussion also serves as a review of factors which may be important to the origin of magnetic anomalies. It is set out as a series of comments and replies.

Comment: The basic assumption of normal and reverse magnetization may not be valid. Reply: It cannot be proved that reverse magnetization is required (Bott 1967; Emilia and Bodvarsson 1969) and typical anomalies can be modelled with varying but only positive magnetization (e.g. Heirtzler and Le Pichon, 1965; Ross 1966; Brakl et al., 1968; Watkins, 1968). Especially in areas of pronounced relief reversals are not required (Woodward, 1973) but there are also places where anything other than reverse magnetization would require extremely unusual structure (Ross, 1966; Talwani et al., 1971). Reversely magnetized material has been sampled from the seafloor (Cox and Doell, 1962; de Boer et al., 1969; Lowrie et al., 1973) and there is no question that field reversals do occur (Bullard, 1968). If seafloor spreading is accepted it is difficult to see how reversely magnetized material could be avoided.

Comment: The assumption of linear blocks extending to infinity either side of a profile is not reasonable. Reply: Provided the along strike length of a block is at least five times the depth to its top the infinite length assumption is a good approximation (Gay, 1963). The topographic trend of abyssal hills is usually parallel to anomaly trends (Menard and Mammerickx, 1967; Moore and Heath, 1967; Spiess and Mudie, 1971) and anomaly lineations are usually very long; thus the assumption of long blocks is realistic. However pronounced topography such as a fracture zone scarp to the side of a profile can have an effect (Rea, 1972; Malahoff and Woollard, 1971). At such places it would not be reasonable to expect a close match between a model profile and an observed profile, even if the seafloor directly underneath is flat.

Comment: The depth to the top of the blocks is not known. Reply: Model studies can be used to estimate the depth to the source (e.g. Smellie, 1956; Naudy, 1971) and although most methods are not very sensitive depths close to the depth of the seafloor are usually obtained (e.g. Ross, 1966). It is usually assumed that the upper surface of the magnetized layer is the top of Layer 2, i.e. the basement. Admittedly model profiles often have gradients sharper than those typically observed, but the inclusion of realistic seafloor structures would produce effects which would smooth calculated profiles. Blocks with tops below Layer 2 are adequate for anomalies observed at sealevel (Bott, 1967; Peter, 1970; Peter et al., 1971) but anomalies observed near the seafloor require sources at or near the seafloor (Luyendyk, 1969; Larson, 1971; Klitgord et al., 1972). There is ample evidence (see later) that the magnetization of Layer 2 is substantial so if sources only below Layer 2 are assumed uniform magnetization of Layer 2 is implied. If seafloor spreading and reversals are assumed it doesn't seem reasonable that Layer 2 should be uniformly magnetized (Luyendyk 1969, 1970b).

Comment: A flat top to the block is unreasonable in view of observed topographic relief of the basement. Reply: This is definitely a valid point for shallow depths and it can be shown that topography alone can produce anomalies (e.g. Vogt and Ostenso, 1966; Talwani et al., 1971). However the depth to basement for the anomalies considered here is 5 km or more and at that depth only extreme topography would have an effect (Hayes and Heirtzler, 1968).

Comment: The configuration of the bottom of the magnetized layer is not known. Reply: The assumed thickness of the blocks, hence the depth to the bottom, is a source of much debate and will be discussed more fully later. Any relief on the bottom surface has less effect than that on the upper surface and so probably isn't very important, especially for this study where the depth to even the top is 5 km.

Comment: Vertical sided blocks are unrealistic. Reply: The faulting and tilting that is apparent at rifts (van Andel and Bowin, 1968; Atwater and Mudie, 1968; Larson, 1971) may produce contacts between successive portions of the crust which aren't vertical. Inclined blocks can be successfully used to model anomalies (e.g. Heirtzler et al., 1966; Watkins and Richardson, 1968) but the models are somewhat complex. Inclined contacts are realistic but they are not required for adequate modelling of typical anomalies.

Comment: Vertical sided blocks imply dykes which terminate at the top with no horizontal flows. Reply: The existence of pillow lavas on the seafloor (Heezen and Hollister, 1971) does suggest some extrusive flow of material.

This might produce a layer of mixed polarity flows which could smear out anomalies due to dykes. However model studies by Watkins and Richardson (1971, 1972) have shown that flows need not have a great effect. Although Harrison (1972b) thought that the models Watkins and Richardson assumed were too simple they do show that for an elementary study surface flows can be ignored.

Comment: Induced magnetization of the source layer is ignored. Reply: The available studies of seafloor material likely to be involved in producing anomalies (summarized in Appendix 6.A) indicate that the natural remanent magnetization (NRM) is high, and almost certainly due to stable thermoremanent magnetization (TRM) acquired at the time of initial cooling (Ade-Hall, 1969). The ratio of permanent to induced magnetization (Koenigsberger ratio, Q) is typically greater than 10, so induced effects can reasonably be ignored. The existence of worldwide correlatable anomaly lineations is in itself support for the importance and stability of remanent magnetization.

Comment: The direction of remanent magnetization is based on the assumption of an axial dipole field. Reply: The magnetic field if averaged over at least a thousand years will probably have been axial dipolar (section 1.3.1). The blocks considered have widths of effectively more than 2000 years so the assumption is valid. It appears that field reversals are complete, i.e. $180^{o}$ inclination change (Opdyke, 1972) so the dipole assumption is valid for both normal and reverse blocks.

Comment: The magnetization is assumed to be uniform with depth in the block. Reply: The variation of magnetization with depth is an important issue which will be discussed more fully later. At this stage it is sufficient to assume that the uniform block represents the average magnetization within the depth range of the block.

Comment: The magnetization is assumed to be uniform horizontally, and since the magnetic properties of materials are affected by petrologic properties uniform petrology is implied. Reply: Petrologic contrasts can produce anomalies (e.g. Watkins and Richardson, 1968; van Andel and Bowin, 1968). At ridge axes and fracture zones, the only seafloor areas extensively sampled, there are clearly very substantial variations in petrology (e.g. van Andel and Bowin, 1968; Irving, 1970; Kay et al., 1970; Thompson and Melson, 1972). Intrusive activity still takes place off the axis (Fisher et al., 1968; Menard, 1969; Luyendyk, 1970a) and such material may vary petrologically from axial material (e.g. Kay et al., 1970; Miyashiro et al. 1970; Gass and Smewing, 1973). Differences in the petrology of normal and reversely magnetized material have been reported (e.g. Wilson, 1966; Wilson and Watkins, 1967; Watkins and Haggerty, 1968). Nevertheless the

existence of world wide correlatable anomalies argues that despite all the possible disruptive effects of petrologic variations such variations are not of major importance. The possibility that systematic variations in petrologic properties between different plate boundaries or tectonic regimes (Thompson and Melson, 1972; Shido and Miyashiro, 1973) may produce systematic regional variations in magnetic properties is worth considering.

Comment: If it is assumed that the normal and reverse blocks are a product of seafloor spreading the assumed uniform horizontal magnetization implies that the field strength was constant. Reply: The implication arises because the magnetization of the source layer is almost certainly due to TRM, the intensity of which would be proportional to the field at the time of cooling (Ade-Hall, 1969). Variations in the strength of the field with time would thus produce variations in the magnetization of the seafloor. The strength of the dipolar magnetic field has varied by up to 100% in the last 10 million years (Cox 1968, 1969; Smith, 1967a; Kono, 1971) and similar variations occurred in earlier periods (Smith 1967b,c; Carmichael 1967). Fluctuations with periods of a few millions of years appear probable and periods as short as thousands of years have been observed (Cox, 1969; Bucha, 1970). Current theories of the origin of the field imply that short period oscillations are likely (Allan, 1962; Cox, 1968). The probability of field variations shows that a very good match of the amplitudes of model and observed profiles throughout an anomaly sequence should not be demanded.

Comment: The assumed blocks imply that reversals are instantaneous. Reply: At a reversal the $180^{\circ}$ change in direction takes place in 2000 years or less (Ninkovitch et al., 1966; Cox, 1969; McElhinny, 1971; Opdyke, 1971) and this is effectively instant in terms of the seafloor record. The field intensity decreased to at least 20% during a reversal (Ninkovitch et al., 1966; Coe, 1967) and the decrease takes place over up to 10,000 years either side of the reversal (Cox and Dalrymple, 1967). The time span of the reduced field could produce some blurring of the edges of polarity intervals of less than 100,000 years, but would have little effect on longer intervals.

Comment: The block model assumes infinitely narrow boundaries between reversals. Reply: If the mode of crustal formation at the ridge axis is injection of narrow dykes it is reasonable to suppose that injection would not take place exactly into the centre of the previous dyke. A spread of injection is more likely, and this would smear out the reversal boundaries. There is much discussion of the likely injection width, and it will be discussed further later. Injection of a hot dyke will heat the surrounding material which will then be remagnetized on cooling. Reheating is unlikely to extend beyond a few metres (Harrison, 1968a; Doell, 1972) and the result is only an effective increase in the width of the intruding dykes.

To conclude: Despite all the limitations discussed above the simple model of reversal blocks is useful. Numerous publications in recent years have shown that simple as it is it does yield anomalies remarkably similar to those observed. If simple models can explain the major factors involved in the source of anomalies more sophisticated models can be used later to study details.

## 6.3 REVERSAL TIME SCALE

### 6.3.1 The SPAC reversal time scale

The magnetic field reversal time scale of Heirtzler et al. (1968) is defined only for anomalies out to number 32, approximately 75 mybp. The identification of anomalies beyond number 32 in the southwest Pacific basin enables the time scale to be extended. The assumptions inherent in the principle of determining a reversal time scale from marine magnetic anomalies have been discussed in section 1.3.2 and will not be repeated here. The general agreement between deep sea drilling results and the Heirtzler et al. (1968) scale is sufficient justification for proposing an extension of the scale.

In practice a time scale can be defined from a single profile as follows. A simple model of normal and reverse blocks is assumed and the positions of the polarity changes are adjusted until the profile calculated from the model blocks agrees with the observed profile to the desired accuracy. Assumption of a spreading rate and a date for one point on the profile enables the spacing of the assumed blocks to be translated into dates of the field reversals.

Fig. 6.1 shows an observed profile from the southwest Pacific, SPAC; the normal and reverse blocks which yield a model profile that fits the profile SPAC; and the time scale for the blocks. The dates of the reversals are given in Table 6.1 overleaf. Justification and discussion of these dates will occupy the remainder of this chapter section.

### 6.3.2 The basis of the SPAC time scale

Although a time scale can be defined from only one profile such a scale is much more credible if the anomaly sequence that defines it has been widely observed. This is so for the SPAC scale of Table 6.1. The anomalies 25 to 32 have been observed in many places throughout the world. The anomalies 33-36, and less definitely 37, are widely observed in the southwest Pacific basin but their existence elsewhere has seldom been referred to. They can however be seen elsewhere as follows.

Table 6.1 Geomagnetic reversal time scale based on profile SPAC

| Anomaly | Interval of normal polarity (mybp) | | |
|---|---|---|---|
| 25 | 62.75 | to | 63.28 |
| 26 | 64.14 | | 64.62 |
| 27 | 66.65 | | 67.10 |
| 28 | 67.75 | | 68.45 |
| 29 | 68.75 | | 69.40 |
| 30 | 70.00 | | 71.50 |
| 31 | 71.60 | | 72.40 |
| 32A | 73.95 | | 74.05 |
| 32 | 74.30 | | 75.60 |
| 33 | 75.80 | | 75.88 |
| 34-36 | 76.20 | | 80.40 |
| 37 | 80.75 | | 81.55 |

Anomaly 33 although small is distinctive. Apart from in the southwest Pacific it can be seen in the north-south lineations of northeast Pacific (Fig. 6.2A), the eastwest lineations south of the Aleutian trench (Fig. 6.2B) and the Indian Ocean (Fig. 6.3A). Anomaly 34 is implied south of the Aleutians (Fig. 6.2B) and in the Indian Ocean (Fig. 6.3A). The whole of the long positive anomaly 34 to 36 can be seen in the northeast Pacific (Fig. 6.2A) and tentatively in the South Atlantic (Fig. 6.3B). Anomaly 37, if present in the northeast Pacific, is not readily apparent (Fig. 6.2A) and in the southwest Pacific it may be a structural anomaly associated with the continental margin. Nevertheless it will be included in the reversal time scale. The prominent anomaly numbered 38 in profile SPAC shown in Fig. 6.1 can be modelled by a simple reversal block model, but it is not included in the time scale because it is not seen elsewhere in the southwest Pacific and it is underlain by prominent topography (Fig. 6.4).

The spacing of the anomaly lineations in the southwest Pacific basin varies across the area, so one type profile was selected from which to determine the time scale. The type profile chosen, SPAC (Fig. 6.1) is a composite of profiles T and W (Fig. 6.5). Profile W, which is adjacent to profile T, was used for anomalies 25 and 26 because anomaly 26 is not clear on profile T. The remainder of SPAC is profile T. These profiles were chosen because the anomalies in that area are well developed and the lineations are undisturbed. The choice was made on the basis of only the magnetic data. The bathymetric data for profile T became available only later and in retrospect a better profile might have been chosen. However the choice appears justifiable because the SPAC time scale gives good linear spreading

rates for other profiles in the southwest Pacific (see later).

The model used for computing the time scale assumed a magnetized layer 2.0 km thick with the upper surface 5.0 km below sea level, the approximate depth to the seafloor at profile T (Fig. 6.4). The calculated anomaly profile in Fig. 6.1 is what would be observed for blocks formed and observed with a field inclination of 90°. The inclination at profile T is approximately 75° but the difference would have no significant effect on the block boundary positions.

The time scale is essentially determined from the close similarity of profile SPAC to the north Pacific profile NPAC (Fig. 6.1). That profile (from Raff 1966) is the type profile that Heirtzler et al., (1968) used for this part of their time scale. The scale they gave (Heirtzler et al., Table 1 and Fig. 3, 1968) does not match their type profile beyond anomaly 31, and presumably because of drafting errors. Their dates for anomalies 25 to 31 give a spreading rate in the north Pacific of 4.74 cm/yr. Comparison of profiles SPAC and NPAC gives 4.37 cm/yr for SPAC. This rate was assumed for the full extent of profile SPAC. The Heirtzler et al. dates were taken for anomalies 25-27 so those blocks were fixed. The remaining blocks were adjusted by trial and error to give a model profile which reasonably matched profile SPAC. The dates of the reversals (Table 6.1) were then determined from the model blocks.

### 6.3.3 Comparison with other time scales

Fig. 6.6 shows several time scales which have been proposed for the anomalies beyond number 25. Vine (1966) didn't give reversal dates but he assigned dates to a composite north Pacific profile on the assumption of a uniform spreading rate of about 4.5 cm/yr prior to 10 mybp. His dates are about 5 my younger than those shown in Fig. 6.6. It is his composite profile that has become the standard profile. Heirtzler et al. (1968) determined their polarity intervals from it but the absolute dates were derived by comparison with an assumed uniform rate in the south Atlantic.

McKenzie and Sclater (1971) independently noticed the errors in the Heirtzler et al. scale beyond anomaly 31. Using a spreading rate of 4.74 cm/yr in the north Pacific they revised the dates of anomalies 31, 32A and 32 and added dates for anomaly 33 and the reverse-normal transition that defines anomaly 34.

The Lamont scale is an unpublished revision of the Heirtzler et al. scale and is used at Lamont-Doherty Geological Observatory.

Larson and Pitman (1972) state that they have extended the Heirtzler et al. scale and that for their scale "The negative interval at 82 to 85 mybp has been added by measuring west of anomaly 32 on Raff's (1966) north Pacific profile at 40° 30' N". That is the standard profile NPAC and Figs 6.1 and

6.6 show that their assumed negative interval would not be as old as they state. The younger boundary of it would be no more than 80.5 mybp.

For the anomalies 25 to 34 the reversal dates of the different scales (excluding Vine's) are not very different. Variations between profiles in a small area are likely to be just as large as the differences between the north and southwest Pacific type profiles. The SPAC dates for anomaly 36 and beyond do not agree with those of Larson and Pitman (1972) but the SPAC dates are preferred.

### 6.3.4 Absolute dates and the Cretaceous normal polarity interval

In previous sections reversal dates have been quoted to 0.01 my. Whilst the lengths of particular polarity intervals may be correct to that accuracy absolute ages are very uncertain. The dates of the Heirtzler et al. scale were based on an extrapolation from 3.35 mybp and the other scales are only revisions relative to that scale. Deepsea drilling results have confirmed that the time scale is at least reasonably correct but the confirmation is not detailed. Van Andel (1972) has discussed the limitations involved in dating the oceanic crust from deepsea drilling results and concludes that a reasonable error estimate for the JOIDES ages in the interval of interest here would be ±5 my. Table 6.2 shows data for sites at which basement was reached and the age was expected from magnetic anomalies at or close to the site to be in the range 60 to 85 mybp. The JOIDES ages are based on paleontological dates of the contact sediment and in general they are younger than the magnetic anomaly dates. The differences are greater than the uncertainties Van Andel suggested and might reflect inaccuracies in the magnetic reversal scale. However it is not difficult to provide plausible reasons which could explain the "discrepancies".

Table 6.2 Basement ages at JOIDES sites

| Site | Location | JOIDES | Magnetic |
|---|---|---|---|
| 2-9 | N. Atlantic | 85 | 81 |
| 3-20 | S. Atlantic | 70-72 | 67 |
| 5-39 | E. Pacific | 50 | 60 |
| 5-41 | Equat. Pacific | 50 | 67 |
| 12-112 | Labrador Sea | 55 | 67 |
| 22-213 | NE Indian | 56 | 63 |
| 24-236 | NW Indian | 55-60 | 68 |
| 25-245 | SW Indian | 63 | 68 |
| 29-283 | Tasman Sea | 65 | 75 |

Data from Van Andel (1972) and JOIDES (1972a,b,c, 1973d).

It is possible that the magnetic anomaly reversal time scale could also be checked by paleomagnetic analysis of dated samples from land. Ordinarily the land record is too discontinuous and dating inaccuracies too great to allow a dated sample of known polarity to be assigned a particular point of the seafloor reversal sequence. However there is a long interval from approximately 80 to 110 mybp during which the field was apparently of constant normal polarity. The paleomagnetic data for this interval, which is referred to as the Cretaceous normal polarity interval, have been discussed by Helsey and Steiner (1969), McElhinny and Burek (1971), Creer (1971) and Irving and Couillard (1973). The most complete and up to date compilation is that of Irving and Couillard (1973) and they state that there are no known reversals between 109 and 82 mybp. If the field was indeed normal throughout this period it provides an important constraint of the reversal time scale.

The existence of anomaly 37 and a reversed period beyond it might be considered equivocal but the existence of the reversed interval immediately beyond anomaly 36 is unequivocal. If there is no reversed polarity beyond 82 mybp the seafloor reversed period must be younger than that. If anomaly 37 is accepted the end of the reversed period beyond it (Fig. 6.1) agrees well with the 82 my age of the start of the Cretaceous normal polarity interval. If the longer reversed interval of Larson and Pitman is taken but correctly calculated from NPAC (Fig. 6.1) the reversed interval ends at about 82.5 my. Either way the seafloor reversal scale agrees with Irving and Couillard's data.

The Cretaceous normal interval provides only an older limit to the seafloor reversal time scale. The reversed anomalies could be younger than 82 mybp. However the general lack of anomalies beyond anomalies 36 and 37 in the northeast Pacific, south Atlantic and possibly the north Atlantic (Vogt and Johnson, 1971) suggests that the mapped anomalies extend to the start of the normal interval and thus the time scale is correct. Detailed surveys in several areas of the anomalies beyond number 32, coupled with deep sea drilling, could better define the upper boundary of the Cretaceous normal interval. As Irving and Couillard (1973) point out, it is a potentially important global time marker.

### 6.3.5 Short polarity intervals

The duration of the normal polarity interval that defines anomaly 33 is only 0.05 my in both the SPAC and McKenzie and Sclater (1971) time scales. There are only six shorter intervals in the 171 intervals of the Heirtzler et al. time scale from 0 to 76 mybp, and none in the 41 intervals of the Larson and Pitman (1972) scale from 115 to 148 mybp. The shortness of this interval is significant in view of the current interest in statistical aspects of the duration of polarity intervals (Cox, 1968, 1969, 1970; Nagata, 1968; Parker 1969, Naidu, 1971; Blakely and Cox, 1972 a, b).

Models which explain reversals of the magnetic field in terms of statistical fluctuations in the core (Cox, 1968; Nagata, 1968; Parker, 1969) lead to the conclusion that reversals as a function of time should be Poisson distributed. Naidu (1968) has shown that the polarity intervals of the Heirtzler et al. (1968) time scale are Poisson distributed for 0 to 45 mybp but prior to that they are not; the number of short intervals being much less than expected. The generally greater depth of old seafloor will diminish the anomaly a short interval produces at the surface, but this is not sufficient to account for the lack of short intervals. Either the short intervals are present but have not been detected for some reason, or they are not present and the proposed models are not applicable for earlier periods. The existence of anomaly 33(duration 0.05 my) shows that at least one short interval does exist. Blakely and Cox (1972b) have applied their (1972a) technique of stacking profiles to six profiles covering the period 54-69 mybp and detected several additional reversals as short as 0.02 my duration. It is probable that similar techniques if applied extensively will detect further short intervals. The existence of anomaly 33 and Blakely and Cox's results show that the lack of short intervals may be only apparent.

## 6.4 PALEO-POSITIONS OF ANOMALY LINEATIONS

If it is assumed that observed anomalies can be adequately modelled by normal and reverse blocks model studies can provide information on the possible positions the anomalies were at the time at which they formed. The form of an anomaly profile observed over lineated normal and reverse blocks depends on the orientation of the lineations with respect to both the direction of the remanent magnetization of the blocks and the present day field direction. Consequently the model studies require as input parameters the strike of the lineations, the inclination and declination of the present field, and the inclination and declination of the remanent magnetization of the blocks. The remanent parameters are not known but it is they which are used to derive paleopositions. The parameters are varied until the calculated anomaly profile best fits the observed profile. If an axial dipole field is assumed the remanent inclination indicates the latitude of the anomalies at the time of magnetization and the declination gives the strike of the lineations. Unfortunately there will be a family of pairs of inclination and declination values which yield the same anomaly pattern (Schouten, 1971) so additional constraints are required to select unique values.

Some model studies have been done to see if it is possible to determine the paleopositions of the anomalies 25-37 of the southwest Pacific basin. From west to east in the area the present field inclination changes from $80^{\circ}$ to $70^{\circ}$, the declination from $040^{\circ}$ to $025^{\circ}$, and the strike of the

anomalies from 075° to 040°. The strike of the anomalies with respect to magnetic north, i.e. the effective declination, changes from 035° in the west to 015° in the east. To limit the number of variables the model studies which are presented assume a present field inclination of 70° and an effective declination of 30°. The SPAC time scale was used with a spreading rate of 4.0 cm/yr. The blocks were 2 km thick with their tops 5 km below sea level.

Fig. 6.7 shows the anomalies which would be observed if the lineations had been formed at approximately their present latitude but at different orientations. The differences for various orientations are small, the main effect being an increase in symmetry as the lineation paleo-strike approaches north-south. Fig. 6.8 shows the anomalies which would be observed if the lineations had formed striking east-west at a different latitude. The differences for various latitudes are slight, the symmetry increasing for higher paleo-latitudes.

The variations in Fig. 6.7 and 6.8 could have been expected from the mathematical description of the anomaly produced by a linear block (See Appendix 6B, part 1). It shows that for a given latitude the degree of symmetry increases as the lineation strike approaches north-south, and for a given strike the symmetry increases for higher latitudes. The Fig. 6.8 profile for latitude 45°S shows the maximum amount of asymmetry likely to be observed in the area as any lineations formed south of 45°S, irrespective of their orientation, would be more symmetric. Similar profiles appear in both diagrams because the strike and latitude are interrelated in their effect on the anomalies. For example lineations formed striking 040° at 55°S would produce the same effect as lineations formed striking east-west at 65°S.

Fig. 6.9 shows that there are considerable variations in the shape of the anomalies observed throughout the area. Almost any individual anomaly could be matched somewhere in the theoretical anomalies shown in Figs 6.7 and 6.8. However compared with the theoretical anomalies the observed anomaly 32 doesn't have a marked northward tilt, anomaly 31 is not very prominent relative to anomaly 30, anomalies 29 and 28 tend to be flat topped rather than spiked, and the dip to the south of anomalies 25-27 is not very pronounced. The overall appearance of the observed anomalies is similar to that of the more symmetrical model profiles. If the lineations formed north of their present position the observed symmetry requires that as well as a southward translation they must have also rotated from a more north-south strike. Even for in situ latitude formation the strike would have to be more north-south than present. A degree of symmetry is more readily achieved if the lineations formed further south. For higher latitudes strike variations have less effect.

When the ideal nature of the assumed model is recalled and the inherent ambiguities recognized, it is clear that these model studies do not provide a precise indication of paleo-position. Nevertheless they suggest that the lineations probably formed south of their present position.

## 6.5 THICKNESS OF THE MAGNETIZED LAYER

### 6.5.1 General

Two important unknowns in present understanding of the source of magnetic anomalies are the thickness of the magnetized layer and the intensity of magnetization of the layer. The two factors are not independent; if either is specified the amplitude of the anomalies determines the other.

Layer thicknesses of 5 km or more were used in some early studies (Vine and Matthews, 1963; Heirtzler and Le Pichon, 1965; Vine and Wilson, 1965), the depth to the base of the layer being chosen mainly from the probable depth of the Curie temperature isotherm. However thinner layers soon became preferred, partly because they gave sharper anomalies but mainly on petrological grounds. Hess (1962, 1965) argued that Layer 3 was likely to be serpentinized peridotite. This probably would not be highly magnetized and has a low Q (Watkins and Paster 1971) and therefore would not contribute much to surface anomalies. Layer 2 was considered to be mainly basalt; rapidly cooled in situ and capable of having a high remanent magnetization. Since Layer 2 is typically 2 km or less many studies have assumed magnetized layer thicknesses of the order of 2 km (e.g. Vine and Wilson, 1965; Vine, 1966; Bott, 1967; Hayes and Heirtzler, 1968; McKenzie and Sclater, 1971). Recently thicknesses of 500 m or less have come into favour (e.g. Irving et al., 1970; Talwani et al., 1971; Weissel and Hayes, 1972; Blakely and Cox, 1972b).

For simple model studies the thickness of the magnetized layer is not very important but for an adequate understanding of the structure and composition of the oceanic crust a knowledge of magnetization distribution is vital. Model studies cannot provide a unique solution but broad constraints are provided by three factors: (1) the shape of anomalies; (2) the amplitude of anomalies; (3) the plausibility of the deduced intensity of magnetization.

### 6.5.2 Thickness and anomaly amplitude and shape

The amplitude and shape of anomalies is affected by the thickness of the magnetized layer. Fig. 6.10 shows some models for different thicknesses in which the magnetizations have been scaled linearly with respect to the thickness to produce similar anomaly amplitudes. The intensities of the thicker layers should have been slightly greater but it is clear that the

thicker the layer the lower the required magnetization. The effect of a change in thickness is not just a uniform change of amplitude; the small anomalies, e.g. 32A and 33, are reduced relative to the major anomalies as the thickness is increased. This is what would be expected from theory (Appendix 6B, part 2) as the small anomalies arise from narrow blocks and so are most affected by thickness. The small anomalies could however be increased for thick blocks by only slight increases in the width of the blocks which produce them. The SPAC time scale was determined using 2 km blocks and the shorter intervals might be altered if a different layer thickness was used.

The most obvious effect of a thicker layer is the smoothing of the anomalies. The sharpness of the anomalies is to a certain extent affected by inclination and declination (Fig. 6.7 and 6.8) but the thickness effect is more pronounced. Typical observed anomalies (Fig. 6.9) are more like the smoother profiles of the 5 km thick layer than the sharper 0.5 km profiles. However most natural crustal effects will tend to smooth anomalies so a thin layer could be acceptable. So many factors can alter the shape of anomalies that it doesn't seem promising to estimate the layer thickness from anomaly shape alone.

### 6.5.3 Thickness and basement relief

An unusual seafloor structure associated with the Tairoa fracture zone that was discussed in section 4.3.3 may provide information on the thickness of the magnetized layer. Fig. 4.11 shows the relevant bathymetric and magnetic profile across the fracture. It is the two sets of anomalies 27-29 which are of special interest. The set on the western side of the fracture is over the raised seafloor but is quite similar to the eastern set, apart from having higher amplitudes. There is no seismic profile record for this profile but other tracks in the area indicate sediment thicknesses of less than 100 m (R.E. Houtz, pers comm., 1972). It is therefore reasonable to assume that the bathymetric profile approximates the basement surface and that the raised block is uplifted or thickened basement.

Fig. 6.11 shows model studies in which the upper surface of the basement has been approximated by flat surfaces at a depth of 4 km for the raised block and 5 km for the surrounding area. In each case the anomalies produced by a uniform layer at 5 km are compared with those produced by the raised block. The two cases for which the magnetized layer is assumed to be uplifted (A and B) produce small increases in the anomalies over the block and both cases are quite similar. When the bottom of the magnetized layer is held constant (C and D) the effects are much more pronounced and the two cases are quite different. Models using a 5 km thick layer produce similar effects

to those shown in Fig. 6.11 but the uplifted and thickened cases are not very different.

Table 6.3 presents a more quantitative assessment of the models. The ratios given are the anomaly amplitude over the raised block divided by the amplitude over the uniform layer. The ratios for the models in which the magnetized layer is uplifted agree well with the ratios observed on the ELT23 profile. For a thickened layer the model ratio of a 5 km layer agrees with the observed ratio but the ratios for 0.5 km and 2 km layers do not agree.

Table 6.3 Ratios of anomaly amplitudes

| Anomaly | ELT23 | Uplifted : flat | | | Thickened : flat | | |
|---|---|---|---|---|---|---|---|
| | west : east | 0.5 km | 2.0 km | 5.0 km | 0.5 km | 2.0 km | 5.0 km |
| 27 | 1.30 | 1.29 | 1.24 | 1.21 | 3.37 | 1.67 | 1.33 |
| 28 | 1.24 | 1.32 | 1.26 | 1.23 | 3.35 | 1.68 | 1.33 |
| 29 | 1.28 | 1.25 | 1.24 | 1.18 | 3.12 | 1.62 | 1.29 |

The model shapes used are admittedly very simple and uniform magnetization is assumed, but it appears that if the magnetized layer thickness is 2 km or less it is necessary to assume that the layer is uplifted rather than thickened. For layers thicker than 2 km it would be less necessary to assume uplift. The model studies do not provide a unique determination of the thickness but a thin layer leads to a much more unusual configuration and so might be considered less preferable. If the layer is only 0.5 km thick the whole layer and several hundred meters of the material below it is potentially exposed on the sides of the block. It would be a good place to dredge for samples of the magnetized layer.

### 6.5.4 Thickness and intensity of magnetization

The interdependence of the thickness and the intensity of magnetization of the magnetized layer has been discussed in section 6.5.2. The amplitudes of anomalies observed in the southwest Pacific basin vary but if a magnetized layer 0.5 km thick is assumed intensities of magnetization of 15 to $20 \times 10^{-3}$ emu/cm$^3$ are required to produce the observed anomalies. For a 2 km layer $5 \times 10^{-3}$ emu/cm$^3$ is sufficient and for a 5 km layer $2 \times 10^{-3}$ emu/cm$^3$ is adequate. Comparison of these derived values of magnetization with observed values is probably the best means of assessing the actual thickness of the magnetized layer.

Knowledge of the magnetization of oceanic crust has been derived mainly from measurements of the magnetization of dredge samples. A summary of data presented in the literature is given in Appendix 6A. Magnetizations of $15 \times 10^{-3}$ emu/cm$^3$ or greater have been reported but such high values are almost completely confined to the ridge axis. Detailed sampling on the Reykjanes ridge (de Boer et al., 1970) and the mid-Atlantic ridge at 45°N (Irving et al., 1970) has shown an almost ten fold decrease in magnetization within 50 km of the ridge axis. From model studies of specially controlled profiles at the Reykjanes ridge Talwani et al., (1971) deduced magnetizations of $30 \times 10^{-3}$ emu/cm$^3$ at the axis, $12 \times 10^{-3}$ at 75 km and $7 \times 10^{-3}$ at 100 km off the axis. Possible reasons for the decrease away from the axis have been discussed by, for example, de Boer et al., (1970), Carmichael (1970), Irving et al., (1970), and Banerjee (1971, 1972). Irrespective of the reason it appears that high magnetization will be present only near the axis.

Samples typical of the ocean basins are difficult to get because of sediment cover but the majority of magnetizations reported from basins are less than $10 \times 10^{-3}$ emu/cm$^3$. Dredge samples may be biased towards unusual features such as fracture zone scarps and seamounts so the deepsea drilling data are particularly important. The range of magnetization from the Mohole (Cox and Doell, 1962) was 1-10 $\times 10^{-3}$ emu/cm$^3$, the higher values being from within one metre of the surface of the flow. JOIDES data from the Caribbean and Atlantic (Lowrie et al., 1973) give a range of 0.1-10 $\times 10^{-3}$ emu/cm$^3$. Five sites from Legs 2 and 3 had a mean of only $1 \times 10^{-3}$ emu/cm$^3$, and Lowrie et al., (1973) pointed out that this would require a magnetized layer 2.5 km thick to produce the observed magnetic anomalies near the sites in the south Atlantic.

The available data suggest that magnetizations in excess of $10 \times 10^{-3}$ emu/cm$^3$ are unlikely in the basins. This sets a minimum thickness of the order of 1 km for the magnetized layer in the southwest Pacific basin. Magnetizations of $5 \times 10^{-3}$ emu/cm$^3$ or less seem more probable which requires the layer thickness to be 2 km or more.

Apart from the difficulties of high magnetization a thin layer also presents the problem that it ignores the magnetic effect of material below it. Away from the axis all of the crust would be above the Curie temperature isotherm and so could be magnetized. All of Layer 2 (approximately the top 2 km) is generally considered to be basaltic and so could have a high remanent magnetization. Only its upper surface is likely to be very highly magnetized, rapidly cooled pillow lavas, but if hydrothermal circulation is as significant as Lister (1972) believes most of Layer 2 would be cooled

rapidly enough to acquire substantial magnetization. Layer 3 may also be magnetized. Cann (1970), Moores and Vine (1971) and others believe that Layer 3 is gabbro-not sepentinized periodotite (Fig. 1.1) and Vine et al. (1973) report magnetizations of $6.5 \times 10^{-3}$ emu/cm$^3$ for ultramafics of the Troodos Complex that are considered to be similar to Layer 3. Watkins and Paster (1971) have reported magnetizations of approximately $5 \times 10^{-3}$ emu/cm$^3$ for harzburgite from the Macquarie ridge. If a substantial thickness of the oceanic crust is significantly magnetized it is not valid to assume a thin magnetized layer thus ignoring other magnetized material.

### 6.5.5 Thickness and crustal formation

The results discussed in the previous sections favour a magnetized layer thickness of 2 km or more. Assumption of this thickness has interesting implications for the crustal formation process.

If the addition of crustal material at the ridge axis takes place by dyke injection the injection is likely to take place over a range of distances from the centre. Model studies by Loncarevic et al., (1966), Matthews and Bath (1967), and Matthews (1969) showed that for a normally distributed injection process a standard deviation $\sigma$ of 5 to 10 km would produce anomalies similar to those observed. A more detailed study by Harrison (1968) showed that for a layer thickness of 1.7 km $\sigma$ = 3 km, or less, was required to preserve small anomalies. Blakely and Cox (1972b) using 0.5 km thick blocks found $\sigma$ = 3 km satisfactory, which is surprising as some of their blocks were only 1 km wide. Values of $\sigma$ of several kilometers conflict with some deeptow results which indicate that $\sigma \leq 400$ m is required (Larson, 1971; Blakely and Cox, 1972b).

If a thin magnetized layer is assumed the anomalies produced by an ideal model ($\sigma$ = 0) produces anomalies which are too sharp. Random injection removes the objection provided $\sigma$ is a few kilometers. A thick magnetized layer produces anomalies which are already smooth so virtually no random injection is required; indeed the need to maintain small anomalies demands a very narrow injection width.

The range of reported standard deviations may not reflect a real range of injection widths. Rather it may reflect differences in the assumed, or actual, thickness of the magnetized layer. Only drilling at least 2 km into the seafloor is likely to produce data capable of resolving the important issue of the thickness of the magnetized layer.

## 6.6 VARIATIONS OF ANOMALY AMPLITUDE

The data density in the southwest Pacific basin is sufficient to permit an analysis of variations in the amplitude of particular anomalies. Fig. 6.12 shows the mean and range in amplitude of the clearly observed anomalies. Some 348 individual amplitude measurements are involved. In view of the discussions in previous sections detailed comparisons of observed amplitudes with model amplitudes are not justified, but some general comparisons are in order.

The mean amplitudes of the observed anomalies 27-36 agree adequately with model amplitudes, especially when the likelihood of variations in the paleo-intensity of the magnetic field is recalled. However the observed amplitudes of anomalies 25 and 26 are lower than models predict. The depth to the seafloor is, if anything, shallower under anomalies 25 and 26 than the older ones so depth to the source is unlikely to be an explanation. A lower field intensity at that time cannot explain it as in NPAC and other north Pacific profiles the amplitudes of anomalies 25 and 26 are not low relative to the older anomalies. In Chapter 4 it was pointed out that there is a change in the general anomaly structure of the area at about anomaly 25. Some effect associated with this change could explain the lower amplitudes. Possible effects are changes in (1) the thickness of the magnetized layer, (2) petrology, (3) thermal conditions at the time of formation of the anomalies. Whatever the cause it appears to be regional.

Substantial variations within the region also occur. The area has been divided into six zones separated by fracture zones (Fig. 6.13). The anomaly amplitudes for each zone are shown in Fig. 6.14. The ranges in each zone are large but zones two and three tend to have lower amplitudes than the other zones. Fig. 6.15 shows it more clearly.

Several possible causes of zone differences can be discounted; (1) Variation in the paleo-intensity of the magnetic field would affect all the zones; (2) Variation of present or paleo-position would produce insufficient effect, even if zones two and three were considered to have originally been substantially displaced relative to the other zones - which is improbable; (3) Depth to the seafloor and basement is not substantially different in any of the zones; (4) Spreading rates do differ between the zones (Fig. 6.16). Fig. 6.17 shows that this could affect the amplitude of anomaly 32A but the major anomalies are not affected. Anomaly 32A is more affected because the width of its "source block", 4 km at 4.0 cm/yr, is in the range where width variations substantially alter the amplitude (Appendix 6B). The major anomalies all have widths beyond the critical range and so their amplitudes do not alter much with spreading rate.

It is probable that the difference between zones two and three and the other zones reflects a thinner magnetized layer and/or a lower intensity of magnetization of the crust in zones two and three. Both could be produced by differences in thermal conditions at and/or subsequent to the time of formation of the anomalies. Thermal differences are an obvious possibility when spreading rates differ. The problem is that the rates in zones two and three do not differ significantly from those in zone one, which does not have low amplitudes. Thermal effects associated with fracture zones could be an explanation, as zones two and three are narrower than the other zones (Fig. 6.13). However throughout the southwest Pacific basin there are no indications that amplitudes of anomalies close to fractures are low.

Weissel and Hayes (1971, 1972) also have found variations in anomaly amplitudes south of Australia. Amplitudes (of the same anomalies) in three zones differed, and in one zone the amplitudes south of the ridge were lower than to the north. The latter suggests that some effect reduced the effective magnetization of the crust after the anomalies had formed and moved away from the ridge axis. Such an effect could explain the lower amplitudes of zones two and three in the southwest Pacific basin. However the differences between zones south of Australia; and the low amplitude of anomalies 25 and 26 throughout the southwest Pacific basin, suggest that regional effects are also required. Systematic differences in petrology between different tectonic regimes and different plate boundaries have been reported by, for example, Melson and Thompson (1971), Thompson and Melson (1972) and Shido and Miyashiro (1973). Such differences may be the source of systematic regional or local variations in the magnetic properties of the crust. Data to confirm this interesting possibility would not be easy to obtain.

# CHAPTER 7

## EARTHQUAKE MAGNITUDE-FREQUENCY RELATIONSHIPS

This chapter is a study of earthquake magnitude-frequency relationships. An introduction (7.1) is followed by a description of the method of analysis (7.2). Then results from previous work (7.3) and from the southwest Pacific area (7.4) are presented. Interpretations of the results are discussed in section 7.5.

This work has been done with R. Feriel Falconer.

### 7.1 INTRODUCTION

The positions of the plate boundaries in the southwest Pacific area are reasonably well delineated by bathymetric, magnetic and epicentral data. In most places the nature of the boundaries is clear but for the Macquarie complex and the Pacific-Antarctic fracture zone the data do not provide a definite indication of the boundary type. It would be useful to have other means of defining the type of boundary.

One possible relationship for characterising a boundary is the relationship between earthquake magnitude and frequency

$$\log N = a - bM \qquad \ldots\ 7.1$$

where N is the number of events of magnitude M or greater, and a and b are constants. The constant a is determined by the level of activity and is not considered here. It is the coefficient b which is of interest. It depends on the proportion of large to small events in a given group of earthquakes. A high b value indicates a greater proportion of smaller events, a low b value indicates a greater proportion of larger events.

The value of b depends on the magnitude scale used but where M is the surface wave magnitude $M_s$, b lies between 0.5 and 1.5, averaging about 0.9 (Gutenberg and Richter, 1954; Isacks and Oliver 1964; Evernden, 1970; Acharya, 1971). Results from several studies suggested that b was constant in both time and space (Isacks and Oliver, 1964; Sykes, 1965) but there is increasing evidence that this is not so (e.g. Utsu, 1965; Francis, 1968a,b; Evernden, 1970; Karnik, 1969, 1971).

The results of Francis (1968a,b) are particularly significant. They show that for the mid-Atlantic Ridge the b values are higher for ridges than fracture zones. It would be very useful if this difference could be shown to be general. It would then be possible to make hypotheses, based on

b values, for boundaries which are either not well surveyed or difficult to interpret. With this in mind an analysis has been made of the b values of the plate boundaries in the southwest Pacific area. The data used were the magnitudes in the USCGS file (Section 3.6) and the area considered is shown in Fig. 7.1. The intention was first to see if b values from clearly understood sections of plate boundary agreed with Francis's results; then to see if anything could be learned about the less well understood sections. Before presenting the results the method of analysis will be described.

## 7.2 ANALYSIS METHOD

Several aspects of b value study are open to discussion. In particular: the formulae to be used for calculating b, the validity of the basic equation, magnitude scales, range of magnitudes, and reliability of data (Evernden, 1970; Karnik, 1971). Many papers do not give full details of the analysis method used, which makes it difficult to compare results.

It appears that b is often determined by visual fitting of a straight line to the graph of log N against M. A more analytical method is preferable but least squares is not very satisfactory (Karnik, 1971; Vere-Jones, pers. comm. 1972). The estimator used here is

$$b = \frac{1}{\Delta} \log \left[ 1 + \frac{\Delta}{\bar{M} - M_o} \right] \qquad \ldots\ldots 7.2$$

where the earthquake magnitudes are given in intervals of $\Delta$, the minimum magnitude considered is $M_o$ and $\bar{M}$ is the mean magnitude of those earthquakes with magnitudes $\geq M_o$. This estimator is a modified form of that given by Utsu (1965), and takes into account the grouping correction discussed by Utsu (1966). Aki (1965) has shown that it is the maximum likelihood estimator for grouped data.

When determining b this way it is assumed that the linear relationship between log N and M is reasonably valid. Fig. 7.2 shows that this is not so for all magnitudes. The lack of linearity for low magnitudes is mainly due to reduced sensitivity of the detection network for low magnitudes (Evernden, 1969), and most studies throughout the world show a similar effect. For this study another possible reason for the low magnitude nonlinearity is that magnitudes are not given for all the earthquakes reported (Table 7.1). This is not a uniform factor throughout the area. For instance magnitudes are given for all of the reported earthquakes east of 140°W (Fig. 7.1) but they are given for only 55% of those on the Indian-Antarctic boundary. For the Eltanin fracture zone area (120°-140°W), the linear relationship holds down to m = 4.7

(Fig. 7.3) whereas for the whole area (Fig. 7.2) it holds only down to m = 5.1. This suggests that the earthquakes elsewhere for which magnitudes are not given are probably the lower magnitude events. When calculating b the minimum magnitude considered ($M_o$) must be chosen such that the linear relationship holds reasonably well for all magnitudes $\geq M_o$. The value $M_o = 5.1$ will be taken throughout. It does mean discarding some information but should give a degree of uniformity between different areas.

Table 7.1 Numbers of reported magnitudes

| Section | Number of earthquakes | With magnitudes | | With magnitudes ≥ 5.1 | | |
|---|---|---|---|---|---|---|
| | | Number | % of total | Number | % of total | % of those with magnitudes |
| Whole area | 297 | 209 | 70 | 124 | 42 | 59 |
| Indian-Antarctic | 102 | 56 | 60 | 33 | 32 | 59 |
| Pacific-Antarctic | 123 | 110 | 85 | 51 | 42 | 47 |
| Indian-Pacific | | | | | | |
| Whole | 72 | 43 | 60 | 40 | 56 | 93 |
| North of 57°S | 56 | 30 | 54 | 29 | 52 | 97 |
| South of 57°S | 16 | 13 | 81 | 11 | 69 | 85 |

The value of b depends on the magnitude scale used. The magnitudes used here are the body wave magnitudes $m_b$ given by the USCGS. The majority of previous studies use either surface wave magnitudes $M_s$ or magnitudes which approximate the surface wave scale (Richter, 1958; Karnik, 1969; Evernden, 1970). The relationship between $m_b$ and $M_s$ is complex, probably depending on factors such as focal region, type of focal mechanism and transmission path. A relationship can be given by

$$M_s = \alpha m_b + \beta \quad \ldots\ldots 7.3$$

where $\alpha$ and $\beta$ are constants (Gupta and Rastogi, 1972). If b' is the value of b in equation 7.1 for $M_s$ and b is the value for $m_b$ equations 7.3 and 7.1 give

$$b = \alpha b' \quad \ldots\ldots 7.4$$

The reported values of $\alpha$ range from 0.70 to 2.63 with a median of 1.20 (Gupta and Rastogi, 1972). Many studies using $M_s$ find b' values close to 0.9 and this value is often referred to as the normal b value. Because of the

uncertainties in $\alpha$ it is difficult to say what the value of b corresponding to b' = 0.9 would be. The value b' = 0.9 seems to apply to world statistics as well as smaller areas so it is reasonable to assume that a value of b (for $m_b$) calculated from world data would be suitable for comparison. For 1970 (1036 earthquakes with $m_b \geq 5.1$) b = 1.35. For 1971 (1193 earthquakes) b = 1.37. The value b = 1.36 will be assumed and be referred to as the world value.

Evernden (1970) has questioned whether the relationship between log N and M is linear for body wave magnitudes, especially for magnitudes greater than 5.5. The nonlinearities that he found may be related to Tsuboi's (1958) observation that superposition may not hold. That is, if log N is linearly related to M with different values of b in a number of areas then log $\Sigma$N is not linearly related to M. A non-linear curve may result from data which consists of two or more sets with different b values. However such data can also yield a good linear curve (Francis, 1968a). The only practical solution is to break the data into different areas and/or time intervals. If subsets of a data set yield b values which are similar the b value of the whole data set should be valid. The mean of subset b values should also be valid. The extent to which data can be subdivided is limited by the need to have sufficient data in a set for the b value to be reliable.

The confidence limits of any b value can be estimated from the fact that the estimator used (equation 7.2) is approximately chi-squared distributed with 2N degrees of freedom, where N is the total number of earthquakes (Utsu, 1966). The b values of two data sets can be compared with the F test. If two sets A and B with $N_A$ and $N_B$ earthquakes respectively have estimates $b_A$ and $b_B$ then for $b_A < b_B$, $b_B/b_A$ is distributed as the F distribution with $2N_A$ and $2N_B$ degrees of freedom (Utsu, 1966). A mean b value calculated from the b values of several data sets can be compared to another mean value with the standard t test.

## 7.3 EARLIER WORK

This b value study involves comparison of results from the southwest Pacific area with results from other areas. Since the southwest Pacific seismicity is associated with only oceanic plate boundaries the results from other oceanic boundaries are of most interest. Not many determinations of b have been made for the mid-oceanic ridge system. Gutenberg and Richter (1954) using surface wave magnitudes of 6.0 and above obtained b' = 1.4 for 27 Atlantic earthquakes, and b' = 1.3 for 19 Indian Ocean events. Sykes (1965) considered 267 events north of 60°N, primarily on the ridge extending

from Iceland through the Arctic Ocean to Siberia. The magnitude-frequency plot was linear for magnitudes (surface wave) from 4.5 to the maximum of 6.9, and b' = 0.91. For ridges in the Indian Ocean Stover (1966) obtained b' = 0.91 from 76 events with surface wave magnitudes greater than 6.0. Stover (1968) also studied, as one data set, the mid-Atlantic ridge south of 4°N, the Southwest Atlantic ridge and part of the Southeast Indian ridge. He found b' = 1.01 for 51 surface wave magnitudes greater than 6.0. For 83 USCGS bodywave magnitudes in the range 4.7 to 5.9 he found b = 1.04.

Francis (1968a,b) using USCGS located earthquakes on the mid-Atlantic ridge has obtained results more detailed than any of the above. He first (1968a) considered bodywave magnitudes of events in areas where the ridge was well mapped. One hundred and fifty-four events gave b = 1.28 (Fig. 7.4 A). He then separated the events into those on fracture zones (75 events) and those on the ridge axis (79 events) and obtained b = 0.99 and b = 1.72 respectively (Fig. 7.4 B). If the data in Fig. 7.4 B are considered linear above magnitude 4.6 the two b values are different at the 95% level. Francis then considered individually the four fracture zones which the fracture zone events represented and got for the mean of the four b = 1.03 ± 0.33*. Similarly three certain ridge axis sections gave b = 1.73 ± 0.65. Inclusion of data from less well mapped areas, 50°S to 55°N gave three more definite fracture zones and nine more ridge axis sections. Adding these to the previous data gives a fracture zone mean b = 1.00 ± 0.31, and a ridge axis mean b = 1.88 ± 0.68. These are different at the 99% level. Francis (1968b) repeated the analysis of the initial four definite fracture zones and three definite ridge axis sections using surface wave magnitudes (Fig. 7.4 C). This gave for fracture zones b' = 0.63 ± 0.14 and for ridge axes b' = 1.08 ± 0.18. These are different at the 95% level.

It is noteworthy that before Francis separated the fracture zone and ridge axis events (Fig. 7.4 A) he obtained a reliable value, b = 1.28, which is close to the world value 1.36. Sykes (1965) and Stover (1966, 1968) obtained values close to the world value for surface waves. Their data encompass both fracture zones and ridge axes. It is quite possible that if they had separated the two they would have found different b values for the two boundary types. It is clear that at the very least boundary types should be separated; further subdivision is preferable.

The plate boundaries in the southwest Pacific area are probably of either fault or ridge type but subduction has been suggested for parts of the Macquarie complex. The most thorough b value analysis of trench areas

---

*Error limits quoted in the text throughout this chapter are one standard deviation.

is that of Acharya (1971). He has analysed many trench sections individually. For shallow seismicity (surface waves) the b' values range from 0.70 to 1.04, but most are between 0.80 and 0.90. Evernden (1970) presented USCGS bodywave magnitude data for the Tonga-Kermadec trench. He considered the data nonlinear but b = 1.40 would fit the data very well. In general the b values for shallow seismicity at trenches appear to be close to "normal". For intermediate and deep seismicity, b values range from normal to well below normal (Acharya, 1971). All of the seismicity in this study is shallow.

## 7.4 THE SOUTHWEST PACIFIC RESULTS

### 7.4.1 Whole area

The seismicity of the area studied is shown in Fig. 7.1. For the whole area there are 124 earthquakes with $m \geq 5.1$. They give b = 1.24 (Fig. 7.2) which is not significantly different from the world value 1.36. A breakdown of the data into the three boundaries concerned is shown in Fig. 7.5 and Table 7.2. The b value of the Pacific-Antarctic boundary (1.41) differs from the complete data b value (1.24) at the 75% level, and the other two boundaries differ from 1.24 at the 90% level. The differences indicate that the whole area should not be considered as one data set. Each boundary is considered separately and in more detail in the following sections.

Table 7.2 Southwest Pacific area b values

| Section | Number of earthquakes | Number with magnitudes | Number with $m \geq 5.1$ | b |
|---|---|---|---|---|
| Whole area | 297 | 209 | 124 | 1.24 ± 0.19* |
| Indian-Antarctic | 102 | 56 | 33 | 1.62 ± 0.47 |
| Pacific-Antarctic | 123 | 110 | 51 | 1.41 ± 0.34 |
| Indian-Pacific | 72 | 43 | 40 | 0.92 ± 0.27 |

*90% confidence limits.

### 7.4.2 The Indian-Antarctic boundary

That part of the Indian-Antarctic boundary east of 135°E is considered (Fig. 7.1). It contains most of the seismicity of the whole boundary (Sykes, 1970a) which in this area consists of short east-west sections of

active spreading ridge offset by north-south fracture zones. The ridge sections are conspicuously aseismic and all the earthquake activity can be considered fracture zone activity.

The b value for the boundary as a whole is 1.62, which is greater than the world value (1.36) at the 75% level, and is greater than Francis's fracture zone value (0.99) at the 98% level.

Most of the epicentres occur in three major sections (Fig. 7.1) which can be considered separately (Table 7.3). The number of epicentres available in each section is insufficient to justify further subdivision even though the 140°E section is definitely two fracture zones and the long section between 54°S and 60°S may be several separate zones. The mean b value of the three sections is 1.54 ± 0.13 which is greater than Francis's mean fracture zone value 1.00 ± 0.31 at the 95% level.

Table 7.3 Indian-Antarctic boundary b values

| Section | Number of earthquakes | Number with magnitudes | Number with $M \geq 5.1$ | b |
|---|---|---|---|---|
| Whole boundary | 102 | 56 | 33 | 1.62 ± 0.47* |
| 50-55°S, 140°E | 28 | 17 | 8 | 1.40 ± 0.89 |
| 55-60°S, 145-150°E | 44 | 24 | 15 | 1.63 ± 0.75 |
| 60-63°S, 155°E | 21 | 11 | 8 | 1.60 ± 1.02 |

*90% confidence limits.

### 7.4.3 Pacific-Antarctic boundary

Since there is no seismicity on the Pacific-Antarctic boundary north of 48°S effectively all of the boundary is considered (Fig. 7.1). East of 150°W the seismicity, although scattered, is all associated with fracture zones which have been mapped from bathymetric and magnetic data (Herron, 1971). The activity between 155°W and 170°W is probably on one or more fracture zones but these have not been mapped. All the areas east of 180° where active spreading ridges have been identified are aseismic, so it is probable that all the seismic activity east of 180° is fracture zone activity. The section from 180° to the triple junction – the Pacific-Antarctic fracture zone, is probably one or more fracture zones. Some of the seismicity there might be associated with short sections of active ridge.

The b value for the boundary as a whole is 1.41 (Table 7.4). This is greater than Francis's fracture zone value (0.99) at the 95% level.

Table 7.4 Pacific-Antarctic boundary b values

| Section | Number of earthquakes | Number with magnitudes | Number with $M \geq 5.1$ | b |
|---|---|---|---|---|
| Whole boundary | 123 | 110 | 51 | 1.41 ± 0.34* |
| 50°S, 115°W | 14 | 14 | 6 | 2.43 ± 1.83 |
| 55°S, 120-140°W (Eltanin F.Z.) | 52 | 52 | 17 | 1.23 ± 0.52 |
| 57°S, 140-145°W | 12 | 11 | 6 | 0.93 ± 0.70 |
| 63°S, 160-170°W | 15 | 12 | 6 | 1.46 ± 1.09 |
| 63°S, 180-163°E (Pacific-Antarctic F.Z.) | 25 | 16 | 14 | 1.62 ± 0.74 |

*90% confidence limits.

Individual sections, some composed of several fracture zones, range from 0.93 to 2.43 (Table 7.4). The mean of the sections is 1.53 ± 0.56 which is greater than Francis's fracture zone mean value (1.00 ± 0.31) at the 90% level.

One of the aims of the b value study was to see if the b value of the Pacific-Antarctic fracture zone would provide any indication of whether its seismicity was associated with fracture zones or ridges. The b value is 1.62 which is not significantly different from the b values of sections on the Indian-Antarctic and Pacific-Antarctic boundaries that are known to be fracture zones (Tables 7.3 and 7.4). There is no seismicity on the ridges in the southwest Pacific area to provide comparative ridge b values, but in the Atlantic Francis (1968a) found a mean ridge b value of 1.88 ± 0.68. The Pacific-Antarctic fracture zone value is not significantly different from that. Thus the b value does not provide an unequivocal indication of the nature of the seismicity on the Pacific-Antarctic fracture zone.

### 7.4.4 Indian-Pacific boundary

The Indian-Pacific boundary from New Zealand southward is well recognized as complex, and elements of ridge, trench and fault have all been suggested. It is clearly quite different from the simple ridge-fault boundaries of the Antarctic plate with the Indian and Pacific plates. Earthquakes north of 48°S may be associated with the New Zealand continental margin so only data south of 48°S are considered.

The b value of the whole boundary is 0.92 (Table 7.5). This is lower than the world, Indian-Antarctic and Pacific-Antarctic values at greater than the 98% significance level.

Table 7.5 Indian-Pacific Boundary b values

| Section | Number of earthquakes | Number of magnitudes | Number with $M \geq 5.1$ | b |
|---|---|---|---|---|
| Whole boundary | 72 | 43 | 40 | 0.92 ± 0.27* |
| South of 57°S | 16 | 13 | 11 | 1.48 ± 0.80 |
| North of 57°S | 56 | 30 | 29 | 0.80 ± 0.26 |
| 48-51°S | 33 | 18 | 17 | 0.84 ± 0.35 |
| 51-57°S | 23 | 12 | 12 | 0.76 ± 0.39 |

*90% confidence limits.

There is a gap in seismicity at about 57°S. The section south of there is characterised by the Hjort trench. Subduction has been suggested but all the earthquakes are shallow. The b value for the section is 1.48 (Fig. 7.6 and Table 7.5); not significantly different from the "normal" world value, 1.36. Shallow seismicity associated with trenches elsewhere appears to have "normal" b values (Section 7.3) so on the basis of b values the section could be a subduction area. The observed b value is comparable to those found for fracture zones on the Pacific-Antarctic and Indian-Antarctic boundaries (Tables 7.3 and 7.4) so from b values the area could also be a fracture zone.

The section north of 57°S has a b value of 0.80 (Fig. 7.6 and Table 7.5). This is different from the southern section at the 95% level and is different from the world, Pacific-Antarctic and Indian-Antarctic values at the 98% level. Within the section north of 57°S there is a gap in seismicity at 51°S. South of there the deeps associated with the Macquarie ridge are east of the ridge, while to the north they are to the west. The b values of the two sections are not significantly different (Table 7.5).

The Indian-Pacific boundary north of 57°S differs from the other sections in several ways. Six of the seven earthquakes of magnitude greater than 6.0 in the whole study occurred there. The only large clusters also occurred there (Section 3.6.4). Only 3% of the earthquakes with magnitudes are less than magnitude 5.1, compared with 41% and 53% on the Indian-Antarctic and Pacific-Antarctic boundaries respectively. The lower the b value the smaller the proportion of low magnitudes relative to higher magnitudes, but the observed number of low magnitudes is too small to be accounted for by the low b alone. It is not likely to be an observational factor as the percentage of earthquakes for which magnitudes are reported is comparable to that of the other boundaries (Table 7.1).

## 7.5 DISCUSSION

Six of the eight fracture zones along the Antarctic boundary studied here have b values higher than the world b value. Six of the seven fracture zones in the Atlantic studied by Francis have b values lower than the world value. The mean for the Antarctic fracture zones, 1.54 ± 0.43, is higher than the Atlantic fracture zone mean, 1.00 ± 0.31, at the 99% level. The Antarctic fracture zone mean is not significantly different from the mean of the active ridge sections of the Atlantic, 1.88 ± 0.68. Obviously the b value alone cannot be used to determine whether a section of plate boundary is a fracture zone.

This result is in itself useful but the differences which have been found between the Atlantic and the southwest Pacific area are probably more useful. They may provide information on the tectonic significance of b values. To facilitate further discussion various factors which have been suggested as important in determining the b value of an area are listed in Table 7.6.

Table 7.6 Factors which may influence b values

| Factor | High b | Low b |
|---|---|---|
| boundary type | rift zone | fracture zone |
| type of faulting | normal | strike-slip |
| space-time sequence | swarm, clustering | nonclustered |
| temperature | high | low |
| mode of deformation | cataclastic | brittle |
| material | heterogeneous | homogeneous |
| stress distribution | nonuniform | uniform |
| stress level | low | high |
| stress drop | small | large |

The b value difference between ridges and fracture zones in the Atlantic is significant irrespective of whether surface waves or body waves are considered (Section 7.3). This indicates that the cause of the difference is source effects, rather than propagation effects such as attenuation in high temperature areas of the ridge axis, or orientation of seismograph stations with respect to the source (Francis, 1968b). One possible source effect is the nature of faulting. Focal mechanism studies indicate that strike-slip

faulting predominates on fracture zones while normal faulting occurs on ridge sections. Francis (1968a) pointed out the possibility that b is a function of the type of faulting; high for normal faulting, low for strike-slip faulting. There are four reliable focal mechanism studies for the Antarctic boundary fracture zones, and each indicates predominantly strike-slip faulting. There is no reason to suppose that the faulting on any of the fracture zones is not strike-slip. The high Antarctic boundary b value thus negates the possibility that strike-slip faulting produces low b values.

In a study of earthquake swarms on midocean ridges (mainly the Atlantic) Sykes (1970b) suggested that the b value of the ridge axis is high because much of the seismic activity is of the swarm type. However Francis and Porter (1971) have shown that nonswarm activity also has a high b value. The Antarctic boundary activity is not of the swarm type (Section 3.6.4) so the high Antarctic b value further supports Francis and Porter's conclusion that high b is not just a swarm effect.

Francis (1968b) suggested that at a ridge axis high temperatures and relatively low pressures lead to cataclastic deformation, which has a high b value (Scholz, 1968a); while at fracture zones temperatures are lower and brittle failure would occur, for which the b value is low. If Francis is correct the high Antarctic boundary b values imply cataclastic deformation along the Antarctic fracture zones. This is not contradictory with the Atlantic fracture zones undergoing brittle fracture if it is the temperature regime, not the boundary type, which determines the mode of fracture. For all the Antarctic boundary fracture zones the lengths of the fracture zones in relation to the spreading rates are such that the age of the seafloor either side of the fractures is less than 10 my. In the Atlantic the age differences across the fracture zones studied are more than 20 my. Since crustal temperature is inversely related to age the Antarctic fracture zones are at higher temperatures. They are still close to ridge axis conditions and so could be expected to behave in a ridge manner. The similarity of the b values of the Antarctic fracture zones and the Atlantic ridge axis could thus be due to similar thermal environments.

The results for the Macquarie ridge complex provide support for several aspects of the preceding discussion. Firstly the section south of 57°S. The seafloor west of the boundary is the northern flank of the Indian-Antarctic ridge. The age of the seafloor ranges from zero at 61.5°S to 20 my at 57°S. The eastern side is a part of the Pacific plate for which the age is not known. From the depth and relationship to the Cretaceous anomalies east of 165°E it is likely to be considerably older than the adjacent Indian plate. Although the age difference across the boundary is probably more than

10 my most of the west side is less than 10 my old. The boundary would therefore still be in a high temperature environment. The relatively high b value (1.48) is consistent with the association of high b with high temperature observed on the Atlantic ridge and Antarctic boundary fracture zones. Secondly the section north of 57°S. The age of the seafloor on the west is 20 my at 57°S, 35 my at 52°N and probably older further north. The age of the eastern side is not known but it is not likely to be young. Although the topography of the Macquarie Ridge probably reflects recent tectonic activity the area is basically a boundary between two old, cold crustal sections. The low b value (0.80) is consistent with the association of low b value with lower temperatures observed on the Atlantic fracture zones.

The association of high b with high temperature areas and low b with low temperature areas appears to be valid, but does not explain the basic cause of the differences in b. The cause probably lies in (1) the nature of the fracture process, (2) the type of material, and (3) the stress conditions in the source region of the earthquakes. All three factors are probably interrelated.

Laboratory measurements of Mogi (1962, 1963a) and Scholz (1968a,b) have shown that nonuniform stress and/or heterogeneous material can produce high b values. Sykes (1970b) suggested that the Atlantic ridge axis high b values could be due to volcanic activity producing both nonuniform stress and heterogeneous structure. Earthquake swarm activity is probably the best indicator of volcanic activity. The USCGS data and T-phase data (Northrop et al., 1970) do not indicate such activity on the Antarctic boundary fracture zones. Thus even if volcanism does produce high b it is not the only reason.

Scholz (1968a) suggested that b reflects the level of stress; low b for high stress and vice-versa. On the Macquarie ridge complex north of 57°S the large numbers of high magnitude earthquakes suggest high stress. In the Atlantic the stress appears to be high on the fracture zones, as they have the highest magnitude earthquakes and account for most of the energy release (Francis, 1968a). Both areas have low b values, in agreement with the high stress, low b relationship. The Atlantic ridge axes also agree with the relationship as they appear to have low stress and their b values are high. Intuitively it might be expected that fracture zones would be high stress areas, and in the Atlantic they appear to be. However if the relationship between stress and b is correct the high b values of the Antarctic boundary fracture zones indicate low stress. The Antarctic ridge axes are aseismic which indicates that they are even less stressed. Thus in both the Atlantic and the southwest Pacific area the fracture zones are relatively higher

stressed than the ridge axes. However it is interesting to note that Lachenbruch and Thompson (1972) conclude from the orthogonality of ridges and fracture zones that fracture zones provide less resistance to motion than ridge axes.

Gibowicz (pers. comm., 1973) has suggested that the b value reflects the mode of stress release rather than the level of stress; low b values indicating high stress drop at each event, high b values indicating lower stress drop. High stress drop at each event leads to a low b value because most of the stress is released as a one shot process and the residual stress, if released at all, is released only in much lower magnitude events. Such a process would explain the lack of low magnitude events on the Macquarie ridge complex north of 57°S, where the b value is very low.

The main conclusion of this study is that several of the suggested relationships between b value and other factors (Table 7.6) are not valid. In particular b does not indicate: (1) boundary type – fracture zones can have high or low b, (2) type of faulting – strike-slip faults can have high or low b, (3) space-time sequence – high b occurs for clustering and non-clustering. The relationship of b value to stress level may apply only to relative stress rather than to absolute stress – the lowest b value areas in a region indicating the highest stressed areas.

The association of high b with high temperatures and low b with low temperatures appears to be clearly established. The b value may fundamentally be related to one or all of the more detailed factors: type of fracture, stress distribution, stress drop, and type of material; but temperature probably has a controlling influence on all of these factors. As more data becomes available further b value studies should provide constraints on the present hypotheses. A detailed study of the relationship between b value and crustal temperature would be useful.

Postscript to Chapter 7

An important paper by Wyss (1973) has become available since the research described in this chapter was completed and typed. Wyss combines magnitude-frequency and magnitude-moment relationships and derives a relationship which shows that b is related to the stress drop and the source area of an earthquake: high b for low stress drop and/or small source area; and conversely low b for high stress drop and/or large source area. Applying his results to Francis's data Wyss estimates that for the mid-Atlantic ridge system the fracture zone events (low b) could have 30% higher stress drops or 20% larger source dimensions than the ridge crest events (high b). He suggests that lower stress drop on the ridge could be due to higher temperatures and weaker crust there; alternatively larger source dimensions on the fracture zones could be due to a greater thickness of brittle crust in the cooler areas away from the ridge crest. Both suggestions are in accord with the chapter 7 conclusion that there is a relationship between b value and temperature - low b for low temperature and high b for high temperature.

# CHAPTER 8

## EPICENTRAL POLES

In this chapter a new method of determining poles of rotation is presented. An introduction (8.1) is followed by a description of the method (8.2). Use of the method to obtain the Indian-Pacific, Pacific-Antarctic and Indian-Antarctic poles is described in section 8.3, and the consistency of the poles is examined in section 8.4. The epicentral results are compared with other results in section 8.5.

### 8.1 INTRODUCTION

The basic principle of plate tectonics is that when plates are considered to be rigid the motion of one plate relative to another can be described by a rotation about a pole. A consequence of this is that any pure slip boundaries between plates (transform faults) must lie on small circles about the pole of rotation. Using this fact the position of the rotation pole can be found from a knowledge of the transform faults.

Several methods for finding the rotation pole have been described in section 1.4.6. A new method dependent only on earthquake epicentres is presented here. It is based on the fact that most transform faults are seismically active, and that the faults should be small circles about the rotation pole. For convenience the method will be referred to as the epicentral method, and the rotation poles determined with the method will be referred to as epicentral poles.

### 8.2 THE EPICENTRAL METHOD

Suppose there is a group of N epicentres which are all associated with one transform fault. Ideally the epicentres would lie along the arc of a circle centred on the rotation pole (Fig. 8.1). In practice they are scattered about the arc, either because the epicentre locations are not accurately determined or because the tectonic activity at the transform fault is not concentrated. If the pole position is known the distance $r_i$ of each epicentre from the pole can be calculated. If the distance of the transform fault (i.e. the arc of the circle) from the pole is R the distance $d_i$ of an epicentre from the arc is

$$d_i = r_i - R \qquad \ldots.8.1$$

In practice the transform fault, i.e. arc, is not precisely defined so R is not known. However if the epicentres are randomly distributed about the arc

a good estimator for R will be the mean distance $\bar{r}$ where

$$\bar{r} = \frac{1}{N} \sum_{i=1}^{N} r_i \qquad \ldots.8.2$$

The standard deviation of the distances $d_i$ of the epicentres from the arc is then given by

$$S = \left[ \frac{1}{N-1} \sum_{i=1}^{N} (r_i - \bar{r})^2 \right]^{\frac{1}{2}} \qquad \ldots.8.3$$

Now suppose that the pole position is not known. The standard deviation S can be calculated about any point but the minimum value of S will be obtained for calculation about the centre of the arc. It is this minimum property that is used to determine the pole position. A pole position is assumed and S calculated and this is repeated for other positions chosen in any way desired, e.g. a regular grid about the initial point. The position that gives the minimum value of S can then be considered the best estimate of the pole position.

In general there may be several transform faults along a boundary, each one an arc about the rotation pole. Each fault may have associated earthquake activity and the method outlined above can be extended to consider all the faults.

Suppose there are k groups of epicentres, each group representing one fault (Fig. 8.2). The mean standard deviation for all the faults is given by

$$S = \frac{1}{k} \sum_{j=1}^{k} S_j \qquad \ldots.8.4$$

where $S_j$, the standard deviation of the j'th fault is given by

$$S_j = \left[ \frac{1}{N_j-1} \sum_{i=1}^{N_j} (r_{ij} - \bar{r}_j)^2 \right]^{\frac{1}{2}} \qquad \ldots.8.5$$

and $\bar{r}_j$ is the mean arc distance of the $N_j$ epicentres associated with the j'th fault.

As before S is calculated for several positions and the pole is given by the position for which S is minimum. The minimum position could be found by a gradient search method from the initial point but in practice it is better to calculate S at a series of grid points. This enables the existence of secondary minima to be identified and contours of S can be used to indicate the uncertainty in the pole position (see later).

The fracture zones may differ and it seems desirable to calculate the mean standard deviation from weighted values of the $S_j$. This gives

$$S = \frac{\sum_{j=1}^{k} h_j S_j}{\sum_{j=1}^{k} h_j} \qquad \ldots.8.6$$

where $h_j$ is the weight for the j'th fault.

Some factors which could be taken into account for determining the weight of a fault are as follows:

(1) The number of epicentres, $N_j$.
(2) The standard deviation, $S_j$.
(3) The length of the fault as defined by the epicentres.
(4) The distribution of the epicentres within the fault zone.
(5) The distance from the pole, $\bar{r}_j$.
(6) The accuracy of the epicentre locations, which may vary along a boundary.

The weighting function used in this study is

$$h_j = \frac{(2N_j)^{\frac{1}{2}}}{S_j} \qquad \ldots.8.7$$

It takes into explicit account only factors (1) and (2) above. More complex weighting functions could be suggested but a simple treatment is preferable, at least initially. The particular function used can be justified on statistical grounds. If the deviations about the j'th fault are normally distributed the standard deviation of $S_j$ will tend towards $\frac{S_j}{(2N_j)^{\frac{1}{2}}}$ for large $N_j$. Thus in using equation 8.6 to determine the mean standard deviation, each $S_j$ is weighted by the inverse of its standard deviation.

The length of a fault is not directly taken into account in the present method. It is however indirectly considered because for a small displacement from the true pole position the standard deviation will increase more rapidly for a long zone than a short zone. Hence the minimum will be sharper for a long zone. Normally several zones at different azimuths from the pole are required to get a tightly constrained pole but a good pole can be determined from only one zone if it is long enough to form a significant arc.

The distributions within the fault zones are important. A distribution such as that in Fig. 8.3A is clearly less suitable than that of Fig. 8.3B. Both distributions will give the same contribution to the mean standard deviation S, but case B will lead to a sharper minimum than case A. The contribution to S will be the same for each of the distributions shown in Fig. 8.4.

However these cases would be distinguished because the standard deviations would show minima at different pole positions.

The basic starting point of the method is a set of epicentres of earthquakes known to be on transform faults. The epicentres are then grouped so that each group consists of epicentres associated with only one fault. This implies some knowledge of the location of the transform faults. For midocean ridge plate boundaries the orthogonality of the ridges and transforms, and in places the aseismicity of the ridges are useful indicators of the transform faults. Other boundaries are usually more difficult as pure transforms may merge into sections with only a component of slip along the boundary. Epicentres are normally scattered which can make it difficult to distinguish one long fault from a series of shorter ones with a different trend. The analysis method is however tolerant of both invalid "nontransform epicentres" and incorrect grouping of epicentres provided not too many incorrect epicentres (or even groups) are included. In fact one of the main benefits of the method is that it will indicate such misinterpreted epicentres.

A particularly important aspect of the method is a careful examination of the distribution of epicentres within each fault zone. The program used lists various data of each zone for the best pole position found. The deviations from the arc for each epicentre are given so that the distribution can be checked. Isolated irregular epicentres can be detected from their large deviations and whole zones which do not fit the calculated pole can be detected. Criteria can be established for rejection of epicentres with large deviations and epicentres can be regrouped for further recalculation.

## 8.3 APPLICATIONS OF THE EPICENTRAL METHOD

### 8.3.1 Indian-Pacific

The boundary between the Indian and Pacific plates extends from southeast Asia to the southern end of the Macquarie complex (Fig. 0.2). From Asia to the northern end of the Tonga trench the boundary is complex and several small plates may be involved (Johnson and Molnar, 1972; Krause, 1973). From the northern end of the Tonga trench to the centre of New Zealand the existence of intermediate and deep earthquakes indicate that subduction is taking place. In the South Island the boundary is generally associated with the Alpine fault and its branches but seismicity is scattered (Evison, 1971) and tectonic activity appears to be distributed over a wide area. In the southwest part of the South Island (Fiordland) intermediate depth earthquakes (Smith, 1971) suggest subduction. Further south the seismicity is associated with the Macquarie complex, the precise nature of which is not clearly defined.

The lack of any clearly defined transform faults on the boundary represents a difficulty for the application of the epicentral method. However when the USCGS epicentres south of New Zealand are plotted on a stereographic projection all those south of about 49°S lie close to the arc of a circle (Fig. 8.5). In a stereographic projection a circle on the map represents a circle on the earth. In plate tectonics a circle about the pole of rotation defines the locus of a possible transform fault. Thus if the earthquakes on the Macquarie complex are considered to be on a circular arc they define a transform fault. They can therefore be used for the epicentral method.

As a starting point it is assumed that all the epicentres south of 49°S are associated with one fault zone. An initial pole is taken at 55°S, 175°E and the epicentral standard deviation S is calculated at two degree intervals for 30-80°S, 150°E-150°W. A single minimum is found at 56°S, 176°E. A search at 0.1 degree intervals about there gives a minimum value of S = 27.1 km at 56.0°S, 175.2°E. The distribution about the arc (Fig. 8.6) is normal when tested with the chi-square test. There are two epicentres close to each other at 53.2°S which are 67 and 69 km respectively from the arc. For a normal distribution with a standard deviation of 27 km there is less than 2% chance of even one deviation as large as 67 km. Since there are only 59 epicentres it is probably justifiable to reject these two epicentres from the calculation. When this is done the epicentral pole for 57 epicentres is found at 56.0°S, 175.6°E with a value of S = 24.0 km. The distribution about the arc is normal (Fig. 8.7).

The contours of S (Figs 8.8 and 8.9) indicate that the pole position is more constrained in the north-south direction than the east-west direction. The confidence limits on S should be an adequate statistic to use for quantitatively assessing the accuracy of the pole. If the deviations about the arc are considered normally distributed (which is acceptable statistically) the 90% confidence upper bound for S is 1.24 S. The contour of 1.25 S is probably a reasonable measure of the accuracy of the pole. The area it encloses will be called the confidence area.

The simple distribution of deviations about the arc (Fig. 8.7) is useful but does not take into account the spatial distribution of the epicentres. If the epicentres represent several faults, not just one as assumed, the deviations about a single arc may be normal but probably would not be random because runs would occur. The latitudinal distribution (Fig. 8.10) is not random when tested with the run test. It is the epicentres from 49°S to 50°S which are not random (Fig. 8.11). Those south of 51°S are random when tested separately.

The epicentral method should be satisfactory if not all of a fracture zone is included. Since there is doubt about the 49-50°S section it can be omitted, leaving 33 epicentres all south of 52°S. They give a pole at 56.2°S, 174.1°E, which is inside the confidence area of the 57 epicentres solution. The epicentral standard deviation is 23.3 km which is less but not significantly (F test) less than the 24.0 km of the 57 epicentres (Table 8.1).

Table 8.1 Indian-Pacific epicentral poles based on Macquarie complex epicentres.

| Data set | Number of epicentres | lat °S | long °E | S(km) |
|---|---|---|---|---|
| USCGS | 57 | 56.0 | 175.6 | 24.0 |
| USCGS south of 52° | 33 | 56.2 | 174.1 | 23.3 |
| Sykes | 47 | 55.8 | 176.4 | 25.1 |
| USCGS-Sykes mix | 61 | 56.0 | 175.8 | 24.4 |
| USCGS 2 zone | 57 | 56.0 | 176.0 | 24.1 |
| USCGS 3 zone | 57 | 55.6 | 175.2 | 23.0 |
| Sykes 2 zone | 47 | 55.8 | 175.9 | 25.3 |
| Sykes 3 zone | 47 | 55.8 | 175.8 | 25.3 |

A second, although not entirely independent, set of data for the area are the Sykes' epicentres. They are fewer in number (Fig. 8.12) but probably more accurately located. A preliminary trial with all those south of 48.5°S yields four epicentres more than three standard deviations from the arc. Eliminating them leaves 47 epicentres which give a pole at 55.8°S, 176.4°E with S = 25.1 km (Table 8.1). The pole is inside the confidence area of the pole of the 57 USCGS epicentres.

The distribution of epicentres between 48°S and 50°S is better for the Sykes epicentres (Fig. 8.13) than for the USCGS epicentres (Fig. 8.11). The arc of the USCGS pole fits the Sykes epicentres well. A data set consisting of Sykes' epicentres north of 51°S and USCGS epicentres south of there gives a pole at 56.0°S, 175.8°E (Table 8.1). The latitudinal distribution of the deviations from the arc for the mixed set is random when tested with the run test.

So far all the epicentres have been assigned to only one zone, which assumes that the Macquarie complex is one fracture zone. A good test of this assumption is to split the area into sections each of which is regarded as an individual fracture zone. The pole can then be computed from the sum of the sections. Results for four data sets are shown in Table 8.1 with

details of each set in Table 8.2. All the pole positions fall within the confidence area of the pole of the 57 USCGS epicentres. The standard deviations of all the sections do not differ significantly (F test). The radii of the individual sections within each data set do not differ significantly (t test), except for the three zone USCGS. The solutions based on more than one zone yield standard deviations comparable to those of the single zone solutions (Table 8.1). But if the zones can be validly considered part of one zone the single zone solution is better because the confidence area is smaller (Fig. 8.14).

Table 8.2 Results for data sets consisting of several zones.

| Data set and zones | Number of epicentres | Radius of arc (deg) | S(km) | Contribution to mean S (%) |
|---|---|---|---|---|
| USCGS 2 zone | 57 | | mean 24.1 | |
| 49.0 - 55.1 | 38 | 9.82 | 22.2 | 64 |
| 56.2 - 61.7 | 19 | 9.82 | 28.2 | 36 |
| USCGS 3 zone | 57 | | mean 23.0 | |
| 49.0 - 52.8 | 29 | 9.15 | 23.9 | 40 |
| 52.8 - 56.9 | 13 | 9.31 | 19.3 | 33 |
| 58.0 - 61.7 | 15 | 9.49 | 26.1 | 27 |
| Sykes 2 zone | 47 | | mean 25.3 | |
| 48.1 - 49.9 | 28 | 9.66 | 25.5 | 54 |
| 50.2 - 61.9 | 19 | 9.59 | 25.1 | 46 |
| Sykes 3 zone | 47 | | mean 25.3 | |
| 48.1 - 49.9 | 28 | 9.66 | 25.5 | 46 |
| 50.2 - 53.0 | 11 | 9.57 | 23.0 | 32 |
| 55.0 - 61.9 | 8 | 9.62 | 29.0 | 22 |

Considering the results of the various data sets (Tables 8.1, 8.2) the following conclusions can be made. The similarity of the standard deviations and radii of the different sections of the Macquarie complex indicates that it is valid to assume that the epicentres south of approximately 48.5°S define one single transform fault. This gives an epicentral pole at approximately 56°S, 176°E. Using the 1.25 S contour as a confidence region the pole position can be given as 56.0 ± 0.3°S, 176.0 ± 3.0°E, or 56.0°S ± 35 km, 176.0°E ± 190 km.

8.3.2 Pacific-Antarctic

The majority of the seismicity on the Pacific-Antarctic boundary occurs in distinct linear sections (Fig. 8.15). The only reliable first motion solution for the whole boundary is in the section at 50°S, 115°W (Forsyth, 1972). It indicates pure strike-slip motion along the trend of the epicentres. A very unreliable solution at 55.4°S, 128.2°W (Sykes, 1967) is compatible with strike-slip motion along the trend of the epicentres there. The bathymetric and magnetic data are sufficient to indicate that east of 180° the epicentre lineations are along active fracture zones. It should be valid to assume that these active fracture zones are transform faults. In the Pacific-Antarctic fracture zone area, 180° - 161°E, the seismicity could be on ridges and/or fracture zones. Since there are sufficient distinct sections of epicentres that are associated with transform faults the epicentral method is readily applicable to the boundary.

The epicentre lineations are approximately east-west (Fig. 8.15) so sections are initially chosen by longitude. The few obviously isolated epicentres are not considered and four sections are taken at 55°S between 118°W and 138°W. The Pacific-Antarctic fracture zone is included and taken as one section. There are eight sections all together. An initial run yields four epicentres (open circles in Fig. 8.15) which have deviations more than 2.5 times the standard deviation of their respective zones. Omitting them leaves 100 epicentres. A search at five degree intervals over a wide area gives a pole at 75°S, 150°E. A one degree search gives a pole at 76°S, 144°E with a standard deviation S = 15.5 km. This pole will be referred to as the eight zone pole; an alternative pole based on ten zones will be discussed later.

A simple means of assessing the pole is to examine the standard deviations of the individual zones used (Table 8.3 overleaf). In section 3.6.3 it was shown that the uncertainty in epicentre locations is likely to be at least 25 km so all the individual standard deviations are satisfactory. The distribution in each zone could be checked with various statistical tests, examples of which were given in the previous section. In practice the rigorous tests are needed only when the interpretation is uncertain. A simple inspection of the distribution about the mean arc of each zone is usually sufficient.

The section at 50°S, 115°W (Fig. 8.16) is remarkably linear. It is 170 km long, the standard deviation is only 5.8 km, and only one of the epicentres is more than 8 km from the arc. The distributions between 118°W and 145°W (Fig. 8.17) also fit the eight zone arcs well. It should be noted that when the pole is calculated from several sections there is no requirement that every section fit the pole well. The distribution at

160°W (Fig. 8.18) is not random about the eight zone arc. The standard deviation is only 18.5 km but a lower standard deviation would be obtained for an arc trending more east-west. Two separate fracture zones would probably be more satisfactory. In the Pacific-Antarctic fracture zone, 180° - 161°E, (Fig. 8.19) the distribution about the eight zone arc is visually reasonable but the run test indicates that it is nonrandom at the 95% level.

Table 8.3 Pacific-Antarctic epicentral poles

| | | 8 zones: 76°S,144°E | | | 10 zones: 71°S,122°E | |
|---|---|---|---|---|---|---|
| Zone | Number of epicentres | $S_j$ (km) | Contrib. to mean S (%) | | $S_j$ (km) | Contrib. to mean S (%) |
| 115°W | 11 | 5.8 | 33 | | 5.8 | 29 |
| 120°W | 3 | 18.9 | 5 | | 19.0 | 5 |
| 125°W | 12 | 23.3 | 9 | | 25.1 | 7 |
| 130°W | 29 | 24.6 | 13 | | 25.0 | 11 |
| 136°W | 5 | 15.3 | 8 | | 15.0 | 7 |
| 142°W | 12 | 17.3 | 11 | | 19.4 | 9 |
| 160°W | 7 | 18.5 | 8 | | 28.1 | 5 |
| Pac-Ant | 21 | 20.8 | 13 | (N) (1) 9 | 25.5 | 6 |
| | | | | (2) 5 | 15.7 | 7 |
| | | | | (3) 6 | 8.2 | 15 |
| | | mean S = 15.5 | | | mean S = 14.9 | |

In the Pacific-Antarctic fracture zone (Fig. 8.19) the gaps in the seismicity suggest that the area could be considered as three zones. When this is done there are ten separate sections on the whole Pacific-Antarctic boundary. They give a pole at 71°S, 122°E. The standard deviation is 14.9 km, a slight but not significant improvement on the 15.5 km of the pole calculated with eight zones.

The arcs about the eight and ten zone poles differ little for the sections east of 150°W (Figs 8.16 and 8.17), and the standard deviations are similar (Table 8.3). At 160°W (Fig. 8.18) the ten zone standard deviation is 28.1 km compared with 18.5 km of the eight zone. However if the section is considered two separate fracture zones the best fitting arcs are those about the ten zone pole.

In the Pacific-Antarctic fracture zone (Fig. 8.19) the differences between the two poles are significant. If there are three separate fracture zones they fit the pole at 71°S, 122°E adequately, especially the western-

most, third zone (Table 8.3). When the likely uncertainties in epicentre locations are considered (Fig. 8.20) three separate zones would also fit the pole at 76°S, 144°E. For that position the standard deviations of zones one and two are virtually the same as for the pole at 71°S, 122°E, but for zone three the standard deviation is 24 km compared with 8 km. If the area is one single zone both poles are not acceptable. For the pole at 71°S, 122°E the standard deviation of the single zone is 98 km, and it is clear from Fig. 8.19 that the single zone strike is too east-west to fit that pole.

Some contours of the epicentral standard deviation for the ten and eight zone data sets are shown in Fig. 8.21. The 90% confidence limit is 17.9 km and 18.6 km respectively which gives confidence areas not much smaller than the area inside the 20 km contour. However the contours may not adequately indicate the confidence limits for the epicentral pole. For example 71°S, 122°E is inside the confidence area of the eight zone data set, but Figs 8.19 and 8.20 indicate that that position is not adequate for the eighth zone of the data set i.e. the Pacific-Antarctic fracture zone as one zone. Thus the 90% confidence area defines an area of adequate standard deviations but not neccessarily adequate distributions. Alternative means of assessing the confidence limits for the pole are required.

To conclude: Fig. 8.21 indicates that the Pacific-Antarctic epicentral pole is not tightly determined, but without discussing any other geophysical data a pole at 71°S, 122°E can be considered preferable. It fits all the epicentre lineations well and it produces the lowest epicentral standard deviation.

### 8.3.3 Indian-Antarctic

For the Indian-Antarctic epicentral pole Sykes' epicentres (Fig. 3.10) are used. Firstly because they show less scatter than the USCGS epicentres (Fig. 3.9). Secondly because the USCGS file was set up with data only east of 135°E, whereas the Sykes file has data for the whole Indian-Antarctic boundary.

The area east of approximately 135°E (Fig. 8.22) is relatively clear so that area is considered first. The available bathymetric and magnetic data indicate that all the seismic activity is associated with fracture zones that offset east-west sections of spreading ridge. Focal mechanism studies (Banghar and Sykes, 1969) for two earthquakes at the northern end of the long zone from 55° to 60°S indicate predominantly strike-slip motion along the trend of the epicentres. It should be valid to assume that all the activity, apart from a few isolated epicentres, is on transform faults.

A longitudinal division into three sections, ignoring the small section at 144°E, is sensible. However in the section at 140°E there is a short length of spreading ridge at 52.3°S, (Weissel and Hayes, 1972), so the 140°E section is considered two sections separated at 52.3°S. This gives a total of four separate sections. They yield an epicentral pole at 26°S, 163°W, with an epicentral standard deviation S = 21.3 km. The standard deviations of the individual zones are between 18 and 25 km. Contours of the epicentral standard deviation are shown in Fig. 8.23. The 90% confidence limit is 25.8 km so the 25 km contour approximates the confidence area. It can be seen that this area is very large, but it probably overestimates the uncertainties in the pole position.

In the long section from 55°S to 60°S (Fig. 8.22) none of the deviations from the arc is more than two standard deviations and the distribution is random with the run test. Nevertheless there is a suggestion that it is more than one zone. Data sets using several different subdivisions of this section produce poles less than four degrees from 30°S, 166°W. However the distributions in the smaller sections are not all random, the short sections lead to large confidence areas, and a "false" secondary minimum occurs near 50°S, 160°E. For that position the Balleny fracture zone (Fig. 8.24) has a standard deviation of 75 km, and it contributes only 8% to the mean standard deviation. The position is obviously unsuitable for the Balleny fracture zone but it is not clearly discrepant for the shorter sections further north. The false minimum is a product of the weighting system used. The standard deviation of the Balleny fracture zone for positions off the "true" pole is such that its weighting compared with the other sections decreases too quickly. It is effectivly weighted out of the sum of all the zones and so has little effect.

Next the boundary west of 135°E is considered. The epicentres between 130° and 120°E (Fig. 3.10) are associated with the Australian-Antarctic discordance and are not considered for the epicentral method. West of 120°E (Fig. 8.25) epicentre lineations are not striking but there are seven small areas with slightly concentrated activity. The six areas west of 100°E are associated with fracture zones which McKenzie and Sclater (1971) have tentatively identified from magnetic and bathymetric data; and the area at 118°E coincides with a fracture zone mapped by Weissel and Hayes (1972). These seven zones give an epicentral pole at 28°S, 162°W, very close to the pole position from data east of 135°E (Table 8.4 overleaf). The standard deviations of the separate zones are between 9 and 20 km.

In the group at 32°S, 78°E, two focal mechanism studies (Banghar and Sykes, 1969) indicate normal faulting not strike slip motion so this area may not be a transform fault and so should not strictly be considered.

The distribution at 118°E is not good and possibly should not be considered. Eliminating these two areas leaves five zones which give a pole at 31°S, 166°W (Table 8.4).

Table 8.4 Indian-Antarctic epicentral poles

| Data set | Number of epicentres | lat °S | long °W | S(km) |
|---|---|---|---|---|
| 4 zones east of 135°E | 80 | 26 | 163 | 21.3 |
| as above : equal weighting | 80 | 26 | 163 | 21.0 |
| USCGS east of 135°E (4 zones) | 91 | 27 | 164 | 24.5 |
| 7 zones east of 120°E | 42 | 28 | 162 | 13.5 |
| 5 zones east of 120°E | 31 | 31 | 166 | 14.4 |
| 9 zones, whole boundary | 111 | 30 | 166 | 16.6 |
| as above : equal weighting | 111 | 30 | 166 | 16.8 |

When the best data east and west of 135°E are combined there are nine zones for the whole boundary. They give a pole at 30°S, 166°W with S = 16.6 km. Contours of the epicentral standard deviation are shown in Fig. 8.26. The 90% confidence limit is 19.5 km so the 20 km contour approximates the confidence area.

For the complete boundary data set the secondary minimum discussed previously is present. One way of "avoiding" it is weight each section equally i.e. use $h_j = 1$ in equation 8.6. This produces an identical epicentral pole position, 30°S, 166°W, and nearly the same mean standard deviation as the more complex weighting system (Table 8.4). The standard deviation contours (Fig. 8.27) are similar in shape and the confidence area (approximately the 20 km contour) is smaller. Equal weighting also gives the same pole as the more complex weighting for the data east of 138°E only (Table 8.4).

The USCGS epicentres east of 135°E (Fig. 3.9) give a pole at 27°S, 164°W; virtually the same as the other poles found using Sykes' data.

To conclude: the results for the Indian-Antarctic boundary reveal deficiencies in the weighting system used but a wide variety of data sets give poles near 30°S, 166°W. The convergence of the different data sets probably indicates that the confidence area as defined here is too conservative an estimate of the uncertainties in the epicentral pole. The Indian-Antarctic epicentral pole is close to 30°S, 166°W.

## 8.4 CONSISTENCY OF THE EPICENTRAL POLES

The epicentral poles for the Indian, Pacific and Antarctic interactions are listed in Table 8.5. It should be noted that each pole has been determined quite independantly.

Table 8.5 Epicentral poles

| Indian-Pacific | Pacific-Antarctic | Indian-Antarctic |
|---|---|---|
| $56^{\circ}S$ $176^{\circ}E$ | $71^{\circ}S$ $122^{\circ}E$ | $30^{\circ}S$ $166^{\circ}W$ |

An important check of the reliability of the poles is that they should form a consistent set. The poles define the directions of the angular rotation vectors of the interacting plates, and if the plates are rigid the vectors should be such that

$$\omega(\text{Pac-Ant}) + \omega(\text{Ant-Ind}) + \omega(\text{Ind-Pac}) = 0 \qquad \ldots\ldots\ldots 8.8$$

A neccessary condition for equation 8.8 to hold is that vectors are coplanar; which means that the rotation poles must lie on a great circle. Fig. 8.28 shows that the epicentral poles very closely satisfy that condition; in fact no pole is more than 35 km from the great circle. The consistency is remarkable considering the uncertainties in each individual pole.

Colinearity of the poles is a necessary condition but it is not sufficient - the vectors must also add correctly. If the pole positions i.e. the vector directions are fixed, the vector magnitudes i.e. rates of angular rotation, must be consistent. The epicentral method does not provide the rotation rate so additional data must be used. A rate of motion at a single point on any one of the boundaries would completely determine the system. Ridge spreading rates will provide rates of movement, and since they are available at several places the system is in theory overdetermined. In practice the uncertainties in the data are considerable and only an approximate check of the consistency is possible.

Before discussing the rotation rate data it is important to point out that the epicentral method provides essentially instantaneous poles. The seismicity data are for the last decade and if all the earthquake fault movements were strike-slip the epicentre lineations indicate the directions of plate motion during the last decade. The epicentral poles therefore apply for motions in the last decade. Most other methods of finding rotation poles provide poles which represent movement during longer intervals; often up to 10 my.

The rates of movement required to check the epicentral poles should strictly be for only the last decade, but that is not practical. New Zealand data of observed fault movements, a geodetic survey, and displacement of $\leq$ 10,000 y old river terraces (Wellman, 1973a) provides some recent data for the Indian-Pacific boundary. However the boundary is a broad zone in most of New Zealand (Evison, 1971; Wellman, 1973a) so it is not possible to be sure that data from several small areas reflect the total movement between the two plates.

The most reliable data for determining the rotation rates are ridge spreading rates determined from magnetic anomalies. They yield an average rate over the anomaly span used. The minimum span is the first reversal at 0.69 mybp but this would be very difficult to use reliably. Probably the best that can be done is to use anomaly 2 (1.79 mybp). If plate motions do not change rapidly the rates calculated over the 1.79 my interval should be adequate. Figs 8.29 and 8.30 show that the considerable scatter in the available data make it difficult to accurately define the rotation rate for either the Pacific-Antarctic or the Indian-Antarctic poles.

Table 8.6 shows the results of several data sets used to check the rotation rates appropriate for the epicentral poles. In each set the rotation rate for one of the poles is assumed and the other two rates are calculated by vector addition.

Table 8.6 Epicentral pole rotation rates

| Set | Pacific-Antarctic | Indian-Antarctic | Indian-Pacific |
|---|---|---|---|
| 1 | 7.4 | 6.9 | 12.6* |
| 2 | 10.5* | 9.8 | 17.9 |
| 3 | 8.6 | 8.1* | 14.8 |
| 4 | 10.2 | 9.5* | 17.4 |

* Indicates rate that was assumed.
Rates in units of $10^{-7}$ deg/y.

Set one uses the New Zealand data to determine the Indian-Pacific rate. Wellman (1973a) concludes that recent movement across the boundary in the South Island is of the order of 3 cm/y. For the Indian-Pacific pole at $56^{\circ}$S, $176^{\circ}$E this gives a maximum rate of 13.5 cm/y at $90^{\circ}$ from the pole, i.e. 12.6 x $10^{-7}$ deg/y rotation rate.

Set two uses the Pacific-Antarctic data of Fig. 8.29. A best fitting straight line through the origin should enable the rotation rate to be determined from the maximum rate at $90^{\circ}$. The data are scattered but the

maximum half spreading rate can be estimated as 5.8 ± 0.6 cm/y. This gives a Pacific-Antarctic rotation rate of approximately $10.5 \times 10^{-7}$ deg/y.

Set three uses the Indian-Antarctic data of Fig. 8.30. The data do not fit a straight line at all well which may be due to inaccuracies in the data or it may indicate that the pole position is not appropriate. A maximum half spreading rate of 4.5 cm/y gives an Indian-Antarctic rotation rate of $8.1 \times 10^{-7}$ deg/y.

Set four uses data from the southeast Indian ridge near the Indian-Antarctic-Pacific triple junction (Section 4.6.2). Anomaly 2 has been clearly identified at several places there. It gives a half spreading rate of 3.4 ± 0.1 cm/y perpendicular to the ridge trending N55°E. For a pole at 30°S, 166°W a ridge perpendicular to the motion would strike N52°E. The rate perpendicular to this gives a maximum half spreading rate of 5.3 cm/y, or a rotation rate of $9.5 \times 10^{-7}$ deg/y for the Indian-Antarctic pole.

The data in the whole of Table 8.6 indicate that it is difficult to check the consistency of the epicentral poles from the rotation rates. For any pole the rates deduced by different methods vary by up to 30%. For the Indian-Pacific pole the "observed" rate (set one) is lower than any of the indirectly calculated rates and the observed rate leads to rates for the two other poles which appear to be too low. The Pacific-Antarctic observed rate (set two) is probably correct to within 10% and only set four agrees with it. However set four is based on an Indian-Antarctic rate which appears too high even for that boundary (Fig. 8.30) and it produces a high rate for the Indian-Pacific boundary.

In conclusion it can be said that it is difficult to fully check the consistency of the epicentral poles. The rotation rates agree to within only 30%, but considering the data used that may well be good agreement. The condition that the poles be on a great circle certainly is very closely met, but considering the uncertainties in the pole positions that agreement may be fortuitous. The requirement that the poles be consistent is based on the assumption that the plates are behaving in a truely rigid manner. This may not be valid. Some of the epicentre scatter at the plate boundaries may reflect local non-rigid behaviour, and some non-rigidity of the Indian plate is indicated by the sediment deformation (Eittreim and Ewing, 1972), and minor seismic activity (Sykes, 1970a), in the northeast Indian ocean. Rather than demand that the epicentral poles be consistent their general consistency may be considered indicative of the rigid behaviour of the plates.

## 8.5 COMPARISONS WITH OTHER DATA

### 8.5.1 General

The examination in the previous section of the consistency of the epicentral poles is one way of assessing the validity of the poles. In this section each pole is assessed individually by comparing predictions based on the epicentral pole with observations independent of the method, and by comparing the epicentral pole with other poles. Before discussing each pole separately the following general points should be noted.

The epicentral method uses epicentres from transform faults and the epicentral pole yields arcs that best fit the epicentres. The arcs define active fracture zones and these will be compared with fracture zones that have been defined independently. Most of the identified fracture zones have been mapped from bathymetric features and offsets of magnetic anomalies and in only a few places were the data from the active portions of the fracture zones. In most places the position and strike of the active portion was inferred from epicentres and from the strike of the fracture zone beyond the active part. If a pole position has moved with time a fracture zone strike defined from inactive portions may be different from the strike of the active transform fault portion.

Harrison (1972a, 1973) has shown that the use of inactive portions of fracture zones for determining pole positions can lead to substantial errors in the pole positions. This could be significant for some of the alternative poles that will be discussed. The epicentral poles are not effected as they use only the true transform portions of the fracture zones.

A complete list of published pole positions is given in Appendix 8A but only the more reliable determinations will be discussed in detail in the following sections.

There will not be detailed discussions of the strike of ridge sections with respect to spreading directions predicted by the epicentral poles. Plate tectonics geometry does not require that ridges be orthogonal to the spreading direction so ridge strikes do not provide definitive data for assessing the epicentral poles. On the Indian-Antarctic and Pacific-Antarctic boundaries the ridges do appear to be orthogonal to the spreading directions.

It is interesting to note that the standard deviation of every individual fracture zone considered on the three boundaries is less than 30 km. The uncertainties in epicentre locations are likely to be of similar order so statistially the fracture zones defined by seismicity could be of "zero width".

8.5.2 Indian-Antarctic

The Indian-Antarctic epicentral pole at 30°S, 166°W was determined with data from two areas: east of 135°E, and west of 100°E. Each of these areas separately gave similar pole positions (Table 8.4), which can be considered good evidence of the continuity of the Indian and Antarctic plates in this area.

For the area east of 135°E the morphology and magnetic anomalies have been described by Hayes and Conolly (1972) and Weissel and Hayes (1972) respectively (Fig. 2.9). Both have identified active fracture zones but there are significant differences in the positions and lengths of individual zones depending on the type of data primarily used. There is therefore little point in a detailed comparison of their fracture zones with those defined by the epicentral method. It is sufficient to say that the strikes of all the alternative fracture zones agree to within 10°. Two focal mechanism studies of Banghar and Sykes (1969) are available in the area (Fig. 8.22). Both solutions are primarily strike-slip and the slip directions agree to within 6° with the direction defined by the epicentral pole.

The structure of the area west of 100°E has been described by McKenzie and Sclater (1971). The fracture zones they identified (Fig. 2.10) are determined from bathymetry and magnetic anomalies but are also very dependent on epicentres. Therefore detailed comparison with the epicentral results is unwarrented. The strike of their fracture zones agree to within 8° with the strikes given by the epicentral pole. Three focal mechanism studies are available from Banghar and Sykes (1969). The slip vector of a strike-slip solution at 46°S, 96°E (Fig. 8.25) is within 8° of the predicted epicentral direction. The directions for two normal faulting solutions at 32°S, 78°E are more divergent, but for both solutions the slip vector is not well determined.

The Indian-Antarctic epicentral pole is well southwest of several alternative poles for the boundary (Fig. 8.31). Weissel and Hayes' (1972) pole is determined from superposition of anomaly 5 (10 mybp) either side of the southeast Indian ridge east of 105°E. They indicate an uncertainty of less than 3° in the pole position. The McKenzie and Sclater (1971) pole is from a matrix method using spreading rates, fracture zone strikes, and focal mechanism slip vectors. Data mainly west of 105°E were used, but some data east of 135°E were also included. Thus contrary to Weissel and Hayes (1972) statement the Weissel and Hayes and McKenzie and Sclater poles are not independent. The Chase (1972) pole is one of the set of similtaneous poles determined with his n-plate method, and is one of the best determined poles

of the set. Seven spreading rates and 14 directions from focal mechanism studies or fracture zones on the Indian-Antarctic boundary were included in the global data set used.

The confidence area of the epicentral pole (Fig. 8.26) is very elongate because the narrow azimuthal distribution of the fracture zones leads to poor control in the direction of perpendiculars to the fracture zones. The alternative poles (Fig. 8.31) are between $17^{o}$ and $26^{o}$ from the epicentral pole but they are close to the axis of minimum epicentral standard deviation, and the standard deviation at all of them is less than 10% greater than at the epicentral pole. At any given point on the Indian-Antarctic boundary the directions of motion predicted by the different poles differ by less than $10^{o}$. Consequently fracture zones provide little control for assessing the merits of the different pole positions.

Spreading rates provide control along the axis of the epicentral confidence area. Table 8.7 lists calculated and observed spreading rates at three widely spaced points on the boundary. The Weissel and Hayes pole and rate appears to be the best fit and the epicentral pole does not fit very well. However the rates at $78^{o}$E and $115^{o}$E are 10 my averages and the rate at $160^{o}$E is a 1.8 my average. What is strictly required for the epicentral pole is the present day rate.

Table 8.7 Observed and calculated spreading rates on the Indian-Antarctic boundary

| Source for rate | $62^{o}$S,$160^{o}$E | $50^{o}$S,$115^{o}$E | $38^{o}$S,$78^{o}$E |
|---|---|---|---|
| Observed | 3.4 | 3.7 | 3.2 |
| Weissel & Hayes (1972) $12^{o}$S, $145^{o}$W $\omega = 6.75 \times 10^{-7}$ $^{o}$/y | 3.4 | 3.7 | 3.4 |
| McKenzie & Sclater (1971) $11^{o}$S, $148^{o}$W $\omega = 6.4 \times 10^{-7}$ $^{o}$/y | 3.1 | 3.5 | 3.2 |
| Chase (1972) $16^{o}$S, $156^{o}$W $\omega = 6.5 \times 10^{-7}$ $^{o}$/y | 2.9 | 3.5 | 3.5 |
| Epicentral $30^{o}$S, $166^{o}$W $\omega = 8.1 \times 10^{-7}$ $^{o}$/y | 2.9 | 3.9 | 4.5 |
| $\omega = 9.5 \times 10^{-7}$ $^{o}$/y | 3.4 | 4.6 | 5.3 |

Spreading rates are half spreading rates in cm/y.

It is difficult to give a definate conclusion on the validity of the Indian-Antarctic epicentral pole position $30^{o}$S, $166^{o}$W. The pole is compatible with the available data on directions of motion but a pole further northeast along the axis of the confidence area may be a better position for rates of movement. More detailed spreading rate data are required to check the epicentral pole.

### 8.5.3 Indian-Pacific

The data used for the Indian-Pacific epicentral pole were selected quite independently of any other geophysical data. The very tight determination of the pole position (Fig. 8.9) could be considered good evidence that the pole is valid, but it is preferable to also examine what the pole predicts on the boundary.

The basic assumption of the method implies pure strike-slip motion along all of the Macquarie complex south of about 49°S. Focal mechanism studies are available from Sykes (1967), Banghar and Sykes (1969), and Johnson and Molnar (1972), (Fig. 8.32). Only two indicate pure strike-slip motion, the others indicate some thrusting of the Pacific plate over the Indian plate. The slip vectors of the thrust solutions are not well determined (Banghar and Sykes, 1969). The thrusting is not necessarily incompatible with regional strike-slip motion because focal mechanisms indicate only local motion. Any structure oblique to the boundary may lead to local motion that is different from the regional one.

The existence of the substantial ridges and troughs that make up the complex could be considered evidence that it is not a simple fault boundary. However the topographic structure may be a result of movement in time of the position of the pole. The pole is close to the boundary so any shift could cause large changes in motion along the boundary leading to the development of major structural features. Changes with time could explain why the southern part of the Hjort trench strikes across the boundary (Fig. 8.32). The scatter of the epicentres and the possibility of systematic errors in epicentre location make it unwise to suggest that the boundary line defined by the epicentral pole (Fig. 8.32) is associated with any particular feature of the complex.

North of about 49°S the epicentres diverge from the single arc (Figs 8.5 and 8.12), so the boundary cannot extend as a continuous strike-slip fault into New Zealand. In the South Island the boundary is generally associated with the Alpine fault which goes offshore from Fiordland. The vector of motion predicted for the area between 49°S and Fiordland implies a component of compression. If some of this compression is taken up by underthrusting the intermediate depth earthquakes observed in Fiordland (Smith, 1971) could be explained. Christoffel and van der Linden (1972) have proposed a model which would reconcile the southeastward dip of the earthquake zone with the northeast direction of relative motion.

At the central part of the Alpine fault at 170°E (Fig. 8.33) the direction of motion predicted from the epicentral pole strikes 20° east of the fault. The component of motion normal to the fault explains the observed uplift and thrust of the eastern side. Further north the Alpine fault branches into

several fault traces (N.Z. Geol. Survey, 1972). The strikes of these faults where they break off from the main trace are within $5^{o}$ of the strike of the epicentral pole vector. After a short distance, however, they reorientate to a more northward trend. The structure of the area may be a consequence of the present motion being oblique to pre-existing structural trends.

The predicted directions of relative motion change from east-west at the northern end of the South Island to $15^{o}$ north of west at the northern end of the Tonga trench. The directions agree well with those given by focal mechanism studies (Johnson and Molnar, 1972), and are compatible with the underthrusting indicated by the distribution of earthquakes (Isacks et al., 1968).

The epicentral pole position is significantly different from other published pole positions (Fig. 8.33). The differences are probably a result of different initial assumptions rather than uncertainties in pole determinations. Christoffel's (1971) pole (DC) is based on the assumption that the Indian-Pacific boundary is a continuous transform fault from the triple junction to the southern end of the Kermadec trench. This seems unlikely. Wellman's (1973a) pole (HW) is a graphical determination based on the direction of the southern and central Alpine fault. Some account was taken of non-pure strike-slip motion and the proximity to the epicentral pole is support for the validity of the epicentral pole position. The McKenzie and Sclater (1971) pole (MS) and the Weissel and Hayes (1972) pole (WH) are indirect poles calculated from Le Pichon's (1968) Pacific-Antarctic pole and their respective Indian-Antarctic poles (Fig. 8.31). Chase's (1972) pole is one of his simultaneous set. It includes data from only three focal mechanism studies on the Indian-Pacific boundary and so is mainly an indirect pole.

All the poles predict predominantly strike-slip motion on the Macquarie complex but the three southern poles (Fig. 8.33) predict some subduction in the Hjort trench area and almost pure strike-slip in the southern and central Alpine fault. There is no positive evidence of subduction at the Hjort trench and there is some evidence for motion oblique to the Alpine fault so the epicentral pole position would appear to be better.

The epicentral method does not give the rate of motion but if the three epicentral poles are assumed to be consistent the rotation rate can be estimated to be 13 to 18 x $10^{-7}$ $^{o}$/y (Table 8.6). A rate of 15 x $10^{-7}$ $^{o}$/y would give 2.8 cm/y strike-slip motion on the Macquarie complex. The component parallel to the central Alpine fault at $170^{o}$E would be 3.5 cm/y which is of the order of that estimated by Wellman (1973a) from geomorphic evidence. The rates predicted by the other poles are similar.

It is reasonable to conclude that the validity of the Indian-Pacific epicentral pole position $56^{o}$S, $176^{o}$E, has been established. The pole predicts

pure strike-slip motion for most of the Macquarie complex. More accurate epicentres might make it possible to determine the role of various features of the complex with regard to this motion.

### 8.5.4 Pacific-Antarctic

The Pacific-Antarctic boundary and rotation poles will be discussed more fully in the next chapter so only a brief discussion is given here.

The Pacific-Antarctic epicentral pole position that has been adopted is 71°S, 122°E, but an alternative pole at 76°S, 144°E is statistically almost as good. The latter pole is based on the Pacific-Antarctic fracture zone being one fault, the former pole assumes that it is at least three faults.

The only reliable focal mechanism solution for the whole Pacific-Antarctic boundary is in the very linear fracture zone at 115°W (Fig. 8.16). The solution (Forsyth, 1972) indicates pure strike-slip motion, with the slip vector only 2° from the direction predicted from the epicentral pole.

East of 150°W directions of motion predicted by the two epicentral poles differ by less than 5°, and the directions of all the mapped fracture zones (Figs 2.11, 4.18) are within 10° of the epicentral directions (Fig. 8.17). The fracture zone at 142°W is of interest because it is the only one that is adequately defined by data from within the active portion. The direction defined by the bathymetric data is exactly the same as that predicted from the adopted epicentral pole, 71°S, 122°E. The alternative pole yields a strike 5° more westerly.

In the area just east of 180° (Fig. 4.22) the directions predicted by the two epicentral poles differ by up to 15° but the fracture zone trends are not reliably enough determined to provide useful comparisons. The ridge at 168°W strikes N40°E. For a ridge orthogonal to the motion the adopted pole predicts N44°E while the alternative pole gives N32°E.

The interpretation of the Pacific-Antarctic fracture zone as several smaller zones striking slightly across the trend of the whole zone is preferred (see later) and the adopted epicentral pole clearly fits this interpretation satisfactorily while the alternative pole doesn't (Fig. 8.19).

Published Pacific-Antarctic pole positions (Appendix 8A) are all near 70°S, 120°E (Fig. 8.31) except for one at 82°S, 120°E (Christoffel, 1971). The latter was based mainly on the strike of the Pacific-Antarctic fracture zone as one fault. All the other poles used data only from east of 180°. Their proximity to the epicentral pole 71°S, 122°E, which uses data from both east and west of 180°, supports the validity of the epicentral pole position.

To conclude: The Pacific-Antarctic epicentral pole at 71°S, 122°E fits the available data well, but positions further southeast cannot be

definitely excluded. Additional data west of 170°W could confirm the preferred epicentral pole position.

### 8.5.5 Changes in pole positions

The positions of the Indian-Antarctic poles shown in Fig. 8.31 form a fairly regular progression from the Weissel and Hayes pole to the epicentral pole. A similar progression is seen in the Indian-Pacific poles (Fig. 8.33) but as some of these poles were indirectly calculated their positions are dependent on the Indian-Antarctic poles and the two progressions may not be independent. The progression of the poles becomes more significant when the basis of each pole is examined.

The Weissel and Hayes pole is from the superposition of anomaly 5 and is an average of 10 my of movement. The McKenzie and Sclater pole uses spreading rates based on anomaly 5, but it also uses fracture zone trends which may be defined from younger data, and focal mechanism slip vectors which are effectively instantaneous data. Chase's method uses a global data set that contains spreading rates, fracture zone directions and many focal mechanism vectors. It probably produces poles which represent average motions over an even shorter time than the McKenzie and Sclater pole. The epicentral method yields instantaneous poles.

The progression of pole positions is thus a uniform progression from a position representing ten million years of movement, through "younger" positions, to the instantaneous position. The progression suggests that with time the Indian-Antarctic pole has moved southwest and the Indian-Pacific pole has moved westward. The Pacific-Antarctic pole has probably not moved significantly.

The constraints of rigid plates mean that if one of the poles moves at least one of the others must also move, except when the movement is along the great circle through the poles. In the latter situation only the rates of rotation need change, in the former the rates needn't necessarily change. Fig. 8.31 shows that the pole movements are not along the great circle so movement of both the Indian-Pacific and Indian-Antarctic poles would be required if the Pacific-Antarctic pole did not move. The fact that the available "older" Indian-Pacific poles are indirect calculations based on the other two poles does not necessarily mean that movement of the Indian-Pacific pole is a consequence of the Indian-Antarctic pole movement. It is not possible to determine whether either movement controls the other, or whether all the movements are produced by effects external to this sytem of interacting plates.

It may be significant that the Indian-Antarctic pole movement is towards the boundary in a direction approximately along the perpendiculars to the boundary fracture zones. Pole movement in this direction means that directions of movement on the boundary do not change much. When a boundary consists of established orthogonal ridges and fracture zones minimum energy considerations suggest that if there are pole movements those which minimize changes of direction would be preferred.

The epicentral method described in this chapter has yielded three pole positions that form a consistent set, and each individual pole has been shown to be reliable. Although further work is required to better determine the accuracy of the epicentral poles it does appear that there are systematic differences between the epicentral poles and poles determined by other means. Further applications of the epicentral method should confirm whether or not it is possible to study detailed movements of rotation poles by comparing the epicentral results with the results of other methods.

# CHAPTER 9

## AN INTERPRETATION OF THE STRUCTURE OF THE SOUTHWEST PACIFIC AREA

This chapter draws on material in the previous chapters to give an interpretation of the tectonic development of the southwest Pacific area. An introduction (9.1) is followed by discussions of several areas: the currently active Pacific-Antarctic boundary 0-10 mybp (9.2); the Indian-Antarctic-Pacific triple junction (9.3); the Cretaceous area of the southwest Pacific basin (9.4); and the area representing 10-63 mybp (9.5). Then the southwest Pacific area is considered as a whole (9.6) followed by a discussion of its relationship to the rest of the world (9.7).

### 9.1 INTRODUCTION

In this chapter the tectonic history of the southwest Pacific area is discussed. Much of the discussion is in terms of plate tectonics so it is worth restating the basic assumptions on which plates are defined. Plates are defined as being rigid areas, which effectively means aseismic areas. The plate boundaries are defined by tectonic activity. Seismic activity is a sufficient indication of a plate boundary, but aseismic boundaries also exist. Many active spreading ridges, which are defined as plate boundaries, are aseismic. The world seismicity shown in Fig. 0.2 clearly indicates the rigid, aseismic nature of large areas of the earth's surface. The plate boundaries defined by seismicity are easy to see, and the positions of the boundaries between the seismic sections can be reliably inferred.

Three of the world's largest plates, the Indian, the Pacific and the Antarctic, intersect in the southwest Pacific area. Fig. 9.1 shows the seismicity in the area and it is clear that the plate boundaries are precisely defined by the epicentres. The aseismic portions linking the epicentres are known in many places to be the axes of spreading ridges. The plate boundaries in the area could also be defined from morphologic features, as Fig. 9.2 shows.

In terms of plate tectonics this study is primarily concerned with the southwest part of the Pacific plate, and its boundary with the Antarctic plate. In plate tectonics the continental Campbell plateau-Chatham rise area is not differentiated from the oceanic southwest Pacific basin - it is all part of the Pacific plate. However this study is concerned only with the oceanic part. The structure of it has been described in detail in Chapter 4; here an attempt is made to understand the origin of that structure. It is convenient to first consider various parts of the area separately, then "put them together" for a view of the evolution of the whole area, then consider the area in relation to the rest of the world.

## 9.2 PACIFIC-ANTARCTIC BOUNDARY 0-10 MYBP

The boundary between the Pacific and Antarctic plates is the axis of the Pacific-Antarctic ridge system. Fig. 9.3 shows the seismicity on the boundary, the places where the axis of an actively spreading ridge has been identified from magnetic anomalies, and the positions of anomaly 5. The data west of 144°W are shown in more detail in Fig. 4.1 and have been discussed in section 4.4. The magnetic data east of 145°W are from Herron (1971), and her interpretation of that area is shown in Fig. 2.12 and has been discussed in section 2.8.

Also shown in Fig. 9.3 are representative arcs about a pole at 70°S, 120°E. It will be shown that this pole is appropriate for the relative motion between the Pacific and Antarctic plates during the interval represented by anomalies 1 to 5. In the time scale of Talwani et al. (1971) the centre of anomaly 5 is 9.32 mybp, and the outer edge is 9.94 mybp. The anomalies from the ridge centre (anomaly 1 = 0 mybp) out to anomaly 5 can thus be loosely referred to as representing the interval 0 to 10 mybp. It is the Pacific-Antarctic boundary for this interval that is discussed in this section.

The structure of the Pacific-Antarctic boundary differs markedly either side of about 175°W. West of 175°W the general trend of the boundary as defined by seismic, magnetic, and bathymetric data is about N70°W. No classical magnetic anomalies have been identified, neither have any lineations. The bathymetric relief is extreme and the whole topographic structure is markedly asymmetric. The boundary can be considered a major fracture zone: the Pacific-Antarctic fracture zone. The general strike of the zone is about N70°W, but it probably consists of several individual fractures striking more northerly, possibly at N45°W.

East of 175°W the boundary consists of a smooth ridge, the axis of which coincides with the classical central magnetic anomaly. Anomalies out to number 5 either side of the axis are clear in most places. The trend of the axis varies from N40°E near 170°W to N15°E at the eastern end of the boundary. Offsets of the axis are evident from offsets of magnetic anomalies and topography. Virtually all the offsets are dextral and most, but not all, are seismically active. The length of offset ranges from 500 to 70 km, but smaller offsets could be present. The ridge axis is aseismic and almost all the seismicity occurs between the offset portions of the axis. One reliable and one poor focal mechanism solution support the logical interpretation that the active offsets are ridge-ridge transform faults. The trends of fracture zones and anomaly lineations away from the axis are seldom determined to better than 10°, but the fracture zones and lineations appear to be orthogonal.

Determinations of the pole of rotation for the relative movement between the Pacific and Antarctic plates have been published by several authors (see Appendix 8A). Morgan, Le Pichon, Chase and Wellman all used effectively the same data; which were spreading rates and fracture zone strikes determined from magnetic anomalies east of 175°W. The data were given by Pitman et al. (1968) and Heirtzler et al. (1968). Chase (1972) also used data from elsewhere in the world for his n-plate pole. It (70°S, 107°E) and Christoffel's pole (82°S, 120°E) are the only poles more than two arc degrees from 70°S, 120°E. Christoffel's pole was based mainly on the overall strike of the Pacific-Antarctic fracture zone.

Christoffel's pole and the epicentral pole are the only poles that use any data west of 175°W. As Morgan (1968) and Le Pichon (1968) have pointed out, accurate determination of the Pacific-Antarctic pole is very dependent on data at the western end of the boundary. The results obtained with the epicentral method (section 8.3.2) emphasise this. When the Pacific-Antarctic fracture zone was assumed to be one zone a pole was obtained at 76°S, 144°E. However when three zones were assumed the pole was almost 8° away at 71°S, 122°E. Numerically the latter pole was marginally better. The epicentral method has also been applied to several Pacific-Antarctic boundary data sets with the Pacific-Antarctic fracture zone excluded. The poles obtained were very ill-defined because the epicentral standard deviation minimum was almost "flat" over an area of tens of degrees.

Clearly the interpretation of the Pacific-Antarctic fracture zone is important. Bathymetric and magnetic data do not yet provide adequate information on any local strikes within the whole zone, and much depends on the seismicity. It should be noted that the seismicity need not necessarily be only on fracture zones. It was mentioned in section 2.7 that ridges are generally aseismic only when the spreading rate is greater than about 3 cm/y. Rates of spreading predicted in the Pacific-Antarctic fracture zone area, from for example Morgan's pole and rotation rate, are between 2.5 and 1.8 cm/y. Thus if there are any sections of ridge in the fracture zone area some of the seismicity may be associated with them. It is interesting to note that the less than 3 cm/y area is west of about 165°W, and just west of 165°W (Fig. 4.21) there is seismicity which could be on a ridge axis.

The b value study in Chapter 7 was partly motivated by the desire to see if b values would indicate whether the Pacific-Antarctic fracture zone seismicity was on fracture zones or ridges. The conclusion reached (section 7.4.3) was that the b value, 1.62, was similar to that of known fracture zones on the Pacific-Antarctic and Indian-Antarctic boundaries. Hence fracture zone activity was possible. However the b value was not

different from the value for slow (< 3 cm/y) ridge axes in the Atlantic; thus ridge axis activity cannot be ruled out.

There are two alternative approaches that could be taken to the related problems of interpreting the Pacific-Antarctic fracture zone and determining the Pacific-Antarctic rotation pole. One is to interpret the structure of the fracture zone and use that structure as a constraint on the pole; the other is to use the pole as a constraint in interpretations of the fracture zone structure. A combination of both approaches appears most useful.

Suppose that the Pacific-Antarctic pole is near 70°S, 120°E, and that the Pacific-Antarctic fracture zone morphology and seismicity defines the western-most part of the boundary. Fig. 8.19 shows that transform faults in the area would strike about N45°W. To accommodate the overall strike of the disturbed zone there would have to be several faults. These would presumably be linked by short spreading ridges which would probably, but not necessarily, strike N45°E. The available tracks are not well orientated for detecting these ridges. The seismicity does fit the predicted structure adequately.

Alternatively, suppose that the Pacific-Antarctic fracture zone is one long fault. If so the Pacific-Antarctic pole cannot be close to 70°S, 120°E. Christoffel (1971) assumed that the fracture zone was a single fault striking N75°W; which, combined with data east of 180°, gave a pole at 82°S, 120°W. The epicentral method puts it at 76°S, 144°W, without any a priori assumption of the strike of the zone. If the Pacific-Antarctic fracture zone is a single fault it would be the longest ridge-ridge transform in the world. That in itself is not a reason to suppose that it isn't one fault, but the considerable width of the whole feature (at least 200 km) does suggest several fracture zones.

The best way of assessing the merits of alternative poles, and therefore indirectly the interpretation of the Pacific-Antarctic fracture zone, is to examine how well the poles fit the structure on the rest of the boundary. As pointed out in sections 8.3.2 and 8.5.2 a pole at 76°S, 144°W would fit the epicentres east of about 150°W just about as well as a pole near 70°S, 120°E. The only fracture zone for which the strike of the active portion is known from anything other than epicentres is the Tairoa fracture zone at 140° to 145°W. Its strike, as determined from bathymetry, is 5° from the direction predicted by the 76°S, 144°E pole, but exactly that of the 70°S, 120°E pole. At 160°W the epicentres favour a pole at 70°S, 120°E (Figs. 4.21, 8.18). Between 165°W and 175°W fracture zones are poorly determined but the ridge direction at 170°W favours the 70°S, 120°E pole.

Possibly the best data for deciding between a pole at 76°S, 144°W and one near 70°S, 120°E are spreading rates. Fig. 8.29 shows that a rotation rate of 10.5 x $10^{-7}$ °/y about a pole near 70°S, 120°E fits the data well. Fig. 9.4 shows that the observed rates do not adequately fit a pole at 76°S, 144°E. A reasonably fitting straight line gives a positive velocity at zero distance from the pole, and suggests that the true pole is of the order of 10° beyond 76°S, 144°E. 70°S, 120°E is 9.1° beyond 76°S, 144°E.

It can be concluded that a pole based on the Pacific-Antarctic fracture zone as one fault does not adequately fit the structure of the whole Pacific-Antarctic boundary. A pole at 70°S, 120°E is adequate, and implies that the Pacific-Antarctic fracture zone is several faults striking across the general trend of the zone.

The Pacific-Antarctic rotation rate determined from anomaly 2, i.e. averaged over the last 1.8 mybp, is 10.5 x $10^{-7}$ °/y, with a probable uncertainty of less than 10%. Rates of 10.8 and 10.3 have been obtained by Le Pichon (1968) and Morgan (1968) respectively, from anomalies formed since 8 mybp. The positions of anomaly 5 on one side of the ridge can be superimposed on those on the other side by a rotation of 10° about 70°S, 120°E. This gives a rotation rate of 10.7 x $10^{-7}$ °/y for the last 9.3 mybp. It is reasonable to conclude that the relative motion between the Pacific and Antarctic plates during the last 10 mybp can be represented by rotation at 10.5 x $10^{-7}$ °/y about 70°S, 120°E. The known structure on the Pacific-Antarctic boundary is in accord with, and can be explained by such a rotation.

## 9.3 THE INDIAN-ANTARCTIC-PACIFIC TRIPLE JUNCTION

### 9.3.1 General

The Indian, Antarctic, and Pacific plates intersect just south of 60°S, near 160°E (Figs. 9.1, 9.2). Major results for the area are summarized in Fig. 9.5. The structure of the area is shown more fully in Fig. 4.30 and has been discussed in section 4.6. The epicentral method results were presented in section 8.3 and discussed in sections 8.4 and 8.5. In this section the structure of the area is considered in terms of plate tectonics. The nature of the three plate boundaries will be discussed first, then plate tectonics models will be examined. It will be shown that the Indian, Pacific, and Antarctic plates intersect near 61.5°S, 161°E, forming a stable triple junction of the ridge-fault-fault type.

### 9.3.2 Indian-Antarctic boundary

The Indian-Antarctic boundary in the triple junction area is a section of the actively spreading southeast Indian ridge. The ridge axis strikes N55°E and magnetic anomaly lineations either side of the axis are parallel to the axis. The anomalies closely match a model profile based on the Talwani et al. (1971) time scale (Fig. 4.31). The spreading rate has been calculated from the satellite-navigation controlled tracks which cross the ridge axis. Least squares fits were made of anomaly distance against age; using the Talwani et al. (1971) time scale and only anomalies out to number 3 (4.57 mybp). The mean rate north of the ridge is 3.40 ± 0.14 cm/y, the rate south is 3.37 ± 0.17 cm/y. A determination based on anomaly 2 (1.79 mybp), which is clearly defined in several places both north and south of the axis gives 3.37 ± 0.08 cm/y.

One of the profiles across the ridge, ELT27b, was examined in the numerical symmetry tests described in section 5.5.3. The results given there confirm the general symmetry of the anomalies about the ridge, but show that over short intervals within the anomaly sequence there may have been up to 10% difference in the spreading rate either side of the ridge.

The eastern end of the spreading southeast Indian ridge is probably a good indication of the position of the triple junction. If so the position is close to 61.5°S, 161°E.

### 9.3.3 Indian-Pacific boundary

The best information on the nature of the Indian-Pacific boundary probably comes from the epicentral results presented in section 8.3.1. It was shown there that the whole of the Macquarie complex south of 49°S can be considered a transform fault. The epicentres at the southern end of the boundary (Fig. 9.5) fit that interpretation well. Note that the arc shown is based on the whole Macquarie complex, not just the area shown.

Prior to the development of the epicentral method, Falconer (1972) had suggested - primarily on the basis of the regional bathymetry - that the boundary in the triple junction area was a fault striking N25°W. The b value study was partly motivated by an attempt to assess this suggestion. The b value obtained for the southern Macquarie complex (1.48) supports the fault hypothesis, but is also acceptable if there is subduction in the area. Subduction has been suggested because of the presence of the Hjort trench (Fig. 4.30) but the "trench" can equally well be interpreted as a fracture zone.

The anomalies east of the boundary (Fig. 9.5) show that the seafloor at 165°E is of Cretaceous age (see later). Between these anomalies and the boundary the depth of the basement and JOIDES results indicate an age of at least 30 mybp (section 2.4). The seafloor immediately west of the southern part of the boundary is young material formed at the southeast Indian ridge. Even at 57°S it is only 20 mybp. Clearly there is a substantial age difference across the boundary. The Pacific plate is effectively a cold fixed boundary for the material forming at the southeast Indian ridge. Sleep and Biehler (1970) have suggested that in such circumstances deeps can form, due to hydrostatic head loss as spreading material binds to the fixed boundary. The Hjort "trench" could therefore be a deep associated with a major fault.

The topography observed across the boundary (profiles ARb and EL36, Fig. 4.3) is just what would be expected if the boundary is a fault between the old, cold, deep, Pacific plate and the younger, hotter and shallower Indian plate. The seismicity indicates that this fault boundary intersects the southeast Indian ridge where the ridge ends, i.e. close to 61.5°S, 161°E.

### 9.3.4 Pacific-Antarctic boundary

The Pacific-Antarctic boundary in the area of the triple junction is the Pacific-Antarctic fracture zone. The Antarctic plate in the junction area is the young flanks of the southeast Indian ridge, while the Pacific plate is old close to the boundary. Bathymetry across the boundary (e.g. profile ARe, Fig. 4.32) although complex, reflects the transition from a young, shallow area to an old, deep area.

The detailed structure of the Pacific-Antarctic fracture zone is not clear and much depends on the seismicity. The overall trend of the zone intersects the junction of the Indian-Antarctic and Pacific-Antarctic boundaries, but in the section 9.2 reasons have been given for preferring the interpretation that the whole fracture zone consists of shorter fractures striking approximately N45°W. The epicentres on the boundary near the junction indicate a fault striking N45°W, but it would not intersect the point of intersection of the other two boundaries. If there is a ridge linking the fault to the junction it is not evident from magnetic anomalies on profiles AA and ODF9b (Figs 4.30, 4.31).

The position of the triple junction defined by the intersection of the Indian-Antarctic and Indian-Pacific boundaries could be quite closely defined as 61.6°S, 160.7°E, but the Pacific-Antarctic boundary is not well defined. The structure where the three plates meet is likely to be complex and it does not seem reasonable to imply that the position of the junction is defined to 0.1°. However it is considered that the junction is within 50 km of 61.5°S, 161°E.

9.3.5 Stability of the junction

In order to discuss the triple junction in terms of plate tectonics it will be assumed that: the junction is at 61.5°S, 161°E; the Indian-Antarctic boundary is a ridge striking N55°E spreading symmetrically at 3.4 cm/y; the Indian-Pacific boundary is a transform fault striking N25°W; and the Pacific-Antarctic boundary is a transform fault striking N45°W. Fig. 9.6A shows the basic data with the assumed directions, and Fig. 9.6B shows the plate configuration. It is acknowledged that the assumed Pacific-Antarctic boundary is not well established.

Fig. 9.6C shows the junction in velocity space following the notation of McKenzie and Morgan (1969). The heavy lines represent the relative plate velocities. For example, line AI is parallel to the motion of the Indian plate relative to the Antarctic plate, and its length is proportional to the relative velocity. The assumption of transform fault boundaries defines the directions but not the rates for the Indian-Pacific (IP) and Pacific-Antarctic (PA) motions. It is assumed that southwest Indian ridge is orthogonal to the Indian-Antarctic motion (IA), so the direction of IA is perpendicular to N55°E. The total spreading rate, 2 x 3.4 cm/y, defines the length of IA. The assumption of rigid plates means that the velocity triangle IPA must close, so the lengths IP and PA are determined. They show that the slipping rates on Indian-Pacific and Pacific-Antarctic transform faults are 3.5 cm/y.

If the geometry of the plate boundaries at the junction does not change with time the junction is said to be stable. Certain velocity relationships between the boundaries must be satisfied for this to be so. The condition in the velocity space diagram is that the lines ai, ap and ip must intersect. Each line represents the velocity locus of points in a reference frame with zero velocity with respect to a boundary. For example a reference frame with a velocity corresponding to any point on ai moves parallel to the ridge. The intersection of ai, ap and ip gives a reference frame in which the triple junction does not change with time. The lines ap and ip are along AP and IP respectively, as these boundaries are assumed transform faults. Since the ridge is spreading symmetrically, ai is the perpendicular bisector of IA. Fig. 9.6C shows that ai, ip and ap do intersect at a point, so the stability condition is satisfied. The triple junction defined in Fig. 9.6B is therefore a stable ridge-fault-fault junction.

The intersection of ap, ip and ai is at P which means that the triple junction is stationary with respect to the Pacific plate. The velocity of the junction relative to the ridge is given by PX which indicates that the active length of the ridge is shortening at 0.6 cm/y. Relative to Antarctica the junction is moving northwest at 3.5 cm/y.

### 9.3.6 Comparison with predictions

The velocity vectors given above have been deduced from data only in the triple junction area. The pole positions and rates of rotation for the plates involved are known so it is possible to calculate the expected velocity vectors at the triple junction. Table 9.1 shows the velocities determined from the most reliably determined poles. The pole sources are listed in Appendix 8A and were discussed in sections 8.5 and 9.2. Since the poles are determined with data from areas other than the triple junction the predicted motions are essentially independent of those determined from the triple junction data.

Table 9.1 Relative velocities at the Indian-Antarctic-Pacific triple junction

| | | | | | |
|---|---|---|---|---|---|
| | India-Antarctica | | | | |
| Source | Junction | IA9 | IA6 | IA5 | IA7 |
| Ridge strike | N55°E | N50°E | N61°E | N60°E | N53°E |
| Half spreading rate cm/y | 3.4 | 3.4 | 3.4 | 3.1 | 2.9 |
| | India-Pacific | | | | |
| Source | Junction | IP10 | IP6 | IP5 | IP7 |
| Fracture zone strike | N25°W | N29°W | 000° | N10°W | N23°W |
| Slipping rate cm/y | 3.5 | 3.3 | 3.4 | 2.7 | 1.8 |
| | Pacific-Antarctica | | | | |
| Source | Junction | PA8 | PA2 | | PA6 |
| Fracture zone strike | N45°W | N48°W | N45°W | | N45°W |
| Slipping rate cm/y | 3.5 | 3.5 | 3.9 | | 4.2 |

Source code letters refer to data in Appendix 8A.

The agreement between the directions deduced from only the triple junction area and those deduced "theoretically" from the poles of rotation is in general good. The rates differ more, especially those of the last column, which are based on Chase's (1972) n plate method. The column two results are from the epicentral poles, and the rates are not independent of the junction area as they are based on the rates of set 4 in Table 8.6, in which the Indian-Antarctic rate was determined from the spreading rate in the junction area. Each of the epicentral poles is determined independently so the directions are independent. It is notable that they form a set satisfying the stability condition.

The most divergent direction is the Indian-Pacific direction IP6 based on the Weissel and Hayes (1972) pole. Strictly the rates and directions given in Table 9.1 are for the relative motions not the motions on the boundaries. Thus if the Indian-Pacific boundary does strike N25°W the 000° velocity vector implies compression on the boundary. Weissel and Hayes (1972) noted this in their discussion of the junction, and they concluded that the junction was of the ridge-trench-fault type. The interpretation given here is preferred.

The fact that the junction is at present a stable ridge-fault-fault junction does not mean that it has always had that form. In view of the complexity of the Pacific-Antarctic boundary it seems probable that the junction will have either had a different form, or will have jumped to its present position from a position further east on that boundary. Is it significant that a stable ridge-fault-fault junction would also be produced by an Indian-Pacific fault boundary striking 000°, and Pacific-Antarctic fault boundary striking N75°W - the strike of the whole Pacific-Antarctic fracture zone near the junction?

## 9.4 THE SOUTHWEST PACIFIC BASIN

### 9.4.1 General

Magnetic anomalies provide the main information on the structure of the southwest Pacific basin. They are shown in Figs 4.1 and 4.3 and some of the key anomalies are shown in Fig. 9.3. The structure of the basin area has been fully described in section 4.3. The southwest New Zealand plateau, which forms the northern margin of the basin, was discussed in section 2.2.

The seafloor and basement structure is relatively uniform throughout the basin. Offsets of the anomaly lineations indicate five long fracture zones and two smaller ones. Apart from the "block" at the Tairoa fracture zone (Fig. 4.11) there are no major topographic or basement features associated with the fractures. The anomaly lineations terminate in the west close to a definite structural boundary with the Emerald basin. The Louisville ridge, probably a seamount chain, appears to form an eastern boundary. Apart from one identification of anomaly 25 there are no reliable identifications of anomalies 25 to 36 east of the Louisville ridge (Fig. 9.3). The single identification of anomaly 25, and anomalies younger than 25, indicate a dextral offset of the order of 1000 km across the ridge. The lack of anomalies beyond 25 on the eastern side suggests that the difference across the Louisville ridge is more than just a substantial offset.

The overall magnetic structure of the southwest Pacific basin is very uniform and it is the minor features that are of most interest. Not specifically for the interpretation of this area, but more because they are indicative of complications that could affect the interpretation of areas either that are more complex or where the data coverage is sparse. Irregularities of anomaly lineation directions and spacings are evident throughout the basin. Some of these are probably due to navigation errors but others are almost certainly due to small offsets or genuine irregularities. Absence of small parts of the sequence are present, while in other places the anomaly sequence is considerably "stretched", even to the extent of a whole extra anomaly. Both affect spreading rate determinations and make it difficult to apply numerical correlation techniques. The Toarahi and Waimori fracture zones indicate that local disturbances can substantially affect a small area within an otherwise uniform area. Such areas could be produced by a brief period of extreme asymmetrical spreading in a short section of a spreading ridge. Variations in the offset along a fracture zone, as are seen on several of the fractures, could also be produced by asymmetrical spreading (see later).

### 9.4.2 Age of the basin and formation of the Bounty trough

A revised and extended magnetic reversal time scale based on the southwest Pacific basin anomalies was presented in section 6.3. It shows that anomalies 25 to 36 represent the interval 63 to 80.5 mybp. Thus most of the oceanic basement of basin formed during that interval. Since the Tertiary-Cretaceous boundary is 63-65 mybp the basin can be referred to as of upper Cretaceous age.

An additional anomaly (number 37) is present in some places but anomaly 36 is the oldest anomaly consistently identified. At the Campbell plateau margin anomaly 36 is generally not more than 100 km from the base of the slope (Fig. 9.7). The basement is flat right to the margin and there are no indications of any subduction, so the Campbell margin can be considered to have formed just prior to anomaly 36. A time of 81 to 83 mybp would be a reasonable estimate from the distance of anomaly 36 from the slope.

East of Bollons seamount anomaly 36 is at least 250 km from the south Chatham slope. However it is close to basement structure (Fig. 4.16) that may mark the boundary of the regular southwest Pacific basin. The interesting question is: what is the crustal structure and age of the area between the boundary and the Chatham rise? It is not a magnetic quiet zone but no anomaly lineations are evident. The basement structure is more complex than off the Campbell margin and basement ridges are present (Fig. 2.3). The area could

be transistional between oceanic and continental crust, like some other areas off complex margins (Talwani and Elholm, 1973). Some relationship to the Bounty trough seems probable.

Several workers have suggested that the Bounty trough is an extensional feature formed by relative rotation between the Chatham rise and Campbell plateau (section 2.2). Rotation of the Chatham rise to close the Bounty trough would also bring the south Chatham slope close to anomaly 36. The continental margin-anomaly 36 relationship would then be similar to that off the Campbell margin. This suggests that the formation of the whole southwest Pacific basin began just prior to anomaly 36. The lack of any distorted sediments at the mouth of the trough suggests that the opening of the trough pre-dates the formation of the basin, i.e. prior to 81-83 mybp.

### 9.4.3 Pole of rotation

The anomaly lineations and the major fracture zones in the southwest Pacific basin are quite uniform, which suggests that it may be possible to describe the origin of the basin in terms of rotation about a pole. Arcs drawn about the pole for the last 10 mybp, i.e. 70°S, 120°E, strike across the fractures at up to 40°, which clearly indicates that that pole is not appropriate for the Cretaceous movements. Hayes and Ewing (1971) fitted the full extent of the Louisville ridge to a pole in the eastern equatorial Pacific at 5°N, 120°W. Christoffel and R.K.H. Falconer (1973) showed that a pole close to there, at 0°S, 120°W would fit the southwest Pacific basin fracture zones well. They noted some irregularities in the spreading rates in the basin, but it was not appreciated that the spreading rates indicate a pole to the west of the basin, not to the northeast in the equatorial area.

The seafloor spreading rates in the basin can be reliably calculated from the anomalies and the revised reversal time scale. In Fig. 6.16 data for the spreading rates in six areas of the basin are shown. The plots indicate very uniform spreading throughout the interval 63 to 81 mybp. However the profiles were chosen from where the lineations are most uniform. Other data would show more irregularity and the rates within each zone vary by up to 15%. Nevertheless there is definite trend of increasing rates to the east. This indicates a pole west of the basin, and the rate of increase of the spreading rates indicates that the pole would be 20 to 30 arc degrees west of the western end of the basin.

By trial and error a pole has been found that will fit the directions of the major fracture zones and the spacings of the anomaly lineations. The pole position is 56°S, 126°E, and the angle of opening for anomaly 36 to 25 is approximately 12°. Fig. 9.8 shows that the pole position fits most

of the fracture zones very well. Before commenting on some details of the fit it is worth emphasising that the anomaly interpretation and the mapping of the fracture zones was completely finalized before this pole position was determined.

The fit of an arc about the pole to the Louisville ridge does not appear very good in Fig. 9.8, but Fig. 9.3 shows that over a longer length to the north the fit is good. The Waimori fracture zone (Fig. 9.8) does not fit but it is obviously an irregular feature anyway. Between the Louisville ridge and the Tairoa fracture zone the anomaly lineations are not orthogonal to the direction of motion, but elsewhere they are.

The Rangirua fracture zone shown in Fig. 9.8 is noticeably "discrepant", but the theoretical fracture zone through there suggests an interesting reinterpretation of the area. Fig. 9.9 shows some of the area in more detail. An interpretation of the long Rangirua fracture zone as following the predicted arc, with the short Toarahi fracture to the west of it is acceptable and in several ways is "tidier". The anomaly lineations are then orthogonal to the fracture zones, and the general uniformity of anomalies 31-36 is preserved either side of the major fracture zone. The northward offset of the small group 32A-32 is still maintained. It is natural to wonder if the presence of the Bollons seamount is important.

Acceptance of the reinterpretation of the Rangirua fracture zone would mean that all of the major fracture zones in the southwest Pacific basin satisfactorily fit a pole at $56^{\circ}$S, $126^{\circ}$E. The irregularity of the spreading rates means that the pole position is not precisely defined, but the position adopted is probably reliable to within five degrees.

## 9.5 SOUTHWEST PACIFIC 10-63 MYBP

The area between the uniform southwest Pacific basin and the axial region of the Pacific-Antarctic boundary was described in section 4.5. The area is bounded by anomalies 5 and 25, so it represents the interval 10 to 63 mybp. This 53 my interval is approximately 65% of the time involved in the formation of the southwest Pacific oceanic crust. Fig. 4.1 shows that it has not been possible to determine detailed structure throughout most of the area, so there is a substantial time interval for which only a very incomplete understanding can be achieved.

In the western part of the area between anomaly 25 and the Pacific-Antarctic fracture zone there are numerous magnetic anomalies but the identification of lineations or characteristic anomalies is very difficult. The few shown in Fig. 4.1 are very tentative. The bathymetry is relatively disturbed. Further east the area between anomalies 5 and 25 is the

relatively gentle northern flanks of the Pacific-Antarctic ridge and some anomaly lineations are reasonably well established (Fig. 4.1). Based largely on the work of Pitman et al. (1968) most of the anomalies in the classical sequence between numbers 5 and 25 have been identified west of the Tairoa fracture zone. That fracture zone is the only one identified throughout the whole 5-25 area. Its exact position is not well determined. In Fig. 4.1 it was drawn so as to join the clearly identified offset in the Cretaceous anomalies with the marked offset in the ridge axis at 56°S, 144°W (see also Fig. 9.3, where the ridge offset is clearer).

East of the Louisville ridge-Eltanin fracture zone line (Fig. 9.3) Herron (1971) has identified some anomalies between 5 and 25 (Fig. 2.12). The directions of the anomaly trends are not well established though (section 2.8).

With so little information on the structure of the area between anomalies 5 and 25 it is difficult to reliably determine whether rotations about poles will adequately explain the structure of the area. Herron (1971) suggested that for the anomalies prior to number 5 east of 150°W, a pole near the end of the Macquarie ridge at 62°S, 165°E was appropriate. Christoffel (1969), considering data west of 150°W, noted the narrowing towards the west of the distance between anomaly 5 and 25, and from it suggested a pole at 64°S, 160°E. Christoffel and R.K.H. Falconer (1973) showed that for that pole an angle of opening for anomaly 25 to anomaly 5 of 21° was satisfactory. A re-examination of the data west of 150°W indicates that a pole at 72°S, 160°E with an angle of opening of 22° is better.

The revised pole was determined by trial and error, with primary control for the direction of the pole being the strike of the Tairoa fracture zone (admittedly ill defined), and the assumption that the anomalies either side of the fracture were orthogonal to the direction of motion. Distances between anomalies 5 and 25 throughout the area provided control for the distance of the pole from the area. Fig. 9.10 shows that the adopted pole position is more satisfactory than the previously assumed position. The angle of opening of 22° is based only on the distances from anomaly 25 to anomaly 5, but Fig. 9.11 shows that at least near the Tairoa fracture zone the rate of spreading was uniform within the 53 my interval.

Formation of the anomaly 5 to 25 area by rotation about a pole at 72°S, 160°E suggests several reasons for why anomaly lineations were identifiable in the east but not in the west. In the east the tracks were mostly orthogonal to the lineations and do not cross fracture zones, which simplifies the identification of lineations. West of about 175°W the strike of fracture zones would vary between N45°W and almost east-west. With predominantly

north-south tracks, lineations - if offset by such fracture zones - would be difficult to detect, especially as the shapes of anomalies in the area are not distinctive. Variations in spreading rates could also contribute to the differences between east and west. In the east, where the lineations are clear, the spreading rate is uniform and about 1.7 cm/y (Fig. 9.11). West of 175°W the rate would be of the order of 1 cm/y. It is frequently difficult to identify anomalies when spreading rates are low (Pitman and Talwani, 1972) especially if the topography is rough, as it is in the west.

In conclusion it can be said that for the interval 10 to 63 mybp a pole at 72°S, 160°E with a rotation of 22° not only satisfies most of what is known of the area, but also provides insight into why it has not been easy to identify structure throughout all of the area.

## 9.6 SOME APPLICATIONS OF PLATE TECTONICS TO THE SOUTHWEST PACIFIC AREA

### 9.6.1 Introduction

In Chapter 4 it was found convenient to describe the structure of the southwest part of the Pacific plate in three sections: the basin, the ridge system axis, and the area inbetween. These subdivisions reflected the contrasts in magnetic and bathymetric structure in the three areas. In the preceding sections of this chapter it has been shown that the structure of each of the areas can be explained by rotation about a different pole. The results are summarized in Table 9.2.

Table 9.2 Rotation data for the southwest part of the Pacific plate

| Anomaly span | Time span (mybp) | Pole position | Angle of opening | Angular rate deg/y x $10^{-7}$ |
|---|---|---|---|---|
| 1-5 | 0-10 | 70°S 120°E | * 5° | 5.3 |
| 5-25 | 10-63 | 72°S 160°E | 22° | 4.1 |
| 25-36 | 63-80 | 56°S 126°E | 12° | 7.1 |

* Half the total angle for anomaly 5 either side of the ridge; symmetry assumed.

In this section features within the southwest Pacific area will be compared with predictions based on plate tectonics theory, using the data in Table 9.2. Reconstructions of the continents will also be discussed. Before proceeding, the limitations need to be clearly recognized.

Movements in the area have extended over at least 80 my, but these movements are described by only three poles with uniform rotation rates for each pole. Whilst movement may take place about a fixed pole for a period

it is unlikely that the transitions between the poles would be by finite "jumps". Continuous movement from one position to the next is more probable. Continuous changes in rotation rate are also more probable.

The three intervals are marked by anomalies 5, 25 and 36, and the dates are referred to as 10, 63 and 80 mybp. The anomaly dates are more precisely defined but as they are not absolute, and the boundaries between the intervals are not exact, integer dates for the intervals are reasonable. Complete transition from one pole to the next, even within ±1 my of the dates, is not implied.

The pole position for the 0-10 mybp interval is based on the whole Pacific-Antarctic boundary, and so assumes rigid behaviour of the Pacific and Antarctic plates in the area, at least for that interval. The poles for the other two intervals apply only to the Pacific plate west of the Louisville ridge, and they assume rigid plate behaviour of that area. The presence of more plates in the area, or non-rigid plate behaviour, clearly could affect both the pole determinations and any conclusions drawn from them.

### 9.6.2 Structure in the southwest part of the Pacific plate

This sub-section could be described as a pot pourri of observations. Some of them possibly trivial, others possibly very significant for this and other areas. All of them could be discussed more fully but they have not yet been investigated thoroughly.

Hayes and Ewing (1971) have described the Louisville ridge as a semi-continuous feature from the Tonga-Kermadec trench to the Eltanin fracture zone (Fig. 0.1). They have fitted it to a pole at $5^{\circ}N$, $120^{\circ}W$. However Fig. 9.3 shows that the ridge at its southern end fits the southwest Pacific poles rather well. Its detailed relationship to the Eltanin fracture zone is not clear, as the fracture zone consists of several fractures and the whole zone has a width of at least 200 km. In places the reported positions of the Louisville ridge also extend across 200 km.

The width (~ 200 km) and length (~ 1000 km) of the whole Eltanin fracture zone is similar to that of the whole Pacific-Antarctic fracture zone, and both consist of several shorter fractures striking across the trend of the whole feature.

The Tairoa fracture zone is the only major fracture in the southwest Pacific basin with a dextral offset. It is also the only one traceable from the southwest Pacific basin to the ridge axis. South of the ridge anomaly 12 is dextrally offset across where a theoretical continuation of the fracture zone goes through (Fig. 9.3). The offset there, ~320 km, is similar to the 310-350 km offsets observed between the ridge axis and

anomaly 31 in the southwest Pacific basin. Further north the offset may be only 150-200 km. Continuation of the fracture zone northward on the 25-36 trend shows it passing close to the end of the Chatham rise.

The changes from one pole to another involve changes in the directions of fracture zones, or more generally changes in the direction of spreading. Changes in rate also occur. Fig. 9.3 shows that for the change at anomaly 25 the direction changes are marked, especially in the west. At the Tairoa fracture zone the direction change is $25^{\circ}$ and the rate decreases (coming forward in time) from 4.5 to 1.7 cm/y. In the west the direction changes are up to $70^{\circ}$, with rates decreasing from about 3 to 1 cm/y. The bathymetric contrast across the anomaly 25 boundary has been noted previously (section 4.5) and the increase to the west in the contrast (Fig. 9.7) probably reflects the increase in the severity of the direction changes.

It is unlikely that changes in movement, especially in direction, would take place in a very short time or could be accommodated in a short distance. In the east, anomalies 25 and 26 are very clear and anomalies 20-23 are reasonably clear, but there is some difficulty inbetween (section 4.5). This may indicate that the major changes took place between anomaly 25 (63 mybp) and anomaly 23 (59 mybp). West of the Tairoa fracture zone (Fig. 9.10) the gradual changes of anomaly trends suggest either a slower change of pole position or a slow readjustment. The marked change shown in the trend of the Tairoa fracture zone is diagrammatic; data are insufficient to define the precise trend.

The changes at anomaly 5 are less than at anomaly 25 (Fig. 9.3). In the east the direction changes are less than $5^{\circ}$, which probably explains why there are no marked contrasts at around anomaly 5. Near the Tairoa fracture zone the expected increase in rate from 1.7 to 3.3 cm/y (coming forward in time) is seen (Fig. 9.11). Near the eastern end of the Pacific-Antarctic fracture zone the direction change is $25^{\circ}$ and the rate increases from 0.9 to 2.8 cm/y. The greater direction change may account for why anomalies beyond number 5 are not clear there.

At places where there are fracture zones changes in movement may be important over longer intervals than normal. For example at the Tairoa fracture zone anomaly 25 on the west is opposite 71 mybp seafloor, while on the east it is opposite 55 mybp seafloor. Consequently a change occurring at about anomaly 25 (63 mybp) could affect crust in the interval 55 to 71 mybp.

Fig. 9.12 shows three sets of arcs which were initially drawn just for interest but which proved instructive. Each arc can be considered a hypothetical fracture zone for the interval 0 to 80 mybp. The anomalies should be orthogonal to the arcs. They clearly show the major change at anomaly 25

with lesser effects at anomaly 5. The two eastern lines also show that the rotations fit the anomaly positions very well. Details of each line are of interest.

The eastern-most one starts at the western side of the aseismic Hangu fracture zone (section 4.4.2) and so should be a fracture zone throughout. There is no fracture zone between anomalies 25 and 32 where the arc goes through, but that is the area where there is the "stretching" between anomalies 29 and 31. The arc is not far from the "irregular" Toarahi fracture zone, and it was this diagram which initiated the re-examination of that area discussed in section 9.4.3.

The centre line (Fig. 9.12) starts from the western end of the fracture zones that have been inferred at 160°W from epicentres alone. It, too, should be a fracture zone throughout. In the area where it intersects anomaly 25 the anomalies 25 and 26 are not very clear and there is some bathymetric disturbance. Further north it passes close to the "irregular" Waimori fracture zone.

The western-most line starts from the eastern end of the Pacific-Antarctic fracture, close to a very tentative identification of the spreading axis. The "misfit" of the line to the anomalies indicates that the ridge is "too far south". The trend of the line towards the end of the Auckland slope is interesting. Of greater interest is the parallelism to the overall trend of the Pacific-Antarctic fracture. Fig. 9.13 shows the area in detail. The arc for 10 to 63 mybp is quite close to the overall trend of the fracture zone. Even if there was a regular transition of the pole from the 0-10 mybp position to the 10-63 mybp position arcs would be between those shown. The arc orientations, and the amount of rotation (Fig. 9.12) show that for up to 63 mybp the Pacific-Antarctic fracture zone area could have been primarily a fracture zone boundary. This could explain the size and complexity of the feature.

### 9.6.3 Fracture zone offsets and asymmetrical spreading

All the fracture zones on the Pacific-Antarctic ridge have dextral offsets; all the major fracture zones in the southwest Pacific basin, except the Tairoa, have sinistral offsets. This observation led to a brief study of how the differing offsets might have arisen in an area in which the rotations appear relatively uniform.

Anomaly offsets across a fracture are normally considered as originating at an offset in the ridge axis (Fig. 1.5). The anomaly offset is equal to the offset of the ridge and irrespective of spreading rate or pole position all anomalies produced will have the same offset, provided the offset of

the ridge stays the same. The southwest Pacific data indicate that in upper Cretaceous times the ridge offsets were sinistral but since then they have changed to dextral.

Change in the offset of a ridge can be produced by two uniformly separating plates if there is some asymmetrical spreading on at least one side of a fracture zone. Fig. 9.14 shows this schematically. At times 1 and 2 the two plates are moving apart at 4V with symmetrically spreading ridges moving at 2V relative to the left plate. Sinistrally offset anomalies are produced either side of the ridge. At time 3 the upper ridge starts moving at 3V relative to the left-hand plate. This gives asymmetrical spreading: 3V to left, V to the right. The lower ridge continues spreading symmetrically at 2V either side. The upper ridge is moving right with respect to the lower ridge at velocity V. By time 4 the ridges are not offset at all, and subsequently the original sinistral offset becomes dextral. By time 6 there are anomalies on the left and right which show offsets that are sinistral, dextral and zero. Throughout the whole sequence the only relative motion is between the offset ridge axes, and the sense of movement there is still that of a conventional fixed offset ridge-ridge transform.

The schema in Fig. 9.14 has obvious applications to the southwest Pacific area, as it shows how the Cretaceous sinistral offsets could be linked with the present dextral ridge offsets. The amount of asymmetry required is very small as most of the observed offsets are of the order of 100 km. A spreading rate difference of only 0.25 cm/y would change a 100 km sinistral offset into a 100 km dextral offset in 80 my. Weissel and Hayes (1971, 1972) have documented differences of up to 0.9 cm/y south of Australia.

In nature the situation could easily be more complex than shown in Fig. 9.14. It isn't necessary that the spreading be symmetrical on one section; all that is required is that the asymmetry be different across the fracture. If a ridge was initially straight it could become offset - this appears to have occurred south of Australia. When two offset ridges become straight the shift of the fault to somewhere else might be favoured. Asymmetry could start, stop, or reverse at various times.

It is clear that even slight asymmetry can produce variable offsets on fracture zones, small sections with opposite offsets, disappearance or appearance of fracture zones, and shifts in the ridge axis. An important point is that none of this violates the basic concepts of plate tectonics, as there is no deformation within the separating plates. Plate tectonics does not require symmetrical spreading.

### 9.6.4 Continental reconstructions

At the margin of the Chatham rise with the southwest Pacific basin there are some basement complexities which may reflect movement between the Chatham rise and the basin south of anomaly 36. At the Campbell plateau margin there are no indications of relative motion between the basin and the plateau, so the plateau can be considered fixed to the oceanic seafloor. As the plateau is part of the New Zealand continental block, the southwest Pacific basin seafloor can be considered to have formed by seafloor spreading arising from relative movement between the continental block and the axis of a spreading ridge. The history of the relative movement is recorded in the seafloor so it is possible to reconstruct the movements. The age of the seafloor at the margin is 81-83 mybp so the relative movement back until then can be determined.

The Antarctic continental margin also appears to be passive so it would be possible to reconstruct the movements between Antarctica and the ridge. The movement of Antarctica relative to the Campbell plateau (loosely referred to as New Zealand) could then be determined. It is not however possible to do this with any certainty because there are insufficient data south of the ridge to determine the movements between Antarctica and the ridge.

If it is assumed that the ridge has not changed shape and that seafloor spreading has been symmetrical it would be possible to determine the movements between New Zealand and Antarctica from only the data north of the ridge. However the results discussed in the previous section indicate that the ridge has changed shape and that an easy way for this to have occurred is by asymmetrical spreading with the rate faster on the north side of the ridge. Fig. 9.14 shows that with data from only the left-hand plate (analagous to the Pacific plate) an assumption of symmetrical motion would over-estimate the movement between the plates, if the data were from an asymmetrical section. An estimate from a symmetrical section would be correct, but the changing offsets can also be produced without any symmetrical sections.

It is difficult to determine how much asymmetry there might be in the southwest Pacific. For the interval 0-10 mybp data are too few west of 160°W, but east of there there are adequate data for both sides of the ridge. At the Hangu fracture zone at 150°W (Fig. 4.18), spreading for anomalies 1 to 5 is symmetrical west of the fracture, but to the east it is 12% faster on the south side. Further east on the boundary (Fig. 2.12) there are places at which the rate is up to 20% (~1cm/y) faster on the south side. Faster spreading on the south is opposite to what is required for the change from sinistral to dextral offsets.

Herron (1971, 1972) has suggested that for the period prior to anomaly 5 the Eltanin fracture zone-Louisville ridge line may have been a plate boundary. That is, the spreading east of the line may have involved different plates from that to the west. It is difficult to prove, so as a conserveative approach only the area west of the Louisville ridge will be considered for prior to 10 mybp. Either side of the Tairoa fracture zone the spreading rate to anomaly 12 is the same north and south of the ridge, which is what would be expected from the relatively uniform offsets along the fracture. Further east the rate to anomaly 25 could be 10% higher on the south side.

For the anomalies prior to number 25 there are no data south of the ridge, and conclusions from the southwest Pacific basin are difficult. Offsets on the Matua and Pahemo fracture zones are constant, on the Rangirua they decrease to the south, and on the Tairoa and Kohiku they increase to the south.

There are obviously considerable spreading rate irregularities throughout the area, which makes it difficult to reliably reconstruct the relative plate movements in the area. However it is of interest to attempt a reconstruction and this has been done. Clearly acknowledging the uncertainty it has been assumed that spreading has been symmetrical throughout the last 80 my. The data for only the Pacific side (Table 9.2) are then sufficient.

Before proceeding, the frames of reference need to be stated. The poles shown in Fig. 9.3 and listed in Table 9.2 are determined from data in the Pacific plate, so fracture zones in the Pacific plate fit those poles. The poles are relative to the Pacific plate. Fracture zones in the Antarctic plate produced by rotation about the same ridge will not fit the Pacific poles, because of rotation of the coordinate system of the poles. Fig. 9.15 shows sample fracture zones based on the Pacific poles being fixed relative to the Pacific plate and the Pacific rotating away from Antarctica. When it is recalled that an arc north of the ridge for a particular interval would originally have formed a continuous small circle with the similar arc to the south, the effects of the plate rotations can be fully appreciated. The effects are particularly marked in this area because the poles are so close to the area.

The poles for the Antarctic fracture zones in Fig. 9.15 are found by rotating the Pacific poles. The anomaly 1 to 5 pole is the same for both; $70^{\circ}S$, $120^{\circ}E$. The 5-25 Antarctic pole is the 5-25 Pacific pole rotated $10^{\circ}$ about $70^{\circ}S$, $120^{\circ}E$, which gives $74^{\circ}S$, $161^{\circ}E$. The 25-36 Antarctic pole is the Pacific 25-36 pole rotated $10^{\circ}$ about $70^{\circ}S$, $120^{\circ}E$, then $44^{\circ}$ about $74^{\circ}S$, $161^{\circ}E$. Anticlockwise rotations about the Antarctic poles will describe the motion of New Zealand with respect to Antarctica. Reversing the rotations will reconstruct the former position of New Zealand with respect to Antarctica. Fig. 9.16 shows the reconstruction for anomaly 36 time (~ 80 mybp). The required poles and angles are given in Table 9.3.

Table 9.3 Rotation data for the movement of New Zealand relative to Antarctica

| Anomaly span | Time span (mybp) | Pole position | | Rotation angle |
|---|---|---|---|---|
| 36-25 | 80-63 | 53°S | 155°E | 24° |
| 25-5 | 63-10 | 74°S | 161°E | 44° |
| 5-1 | 10-0 | 70°S | 120°E | 10° |

Considering the assumptions required to obtain the reconstruction shown in Fig. 9.16 there is little point in very detailed discussion of it. Some general comments are however in order.

that there may have been a large component of shear when New Zealand and Antarctica separated. The initial direction of motion between New Zealand and Antarctica is shown by the fracture zones at the Antarctic margin in Fig. 9.15. Although there are components of shear the motion is primarily directly away from the margins. The basement difference may instead be due to different thermal conditions at break-up. It is noticeable that there are magnetic quiet zones at the Australian and east Antarctic margins but not at the New Zealand margin. This might reflect thermal differences. Quiet zones may also be related to thick sediment, which is present off Australia and east Antarctica but not off New Zealand. Magnetic data from the Ross shelf margin east of Iselin bank would be interesting as the basement depth and sediment thickness there is intermediate between that of the Campbell plateau and that of the Australian-Antarctic margins (section 2.3).

Quantitative reconstructions of New Zealand and Antarctica have also been given by Christoffel and Falconer (1973) and Hayes and Ringis (1973). The Christoffel and Falconer one (Fig. 9.17) is based on the three anomaly intervals used for Fig. 9.16. For the anomaly intervals 1-5 and 5-25 the poles and angles were similar to those used here, but for 25-36 the pole was in the equatorial eastern Pacific. It is not now considered that that pole is reliable, but it is interesting that such a divergent pole produces a plausible reconstruction.

The Hayes and Ringis (1973) reconstruction (Fig. 9.18) was constructed as follows. The Tasman basin opened between anomaly 36 and anomaly 24 (section 2.6) so closing up this gave the position of western New Zealand and the Lord Howe rise relative to eastern Australia at anomaly 36 time. Australia, with New Zealand attached, was then closed to Antarctica, and finally eastern New Zealand was moved along the Alpine fault 480 km northwards with respect to western New Zealand. The resulting indirectly determined position of the Campbell plateau with respect to Antarctica should be valid for anomaly 36 time. It is clear that it differs considerably from that determined more directly from the southwest Pacific data (Fig. 9.16). If the Fig. 9.16 position for the Campbell plateau-Chatham rise area is correct, and the Hayes and Ringis position for western New Zealand is also correct, there must have been substantial gaps between parts of New Zealand at 80 mybp.

Another reconstruction is shown in Fig. 9.19. It is not based on any quantitative method but it would not be difficult to achieve by plausible rotations. The reconstruction was done by fitting the Campbell plateau to Antarctica in a position that avoids overlaps of continental areas. An unintentional by-product is that closing up the Bounty trough by rotation of the Chatham rise towards the Campbell plateau brings the western end of the

Chatham rise nicely against the Antarctic continent. Bollons seamount can, with only a small amount of movement with respect to the Campbell plateau, "fill up" the small gap between the major continental areas. Orphan Knoll, a feature off Newfoundland similar in form to Bollons seamount, has been shown to be continental (JOIDES, 1970). Bollons seamount could be a similar continental fragment, so it is appropriate to retain it in the continental reconstruction. It is probably related to the formation of the Bounty trough and it fits well in the area.

The south Tasman rise is another continental fragment (JOIDES, 1973d). For clarity it was omitted from Fig. 9.18 but if retained in its present position with respect to Australia it overlaps Iselin bank and part of the Ross shelf. There is plenty of room for it in any of the reconstructions offered, if either it or Iselin bank is permitted to move relative to the major continental areas. The margins of the south Tasman rise (Houtz and Markl, 1972) and the western side of Iselin bank (Houtz and Davey, 1973) are complex, which may reflect complex movements of these features.

In the reconstructions shown Antarctica has been kept stationary at its present position. This is somewhat arbitrary as the seafloor data provide information on only the relative movements. Paleomagnetic data (Francheteau and Sclater, 1969; McElhinny, 1973b) suggest that east and west Antarctica have been within 5-10° of their present latitudes since the upper Cretaceous so major movement of Antarctica does not seem likely.

Hayes and Ringis (1973) noting their overlap of the Campbell plateau onto west Antarctica (Fig. 9.18) suggested that relative movement between east and west Antarctica would remove the inconsistency. The reconstruction shown in Fig. 9.16 is probably more reliable for the Campbell plateau relative to west Antarctica. It too shows some overlap, but only a small amount of movement of west Antarctica would remove the overlap. The reconstructions all however have limitations, mainly due to insufficient data, and they cannot be considered definitive. Movements between east and west Antarctica are not as yet "demanded" by the seafloor data.

## 9.7 SOUTHWEST PACIFIC MOVEMENTS AND MOVEMENTS ELSEWHERE

### 9.7.1 Introduction

The previous sections have been primarily concerned with the structure of the southwest part of the present Pacific plate, and relative movements between the New Zealand and Antarctic continents. At present the New Zealand-Antarctica movement is part of the movement between the Pacific and Antarctic plates. It is possible that prior to 10 mybp the southwest Pacific basin and

New Zealand were separate from the large Pacific plate; the boundary being along the Louisville ridge. Movements west of the ridge would then be part of the movement between the Antarctic plate and a smaller southwest Pacific plate. These movements can be described from data in the area without considering other areas. However one of the important aspects of plate tectonics is that with the earth's surface consisting of several rigid plates, two plates cannot move in isolation. The movements of two plates influence, and can be influenced by, movements of at least some of the other plates. It is therefore worth considering the southwest Pacific movements in relation to other movements. A geometrical analysis would be difficult but a consideration of just the timing of movements is relatively easy and provides valuable information.

### 9.7.2 Plate movements in the southwest Pacific area

The structure of the southwest part of the Pacific plate, and the movements between New Zealand and Antarctica are probably most influenced by plate movements in the immediate area. Several interesting inter-relationships are apparent.

At about 81-83 mybp (just prior to anomaly 36 time) the Campbell plateau and the Chatham rise were adjacent to west Antarctica, the exact details of New Zealand are unclear but most of the Tasman basin was closed up, and Australia was adjacent to east Antarctica. Larson and Chase (1972) consider that east of the Louisville ridge there has been spreading between the Pacific and Antarctic plates since 150 mybp, so at 83 mybp motion had been taking place east of the New Zealand-Antarctica-Australia block for some time. The motion apparently slowed down very considerably at about 82 mybp* (Larson and Pitman, 1972). This time coincides with the start of separation of the Campbell plateau from west Antarctica. The Chatham rise may have prior to then moved a little relative to west Antarctica and the Campbell plateau to open up the Bounty trough, or it may have moved relative to the Campbell plateau as the major separation from west Antarctica began. However the Campbell plateau and Chatham rise predominantly move together, starting at 81-83 mybp. At the same time the Tasman basin also started to open, separating the Lord Howe rise and western New Zealand from eastern Australia.

After 82 mybp movements in the southwest Pacific and the Tasman basin continued smoothly for about 20 my. Then at about 63-58 mybp (anomalies 25-23) there was a change in the southwest Pacific: the rotation pole shifted and

---

*Larson and Pitman (1972) give the date of this change as 85 mybp, on the basis of their extension of the reversal time scale. In section 6.3.3 it was shown that their scale needs revision, which brings their date of 85 mybp to about 82 mybp.

the spreading rate slowed. At the same time the Tasman basin stopped spreading. Between Australia and Antarctica the oldest identifiable anomaly is 21 or 22 (~ 55 mybp) but there is a gap of 300-400 km. With the spreading rate at anomaly 21 time the gap would represent 6-8 my so Australia and Antarctica may have started to separate at close to 60 mybp, coincident with the halt in the Tasman basin and the changes in the southwest Pacific.

After 60 mybp movements between Australia and Antarctica and New Zealand and Antarctica continued smoothly for about 50 my. Then at about 10 mybp (anomaly 5) there were several changes. The pole for the southwest Pacific moved again and the spreading rates increased. The Australian-Antarctic pole, which had been moving smoothly, changed direction, and spreading rates increased (Weissel and Hayes, 1972). East of the Louisville ridge there were some changes and it appears that from then on the southwest Pacific did not move separately from the major Pacific plate. In New Zealand the major movement on the Alpine fault may also have commenced at about 10 mybp.

### 9.7.3 Global plate movements

It is clear that the major changes in movement of the southwest part of the Pacific plate are associated with major changes in plate movements in the whole southwest Pacific area. A brief survey of the literature indicates that there may be synchronous changes throughout the world.

Some major events at 81-83 mybp are as follows. Changes in the directions of movement between America and Europe, and America and Africa (Pitman and Talwani, 1972). Slowing of spreading in the south Atlantic (Mascle and Phillips, 1972). Labrador sea starts to open (Le Pichon et al., 1971c). Tasman basin starts (Hayes and Ringis, 1973). Changes of movements in the central Pacific (Larson and Chase, 1972). Changes of directions in the northeast Pacific (Vacquier, 1972). Change from extremely fast to average rates for Pacific-Antarctic spreading (Larson and Pitman, 1972). Separation of New Zealand from Antarctica.

At about 60 mybp the following events are reported. Spreading in the Indian ocean slows down (McKenzie and Sclater, 1971). Changes in movements between America and Europe, and America and Africa (Pitman and Talwani, 1972). Labrador sea ceases or slows (Le Pichon et al., 1971). Norwegian sea starts (Avery et al., 1968). Changes of direction in the northeast Pacific (Atwater and Menard, 1970; Peter et al., 1971). Changes on the east Pacific rise (Herron, 1972). Tasman basin stops (Hayes and Ringis, 1973). Australia separates from Antarctica (Weissel and Hayes, 1972). Changes in the southwest Pacific.

Some major events at 10 mybp are as follows. Reorganization on the Chile ridge (Herron and Hayes, 1969). Changes on the east Pacific rise (Herron, 1972). Increase in spreading rates throughout the Indian ocean (McKenzie and Sclater, 1971). Changes in the northeast Pacific (Atwater and Menard, 1970; Chase et al., 1970). Changes of direction in the north Atlantic (Pitman and Talwani, 1972). Spreading rates change south of Australia (Weissel and Hayes, 1972). Changes in the southwest Pacific.

There are changes in various places at times other than 82, 60 and 10 mybp, but in most areas the most significant changes are those that occurred close to those times. The change at 82 mybp is very major as it involves virtually all of the Pacific and Atlantic oceans, and is a change from very rapid movements (up to 18 cm/y) to more normal rates (3-6 cm/y). Larson and Chase (1972) have pointed out that the period of rapid movements (~ 125 to 82 mybp) coincides with extensive volcanic and tectonic activity in the circum-Pacific area. The change near 60 mybp is probably the most widely referred to event, and it is interesting to note that it is close to the Cretaceous-Tertiary boundary - a major geological and evolutionary boundary.

### 9.7.4 Causes of movement

The marine geophysical data in the southwest Pacific area provide a reasonably good picture of the structure of at least the oceanic area. With the aid of plate tectonics it is possible to reconstruct movements in the area and understand some of the tectonics of the area. Knowledge of the movements does not, however, explain the origin of them. It is clear that the southwest Pacific movements could be described as being a response to movements elsewhere, but that does not help explain why such movements occur. The basic causes of plate movements and the driving forces for them are subjects of considerable interest, but they have not been a part of this study. Some of the structure in the southwest Pacific area is however of interest with respect to possible causes of plate movements.

Mantle plumes (section 1.3.4) have been suggested as a driving force for plates. The locations of the plumes can be inferred from the presence of volcanic activity away from the mid-ocean ridge crest (e.g. Hawaii) or pronounced activity at the crest (e.g. Iceland). Morgan (1972a, b) has noted the presence of the volcanic Balleny Islands and assumed a plume in the area. The unusually large number of seamounts in the Balleny basin supports the idea of pronounced volcanic activity in the area. So, too, does Scott Island and the very large features near to it.

Regional depths also support the idea of a plume in the area. Morgan (1972a, b) concludes that one feature of places where plumes are evident

is that seafloor depths are shallower than usual, presumably because of the thermal upwelling. The section of the southeast Indian ridge adjacent to the triple junction increases in depth away from the axis in a similar way to typical midocean ridges (Fig. 1.7), but the depth of the whole feature is abnormally shallow. The ridge axis near 170°W (Fig. 4.24) also has the "right shape" but is 400-500 m shallower than normal. The depth to basement in the Balleny basin is 3 to 4 km, and the depth-age relationship (Fig. 1.7) suggests an age of less than about 15 my for this depth. Anomalies back to 10 my are very clear north of the Balleny Islands. It is likely that much of the basin further southeast was also produced by seafloor spreading from the southeast Indian ridge, and so would be considerably older than 10 mybp. A JOIDES site in the east of the basin (Fig. 2.2) yielded an age of at least 40 mybp. The depth throughout the basin therefore seems to be shallower than would be expected from its probable age. This is further support for the idea of a plume in the area.

It is difficult to determine how long such a plume would have been active and how much effect it would have on plate motions in the area. An interesting observation is that Morgan (1972b) suggests that asymmetrical spreading will occur if there is spreading from a plume-fed ridge, and one of the plates is not free to move away from the plume (Fig. 1.6). Weissel and Hayes (1972) have noted that the eastern-most sections of the southeast Indian ridge (those nearest the triple junction) are too far south to permit symmetrical spreading either side of the ridge for the time interval represented in the anomalies north of the ridge. The schema in Fig. 1.6C suggests that if the Antarctic plate has been stationary for some time and the Balleny plume is stationary with respect to the mantle, symmetrical spreading would not be expected. Spreading that was asymmetrical but not completely one sided would lead to the observed configuration of the ridges.

Plumes are believed to be the origin of many linear chains of seamounts, and the Louisville ridge does appear to be either a long chain of seamounts or a discontinuous ridge of volcanic origin. It is possible that it is related to a plume, presumably at its southern end in the vicinity of the major Eltanin fracture zone. The origin of the Louisville ridge may, however, lie in activity associated with its suggested role as a major plate boundary. Ridge depths in the area of the Eltanin fracture zone are not shallow which tends to support a non-plume origin of the Louisville ridge.

These brief discussions of the Balleny plume and the Louisville ridge are illustrations of contributions that the concept of plumes could make towards a better understanding of the structure of the southwest Pacific area. and the reasons for that structure. Equally well the knowledge of the

structure of the area could contribute much towards understanding plumes and their effects. In particular it would be of interest to know whether or not the structure and plate movements will indicate how long a plume may have been active in the area. A knowledge of this could provide information on the general problem of how much effect the initiation and continued activity of any plume has on plate movements.

# CHAPTER 10

## REVIEW AND FUTURE WORK

This chapter is a very brief review with comments on possible future work. It is not intended to be a complete review, neither is it intended to be a complete list of possible work. The structure of the area is discussed first (10.1) then the special studies that were part of the overall study are discussed: numerical correlation (10.2), magnetic anomaly model studies (10.3), the b value study (10.4), and the epicentral method (10.5).

### 10.1 Southwest Pacific structure

The geophysical data available for this study have made it possible to describe the structure of the southwest part of the Pacific plate in more detail than was previously possible, and the Indian-Antarctic-Pacific triple junction can also be better understood. There is no point reviewing all the findings here as they have been discussed in the previous chapter. With respect to possible future work, two main areas can be suggested. One is the collection of more data in the area, the other is further work on the available data.

First, the collection of more data. Two approaches are possible and both would be useful. One is very detailed work in small areas, the other is more reconnaissance surveying. The latter could be accomplished quite effectively from ships in transit through the area. There are large gaps in track coverage between about 170°W and 155°W and data from this area would considerably assist in deciphering the area north of the ridge between anomalies 5 and 25. A single zig-zag track in the ridge crest area near 160°W (Fig. 4.21) would be a good test of the whole principle of plate tectonics, as it is possible to predict for that area the almost exact location and strike of the ridge crest sections, and the amount of offset of them. A few tracks across the Pacific-Antarctic fracture zone just east of the triple junction would also considerably improve knowledge of that important boundary. It is obvious that any tracks south of the Pacific-Antarctic ridge east of 180° would be very useful. That area should be a top priority area for any reconnaissance work as without a knowledge of the older anomalies in the area it is difficult to assess various possible reconstruction positions of New Zealand and Antarctica.

Detailed surveys of smaller areas would also be very valuable as it is fair to say that nowhere is there a detailed knowledge of the small scale structure. There are too many areas of interest to discuss them all here but the following appear most profitable. The Louisville ridge: Is it really

continuous? What is the age of various sections and what is the petrological nature? These are important for the hotspot origin. How extensive is the flat basement and is it basement or ash? Are there anomaly lineations east of it? If so, they could be in the important normal interval beyond 82 mybp. The Bollons seamount: Where is it and what is its extent? Is it continental? Dredging might show but drilling seems to be the only conclusive means. What are the precise trends and offsets of the anomalies just east of it at the Toarahi and Rangirua fracture zones? The Pacific-Antarctic fracture zones: detailed surveys are required to verify the existence of the predicted short sections of spreading ridge, micro-earthquake surveys would provide valuable data on the probable fracture zone trends. Micro-earthquake surveys on the Macquarie ridge complex would also be very useful. The western termination of the southwest Pacific Cretaceous anomalies also needs to be determined to understand the boundary between the southwest Pacific and the Emerald basin area. A better knowledge of the Emerald basin-Solander trough area is vital to the continental reconstructions.

Much valuable work can be done without collecting any more data. The data could well be looked at again in the light of the plate tectonics conclusions given here. The structures mapped here were not based on plate tectonics conclusions, and the approach taken was conservative. It may be possible to detect trends in some areas when possible trends have been suggested. In particular the data between the Pacific-Antarctic fracture zone and the southwest Pacific basin could be examined with the idea of fracture zones trending very obliquely across the area. The data in the Balleny basin could also be re-examined. In both of these areas a three-dimensional perspex model like that used by Christoffel and R.F. Falconer (1973) would be very useful. Poles of rotation could be determined in shorter time intervals (T.M. Geddes is starting this). New Zealand Oceanographic Institute are working on some of the bathymetric maps for the Pacific-Antarctic fracture zone and the completion of detailed maps for all the area is very important.

## 10.2 NUMERICAL CORRELATION

The numerical correlation studies described in Chapter 5 were aimed at studying the application of numerical techniques to correlation of magnetic anomalies. The results are applicable to any correlation problem. The main conclusions reached were that the exact form of correlation coefficient is probably not important, and that horizontal scale variations and any missing or duplicated sections can have a critical effect. The use of short sweeping sections partially overcomes the problems of missing sections, and variable length correlation can overcome scale variations. Statistical uncertainty

estimates based on the autocorrelation functions of the records appear to be reliable and quick estimates based on the number of maxima are probably adequate.

The numerical techniques appear to be well suited to the situation where one profile is controlled, such as in a model study where it is desired to find the model that best fits the data. Numerical correlation techniques should be applied to the final results of the sophisticated model studies and profile manipulations that are now being published. Numerical correlations can also be used to more objectively assess symmetry in profiles. Since a symmetry study would usually involve fewer profiles than general correlation studies a rigorous analysis can be done in a reasonably short time. Overlapping long and short sweeping sections could be used, coupled with variable horizontal scaling and completely quantitative error estimates. Some form of estimate should accompany all correlation results.

## 10.3 MAGNETIC ANOMALY MODEL STUDIES

The magnetic anomaly model studies presented in Chapter 6 were really a series of separate studies, but all were based on the same model of normally and reversely magnetized blocks. The model was critically discussed and although recognized as simple it was considered useful. The results obtained support the simplified approach.

First a revised and extended geomagnetic reversal time scale for the upper Cretaceous was presented. The validity of dating anomaly 33 and the extension to anomaly 36 and a reverse interval beyond it have been confirmed by the independent recognition of these features by McKenzie and Sclater (1971) and Larson and Pitman (1972). The briefness of anomaly 33 (0.05 my) places constraints on models of the mode of formation of the seafloor and of the thickness of the magnetized layer. It also supports other evidence for short polarity intervals in the lower Tertiary and upper Cretaceous; it has been thought that short intervals were not present. The uniformity of the southwest Pacific Cretaceous anomalies suggests that they would be useful for further refinements of the reversal time scale and the detection of other short polarity intervals, using the profile averaging and processing techniques of Blakely and Cox (1972a, b).

The possible positions of formation of the Cretaceous anomalies were briefly studied, but the results were not very conclusive. The more sophisticated techniques now available could be more useful.

The thickness of the magnetized layer was studied and it was concluded from several lines of evidence that a layer thickness of at least 2 km would

be most suitable. This is somewhat thicker than is frequently assumed. Deepsea drilling at least 2 km into the basement at many sites could help resolve the issue, but model studies of anomalies away from the ridge axis elsewhere would be easy to do and would partially check the conclusions reached from the southwest Pacific.

Variations in anomaly amplitudes within the area were shown to exist. Similar variations have been documented south of Australia. Further studies elsewhere could confirm whether the variations are produced at the time of formation, or subsequently, or whether they reflect petrological differences. The anomalies between numbers 5 and 25 have amplitudes considerably less than would be produced if the magnetized layer properties were similar to those of the older anomalies. Global studies of relative amplitudes in anomaly sequences could determine whether such effects are due to total field variations.

## 10.4 THE b VALUE STUDY

Earthquake magnitude - frequency relationship b values were determined for the plate boundaries in the southwest Pacific area. The northern and central Macquarie ridge complex was found to have a low b value (~ 0.9), while all the other areas had high b values (~ 1.6). Comparison with results from the mid-Atlantic ridge showed that contrary to previous suggestions b values are not determined by: the nature of the boundary - ridge or fault; the type of faulting - normal or strike-slip; clustering or non-clustering. An association of high b with high temperature and low b with low temperature is indicated.

The b value study is one study which is readily amenable to further work. It is planned to repeat the study with the International Seismological Centre (ISC) data which are probably more consistent than the USCGS data used. Statistical uncertainties due to lack of data made useful comparisons of individual fracture zones difficult, but more data are becoming available all the time. It should soon be possible to check the suggested b value - temperature relationship by considering a series of fracture zones that have different crustal ages juxtaposed. This should give a range of temperature environments.

## 10.5 THE EPICENTRAL METHOD

In Chapter 8 a new method for determining poles of rotation was presented. The only data required are epicentre locations from one or more transform faults. An application of the method to the Macquarie ridge complex showed that the whole feature south of about 49°S could be considered a single transform fault boundary. This yielded a very tightly defined Indian-Pacific pole

position - the first quantitative determination of this pole position not based on other poles. The Pacific-Antarctic and Indian-Antarctic poles were also independently determined. According to plate tectonics theory the three poles should form a consistent set, and they did.

The results obtained with the method are in agreement with independent data on the three boundaries. The Pacific-Antarctic results highlighted the difficulties of interpreting the Pacific-Antarctic fracture zone but provided valuable quantitative support for the interpretation of the area, and other determinations of the Pacific-Antarctic rotation pole.

The method yields effectively instantaneous poles, and comparisons with pole positions determined by other methods yield information on movements of the poles during the last 10 mybp. This feature of the method is of considerable interest. Further applications of the epicentral method to poles elsewhere in the world should confirm whether it is possible to reliably investigate pole movements this way.

The method also provides some information on the processes occurring at transform faults as it yields quantitative values of the scatter of the earthquake activity. The results obtained suggest that the activity is in general very closely confined to a single line. Applications of the method to only well located epicentres should not only verify this but should provide much better located pole positions.

The epicentral method needs more study, particularly the aspects of weighting individual fracture zones, and determining the best parameter to use for statistically assessing the confidence area of the pole position. One of its main advantages is that continual improvements in pole positions will be possible as more data and better locations become available. The method has already provided some predictions which have important implications for the southwest Pacific area. It appears probable that it can become an important new tool for investigating plate movements and tectonics of plate boundaries.

---

This thesis is a contribution towards a better knowledge and understanding of the southwest Pacific area. The area is only a small part of the earth's surface but it is hoped that the study will also contribute to a better understanding of the whole earth.

---

# APPENDIX 1A

## BIBLIOGRAPHIC NOTE ON THE VINE AND MATTHEWS HYPOTHESIS

The hypothesis that the magnetic anomalies observed at sea are caused by normally and reversely magnetised blocks clearly originates with Vine and Matthews (1963). However they did not state the important corollary that the anomalies could be used to date the seafloor nor did they explicitly state that symmetrical anomalies would be produced.

Morley and Larochelle (1964) very clearly state the same hypothesis as Vine and Matthews (1963) and they note that Morley stated it at a conference in 1963. They give the corollary of determining reversal dates from magnetic anomalies (not stated by Vine and Matthews) and they also give a further important extension. They state

> "If this figure (seafloor spreading rate) could be determined accurately for the various geological periods, it would then be possible using the data from a magnetometer survey of the ocean basin floors to reconstruct not only the history of reversals of the earth's field but also the direction and rate of the drift of the continents."

There is an earlier account which although not very explicit suggests the possibility of determining the age of seafloor from anomalies. It is in the Geomagnetism section of Operation Deep Freeze Report 61 (U.S. Navy Hydrographic Office, 1962) written by R.H. Higgs and R.W. Seaton (Higgs, pers. comm. 1973). After noting magnetic lineations parallel to the Pacific-Antarctic Ridge and in places an inverse relationship between bathymetric and magnetic relief they suggest as a possible explanation

> "The rock comprising the bathymetric relief is in actual fact reversely magnetised. This would indicate that there probably has been a reversal of the earth's magnetic field since the time of original solidification of the rock. .....In such cases the direction of remanent magnetism derived from magnetic data in the ocean areas then can be compared with paleomagnetic data from land areas. The combined data then might make it possible to draw inferences concerning the age of oceanic crustal rocks."

This important principle is not stated by Vine and Matthews (1963) or Morley and Larochelle (1964). It was Vine and Wilson who first used it in 1965, without explicitly stating it.

# APPENDIX 3A

## PUBLISHED DATA REPORTS

Fifteen of the tracks used in this study have been published in data reports. Details are given below.

Track: V16.
Reference: Heirtzler (1961), Vema Cruise No. 16 Geomagnetic Measurements.
Data format: Track charts with mileage annotated. Total field and bathymetry profiles, linear with mileage.

Track: ODF3, ODF5, ODF6, ODF8.
Reference: U.S. Navy Hydrographic Office (1962), Operation Deep Freeze 1960-1961 Marine Geophysical Investigations.
Data format: One track chart with magnetic anomalies plotted perpendicular to tracks. Also one diagram with bathymetric and total magnetic field profiles of part of ODF3.

Track: ODF9
Reference: U.S. Naval Oceanographic Office (1965), Operation Deep Freeze 1961-1962.
Data format: Diagrams with total field and bathymetry profiles plotted in relation to sections of track chart.

Track: ELT16, ELT17, ELT19.
Reference: Heirtzler et al. (1969) USNS Eltanin cruises 16-21, Navigation bathymetric and geomagnetic measurements.
Data format: Track charts; listing of navigation information; bathymetric and magnetic anomaly profiles plotted with respect to distance.

Track: ELT23, ELT25, ELT26, ELT27.
Reference: Hayes et al. (1969) USNS Eltanin cruises 22-27, Navigation bathymetric and geomagnetic measurements.
Data format: As for ELT 16-21.

Track: ELT28, ELT32.
Reference: Hayes et al. (1972b) USNS Eltanin cruises 28-32, Navigation, bathymetric, geomagnetic, gravity and seismic reflection measurements.
Data format: As for ELT 16-27 but free air gravity anomaly profiles also given, and photo reductions of seismic reflection profiles.

# APPENDIX 3B

## THE MAGNETIC EFFECT OF HMNZS ENDEAVOUR

The magnetic effect of a ship will vary with the position of the sensor relative to the ship, the ship's heading, and the ambient field. It is convenient to assume that the magnetization of the ship can be divided into two parts; one, a permanent magnetization independent of the field, the other, an induced magnetization proportional to the applied field (Bullard and Mason, 1961). To the first order the field due to the ship can then be expressed by

$$F = A + B\cos\theta + C\cos 2\theta \qquad \ldots\ldots 3B.1$$

where $\theta$ is the magnetic heading of the ship, and A, B and C are constants related to the permanent and induced magnetization. A theoretical description of the variation of the field with distance from the ship requires a model of the distribution of magnetization within the ship. Bullard and Mason (1961) discuss a plausible model which enabled them to determine the coefficients of equation 3B.1 for a particular ship. Their model should be applicable generally, but to determine the coefficients data are required from two sensors at various distances from the ship and on various headings. Such data are not available for HMNZS Endeavour. However some information on the effect of the ship has been obtained from a set of data that was taken while routinely underway.

The test was carried out in the Ross Sea starting at $74.7^{\circ}$S, $172.5^{\circ}$E and extending over 60 km. The ship's heading was N$80^{\circ}$W magnetic, with the ambient field strength approximately 66,000 nT and inclination $85^{\circ}$. Two sensors A and B were streamed astern. A was kept at 140 m while B was varied in steps of approximately 8 m between 45 m and 100 m, the maximum length available. At each distance the sensors were alternately connected to the same magnetometer electronics to give between six and eight sets of readings for each sensor. Each set consisted of four to six individual readings. Use of the same electronics eliminated any errors of calibration in the system.

Fig. 3B.1 shows all the readings for one distance. In some sets there is a range of up to 50 nT that was probably due to noise in the system (both sensor systems were below par), and to ionespheric effects. It was discovered afterwards that at the time the test was underway the $K_p$ index was five, which could have given short period variations of up to 350 nT in the area. Despite the scatter in the readings there is a clear difference between the field measured by the two sensors. The increasing trend for both sensors is

probably due to a crustal anomaly. This effect can be adequately eliminated by calculating the mean of adjacent sets for one sensor and taking the difference between this and the mean of the intervening set of the other sensor. This gives several differences from which the mean difference and standard deviation can be calculated. Fig. 3B.2 shows how the field difference between the two sensors varies with the distance astern of the closer sensor. Since the difference appears to approach zero while the sensors are still apart, the sensor at 140 m is probably free of any influence of the ship. Fig. 3B.2 is thus effectively a plot of the effect of the ship with distance. The field at 140 m was always greater than that closer to the ship, that is, the effect of the ship was to reduce the total field.

On one other cruise two magnetometers were run simultaneously on several separate occasions. The results are not directly comparable to those described above because in this case the two sensors were connected to separate electronics. Unfortunately the distances of the two sensors are not known but they were not varied during each occasion (D.A. Christoffel pers. comm.). There were consistent differences between the sensors of up to 90 nT. As in the more detailed study described above, the effect of the ship was to reduce the total field.

The available data (Fig. 3B.2) indicate that the effect of the ship would be significant at distances less than 80 m but would probably be insignificant at 100 m or more. It is not possible to tell how much of the effect is due to induced magnetization, hence dependant on the ship's position and heading, and how much is due to permanent magnetization. The constants B and C in equation 3B.1 are proportional to cosI, where I is the inclination of the earth's field. The field inclination in the region studied varies between $70^{\circ}$ and $85^{\circ}$ so any effect due to the ship's heading is not likely to be large. Also, Endeavour tracks generally involved long sections (hundreds of km) on near constant course so heading effects would not produce significant anomalies of crustal wavelengths. They could, however, produce long wavelength anomalies. The constant A in equation 3B.1 is dependant on induced as well as permanent magnetization so even if heading effects were insignificant there may still have been effects which varied with the position of the ship.

# APPENDIX 3C

## REGIONAL MAGNETIC ANOMALIES

Ross (1966) produced magnetic anomaly profiles from total field profiles by removing a visually estimated long wavelength regional field. He noted that the anomaly profiles thus produced contained long wavelength anomalies; in addition to the typical short wavelength crustal anomalies. The long wavelength anomalies had amplitudes of up to 350 nT and lengths of 100 km to 300 km. New methods of analysis indicate that although some regional anomalies may be present they are probably different to those that Ross mapped.

The important new factor is the use of an independently defined regional field when producing anomaly profiles from the observed total field data. Fig. 3C.1 shows an anomaly profile that was produced by subtracting a regional field defined by the IGRF. Long wavelength oscillations are evident in the anomaly profile and the heavy line is a base-line which could be taken as the zero level. This base-line is only sketched, it is not quantitatively determined. Differences between the baseline and the zero line of the IGRF define regional anomalies. Below the anomaly profile in Fig. 3C.1 is the corresponding regional anomaly profile given by Ross (1966). His regional anomalies differ considerably from those suggested in the anomaly profile. The primary reason for the differences is that Ross assumed that the majority of the observed short wavelength anomalies were positive. This had a considerable influence on his choice of regional field and regional anomaly. Regional anomalies that he defined in other profiles are similar to those shown in Fig. 3C.1.

The subjective element in Ross's method is too great to justify detailed analysis of the particular regional anomalies that he defined. However long wavelength anomalies are present in the profile of Fig. 3C.1 and similar variations can be seen in other profiles. The variations are not due to deficiences in the IGRF as it is defined up to only degree and order eight and so does not contain wavelengths as short as those shown. Some factors which could contribute to the regional anomalies are as follows.

(1) For New Zealand data the possibility that the effect of the ship is present in some of the records has to be admitted.

(2) Navigational errors: The regional field is calculated for an assumed position and if the actual position was different the regional field would be wrong. For example at $55^{o}$S, $180^{o}$ if the true position was 25 km north of the assumed position the assumed regional field would be 100 nT too high. The effects of a navigational error distributed over several hundred kilometers would produce a long wavelength anomaly.

(3) Temporal variations. Field variations with periods of a few hours up to diurnal could produce long wavelength anomalies. It has been assumed (e.g. Hayes et al., 1969; Heirtzler et al., 1969) that diurnal variations in the area would be of the order of 50 nT. However Davey (pers. comm. 1973) has found that diurnal variations are up to 180 nT in the Ross Sea area. Although variations are likely to be reduced in deep water (Bullard and Parker, 1971) local topography can be important. Roden (1964) has shown that temporal variations can be amplified by 200% at the edge of the continental shelf, and Duba and Lilley (1973) showed that a typical midocean ridge structure could produce amplification of 75%. Long period temporal variations in excess of 100 nT could therefore be present in some of the area.

Discussion of these factors is not meant to imply that all the regional anomalies observed are in fact only pseudo-anomalies. Regional anomalies due to crustal or upper mantle variations may well be present, and such anomalies are of considerable interest. The point of the discussion is that a very careful, and probably complex, analysis is required to validly extract true regional anomalies from the existing data. A possible approach would include all or some of the following. (1) Production of anomaly profiles only by subtracting an explicitly defined field such as the IGRF. (2) Digital filtering of the anomaly profiles to extract regional anomalies in an unbiased manner. (3) Consideration of ionespheric disturbances and diurnal effects especially with regard to topographic structures. (4) Analysis of any track crossovers. (5) Analysis of model profiles for various crustal structures. The initial data would probably have to be only from satellite-navigated tracks and of unquestionable quality.

# APPENDIX 3D

## SECULAR VARIATION

The magnetic anomaly profiles produced by subtracting a regional field based on the data itself have mean values which are constant and approximately zero. This implies that the assumed regional field is a good representation of the actual regional field. Regional field maps produced from the data for epochs 1966.0 and 1967.0 are shown in Figs. 3D.1 and 3.8 respectively. They are at least superficially similar to the calculated GSFC field shown in Fig. 3D.2, and the IGRF field is not very different from the GSFC field. A more detailed comparison (Fig. 3D.3) shows that at least for that specific comparison the IGRF is closer to the observed field than the GSFC. Throughout the area the IGRF appears to be a better fit as anomaly profiles produced with it have mean values closer to zero. A regional field determined from the data is probably a better estimate of the actual regional field than the IGRF or GSFC fields.

Regional field maps determined from data in the area have been given by Christoffel (1961b) and Ross (1967a). Christoffel's map, for epoch 1959.0, was based on two tracks in the summer 1958/59. Ross's map, for epoch 1964.5, was based on two tracks in 1963/64 and two in 1964/65. Ross (1967a) noted that the two maps were different and he interpreted the difference in terms of westward drift of the nondipole field. To superimpose some of the field lines of the two maps required a drift of $0.25^{\circ}$/yr for between $50^{\circ}$S and $60^{\circ}$S, and nearly $1^{\circ}$/yr south of $60^{\circ}$S. Ross's (1967a) analysis was not strictly valid as he assumed that the differences between the maps were due only to westward drift of the field lines. That this is not necessarily so can be seen as follows.

Suppose that at a particular place the east-west field gradient is $\frac{dF}{dL}$ nT/degree and the rate of change of field (secular variation) is $\frac{dF}{dt}$ nT/yr. Then if the whole field pattern drifts without change the rate of drift is given by

$$\frac{dL}{dt} = \frac{dF}{dt} \cdot \frac{dL}{dF} \qquad \ldots\ldots \text{ 3D.1}$$

If however the field gradient changes with time an observed westward drift of a field line does not necessarily indicate drift of the whole pattern. For example the isoporic centre is west of the area (Fig. 3D.1) and a general decrease in field intensity will appear as a collapse of the field lines towards the centre. This gives an apparent westward drift in the area; but west of the isoporic centre it would give an eastward drift. The IGRF and GSFC further illustrate the limitations of extending secular variation

to westward drift. Secular variation as given by the IGRF is shown in Fig. 3D.4 and as given by the GSFC in Fig. 3D.5. Table 3D.1 shows values of westward drift deduced from field gradients and the secular variation using equation 3D.1. Clearly the westward drift so determined is very dependent on the secular variation distribution. Even when the secular variation is adequately known it is not valid to directly determine westward drift from it (Nagata, 1967).

Table 3D.1 Westward drift from secular variation

Westward drift in degrees/yr.

| | 160°E | | 170°E | | 180° | |
|---|---|---|---|---|---|---|
| | IGRF | GSFC | IGRF | GSFC | IGRF | GSFC |
| 40°S | 0.11 | 0.11 | 0.10 | 0.14 | 0.15 | 0.17 |
| 50°S | 0.17 | 0.17 | 0.20 | 0.15 | 0.21 | 0.26 |
| 60°S | 0.40 | 0.10 | 0.37 | 0.10 | 0.18 | 0.42 |
| 70°S | 1.38 | 0 | 0.97 | 0.07 | 0.18 | 0.85 |

When data are available from only a small area it is preferable to analyse only the secular variation. In the southwest Pacific area secular variation data are available from several magnetic observatories (Fig. 3.5). Malin (1969) has given data from Amberley and Macquarie for the interval 1957.5 to 1962.5, and Cullington (1968) has given data from Scott for 1958 to 1965, and Hallet for 1961 and 1962. The IGRF and GSFC are not defined for prior to 1965 but comparisons of their secular variations with the observatory data should be reasonably valid. Figs 3D.4 and 3D.5 indicate that a better fit to the observed secular variation is obtained with the IGRF than with the GSFC. It is of obvious interest to also consider the marine magnetic data. Williams (1967) and Whitmarsh and Jones (1969) have determined secular variation from track crossovers but that method has not been used for this area as there are insufficient crossovers, as well as problems of navigation uncertainties and diurnal variations. Instead regional field maps have been considered. The results are not very satisfactory.

First Ross's epoch 1964.5 map (Fig. 3D.6) was compared with the 1967.0 map (Fig. 3.8). Field differences between the two maps were determined on longitude 175°E between 45°S and 65°S, where control is good in both maps.

The secular variation values deduced were irregular with respect to latitude but all were between -50 and -80 nT/yr. However when the 1966.0 map (Fig. 3D.1) was compared with the 1964.5 map the secular variations on the same meridian were between -90 and -160 nT/yr. Comparison of the 1966.0 and 1967.0 maps throughout the area gave variations ranging from -190 to +70 nT/yr.

Clearly the existing maps are not adequate for determining secular variation. That does not necessarily mean that the existing data are inadequate. A more careful analysis may provide good secular variation data. The major difficulty is probably the long wavelength anomalies discussed previously as they represent pronounced local anomalies in the regional field.

# APPENDIX 3E

## BATHYMETRIC CHARTS

The following bathymetric charts which cover all or part of the area were used:

Chart: General Bathymetric Map of the Ocean:Pacific Ocean
Area: All of the area west of 140°E
Reference: Udintsev (1964).

Chart: Bathymetry and Seismicity
Area: Equidistant projection of all areas south of 40°S
Reference: Tolstikov (1966).

Chart: New Zealand Region Bathymetry
Area: 24°S-57.5°S, 157°E-167°W
Reference: Lawrence (1967).

Chart: New Zealand to Cape Adare, Antarctica
Area: 41°S-71.5°S, 157°E-166°W
Reference: U.S. Naval Oceanographic Office (1967).

Chart: Bathymetry of the Southwest Indian Ocean
Area: 30°S-69°S, 110°E-168°E
Reference: Hayes and Conolly (1972).

Chart: Macquarie Ridge Complex
Area: 42°S-60°S, 150°E-169°E
Reference: Hayes and Talwani (1972).

Chart: Emerald Sheet
Area: 57.5°S-61.5°S, 157°E-169°E
Reference: Hurley and Krause (1973a).

Chart: Hjort Sheet
Area: 61.5°S-65°S, 157°E-169°E.
Reference: Hurley and Krause (1973b)

Chart: Balleny Sheet
Area: 65°S-68°S, 157°E-169°E
Reference: Dawson (1970).

Chart: Chatham Sheet

Area: 42°S-49°S, 179°W-167°W

Reference: Cullen (1969a).

Chart: Submarine and subglacial topography.

Area: All the southern oceans south of 35°S.

Reference: Heezen and Tharp (1972).

(This map did not become available until after the study was virtually completed.)

# APPENDIX 3F

## COMPUTER PROGRAMS

Computer programs which were developed are listed below. All are written in ALGOL for use on the Elliott 503 computer of the Applied Mathematics Division, DSIR. Some details of the formulae are given in the relevant chapters.

### GENERAL PURPOSE

#### Card to tape

Reads cards and produces compacted paper tape copy and lineprinter listings. Useful for preparing data files or programs on card and then converting to paper tape for the Elliott 503 which has fast paper tape readers but a slow card reader. Also useful for interchange between Elliott 503, IBM 1130, and PDP 15 computers, all of which were used.

#### Plot and list profile

Reads a data string (profile), plots it on the plotter, and lists and plots it on the lineprinter. Also calculates mean and standard deviation. Useful data checking program.

#### Draw maps

A collection of programs that draw a grid and plot data. Data can be either continuous e.g. coastlines, or point e.g. epicentres. Data can be selected by area so that for instance only part of a complete epicentre file is plotted. Different programs for stereographic, equidistant, equal area, and mercator projections.

### TOTAL FIELD Section 3.4.4

#### Total field

Calculates total field from spherical harmonic coefficients. Calculates and prints a table of values for a specified epoch for specified grid points. Any set of harmonic coefficients can be used. The basic routine was provided by D.J. Woodward, Geophysics Division, DSIR.

### NUMERICAL CORRELATION Chapter 5

#### Second moment cross-correlation

Reads two data strings (profiles) and cross-correlates the shorter one with the longer one for all possible alignment positions of the profiles.

Variable second moment

Modification of the above program so that the length of the shorter profile can be altered to any desired length, then cross-correlated.

First moment correlation

Two programs similar to the above two but calculating the first moment correlation coefficient rather than the second moment.

Non-normalized correlation

Modifications of above programs to calculate non-normalized correlation coefficients.

Symmetry hunt

Programs similar to all the above but the shorter profile is inverted before correlation with the longer profile.

EPICENTRAL METHOD Chapter 8

Epicentral pole

Performs epicentral pole calculation. Reads groups of epicentres, and calculates and prints epicentral standard deviation at a series of grid points about a specified point. Grid size and spacing variable. For position of minimum standard deviation prints various data for each epicentre.

# APPENDIX 6A

## MAGNETIC PROPERTIES OF OCEANIC BASEMENT

The accompanying table lists data reported for seafloor samples that were believed to be non-erratic and therefore representative of oceanic basement. Ranges and/or means are given only where stated in the references.

| Reference | Magnetization Intensity J $\times 10^3$ emu/cm$^3$. | | Koenigsberger Ratio Q | | Comments |
|---|---|---|---|---|---|
| | Range | Mean | Range | Mean | |
| Matthews 1961, 1971 | 1-10 | 5 | 8-34 | 21 | Iberia abyssal plain 4960m. Highly altered basalt from abyssal hill. Believed nonerratic. |
| Cox, Doell 1962 | 2.2-10.1 | 5.4 | 15-105 | 40 | Mohole. Reversely magnetized basalt flow. High J at surface, lower below 1m. |
| Ade-Hall 1964 | <3-43 | 65% >10 | 0-75 | 61% >10 | 18 Pacific, 9 Atlantic sites. 90 samples. 40-5000m depth. Site details not given. |
| Vogt, Ostenso 1966 | 2-11 | 7 | 5-120 | 60 | Mid-Atlantic Ridge at 44.5°N. 2 sites. Flanks of the rift. |
| Luyendyk, Melson 1967 | 3.6-11.3 | 6.3 | 3-29 | 12 | Mid-Atlantic Ridge at 22.5°N. Fresh basalt. |
| | 0.5-2 | 0.7 | 1-7 | 3 | Basalt breccias. |
| Opdyke, Hekinian 1967 | 1.9-40 | 29 | <1-80 | 32 | Mid-Atlantic Ridge at 30°-32°N. 5 sites. Other highly altered basalts with J < 1. |
| Ozima et al. 1968 | 0.2-6.7 | | 1-57 | | North Pacific seamounts. 9 sites. Ages 25 - 95mybp. |
| de Boer et al. 1970 | 5.5-133 | 50 | 15-498 | | Reykjanes Ridge. Highest values only at axis, 50km off axis J was 5.5 -9.0. |
| Irving et al. 1970 | 3-100 | 9.2 | | | Mid-Atlantic Ridge at 45°N. In rift (9 sites) mean J = 57. Off axis mean J = 4.1. |
| Marshall, Cox 1971 | 1-36 | 14 | | | Fresh pillows from J. de Fuca and Central Ind. Ridges. Includes internal measurements. Mean is their estimate for typical fresh pillows. |
| Watkins, Paster 1971 | 11-95* | 22* | 1-50 | | South Pacific, mostly from >3000m. Includes internal measurements. |
| | 5.1-4.3* | | 7-11 | | Harzburgite from Macquarie Ridge. 2 sites. |
| | | | | | * Original values in emu/g, density 2.7g/cm$^3$ assumed. |
| Vine et al. 1973 | | 7.2 | | 5.6 | Troodos. Lower pillow lavas. (Axial type) |
| | | 1.2 | | 4.7 | Upper pillow lavas. (Off axial type) |
| | | 6.6 | | 9.3 | Pyroxine dunite ultramafics. |
| Lowrie et al. 1973 | 0.1-10 | 1 | 1-50 | 5.9 | JOIDES basalts. 5 Atlantic sites. 21 - 85mybp. |

# APPENDIX 6B

## THEORETICAL ANALYSIS OF ANOMALIES

The following results apply for the anomaly produced by a single block. They would not necessarily apply exactly in the typical situation of a sequence of adjacent blocks. The equations are from Schouten (1971) who based his formulation of the problem on Bott (1967) and Gay (1963).

### 6B.1 Symmetry

The symmetry of the anomaly produced by an infinitely long block is dependent on a phase factor $\theta$ given by

$$\theta = 180 - 2I'$$

where I', the effective inclination, is given by

$$I = \tan^{-1}\left[\tan I/\sin\alpha\right]$$

and I = field inclination

$\alpha$ = strike of block with respect to magnetic north.

Complete symmetry is produced when $\theta = 0$, asymmetry for $\theta = 45^{\circ}$, and antisymmetry for $\theta = 90^{\circ}$. For all lineations striking north-south $\alpha = \theta$ so $\theta = 0$ and the anomalies are symmetrical. The greatest degree of non-symmetry at a given latitude (i.e. given I) is for east-west striking lineations.

Some examples:

(1) Latitude = $55^{\circ}$ hence I = $71^{\circ}$
Lineation strike $\alpha = 040^{\circ}$
Effective inclination I' = $72^{\circ}$
Phase factor $\theta = 26^{\circ}$

(2) Latitude = $65^{\circ}$ hence I = $77^{\circ}$
East-west lineation $\alpha = 090^{\circ}$
$I' = I = 77^{\circ}$
$\theta = 26^{\circ}$

The two situations have the same phase factor and so produce the same shaped anomalies.

(3) Latitude = $45^{o}$ I = $63^{o}$

East-west lineation $\alpha = 090^{o}$

$I' = I = 63^{o}$

$\theta = 54^{o}$

(4) Latitude = $45^{o}$ I = $63^{o}$

North-south lineation $\alpha = 000^{o}$

$I' = 90^{o}$

$\theta = 0$

6B.2 Amplitude

The amplitude over an infinitely long block is proportional to a factor A(w) given by

$$A(w) = Cp \left[\exp(-2a/w) - \exp(-2b/w)\right] \qquad \ldots\ldots 6B.1$$

where $Cp = (\sin I/\sin I')^2$

a = depth to the top of the block

b = depth to the bottom of the block

w = width of the block.

The factor Cp depends on the inclinations and the strike of the lineations. In the southwest Pacific area it is not very important because the inclination is high. For example at $45^{o}$S the values of I and I' calculated in examples (3) and (4) above show that the amplitude of north-south lineations would be 79% of the amplitude of east-west lineations. This is the maximum possible amplitude effect due to strike variations at that latitude. For all latitudes further south the effect would be less as the maximum possible I' is $90^{o}$ and I would be greater than $63^{o}$. Thus south of $45^{o}$S differences of latitude or strike should produce less than 20% variation in the amplitude of a given anomaly.

The term in the brackets in equation 6B.1 is dependent on the width of the block in relation to its depth a, and thickness b-a. Fig. 6B.1 shows how the amplitude varies with block width for several block thicknesses, all cases for a depth of 5 km. The curves are broadly similar but the differences are significant for narrow blocks (Fig. 6B.2). For example with a 3 km wide block the relative amplitude for a 5.0 km thickness is half that for a 0.5 km thickness. A block 3 km wide and 5.0 km thick would have the same relative amplitude as a block 2.4 km wide and 0.5 km thick. Clearly for narrow blocks a substantial change in amplitude can be produced by either a change in thickness or a change in width.

The anomaly produced by a thick block is larger than that produced by a thinner block if the magnetization of the two is the same. To yield the same anomaly amplitude the intensities can be scaled. Fig. 6B.3 shows the factor by which the magnetization appropriate for a 0.5 km thick block would have to be divided to produce the same anomaly amplitudes if a thicker block is used. The scaling is not linear and also depends on the width of the block. As the thickness is increased narrow blocks require relatively higher magnetizations than wide blocks. The effect is that increasing the block thickness does not have a linear effect - the anomalies of narrow blocks are more attenuated than those of wide blocks.

# APPENDIX 8A

## PUBLISHED POLE POSITIONS

| Code | Reference | Rotation Pole Lat | Rotation Pole Long | Rotation Rate $\omega \times 10^{-7}$ °/y | Method for Pole position |
|---|---|---|---|---|---|
| **PACIFIC-ANTARCTIC** | | | | | |
| PA1 | Morgan(1968) | 71°S | 118°E | 10.3 | Fracture zones and spreading rates |
| PA2 | Le Pichon(1968) | 70°S | 118°E | 10.8 | Fracture zones |
| PA3 | Le Pichon(1968) | 68°S | 123°E | 10.8 | Spreading rates |
| PA4 | Christoffel(1971) | 82°S | 120°E | 10.3 | Fracture zones |
| PA5 | Chase(1971) | 70°S | 118°E | 10.8 | Fracture zones |
| PA6 | Chase(1972) | 70°S | 107°E | 9.76 | n-plate |
| PA7 | Wellman(1973a) | 70°S | 120°E | 10.8 | Spreading rates and one fracture zone |
| PA8 | This study | 71°S | 122°E | | Epicentral |
| **INDIAN-ANTARCTIC** | | | | | |
| IA1 | Le Pichon(1968,1970) | 4.7°N | 172.7°W | 5.71 | 4 term sum |
| IA2 | Christoffel(1971) Model (1) | 30°S | 160°W | 10.5 | Fracture zones |
| IA3 | Model (2) | 21°S | 167°W | 10.4 | PA4 + IP3 |
| IA4 | Chase(1971) | 7°N | 136°W | 5.86 | Fracture zones and focal mechanisms |
| IA5 | McKenzie & Sclater(1971) | 11°S | 148°W | 6.40 | Rates, fracture zones & focal mechanisms |
| IA6 | Weissel & Hayes(1972) | 12°S | 145°W | 6.75 | Superposition anom. 5 |
| IA7 | Chase(1972) | 16°S | 156°W | 6.50 | n-plate |
| IA8 | Wellman(1973a) | 10°S | 150°W | 7.0 | PA7 + IP9 |
| IA9 | This study | 30°S | 166°W | | Epicentral |
| **INDIAN-PACIFIC** | | | | | |
| IP1 | Le Pichon(1968,1970) | 51.2°S | 161.1°E | 12.4 | 5 term sum |
| IP2 | Christoffel(1971) Model (1) | 58°S | 169°W | 18.3* | PA4 + IA2 |
| IP3 | Model (2) | 53°S | 180° | 18.3 | Macquarie - N.Z. one fault |
| IP4 | Chase(1971) | 58°S | 172°W | 11.1 | PA5 + IA4 |
| IP5 | McKenzie & Sclater(1971) | 58.2°S | 179.5°W | 13.4 | PA2 + IA5 |
| IP6 | Weissel & Hayes(1972) | 59.0°S | 173.0°W | 13.6 | PA2 + IA6 |
| IP7 | Chase(1972) | 58°S | 174°E | 12.9 | n-plate |

* Published rate (20.8) is an error (Christoffel, pers. comm.).

Continued overleaf

| Code | Reference | Rotation Pole Lat | Long | Rotation Rate $\omega \times 10^{-7}$ °/y | Method for Pole position |
|---|---|---|---|---|---|
| INDIAN-PACIFIC Continued. | | | | | |
| IP8 | Falconer(1973a) | 55.8°S | 174.7°E | | Preliminary epicentral |
| IP9 | Wellman(1973a) | 55°S | 180° | 13.9 | Alpine fault |
| IP10 | This study | 56°S | 176°E | | Epicentral |

Note: Hayes and Talwani (1972) have listed several other Indian-Pacific poles based on different pairs of PA2 or 4 and IA1, 2, 3, 5 or 6.

---

Note: Most poles and rates are not as accurate as the number of significant figures imply. Values given are as in the original references.

# REFERENCES


Acharya,H., 1971, Magnitude frequency relation and deep-focus earthquakes, Bull. Seismol. Soc. Amer., 61, 1345.

Adams,R.D., 1962, Thickness of the earth's crust beneath the Campbell Plateau, N.Z.J. Geol. Geophys., 5, 74.

Adams,R.D., 1964, Thickness of the earth's crust beneath the Pacific-Antarctic ridge, N.Z.J. Geol. Geophys., 7, 529.

Adams,R.D., 1972a, Dispersion-wave studies in Antarctica, in Antarctic Geology and Geophysics, edited by Adie,R.J., Universitetsforlaget, Oslo, 473.

Adams,R.D., 1972b, Local earthquakes in Victoria Land, in Antarctic Geology and Geophysics, edited by Adie,R.J., Universitetsforlaget, Oslo, 495.

Adams,R.D., and Christoffel,D.A., 1962, Total magnetic field surveys between New Zealand and the Ross Sea, J. Geophys. Res., 67, 805.

Ade-Hall, J.M., 1964, The magnetic properties of some submarine oceanic lavas, Geophys. J.R. astr. Soc., 9, 85.

Ade-Hall,J.M., 1969, Opaque petrology and the stability of natural remanent magnetism in basaltic rocks, Geophys. J.R. astr. Soc., 18, 93.

Adie,R.J., 1962, The geology of Antarctica, A.G.U. Monograph, 7, 26.

Aggarwal,Y.P., Barazangi,M., and Isacks,B., 1972, P and S traveltimes in the Tonga-Fiji region: a zone of low velocity in the uppermost mantle behind the Tonga island arc, J. Geophys. Res., 77, 6427.

Aki,K., 1965, Maximum likelihood estimate of b in the formula log N = a - bM and its confidence limits, Bull. Earthquake Res. Inst., Tokyo Univ., 43, 237.

Allan,D.W., 1962, On the behaviour of systems of coupled dynamos, Proc. Camb. Phil. Soc., 58, 671.

Alldredge,L.R., and Van Voorhis,G.D., 1961, Depth to source of magnetic anomalies, J. Geophys. Res., 66, 3793.

Alldredge,L.R., Van Voorhis,G.D., and Davis,T.M., 1963, A magnetic profile around the world, J. Geophys. Res., 68, 3679.

Anderson,R.N., and Sclater,J.E., 1972, Topography and evolution of the East Pacific Rise between 5°S and 20°S, Earth Planet. Sci. Lett., 14, 433.

Anderson,R.N., McKenzie,D., and Sclater,J.G., 1973, Gravity, bathymetry and convection in the earth, Earth Planet. Sci. Lett., 18, 391.

Atwater,T., 1970, Implications of plate tectonics for the Cenozoic tectonic evolution of western north America, Geol. Soc. Amer. Bull., 81, 3513.

Atwater,T., and Menard,H.W., 1970, Magnetic lineations in the north-east Pacific, Earth Planet. Sci. Lett., 7, 445.

Atwater,T.M., and Mudie,J.D., 1968, Block faulting on the Gorda Rise, Science, 159, 729.

Austin,P.M., Sprigg,R.C., and Braithwaite,J.C., 1973, Structural development of the eastern Chatham rise and of the New Zealand region, in Oceanography of the South Pacific 1972, comp. Fraser,R., N.Z. Nat. Comm. UNESCO, 201.

Avery,O.E., Burton,G.D., and Heirtzler,J.R., 1968, An aeromagnetic survey of the Norwegian Sea, J. Geophys. Res., 73, 4583.

Awe,O., 1964, Errors in correlation between time series, J. Atmos. Terr. Phys., 26, 1239.

Banerjee,S.K., 1971, Decay of marine magnetic anomalies by ferrous ion diffusion, Nature, 229, 181.

Banerjee,S.K., 1972, Rock magnetic aspects of marine magnetic anomalies, Comments on Earth Sciences: Geophysics, 2, 169.

Banghar,A.R., and Sykes,L.R., 1969, Focal mechanisms of earthquakes in the Indian ocean and adjacent regions, J. Geophys. Res., 74, 632.

Barazangi,M., and Dorman,J., 1969, World seismicity maps compiled from ESSA, Coast and Geodetic Survey, epicentre data, 1961 - 1967, Bull. Seismol. Soc. Amer., 59, 369.

Barker,P.F., 1972, A spreading centre in the East Scotia Sea, Earth Planet. Sci. Lett., 15, 123.

Barrett,D.L., 1968, Frequency modulation of a shipborne proton magnetometer signal due to the hydrodynamic instability of the towed vehicle, J. Geophys. Res., 73, 5327.

Bartlett,M.S., 1935, Some aspects of the time-correlation problem in regard to tests of significance, J.R. Stats. Soc., 98, 536.

Bartlett,M.S., 1955, An Introduction to Stochastic Processes, Cambridge Univ. Press.

Beloussov,V.V., 1968a, Some problems of development of the earths crust and upper mantle of oceans, A.G.U. Monograph, 12, 449.

Beloussov,V.V., 1968b, An open letter to J. Tuzo Wilson, Geotimes,13::10, 17.

Beloussov,V.V., 1970, Against the hypothesis of ocean-floor spreading, Tectonophysics, 9, 489.

Ben-Avraham,Z., Bowin,C., and Segawa,J., 1972, An extinct spreading centre in the Phillipine Sea, Nature, 240, 453.

Benkova,N.P., Khramov,A.N., Cherevko,T.N., and Adam,N.V., 1973, Spherical harmonic analyses of the palaeomagnetic field, Earth Planet. Sci. Lett., 18, 141.

Berggren,W.A., 1969, Cenozoic chronostratigraphy, planktonic foraminiferal zonation and the radiometric time scale, Nature, 224, 10722.

Bergh,H., 1971, Sea floor spreading in the south-west Indian Ocean, J. Geophys. Res., 76, 6275.

Berninghausen,W.H., and van Padang,M.N., 1960, Catalogue of the Active Volcances of the World, Part X, Antarctica.

Blakely,R., and Cox,A., 1972a, Identification of short polarity events by transforming marine magnetic profiles to the pole, J. Geophys. Res., 77, 439.

Blakely,R.J., and Cox,A., 1972b, Evidence for short geomagnetic polarity intervals in the early cenozoic, J. Geophys. Res., 77, 7065.

Bond,F.R., and Jacka,F., 1960, Distribution of auroras in the southern hemisphere, Aust. J. Physics, 13, 610.

Bott,M.H.P., 1967, Solution of the linear inverse problem in magnetic interpretation with application to oceanic magnetic anomalies, Geophys. J.R. astr. Soc., 13, 313.

Bott,M.H.P., and Hutton,M.A., 1970a, A matrix method for interpreting oceanic magnetic anomalies, Geophys. J.R. astr. Soc., 20, 149.

Bott,M.H.P., and Hutton,M.A., 1970b, Limitations on the resolution possible in the direct interpretation of marine magnetic anomalies, Earth Planet. Sci. Lett., 8, 317.

Bott,M.H.P., and Ingles,A., 1972, Matrix methods for joint interpretation of two-dimensional gravity and magnetic anomalies with application to the Iceland-Faero Ridge, Geophys. J.R. astr. Soc., 30, 55.

Brakl,J., Clay,C.S., and Rona,P.A., 1968, Interpretation of a magnetic anomaly on the continental rise off Cape Hatteras, J. Geophys. Res., 73, 5313.

Brodie,J.W., 1964, Bathymetry of the New Zealand region, N.Z. D.S.I.R. Bull., 161.

Brune,J.N., 1968, Seismic moment, seismicity and rate of slip along major fault zones, J. Geophys. Res., 73, 777.

Bucha,V., 1970, Changes in the earths magnetic field during the archeological past, Comments on Earth Sciences: Geophysics, 1, 20.

Bullard,E.C., 1967, The removal of trend from magnetic surveys, Earth Planet. Sci. Lett., 2, 293.

Bullard,E., 1968, Reversals of the earths field, Phil. Trans. Roy. Soc., A 263, 481.

Bullard,E.C., and Gellman,H, 1954, Homogeneous dynamos and terrestrial magnetism, Phil. Trans. Roy. Soc., A 247, 213.

Bullard,E.C., and Mason,R.G., 1961, The magnetic field astern of a ship, Deep Sea Res., 8, 20.

Bullard,E.C., and Mason,R.G., 1963, The magnetic field over the oceans, in The Sea, Volume 3, edited by Hill,M.N., 175.

Bullard,E.C., and Parker,R.L., 1971, Electromagnetic induction in the oceans, in The Sea, Volume 4, Part I, edited by Maxwell,A.E., 695.

Burnaby,T.P., 1953, A suggested alternative to the correlation coefficient for testing significance of agreement between pairs of time series, and its application to geological data, Nature, 172, 210.

Cain,J.C., Hendricks,S.J., Langel,R.A., and Hudson,W.V., 1967, A proposed model for the International Geomagnetic Reference Field - 1965, J. Geomag. Geoelec., 19, 335.

Cann,J.R., 1968, Geological processes at mid-ocean ridge crests, Geophys. J.R. astr. Soc., 15, 331.

Cann,J.G., 1970, New model for the structure of the ocean crust, Nature, 226, 928.

Carmichael,C.M., 1967, An outline of the Intensity of the paleomagnetic field of the earth, Earth Planet. Sci. Lett., 3, 351.

Carmichael,C.M., 1970, The mid-Atlantic Ridge near 45°N. VII Magnetic properties and opaque mineralogy of dredged samples, Can. J. Earth Sci., 7, 239.

Carter,R.M., and Landis,C.A., 1972, Correlative Oligocene unconformities in southern Australasia Nature Phys. Sci., 237, 12.

Chase,C.G., 1971, Tectonic history of the Fiji Plateau, Geol. Soc. Amer. Bull., 82, 3087.

Chase,C.G., 1972, The N plate problem of plate tectonics, Geophys. J.R. astr. Soc., 29, 117.

Chase,C.G., Menard,H.W., Larson,R.L., Sharman,G.F., and Smith,S.M., 1970, History of the sea-floor spreading west of Baja California, Bull. Geol. Soc. Amer., 81, 4491.

Christoffel,D.A., 1961a, Total magnetic field measurements between New Zealand and Antarctica, Nature, 190, 776.

Christoffel,D.A., 1961b, A total field magnetic survey conducted between New Zealand and Antarctica and in the Ross Sea, Univ. British Columbia Geophys. Lab. Sci. Report, 3.

Christoffel,D.A., 1969, Sea floor spreading in the southwest Pacific and cenozoic drifting pattern of southern continents, (Abstract) Trans. Am. Geophys. Union, 185.

Christoffel,D.A., 1971, Motion of the New Zealand Alpine fault deduced from the pattern of sea-floor spreading, in Recent Crustal Movements, Roy. Soc. N.Z. Bull., 9, 25.

Christoffel,D.A., and Falconer,R.F., 1973, Magnetic measurements in the Macquarie Ridge region, Oceanography of the South Pacific, 1972, comp. Fraser,R., N.Z. Nat. Comm. UNESCO, 233.

Christoffel,D.A., and Falconer,R.K.H., 1972, Marine magnetic measurements in the south-west Pacific Ocean and the identification of new tectonic features, Ant. Res. Ser., 19, 197.

Christoffel,D.A., and Falconer,R.K.H., 1973, Changes in the direction of sea floor spreading in the south-west Pacific, Oceanography of the South Pacific, 1972, comp. Fraser,R., N.Z. Nat. Comm. UNESCO, 233.

Christoffel,D.A., and Ross,D.I., 1965, Magnetic anomalies south of the New Zealand plateau, J. Geophys. Res., 70, 2857.

Christoffel,D.A., and Ross,D.I., 1970, A fracture zone in the south west Pacific basin south of New Zealand and its implications for sea floor spreading, Earth Planet. Sci. Lett., 8, 125.

Christoffel,D.A., and van der Linden,W.J.M., 1972, Macquarie Ridge - New Zealand Alpine fault transition, Ant. Res. Ser., 19, 235.

Coe,R., 1967, Paleointensities of the earths magnetic field determined from Tertiary and Quaternary rocks, J. Geophys. Res., 72, 3247.

Collette,B.J., and Rutten,K.W., 1972, Crest and fracture zone geometry of the mid-Atlantic Ridge between 10 and 16 N, Nature, Phys. Sci., 237, 131.

Cox,A., 1968, Lengths of geomagnetic polarity intervals, J. Geophys. Res., 73, 3247.

Cox,A., 1969, Geomagnetic reversals, Science, 163, 237.

Cox,A., 1970, Reconciliation of statistical models for reversals, J. Geophys. Res., 75, 7501.

Cox,A., and Dalrymple,G.B., 1967, Statistical analysis of geomagnetic reversal data and the precision of K-Ar dating, J. Geophys. Res., 72, 2603.

Cox,A., and Doell,R.R., 1962, Magnetic properties of the basalt in hole EM7, Mohole Project, J. Geophys. Res., 67, 3997.

Cox,A., Doell,R.R., and Dalrymple,G.B., 1963, Geomagnetic polarity epochs and Pleistocene geochronometry, Nature, 198, 1049.

Creer,K.M., 1970, A review of paleomagnetism, Earth Sci. Rev., 6, 369.

Creer,K.M., 1971, Mesozoic palaeomagnetic reversal column, Nature, 233, 545.

Cullen,D.J., 1965, Autochthonous rocks from the Chatham rise, east of New Zealand, N.Z. J. Geol. Geophys., 8, 465.

Cullen,D.J., 1967a, The Antipodes Fracture Zone, a major structure of the south west Pacific, N.Z.J. Marine and Freshwater Res., 1, 16.

Cullen,D.J., 1967b, Island arc development in the south west Pacific, Tectonophysics, 4, 163.

Cullen,D.J., 1969a, Chatham Bathymetry, N.Z. Oceanogr. Inst. Chart, Oceanic Series, 1:1,000,000.

Cullen,D.J., 1969b, Quaternary volcanism at the Antipodes Islands: its bearing on structural interpretation of the southwest Pacific, J. Geophys. Res., 74, 4213.

Cullen,D.J., 1970, A tectonic analysis of the south-west Pacific, N.Z. J. Geol. Geophys., 13, 7.

Cullington,A.L., 1968, The magnetic secular variation at Scott Base and Hallett Station, N.Z.J. Geol. Geophys., 11, 982.

Davies,D., and Francis,T.J.G., 1964, The crustal structure of the Seychelles Bank, Deep Sea Res., 11, 921.
Davies,D., and McKenzie,D.P., 1969, Seismic travel-time residuals and plates, Geophys. J.R. astr. Soc., 18, 51.
Dawson,E.W., 1970, Balleny Bathymetry, N.Z. Oceanogr. Inst. Chart, Oceanic Series, 1:1,000,000.
de Boer,J., Schilling,J-G., and Krause,D.C., 1969, Magnetic polarity of pillow basalts from Reykjanes Ridge, Science, 166, 996.
de Boer,J., Schilling,J-G., and Krause,D.C., 1970, Reykjanes Ridge: Implication of magnetic properties of dredged rock, Earth Planet. Sci. Lett., 9, 55.
Dementskaya,R.M., and Karasik,A.M., 1969, The active rift system of the Arctic Ocean, Tectonophysics, 8, 345.
Den,N., Ludwig,W.J., Murauchi,S., Ewing,J.I., Hotta,H., Edgar,N.T., Yoshi,T., Asanuma,T., Hagiwara,K., Sato,T., and Ando,S., 1969, Seismic refraction measurements in the northwest Pacific basin, J. Geophys. Res., 74, 1421.
Dewey,J.F., and Bird,J.M., 1970, Mountain belts and the new global tectonics, J. Geophys. Res., 75, 2625.
Dickson,G.O., Pitman,W.C., and Heirtzler,J.R., 1968, Magnetic anomalies in the South Atlantic and sea floor spreading, J. Geophys. Res., 73, 2187.
Dietz,R.S., 1961, Continental and ocean bottom evolution by spreading of the sea floor, Nature, 190, 854.
Dietz,R.S., and Holden,J.C., 1970, Reconstruction of Pangaea: breakup and dispersion of continents, Permian to present, J. Geophys. Res., 75, 4939.
Dixon,W.J., and Massey,F.J., 1969, Introduction to Statistical Analysis, 3rd Ed., McGraw-Hill.
Doell,R.R., 1972, Palaeomagnetic studies of Icelandic lava flows, Geophys. J.R. astr. Soc., 26, 459.
du Toit,A.L., 1927, A geological comparison of South America with South Africa, Carnegie Institute, Washington, 158.
du Toit,A.L., 1937, Our Wandering Continents, Oliver and Boyd, Edinburgh.
Duba,A., and Lilley,F.E.M., 1973, Effect of an ocean ridge model on geomagnetic variations, J. Geophys. Res., 77, 7100.

Eittreim,S.L., and Ewing,J., 1972, Mid-plate tectonics in the Indian Ocean, J. Geophys. Res., 77, 6431.
Elsasser,W.M., 1971, Sea-floor spreading as thermal convection, J. Geophys. Res., 76, 1101.
Emilia,D.A., and Bodvarsson,G., 1969, Numerical methods in the direct interpretation of marine magnetic anomalies, Earth Planet. Sci. Lett., 7, 192.
Emilia,D.A., and Bodvarsson,G., 1970, More on the interpretation of magnetic anomalies, Earth Planet. Sci. Lett., 8, 320.
Erickson,B.H., Naugler,E.P., and Lucas,W.H., 1970, Emperor Fracture Zone:: a newly discovered feature in the central north Pacific, Nature, 225, 53.
Evernden,J.F., 1969, Precision of epicentres obtained by small numbers of World-Wide stations, Bull. Seismol. Soc. Amer., 59, 1365.
Evernden,J.F., 1970, Study of regional seismicity and associated problems, Bull. Seismol. Soc. Amer., 60, 393.
Evison,F.F., 1967, Note on the aseismicity of Antarctica, N.Z. J. Geol. Geophys., 10, 479.
Evison,F.F., 1971, Seismicity of the Alpine fault, New Zealand, in Recent Crustal Movements, Roy. Soc. N.Z. Bull., 9, 161.

Evison,F.F., Ingham,C.E., Orr,R.H., and Le Fort,J.H., 1960, Thickness of the earth's crust in Antarctica and the surrounding oceans, Geophys. J.R. astr. Soc., 3, 289.

Ewing,J., and Ewing,M., 1967, Sediment distribution on the mid-ocean ridges with respect to spreading of the sea floor, Science, 156, 1590.

Ewing,J., and Ewing,M., 1971, Seismic reflection, in The Sea, Vol. 4, Part I, edited by Maxwell,A.E., 1.

Ewing,M., and Heezen,B.C., 1956, Some problems of Antarctic submarine geology, A.G.U. Monograph, 1, 75.

Ewing,M., Carpenter,C., Windisch,C., and Ewing,J., 1973, Sediment distribution in the oceans: the Atlantic, Geol. Soc. Amer. Bull., 84, 71.

Ewing,M., Houtz,R., and Ewing,J., 1969, South Pacific sediment distribution, J. Geophys. Res., 74, 2477.

Ewing,J., Windisch,C., and Ewing,M., 1970, Correlation of Horizon A with Joides bore-hole results, J. Geophys. Res., 75, 5645.

Falconer,R.K.H., 1972, The Indian-Antarctic-Pacific triple junction, Earth Planet. Sci. Lett., 17, 151.

Falconer,R.K.H., 1973a, Indian-Pacific rotation pole determined from earthquake epicentres, Nature Phys. Sci., 243, 97.

Falconer,R.K.H., 1973b, Numerical studies of Cretaceous magnetic anomalies in the south-west Pacific Ocean, Oceanography of the South Pacific, 1972, comp. Fraser,R., N.Z. Nat. Comm. UNESCO, 257.

Fischer,A.G., Heezen,B.C., Boyce,R.E., Bukry,D., Douglas,R.G., Garrison,R.E., Kling,S.A., Krasheninnikov,V., Lisitzin,A.P., and Pimm,A.C., 1970, Geological history of the western north Pacific, Science, 168, 1210.

Fisher,D.E., Bonatti,E., Joensuu,O., and Funkhouser,J., 1968, Ages of Pacific deep-sea basalts and spreading of the sea floor, Science, 160, 1106.

Fisher,R.A., 1970, Statistical Methods for Research Workers, 14th Ed., Oliver and Boyd, Edinburgh.

Fisher,R.L., and Hess,H.H., 1963, Trenches, in The Sea, Volume 3, edited by Hill,M.N., 411.

Fleming,C.A., 1969, The Mesozoic of New Zealand: chapters in the history of the circum-Pacific mobile belt, Q. Jl geol. Soc. 125, 125.

Forsyth,D.W., 1972, Mechanisms of earthquakes and plate motions in the east Pacific, Earth Planet. Sci. Lett., 17, 189.

Francheteau,J., and Sclater,J.G., 1969, Paleomagnetism of the southern continents and plate tectonics, Earth Planet. Sci. Lett., 6, 93.

Francheteau,J., Harrison,C.G.A., Sclater,J.G., and Richards,M.L., 1970, Magnetisation of Pacific seamounts: a preliminary polar curve for the northeastern Pacific, J. Geophys. Res., 75, 2035.

Francheteau,J., Sclater,J.G., and Craig,H., 1969, Magnetization of a recently discovered seamount in the central Pacific, Geophysics, 34, 645.

Francis,T.J.G., 1968a, The detailed seismicity of mid-oceanic ridges, Earth Planet. Sci. Lett., 4, 39.

Francis,T.J.G., 1968b, Seismicity of mid-oceanic ridges and its relation to the properties of the upper mantle and crust, Nature, 220, 899.

Francis,T.J.G., and Porter,I.T., 1971, A statistical study of Mid-Atlantic Ridge earthquakes, Geophys. J.R. astr. Soc., 24, 31.

Fuller,M.D., 1964, Expression of E-W fractures in magnetic surveys in parts of U.S.A., Geophysics, 29, 602.

Gass,I.G., and Smewing,J.D., 1973, Intrusion, extrusion and metamorphism at constructive margins: evidence from Troodos Massif, Cyprus, Nature, 242, 26.
Gay,S.P., 1963, Standard curves for interpretation of magnetic anomalies over long tabular bodies, Geophysics, 28, 161.
Gibson,G.D., 1950, A rapid method for ascertaining serial lag correlations, Biometrika, 37, 288.
Goodell,H.G., 1973, The sediments, Antarctic Map Folio Series, 17, 1.
Gordon,A.L., 1972, On the interaction of the Antarctic circumpolar current and the Macquarie ridge, Ant. Res. Ser., 19, 71.
Green,A.G., 1972, Seafloor spreading in the Mozambique Channel, Nature Phys. Sci., 236, 19.
Griffiths,J.R., 1971, Reconstruction of the south-west Pacific margin of Gondwanaland, Nature, 234, 203.
Griffiths,J.R., and Varne,R., 1972, Evolution of the Tasman Sea, Macquarie Ridge and Alpine Fault, Nature Phys. Sci., 235, 83.
Griggs,D.A., 1939, A theory of mountain building, Amer. J. Science, 237, 611.
Grim,P.J., and Erickson,B.H., 1969, Fracture zones and magnetic anomalies south of the Aleutian trench, J. Geophys. Res., 74, 1488.
Guier,W.H., 1966, Satellite navigation using integral Doppler data, the AN/SRN-9 equipment, J. Geophys. Res., 71, 5903.
Guilcher,A., 1963, Continental shelf and slope (continental margin), in The Sea, Volume 3, edited by Hill,M.N., 281.
Gupta,H.K., and Rastogi,B.K., 1972, Earthquake m vs Ms relations and source multiplicity, Geophys. J.R. astr. Soc., 28, 65.
Gutenberg,B., and Richter,C.F., 1954, Seismicity of the Earth and Associated Phenomena, 2nd Ed., Princeton Univ. Press.

Hales,A.L., 1969, Gravitational sliding and continental drift, Earth Planet. Sci. Lett., 6, 31.
Hamilton,E.L., 1967a, Marine geology of abyssal plains in the Gulf of Alaska, J. Geophys. Res., 72, 4189.
Hamilton,W., 1967b, Tectonics of Antarctica, Tectonophysics, 4, 555.
Hamilton,R.M., and Evison,F.F., 1967, Earthquakes at intermediate depths in southwest New Zealand, N.Z.J. Geol. Geophys., 10, 1319.
Hamilton,R.M., and Gale,A.W., 1968, Seismicity and structure of North Island, New Zealand, J. Geophys. Res., 73, 3859.
Harrison,C.G.A., 1968, Formation of magnetic anomaly patterns by dyke injection, J. Geophys. Res., 73, 2137.
Harrison,C.G.A., 1971, A seamount with a nonmagnetic top, Geophysics, 30, 349.
Harrison,C.G.A., 1972a, Poles of Rotation, Earth Planet. Sci. Lett., 14, 31.
Harrison,C.G.A., 1972b, Comments on a paper by Watkins and Richardson: 'Intrusives, extrusives and linear magnetic anomalies', Geophys. J.R. astr. Soc., 28, 187.
Harrison,C.G.A., 1973, Reply to 'Comments on poles of rotation', Earth Planet. Sci. Lett., 19, 242.
Harrison,C.G.A., and Sclater,J.G., 1972, Origin of the disturbed magnetic zone between the Murray and Molokai Fracture Zones, Earth Planet. Sci. Lett., 14, 419.
Hayes,D.E., 1972, Introduction: Marine geophysics of the southeast Indian ocean, Ant. Res. Ser., 19, 119.
Hayes,D.E., and Conolly,J.R., 1972, Morphology of the southeast Indian Ocean, Ant. Res. Ser., 19, 125.
Hayes,D.E., and Ewing,M., 1970, North Brazilian Ridge and adjacent continental margin, Bull. Amer. Assoc. Pet. Geol., 54, 2120.

Hayes,D.E., and Ewing,M., 1971, Pacific boundary structure, The Sea, Vol. 4, Part II, Edited by Maxwell,A.E., 29.

Hayes,D.E., and Heirtzler,J.R., 1968, Magnetic anomalies and their relation to the Aleutian Arc system, J. Geophys. Res., 73, 4637.

Hayes,D.E., and Ringis,J., 1973, Sea floor spreading in the Tasman Sea, Nature, 243, 454.

Hayes,D.E., and Talwani,M., 1972, Geophysical investigation of the Macquarie Ridge Complex, Ant. Res. Ser., 19, 211.

Hayes,D.E., Heirtzler,J.R., Herron,E.M., and Pitman,W.C., 1969, Preliminary report USNS Eltanin cruises 22-27: Navigation; bathymetric and geomagnetic measurements, Lamont-Doherty Geol. Observ. Tech. Rep. No. 2-CU-2-69.

Hayes,D.E., Talwani,M., and Christoffel,D.A., 1972a, The Macquarie ridge complex, in Antarctic Geology and Geophysics, edited by Adie,R.J., Universitetsforlaget, Oslo, 767.

Hayes,D.E., Talwani,M., Houtz,R., and Pitman,W.C., 1972b, Preliminary report USNS Eltanin cruises 28-32: Navigation; bathymetric, geomagnetic, gravity and seismic reflection profiles, Lamont-Doherty Geol. Observ. Tech. Rep. No. CU-1-72, 1.

Heezen,B.C., 1969, The world rift system: An introduction to the symposium, Tectonophysics, 8, 269.

Heezen,B.C., and Ewing,M., 1963, The mid-oceanic ridge, in The Sea, Volume 3, edited by Hill,M.N., 388.

Heezen,B.C., and Hollister,C.D., 1971, The Face of the Deep, O.U.P.

Heezen,B.C., and Menard,H.W., 1963, Topography of the deep-sea floor, in The Sea, Volume 3, edited by Hill,M.N., 233.

Heezen,B.C., and Nafe,J.E., 1964, Vema Trench: western Indian Ocean, Deep Sea Res., 11, 79.

Heezen,B.C., and Tharp,M., 1972, Morphology of the sea floor, Antarctic Map Folio Series, 16, 1.

Heezen,B.C., Bunce,E.T., Hersey,J.B., and Tharp,M., 1964a, Chain and Romanche Fracture Zones, Deep Sea Res., 11, 11.

Heezen,B.C., Ewing,M., and Miller,E.T., 1953, Trans Atlantic profile of total magnetic intensity and topography, Dakar to Barbados, Deep Sea Res., 1, 25.

Heezen,B.C., Gerard,R.D., and Tharp,M., 1964b, Vema Fracture Zone in the equatorial Atlantic, J. Geophys. Res., 69, 733.

Heezen,B.C., MacGregor,I.D., Foreman,H.P., Fomstaf,G., Hekel,H., Hesse,R., Hoskins,R.H., Jones,E.J.W., Kaneps,A., Krasheninnikov,V.A., Okada,H., and Ruef,M.H., 1973, Diachronous deposits: a kinematic interpretation of the post Jurassic sedimentary sequence on the Pacific plate, Nature, 241, 25.

Heezen,B.C., Tharp,M., and Ewing,M., 1959, The floors of the ocean. 1. The North Atlantic, Geol. Soc. Amer. Special Paper, 65.

Heirtzler,J.R., 1961, Vema Cruise No. 16. Geomagnetic measurements, Lamont Geological Observatory Tech. Rep. 2, CU-3-61 Nonr-Geology.

Heirtzler,J.R., 1968, Evidence for ocean floor spreading across the ocean basins, The History of the Earths Crust, Edited by Phinney,R.A., Princeton Univ. Press, 90.

Heirtzler,J.R., and Le Pichon,X., 1965, Crustal structure of Mid-Ocean Ridges (3) Magnetic anomalies over the mid Atlantic Ridge, J. Geophys. Res., 70, 4013.

Heirtzler,J.R., Dickson,G.O., Herron,E.M., Pitman,W.C., Le Pichon,X., 1968, Marine magnetic anomalies, geomagnetic field reversals and motions of the ocean floor and continents, J. Geophys. Res., 73, 2119.

Heirtzler,J.R., Hayes,D.E., Herron,E.M., and Pitman,W.C., 1969, Preliminary report USNS Eltanin cruises 16-21: Navigation; bathymetric and geomagnetic measurements, Lamont-Doherty Geol. Observ. Tech. Rep. No. 3-CU-3-69.

Heirtzler,J.R., Le Pichon,X., and Baron,J.G., 1966, Magnetic anomalies over the Reykjanes Ridge, Deep Sea Res., 13, 427.
Heirtzler,J.R., Peter,G., Talwani,M., and Zurflueh,E.G., 1962, Magnetic anomalies caused by a two dimensional structure: Their computation by digital computors and their interpretation, Lamont Geological Observatory, Tech. Rep. No. 6, CU-6-62, Nonr-Geology.
Helsley,E., and Steiner,M.B., 1969, Evidence for long intervals of normal polarity during the Cretaceous period, Earth Planet. Sci. Lett., 5, 325.
Herron,E.M., 1971, Crustal plates and sea floor spreading in the southeastern Pacific, Ant. Res. Ser., 15, 229.
Herron,E.M., 1972, Sea-floor spreading and the Cenozoic history of the east-central Pacific, Geol. Soc. Amer. Bull., 83, 1671.
Herron,E.M., and Hayes,D.E., 1969, A geophysical study of the Chile Ridge, Earth Planet. Sci. Lett., 8, 77.
Herron,E.M., and Heirtzler,J.R., 1968, Sea-floor spreading near the Galapagos, Science, 158, 775.
Herron,E.M., and Talwani,M., 1972, Magnetic anomalies on the Reykjanes Ridge, Nature, 238, 390.
Hersey,J.B., 1963, Continuous reflection profiling, in The Sea, Volume 3, edited by Hill,M.N., 47.
Hess,H.H., 1962, History of ocean basins, in Petrologic Studies: A volume to honour A.F. Buddington, Geol. Soc. Amer., 599.
Hess,H.H., 1965, Mid-oceanic ridges and tectonics of the sea-floor, in Submarine Geology and Geophysics, Proc. 17th Symp. Colston Res. Soc., 317.
Hill,M.N., 1963, Editor of The Sea, Volume 3, Wiley.
Holmes,A., 1931, Radioactivity and earth movements, Trans. Geol. Soc. Glasgow, 18, 559.
Holmes,M.L., von Huene,R., and McManus,D.A., 1972, Seismic reflection evidence supporting underthrusting beneath the Alutian Arc near Amchitka Island, J. Geophys. Res., 77, 959.
Houtz,R., and Davey,F., 1973, Seismic profiler and sonobuoy measurements in Ross Sea, Antarctica, J. Geophys. Res., 78, 3448.
Houtz,R.E., and Markl,R.G., 1972, Seismic profiler data between Antarctica and Australia, Ant. Res. Ser., 19, 147.
Houtz,R., and Meijer,R., 1970, Structure of the Ross Sea from profiler data, J. Geophys. Res., 75, 6592.
Houtz,R., Ewing,J., and Buhl,P., 1970, Seismic data from sonobouy stations in the northern and equatorial Pacific, J. Geophys. Res., 75, 5093.
Houtz,R., Ewing,J., and Embley,R., 1971, Profiler data from the Macquarie Ridge area, Ant. Res. Ser., 15, 239.
Houtz,R., Ewing,J., Ewing,M., and Lonardi,A.G., 1967, Seismic reflection profiles of the New Zealand Plateau, J. Geophys. Res., 72, 4713.
Houtz,R., Ewing,M., Hayes,D., and Naini,B., 1973, Sediment isopachs in the Indian and Pacific ocean sectors (105°E to 70°W), Antarctic Map Folio Series, 17, 9.
Houtz,R.E., Ewing,J., and Le Pichon,X., 1968, Velocity of deep-sea sediments from sonobuoy data, J. Geophys. Res., 73, 2615.
Huang,T.C., Watkins,N.D., Shaw,D., and Kennett,J.P., 1972, Volcanic particulate input in high latitudes of the southern Pacific Ocean, (Abstract) Trans. Am. Geophys. Union, 53, 1029.
Hurley,D.E., and Krause,D.C., 1973a, Emerald Bathymetry, N.Z. Oceanogr. Inst. Chart, Oceanic Series, 1:1,000,000, in prep.
Hurley,D.E., and Krause,D.C., 1973b, Hjort Bathymetry, N.Z. Oceanogr. Inst. Chart, Oceanic Series, 1:1,000,000, in prep.
Hurwitz,L., Knapp,D.G., Nelson,J.H., and Watson,D.E., 1966, Mathematical model of the geomagnetic field for 1965, J. Geophys. Res., 71, 2373.

IAGA Commission 2, Working group 4, 1969, International Geomagnetic Reference Field 1965.0, J. Geophys. Res., 74, 4407.
Irving,E., 1964, Paleomagnetism and its application to Geological and Geophysical Problems, Wiley.
Irving,E., 1970, The mid-Atlantic Ridge at 45°N. XIV Oxidation and magnetic properties of basalt; review and discussion, Can. J. Earth Sci., 7, 1528.
Irving,E., and Couillard,R.W., 1973, Cretaceous normal polarity interval, Nature Phys. Sci., 244, 10.
Irving,E., Park,J.K., Haggerty,S.E., Aumento,F., and Loncarevic,B., 1970, Magnetism and opaque mineralogy of basalts from the Mid-Atlantic Ridge at 45 N, Nature, 228, 974.
Isacks,B., and Oliver,J., 1964, Seismic waves with frequencies from 1 to 100 cycles per second recorded in a deep mine in northern New Jersey, Bull. Seismol. Soc. Amer., 54, 1941.
Isacks,B., Oliver,J., and Sykes,L.R., 1968, Seismology and the new global tectonics, J. Geophys. Res., 73, 5855.

Jacobs,S.S., Bruchausen,P.M., and Bauer,E.B., 1970, Eltanin reports cruises 32 - 36, hydrographic stations, bottom photographs, current measurements.
Jacobs,J.A., Russell,R.D., and Wilson,J.T., 1959, Physics and Geology, McGraw-Hill.
Jacoby,W.R., 1970, Instability in the upper mantle and global plate movements, J. Geophys. Res., 75, 5671.
James,D.E., and Steinhart,J.S., 1966, Structure beneath continents: a critical review of explosion studies 1960-65, A.G.U. Monograph, 10, 293.
Jefferys,H., 1924, 1959, The Earth, its Origin, History, and Physical Constitution, Cambridge Univ. Press, 1st Ed. 1924, 4th Ed. 1959.
Jenkins,G.M., and Watts,D.G., 1968, Spectral Analysis and its Applications, Holden Day.
Johnson,R.H., 1970, Active submarine volcanism in the Austral Islands, Science, 167, 977.
Johnson,T., and Molnar,P., 1972, Focal mechanisms and plate tectonics of the southwest Pacific, J. Geophys. Res., 77, 5000.
JOIDES Scientific Staff, 1970, Leg 12, Geotimes, 15:9, 10.
JOIDES Scientific Staff, 1971a, Leg 4, Science, 172, 1197.
JOIDES Scientific Staff, 1971b, Leg 16, Geotimes, 16:6, 12.
JOIDES Scientific Staff, 1971c, Leg 18, Geotimes, 16:10, 12.
JOIDES Scientific Staff, 1972a, Leg 22, Geotimes, 17:6, 15.
JOIDES Scientific Staff, 1972b, Leg 24, Geotimes, 17:9, 17.
JOIDES Scientific Staff, 1972c, Leg 25, Geotimes, 17:11, 21.
JOIDES Scientific Staff, 1973a, Leg 26, Geotimes, 18:3, 16.
JOIDES Scientific Staff, 1973b, Leg 27, Geotimes, 18:4, 16.
JOIDES Scientific Staff, 1973c, Leg 28, Geotimes, 18:6, 19.
JOIDES Scientific Staff, 1973d, Leg 29, Geotimes, 18:7, 14.
Jones,J.G., 1971, Australia's Caenozoic drift, Nature, 230, 237.
Jones,E.J.W., Mitchell,J.G., Shido,F., and Phillips,J.D., 1972, Igneous rocks dredged from the Rockall Plateau, Nature Phys. Sci., 237, 118.

Kanamori,H., and Press,F., 1970, How thick is the lithosphere? Nature, 226, 330.
Karig,D.E., 1970, Ridges and basins of the Tonga-Kermadec island arc system, J. Geophys. Res., 75, 239.
Karig,D.E., 1971, Origin and development of marginal basins in the western Pacific, J. Geophys. Res., 76, 2542.
Karnik,V., 1969, Seismicity of the European Area, Part 1, Reidel.
Karnik,V., 1971, Seismicity of the European Area, Part 2, Reidel.
Kasameyer,P.W., von Herzen,R.P., and Simmons,G., 1972, Heat flow, bathymetry, and the Mid-Atlantic Ridge at 43°N, J. Geophys. Res., 77, 2535.
Kay,R., Hubbard,N.J., and Gast,P.W., 1970, Chemical characteristics and origin of oceanic ridge volcanic rocks, J. Geophys. Res., 75, 1585.
Keen,M.J., 1969, Possible edge effect to explain magnetic anomalies off the eastern seaboard of the U.S., Nature, 222, 72.
Keen,M.J., and Manchester,K.S., 1970, The Mid-Atlantic Ridge near 45°N, X. Sediment distribution and thickness from seismic reflection profiling, Can. J. Earth Sci., 7, 735.
Kennett,J.P., Burns,R.E., Andrews,J.E., Churkin,M., Davies,T.A., Dumitrica,P., Edwards,A.R., Galehouse,J.S., Packham,G.H., and van der Lingen,G.J., 1972, Australian-Antarctic continental drift palaeocirculation changes and Oligocene deep-sea erosion, Nature Phys. Sci., 239, 51.
Kibblewhite,A.C., 1966, The acoustic detection and location of an underwater volcano, N.Z.J. of Science, 9, 178.
Kibblewhite,A.C., and Denham,R.N., 1967, The bathymetry and total magnetic field of the south Kermadec ridge seamounts, N.Z.J. of Science, 10, 52.
Klitgord,K.D., Mudie,J.D., and Normark,W.R., 1972, Magnetic lineations observed near the ocean floor and possible implications on the geomagnetic chronology of the Gilbert epoch, Geophys. J.R. astr. Soc., 28, 35.
Kono,M., 1971, Intensity of the earths magnetic field during the Pliocene and Pleistocene in relation to the amplitude of mid-ocean ridge magnetic anomalies, Earth Planet. Sci. Lett., 11, 10.
Krause,D.C., 1966, Geology and geomagnetism of the Bounty region east of the South Island, New Zealand, N.Z. D.S.I.R. Bull., 170.
Krause,D.C., 1973, Crustal plates of the Bismarck and Solomon seas, in Oceanography of the South Pacific 1972, comp. Fraser,R., N.Z. Nat. Comm. UNESCO, 271.
Krause,D.C., and Watkins,N.D., 1970, North Atlantic crustal genesis in the vicinity of the Azores, Geophys. J.R. astr. Soc., 19, 261.
Krumbein,W.C., and Graybill,F.A., 1965, An Introduction to Statistical Models in Geology, McGraw Hill.

Lachenbruch,A.H., and Thompson,G.A., 1972, Oceanic ridges and transform faults: their intersection angles and resistance to plate motion, Earth Planet. Sci. Lett., 15, 116.
Langseth,M.G., and von Herzen,P., 1971, Heat flow through the floor of the worlds oceans, in The Sea, Volume 4, Part I, edited by Maxwell,A.E., 299.
Larson,R.L., 1971, Near-bottom geologic studies of the East Pacific Rise crest, Geol. Soc. Amer. Bull., 82, 823.
Larson,R.L., and Chase,C.G., 1972, Late Mesozoic evolution of the western Pacific Ocean, Geol. Soc. Amer. Bull., 83, 3627.

Larson,R.L., and Pitman,W.C., 1972, Worldwide correlation of Mesozoic magnetic anomalies, and its implications, Geol. Soc. Amer. Bull., 83, 3645.

Larson,R.L., Menard,H.W., and Smith,S.M., 1968, Gulf of California: a result of ocean floor spreading and transform faulting, Science, 161, 781.

Laughton,A.S., Matthews,D.H., and Fisher,R.L., 1971, The structure of the Indian Ocean, in The Sea, volume 4, part II, edited by Maxwell,A.E., 543.

Laughton,A.S., Whitmarsh,R.B., Rusby,J.S.M., Somers,M.L., Revie,J., McCartney,B.S., and Nafe,J.E., 1972, A continuous east-west fault on the Azores-Gibraltar Ridge, Nature, 237, 217.

Lawrence,P., 1967, New Zealand region: bathymetry, 1:6,000,000, N.Z. Oceanogr. Inst. Chart, Miscellaneous Series, 15.

Le Pichon,X., 1968, Sea-floor spreading and continental drift, J. Geophys. Res., 73, 3661.

Le Pichon,X., 1970, Correction to paper by Xavier Le Pichon 'Sea-floor spreading and continental drift', J. Geophys. Res., 75, 2793.

Le Pichon,X., and Hayes,D.E., 1971, Marginal offsets, fracture zones, and the early opening of the south Atlantic, J. Geophys. Res., 76, 6283.

Le Pichon,X., and Langseth,M.E., 1969, Heat flow from the mid-ocean ridges and sea-floor spreading, Tectonophysics, 8, 319.

Le Pichon,X., Eittreim,S.L., and Ludwig,W.J., 1971a, Sediment transport and distribution in the Argentine basin: I. Antarctic bottom current passage through the Falkland Fracture Zone, Phys. Chem. Earth, 8, 1.

Le Pichon,X., Ewing,J., and Houtz,R.E., 1968, Deep-sea sediment velocity determination made while reflection profiling, J. Geophys. Res., 73, 2597.

Le Pichon,X., Ewing,M., and Truchan,M., 1971b, Sediment transport and distribution in the Argentine basin: 2. Antarctic bottom current into the Brazil basin, Phys. Chem. Earth, 8, 31.

Le Pichon,X., Houtz,R.E., Drake,C.L., and Nafe,F.E., 1965, Crustal structure of mid ocean ridges: (1) seismic refraction measurements, J. Geophys. Res., 70, 319.

Le Pichon,X., Hyndman,R.D., and Pautot,G., 1971c, Geophysical study of the opening of the Labrador sea, J. Geophys. Res., 76, 4724.

Lilley,F.E.M., 1970, Geomagnetic reversals and the position of the north magnetic pole, Nature, 227, 1336.

Lincoln,J.V., 1966, Geomagnetic and solar data, J. Geophys. Res., 71, 3337.

Lincoln,J.V., 1967, Geomagnetic Indices, in Physics of Geomagnetic Phenomena, edited by Matsushita,S., and Campbell,W.H., Volume 1, 67.

Lisitzin,A.P., 1962, Bottom sediments of the Antarctic, A.G.U. Monograph, 7, 81.

Lister,C.R.B., 1972, On the thermal balance of a mid-ocean ridge, Geophys. J.R. astr. Soc., 26, 515.

Lonardi,A.G., and Ewing,M., 1971, Sediment transport and distribution in the Argentine Basin: 4. Bathymetry of the continental margin, Argentine Basin and other related provinces: Canyons and sources of sediments, Phys. Chem. Earth, 8, 81.

Loncarevic,B.D., and Parker,R.L., 1971, Mid-Atlantic Ridge near 45°N: XVII. Magnetic anomalies and oceanfloor spreading, Can. J. Earth Sci., 8, 883.

Loncarevic,B.D., Mason,C.S., and Matthews,D.H., 1966, Mid-Atlantic Ridge near 45°N: I. The median valley, Can. J. Earth Sci., 3, 327.

Lowrie,W., Lovlie,R., and Opdyke,N.D., 1973, The magnetic properties of deep sea drilling project basalts from the Atlantic Ocean, Earth Planet. Sci. Lett., 17, 338.

Ludwig,W.J., Ewing,J.I., Ewing,M., Murauchi,S., Den,N., Asano,S., Hotta,H., Hayakawa,HM., Asanuma,T., Ichikawa,K., and Noguchi,I., 1966, Sediments and structure of the Japan Trench, J. Geophys. Res., 71, 2121.

Ludwig,W.J., Nafe,J.E., and Drake,C.L., 1971, Seismic refraction, in The Sea, Volume 4, Part I, edited by Maxwell,A.E., 53.

Luyendyk,B.P., 1969, Origin of short wavelength magnetic lineations observed near the ocean bottom, J. Geophys. Res., 74, 4869.

Luyendyk,B.P., 1970a, Origin and history of abyssal hills in the northeast Pacific Ocean, Geol. Soc. Amer. Bull., 81, 2237.

Luyendyk,B.P., 1970b, Reply to Peter's (1970) discussion of Luyendyk (1969), J. Geophys. Res., 75, 6621.

Luyendyk,B.P., and Melson,W.G., 1967, Magnetic properties and petrology of rocks near the crest of the Mid-Atlantic Ridge, Nature, 215, 147.

Luyendyk,B.P., and Phillips,J.D., 1970, Geophysical profiles over the northwestern African continental margin, (abstract) Trans. Am. Geophys. Union, 51, 316.

Luyendyk,B.P., Mudie,J.D., and Harrison,C.G.A., 1968, Lineations of magnetic anomalies in the northeast Pacific observed near the ocean floor, J. Geophys. Res., 73, 5951.

McElhinny,M.W., 1971, Geomagnetic polarity transitions, Comments on Earth Sciences: Geophysics, 1, 150.

McElhinny,M.W., 1973a, Mantle plumes, palaeomagnetism and polar wandering, Nature, 241, 523.

McElhinny,M.W., 1973b, Palaeomagnetism and plate tectonics, Cambridge Univ. Press.

McElhinny,M.W., and Burek,P.J., 1971, Mesozoic palaeomagnetic stratigraphy, Nature, 232, 98.

McElhinny,M.W., and Luck,G.R., 1970, Paleomagnetism and Gondwanaland, Science, 168, 830.

McElhinny,M.W., and Wellman,P., 1969, Polar wandering and sea-floor spreading in the southern Indian ocean, Earth Planet. Sci. Lett., 6, 198.

McKenzie,D.P., 1972a, Plate tectonics, in The Nature of the Solid Earth, edited by Robertson,E.C., 323.

McKenzie,D.P., 1972b, Active tectonics of the Mediterranean area, Geophys. J.R. astr. Soc., 30, 109.

McKenzie,D.P., and Morgan,W.J., 1969, Evolution of triple junctions Nature, 222, 125.

McKenzie,D.P., and Parker,R.L., 1967, The north Pacific: an example of tectonics on a sphere, Nature, 216, 1276.

McKenzie,D.P., and Sclater,J.G., 1969, Heat flow in the eastern Pacific and sea floor spreading, Bull. Volcanologique, 33, 101.

McKenzie,D.P., and Sclater,J.G., 1971, The evolution of the Indian Ocean since the late Cretaceous, Geophys. J.R. astr. Soc., 24, 437.

McMullan,R., 1967, A magnetic survey of the Campbell Plateau, Victoria Univ. of Wellington, MSc thesis.

Malahoff,A., and Woollard,G.P., 1971, Geophysical studies of the Hawaiian Ridge and Murray Fracture Zone, in The Sea, Volume 4, Part II, edited by Maxwell,A.E., 73.

Malin,S.R.C., 1969, Geomagnetic secular variation and its changes, 1942.5 to 1962.5, Geophys. J.R. astr. Soc., 17, 415.

Marshall,M., and Cox,A., 1971, Magnetism of pillow basalts and their petrology, Geol. Soc. Amer. Bull., 82, 537.

Mascle,J., and Phillips,J.D., 1972, Magnetic smooth zones in the south Atlantic, Nature, 240, 80.

Mason,R.G., 1958, A magnetic survey off the west coast of U.S.A. between 32°N and 36°N, and 121° and 128°W, Geophys. J.R. astr. Soc., 1, 320.

Matsushita,S., 1967, Geomagnetic disturbances and storms, in Physics of Geomagnetic Phenomena, Volume 2, edited by Matsushita,S., and Campbell,W.H., 793.

Matthews,D.H., 1961, Lavas from an abyssal hill of the floor of the north Atlantic Ocean, Nature, 190, 158.

Matthews,D.H., 1969, Model study of the magnetic anomaly pattern across the Mid-Atlantic Ridge at 45°North, Tectonophysics, 8, 353.

Matthews,D.H., 1971, Altered basalts from Swallow Bank, an abyssal hill in the northeast Atlantic and from a nearby seamount, Phil. Trans. Roy. Soc., A 268, 551.

Matthews,D.H., and Bath,J., 1967, Formation of magnetic anomaly pattern of Mid-Atlantic Ridge, Geophys. J.R. astr. Soc., 13, 349.

Matthews,D.H., Williams,C., and Laughton,A.S., 1967, Mid-ocean ridge in the mouth of the Gulf of Aden, Nature, 215, 1052.

Maxwell,A.E., 1971, Editor of The Sea, Volume 4, Parts I and II, Wiley.

Maxwell,A.E., von Herzen,R.P., Hsu,K.J., Andrews,J.E., Saito,T., Percival,S.F., Milow,E.D., and Boyce,R.E., 1970, Deep sea drilling in the south Atlantic, Science, 168, 1047.

Melson,W.G., and Thompson,G., 1971, Petrology of a transform fault zone and adjacent ridge segments, Phil. Trans. Roy. Soc., A 268, 423.

Menard,H.W., 1964, Marine Geology of the Pacific, McGraw Hill.

Menard,H.W., 1967a, Transition types of crust under small ocean basins, J. Geophys. Res., 72, 3061.

Menard,H.W., 1967b, Sea floor spreading, topography and the Second layer, Science, 157, 923.

Menard,H.W., 1969, Growth of drifting volcanoes,J. Geophys. Res., 74, 4827.

Menard,H.W., and Atwater,T., 1968, Changes in direction of sea floor spreading, Nature, 219, 463.

Menard,H.W., and Atwater,T., 1969, Origin of fracture zone topography, Nature, 222, 1037.

Menard,H.W., and Chase,T.E., 1971, Fracture zones, in The Sea, Volume 4, Part I, edited by Maxwell,A.E., 421.

Menard,H.W., and Ladd,H.S., 1963, Oceanic islands, seamourts, guyots and atolls, in The Sea, Volume 3, edited by Hill,M.N., 365.

Menard,H.W., and Mammerickx,J., 1967, Abyssal hills, magnetic anomalies and the East Pacific Rise, Earth Planet. Sci. Lett., 2, 465.

Menard,H.W., and Smith,S.M., 1966, Hypsometry of ocean basin provinces, J. Geophys. Res., 71, 4305.

Meyerhoff,A.A., and Meyerhoff,H.A., 1972a, 'The new global tectonics': major inconsistencies, Bull. Amer. Soc. Pet. Geol., 56, 269.

Meyerhoff,A.A., and Meyerhoff,H.A., 1972b, 'The new global tectonics': age of linear magnetic anomalies of ocean basins, Bull. Amer. Soc. Pet. Geol. 56, 337.

Miller,R.L., and Kahn,J.S., 1962, Statistical Analysis in the Geological Sciences, Wiley.

Miyashiro,A., Shido,F., and Ewing,M., 1970, Petrologic models for the Mid-Atlantic Ridge, Deep Sea Res., 17, 109.

Mogi,K., 1962, Study of elastic shocks caused by the fracture of heterogeneous materials and its relations to earthquake phenomena, Bull. Earthquake Res. Inst., Tokyo Univ., 40, 125.

Mogi,K., 1963a, The fracture of a semi-infinite body caused by an inner stress origin and its relation to earthquake phenomena ; 2. The case of materials having some heterogenous structures, Bull. Earthquake Res. Inst., Tokyo Univ., 41, 595.

Mogi,K., 1963b, Some discussion on aftershocks, foreshocks, and earthquake swarms - The fracture of a semi-infinite body caused by an inner stress origin and its relation to the earthquake phenomena, Bull. Earthquake Res. Inst., Tokyo Univ., 41, 615.

Moore,T.C., and Heath,G.R., 1967, Abyssal hills in the central equatorial Pacific: detailed structure of the sea floor and sub-bottom reflectors, Marine Geology, 5, 161.

Moores,E.M., and Vine,F.J., 1971, The Troodos Massif, Cyprus and other ophiolites as oceanic crust: evaluation and implications, Phil. Trans. Roy. Soc., A 268, 443.

Morgan,W.J., 1968, Rises, trenches, great faults, and crustal blocks, J. Geophys. Res., 73, 1959.

Morgan,W.J., 1971, Convection plumes in the lower mantle, Nature, 230, 42.

Morgan,W.J., 1972a, Plate motions and deep mantle convection, Geol. Soc. Amer. Memoir, 132, 7.

Morgan,W.J., 1972b, Deep mantle convection plumes and plate motions, Bull. Amer. Soc. Pet. Geol., 56, 203.

Morgan,W.J., and Johnson,G.L., 1970, The triple junction in the south Atlantic, (abstract) Trans. Amer. Geophys. Union, 51, 329.

Morgan,W.J., and Loomis,T.P., 1969, Correlation coefficients and sea-floor spreading - an automated analysis of magnetic profiles, unpublished report, Princeton University.

Morley,L.W., and Larochelle,A., 1964, Paleomagnetism as a means of dating geological events, in Geochronology in Canada, Roy. Soc. Canada Special Publication, 8, 39.

Nagata,T., 1967, Westward drift (of the geomagnetic non-dipole field), Int. Dict. Geophys., 1667.

Nagata,T., 1968, Length of geomagnetic polarity intervals, J. Geomag. Geoelec., 21, 701.

Naidu,P., 1968, Statistical analysis of east Pacific Rise heat flow data, Earth Planet. Sci. Lett., 4, 131.

Naidu,P.S., 1971, Statistical structure of geomagnetic field reversals, J. Geophys. Res., 76, 2649.

Naudy,H., 1971, Automatic determination of depth on aeromagnetic profiles, Geophysics, 36, 712.

Naugler,F.P., and Rea,D.K., 1970, Abyssal hills and sea-floor spreading in the central north Pacific, Geol. Soc. Amer. Bull., 81, 3123.

Nelson,T.H., and Temple,P.G., 1972, Mainstream mantle convection: a geologic analysis of plate motion, Bull. Amer. Assoc. Pet. Geol., 56, 226.

N.Z. Geol. Survey, 1972, South Island Geological Map of New Zealand, 1:1,000,000, N.Z. D.S.I.R.

Ninkovich,D., Opdyke,N., Heezen,B.C., and Foster,J.H., 1966, Paleomagnetic stratigraphy, rates of deposition and tephrachronology in the north Pacific deep-sea sediments, Earth Planet. Sci. Lett., 1, 476.

Northrop,J., 1973, Seismicity gaps in the Pacific-Antarctic ridge and East Pacific rise, in Oceanography of the South Pacific 1972, comp. Fraser,R., N.Z. Nat. Comm. UNESCO, 285.

Northrop,J., Morrison,M.F., and Duennebier,F.K., 1970, Seismic slip rate versus sea-floor spreading rate on the eastern Pacific Rise and the Pacific Antarctic Ridge, J. Geophys. Res., 75, 3285.

Oliver,J., and Dorman,J., 1963, Exploration of sub-oceanic structure by the use of seismic surface waves, in The Sea, volume 3, edited by Hill,M.N., 110.
Oliver,J., and Isacks,B.L., 1967, Deep earthquake zones, anomalous structure in the upper mantle, and the lithosphere, J. Geophys. Res., 72, 4259.
Oliver,J., and Murphy,L., 1971, WWNSS: Seismology's global network of observing stations, Science, 174, 254.
Opdyke,N.D., 1971, Paleomagnetism, in The Sea, Volume 4, Part I, edited by Maxwell,A.E., 157.
Opdyke,N.D., 1972, Paleomagnetism of deep-sea cores, Revs. Geophys. Space Phys., 10, 213.
Opdyke,N.D., and Hekinian,R., 1967, Magnetic properties of some igneous rocks from the Mid-Atlantic Ridge, J. Geophys. Res., 72, 2257.
Opdyke,N.D., and Henry,K.W., 1969, A test of the dipole hypothesis, Earth Planet. Sci. Lett., 6, 139.
Ozima,M., Ozima,M., and Kaneoka,I., 1968, K-Ar ages and magnetic properties of some dredged submarine basalts and their geophysical implications, J. Geophys. Res., 73, 711.

Packham,G.H., and Falvey,D.A., 1971, An hypothesis for the formation of marginal seas in the western Pacific, Tectonophysics, 11, 79.
Parker,E.N., 1969, The occasional reversal of the geomagnetic field, Astrophys. J., 158, 815.
Peter,G., 1970, Discussion of paper by B.P. Luyendyk 'Origin of short wavelength magnetic lineations observed near the ocean bottom', J. Geophys. Res., 75, 6717.
Peter,G., Erickson,B.H., and Grim,P.J., 1971, Magnetic structure of the Aleutian Trench and northeast Pacific Basin, in The Sea, Volume 4, Part II, edited by Maxwell,A.E., 191.
Pitman,W.C., and Heirtzler,J.R., 1966, Magnetic anomalies over the Pacific-Antarctic Ridge, Science, 154, 1164.
Pitman,W.C., and Talwani,M., 1972, Sea-floor spreading in the north Atlantic, Geol. Soc. Amer. Bull., 83, 619.
Pitman,W.C., Herron,E.M., and Heirtzler,J.R., 1968, Magnetic anomalies in the Pacific and sea floor spreading, J. Geophys. Res., 73, 2069.
Pratt,R.M., and Heezen,B.C., 1964, Topography of Blake Plateau, Deep Sea Res., 11, 721.
Press,F., 1970, Regionalised earth models, J. Geophys. Res., 75, 6575.

Raff,A.D., 1966, Boundaries of an area of very long magnetic anomalies in the northeast Pacific, J. Geophys. Res., 71, 2631.
Raff,A.D., 1968, Sea floor spreading - another rift, J. Geophys. Res., 73, 3699.
Raitt,R.W., 1963, The crustal rocks, in The Sea, Volume 3, edited by Hill,M.N., 85.
Rea,D.K., 1972, Magnetic anomalies along fracture zones, Nature Phys. Sci., 236, 58.
Rea,D.K., and Naugler,F.P., 1971, Musicians seamount province and related crustal structures north of the Hawaiian Ridge, Marine Geology, 10, 89.
Reid,J., Stommel,H., Stroup,E.D., and Warren,B.A., 1968, Detection of a deep boundary current in the western south Pacific, Nature, 217, 937.
Richter,C.F., 1958, Elementary Seismology, Freeman.
Roberts,E.B., and Knapp,D.G., 1958, Background and technical objectives in geomagnetism, A.G.U. Monograph, 2, 55.

Roden,R.B., 1964, The effect of an ocean on magnetic diurnal variations, Geophys. J.R. astr. Soc., 8, 375.
Ross,D.I., 1966, A magnetic survey of the south-west Pacific Ocean, Victoria Univ. of Wellington, Ph.D. thesis.
Ross,D.I., 1967a, A total magnetic field map of the southwest Pacific Ocean between New Zealand and Antarctica, N.Z.J. Geol. Geophys., 10, 1230.
Ross,D.I., 1967b, Magnetic and bathymetric measurements across the Pacific-Antarctic Ridge south of New Zealand, N.Z.J. Geol. Geophys., 10, 1452.
Runcorn,S.K., 1956, Paleomagnetic survey in Arizona and Utah: preliminary results, Geol. Soc. Amer. Bull., 67, 301.
Runcorn,S.K., 1962, Palaeomagnetic evidence for continental drift, in Continental Drift, edited by Runcorn,S.K., 1.
Runcorn,S.K., 1965, Palaeomagnetic comparisonc between Europe and north America, in A symposium on Continental Drift, Phil. Trans. Roy. Soc., A 528, 1.

Sato,T., 1965, Long-period geomagnetic oscillations in southern high latitudes, Ant. Res. Ser., 4, 173.
Schlich,R., and Patriat,Ph., 1967, Profils magnetiques sur la dorsale medio-oceanique 'Indo-Pacifique', Annales de Geophysique, 23, 629.
Scholl,D.W., Christensen,M.N., von Huene,R., and Marlow,M.S., 1970, Peru-Chile trench sediments and sea floor spreading, Geol. Soc. Amer. Bull., 81, 1339.
Scholz,C., 1968a, The frequency magnitude relation of microfracturing in rock and its relation to earthquakes, Bull. Seismol. Soc. Amer., 58, 399.
Scholz,C., 1968b, Microfracturing and the inelastic deformation of rock in compression, J. Geophys. Res., 73, 1417.
Schopf,J.M., 1969, Ellsworth Mountains: position in West Antarctica due to sea-floor spreading, Science, 164, 63.
Schouten,J.A., 1971, A fundamental analysis of magnetic anomalies over oceanic ridges, Marine Geophysical Researches, 1, 111.
Schouten,H., and McCamy,K., 1972, Filtering marine magnetic anomalies, J. Geophys. Res., 77, 7089.
Sclater,J.G., 1972, Heat flow and elevation of the marginal basins of the western Pacific, J. Geophys. Res., 77, 5705.
Sclater,J.G., and Francheteau,J., 1970, The implications of terrestrial heat flow observations on current tectonic and geochemical models of the crust and upper mantle of the earth, Geophys. J.R. astr. Soc., 20, 509.
Sclater,J.G., Anderson,R.N., and Bell,M.L., 1971, Elevation of ridges and evolution of the central eastern Pacific, J. Geophys. Res., 76, 7888.
Scrutton,R.A., and du Plessis,A., 1973, Possible marginal fracture ridge south of South Africa, Nature, 242, 180.
Shido,F., and Miyashiro,A., 1973, Compositional difference between abyssal tholeiites from north and south of the Azores on the mid-Atlantic ridge, Nature Phys. Sci., 245, 59.
Shor,G.G., Kirk,H.K., and Menard,H.W., 1971b, Crustal structure of the Melanesian area, J. Geophys. Res., 76, 2562.
Shor,G.G., Menard,H.W., and Raitt,R.W., 1971a, Structure of the Pacific basin, in The Sea, Volume 4, Part II, edited by Maxwell,A.E., 3.
Sleep,N.H., 1972, Thermal effects of the formation of Atlantic continental margins by continental breakup, Geophys. J.R. astr. Soc., 24, 325.
Sleep,N.H., and Biehler,S., 1970, Topography and tectonics at the intersections of fracture zones with central rifts, J. Geophys. Res., 75, 2748.

Smellie,D.W., 1956, Elementary approximations in aeromagnetic interpretation, Geophysics, 21, 1021.
Smith,P.J., 1967a, The intensity of the Tertiary geomagnetic field, Geophys. J.R. astr. Soc., 12, 239.
Smith,P.J., 1967b, Intensity of the Earth's magnetic field in the geological past, Nature, 216, 989.
Smith,P.J., 1967c, The intensity of the ancient geomagnetic field: A review and analysis, Geophys. J.R. astr. Soc., 12, 321.
Smith,W.D., 1971, Earthquakes at shallow and intermediate depths in Fiordland, New Zealand, J. Geophys. Res., 76, 4901.
Smith,A.G., and Hallam,A., 1970, The fit of the southern continents, Nature, 225, 139.
Spiess,F.N., and Mudie,J.D., 1971, Small scale topographic and magnetic features, in The Sea, Volume 4, Part I, edited by Maxwell,A.E., 205.
Sproll,W.P., and Dietz,R.S., 1969, Morphological continental drift fit of Australia and Antarctica, Nature, 222, 345.
Stehli,F.G., 1968, A paleoclimatic test of the hypothesis of an axial dipolar magnetic field, in The History of the Earths Crust, edited by Phinney,R.A., Princeton Univ. Press, 195.
Stehli,F.G., 1970, A test of the earths magnetic field during Permian times, J. Geophys. Res., 75, 3325.
Stover,C.W., 1966, Seismicity of the Indian Ocean, J. Geophys. Res., 71, 2575.
Stover,C.W., 1968, Seismicity of the south Atlantic Ocean, J. Geophys. Res., 73, 3807.
Suggate,R.P., 1963, The Alpine fault, Trans. R. Soc. N.Z. (Geol.), 2, 105.
Suggate,R.P., 1972, Mesozoic-cenozoic development of the New Zealand region, Pacific Geology, 4, 113.
Summerhayes,C.P., 1967, New Zealand region volcanism and structure, Nature, 215, 610.
Summerhayes,C.P., 1969, Marine geology of the New Zealand subantarctic seafloor, N.Z. D.S.I.R. Bull., 190.
Sykes,L.R., 1963, Seismicity of the south Pacific Ocean, J. Geophys. Res., 68, 5999.
Sykes,L.R., 1965, The seismicity of the Arctic, Bull. Seismol. Soc. Amer., 55, 501.
Sykes,L.R., 1967, Mechanism of earthquakes and nature of faulting on the mid-oceanic ridges, J. Geophys. Res., 72, 2131.
Sykes,L.R., 1968, Seismological evidence for transform faults, sea floor spreading, and continental drift, in The History of the Earths Crust, edited by Phinney,R.A., Princeton Univ. Press, 120.
Sykes,L.R., 1970a, Seismicity of the Indian Ocean and a possible nascent island arc between Ceylon and Australia, J. Geophys. Res., 75, 5041.
Sykes,L.R., 1970b, Earthquake swarms and sea floor spreading, J. Geophys. Res., 75, 6598.

Takeuchi,H., Uyeda,S., and Kanamori,H., 1970, Debate About The Earth, Revised edition, Freeman, Cooper and Co.
Talwani,M., 1969, A computer system for the reduction, storage and display of underway data acquired at sea, Lamont Geol. Observ. Tech. Rep. 1, CU-1-69, NOO14-67-A-0108-004.
Talwani,M., and Eldholm,O., 1972, Continental margin off Norway: a geophysical study, Geol. Soc. Amer. Bull., 83, 3575.
Talwani,M., and Eldholm,O., 1973, Boundary between continental and oceanic crust at the margin of rifted continents, Nature, 241, 325.
Talwani,M., and Meijer,R.R., 1972, Gravity measurements Eltanin cruises 28-32, Lamont-Doherty Geol. Observ. Tech. Rep. No. CU-1-72, 200.

Talwani,M., Dorman,J., Worzel,J.L., and Bryan,G.M., 1966, Navigation at sea by satellite, J. Geophys. Res., 71, 5891.
Talwani,M., Windisch,C.C., and Langseth,M.G., 1971, Reykjanes Ridge Crest: a detailed geophysical study, J. Geophys. Res., 76, 473.
Taylor,F.B., 1910, Bearing of Tertiary mountain belt on the origin of the earth's plan, Geol. Soc. Amer. Bull., 21, 179.
Taylor,P.T., Brennan,J.A., and O'Neill,N.J., 1971, Variable sea floor spreading off Baja California, Nature, 229, 396.
Thompson,G., and Melson,W.G., 1972, The petrology of oceanic crust across fracture zones in the Atlantic Ocean: evidence of a new kind of sea floor spreading, J. of Geology, 80, 526.
Thomson,A.A., and Evison,F.F., 1962, Thickness of the earth's crust in New Zealand, N.Z.J. Geol. Geophys., 5, 29.
Tobin,D.G., and Sykes,L.R., 1968, Seismicity and tectonics of the northeast Pacific Ocean, J. Geophys. Res., 73, 3821.
Tolstikov,E.T., 1966, Editor of Atlas Antarktiki, Glavnoe upravlenie geodezii i kartografii, MGSSSR.
Tsuboi,T., 1958, On seismic activities in and near Japan, in Contributions in Geophysics in Honour of Beno Gutenberg, Pergamon Press, 87.

Udintsev,G.V., 1964, Editor, Bathymetric Map of the Pacific Ocean, Institute of Oceanology, Academy of Science, U.S.S.R.
U.S. Naval Oceanographic Office, 1965, Operation Deep Freeze 62, 1961-1962 Marine Geophysical Investigations, TR-118.
U.S. Naval Oceanographic Office, 1967, New Zealand to Cape Adare, 2nd Ed., H.O. 6710.
U.S. Navy Hydrographic Office, 1962, Operation Deep Freeze 61, 1960-1961 Marine Geophysical Investigations, TR-105.
Utsu,T., 1965, A method for determining the value of b in a formula log n = a - bM showing the magnitude frequency relation for earthquakes (in Japanese with English abstract). Geophys. Bull. Hokkaido Univ., 13, 99.
Utsu,T., 1966, A statistical significance test of the difference in b-value between two earthquake groups, J. Physics of the Earth, 14, 37.

Vacquier,V., 1972, Geomagnetism in Marine Geology, Elsevier.
van Andel,T.H., 1971, Fracture zones, Comments on Earth Sciences: Geophysics, 1, 159.
van Andel,T.H., 1972, Establishing the age of the oceanic crust, Comments on Earth Sciences: Geophysics, 2, 157.
van Andel,T.H., and Bowin,C.O., 1968, Mid-Atlantic Ridge between 22 and 23 north latitude and the tectonics of mid-ocean rises, J. Geophys. Res., 73, 1279.
van den Akker,F.B., Harrison,C.G.A., and Mudie,J.D., 1970, Even more on the direct interpretation of magnetic anomalies, Earth Planet. Sci. Lett., 9, 405.
van der Linden,W.J.M., 1969, Rotation of the Melanesian complex and of West Antarctica - a key to the configuration of Gondwana?, Palaeogeog. Palaeoclimatol. Palaeoecol., 6, 37.
Varne,R., and Rubenach,M.J., 1972, Geology of Macquarie island and its relationship to oceanic crust, Ant. Res. Ser., 19, 251.
Varne,R., Gee,R.D., and Quilty,P.G.J., 1969, Macquarie Island and the cause of oceanic linear magnetic anomalies, Science, 166, 230.
Vestine,E.H., 1967, Main geomagnetic field, in Physics of Geomagnetic Phenomena, edited by Matsushita,S., and Campbell,W.H., 181.

Vine,F.J., 1966, Spreading of the ocean floor: new evidence, Science, 154, 1405.
Vine,F.J., and Matthews,D.H., 1963, Magnetic anomalies over ocean ridges, Nature, 199, 947.
Vine,F.J., and Moores,E.M., 1972, A model for the gross structure, petrology, and magnetic properties of oceanic crust, Geol. Soc. Amer. Memoir, 132, 195.
Vine,F.J., and Wilson,J.T., 1965, Magnetic anomalies over a young oceanic ridge off Vancouver Island, Science, 150, 485.
Vine,F.J., Poster,C.K., and Gass,I.G., 1973, Aeromagnetic survey of the Troodos Igneous Massif, Cyprus, Nature Phys. Sci., 244, 34.
Vogt,P.R., 1972, Evidence for global synchronism in mantle plume convection, and possible significance for geology, Nature, 240, 338.
Vogt,P.R., and Johnson, 1971, Cretaceous seafloor spreading in the western north Atlantic, Nature, 234, 22.
Vogt,P.R., and Johnson,G.L., 1973, A longitudinal seismic reflection profile of the Reykjanes Ridge: Part II - Implications for the mantle hot spot hypothesis, Earth Planet. Sci. Lett., 18, 49.
Vogt,P.R., and Ostenso,N.A., 1966, Magnetic survey over the Mid-Atlantic Ridge between 42°N and 46°N, J. Geophys. Res., 71, 4389.
Vogt,P.R., Anderson,C.N., and Bracey,D.R., 1971a, Mesozoic magnetic anomalies, sea-floor spreading and geomagnetic reversals in the southwestern north Atlantic, J. Geophys. Res., 76, 4796.
Vogt,P.R., Anderson,C.N., Bracey,D.R., and Schneider,E.D., 1970, North Atlantic quiet zones, J. Geophys. Res., 75, 3955.
Vogt,P.R., Avery,O.E., Schneider,E.D., Anderson,C.N., and Bracey,D.R., 1969, Discontinuities in sea-floor spreading, Tectonophysics, 8, 285.
Vogt,P.R., Johnson,G.L., Holcombe,T.L., Gile,J.G., and Avery,O.E., 1971b, Episodes of seafloor spreading recorded by the north Atlantic basement, Tectonophysics, 12, 211.
von Huene,R., 1972, Structure of the continental margin and tectonism at the eastern Aleutian Trench, Geol. Soc. Amer. Bull., 83, 3613.

Warren,B.A., 1973, Transpacific hydrographic sections at lats 43°S and 28°S : the Scorpio expedition - II Deep water, Deep Sea Res., 20, 9.
Watkins,N.D., 1968, Comments on the interpretation of linear magnetic anomalies, Pure and Applied Geophysics, 69, 179.
Watkins,N.D., and Haggerty,S.E., 1968, Oxidation and magnetic polarity in single Icelandic lavas and dykes, Geophys. J.R. astr. Soc., 15, 305.
Watkins,N.D., and Kennett,J.P., 1972, Regional sedimentary disconformities and upper Cenozoic changes in bottom water velocities between Australasia and Antarctica, Ant. Res. Ser., 19, 273.
Watkins,N.D., and Paster,T.P., 1971, The magnetic properties of igneous rocks from the ocean floor, Phil. Trans. Roy. Soc., A 268, 507.
Watkins,N.D., and Richardson,A., 1968, Comments on the relationships between anomalies, crustal spreading and continental drift, Earth Planet. Sci. Lett., 4, 257.
Watkins,N.D., and Richardson,A., 1971, Intrusives, extrusives and linear magnetic anomalies, Geophys. J.R. astr. Soc., 23, 1.
Watkins,N.D., and Richardson,A., 1972, Reply to a paper by C.G.A. Harrison 'Comments on a paper by Watkins and Richardson: Intrusives, extrusives and linear magnetic anomalies', Geophys. J.R. astr. Soc., 28, 191.
Wegener,A., 1929, The Origin of Continents and Oceans, Methuen 1969 translation of 4th edition.
Weissel,J.K., and Hayes,D.E., 1971, Asymmetric seafloor spreading south of Australia, Nature, 231, 518.

Weissel,J.K., and Hayes,D.E., 1972, Magnetic anomalies in the southeast Indian ocean, Ant. Res. Ser., 19, 165.
Wellman,H.W., 1956, Structural outline of New Zealand, N.Z. D.S.I.R. Bull., 121.
Wellman,H.W., 1972, Rate of horizontal fault displacement in New Zealand, Nature, 237, 275.
Wellman,H.W., 1973a, New Zealand fault zones and sea-floor spreading, in The Western Pacific: Island Arcs, Marginal Seas, Geochemistry, edited by Coleman,P.J., Univ. Western Australia Press.
Wellman,H.W., 1973b, The Stokes magnetic anomaly, Geol. Mag., 110, 419.
Wellman,P., and Cooper,A., 1971, Potassium-Argon age of some New Zealand lamprophyre dikes near the Alpine fault, N.Z.J. Geol. Geophys., 14, 341.
Whitmarsh,R.B., and Jones,M.T., 1969, Daily variation and secular variation of the geomagnetic field from shipboard observations in the Gulf of Aden, Geophys. J.R. astr. Soc., 18, 477.
Williams,C., 1967, Rates of secular variation in the north-east Atlantic, Naturo, 215, 1468.
Williams,C.A., and McKenzie,D., 1971, The evolution of the north-east Atlantic, Nature, 232, 168.
Williamson,P., and Rubenach,M.J., 1972, Preliminary report on geological studies of Macquarie island, Ant. Res. Ser., 19, 243.
Wilson,R.L., 1962, The palaeomagnetism of baked contact rocks and reversal of the earths magnetic field, Geophys. J.R. astr. Soc., 7, 194.
Wilson,J.T., 1963, Hypothesis of Earth's behaviour, Nature, 198, 923.
Wilson,J.T., 1965, A new class of faults and their bearing on continental drift, Nature, 197, 343.
Wilson,R.L., 1966, Further correlations between petrology and the natural magnetic polarity of basalts, Geophys. J.R. astr. Soc., 10, 413.
Wilson,R.L., 1971, Dipole offset - the time average palaeomagneic field over the past 25 million years, Geophys. J.R. astr. Soc., 22, 491.
Wilson,R.L., and Watkins,N.D., 1967, Correlation of petrology and natural magnetic polarity in Columbia plateau basalts, Geophys. J.R. astr. Soc., 12, 405.
Woodward,D.J., 1973, Gravity and magnetic anomalies over the Macquarie Ridge, in Oceanography of the South Pacific 1972, comp. by Fraser,R., N.Z. Nat. Comm. UNESCO, 325.
Woolard,G.P., 1962, Crustal structure in Antarctica, A.G.U. Monograph, 7, 53.
Worzel,J.L., 1965, Deep structure of coastal margins and mid-ocean ridges, in Submarine Geol. Geophys., Proc. 17th Symp. Colston Res. Soc., 335.
Wyllie,P.J., 1971, The Dynamic Earth, Wiley.
Wyss,M., 1973, Towards a physical understanding of the earthquake frequency distribution, Geophys. J.R. astr. Soc., 31, 341.

Yule,G.U., 1921, On the time-correlation problem with especial reference to the variate-difference correlation method, J.R. Stats. Soc., 84, 497.

Zhivago,A.V., 1962, Outlines of Southern Ocean geomorphology, A.G.U. Monograph, 7, 74.


HMNZS ENDEAVOUR

# GEOPHYSICAL STUDIES IN THE SOUTHWEST PACIFIC:

## PRIMARILY STUDIES OF CRUSTAL STRUCTURE BETWEEN NEW ZEALAND AND ANTARCTICA

VOLUME 2

ROBIN KEITH HALCRO FALCONER

Submitted for the degree of

Doctor of Philosophy in Physics

Victoria University of Wellington

New Zealand

February 1974

# CONTENTS

VOLUME 2

# FIGURES

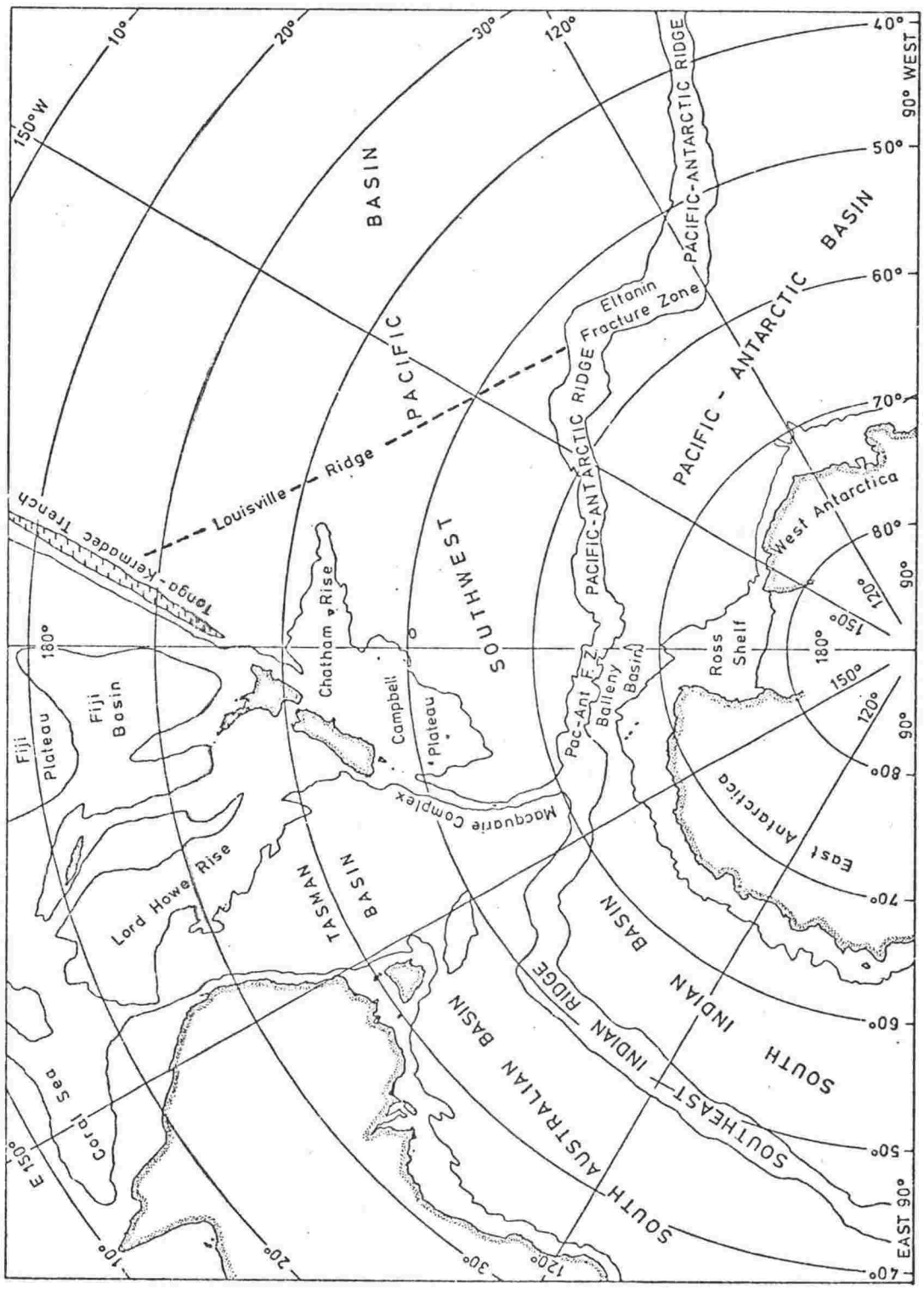


Fig. 0.1 The southwest Pacific area. Generalised 3000 m isobath outlines all the major features.

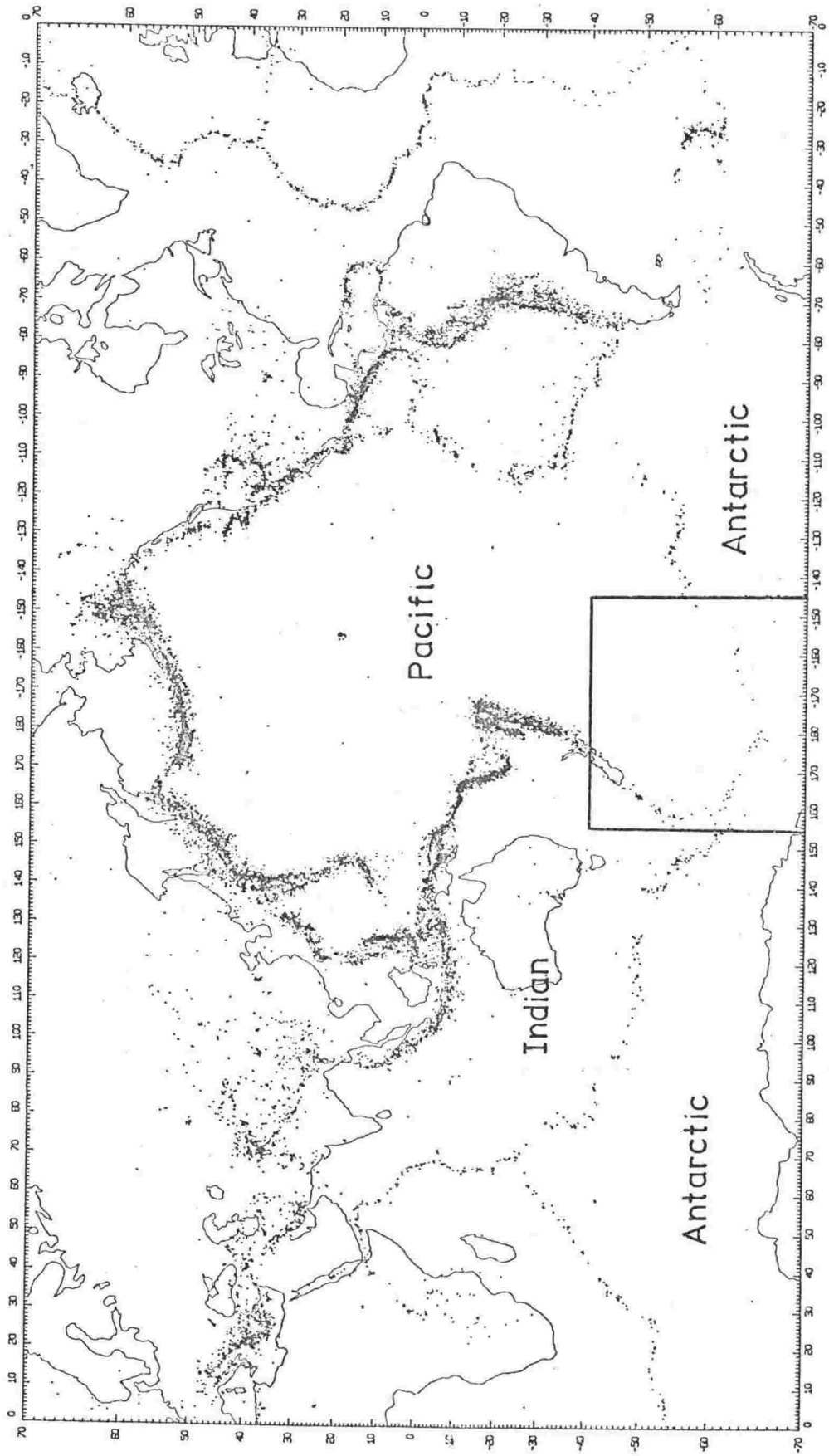


Fig. 0.2 World seismicity with the primary area of study outlined. The seismicity outlines the worlds major plates. The Indian, Pacific, and Antarctic plates intersect in the area studied.

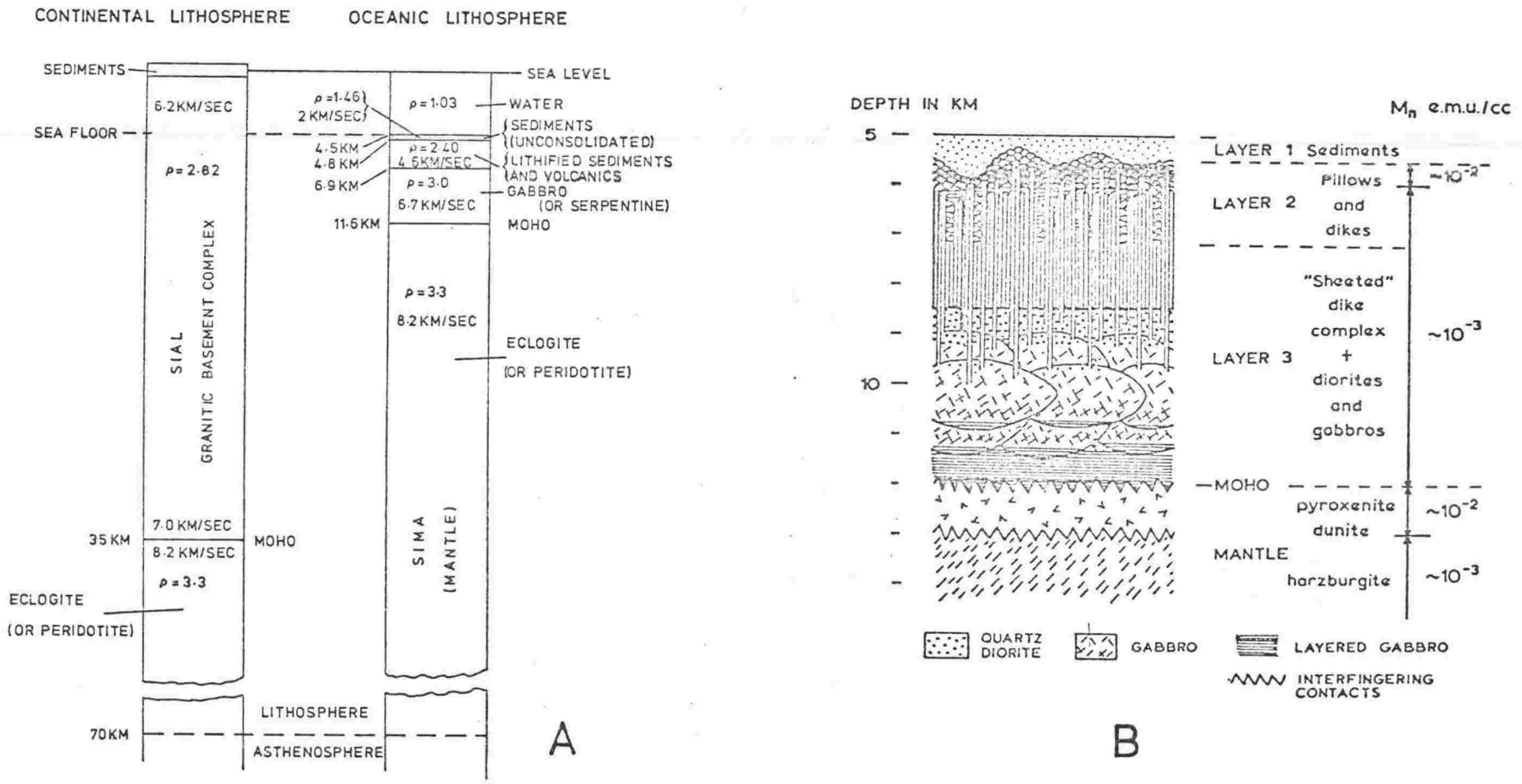


Fig. 1.1 Models for the earths crust. A, from Dietz (1961, Fig. 1), shows the earliest "seafloor spreading" oceanic model. B, from Vine and Moores (1972, Fig. 1), is a recent oceanic model based on the structure of the Troodos massif, Cyprus.

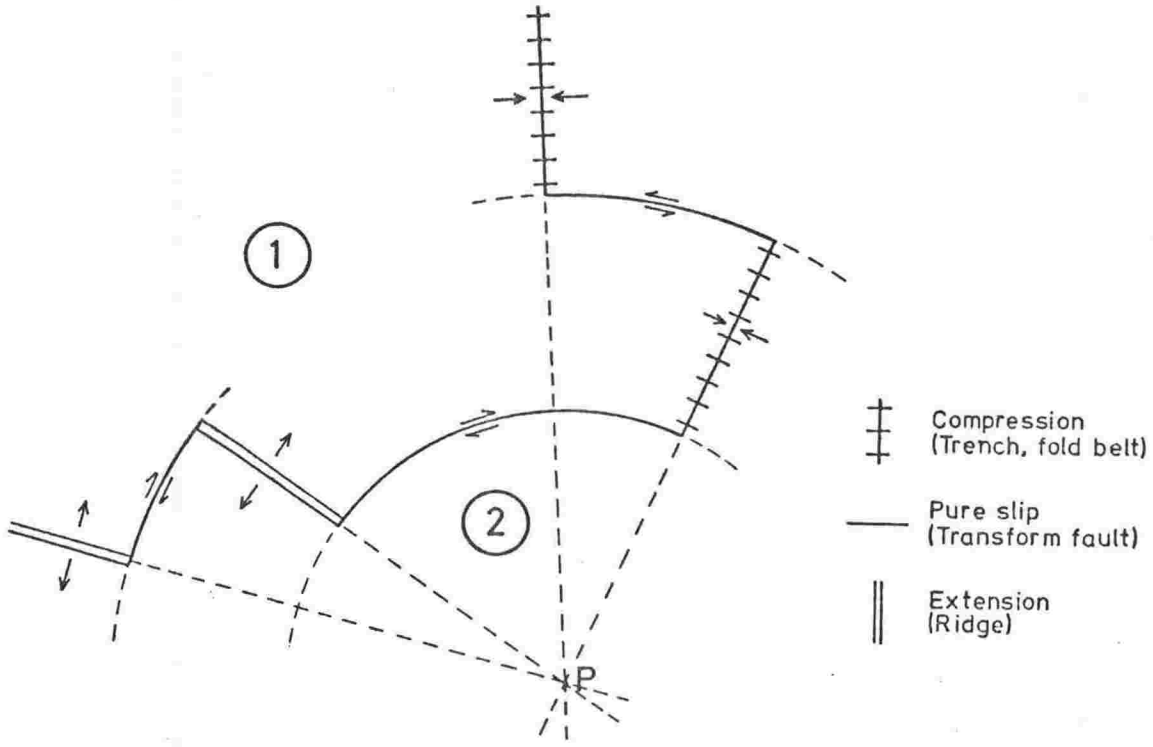


Fig. 1.2 Plate movements and types of plate boundary. Plate 1 rotating clockwise with respect to plate 2 about pole at P.

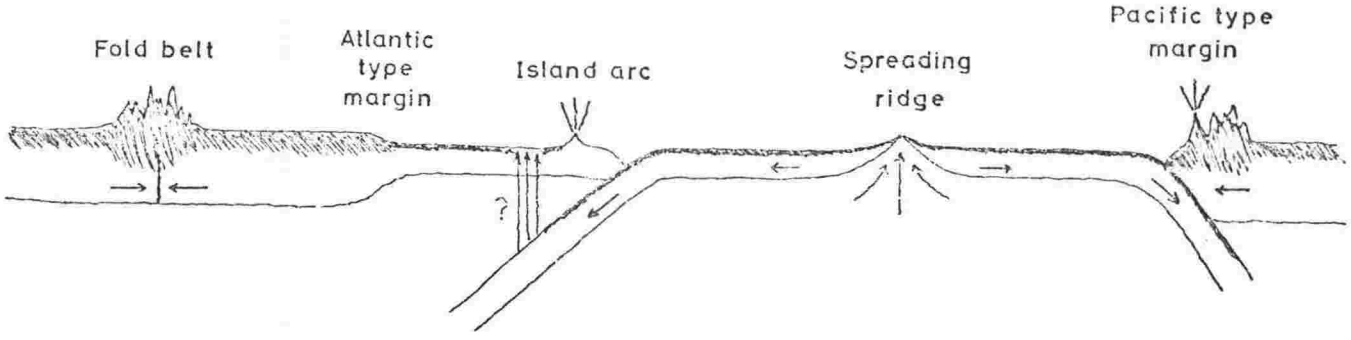


Fig. 1.3 Plate boundaries and tectonic features. Shaded parts of plates indicate the crust. Substantial vertical exaggeration.

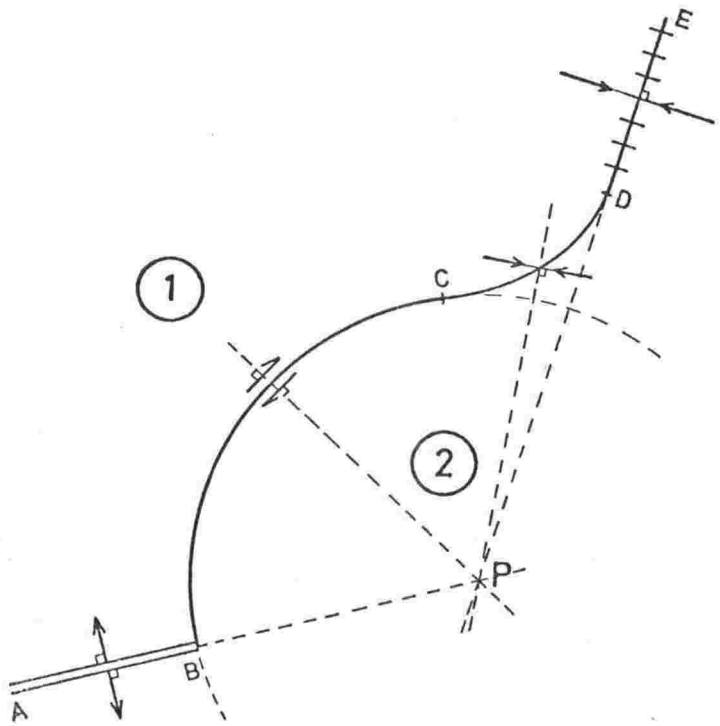


Fig. 1.4 A ridge to trench transformation. Plate 1 rotating clockwise with respect to plate 2 about pole at P.

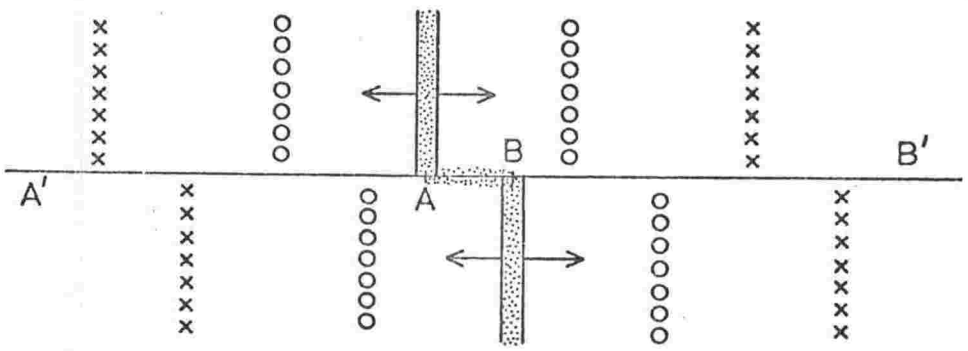


Fig. 1.5 An offset spreading ridge. Crosses and circles indicate magnetic anomalies produced at the ridge crests. Stippled areas indicate seismically active areas.

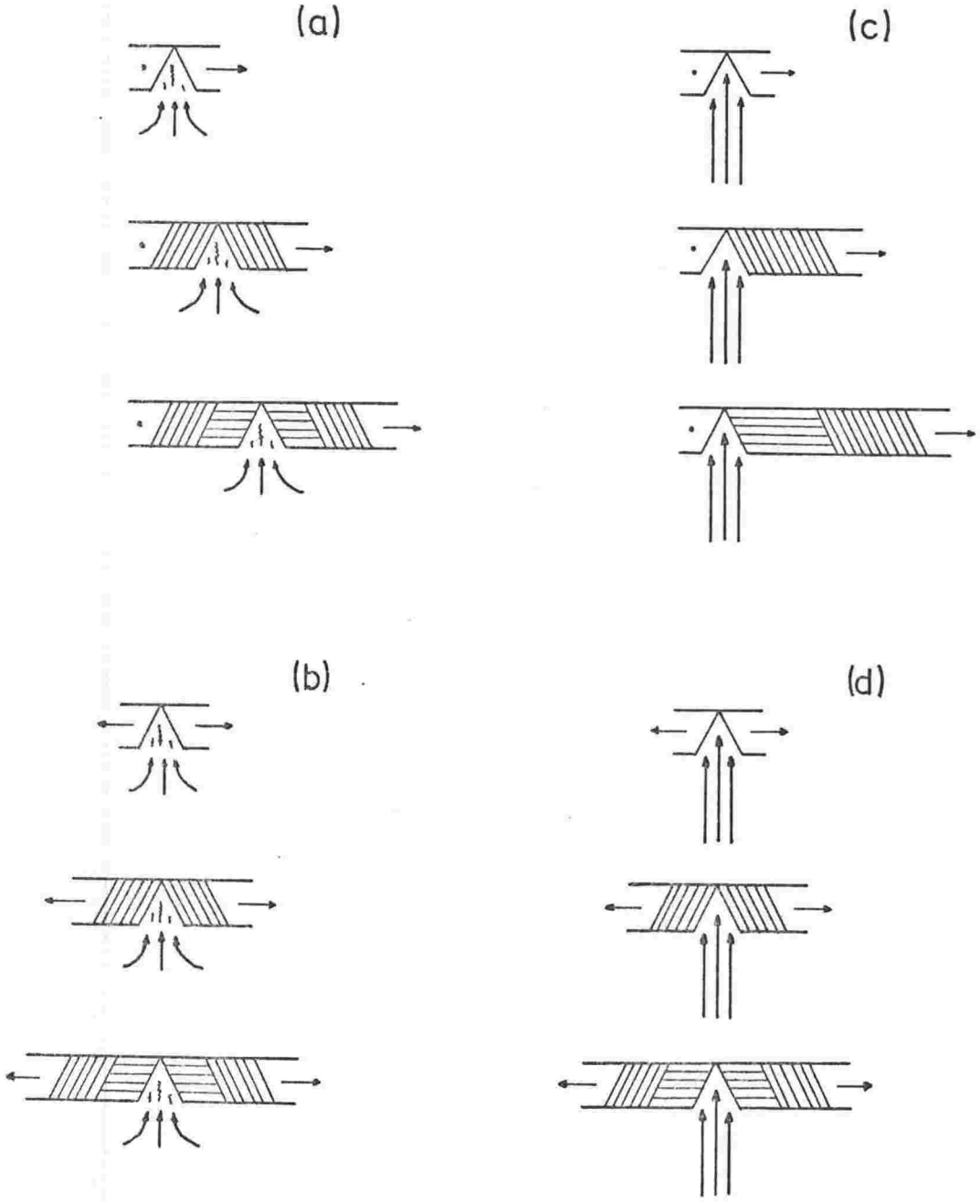


Fig. 1.6 Formation of symmetrical and asymmetrical seafloor spreading. For a and c the left plate is fixed in position. All four cases produce the same amount of seafloor in the same time.

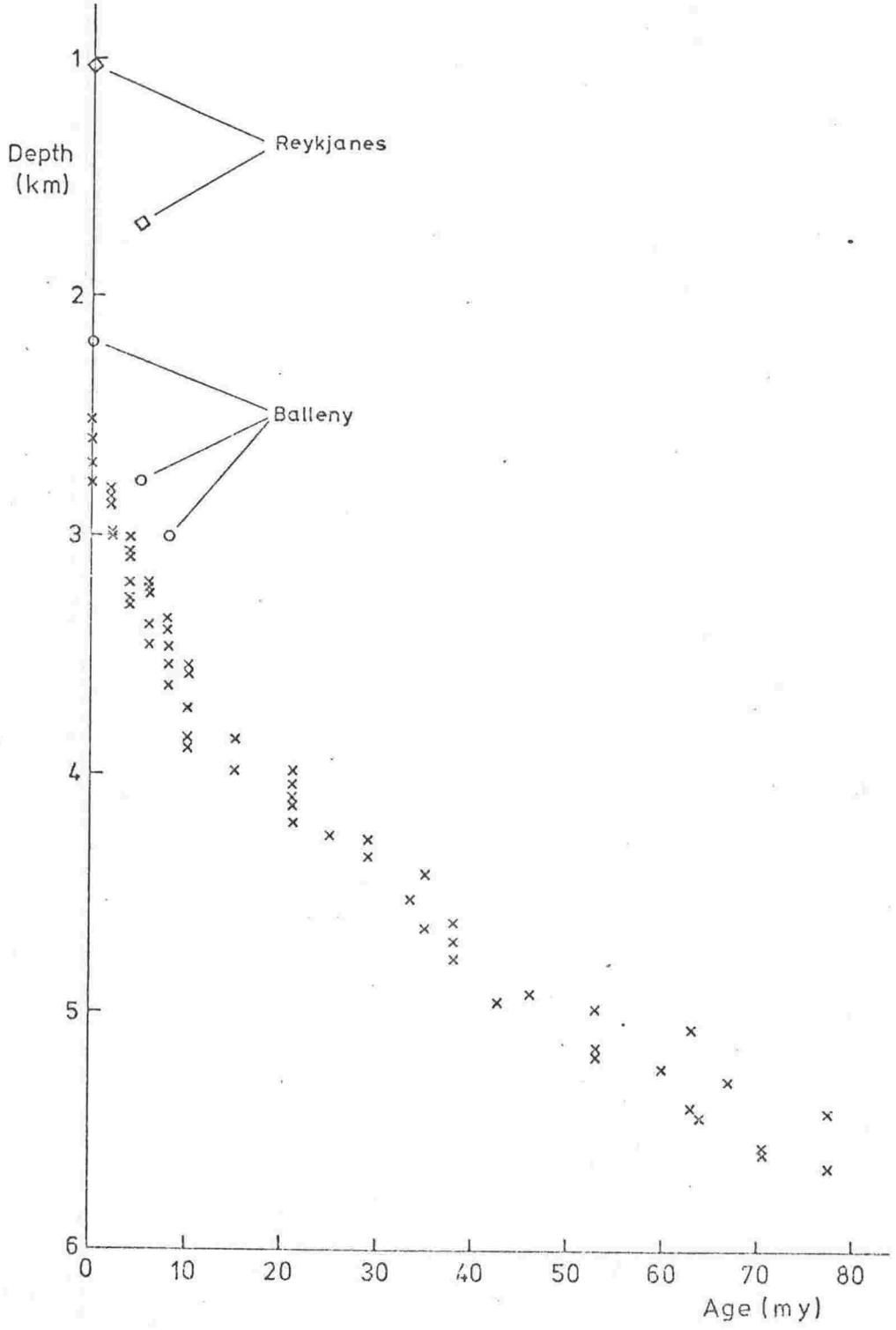


Fig. 1.7 Depth of the seafloor v. age. Data shown by crosses are from the Pacific, Indian, and Atlantic oceans (from Sclater et al., (1971)). Reykjanes ridge from Talwani et al. (1971), and Balleny area from this study.

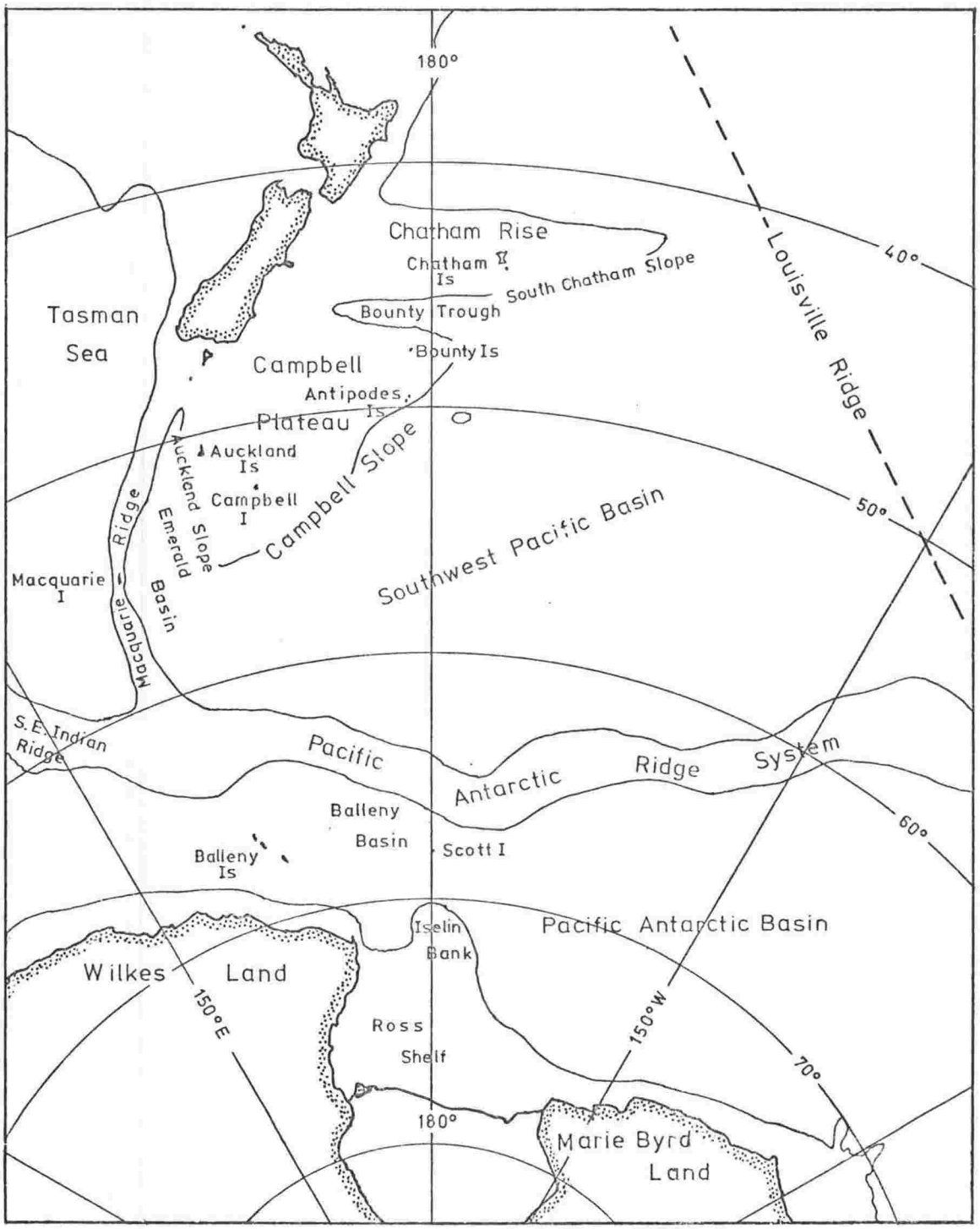


Fig. 2.1 The primary area of study. Generalised bathymetric contours outline the major morphologic features. Contours are 2000 m for continents, 3000 m for ridge systems.

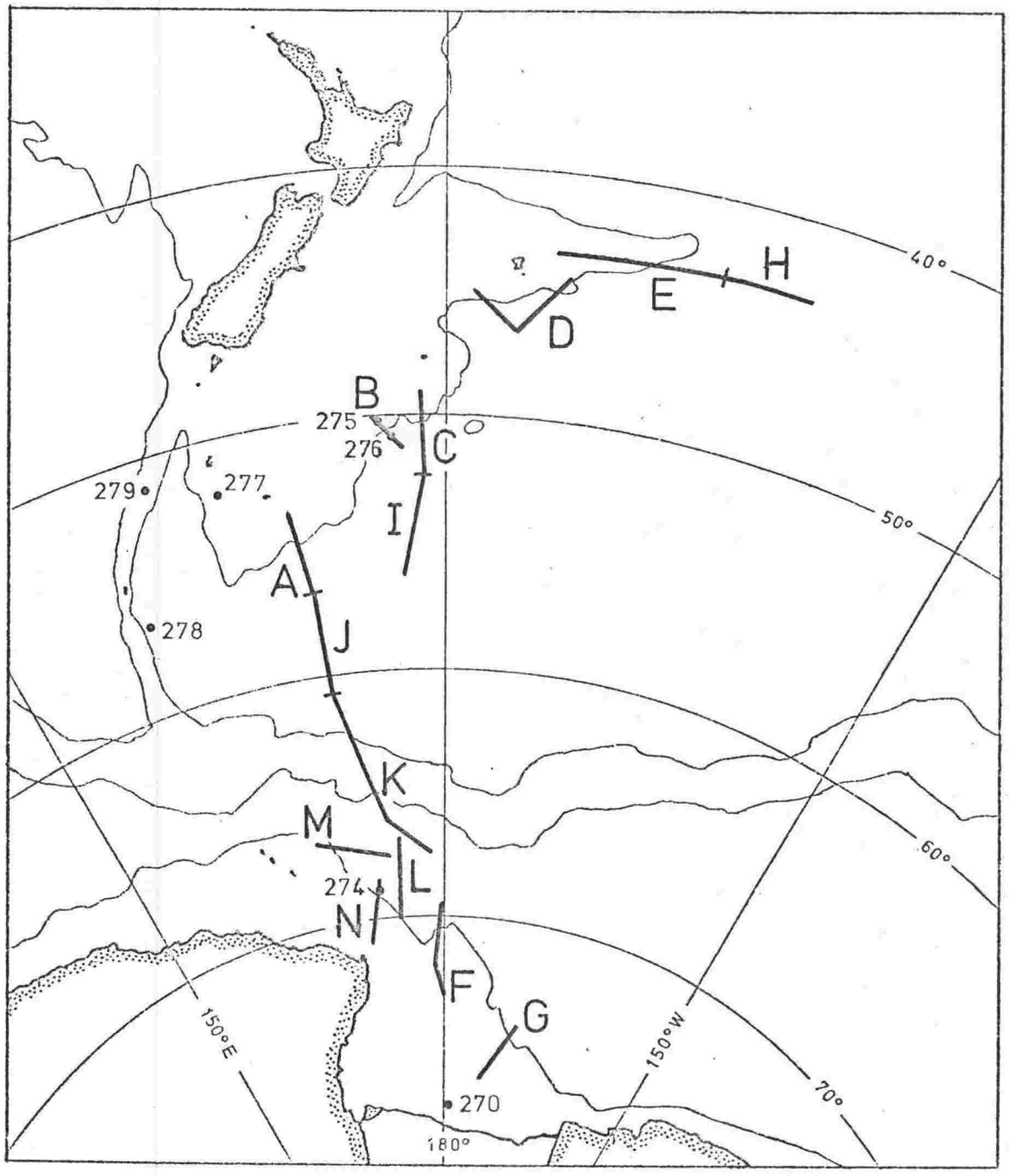


Fig. 2.2 Seismic profiles and JOIDES sites. Numbers indicate the positions of JOIDES drilling sites. Labelled lines indicate the positions of seismic profiles shown in subsequent figures.

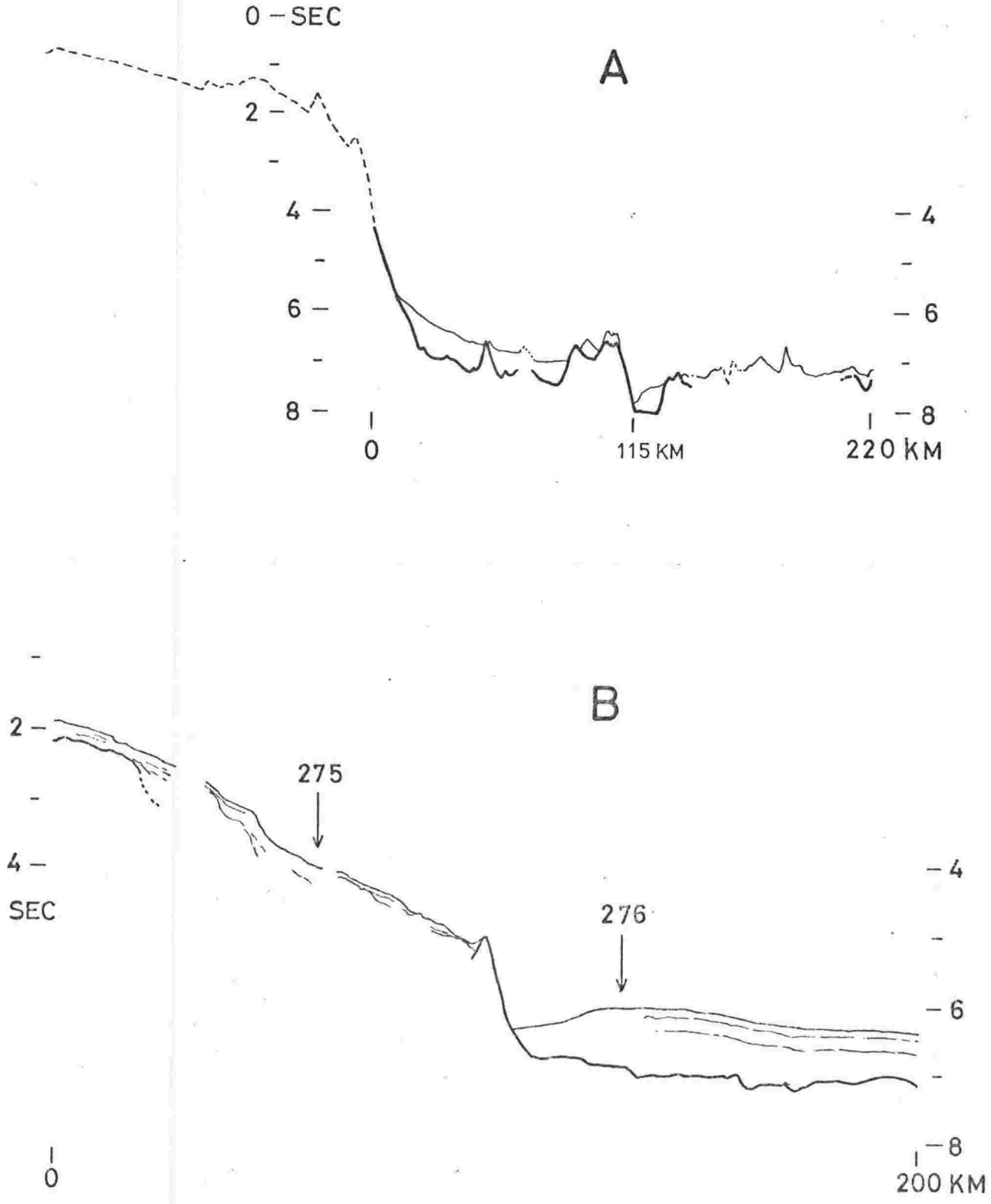


Fig. 2.3 Seismic reflection profiles across the Campbell plateau and Chatham rise margins. Location of profiles shown in Fig. 2.2. Vertical scale in units of twoway travel time. One second represents ∿ 750 m for water, ∿ 1000 m for sediment. Sections A, C, and E redrawn from Hayes et al. (1972b). Section B redrawn from Houtz and Markl (1972, Fig. 10). Section D from Houtz et al. (1967, Fig. 4). Numbered arrows in section B are the approximate locations of JOIDES drilling sites 275 and 276.

Continued overleaf.

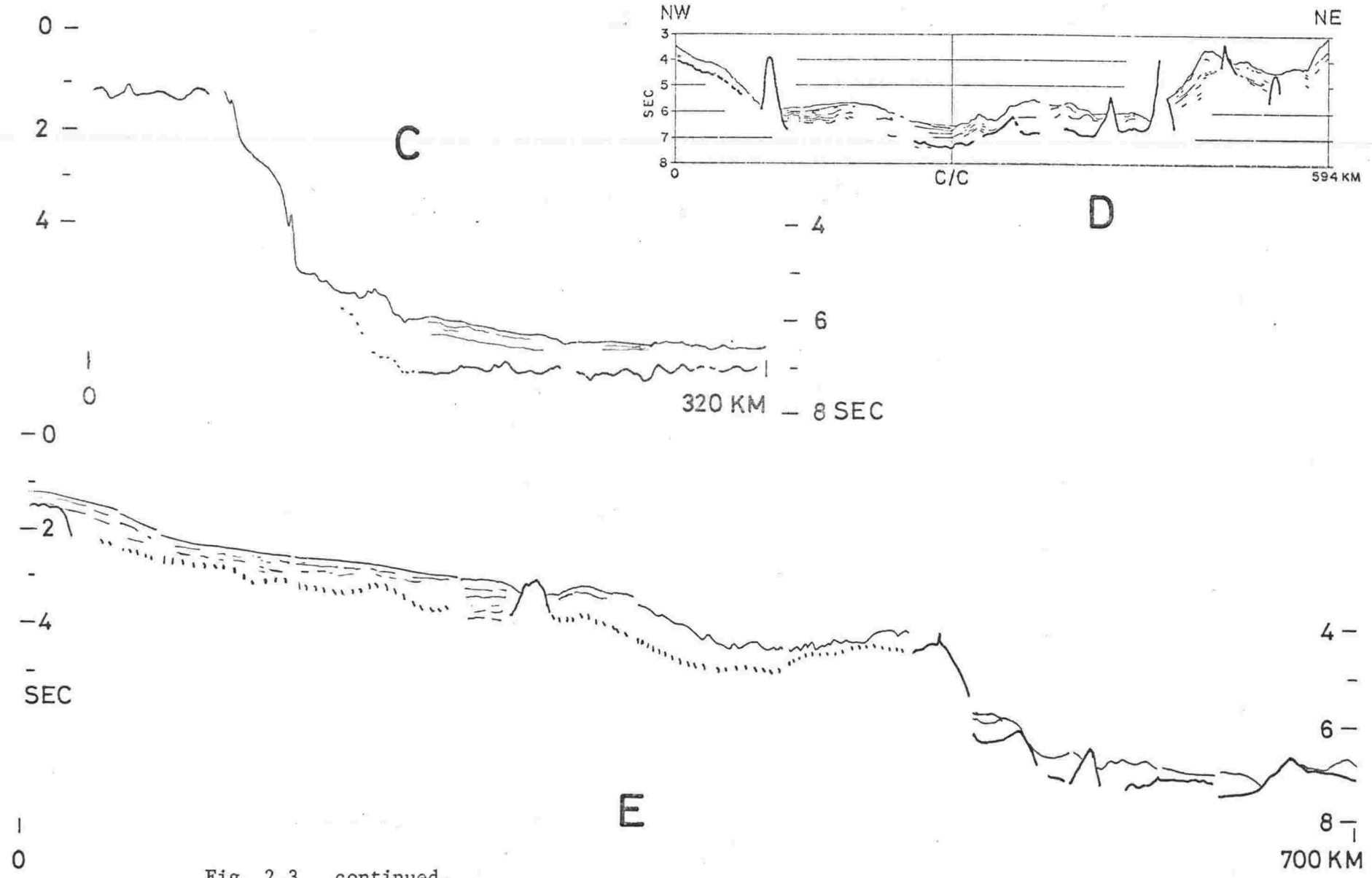


Fig. 2.3 continued.

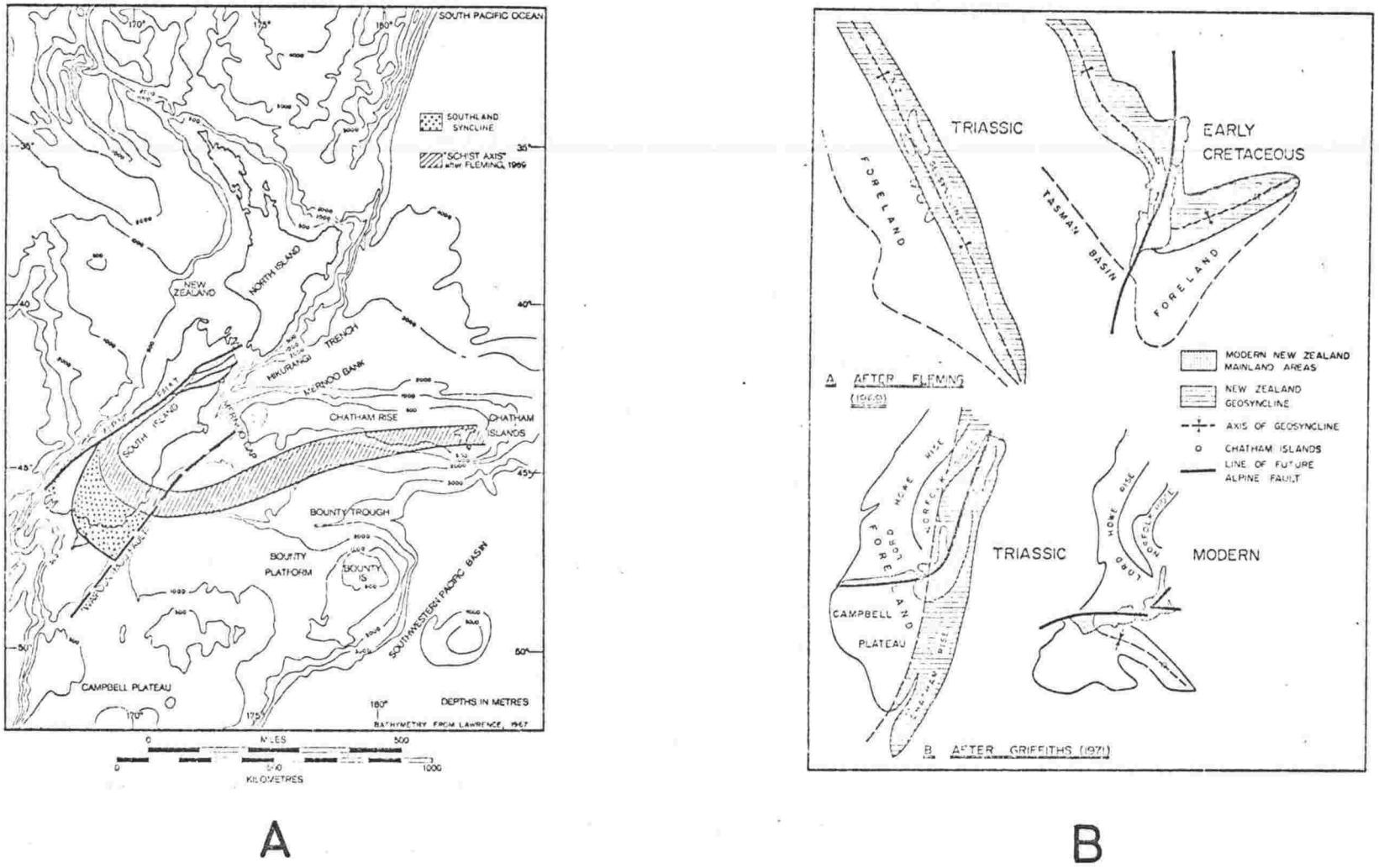


Fig. 2.4 A: New Zealand region structure, modified from Austin et al. (1973, Fig. 1).
B: Paleographic reconstruction of the New Zealand region, from Austin et al. (1973, Fig. 9).

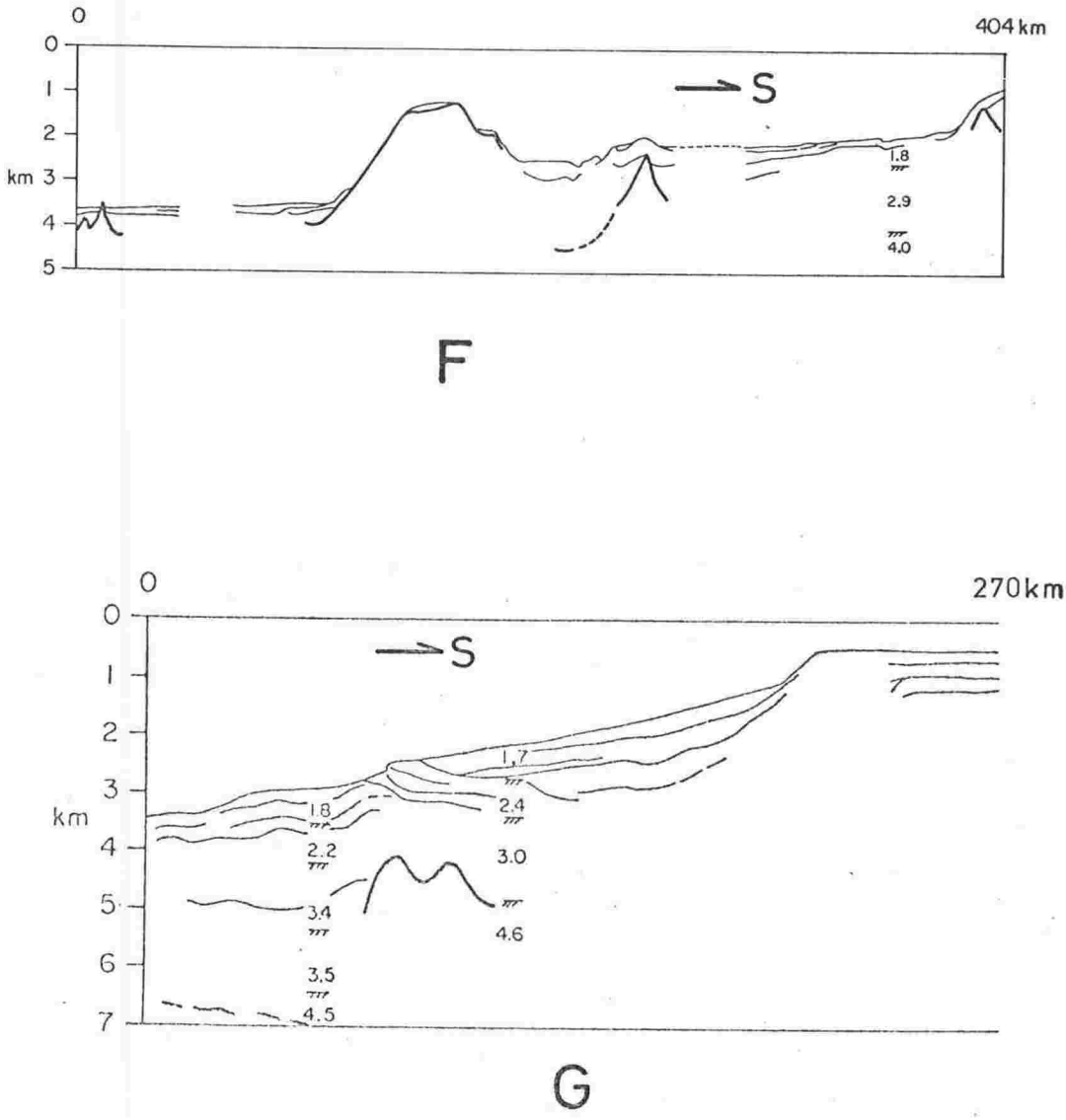


Fig. 2.5 Seismic reflection profiles across the Ross shelf margin. Locations of profiles shown in Fig. 2.2. Numbers and hatching in profiles are velocities and layers determined from sonobuoys. From Houtz and Davey (1973, Figs 11 and 14).

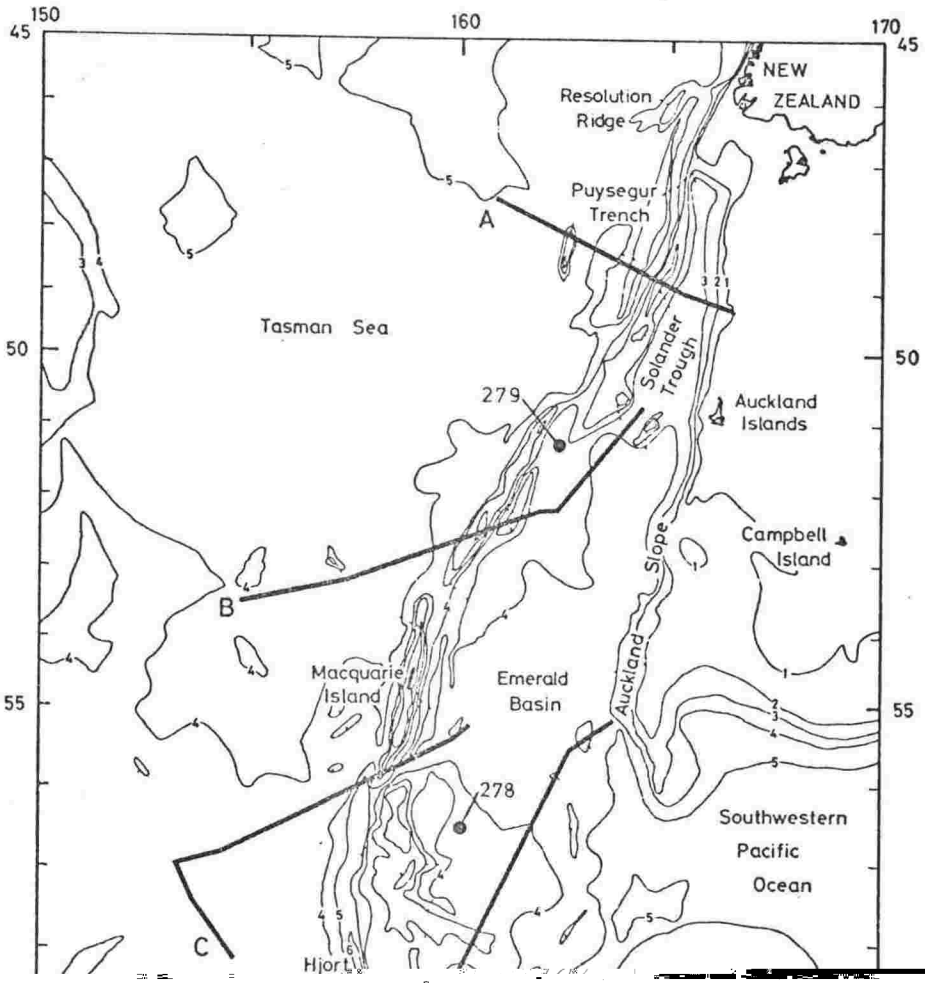
150
160
170
45
50
55
NEW
ZEALAND
Resolution
Ridge
Puysegur
Trench
A
Tasman Sea
Solander
Trough
279
Auckland
Islands
Campbell
Island
Slope
B
Macquarie
Island
Emerald
Basin
Auckland
278
Southwestern
Pacific
Ocean
C
Hjort

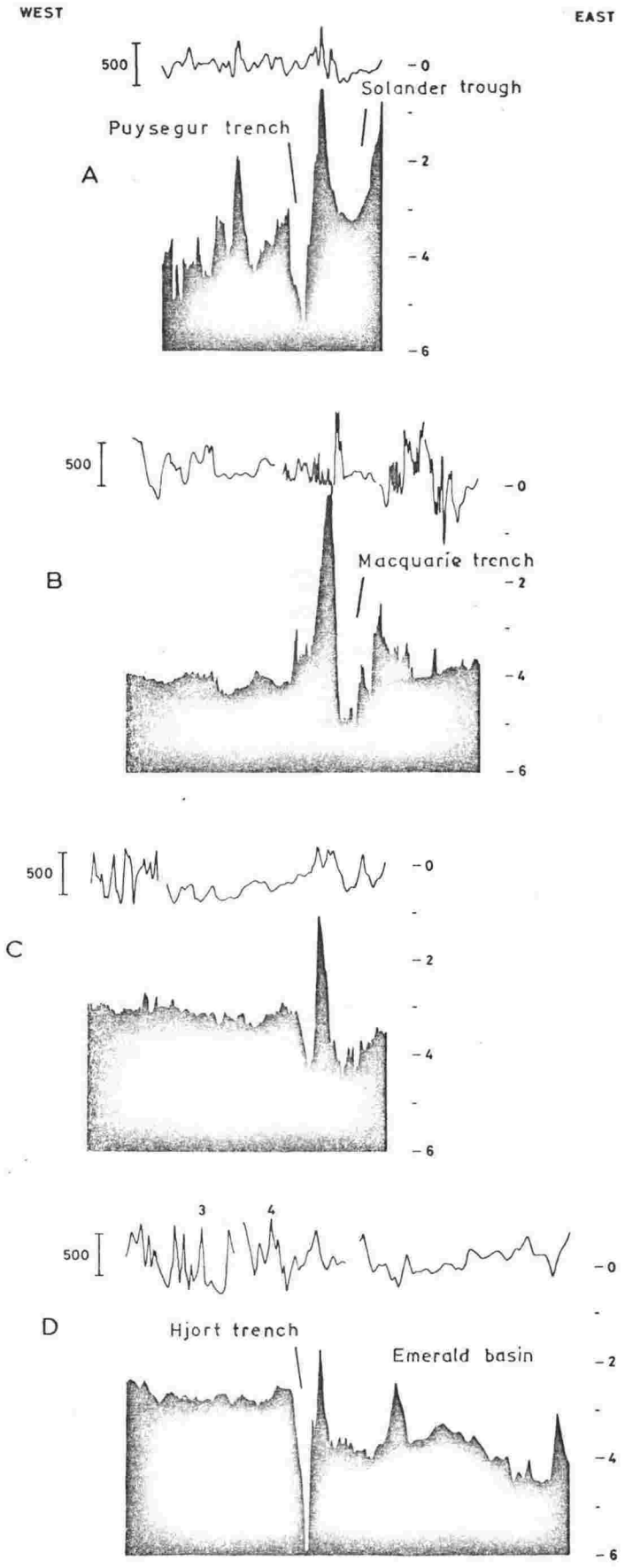


Fig. 2.7 Bathymetric and magnetic profiles across the Macquarie ridge complex, from Christoffel and R.F. Falconer (1973, Fig. 2). Bathymetric scale in kilometres, vertical exaggeration 100:1. There was a severe ionespheric storm for the right hand half of section B.

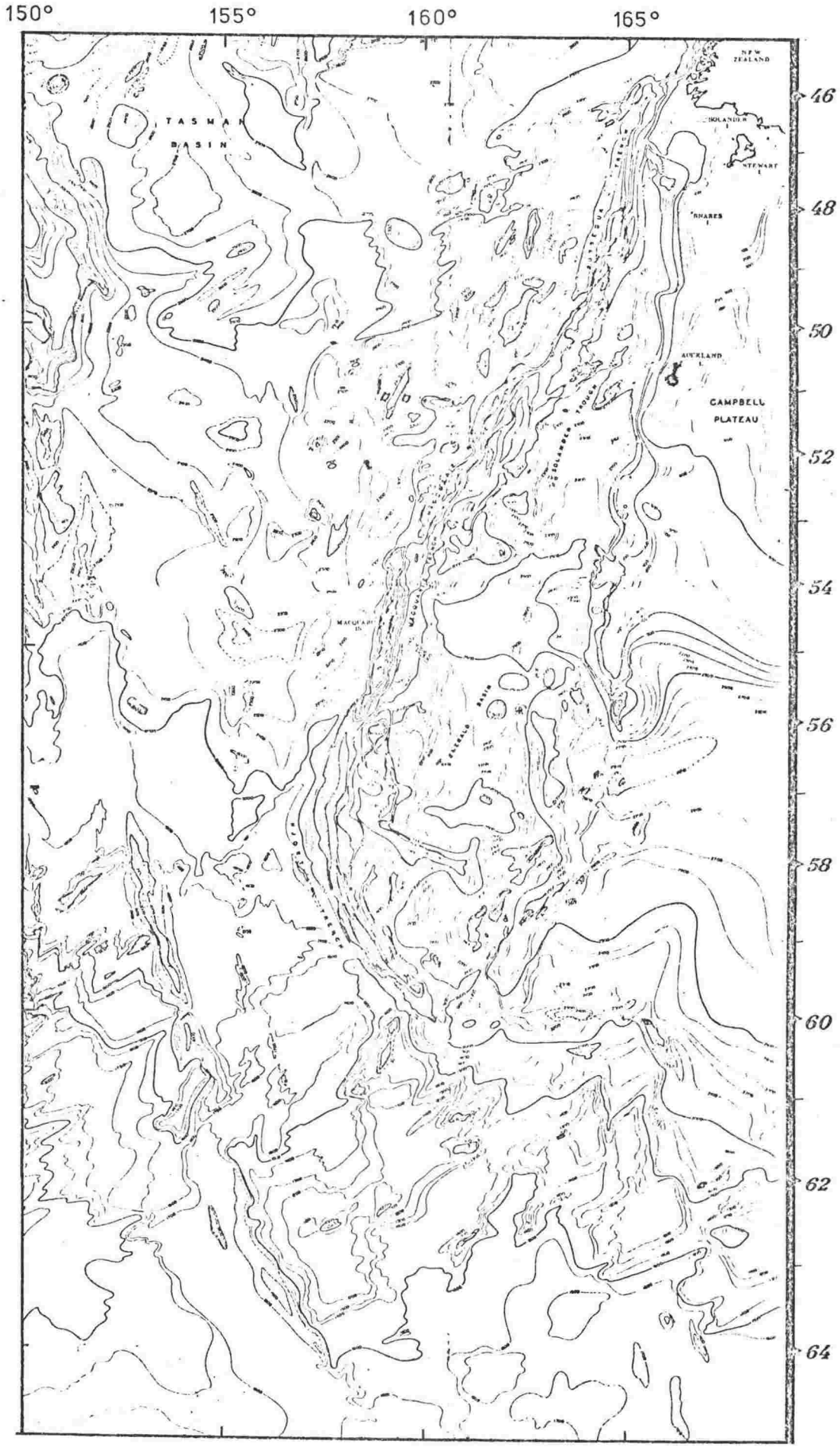


Fig. 2.8 Bathymetry of the Macquarie ridge complex. A very reduced copy of a section of Fig. 1 of Hayes and Conolly (1972). Contours in fathoms.

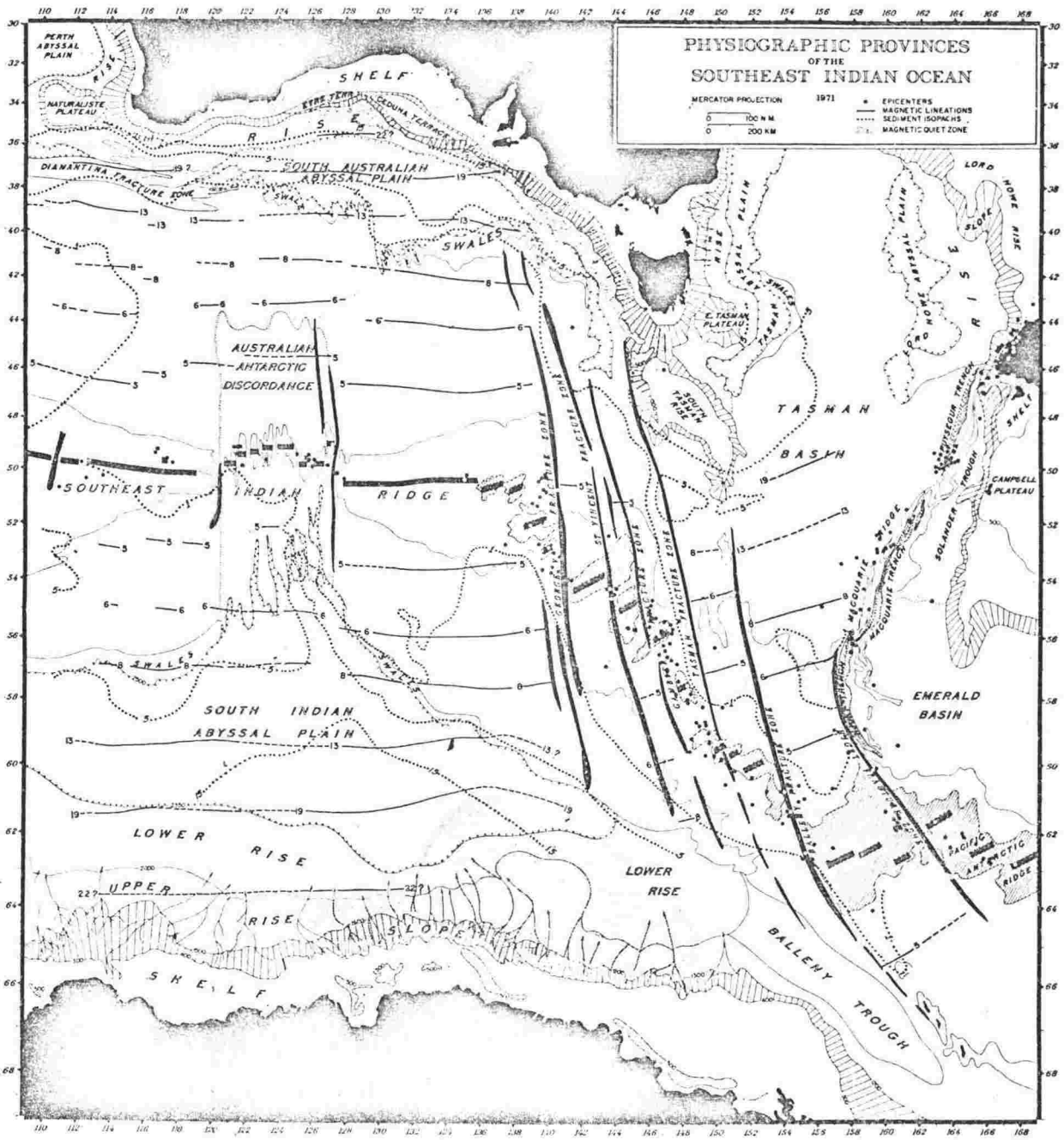


Fig. 1. Physiographic provinces of the southeast Indian Ocean modified from *Hayes and Conolly* [this volume]. Magnetic lineations are taken from *Weissel and Hayes* [this volume]. Selected sediment isopachs in tenths of a second of reflection time (0.1 sec ≈ 100 meters of sediment) are taken from *Houtz and Markl* [this volume]. Epicenters (darkened circles) are from the *Barazangi and Dorman* [1969] file. Mercator projection.

Fig. 2.9 The eastern part of the southeast Indian ocean.

From Hayes (1972, Fig. 1).

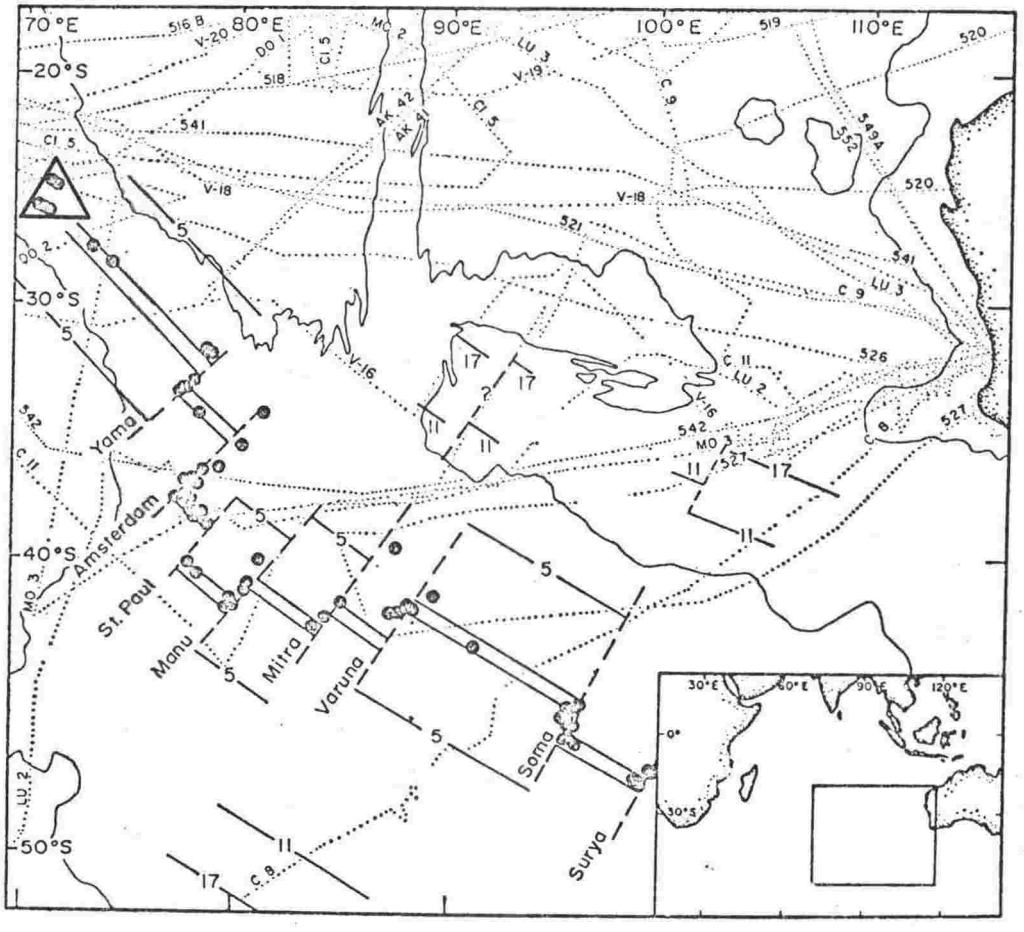


FIG. 28. Ship tracks, 4-km contour, epicentres, fracture zones, coastlines and recognizable magnetic lineations in the south-east Indian Ocean.

Fig. 2.10 The western part of the southeast Indian ocean, from McKenzie and Sclater (1971, Fig. 28). Triangle indicates the central Indian ocean triple junction.

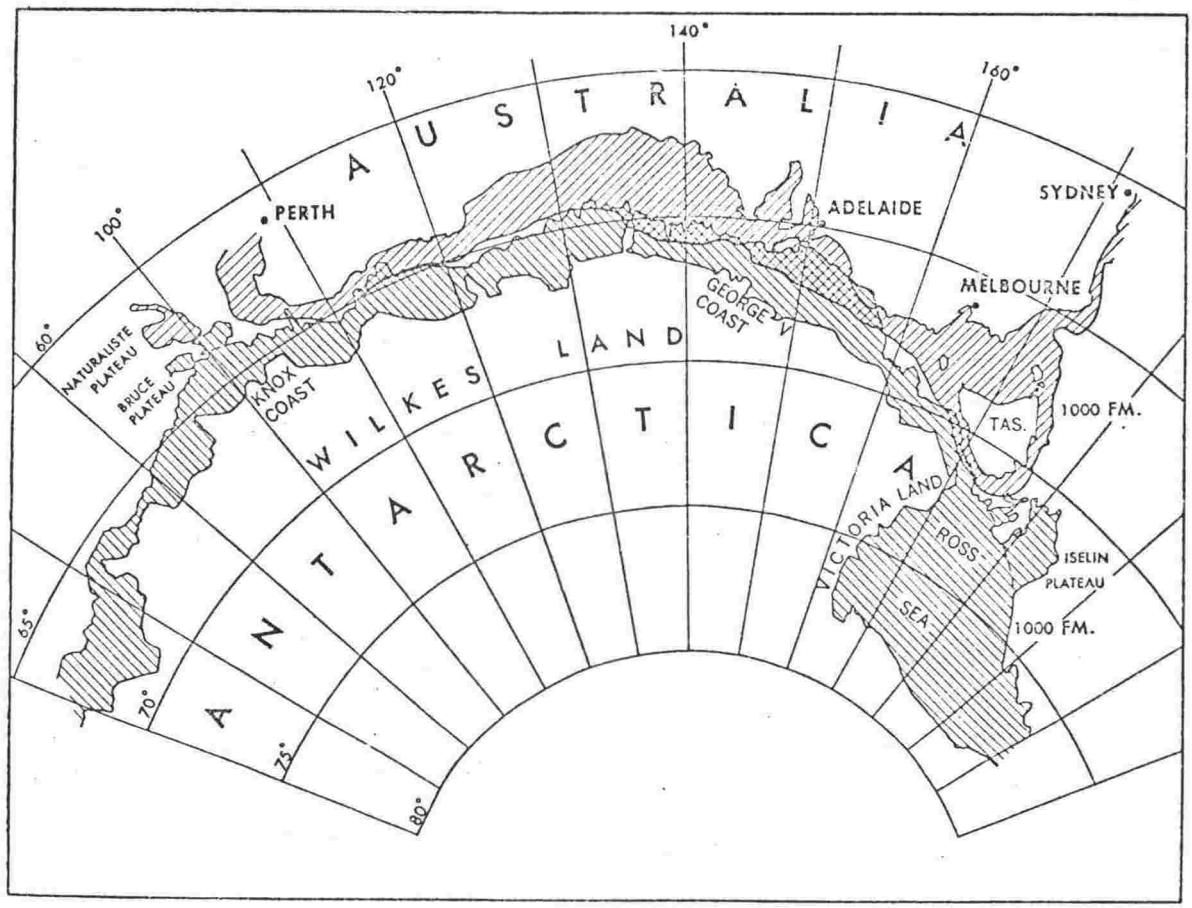


Fig. 3. The best fit of Australia with respect to Antarctica by computerized matching of the 1,000 fathom isobaths. Ruled line pattern indicates continental shelf and slope from shoreline (inner contour) to the 1,000 fathom isobath (outer contour). Overlap areas are cross-ruled and underlap areas are blank.

Fig. 2.11 Reconstruction of Australia and Antarctica, from Sproll and Dietz (1969, Fig. 3).

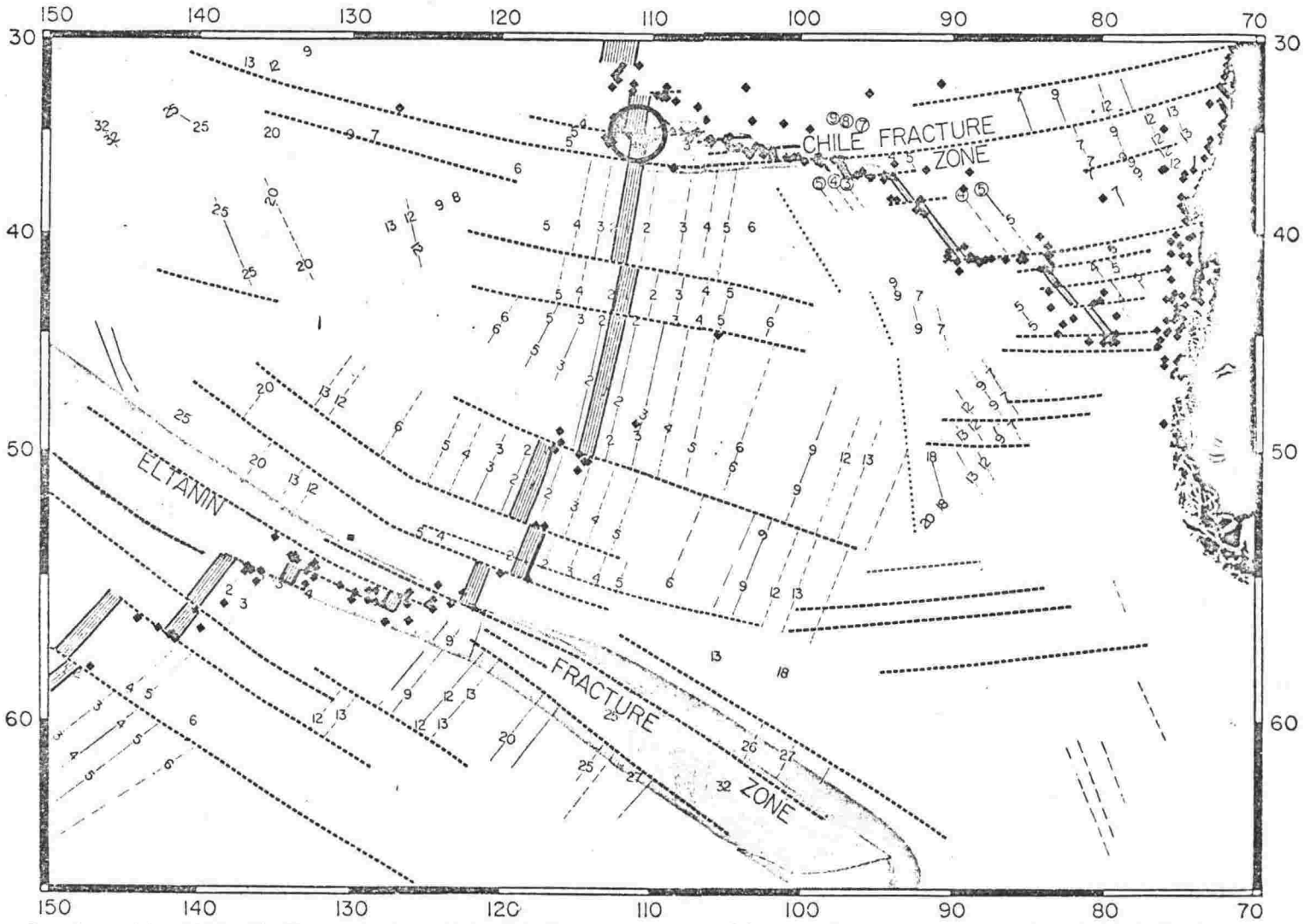


Fig. 4. Summary of the crustal features inferred from magnetic and topographic data. Earthquake epicenters taken from *Barazangi and Dorman* [1969] have been plotted as closed diamonds. Numbers indicate magnetic anomalies according to the *Pitman et al.* [1968] nomenclature. Heavy dashed lines indicate fracture zones inferred from topographic, magnetic, and seismicity data. Note that the axis of the Chile Rise lies oblique to the fracture zones crossing the rise axis. The dotted lines mark the approximate boundary between the Albatross Cordillera and the Chile Rise. Circled anomaly numbers are taken from *Morgan et al.* [1969]. Each anomaly number corresponds to an observation point. Solid connecting lines are drawn only where there are at least two points to define the lineation trend. Where the identification or correlation is tentative, light dashed lines have been used.

Fig. 2.12 The south Pacific east of 150°W, from Herron (1971, Fig. 4). Circle indicates the Pacific - Antarctic - Nazca triple junction.

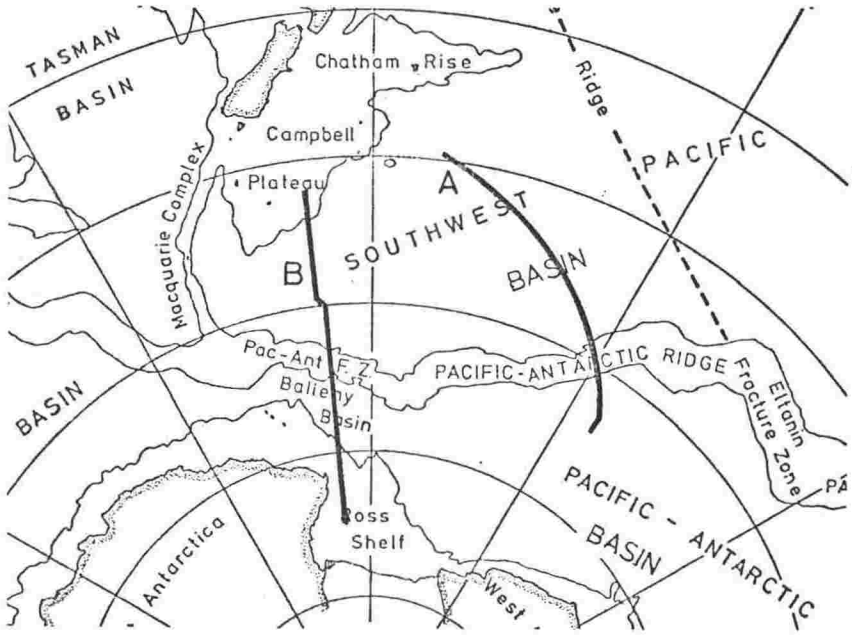


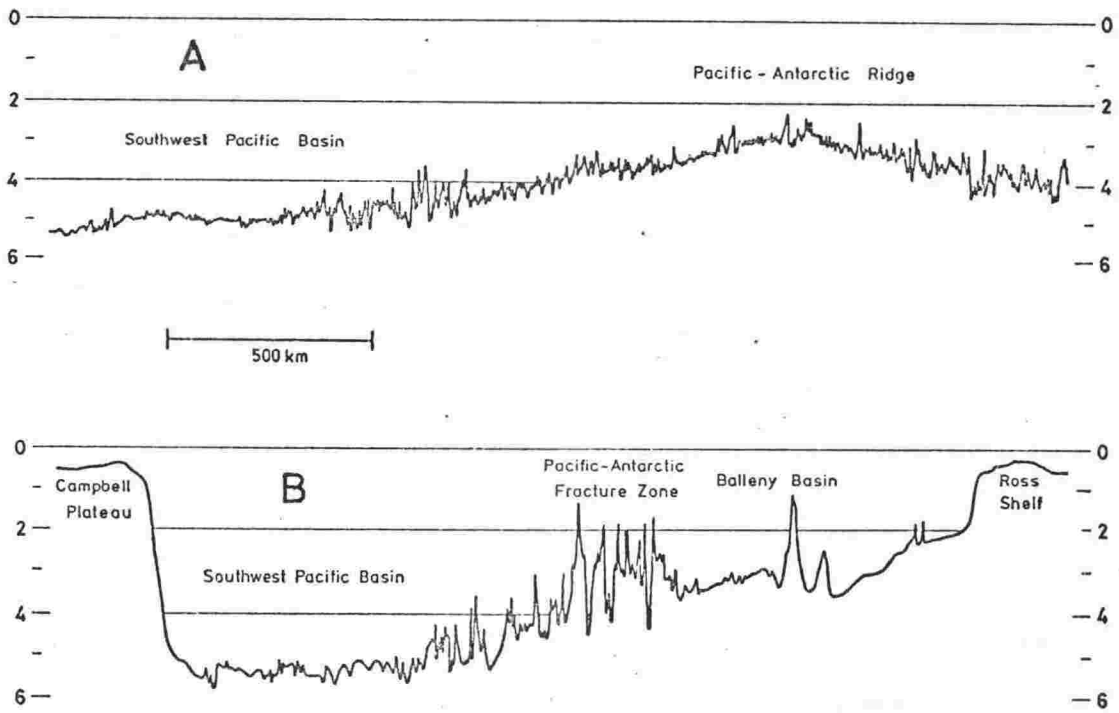


Fig. 2.13 Two representative bathymetric profiles of the southwest Pacific area. Depths in kilometres, vertical exaggeration 100:1.

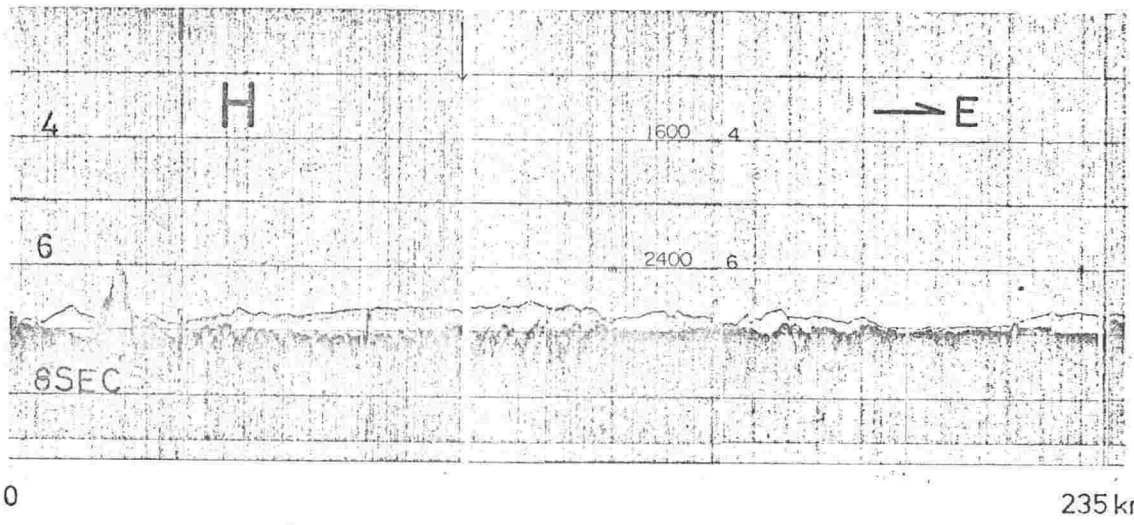


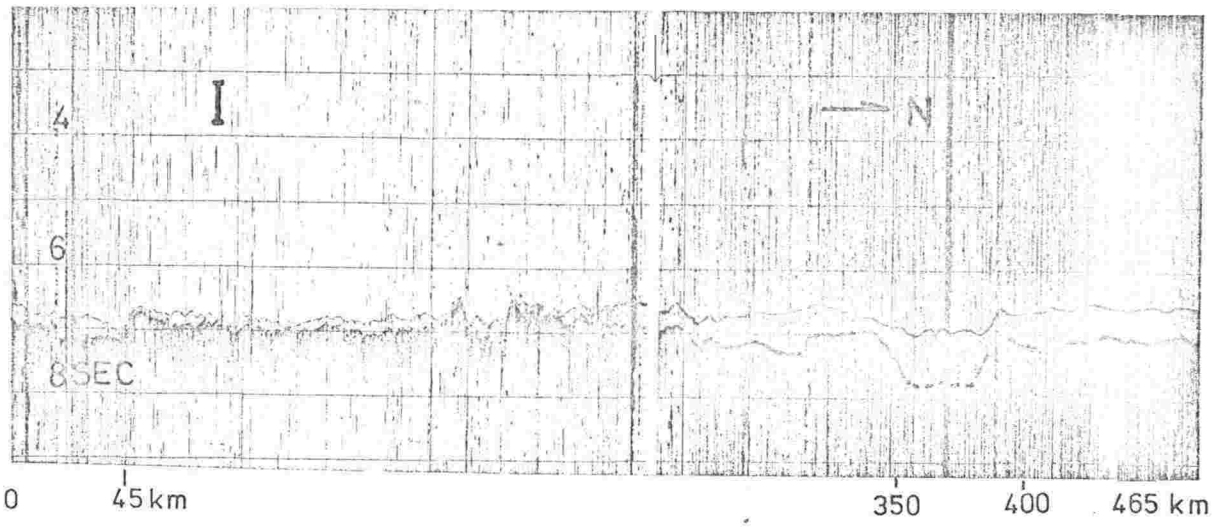


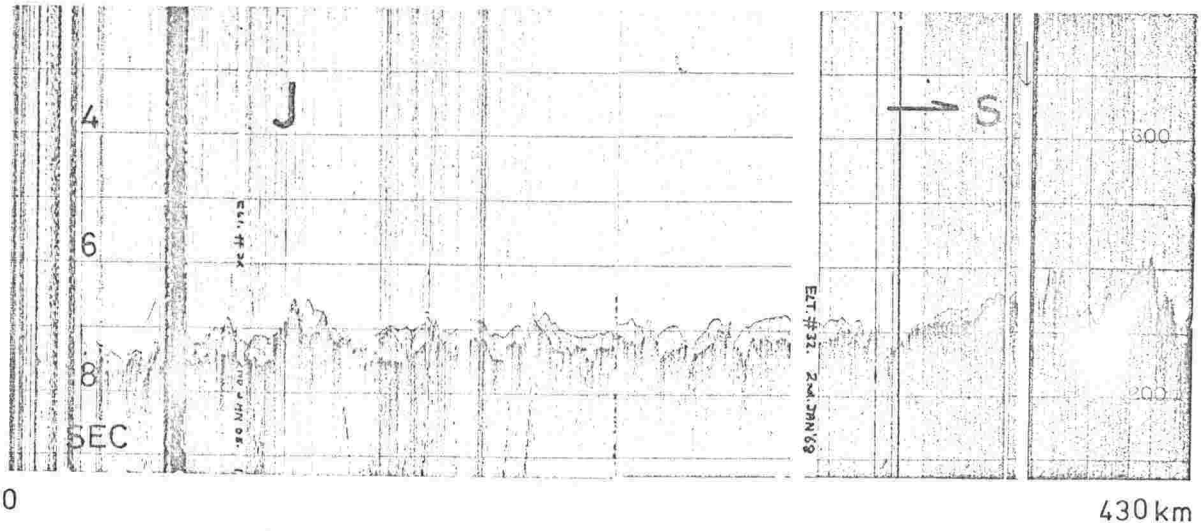


Fig. 2.14 Seismic reflection profiles in the southwest Pacific basin. Locations shown in Fig. 2.2. Vertical exaggeration ∿ 30:1. From Hayes et al. (1972b). Some of profile I touched up.

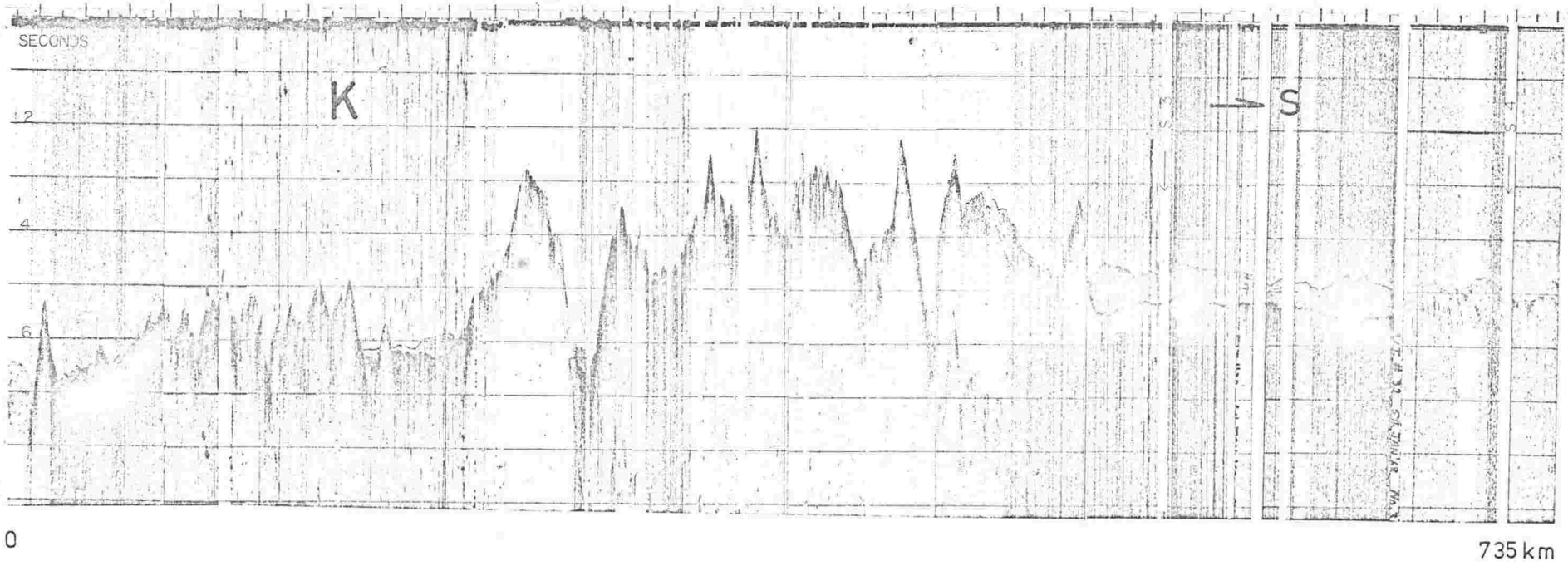


Fig. 2.15 Seismic reflection profile across the Pacific-Antarctic fracture zone. Location shown in Fig. 2.2. From Hayes et al. (1972b). Vertical exaggeration ∿ 30:1. Some of the southern end touched up.

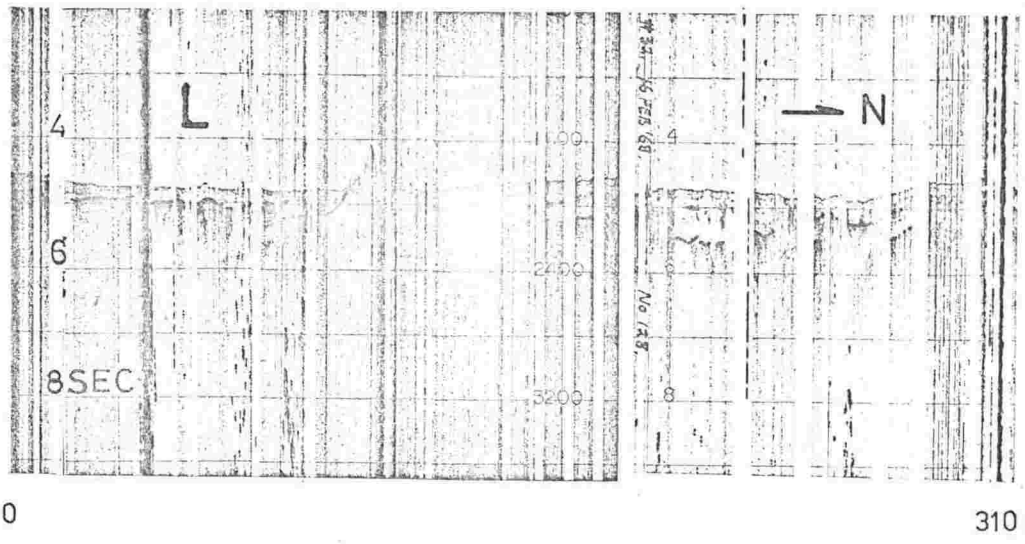


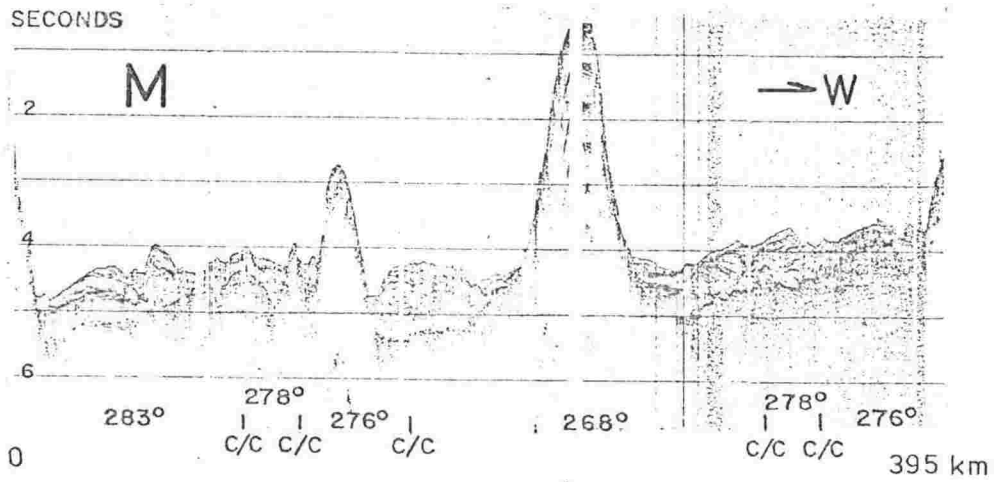


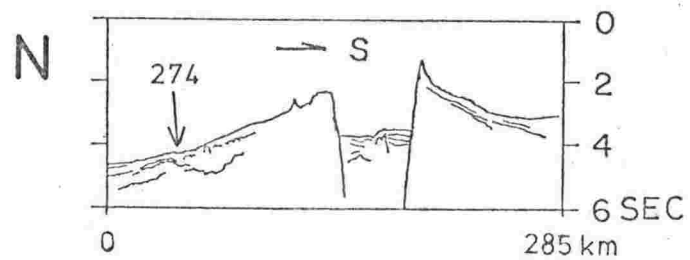


Fig. 2.16 Seismic reflection profiles in the Balleny basin. Locations shown in Fig. 2.2. Vertical exaggeration ∿ 30:1. Profile L from Hayes et al. (1972b). Profile M from Ewing and Ewing (1971, Fig. 60). Profile N from Ewing et al. (1969, Fig. 16). Some of profile L touched up. Approximate location of JOIDES site 274 shown in profile N.

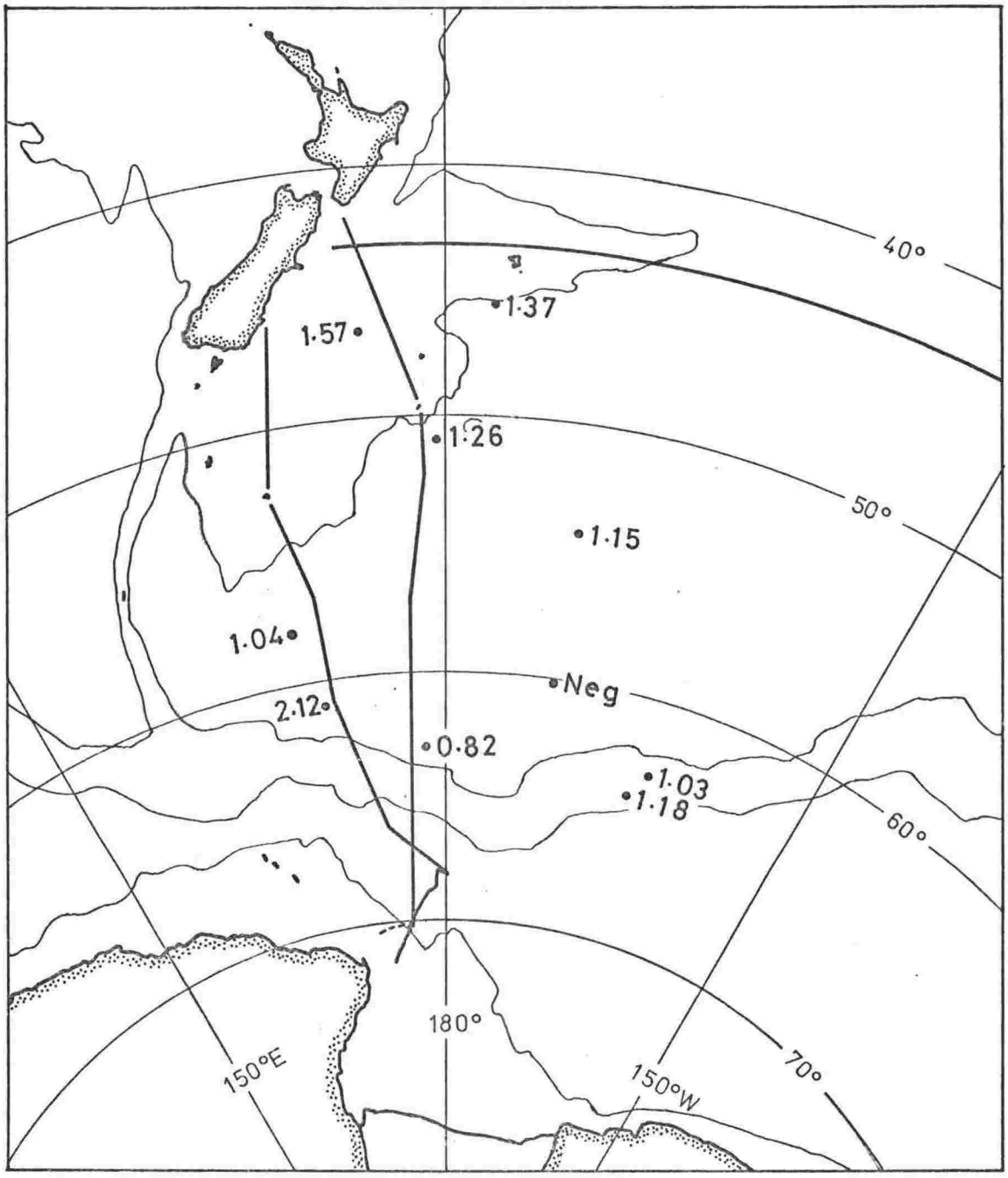


Fig. 2.17 Heat flow and gravity data in the southwest Pacific area. Heavy lines indicate the tracks for which gravity data have been published (Hayes et al., 1972b). Numbers indicate measured heat flow in units of $\mu cal.cm^{-2}.sec^{-1}$; data from von Herzen (pers. comm., 1973).

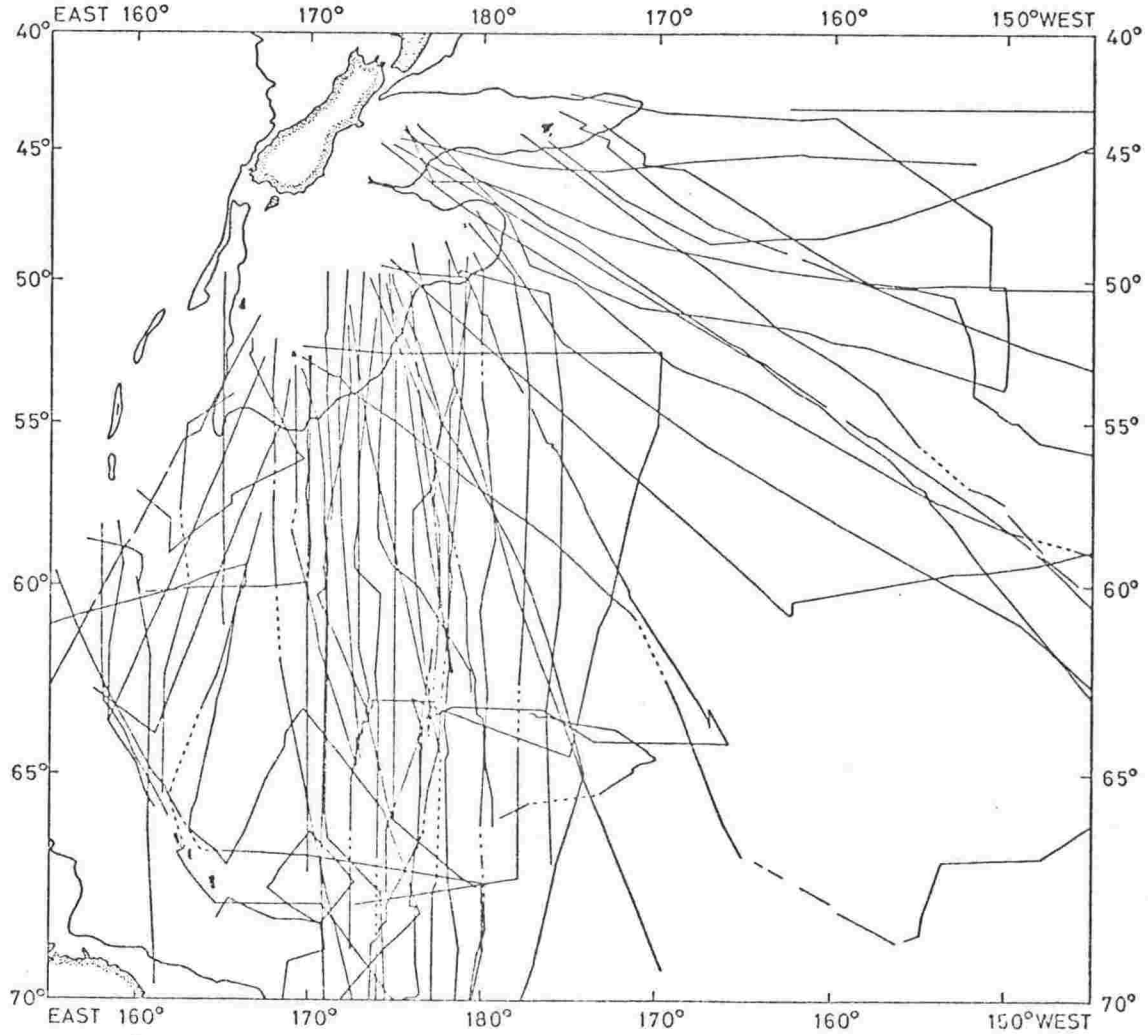


Fig. 3.1 Tracks for which magnetic data were analysed. Major sections of track for which there are no data are shown by dashes or gaps; minor gaps are not shown.

| Time | Day | Mon. | Time Zone | Lat. | Long | Distance n. miles | Calc. field (nT) | Obs. field (nT) | Anomaly (nT) | Year + code | |
|---|---|---|---|---|---|---|---|---|---|---|---|
| 235 | 23 | 1 | -12.0 | -55.618 | -177.431 | 1409.5 | 62865. | 62748. | 116. | 68ENDT | A |
| 239 | 23 | 1 | -12.0 | -55.606 | -177.430 | 1410.2 | 62913. | 62743. | 169. | 68ENDT | |
| 243 | 23 | 1 | -12.0 | -55.594 | -177.430 | 1411.0 | 62949. | 62738. | 210. | 68ENDT | |
| 248 | 23 | 1 | -12.0 | -55.578 | -177.429 | 1411.9 | 62991. | 62733. | 257. | 68ENDT | |
| 258 | 23 | 1 | -12.0 | -55.548 | -177.429 | 1413.7 | 63009. | 62721. | 287. | 68ENDT | |
| 303 | 23 | 1 | -12.0 | -55.533 | -177.428 | 1414.6 | 63021. | 62715. | 305. | 68ENDT | |
| 308 | 23 | 1 | -12.0 | -55.517 | -177.428 | 1415.5 | 63026. | 62709. | 316. | 68ENDT | |
| 313 | 23 | 1 | -12.0 | -55.502 | -177.427 | 1416.4 | 63029. | 62703. | 325. | 68ENDT | |
| 318 | 23 | 1 | -12.0 | -55.487 | -177.427 | 1417.4 | 63029. | 62697. | 331. | 68ENDT | |
| 323 | 23 | 1 | -12.0 | -55.472 | -177.426 | 1418.3 | 63026. | 62691. | 334. | 68ENDT | |
| 328 | 23 | 1 | -12.0 | -55.457 | -177.426 | 1419.2 | 63015. | 62685. | 329. | 68ENDT | |
| 332 | 23 | 1 | -12.0 | -55.444 | -177.426 | 1419.9 | 63006. | 62680. | 325. | 68ENDT | |
| 339 | 23 | 1 | -12.0 | -55.423 | -177.425 | 1421.2 | 62991. | 62671. | 319. | 68ENDT | |
| 344 | 23 | 1 | -12.0 | -55.408 | -177.425 | 1422.1 | 62937. | 62665. | 271. | 68ENDT | |
| 349 | 23 | 1 | -12.0 | -55.393 | -177.424 | 1423.0 | 62871. | 62659. | 211. | 68ENDT | |
| 353 | 23 | 1 | -12.0 | -55.381 | -177.424 | 1423.8 | 62794. | 62655. | 139. | 68ENDT | |
| 356 | 23 | 1 | -12.0 | -55.372 | -177.424 | 1424.3 | 62718. | 62651. | 66. | 68ENDT | |
| 358 | 23 | 1 | -12.0 | -55.366 | -177.423 | 1424.7 | 62629. | 62649. | -20. | 68ENDT | |
| 402 | 23 | 1 | -12.0 | -55.353 | -177.423 | 1425.4 | 62545. | 62644. | -99. | 68ENDT | |
| 405 | 23 | 1 | -12.0 | -55.344 | -177.423 | 1425.9 | 62477. | 62640. | -163. | 68ENDT | |
| 410 | 23 | 1 | -12.0 | -55.329 | -177.422 | 1426.9 | 62412. | 62634. | -222. | 68ENDT | |
| 416 | 23 | 1 | -12.0 | -55.311 | -177.422 | 1428.0 | 62385. | 62627. | -242. | 68ENDT | |
| 424 | 23 | 1 | -12.0 | -55.286 | -177.421 | 1429.4 | 62468. | 62617. | -149. | 68ENDT | |
| 429 | 23 | 1 | -12.0 | -55.271 | -177.421 | 1430.3 | 62558. | 62611. | -53. | 68ENDT | |
| 435 | 23 | 1 | -12.0 | -55.253 | -177.420 | 1431.4 | 62635. | 62604. | 30. | 68ENDT | |
| 441 | 23 | 1 | -12.0 | -55.235 | -177.420 | 1432.5 | 62708. | 62597. | 110. | 68ENDT | |
| 448 | 23 | 1 | -12.0 | -55.213 | -177.419 | 1433.8 | 62765. | 62588. | 176. | 68ENDT | |
| 456 | 23 | 1 | -12.0 | -55.189 | -177.418 | 1435.2 | 62812. | 62579. | 232. | 68ENDT | |
| 505 | 23 | 1 | -12.0 | -55.162 | -177.418 | 1436.9 | 62838. | 62568. | 269. | 68ENDT | |
| 514 | 23 | 1 | -12.0 | -55.134 | -177.417 | 1438.5 | 62838. | 62557. | 280. | 68ENDT | |
| 523 | 23 | 1 | -12.0 | -55.107 | -177.416 | 1440.2 | 62836. | 62546. | 289. | 68ENDT | |
| 532 | 23 | 1 | -12.0 | -55.079 | -177.415 | 1441.8 | 62855. | 62535. | 319. | 68ENDT | |
| 540 | 23 | 1 | -12.0 | -55.055 | -177.415 | 1443.3 | 62866. | 62526. | 339. | 68ENDT | |
| 546 | 23 | 1 | -12.0 | -55.037 | -177.414 | 1444.4 | 62811. | 62518. | 292. | 68ENDT | |
| 551 | 23 | 1 | -12.0 | -55.022 | -177.414 | 1445.3 | 62725. | 62512. | 212. | 68ENDT | |
| 554 | 23 | 1 | -12.0 | -55.013 | -177.413 | 1445.8 | 62637. | 62509. | 127. | 68ENDT | |
| 557 | 23 | 1 | -12.0 | -55.003 | -177.413 | 1446.4 | 62570. | 62505. | 64. | 68ENDT | |
| 600 | 23 | 1 | -12.0 | -54.994 | -177.413 | 1446.9 | 62489. | 62502. | -13. | 68ENDT | |
| 602 | 23 | 1 | -12.0 | -54.988 | -177.413 | 1447.3 | 62447. | 62499. | -52. | 68ENDT | |
| 607 | 23 | 1 | -12.0 | -54.974 | -177.412 | 1448.2 | 62361. | 62493. | -132. | 68ENDT | |
| 614 | 23 | 1 | -12.0 | -54.953 | -177.412 | 1449.4 | 62281. | 62485. | -204. | 68ENDT | |
| 619 | 23 | 1 | -12.0 | -54.938 | -177.411 | 1450.3 | 62244. | 62479. | -235. | 68ENDT | |
| 625 | 23 | 1 | -12.0 | -54.920 | -177.411 | 1451.4 | 62231. | 62472. | -241. | 68ENDT | |
| 630 | 23 | 1 | -12.0 | -54.906 | -177.410 | 1452.3 | 62223. | 62466. | -243. | 68ENDT | |
| 635 | 23 | 1 | -12.0 | -54.891 | -177.410 | 1453.2 | 62204. | 62460. | -256. | 68ENDT | |
| 639 | 23 | 1 | -12.0 | -54.879 | -177.410 | 1453.9 | 62171. | 62456. | -285. | 68ENDT | |
| 644 | 23 | 1 | -12.0 | -54.864 | -177.409 | 1454.8 | 62137. | 62450. | -313. | 68ENDT | |
| 649 | 23 | 1 | -12.0 | -54.849 | -177.409 | 1455.7 | 62097. | 62444. | -347. | 68ENDT | |
| 653 | 23 | 1 | -12.0 | -54.837 | -177.408 | 1456.4 | 62073. | 62439. | -366. | 68ENDT | |
| 658 | 23 | 1 | -12.0 | -54.823 | -177.408 | 1457.2 | 62105. | 62433. | -328. | 68ENDT | |
| 703 | 23 | 1 | -12.0 | -54.808 | -177.408 | 1458.1 | 62150. | 62427. | -277. | 68ENDT | |
| 707 | 23 | 1 | -12.0 | -54.796 | -177.407 | 1458.8 | 62206. | 62423. | -217. | 68ENDT | |
| 709 | 23 | 1 | -12.0 | -54.790 | -177.408 | 1459.2 | 62257. | 62420. | -163. | 68ENDT | |
| 712 | 23 | 1 | -12.0 | -54.780 | -177.410 | 1459.8 | 62316. | 62417. | -101. | 68ENDT | |
| 714 | 23 | 1 | -12.0 | -54.774 | -177.411 | 1460.2 | 62360. | 62414. | -54. | 68ENDT | |
| 717 | 23 | 1 | -12.0 | -54.765 | -177.412 | 1460.7 | 62415. | 62411. | 3. | 68ENDT | |
| 720 | 23 | 1 | -12.0 | -54.756 | -177.414 | 1461.3 | 62467. | 62408. | 58. | 68ENDT | |
| 723 | 23 | 1 | -12.0 | -54.746 | -177.415 | 1461.8 | 62503. | 62404. | 98. | 68ENDT | |
| 727 | 23 | 1 | -12.0 | -54.734 | -177.417 | 1462.6 | 62526. | 62399. | 126. | 68ENDT | |
| 734 | 23 | 1 | -12.0 | -54.713 | -177.420 | 1463.9 | 62511. | 62391. | 119. | 68ENDT | |
| 739 | 23 | 1 | -12.0 | -54.697 | -177.423 | 1464.8 | 62499. | 62386. | 112. | 68ENDT | B |

Fig. 3.2 Reduced copy of computer listing of data for part of profile T.

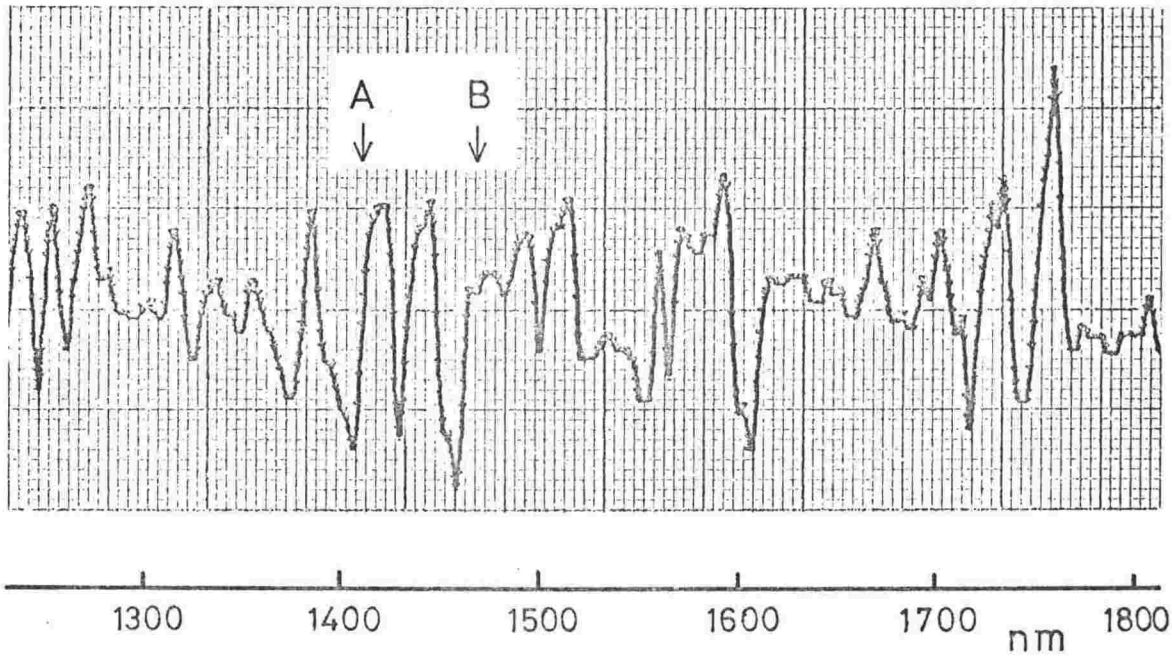


Fig. 3.3 Annotated copy of computer-drawn linear anomaly profile of part of profile T. Labels indicate the section listed in Fig. 3.2.

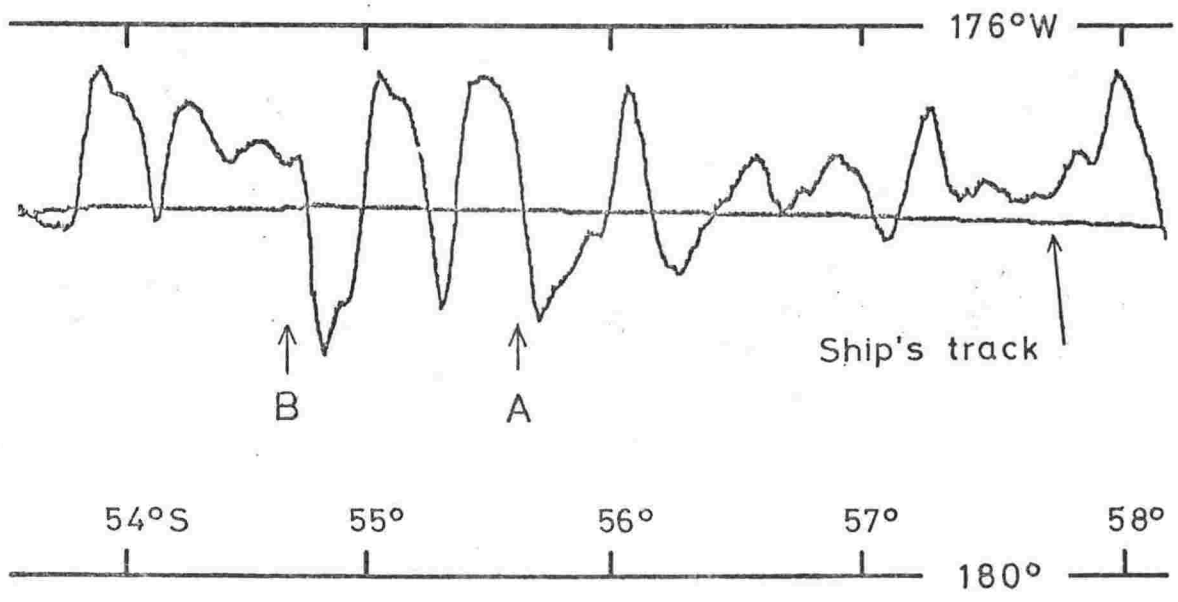


Fig. 3.4 Annotated copy of computer-drawn mercator projection of part of profile T. Ship track was the anomaly zero level and anomalies are plotted with positive to the east. Labels indicate section shown in Figs 3.2 and 3.3.

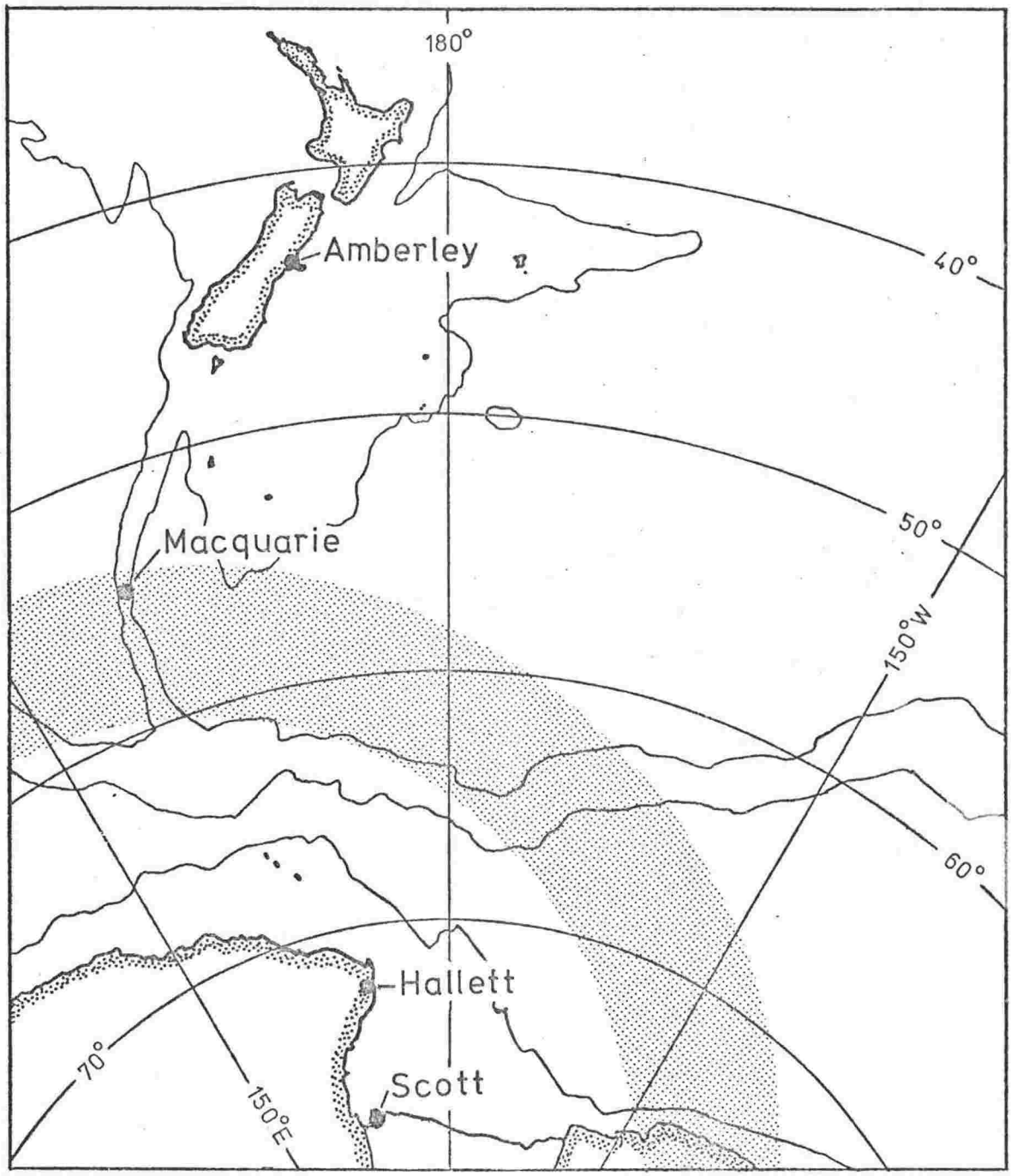


Fig. 3.5 The auroral zone (from Bond and Jacka, 1960) and the locations of magnetic field recording stations. Hallett did not operate after March 1964.

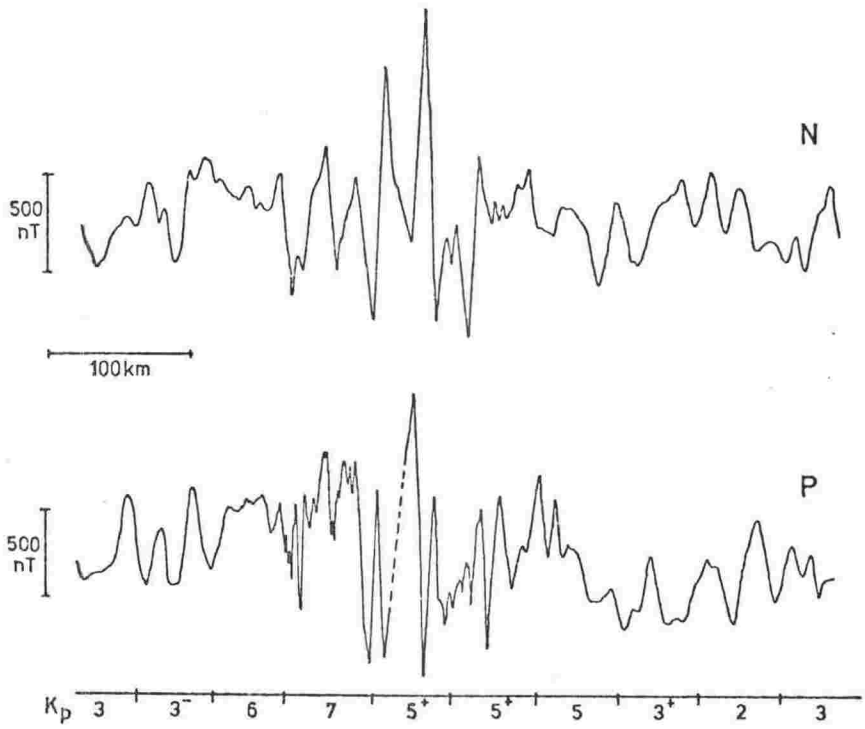


Fig. 3.6 Sections of magnetic anomaly profiles N and P. Three hour intervals and associated Kp index values shown for profile P. For profile N Kp = 2 throughout.

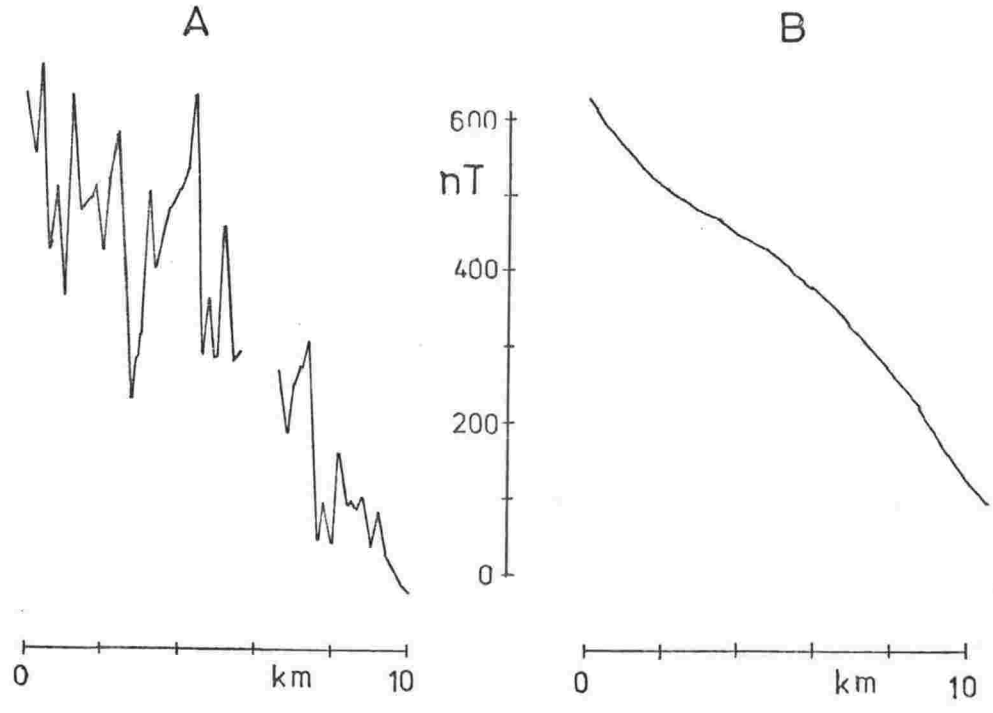


Fig. 3.7 Two sections of profile P for which Kp = 5.

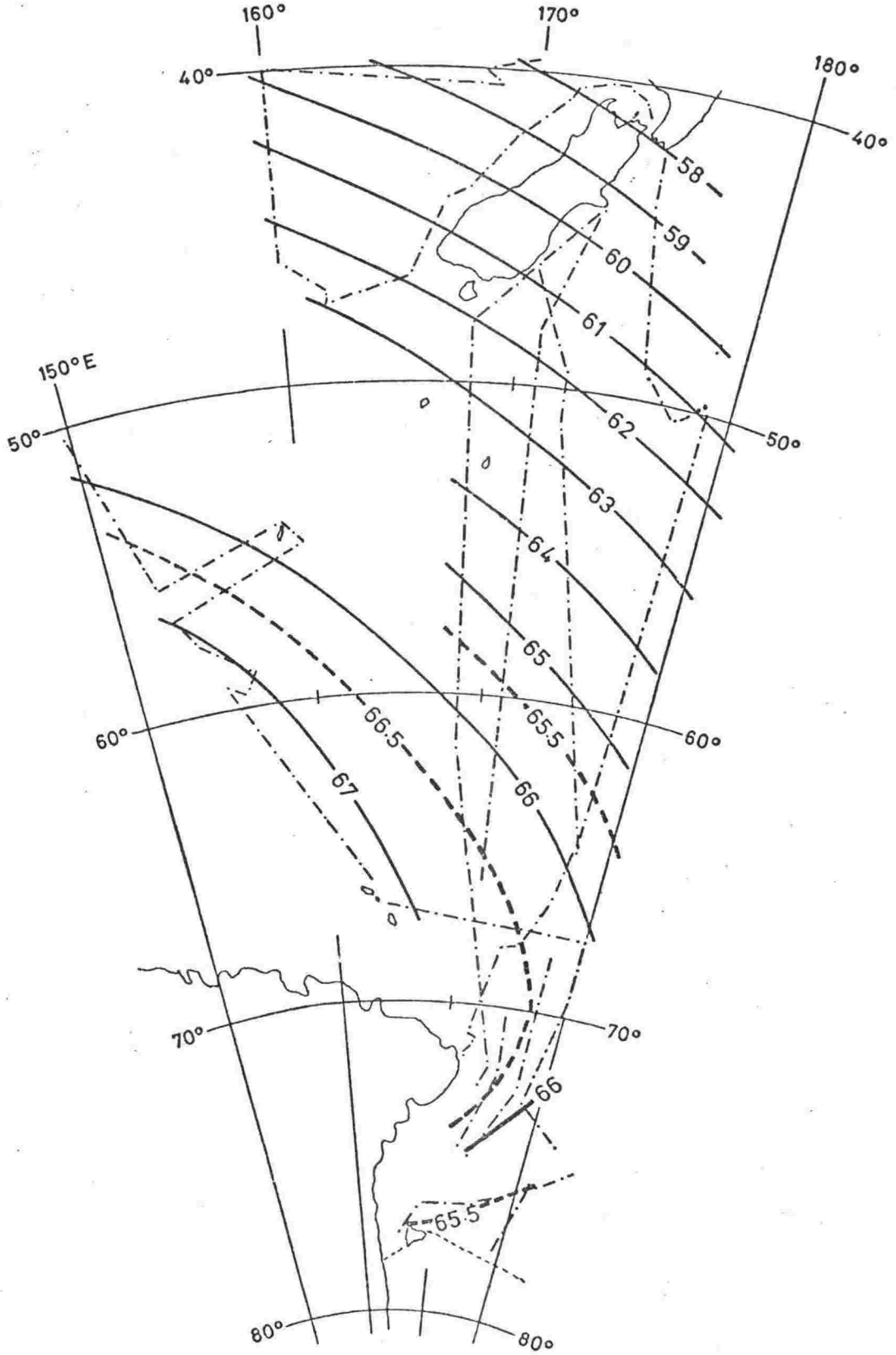


Fig. 3.8 Total field map for 1967.0. Compiled from data obtained during Dec 1966-Feb 1967 along the tracks shown dashed and dotted. Contour units: thousands of nanotesla.

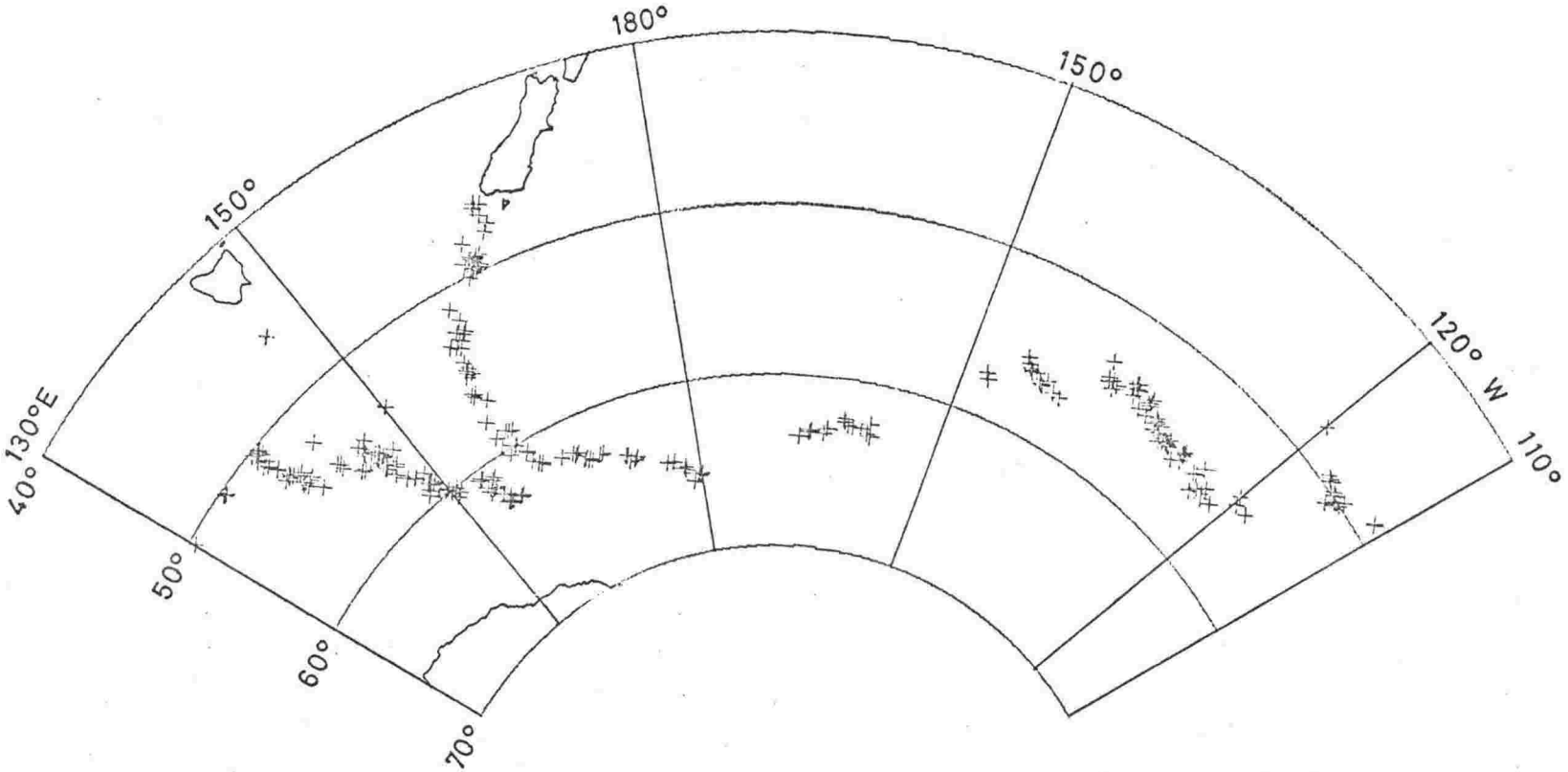


Fig. 3.9 Epicentres of the USCGS file. USCGS data for period Jan 1964-Dec 1972, 130°E-110°W, south of 46°S.

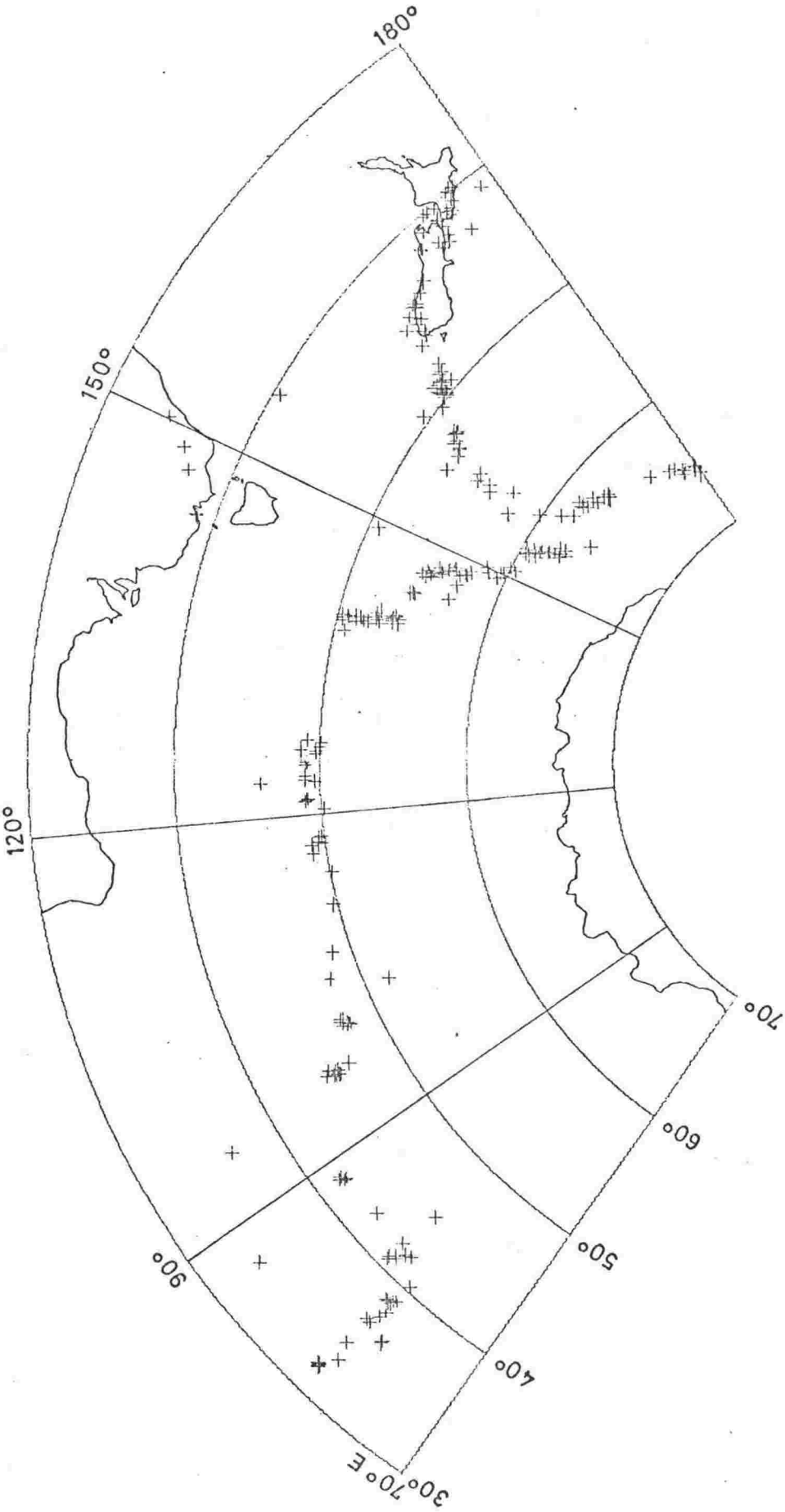


Fig. 3.10 Epicentres of the Sykes file. Sykes' (1970a) data for period 1950-1966, 70°E-180°, south of 30°S except for New Zealand where south of 40°S.

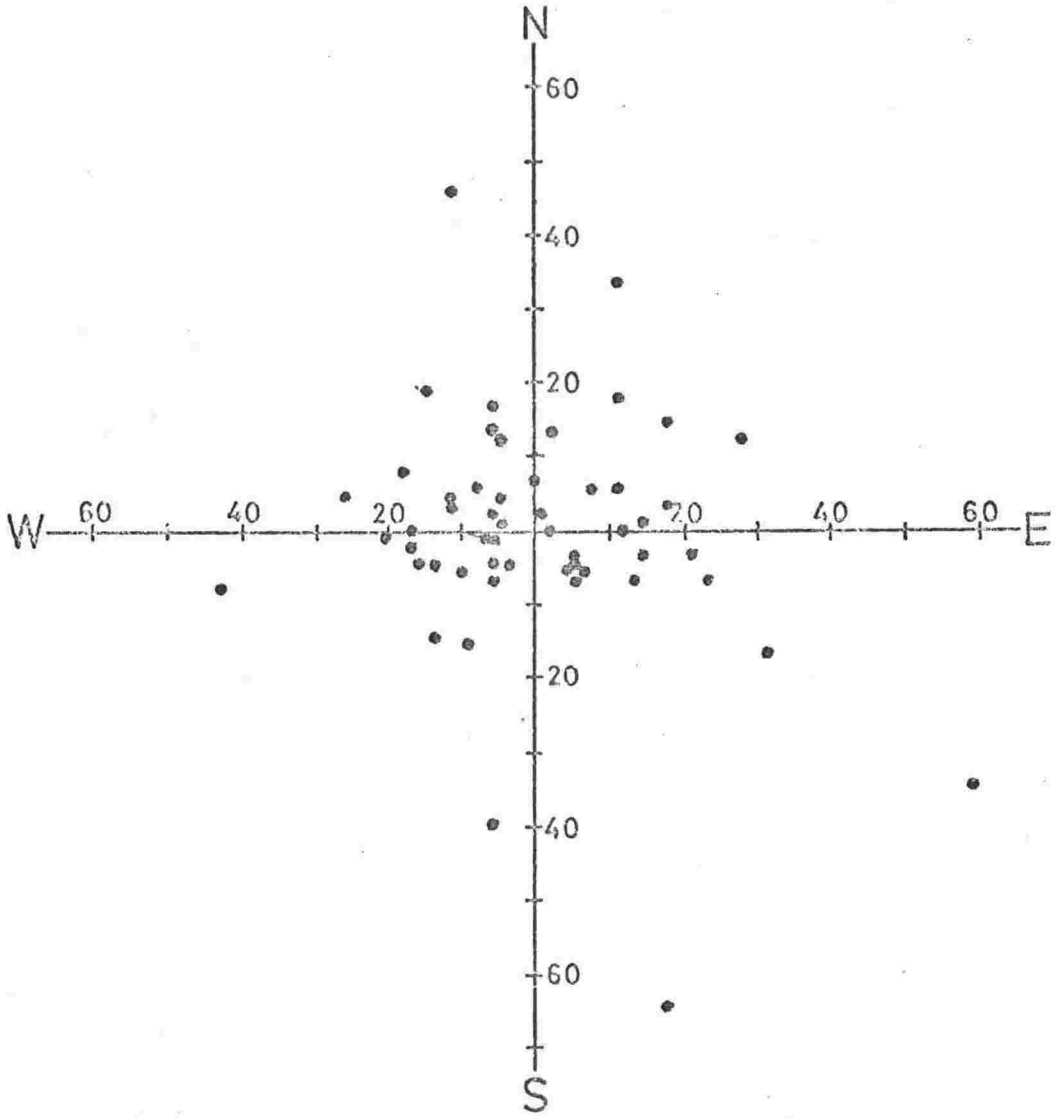


Fig. 3.11 Location of Sykes epicentres with respect to USCGS epicentres. Distances in km.

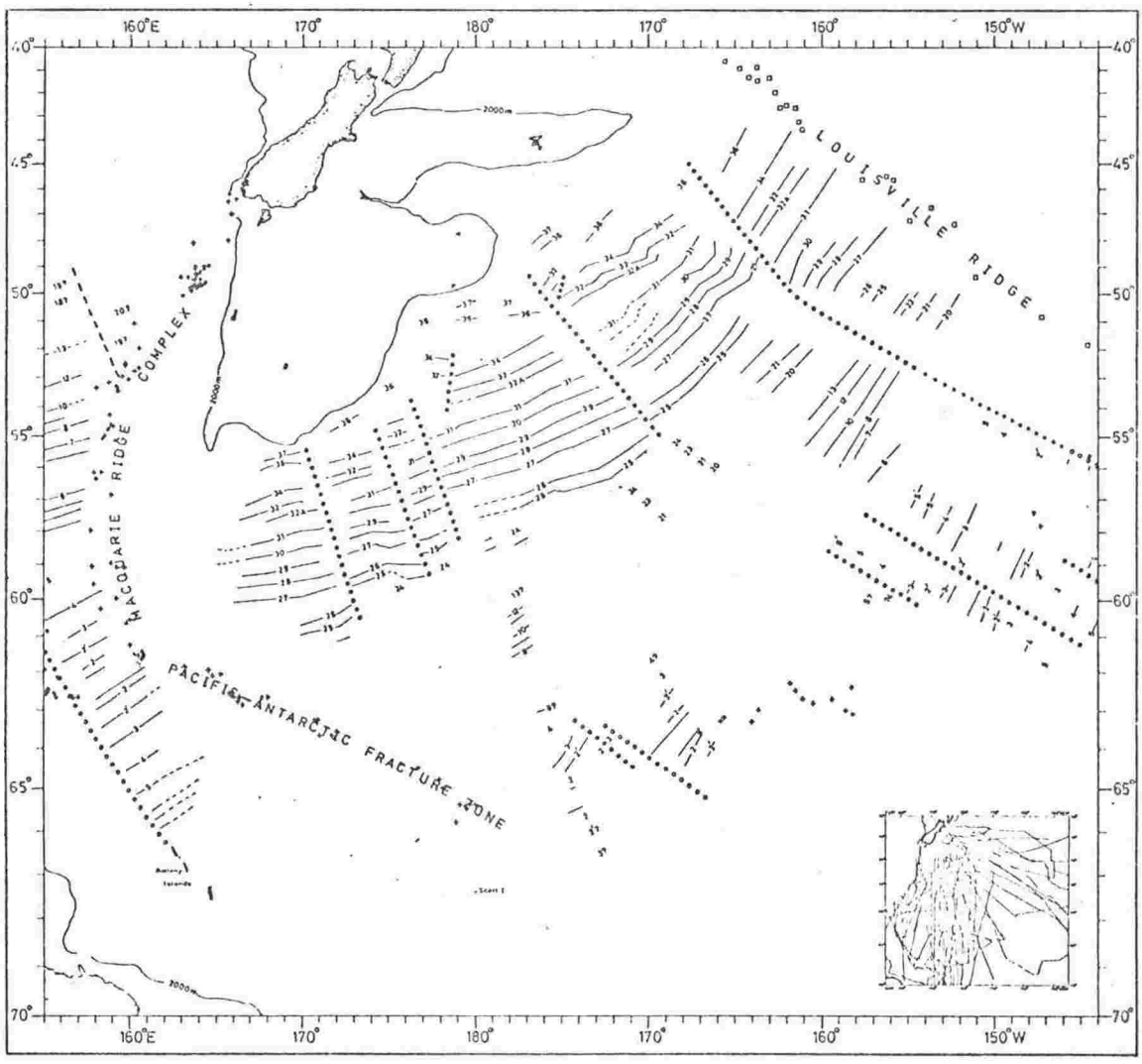


Fig. 4.1 Reduced copy. See pocket for full size diagram.

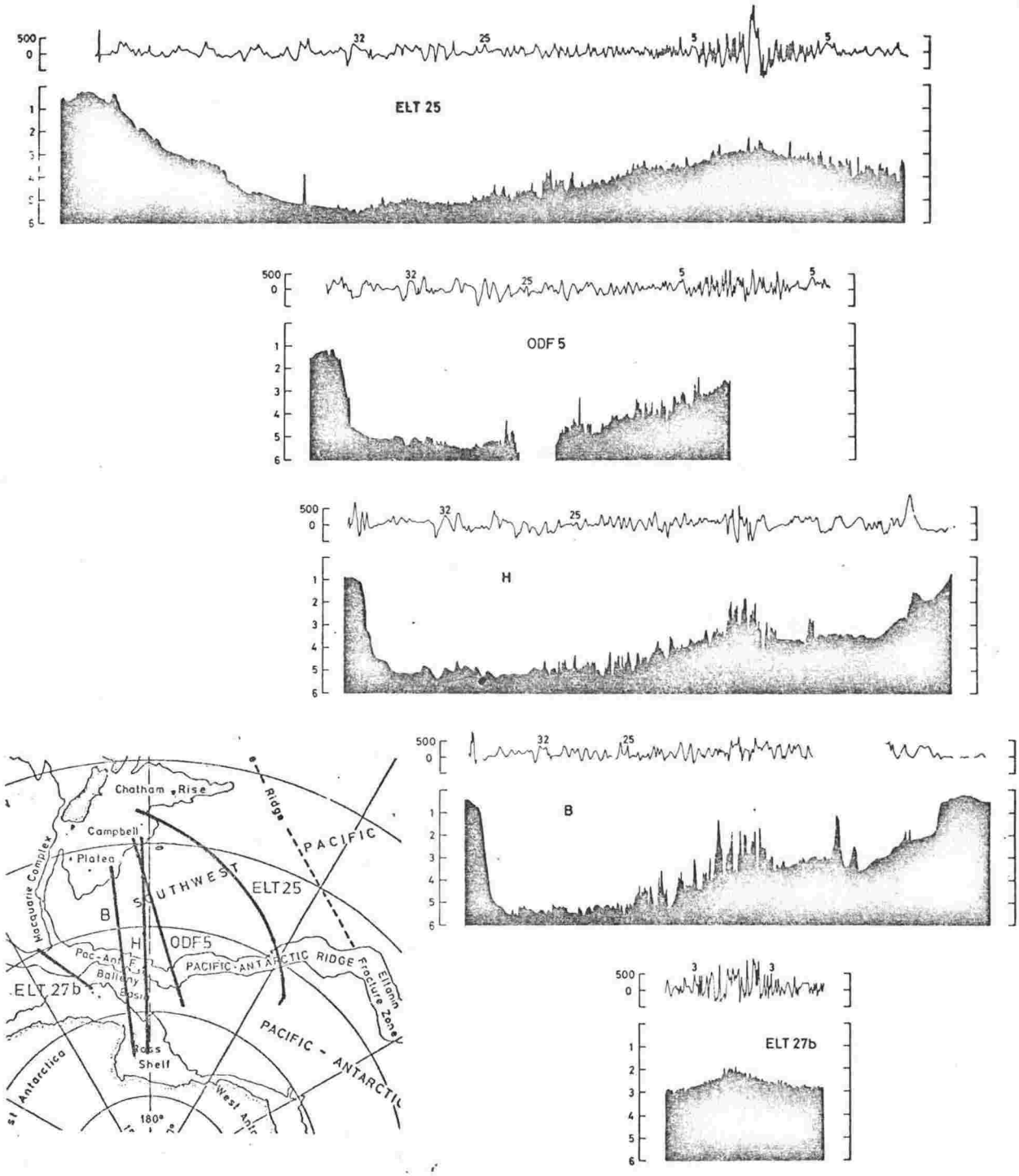


Fig. 4.2 Representative bathymetric and magnetic profiles for five tracks in the southwest Pacific basin area. Depths in km, vertical exaggeration 100:1.

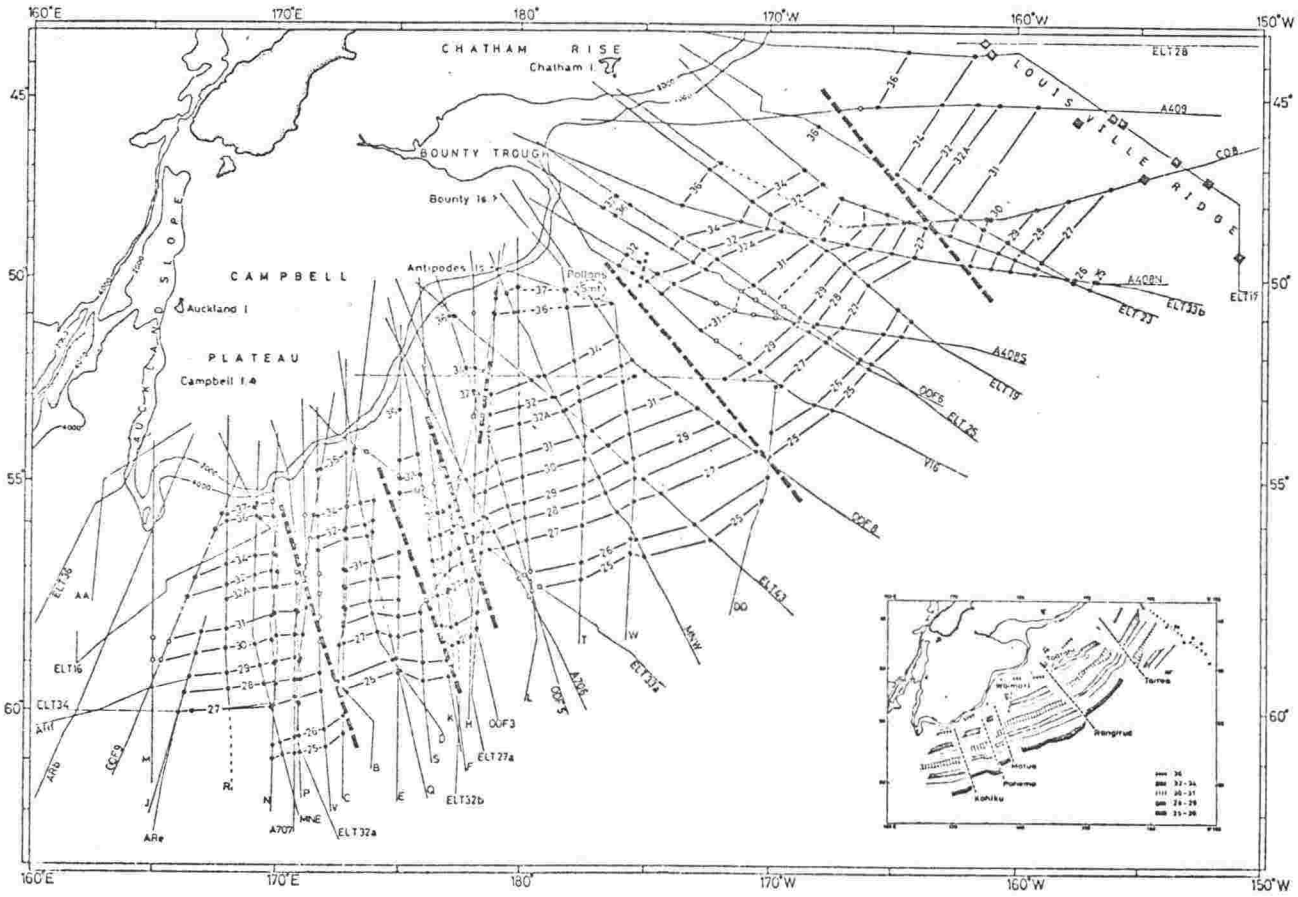


FIG. 4.3 MAGNETIC ANOMALIES IN THE SOUTHWEST PACIFIC BASIN.

Tracks for which magnetic data were available are shown. Closed circles are definite identifications of anomalies within the numbering system used. Open circles are either tentative identifications or prominent anomalies not assignable to the numbered sequence. Fracture zones inferred from offsets of the anomalies are shown by dashed lines. Squares are positions of the Louisville ridge, from Hayes and Ewing (1971) and this study. Inset shows the names given to the fracture zones.

Fig. 4.3 Reduced copy. See pocket for full size diagram.

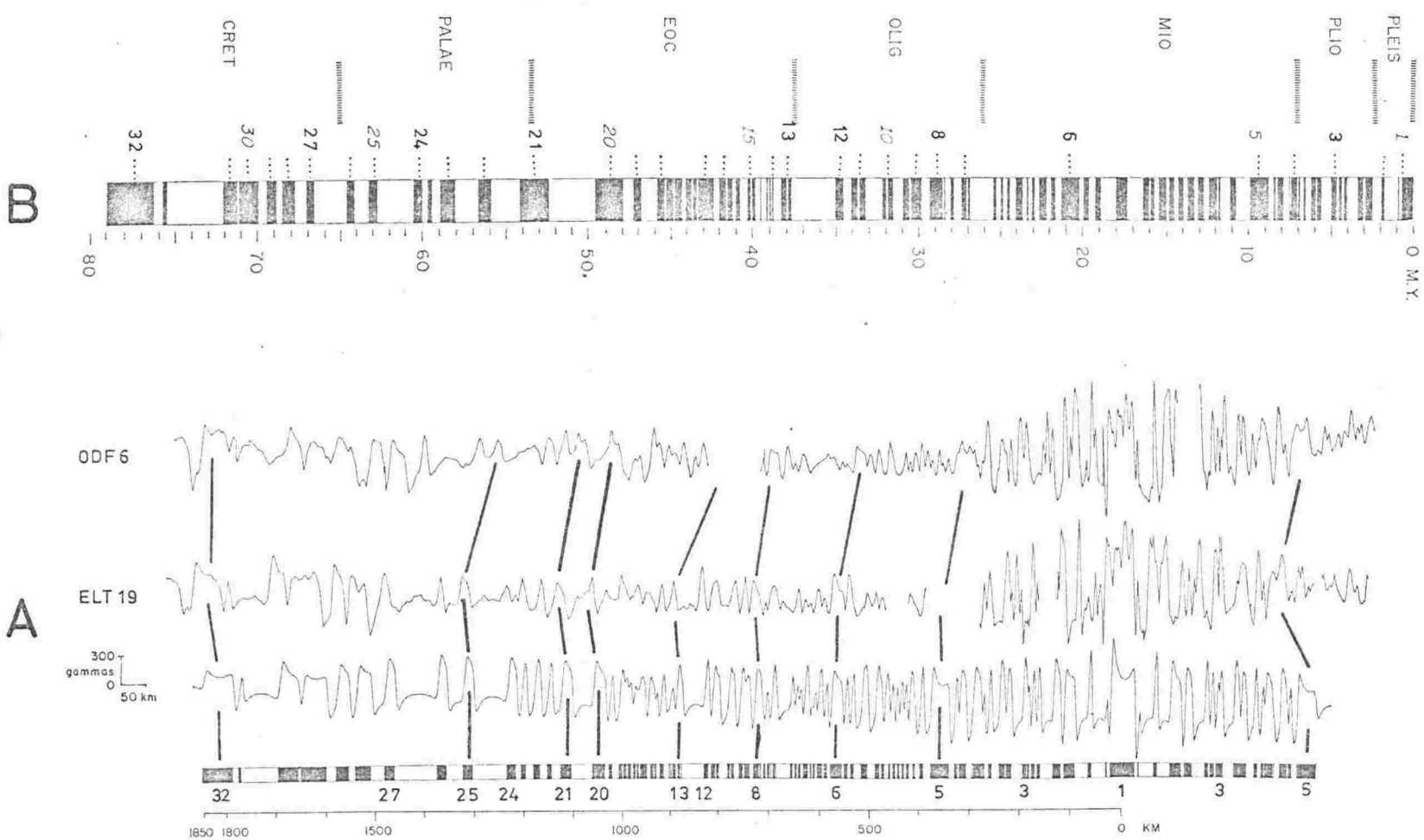


Fig. 4.4 A: Two magnetic profiles from the southwest Pacific, and below them a model profile calculated from the sequence of normally and reversely magnetized blocks shown underneath. Normal polarity black; intervals based on reversal time scale. From Pitman et al. (1968, Fig. 9). B: The geomagnetic reversal time scale from Heirtzler et al. (1968, Fig. 3). From right to left: age; polarity intervals, normal black; anomaly numbers; geological periods. Centre of normal interval for anomaly 32 should be about 75 mybp (see later).

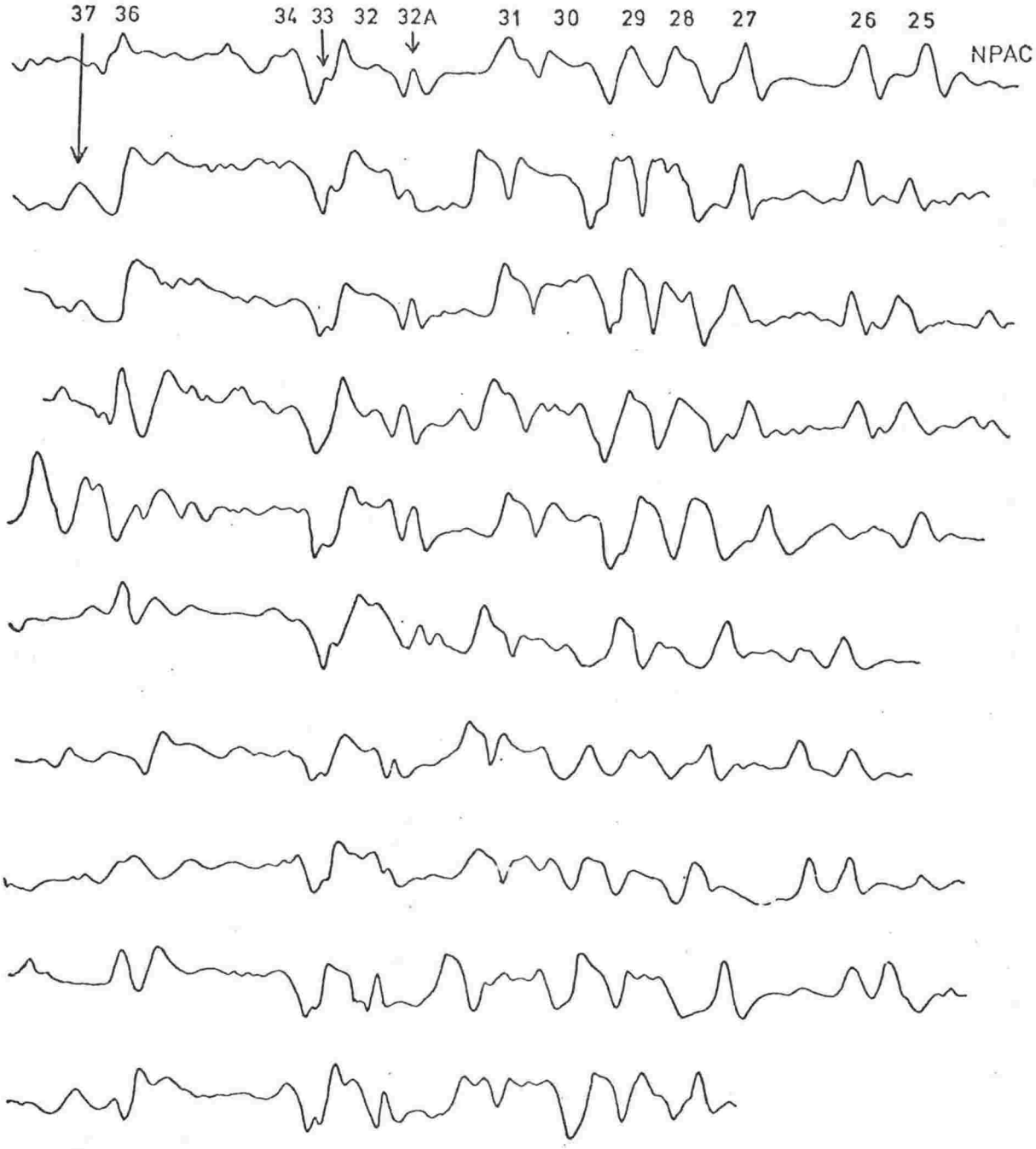


Fig. 4.5 Profile NPAC from the north Pacific, and typical profiles from the southwest Pacific basin. Some profiles composite; eastern most one at the top. Profile NPAC is the type profile for the Heirtzler et al. (1968) geomagnetic time scale. Numbers above NPAC indicate the anomaly numbering system.

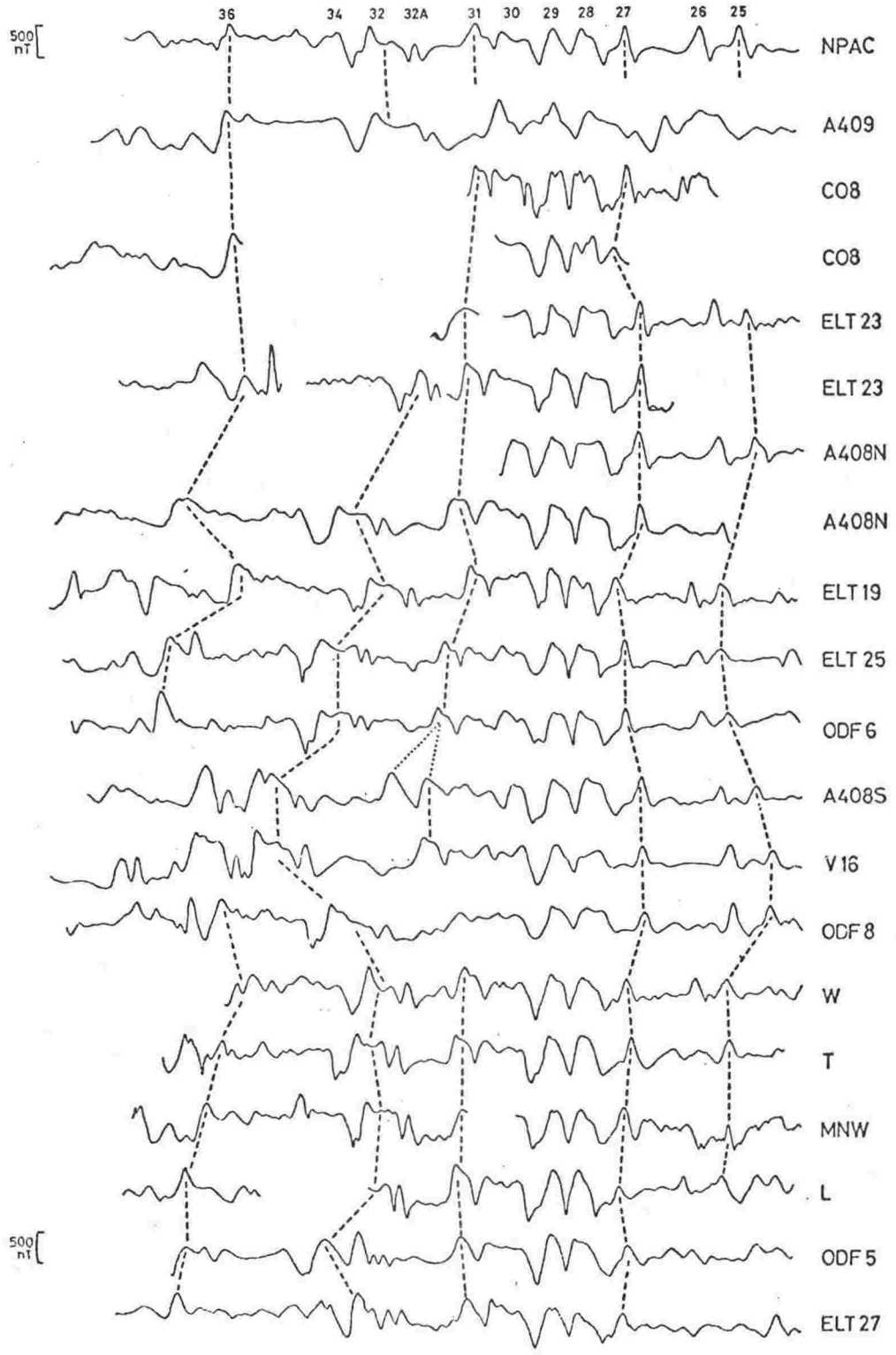


Fig. 4.6 Magnetic anomaly profiles from the southwest Pacific basin east of about 180°. Profiles aligned on anomalies 27 - 31. The track azimuths vary considerably and the profiles were projected to yield approximately the same length of the anomaly sequence.

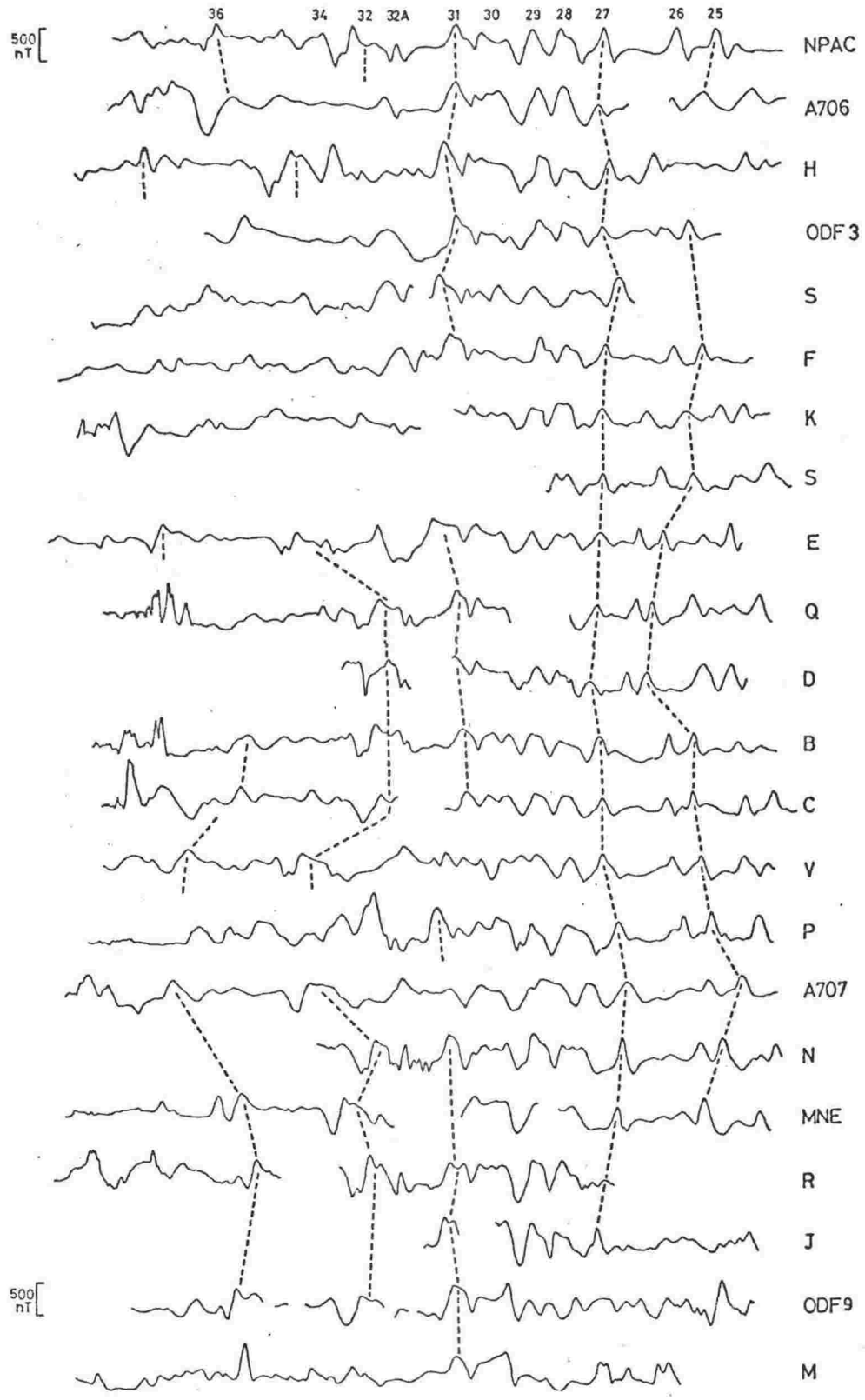


Fig. 4.7 Magnetic anomaly profiles west of about 180°. Arranged as in Fig. 4.6.

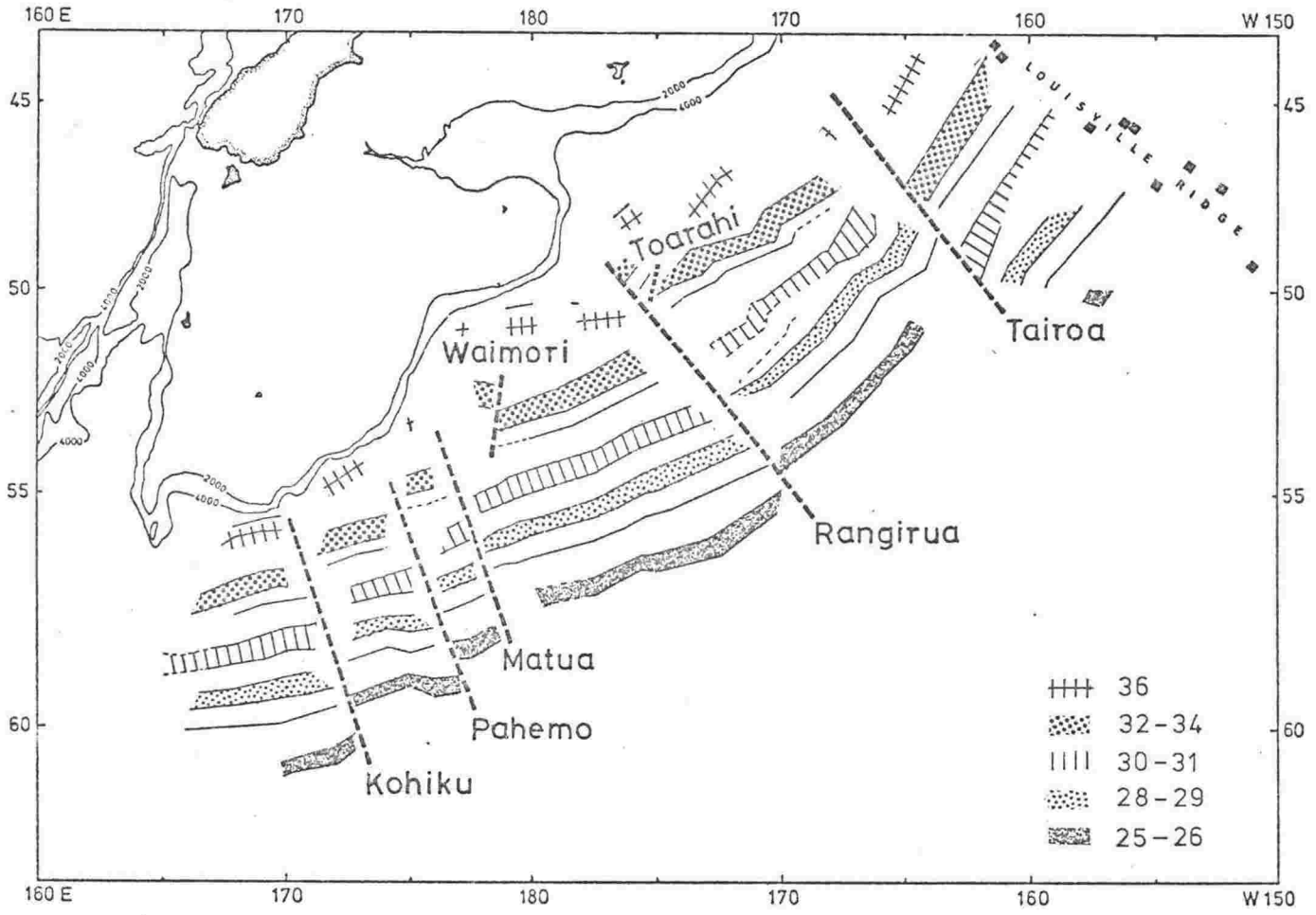


Fig. 4.8 Magnetic anomaly trends and fracture zones in the southwest Pacific basin.

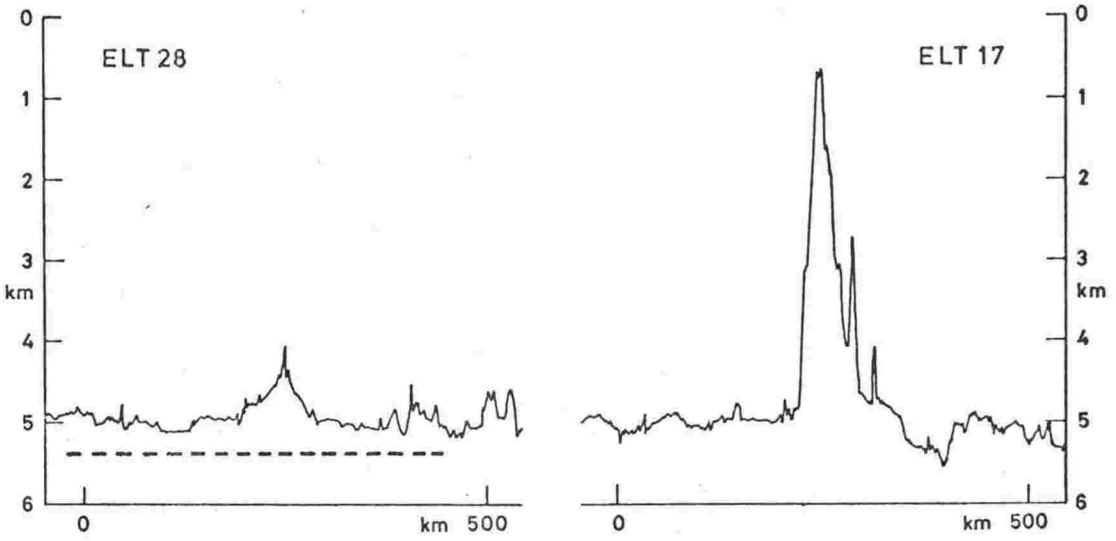


Fig. 4.9 Two east-west bathymetric profiles across the Louisville ridge. ELT17 on 43.6°S. ELT28 on 43.2°S, section above dashed line shown in Fig. 4.10.

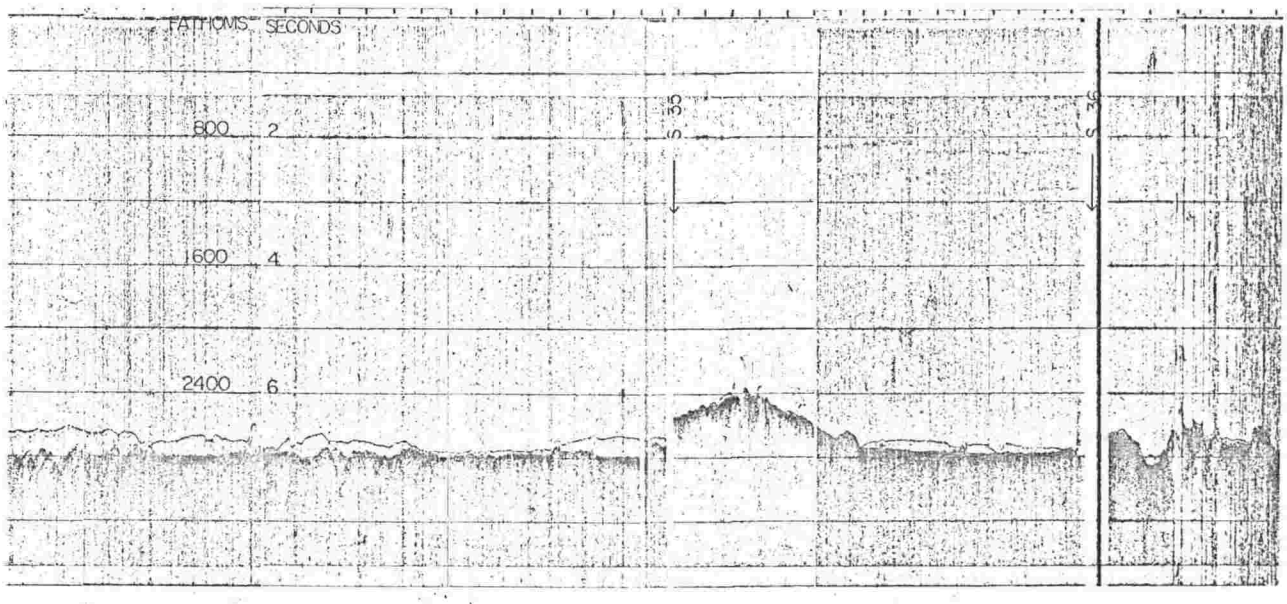


Fig. 4.10 Seismic reflection profile ELT28 across the Louisville ridge. From Hayes et al. (1972b).

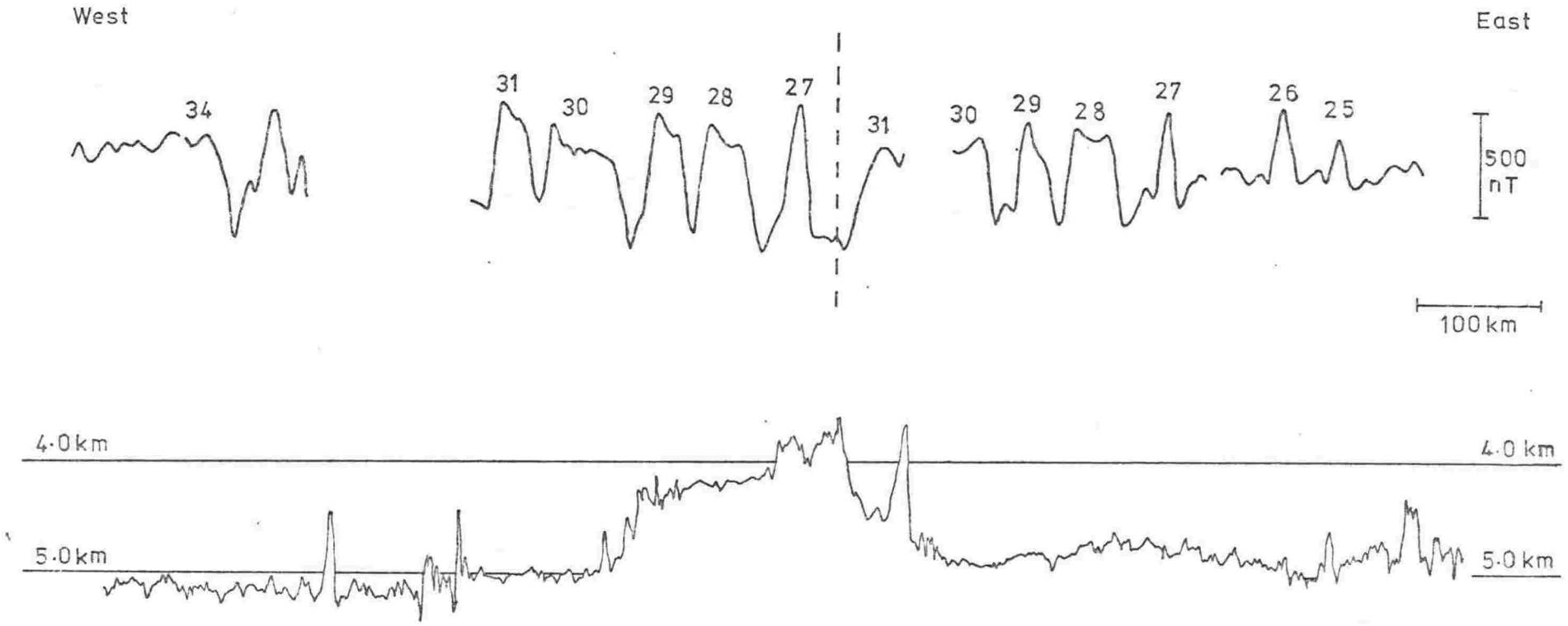


Fig. 4.11 ELT23 bathymetric and magnetic profiles across the Tairoa fracture zone. The track is not straight in the magnetic data gap on the north, and spatially anomaly 34 is about 100 km closer to anomaly 31 than the profile indicates.

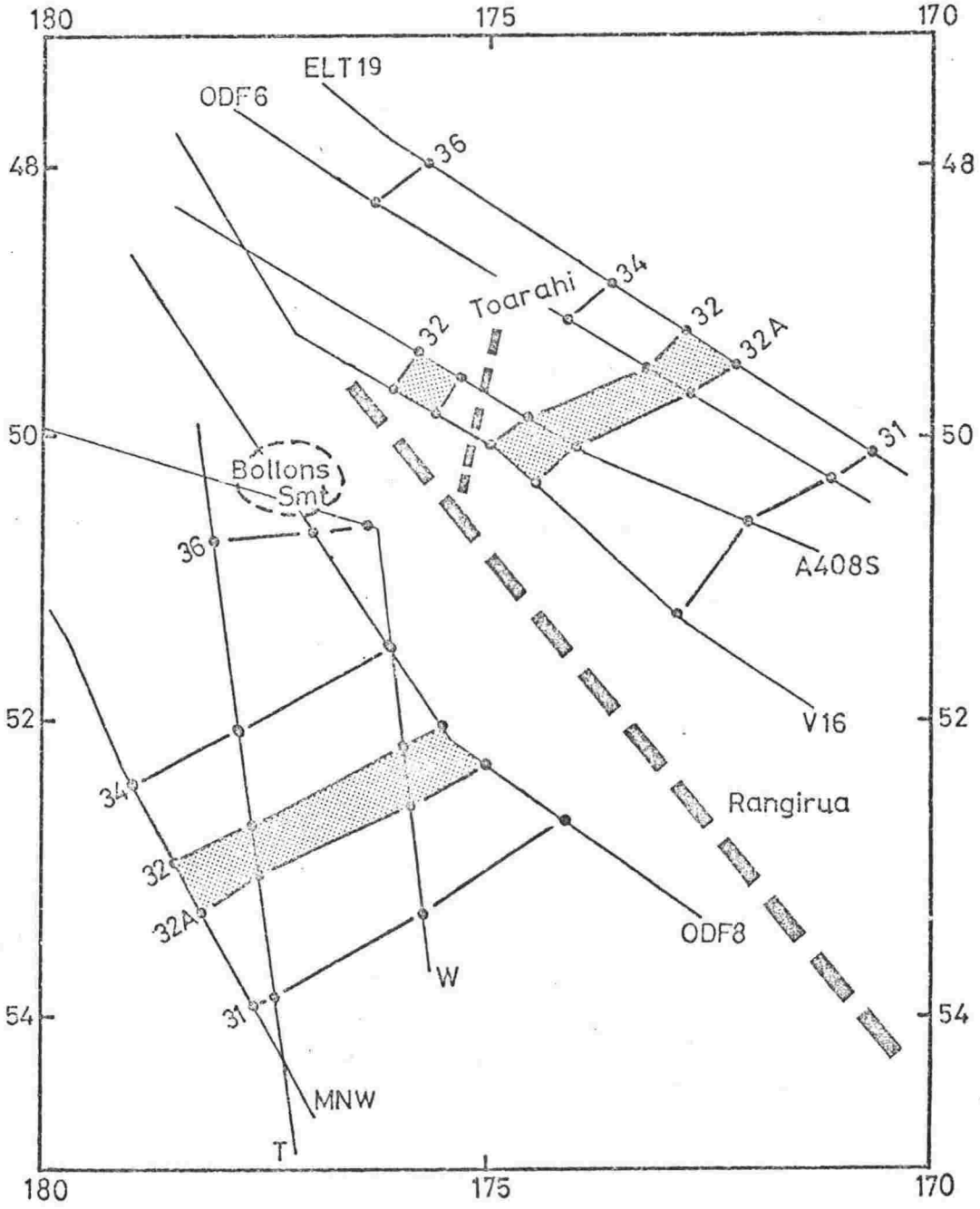


Fig. 4.12 Anomaly lineations and the Toarahi and Rangirua fracture zones based on the offsets of the lineations.

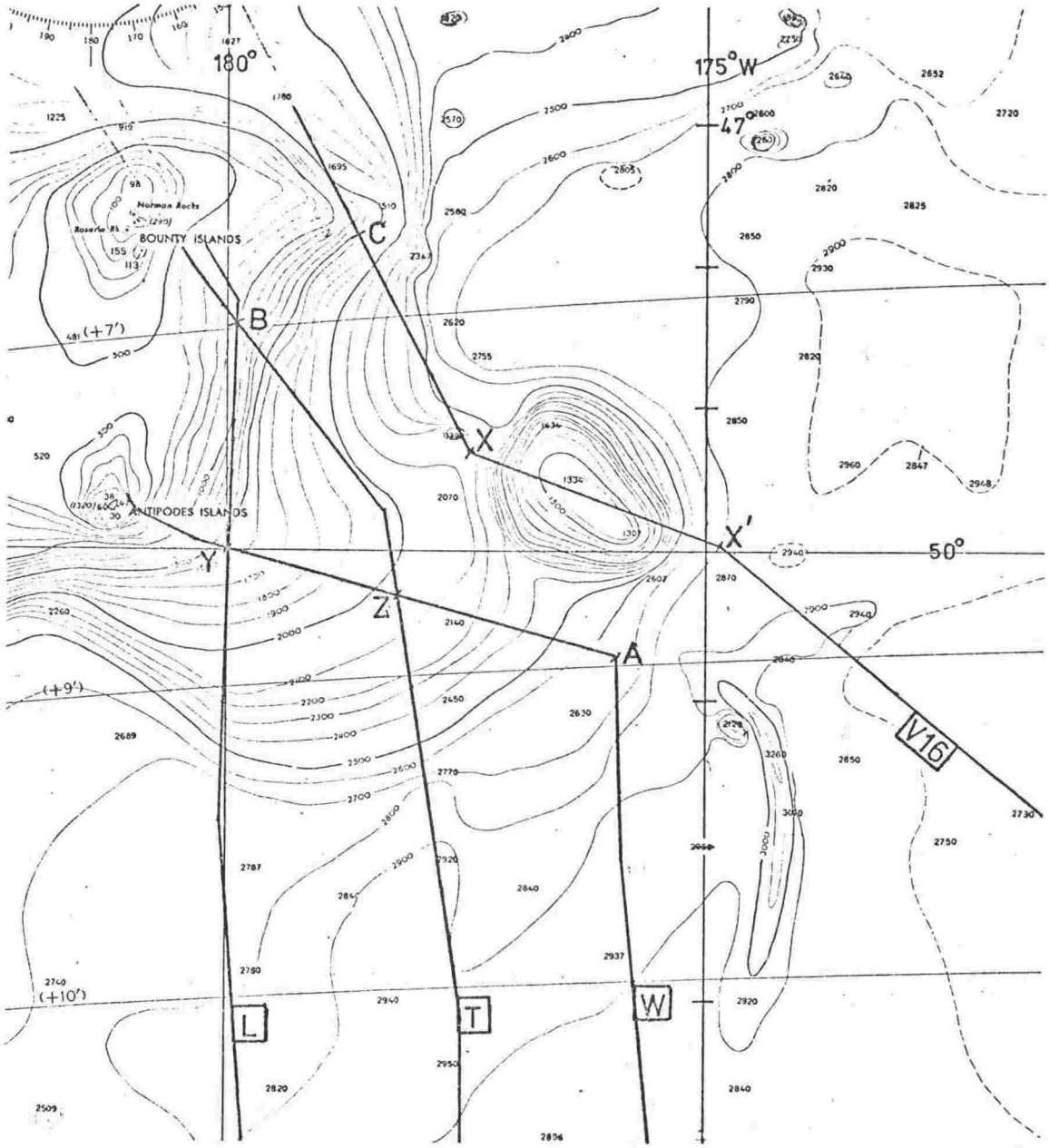


Fig. 4.13 Bathymetry of the Bollons seamount area, from New Zealand to Cape Adare chart (U.S. Naval Oceanographic Office, 1967). Contours in fathoms. Tracks indicate positions of profiles shown in Fig. 4.14.

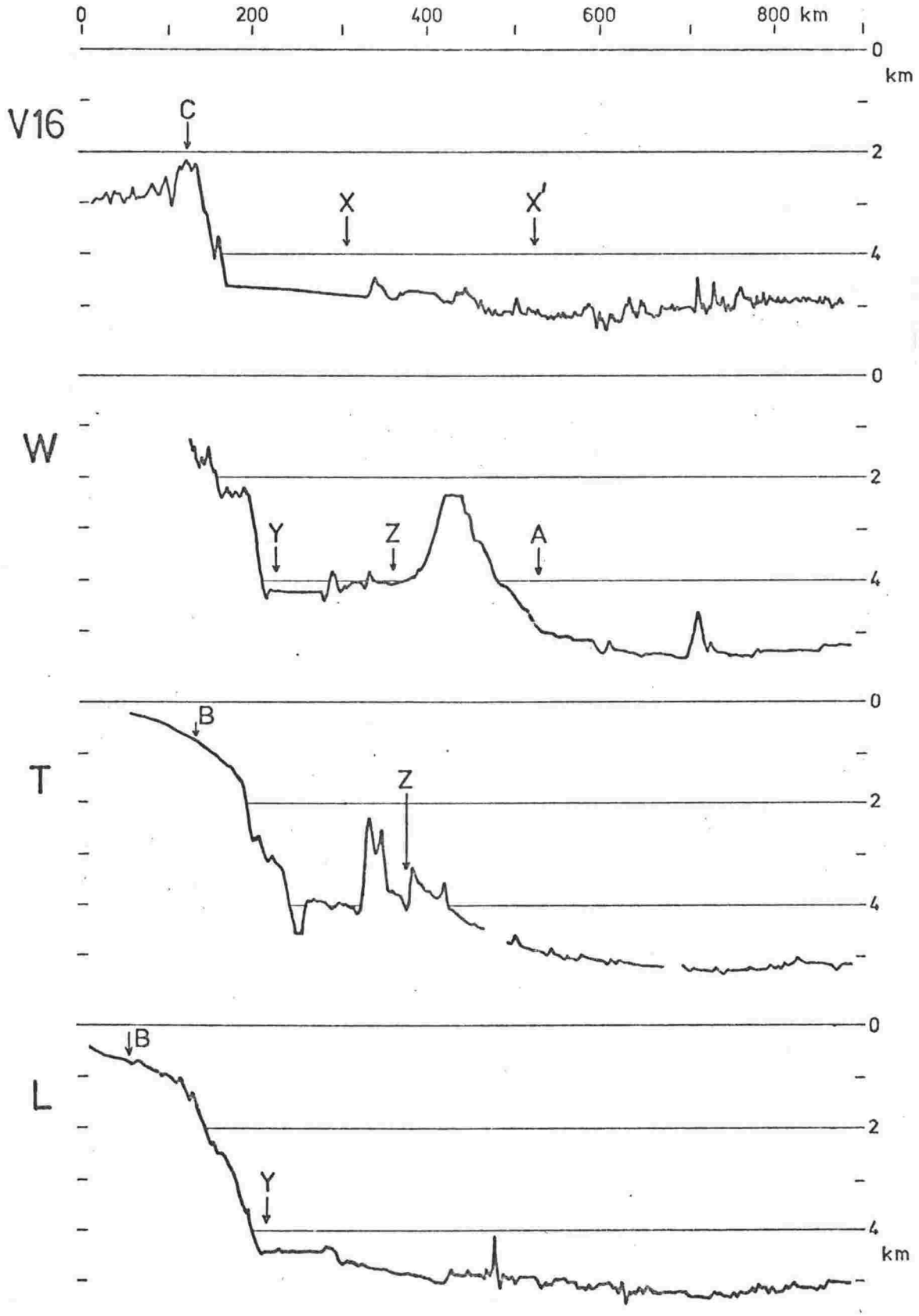


Fig. 4.14 Bathymetric profiles in the Bollons seamount area. Positions of tracks and labelled points shown in Fig. 4.13. Vertical exaggeration 60:1.

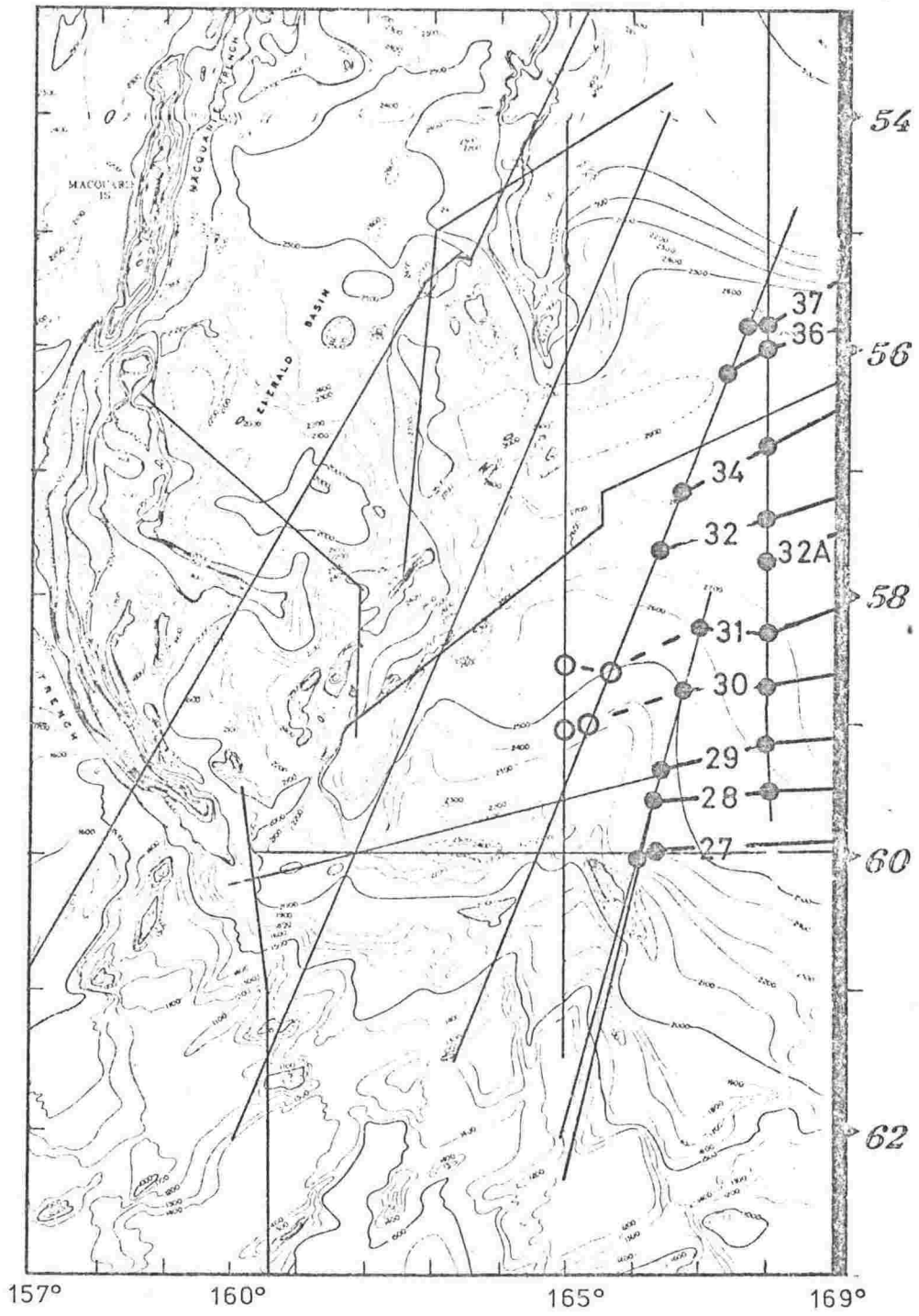


Fig. 4.15 Magnetic anomalies at the western end of the southwest Pacific basin. Tracks for which magnetic data were available are are shown. Definite anomaly identifications are shown by closed circles, tentative identifications by open circles. Bathymetry (in fathoms) from Hayes and Conolly (1972, Fig. 1).

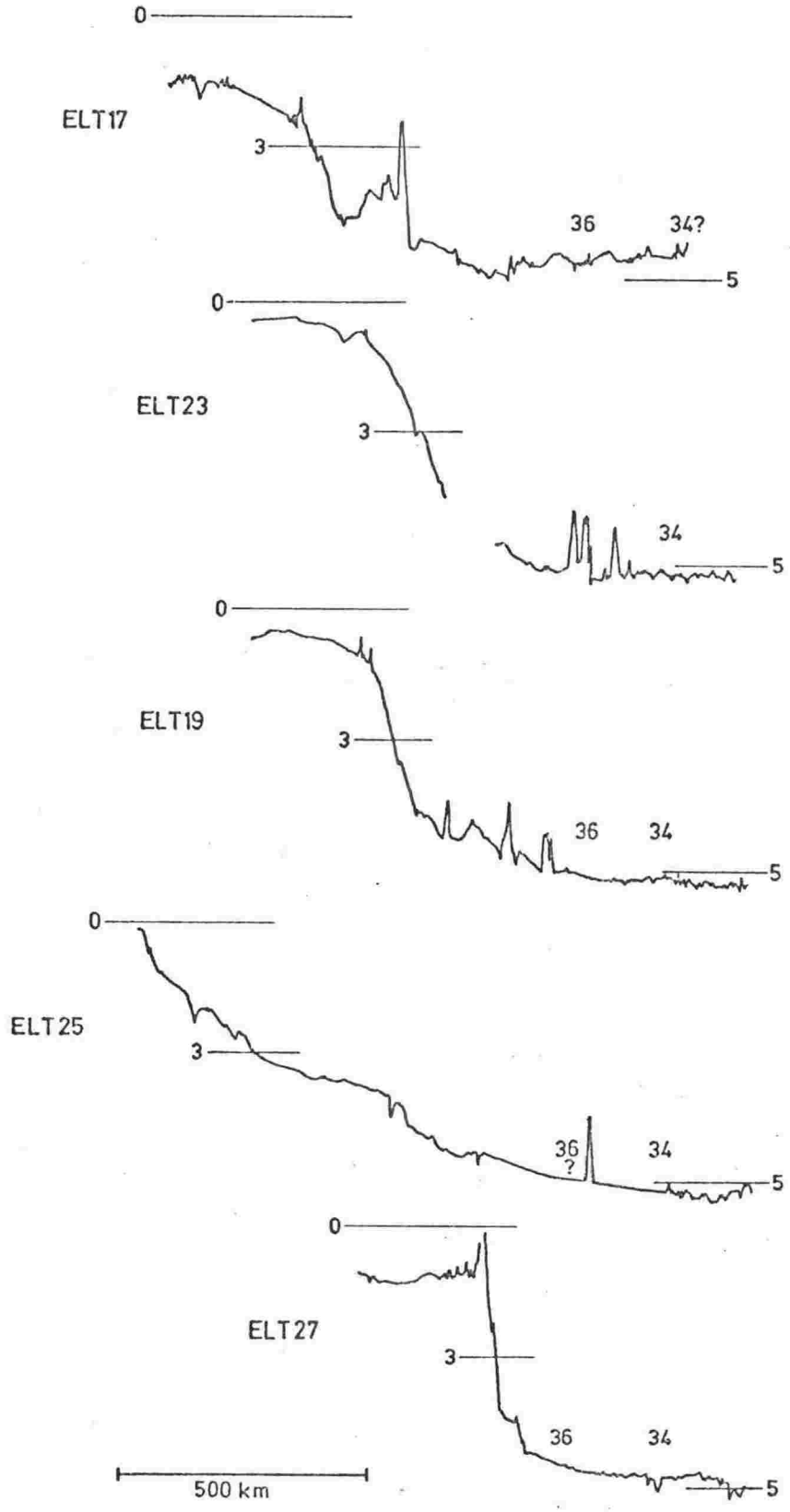


Fig. 4.16 Bathymetric profiles across the south Chatham slope; except ELT27 which is across the Campbell slope at the Antipodes Islands. Depths in km, vertical exaggeration 80:1. Numbers indicate the positions of anomalies 34 and 36. Profiles aligned on these anomalies.

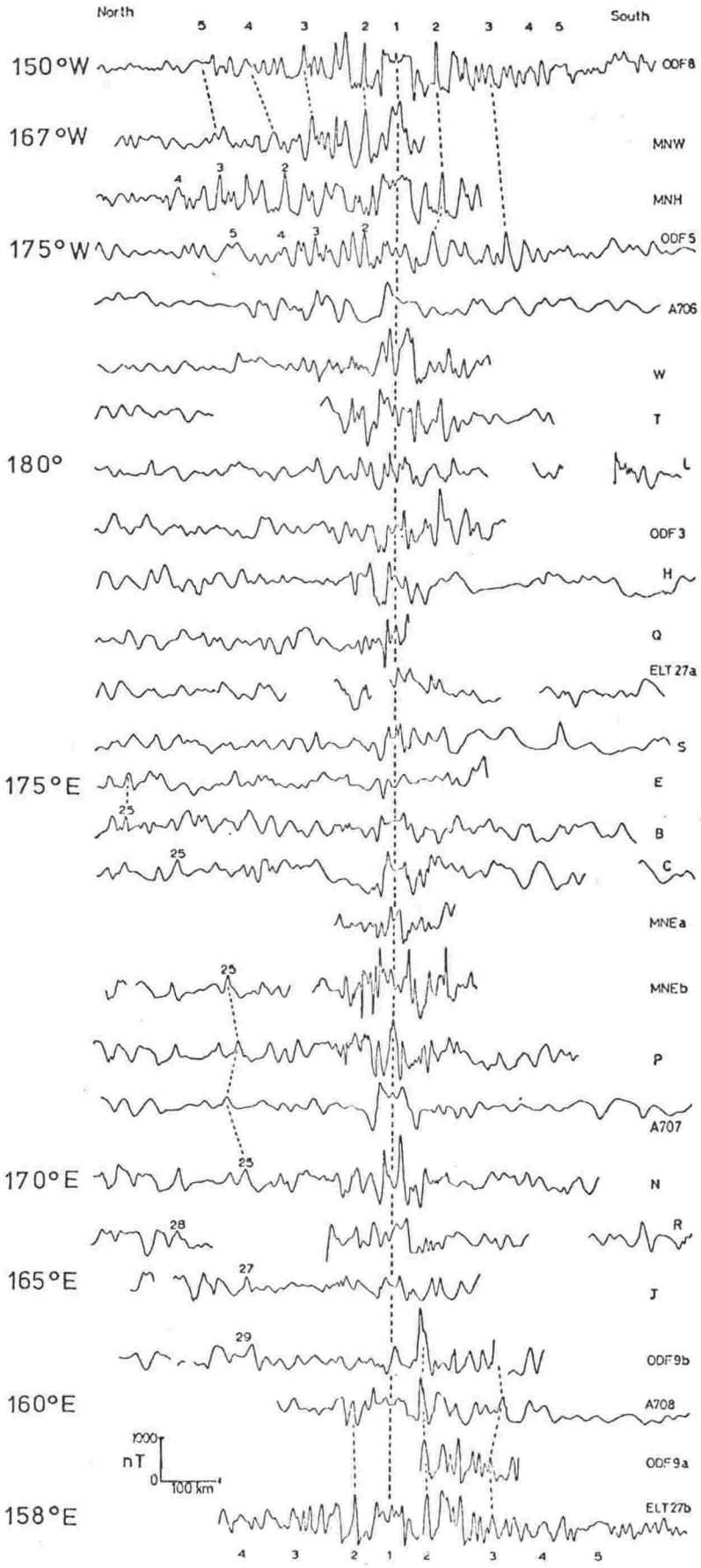


Fig. 4.17 Magnetic anomaly profiles across the Pacific-Antarctic ridge system between 150°W and 161°E, and across the Indian-Antarctic ridge between 160° and 158°E. Eastern most track at the top, with the longitude at the crossing of the axis shown for selected tracks. Profiles aligned on the axis of the ridge system. Identifiable anomalies numbered or correlated.

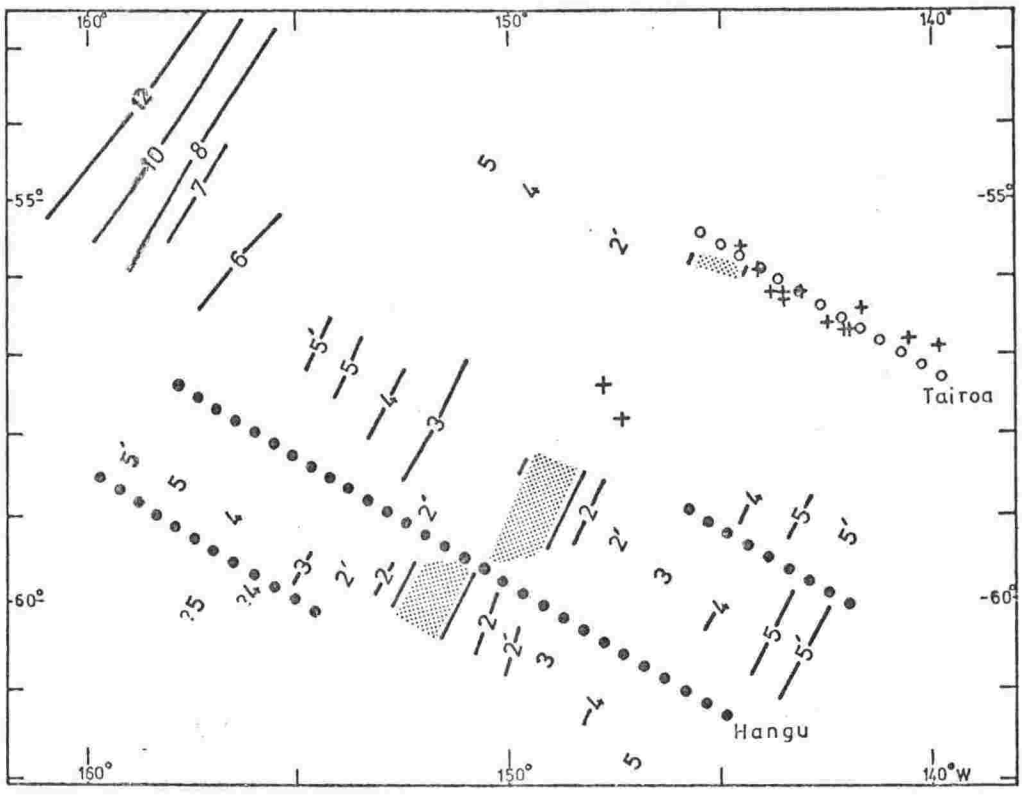


Fig. 4.18 Pacific-Antarctic ridge near 150°W: magnetic anomaly lineations and fracture zones. Numbered lineations are determined from two or more tracks; single numbers represent an anomaly identification from only one track. Central anomaly shown shaded. Filled circles : fracture zones from offset of lineations. Open circles : fracture zones from bathymetry. Crosses : USCGS epicentres 1964 - 1972.

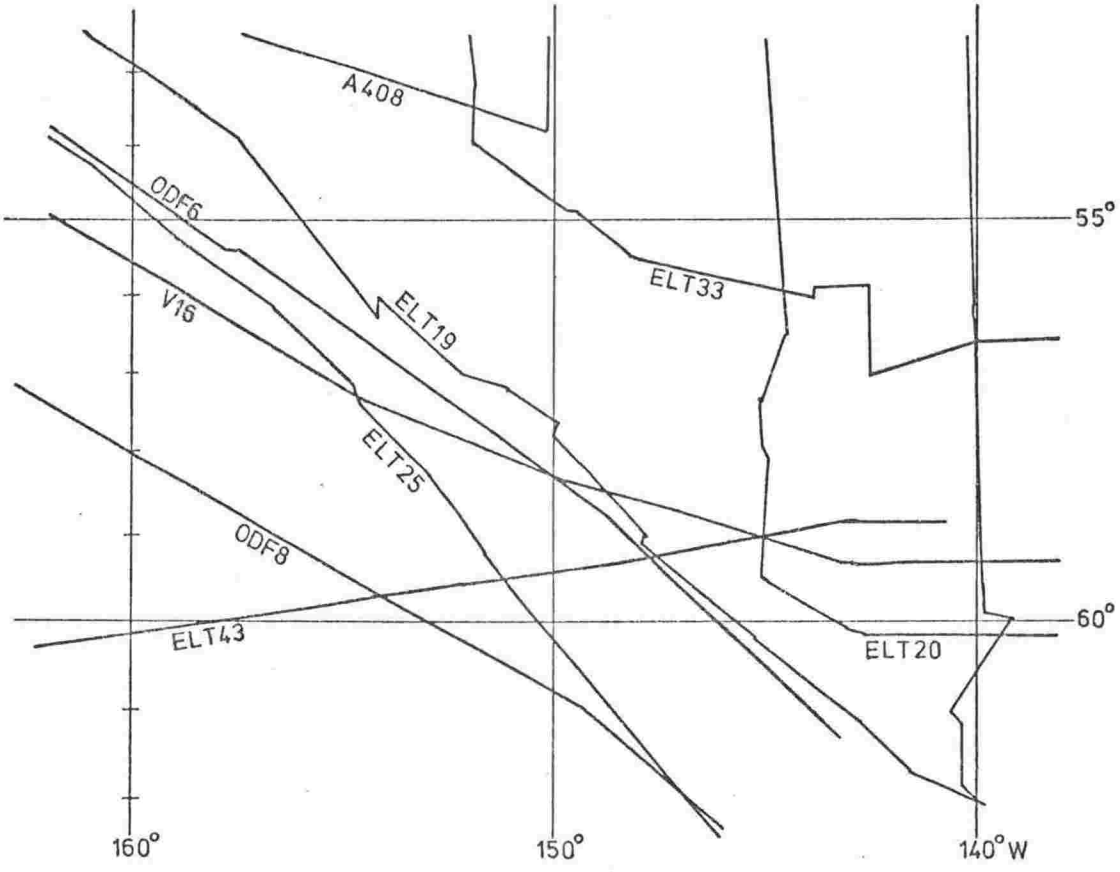


Fig. 4.19 Track control for the interpretation shown in Fig. 4.18. Bathymetric data not available for all tracks.

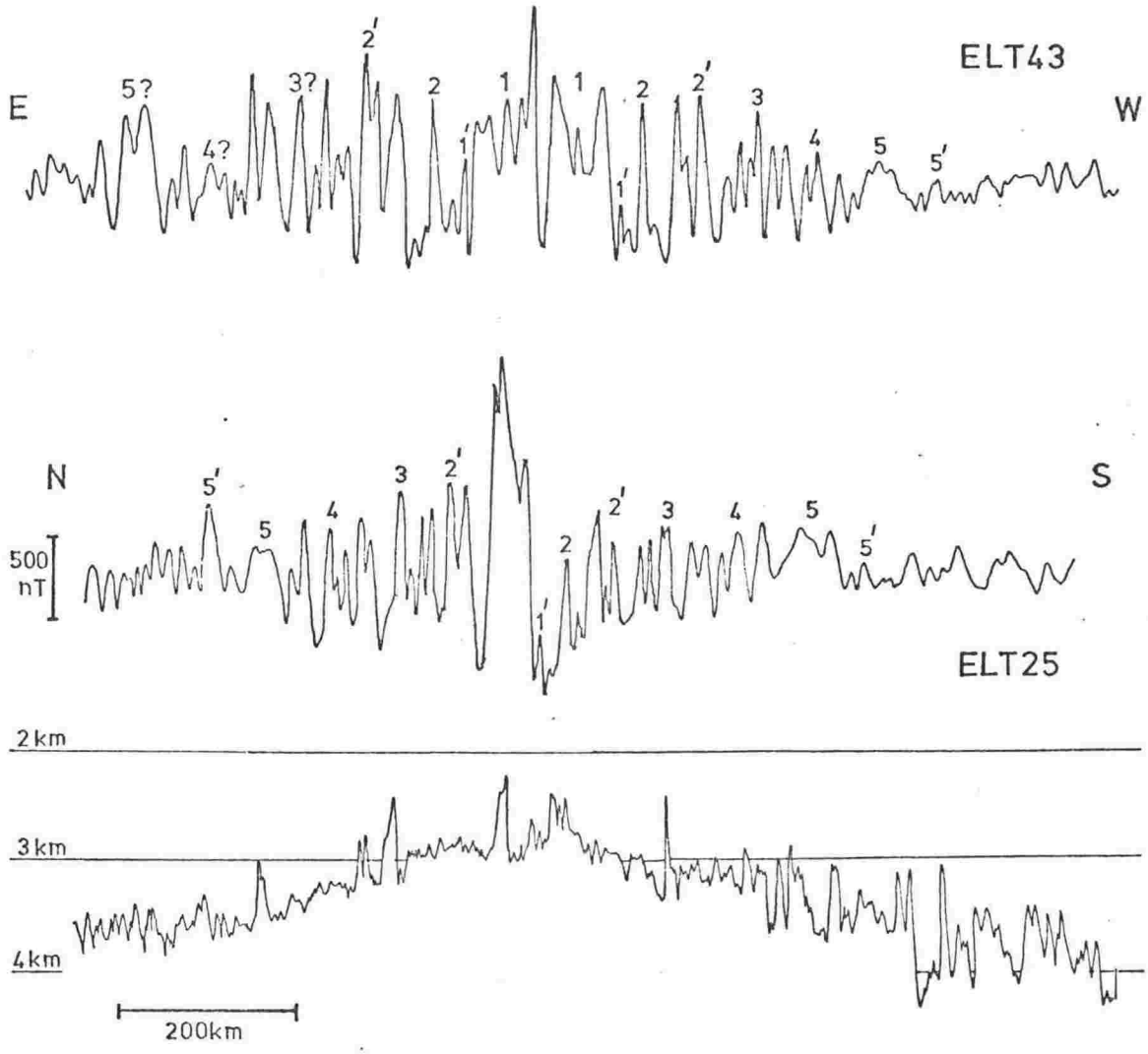


Fig. 4.20 Bathymetric and magnetic profiles from tracks across the Hangu fracture zone. Lower profile is the ELT25 bathymetry. Bathymetry not available for ELT43.

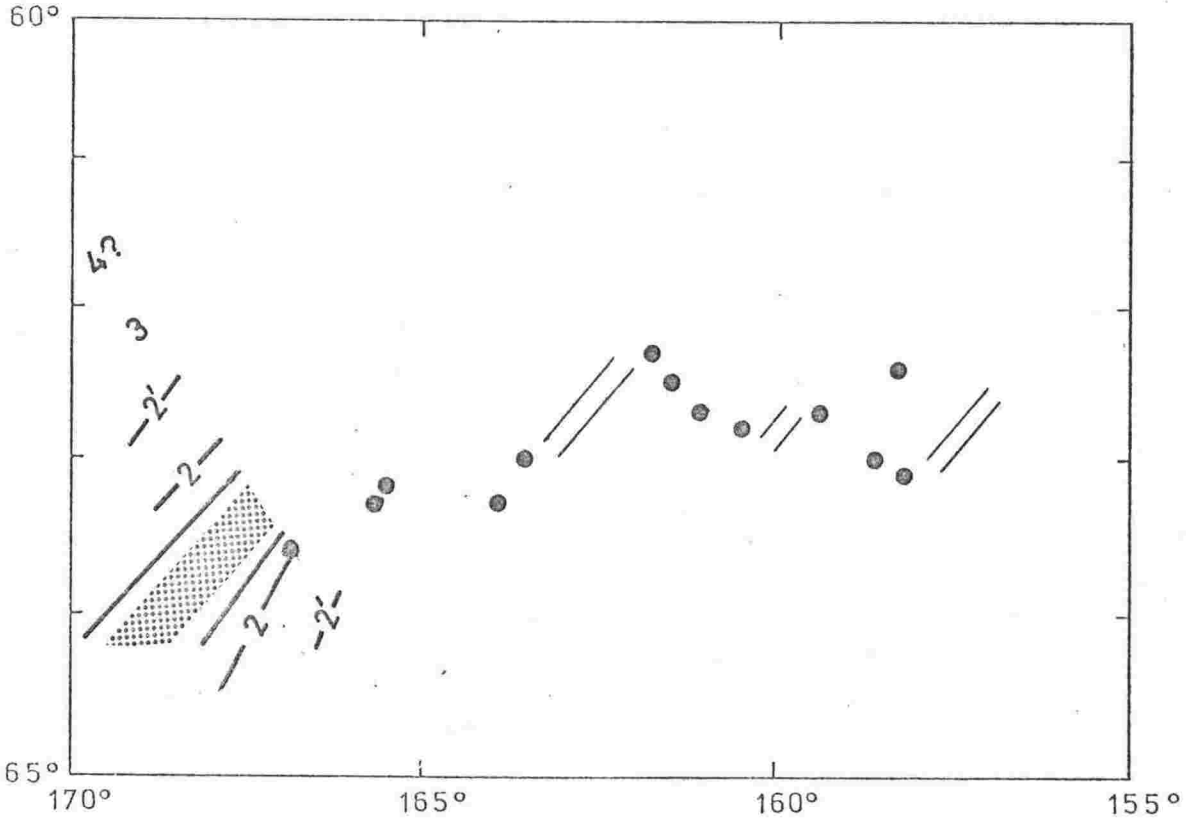


Fig. 4.21 Pacific-Antarctic ridge system 155° to 170°W. Dots are USCGS epicentres 1964 - 1972. Double lines indicate possible ridge axes. Note: These postulated ridge axes are based only on the seismicity data, not on any bathymetric or magnetic data.

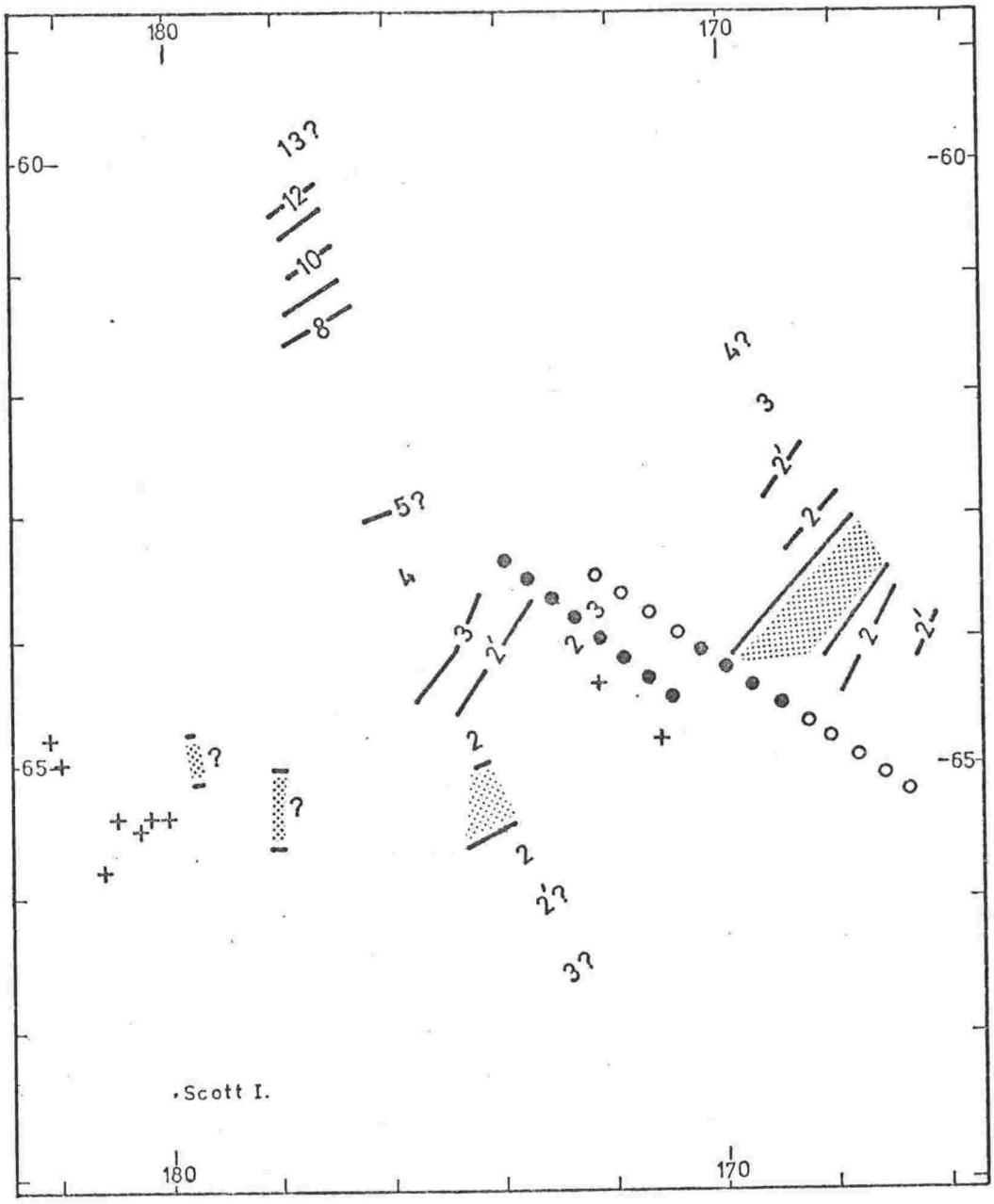


Fig. 4.22 Pacific-Antarctic ridge system just east of 180°: magnetic anomaly lineations and fracture zones. Numbered lineations are determined from two or more tracks; single numbers represent an anomaly identification from only one track. Central anomaly shown shaded. Filled circles : fracture zones from offset of lineations. Open circles : fracture zones from bathymetry. Crosses : USCGS epicentres 1964 - 1972.

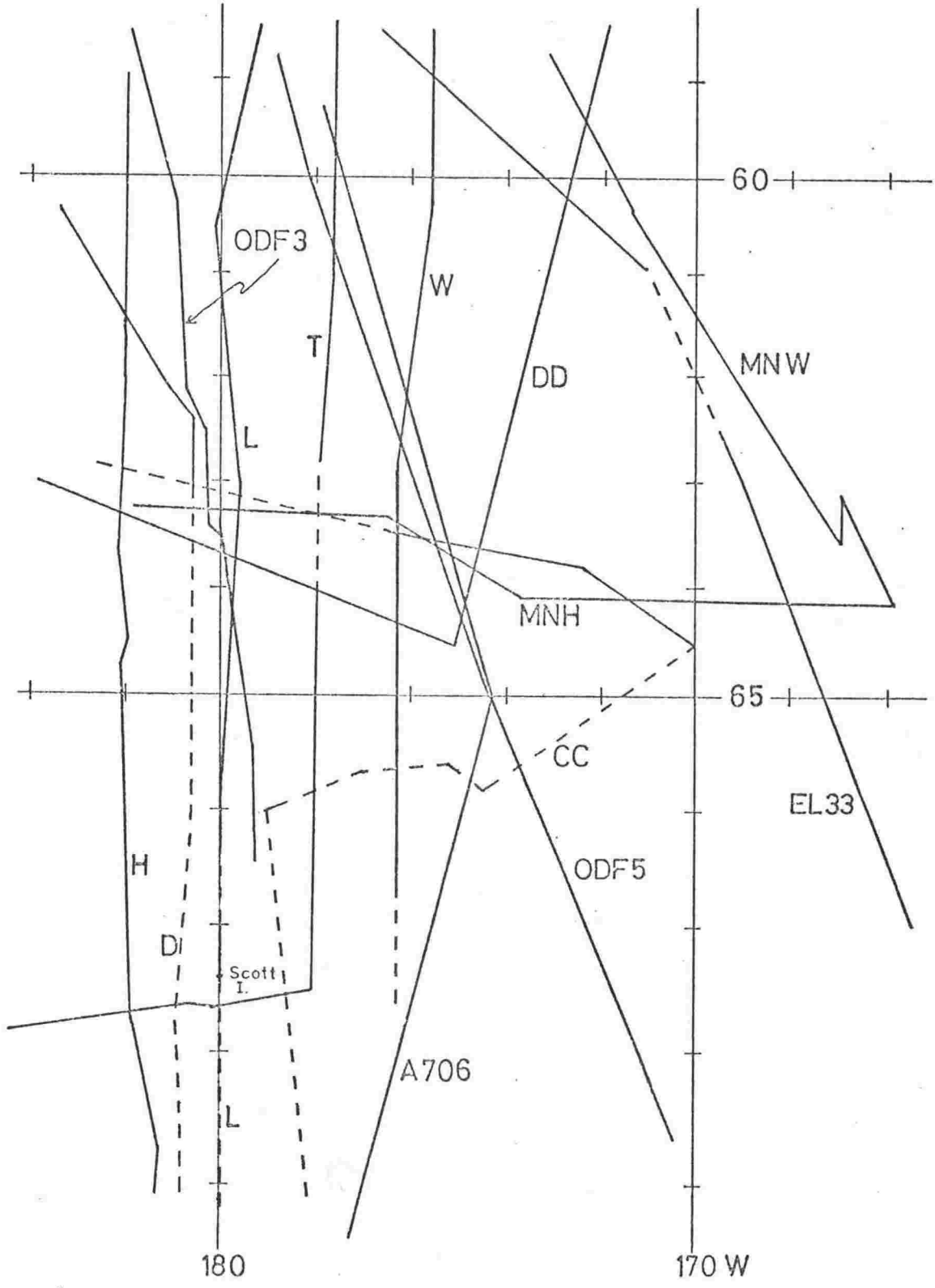


Fig. 4.23 Track control for interpretation shown in Fig. 4.22. Dotted portions indicate bathymetry only, but bathymetry was not available for all the other tracks.

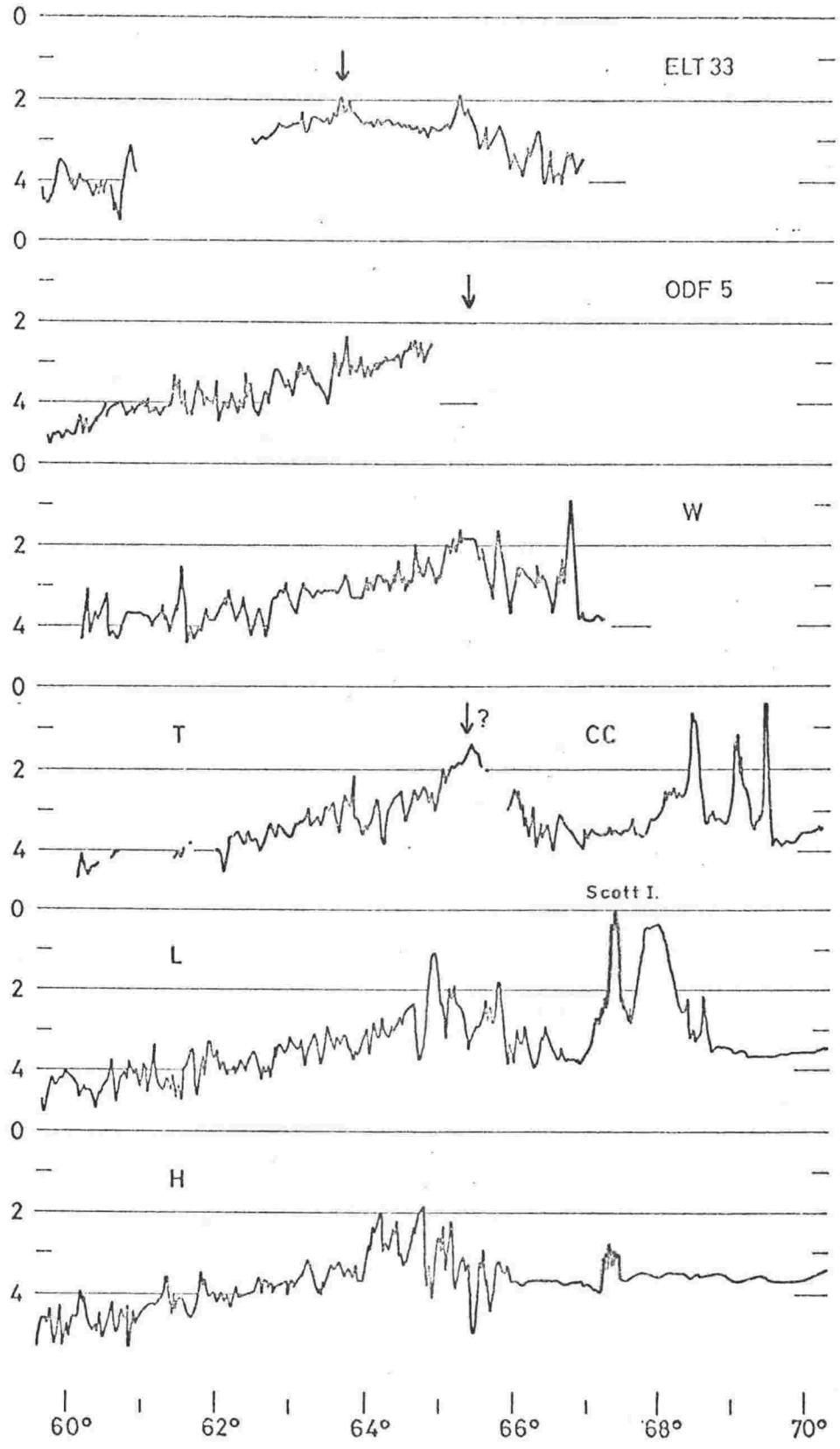


Fig. 4.24 Bathymetric profiles across the Pacific-Antarctic ridge system between 168°W and 178°E. Eastern most track at the top, tracks shown in Fig. 4.23. Arrows indicate the axis of spreading for the profiles in which it has been identified from magnetic anomalies.

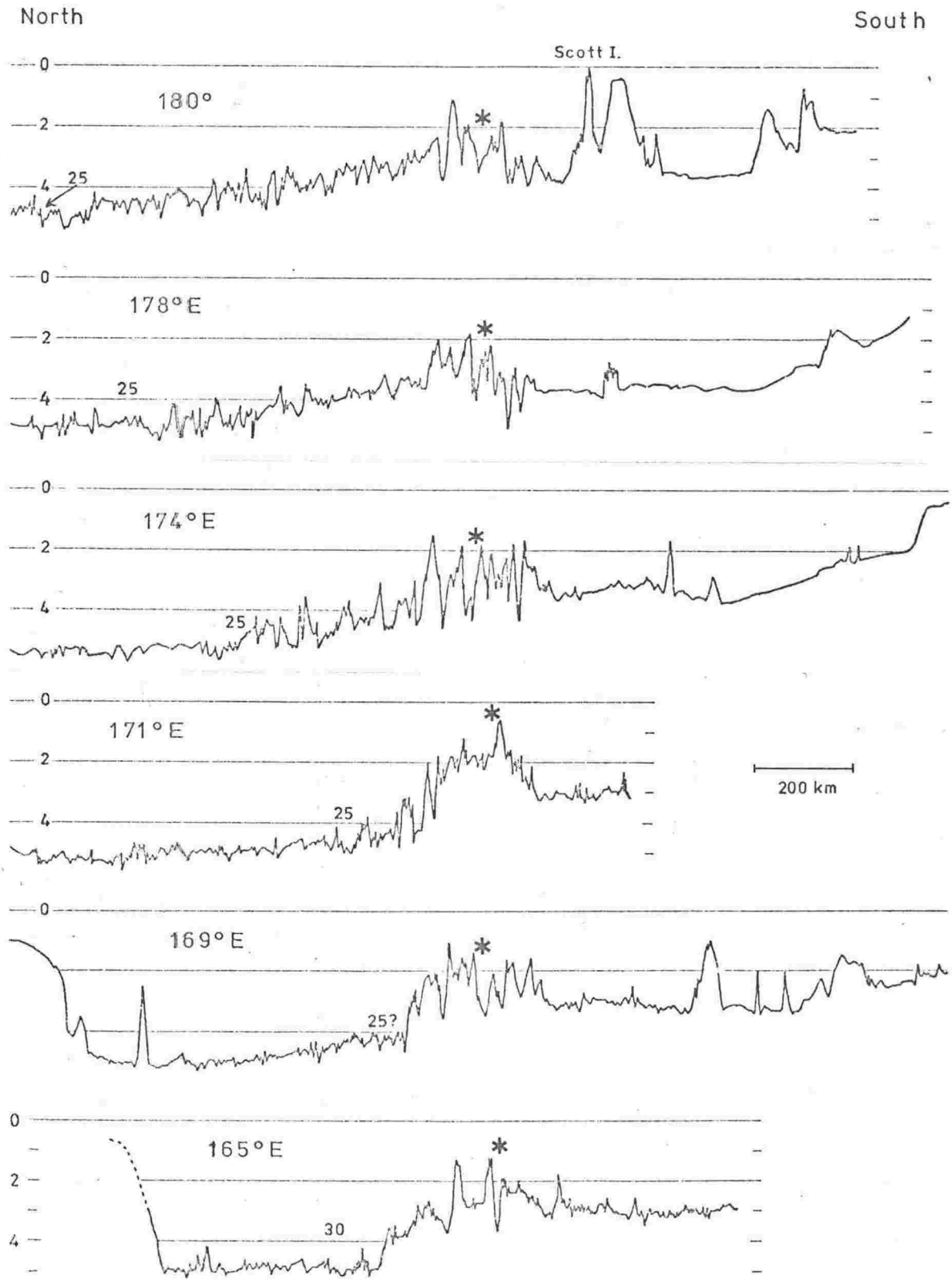


Fig. 4.25 Bathymetric profiles across the Pacific-Antarctic fracture zone. The profiles, which are approximately north-south, are aligned on the topographic axis and the labels indicate the longitude at the axis. Asterisks indicate the approximate position of seismicity adjacent to the profile. Numbers on profiles indicate position of the southern most easily identified anomaly.

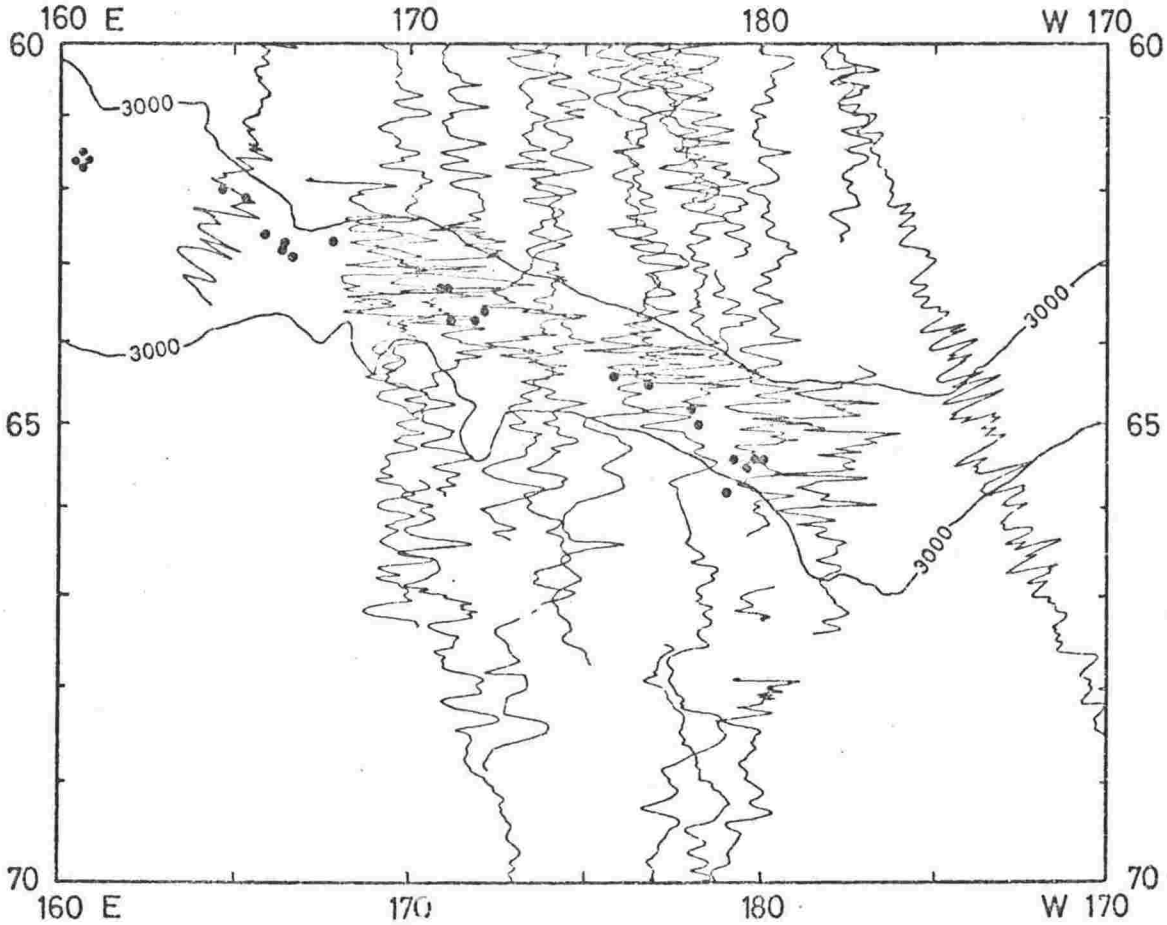


Fig. 4.26 The Pacific-Antarctic fracture zone area: magnetic anomaly profiles, the 3 km bathymetric contour; and USCGS epicentres 1964-1972.

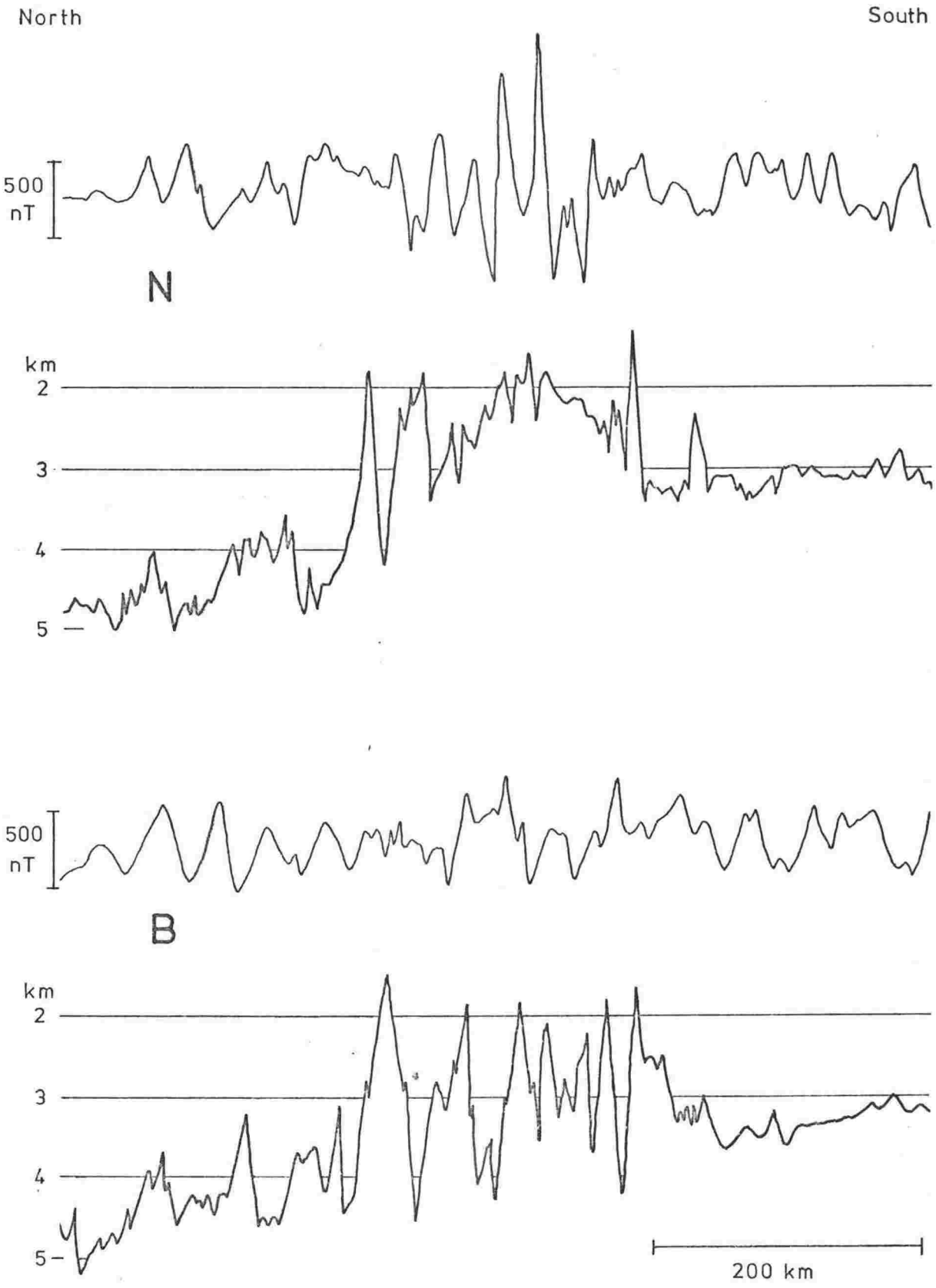


Fig. 4.27 Bathymetric and magnetic profiles from two north-south tracks across the Pacific-Antarctic fracture zone. N at 170°E. B at 174°E.


Fig. 4.28 Magnetic anomaly profiles over the northern flanks of the Pacific-Antarctic ridge east of 170°W. Eastern most profile at the top. Profiles projected to give about the same length of the anomaly sequence. Distance on profile ODF6 from anomaly 25 to anomaly 5 is approximately 950 km.

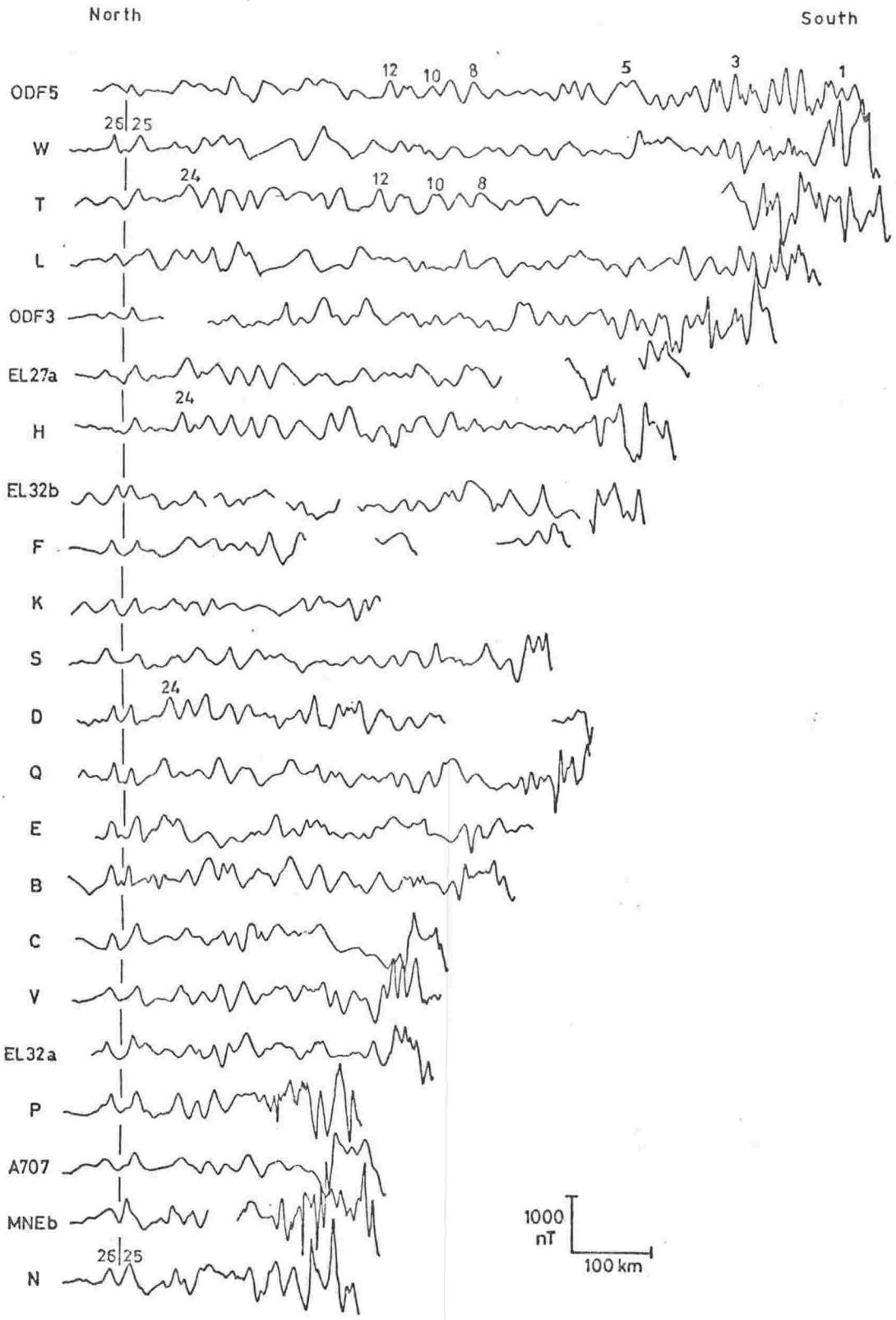


Fig. 4.29 Magnetic anomaly profiles north of the Pacific-Antarctic fracture zone between 170°E and 175°W. Eastern most profile at the top. Profiles are aligned at the left on anomalies 25 - 26, and extend (where complete) to the axis of the Pacific-Antarctic fracture zone.

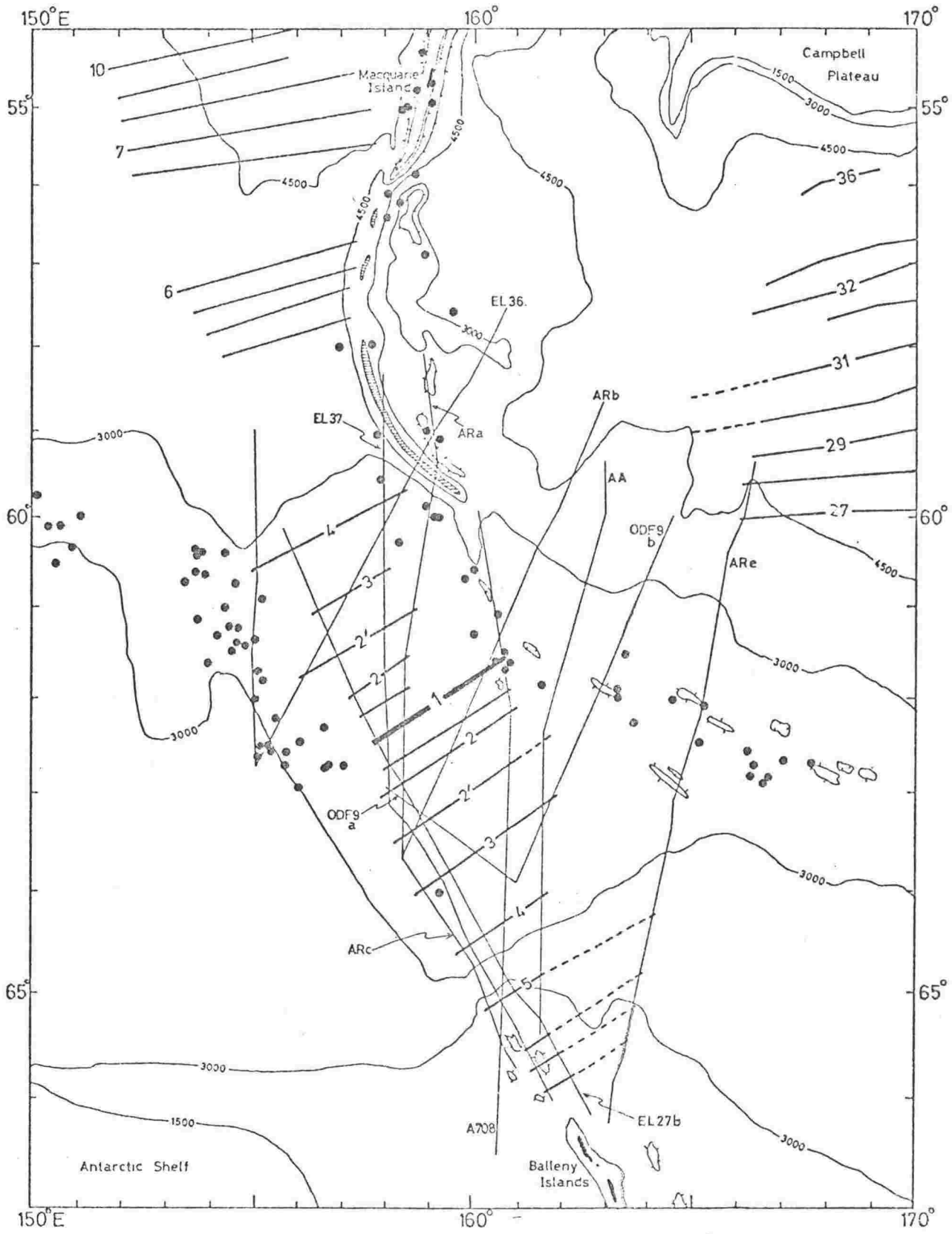


Fig. 4.30 The Indian-Antarctic-Pacific triple junction area. Anomaly lineations south of 60°S are based on magnetic data on the tracks shown. Lineations west of the Macquarie complex north of 60°S are from Christoffel and R.F. Falconer (1973). Epicentres (dots) are from the USCGS for 1964 to 1972 and Sykes (1970) for 1950 to 1966; for duplicated earthquakes the Sykes locations were taken. Bathymetry, in metres, from Hayes and Conolly (1972) and Hurley and Krause (1973a,b).

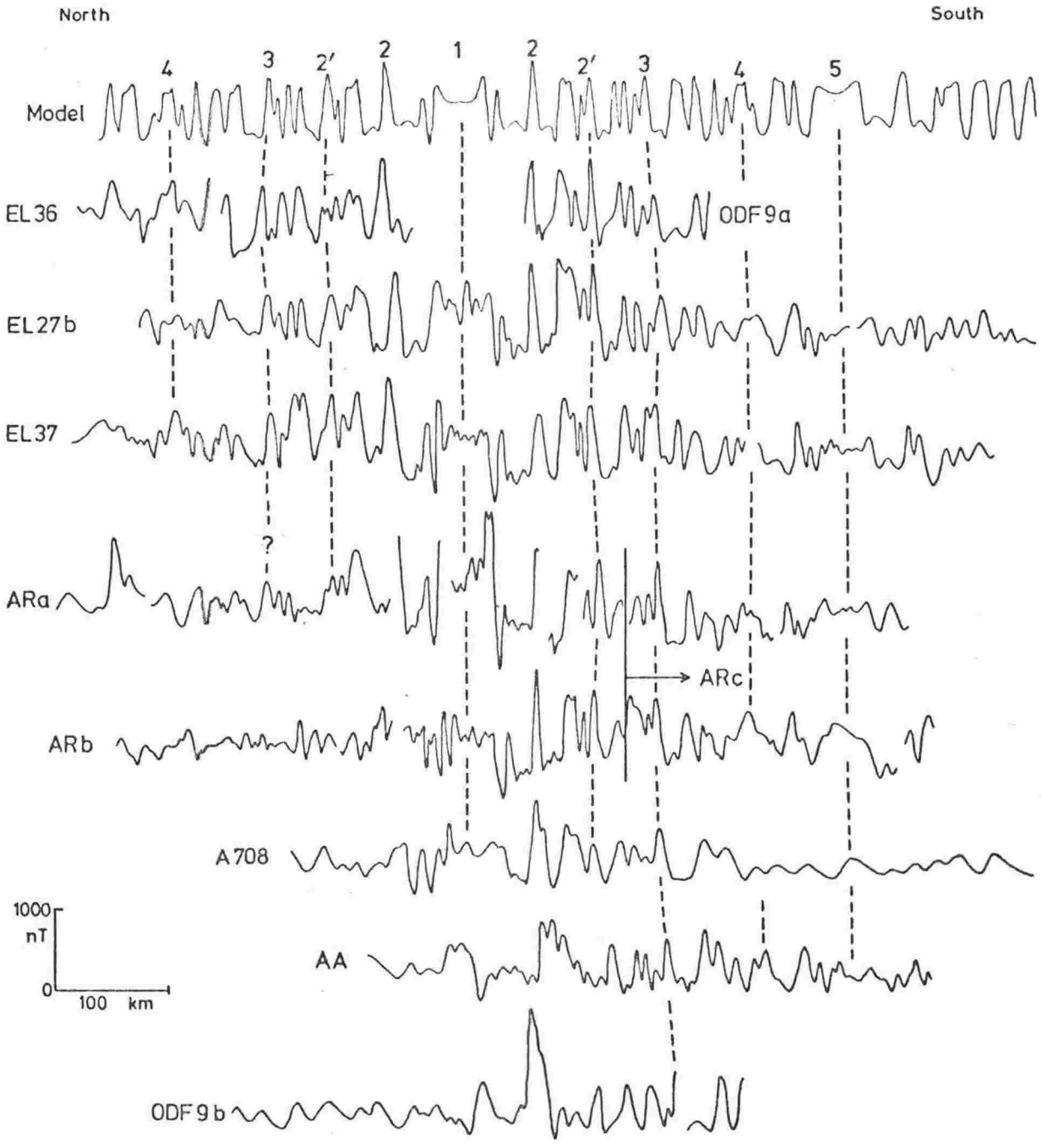


Fig. 4.31 Magnetic anomaly profiles in the triple junction area. Profiles projected perpendicular to the southeast Indian ridge. Model profile based on the time scale of Talwani et al. (1971), with a half-spreading rate of 3.4 cm/y.

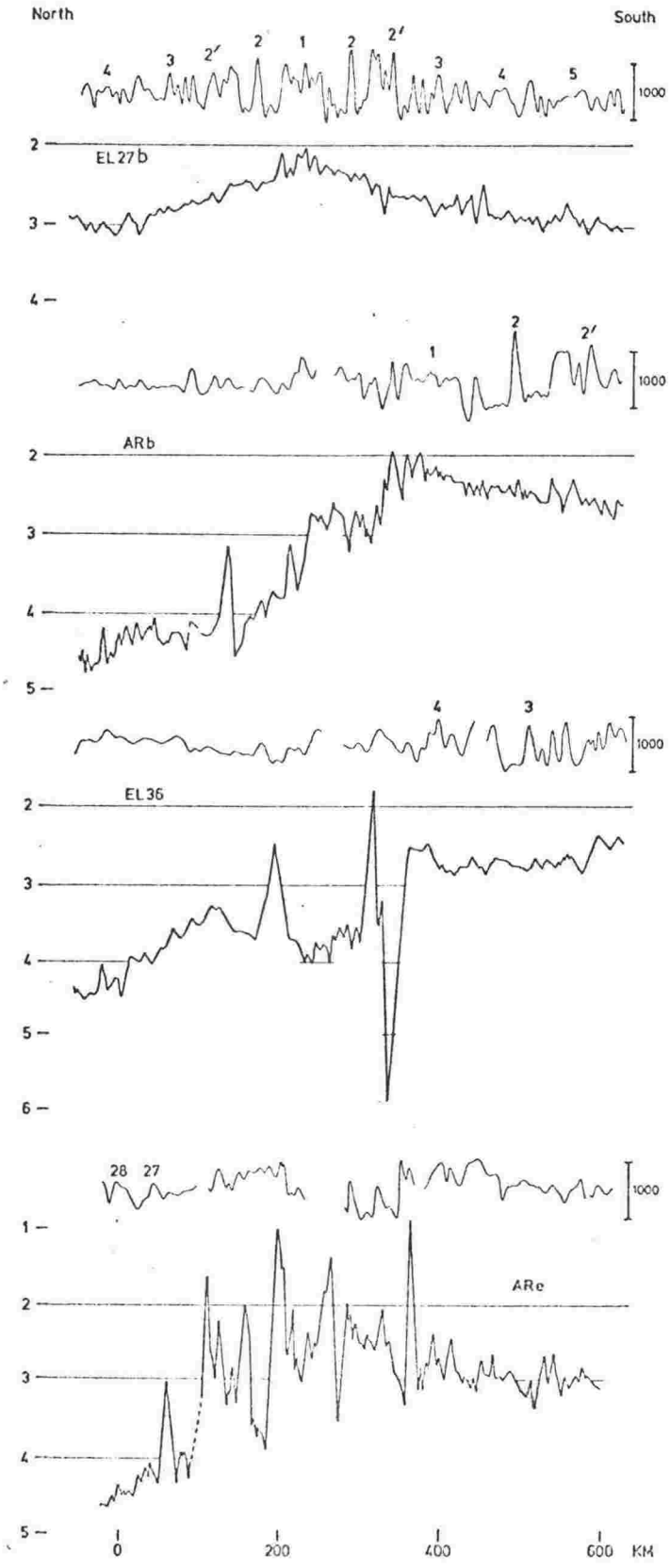


Fig. 4.32 Bathymetric and magnetic profiles from tracks across the major features in the triple junction area. For each track the upper profile is magnetic anomalies in nT, and the lower profile is bathymetry in km. Track locations shown in Fig. 4.30.

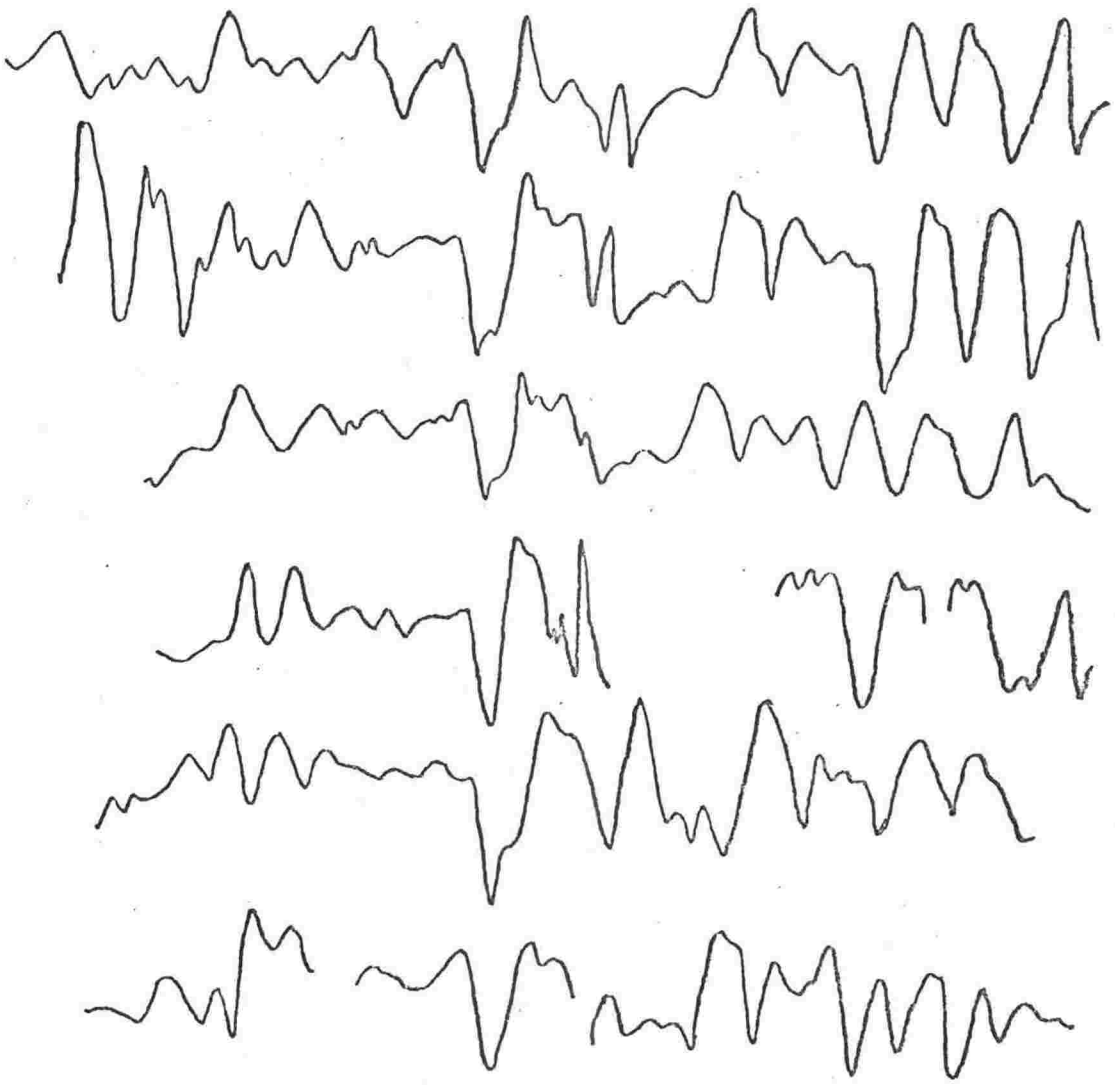

Fig. 5.1 Profiles given to students for correlation study.
The actual size given to students was twice that shown here.

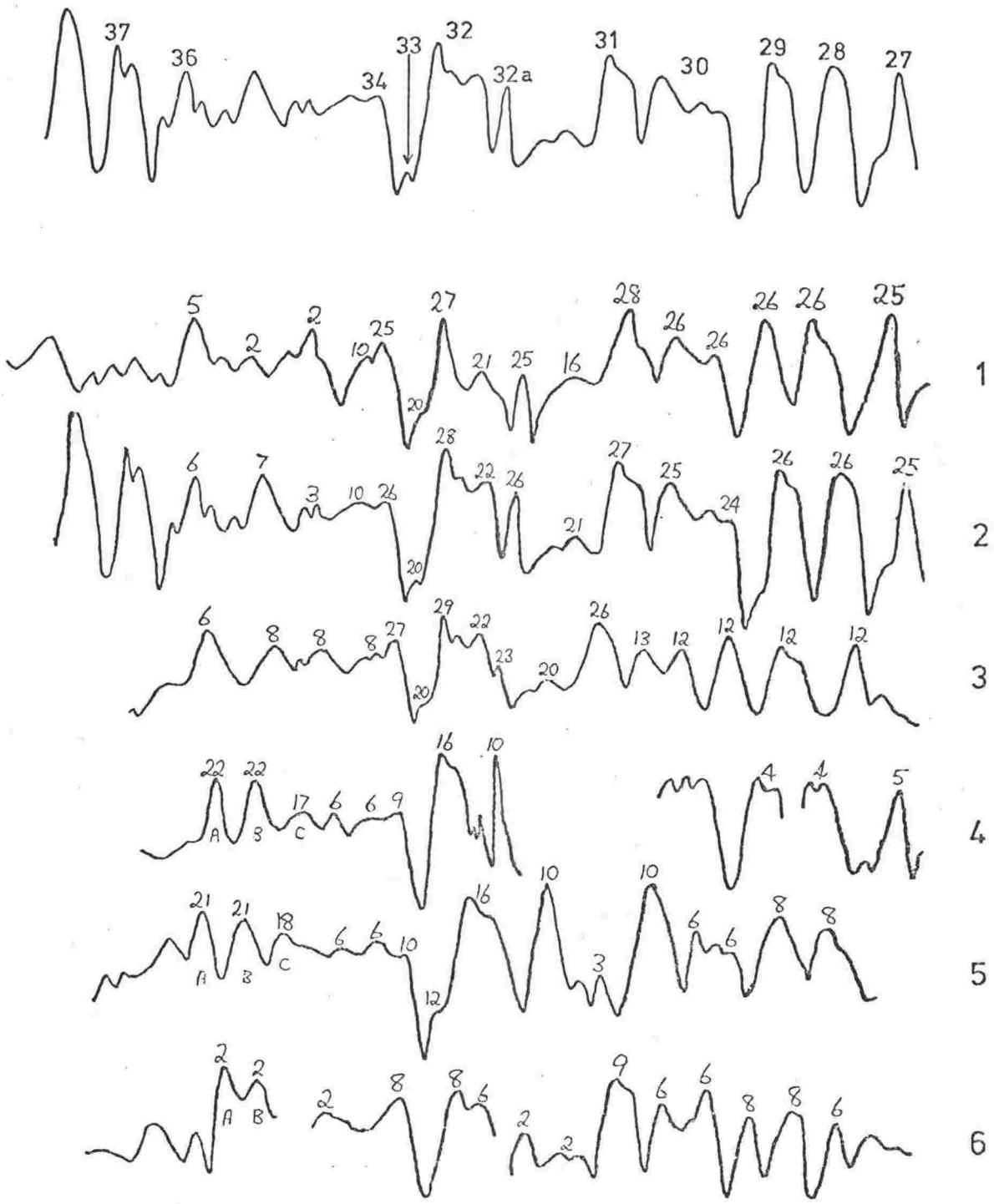


Fig. 5.2 Results of student correlation tests. Upper profile is a type profile with anomaly numbers. Profiles 1-6 are the student profiles of Fig. 5.1. Numbers above peaks indicate the number times each peak was chosen. Total number of students was 34.

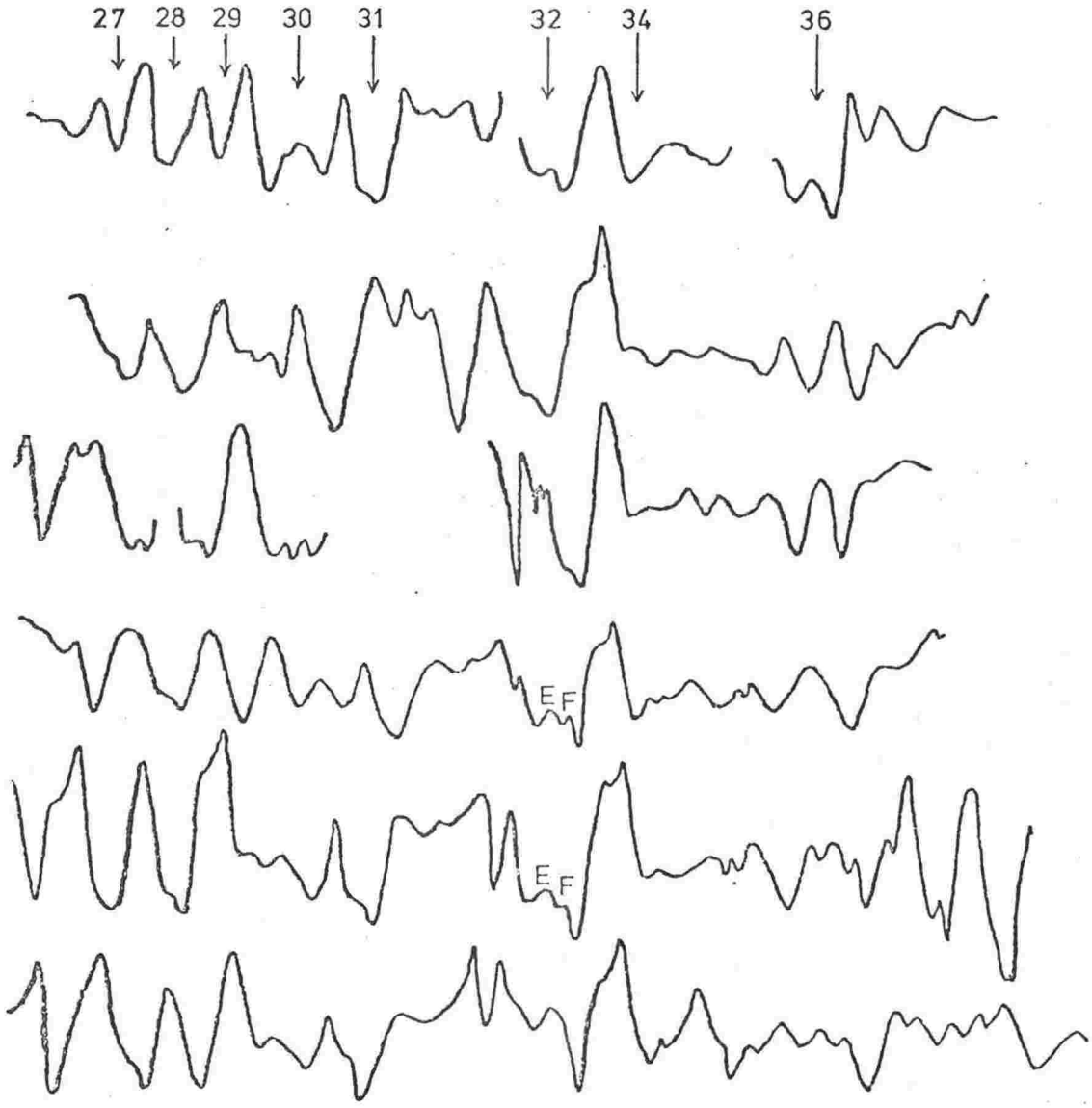


Fig. 5.3 Profiles given to a fourth group of students. Same data as Fig. 5.1 but upside down.

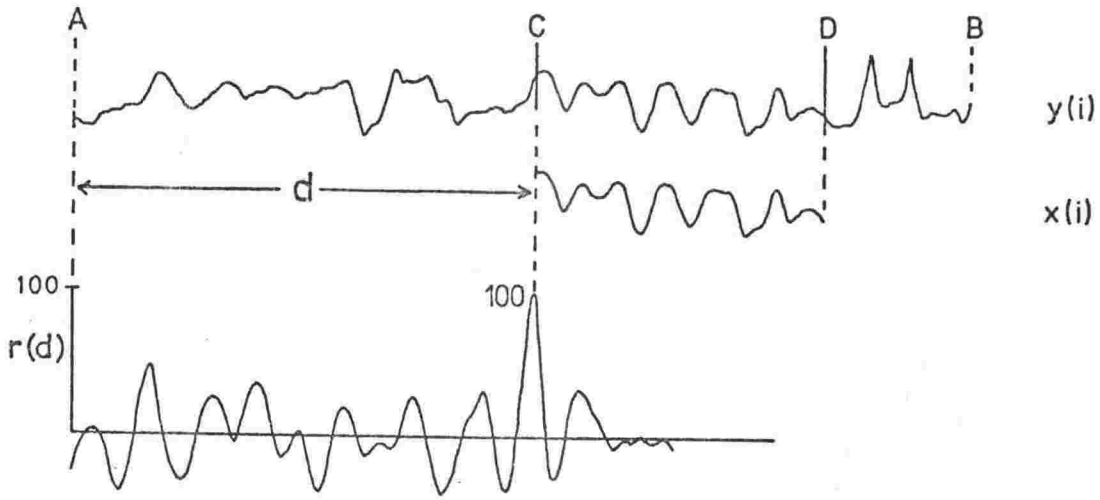


Fig. 5.4 Cross-correlation of profile x with profile y. Profile x in the alignment position at which the correlation function r(d) is maximum.

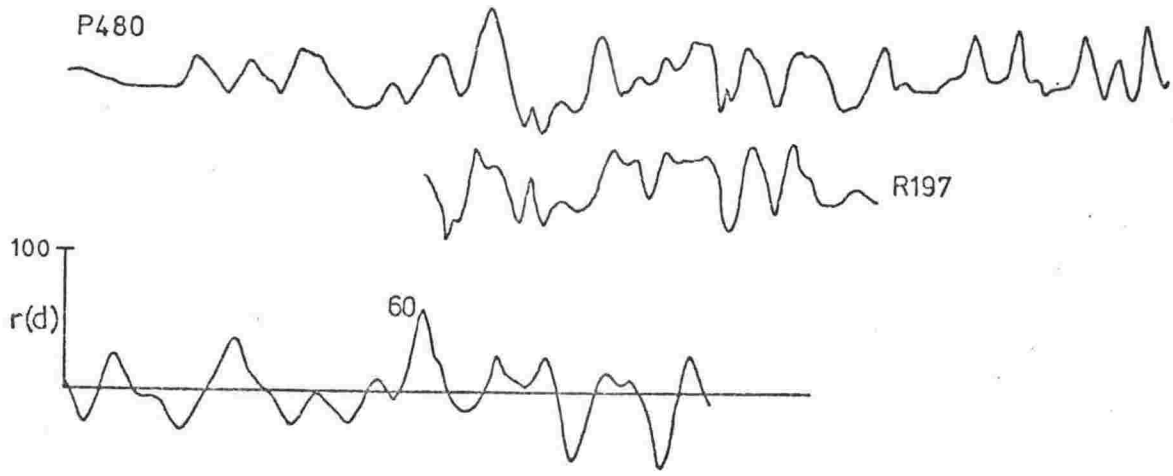


Fig. 5.5 Correlation of profile R197 with profile P480. R197 in the position determined by the maximum value (60) of r(d).

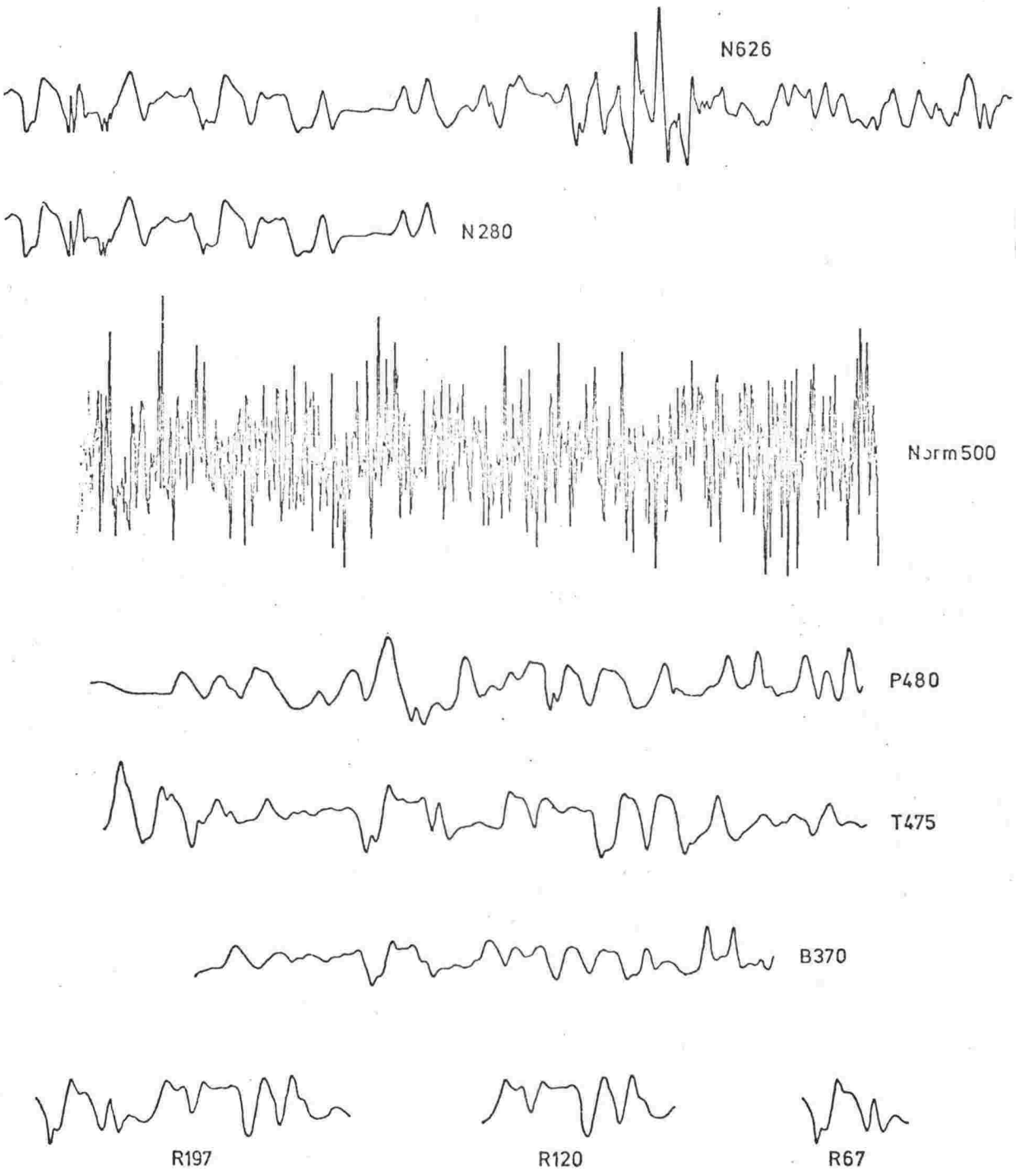


Fig. 5.6 Some profiles used in the numerical correlation study. Profile NORM500 is 500 normally distributed random numbers.

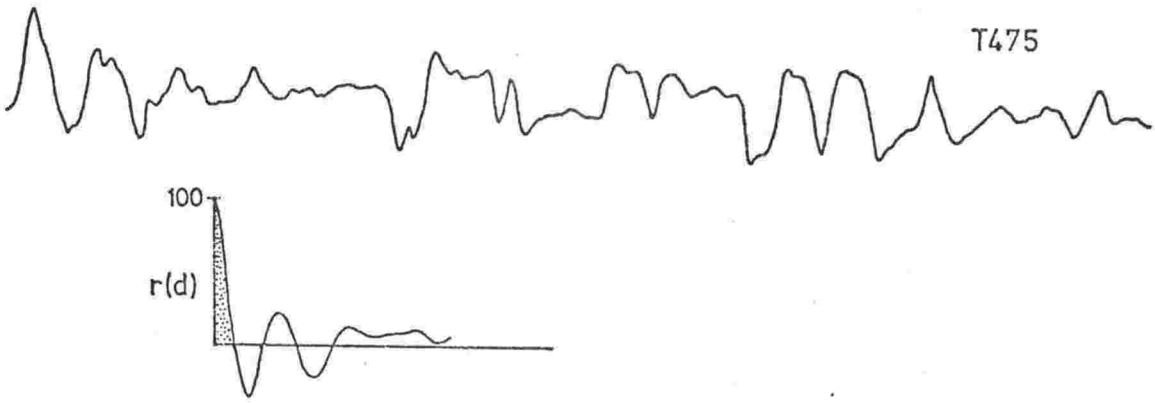


Fig. 5.7 Profile T475 and part of its autocorrelation function r(d). The autocorrelation is calculated out to only d = 20% of 475 and the symmetrical part for -ve d is not shown. The shaded area is the part used for calculating the correlation length L.

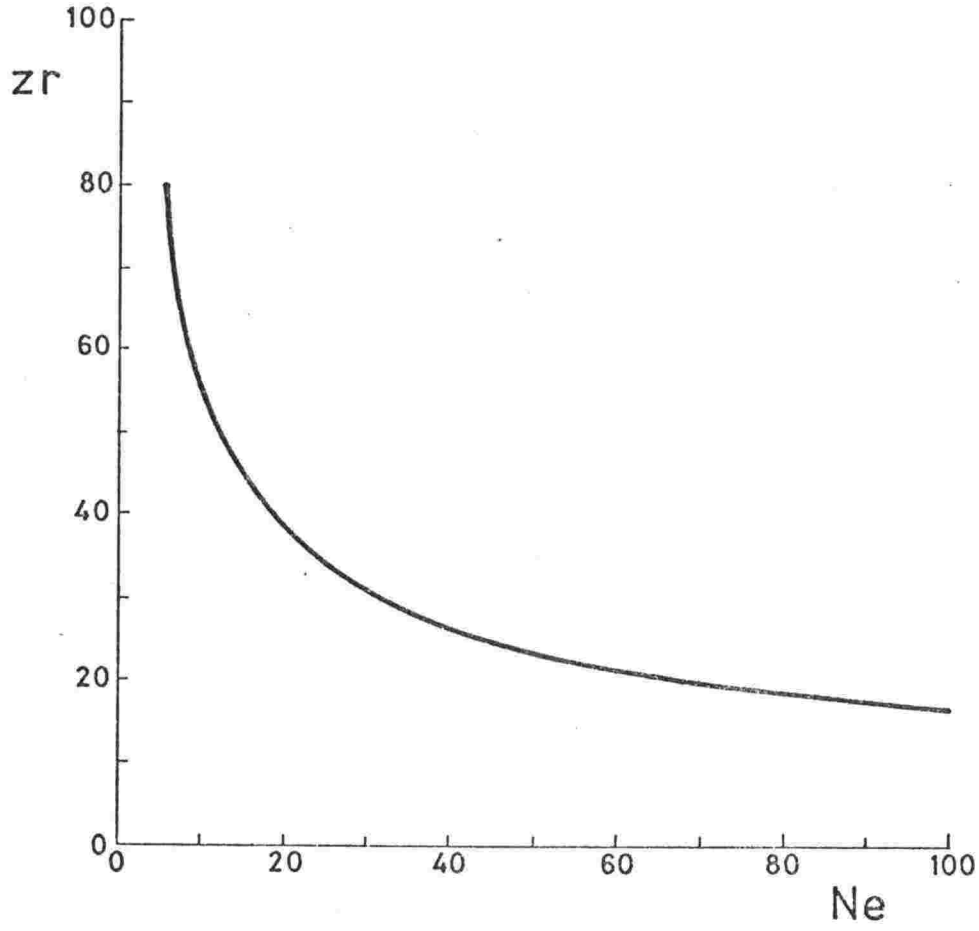


Fig. 5.8 Variation of zr, the 95% confidence level for zero correlation, with the effective number of independent points, Ne.

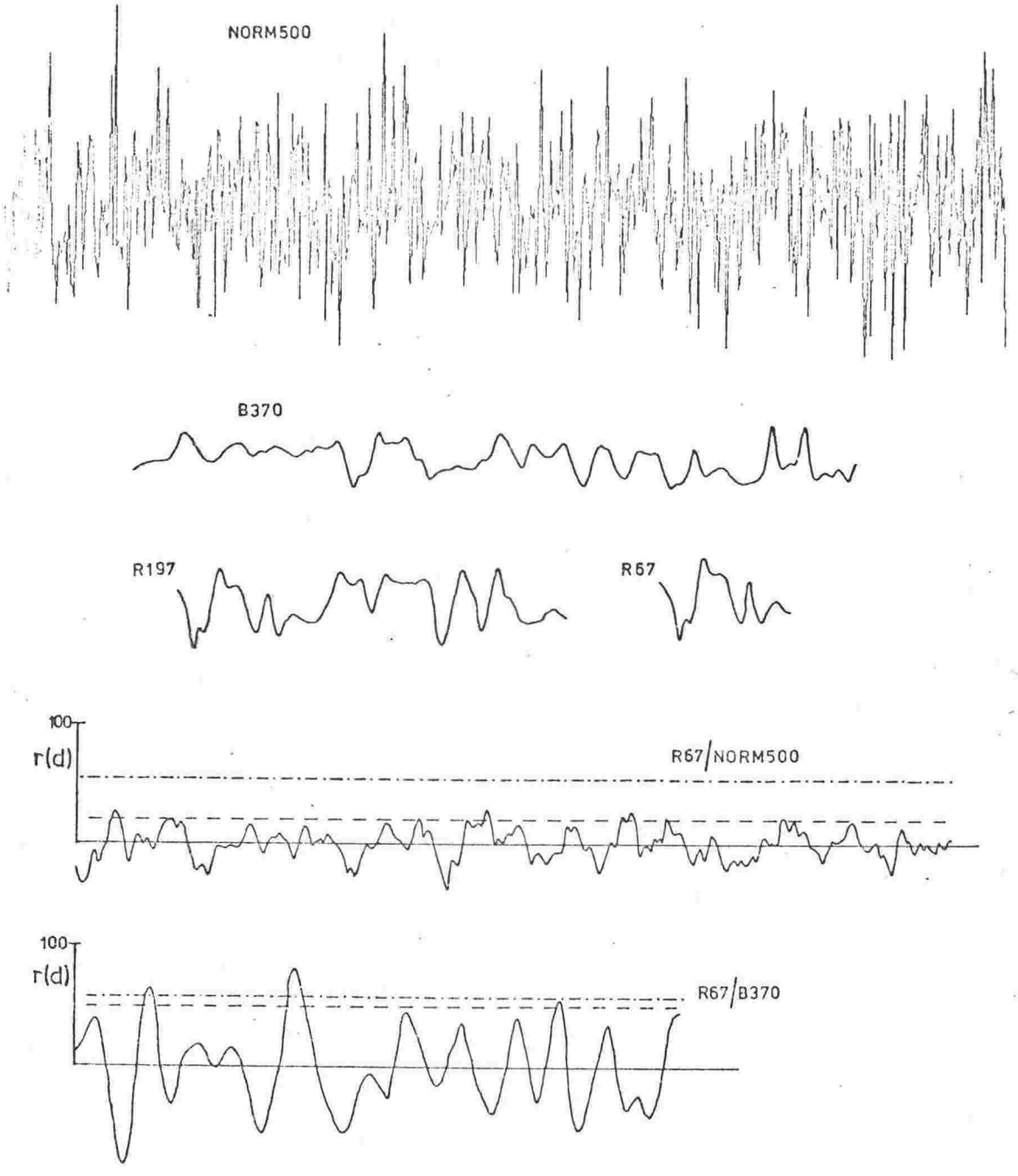


Fig. 5.9 Illustrative profiles and their correlation functions. The dash-dotted and dashed lines on the plots of r(d) are respectively the maximum and minimum values of zr.

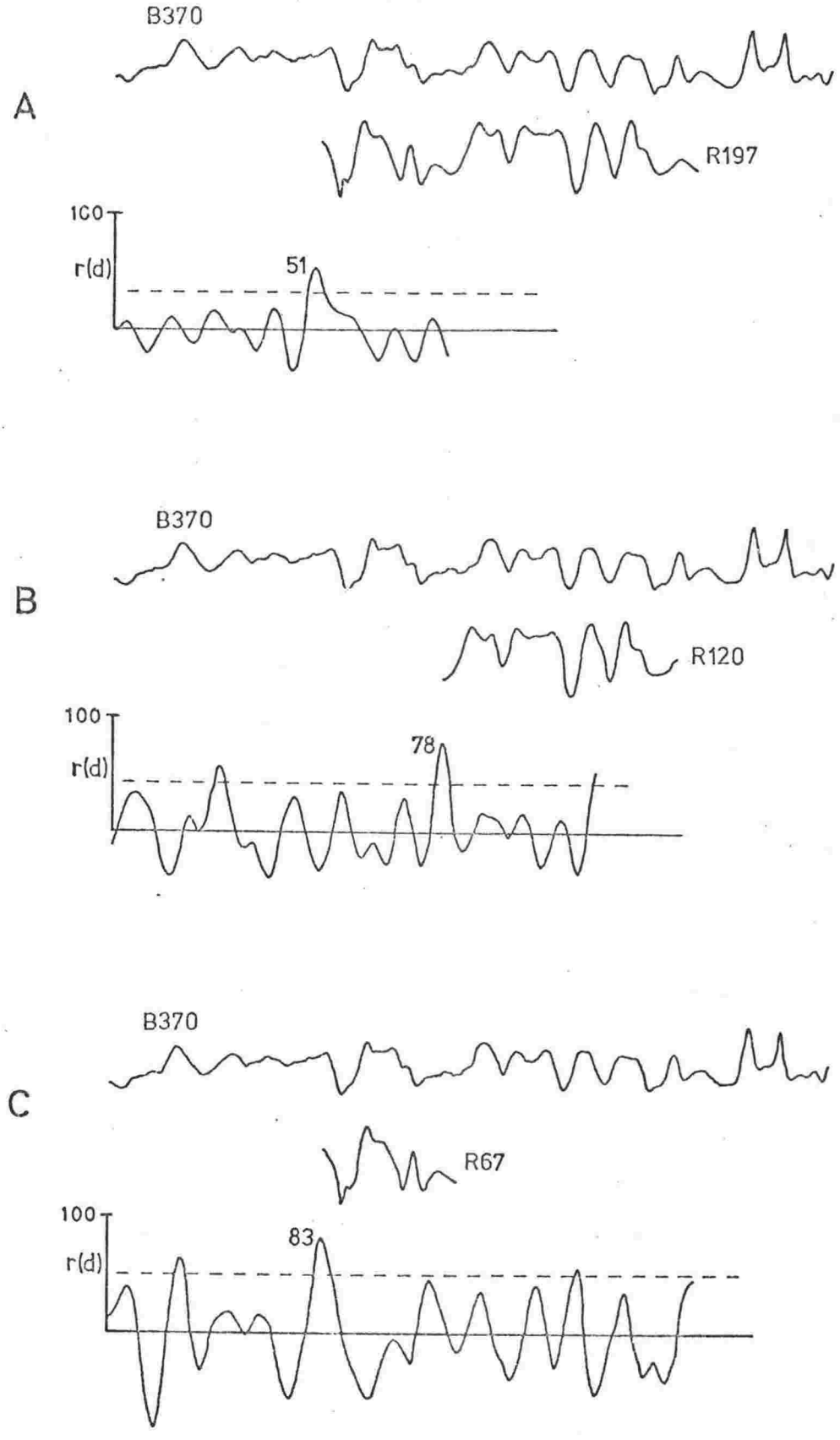


Fig. 5.10 Correlations of profile B370 with profile R197 and its subsections R120 and R67. Dashed lines on the plots of r(d) are the noncorrelation level.

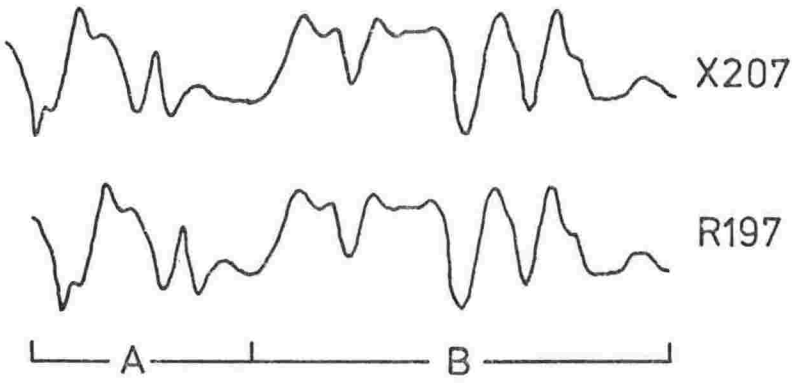


Fig. 5.11 Profiles X207 and R197.

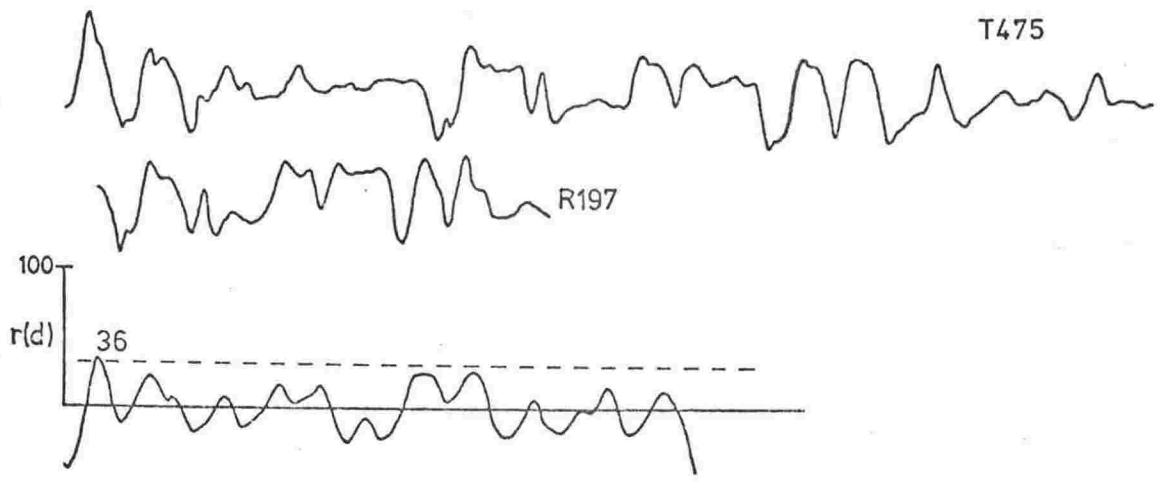


Fig. 5.12 Correlation of R197 and T475.

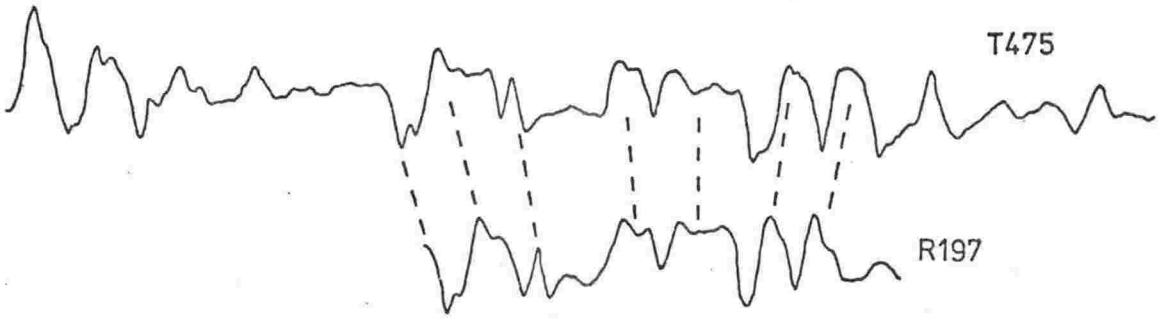


Fig. 5.13 Preferred alignment position of profiles R197 and T475.

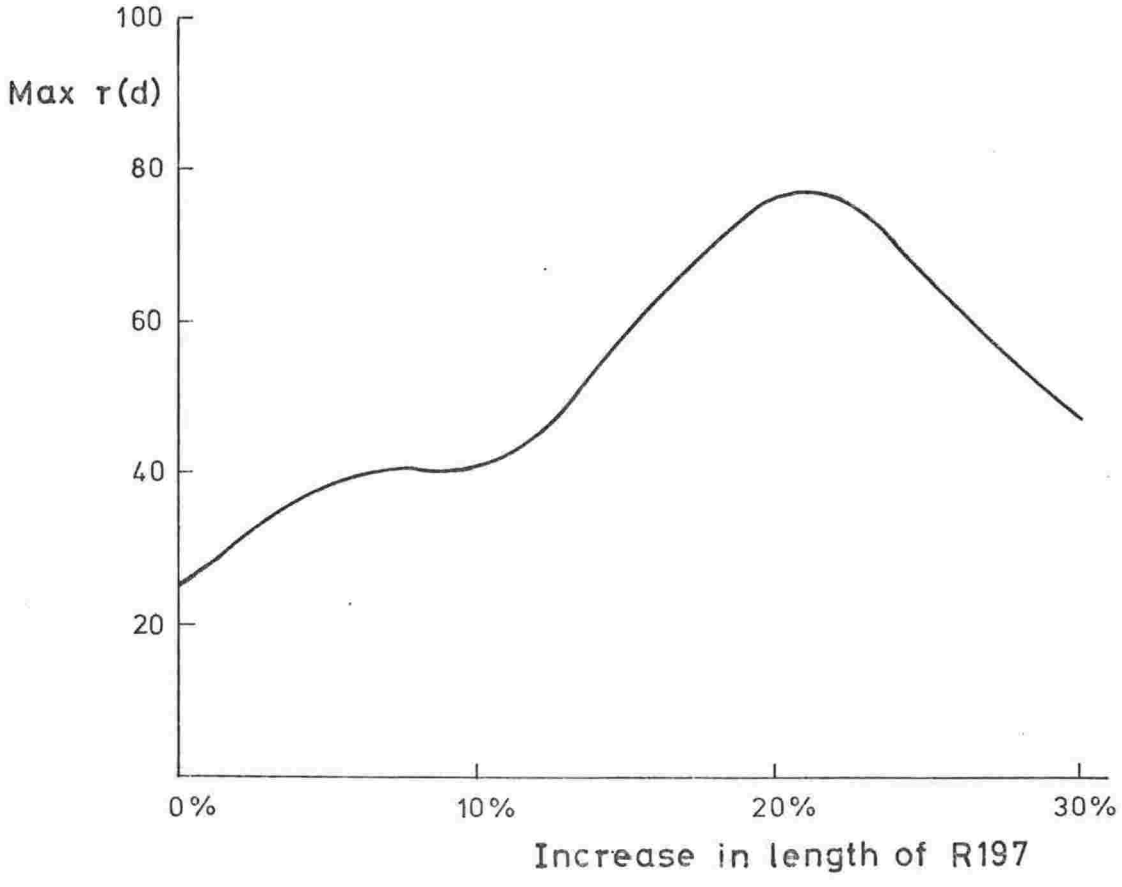


Fig. 5.14 Correlation of R197 on T475: variation of the correlation value at the position shown in Fig. 5.13 as the length of R197 is increased.

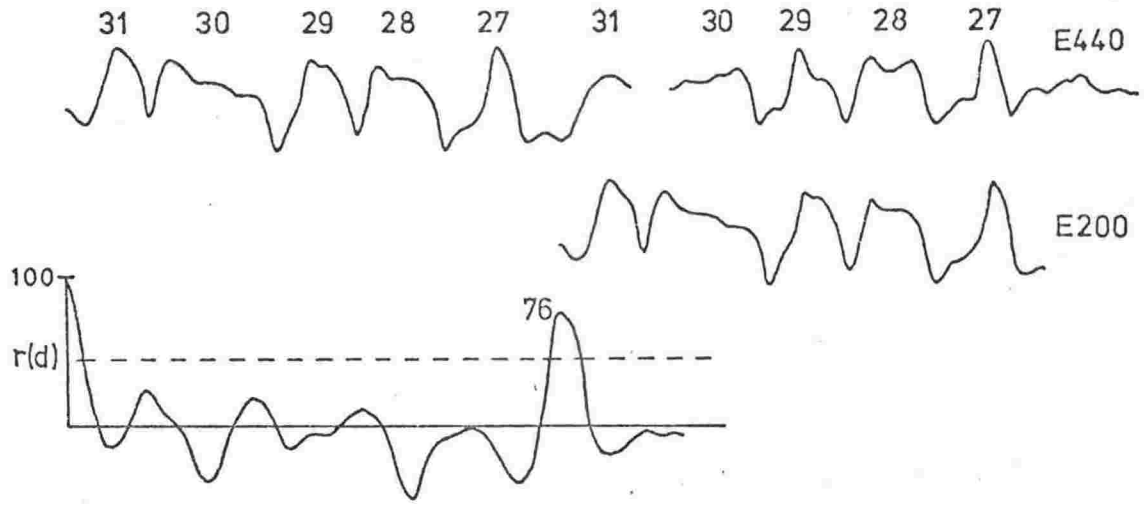


Fig. 5.15 Correlation in the ELT23 profile across the Tairoa fracture zone. Profile E200 is the left hand set of anomalies 27-31 in profile E440.

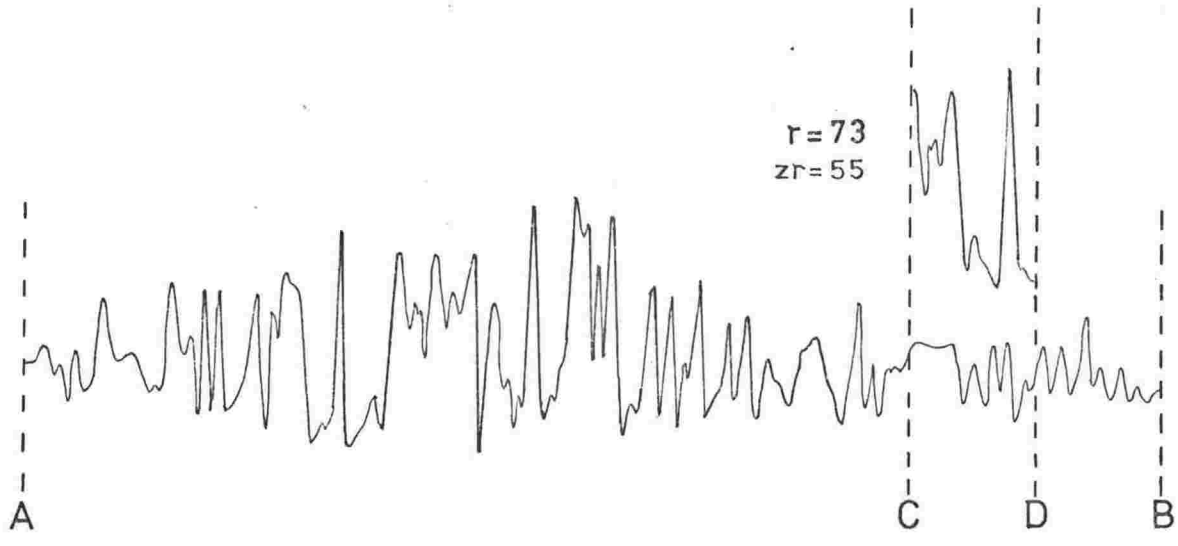


Fig. 5.16 Correlation position which visually would probably not be considered because of the difference in amplitudes.

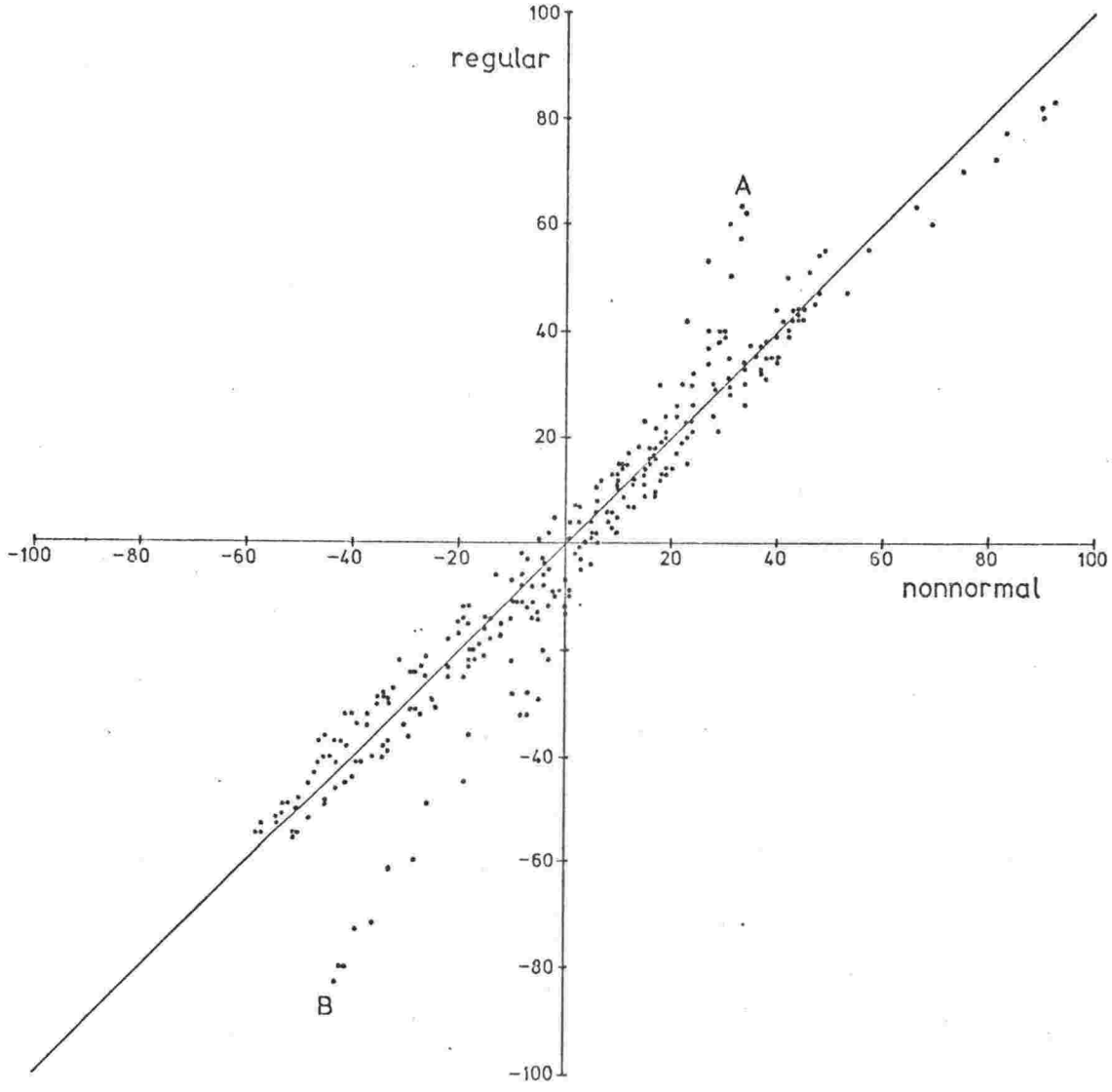


Fig. 5.17 Comparison of r(d) values calculated in regular manner to those found by non-normalized correlation. R67 on B370, all r(d) values plotted. Note large deviations from 1:1 relationship at A and B.

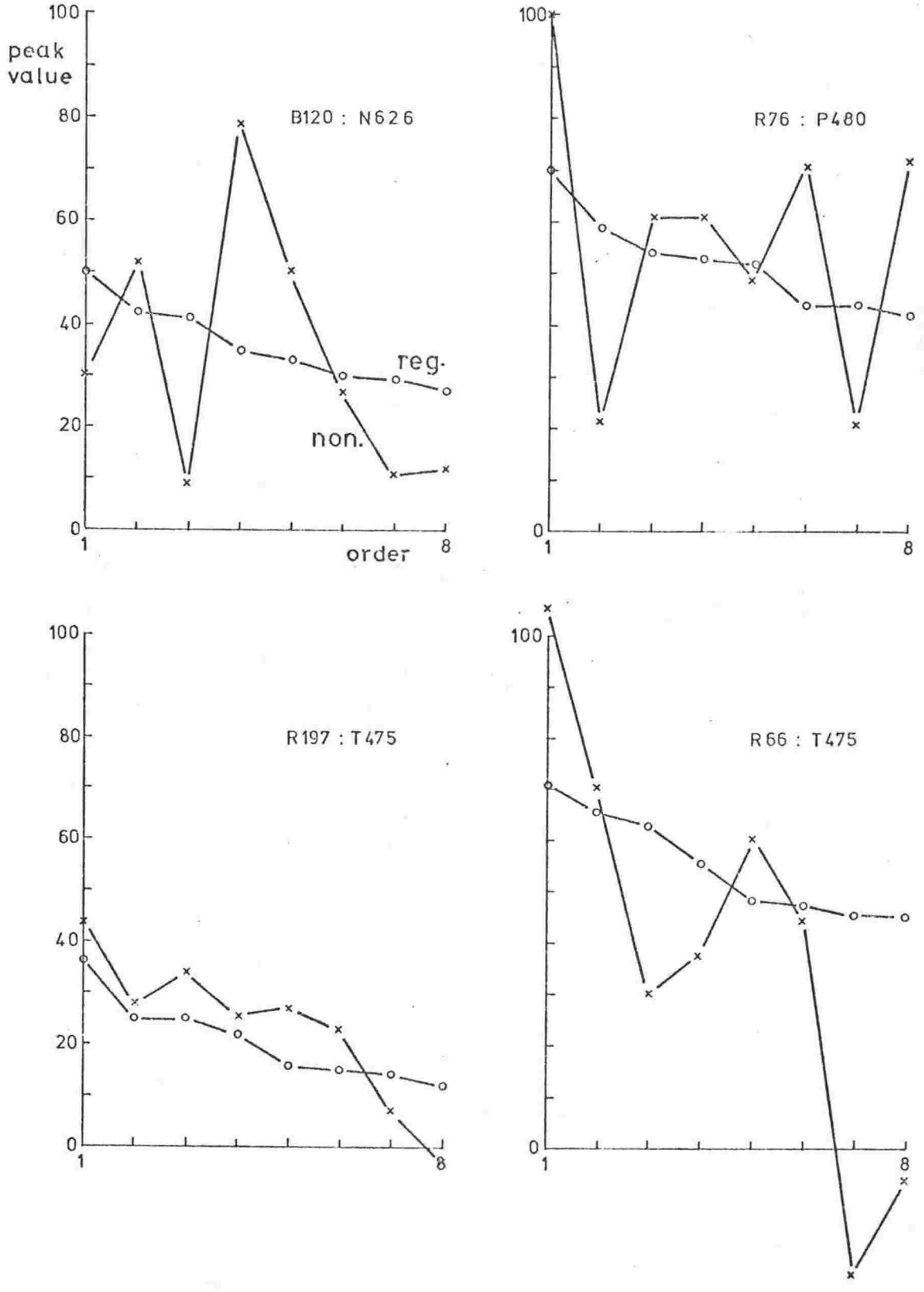


Fig. 5.18 Comparison of peak values of regular and non-normalized correlation. For each pair of profiles the eight highest regular values (open circles) are plotted in descending order, with the associated non-normalized value (crosses) for that alignment position.

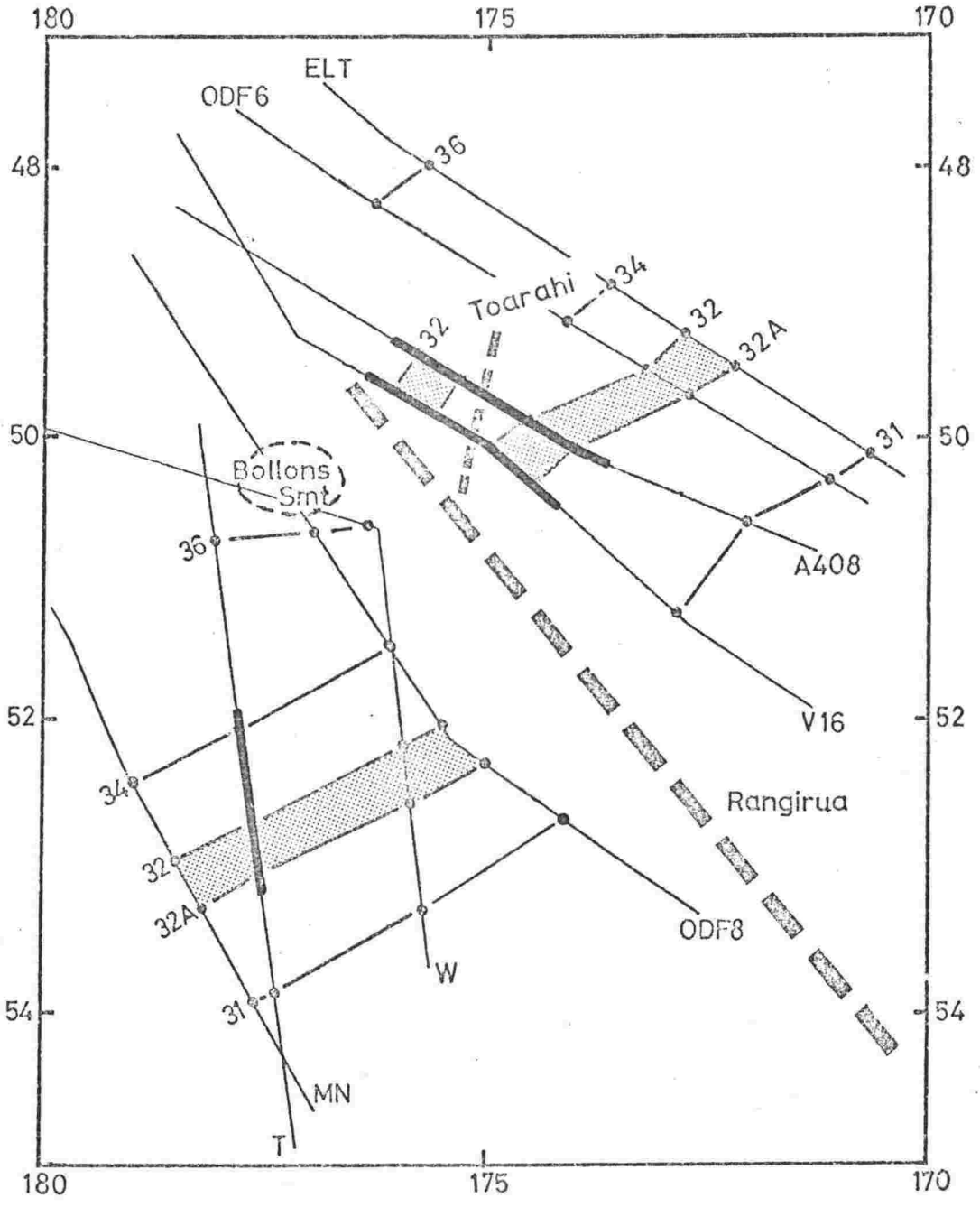


Fig. 5.19 The Toarahi and Rangirua fracture zones. Heavy lines indicate the sections of profiles T, V16 and A408 shown in Fig. 5.20 and used in the numerical correlation study.

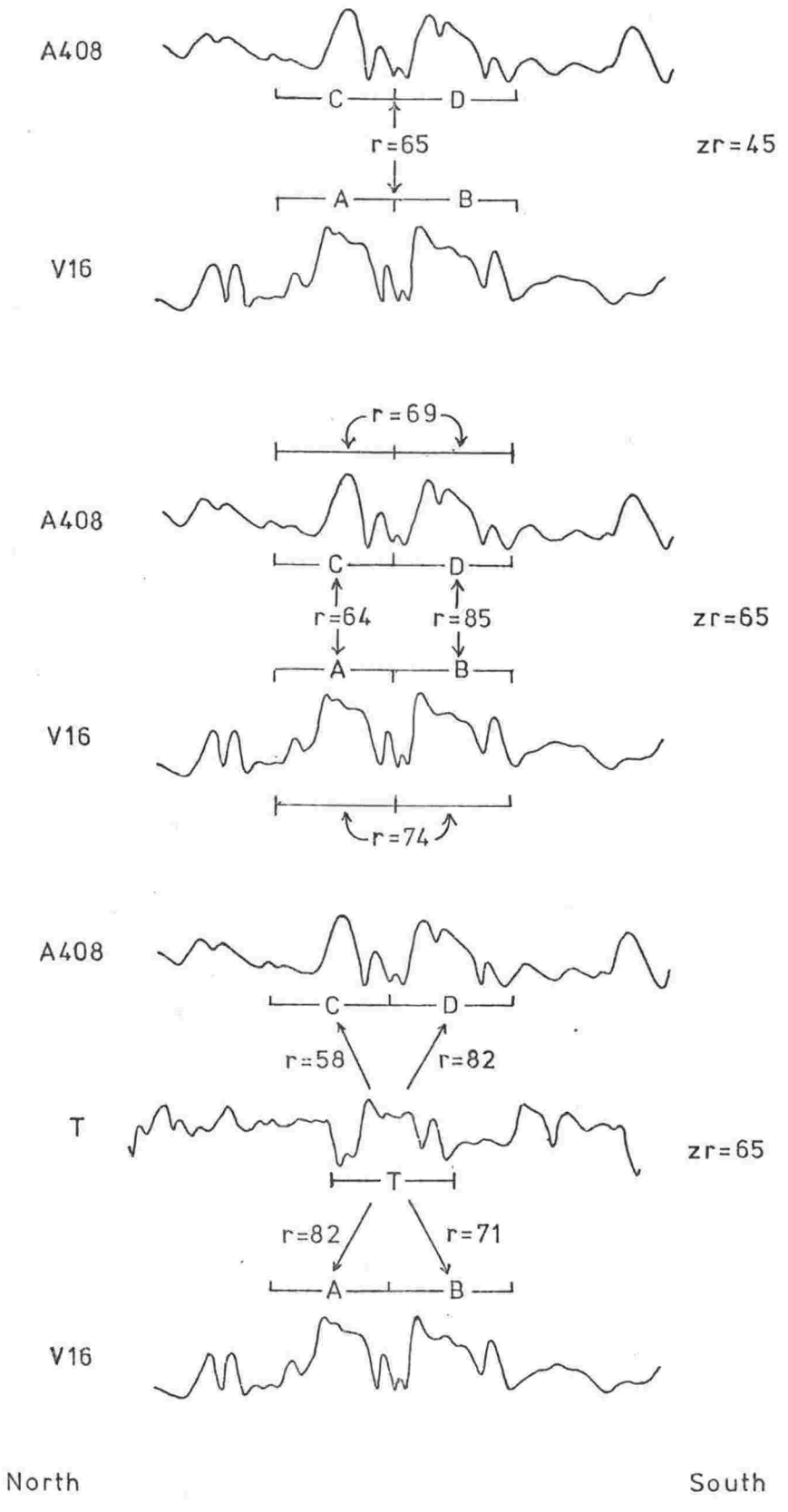


Fig. 5.20 Numerical correlations for the Toarahi and Rangirua fracture zones.

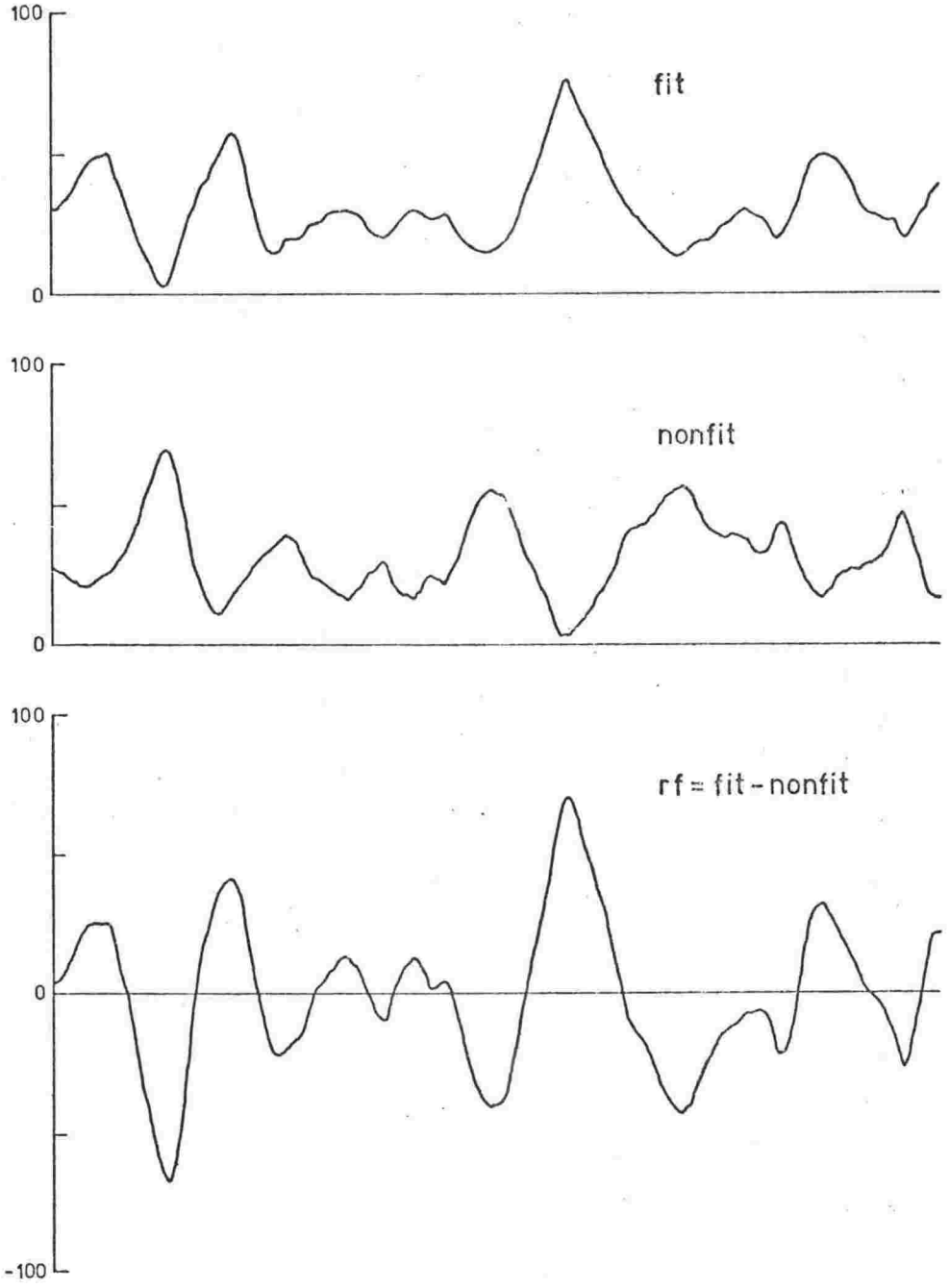


Fig. 5.21 First moment correlation variation with d of fit, nonfit, and rf for R67 on B370.

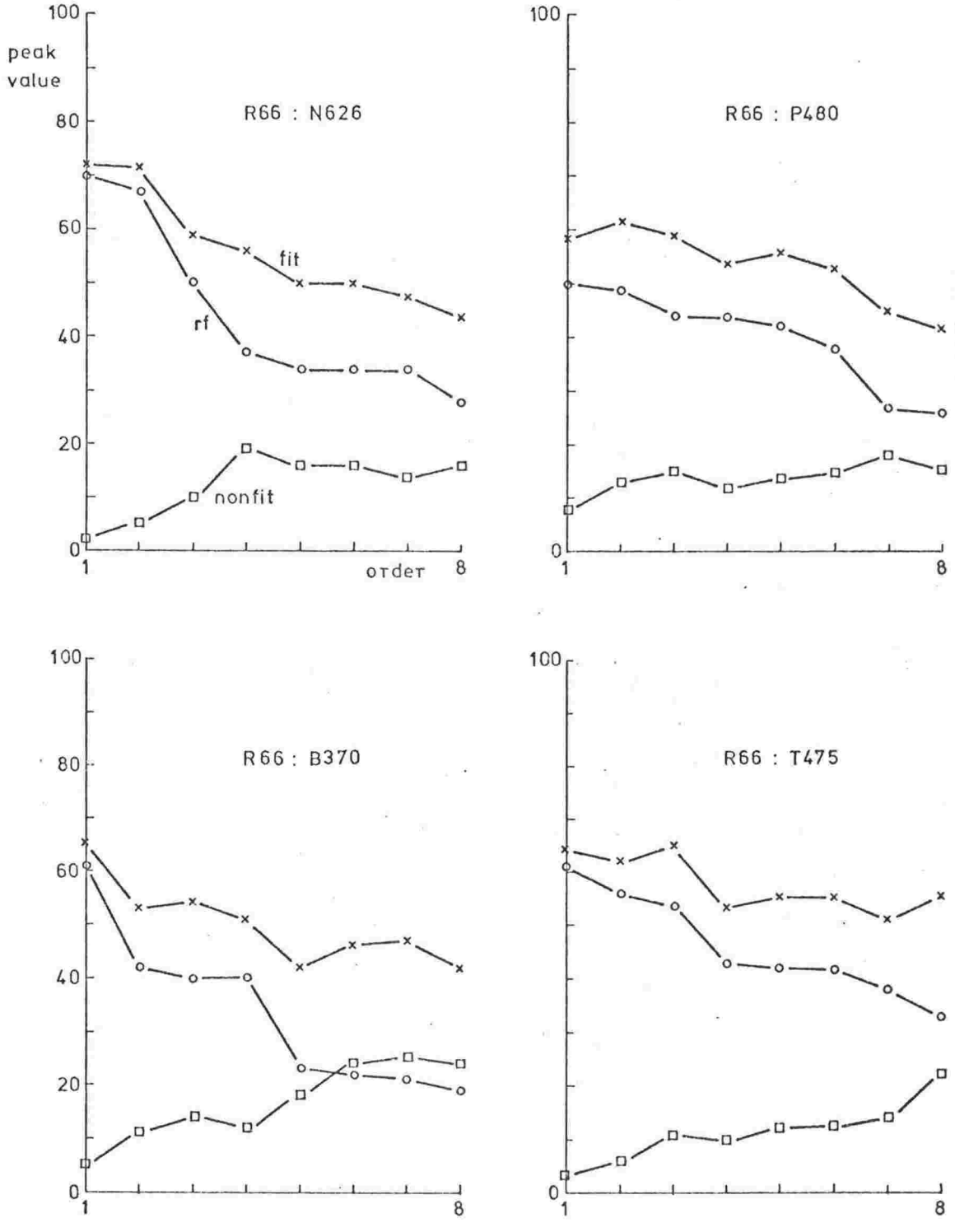


Fig. 5.22 First moment correlation. For each pair of profiles the eight best peak correlation values (circles) are plotted in descending order with their associated fit (crosses) and nonfit (squares) values.

Continued overleaf.

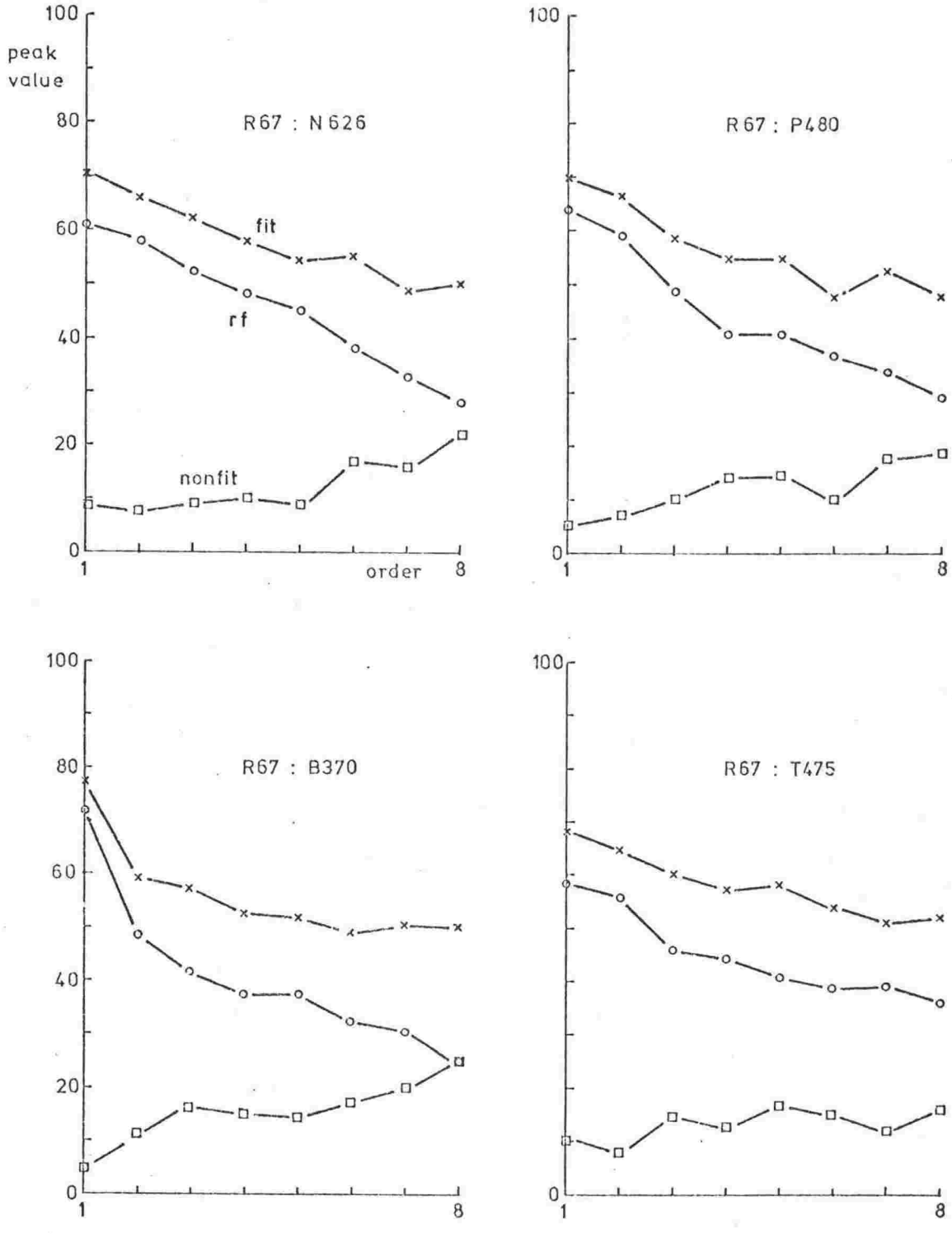


Fig. 5.22 continued.

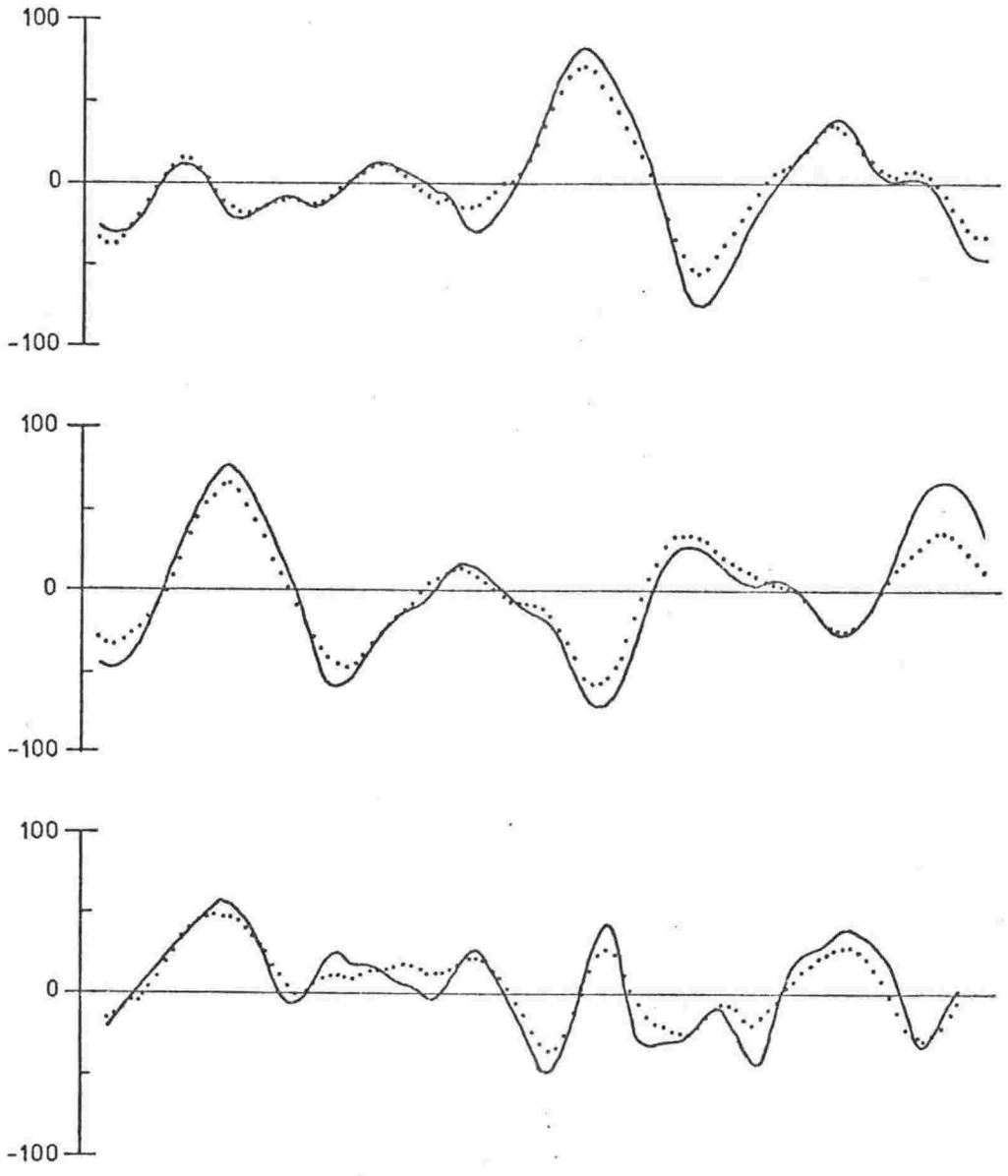


Fig. 5.23 Variation with d of second moment correlation (full lines) and first moment correlation (dotted lines) for three sections of R67 on N626.

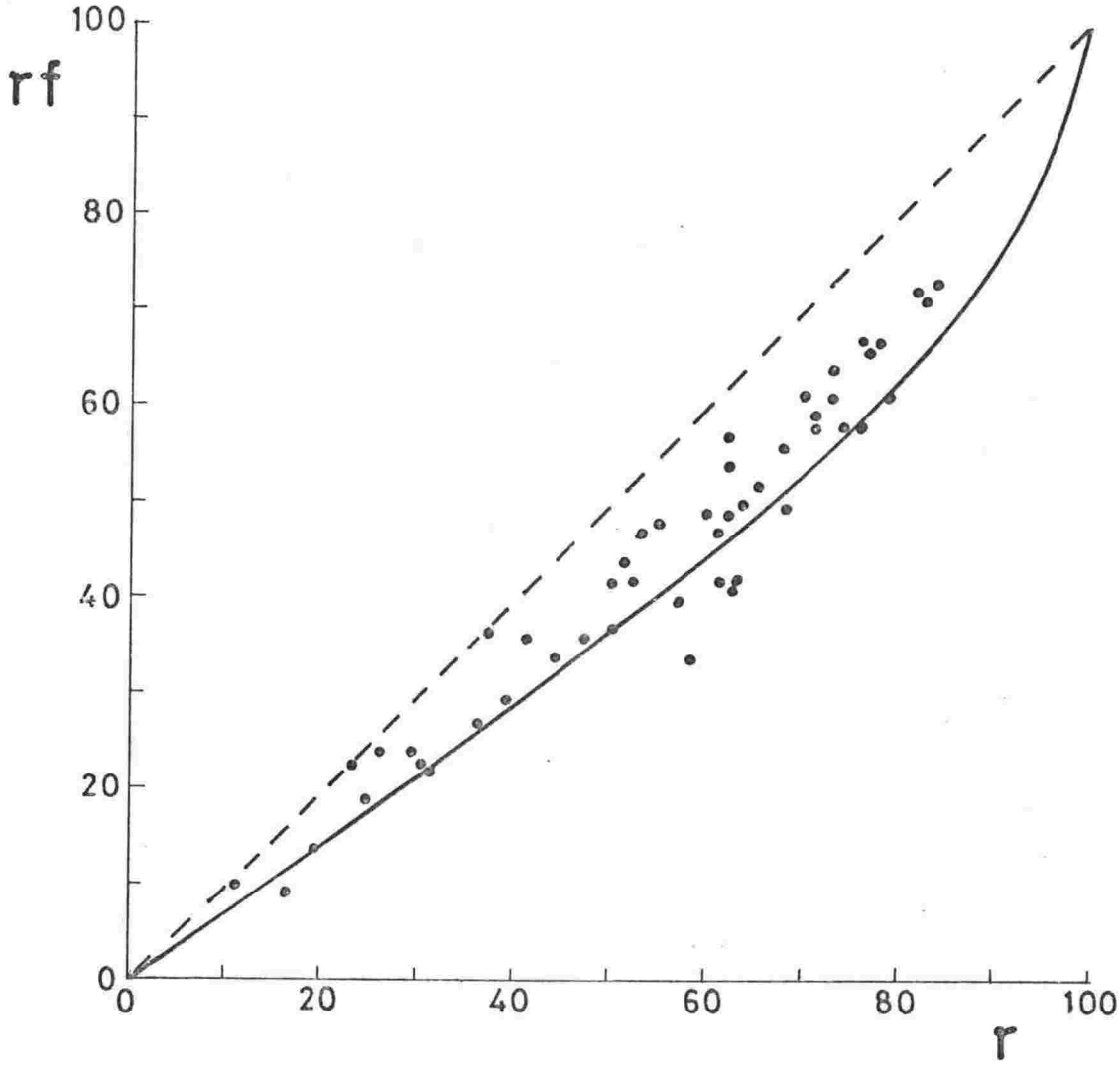


Fig. 5.24 Comparison of peak correlation values determined with first moment (rf) and second moment (r) correlation. Dotted line is 1:1 relationship, solid line is the relationship predicted by equation 5.14.

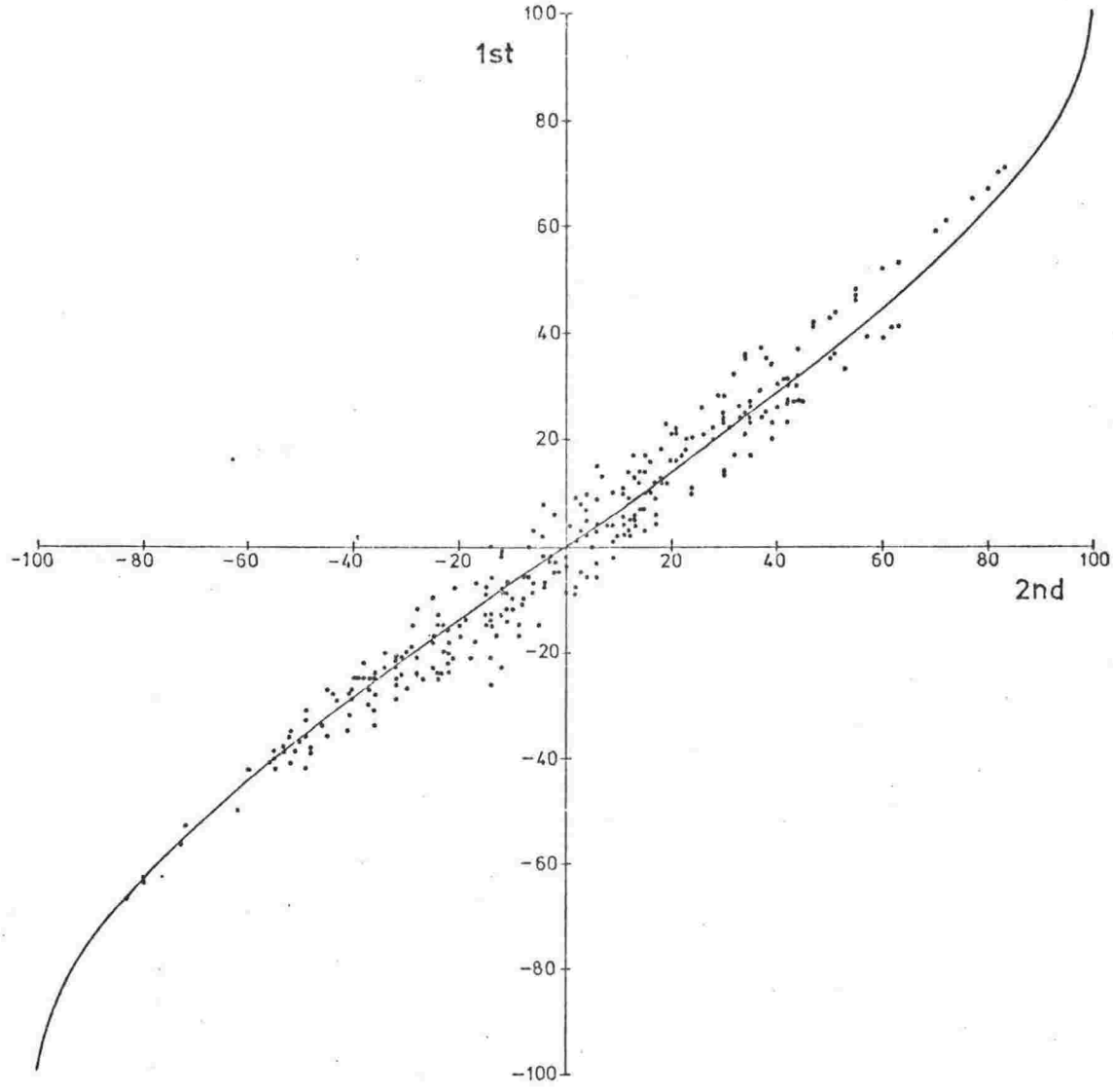


Fig. 5.25 Comparison of first and second moment correlation values for all positions of R67 on B370. Solid line is the relationship predicted by equation 5.14.

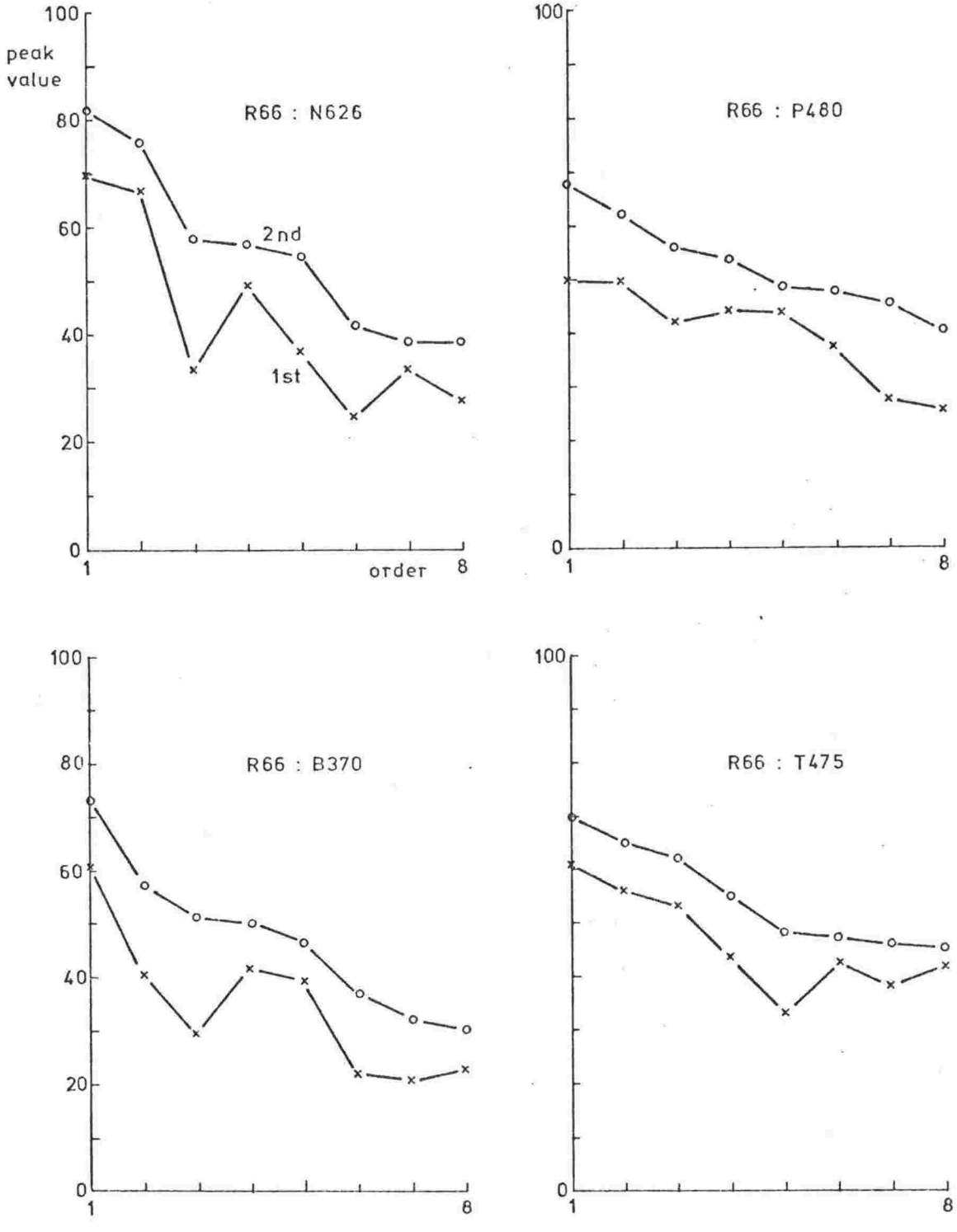


Fig. 5.26 Comparison of peak values of correlation. For each pair of profiles the eight best second moment values (circles) are plotted in descending order with their corresponding first moment values (crosses).

Continued overleaf.

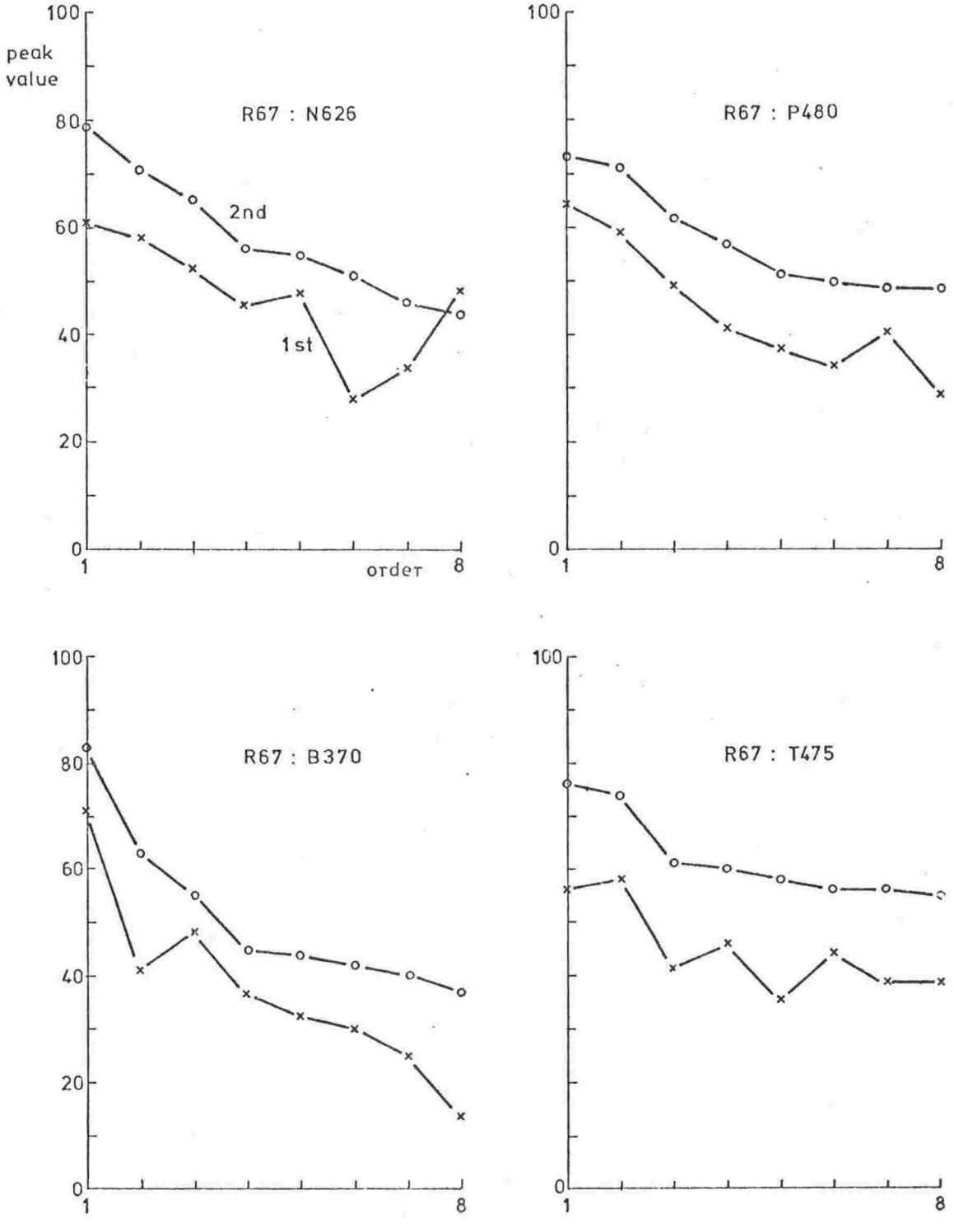


Fig. 5.26 continued.

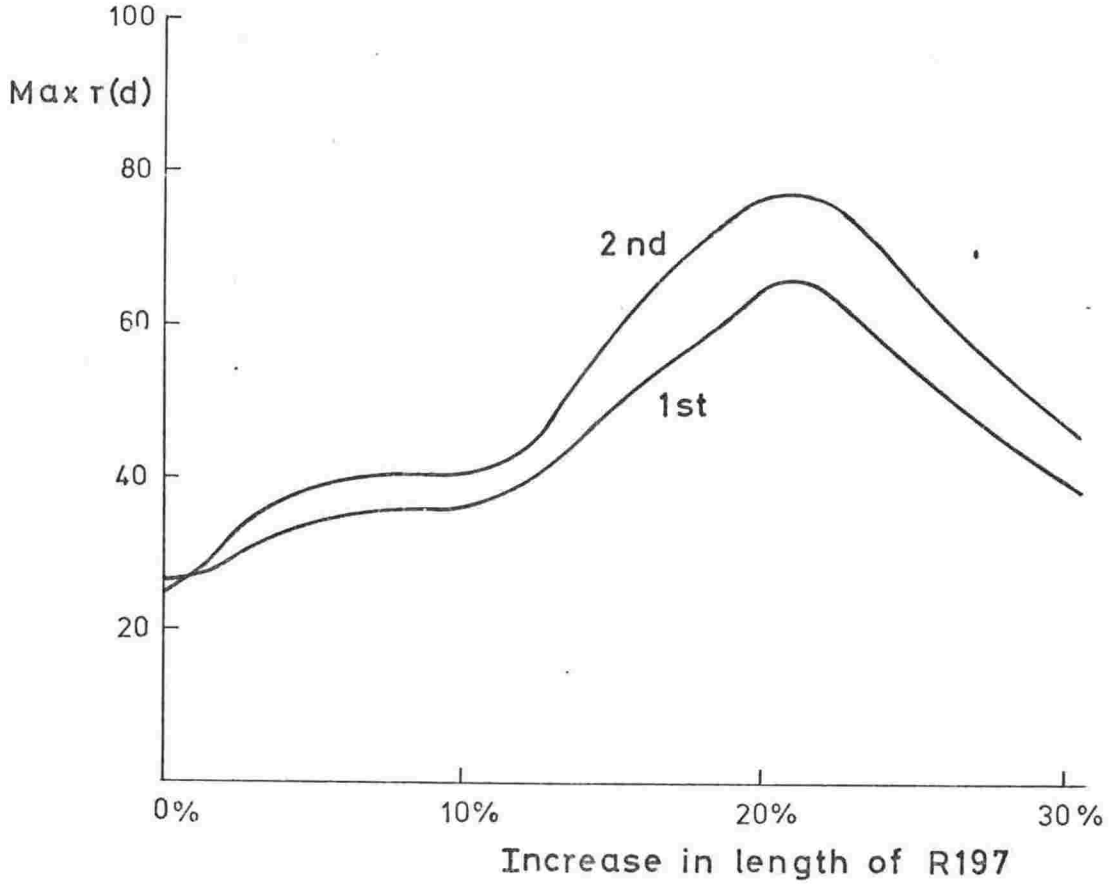


Fig. 5.27 Variation in correlation value at the best visual alignment position of profile R197 on T475.

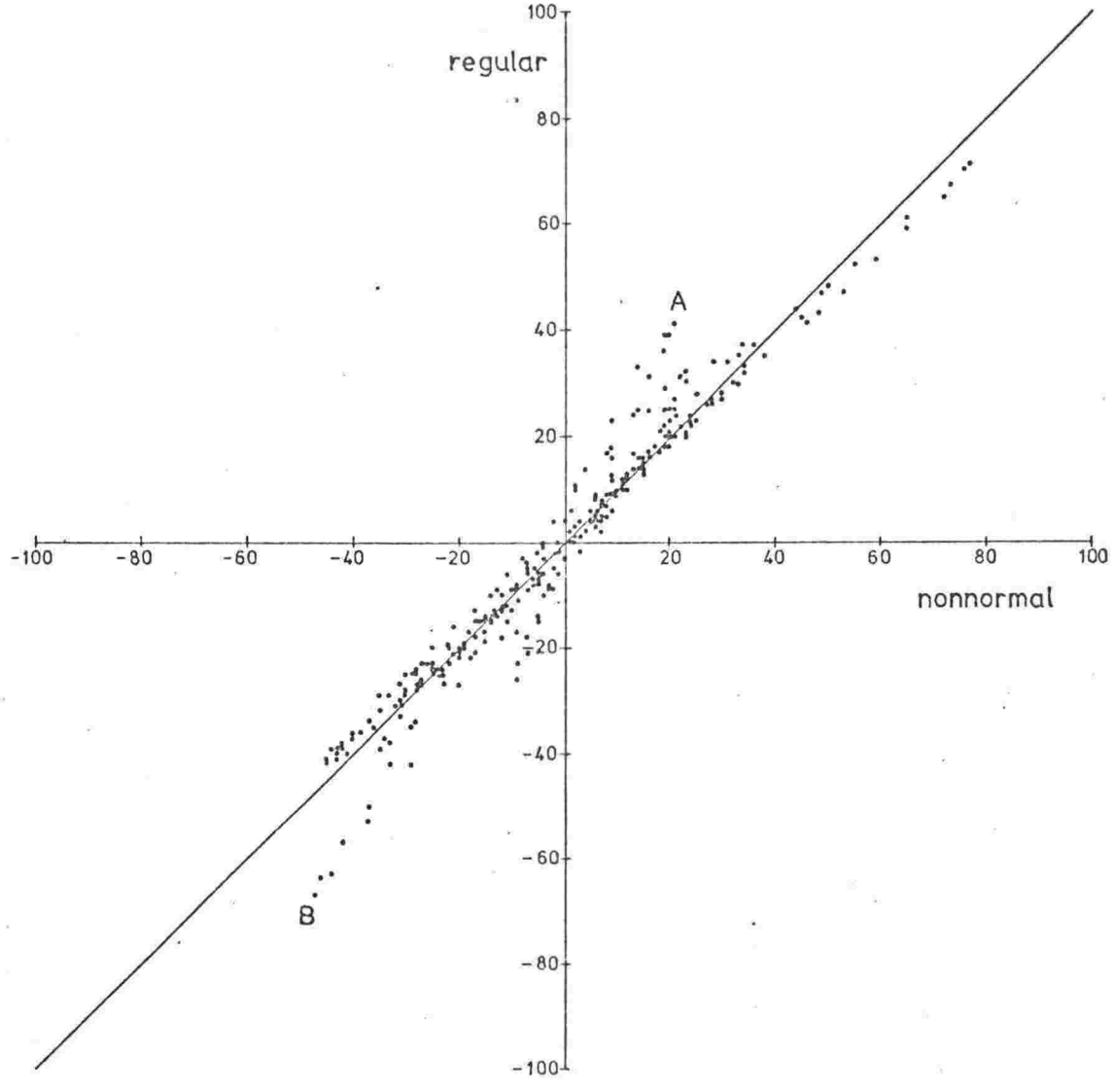


Fig. 5.28 First moment correlation: comparison of rf(d) values calculated in regular manner with those found by non-normalized correlation. R67 on B370. Compare with second moment results in Fig. 5.17.

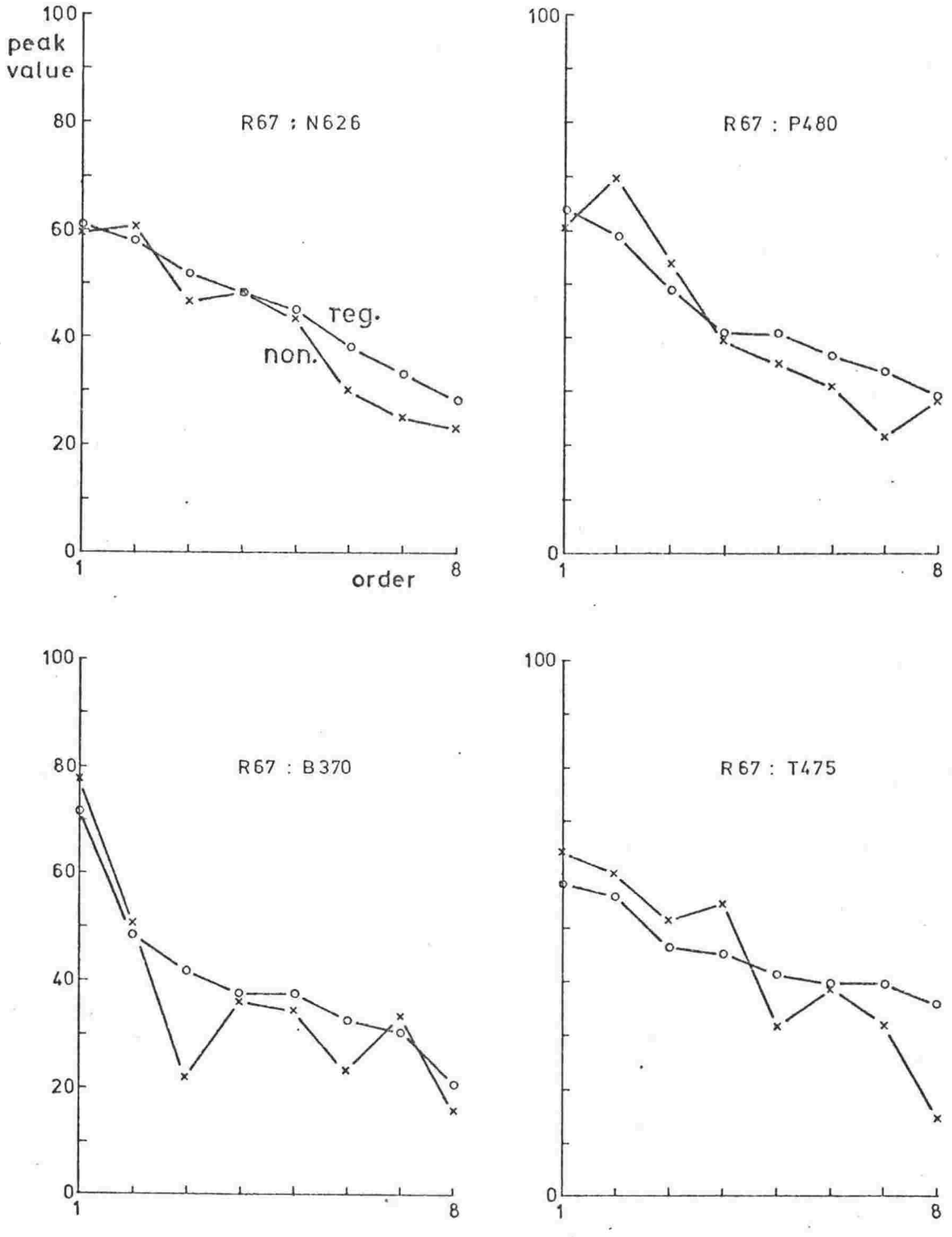


Fig. 5.29 First moment correlation: comparison of peak values of regular correlation (circles) with non-normalized correlation (crosses).

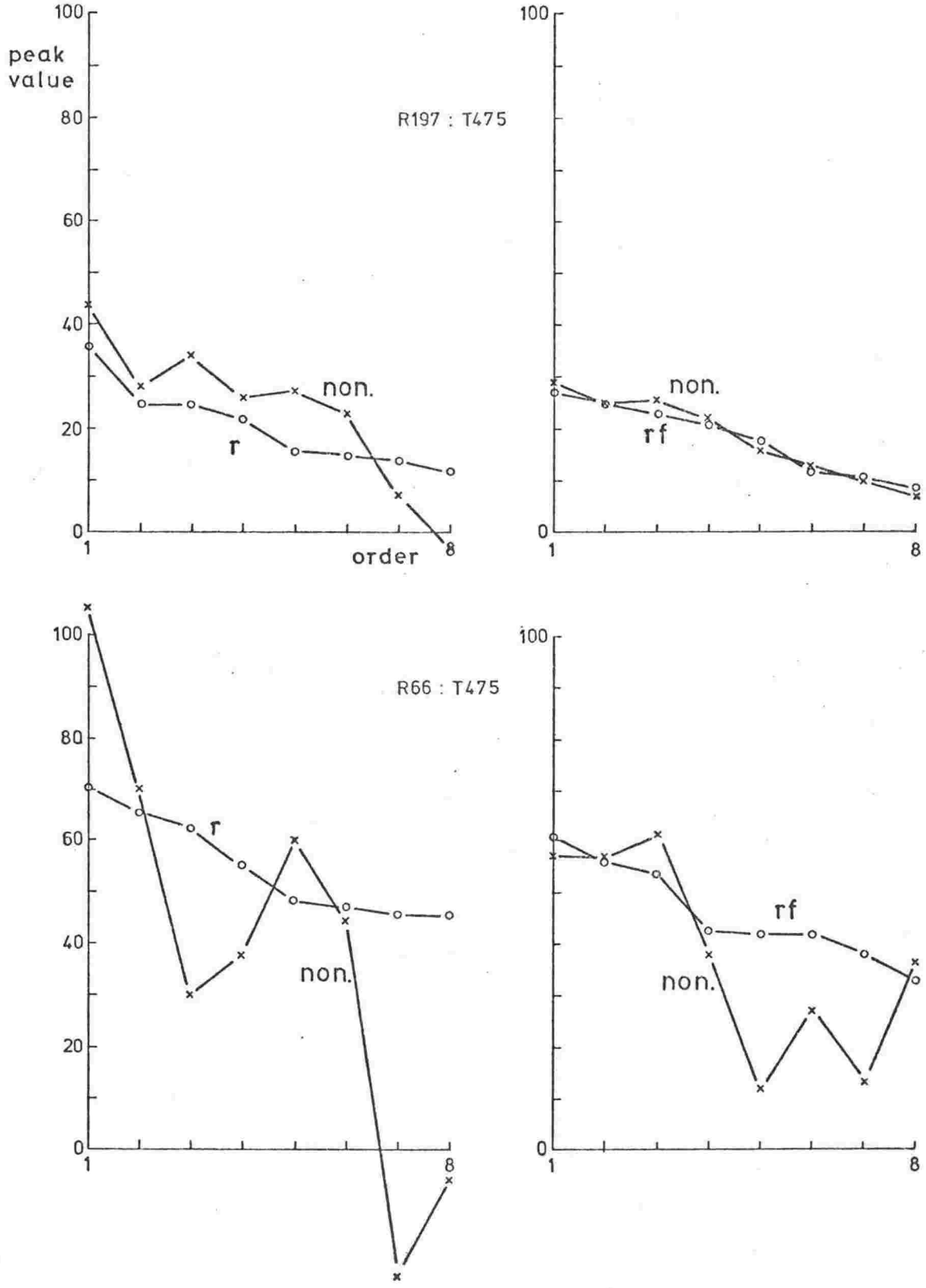


Fig. 5.30 Peak values of regular correlation (circles) viz non-normalized correlation (crosses) for both second moment (r) and first moment (rf) correlation.

Continued overleaf.

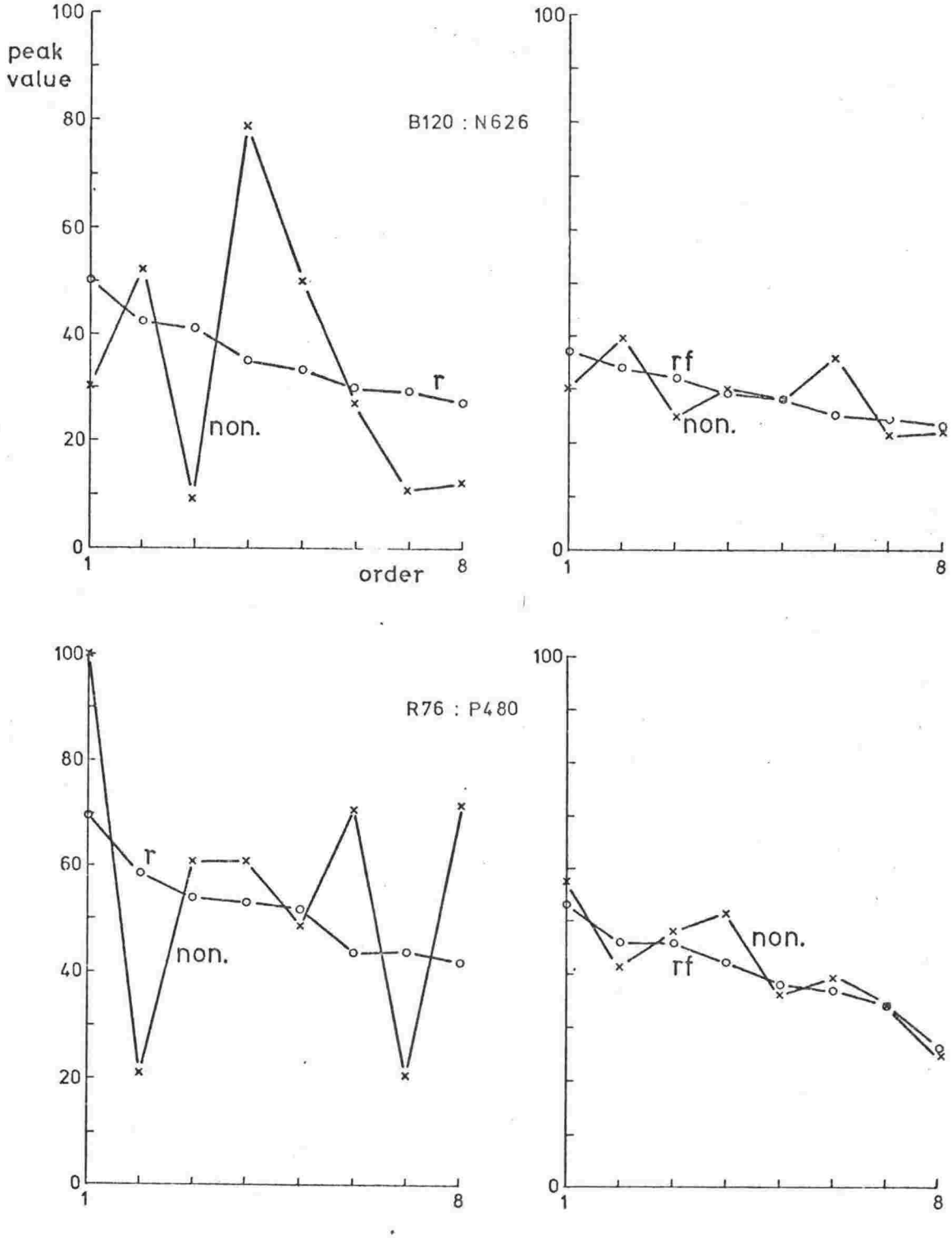


Fig. 5.30 continued.

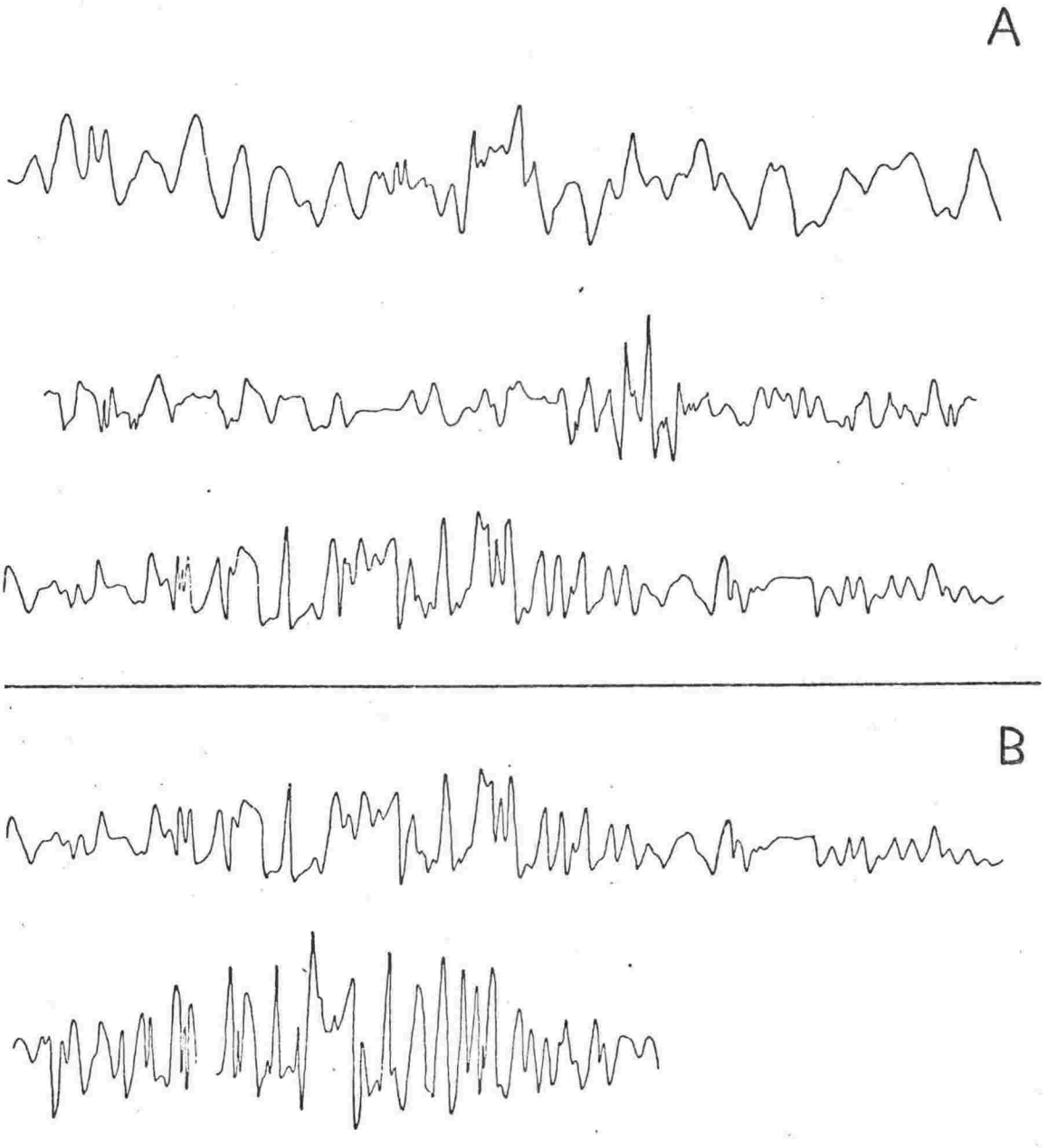


Fig. 5.31 Data given to students for symmetry tests. The actual size given to students was twice that shown here. 41 students received A, 23 students B.

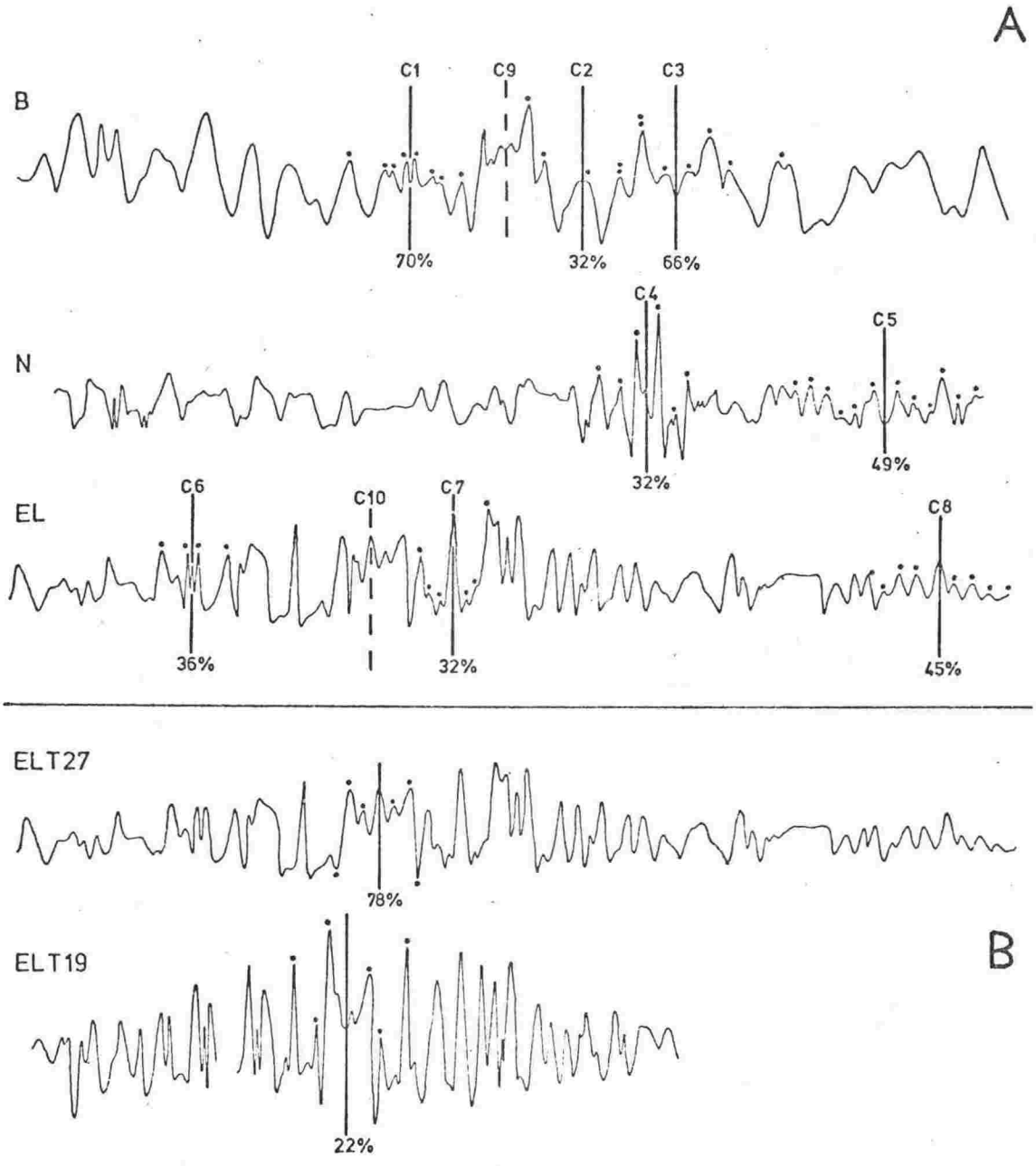


Fig. 5.32 Results of student symmetry tests. Centres picked by more than 20% of the students are shown, with the number (in per cent) that chose each centre. Dots either side of centres indicate the peaks marked by students.

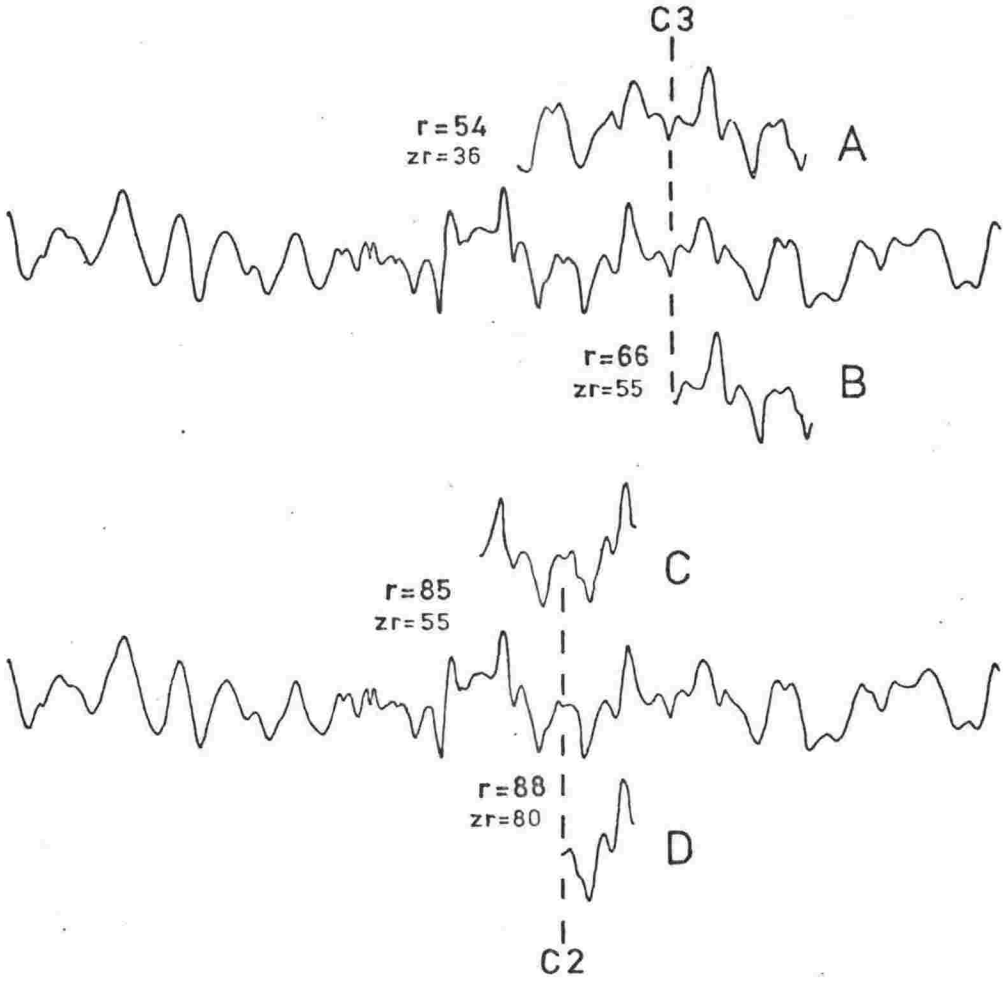


Fig. 5.33 Numerical symmetry correlation: profile B. Inverted sections of B are shown above and below the parent profile at positions which were maxima in the correlation function r(d).

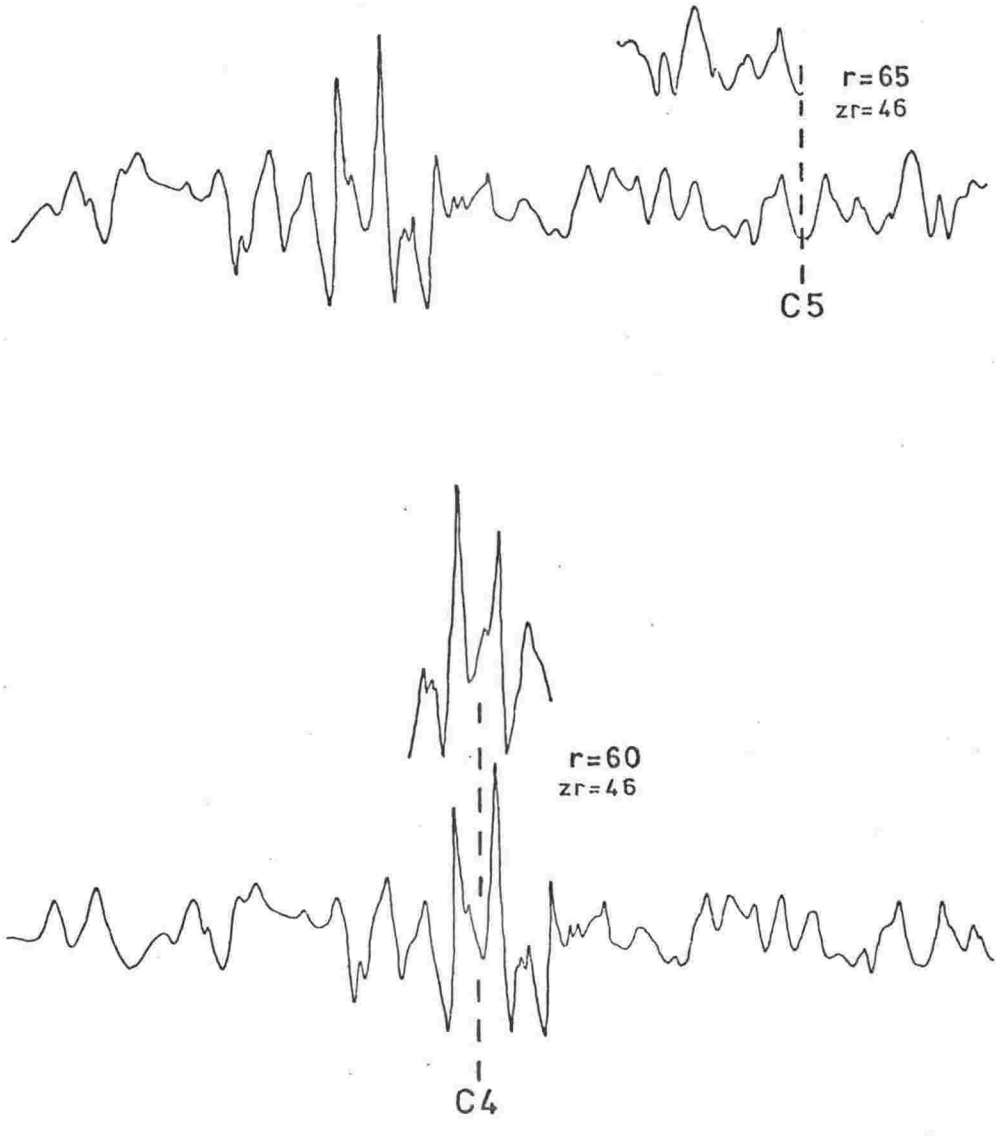


Fig. 5.34 Numerical symmetry correlation: profile N, centres C4 and C5.

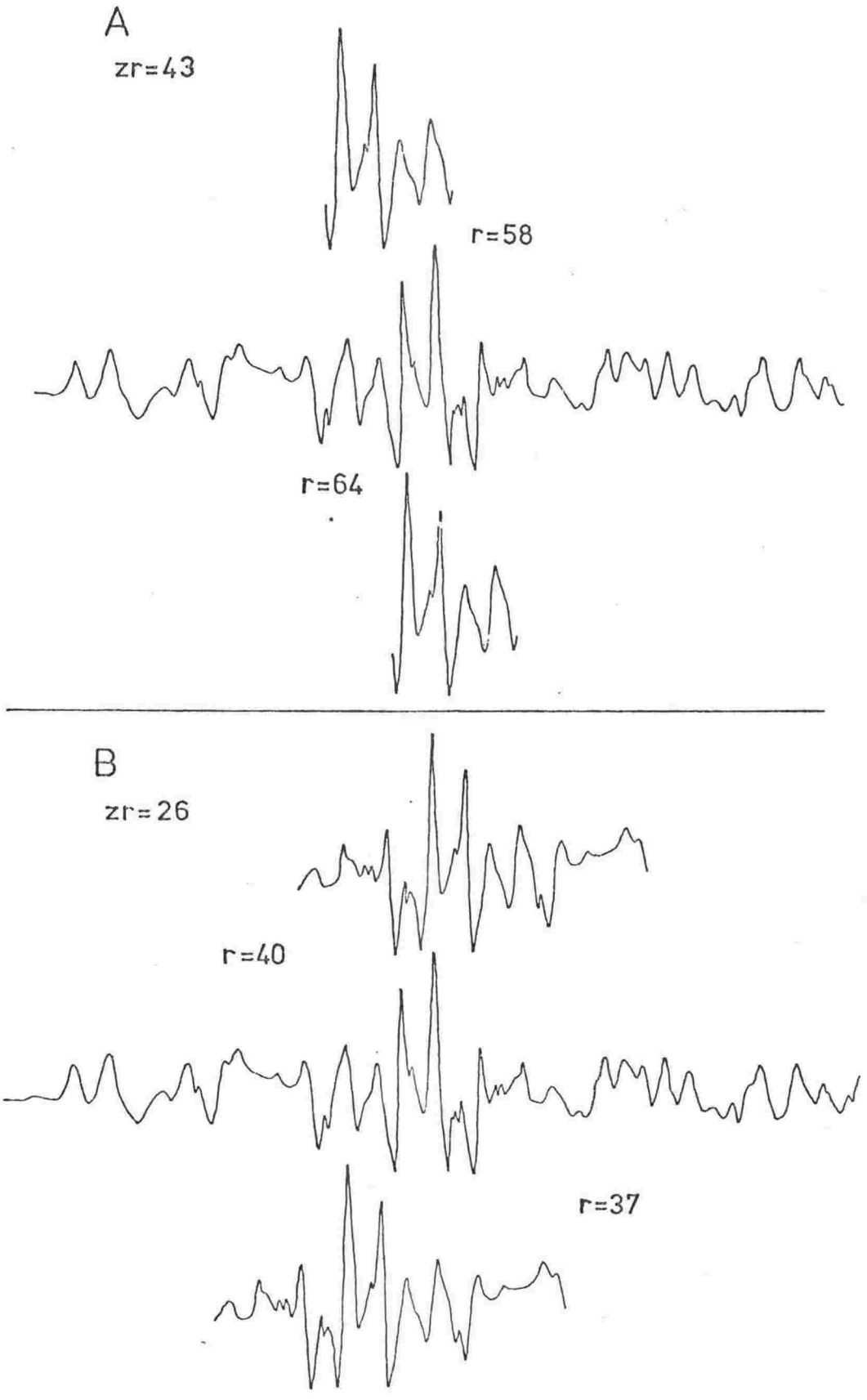


Fig. 5.35 Numerical symmetry correlation: profile N.

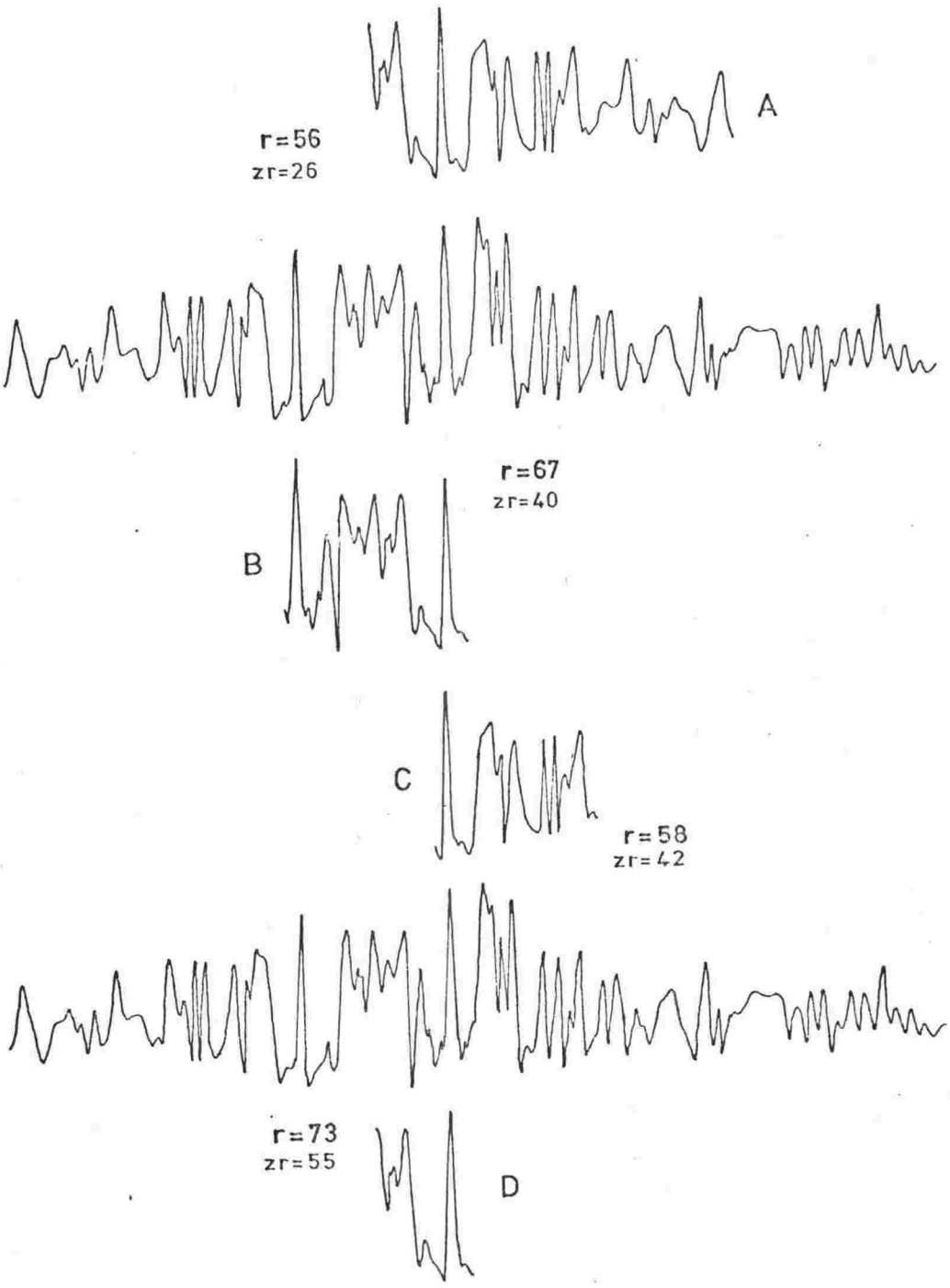


Fig. 5.36 Numerical symmetry correlation: profile ELT27.

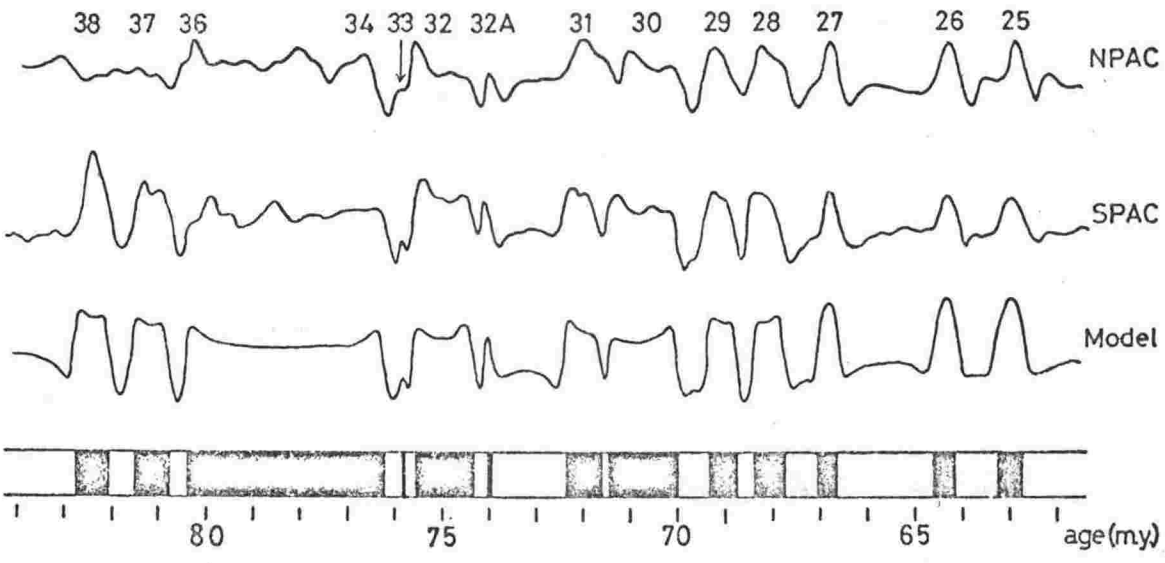


Fig. 6.1 The SPAC reversal time scale and observed and calculated magnetic anomaly profiles. NPAC - the northeast Pacific type profile. SPAC - the southwest Pacific type profile. MODEL - profile calculated from the polarity intervals shown underneath assuming remanent and present field inclination of $90^{o}$. Polarity intervals based on profile SPAC, normal polarity shaded.

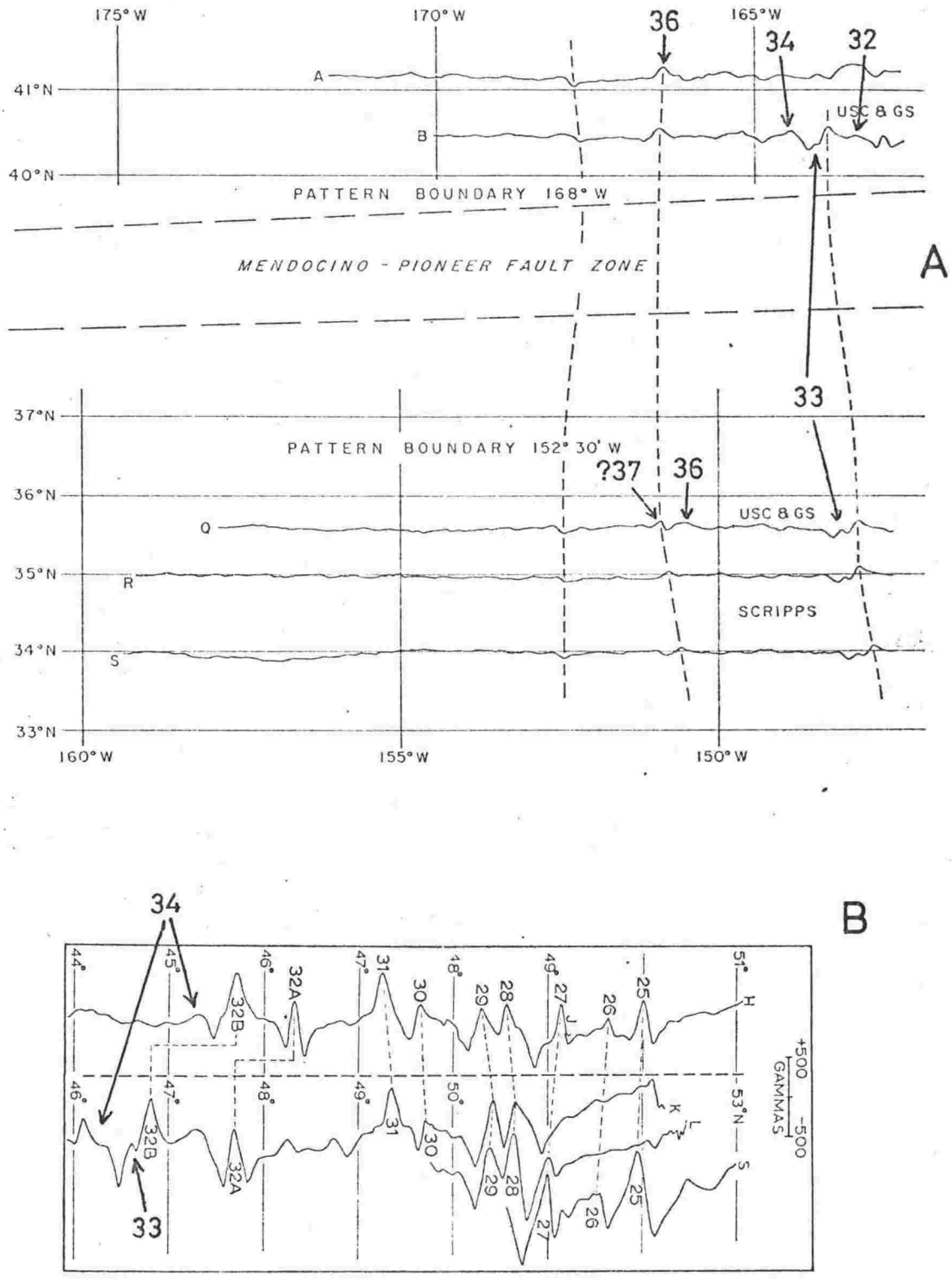


Fig. 6.2 Examples of magnetic anomalies 32 and beyond. A: North-south lineations in the northeast Pacific, from Raff (1966, Fig. 2). B: East-west lineations south of the Aleutian trench, from Grim and Erickson (1969, Fig. 5).

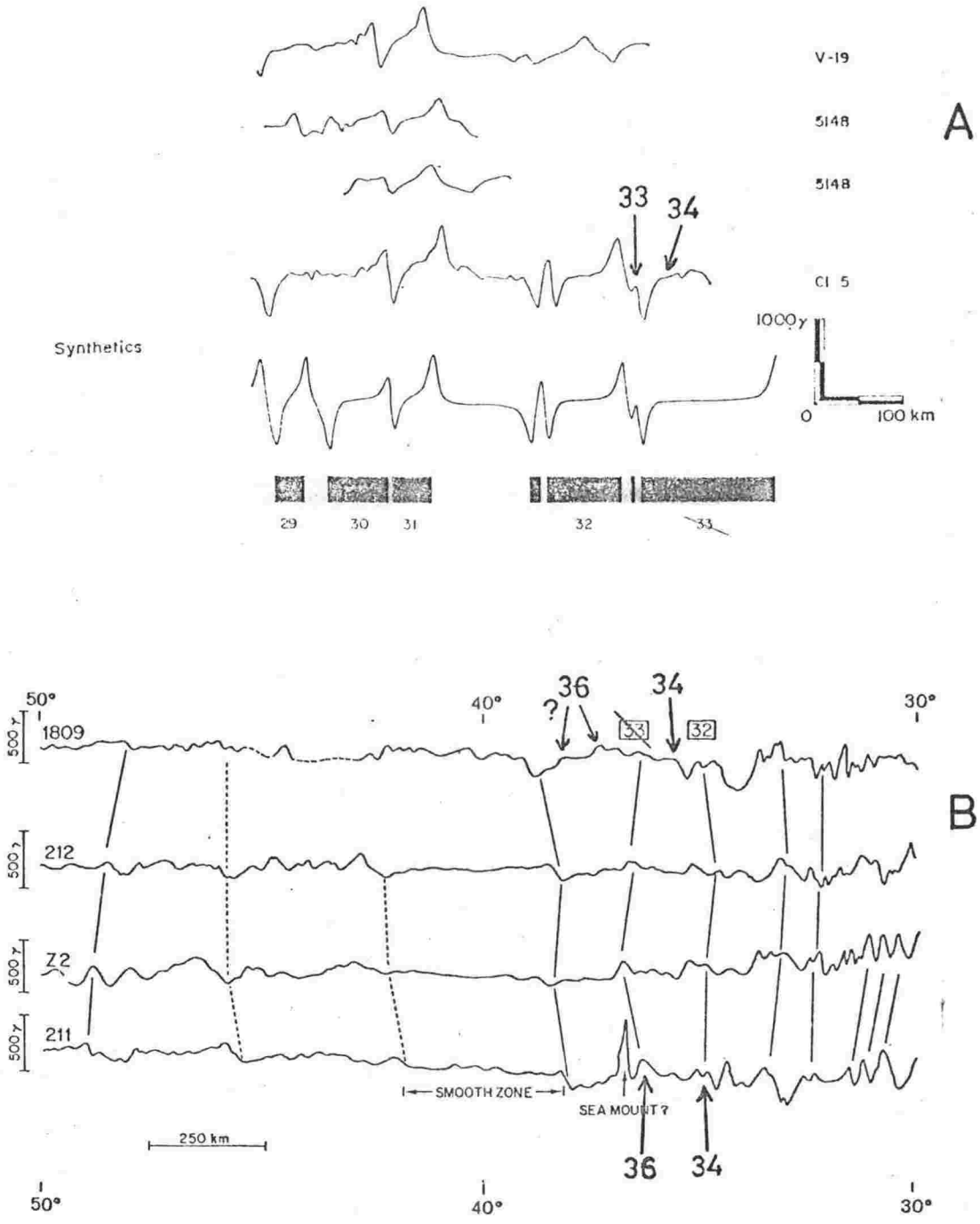


Fig. 6.3 Further examples of magnetic anomalies 32 and beyond A: Northeast Indian ocean, from McKenzie and Sclater (1971, Fig. 22). B: Western south Atlantic, from Mascle and Phillips (1972, Fig. 4). The anomaly labelled 33 in both figures is designated 34-36 in this study.

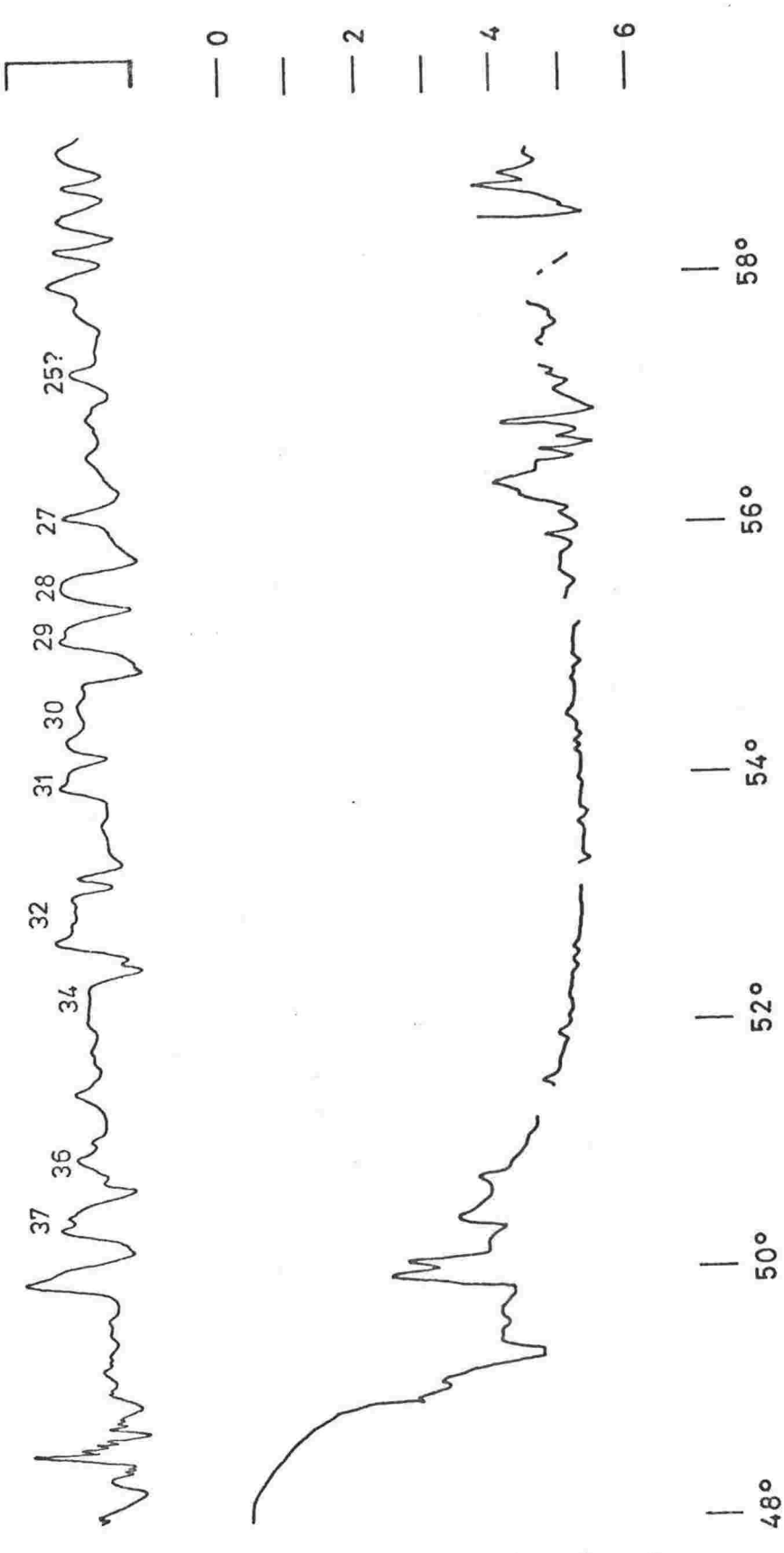


Fig. 6.4 Profile T: bathymetry and magnetic anomalies. The magnetic type profile SPAC is profile T for anomalies 27 to 37.

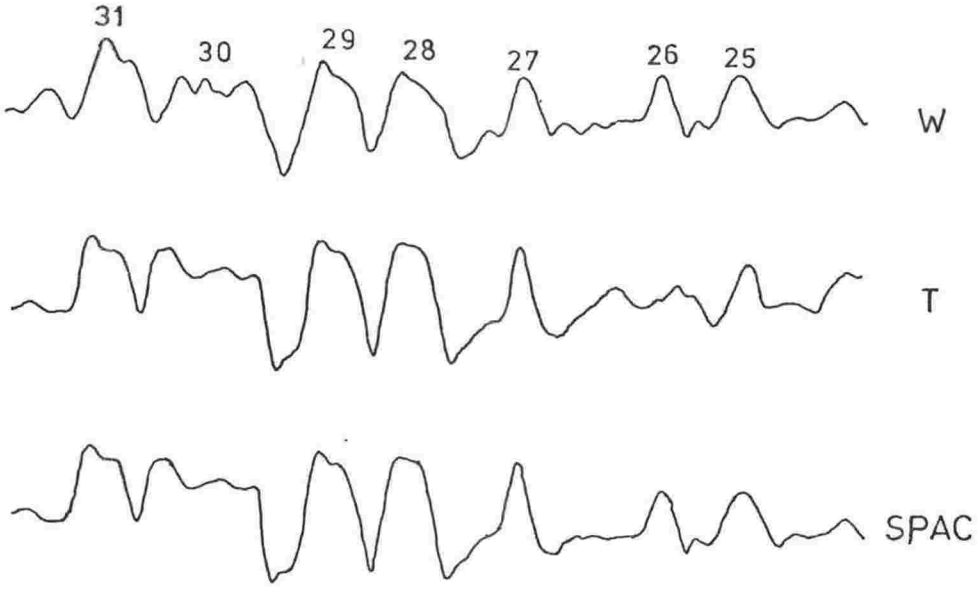


Fig. 6.5 Magnetic anomaly profiles W, T and SPAC for the composite portion of SPAC. Anomalies 25 and 26 in SPAC are from profile W, remainder of SPAC is profile T.

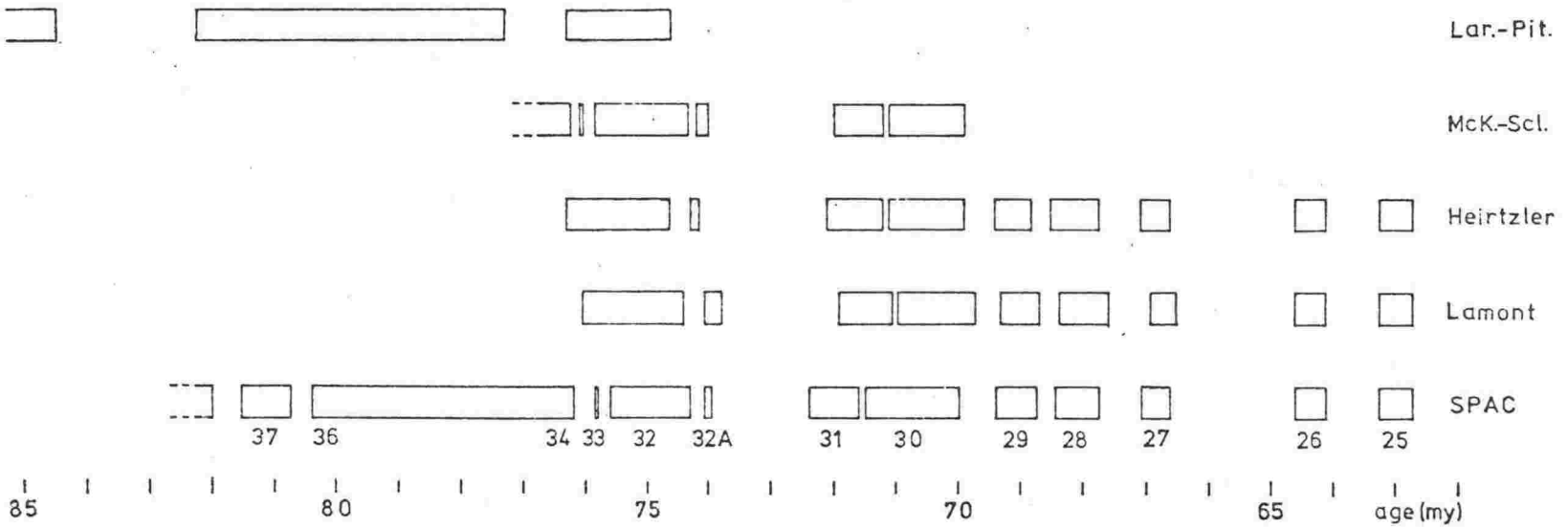


Fig. 6.6 Alternative reversal time scales for anomalies 25 and beyond. Blocks show the the normal polarity intervals. Sources as follows. Lar.-Pit.: Larson and Pitman (1972, Fig. 5). McK.-Scl.: McKenzie and Sclater (1971, Table 1). Heirtzler: Heirtzler et al. (1968, Table 1). Lamont: Lamont-Doherty Geological Observatory (unpublished). SPAC: this study.

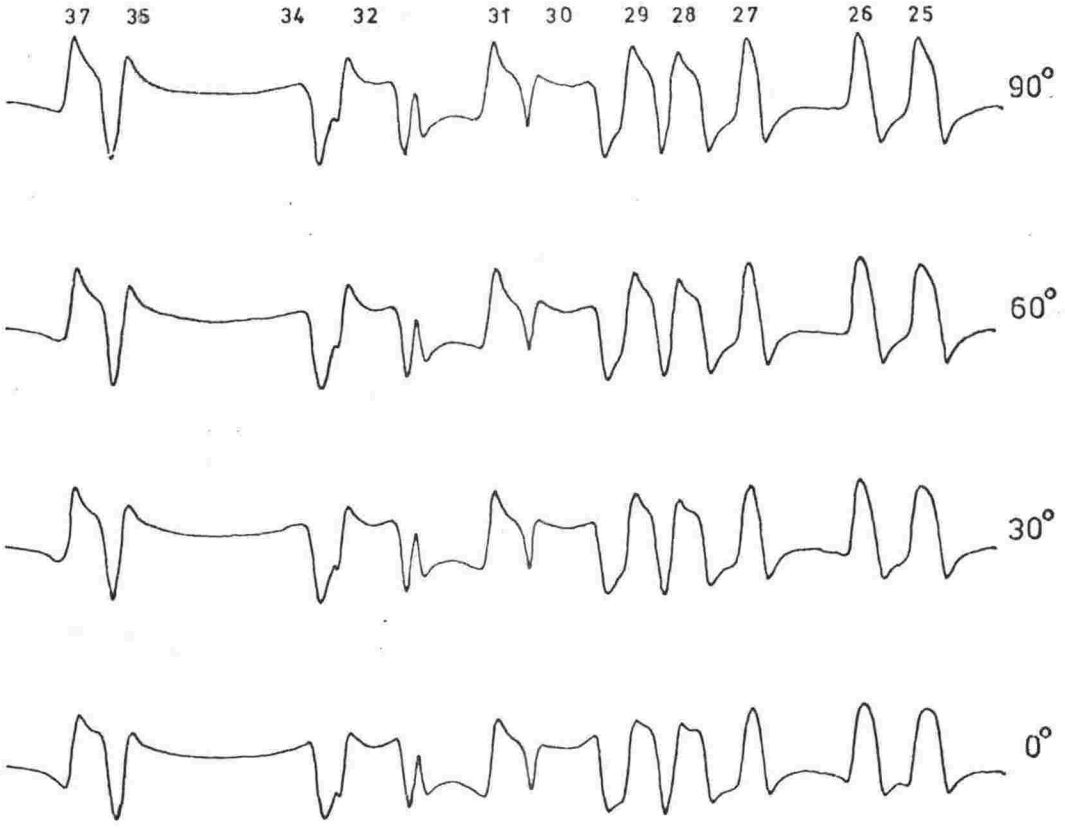


Fig. 6.7 Profiles for lineations formed with the strike east or west of north as labelled, and subsequently rotated to the present orientation (N30°E). Initial and final latitude as at present (Lat = 55°, I = 70°).

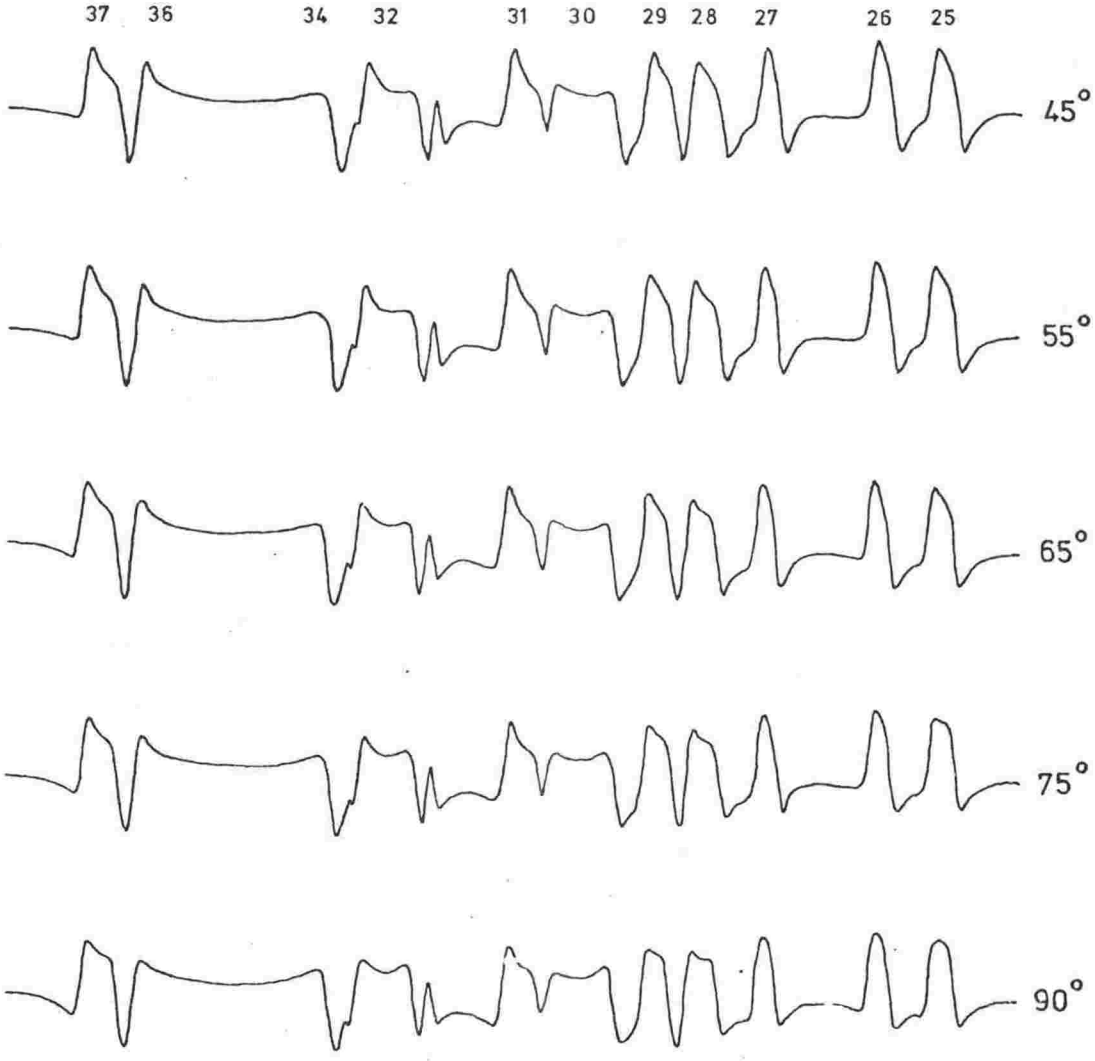


Fig. 6.8 Profiles for lineations formed at the latitudes as labelled and subsequently moved to present latitude ($55^{o}$). Initial strike east-west, present strike N$30^{o}$E.

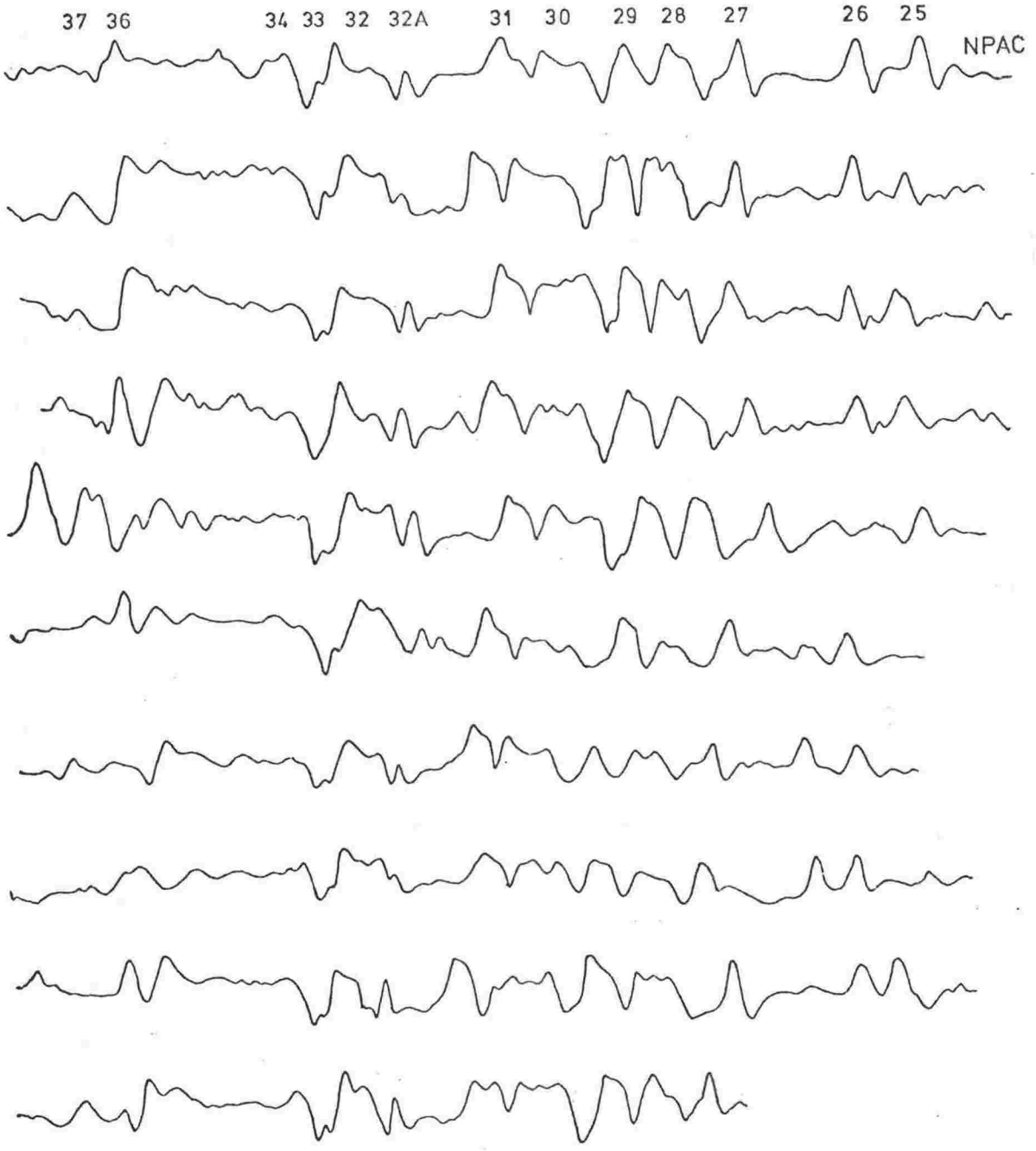


Fig. 6.9 Profile NPAC and typical profiles from the southwest Pacific basin. Some profiles composite; eastern most one at the top.

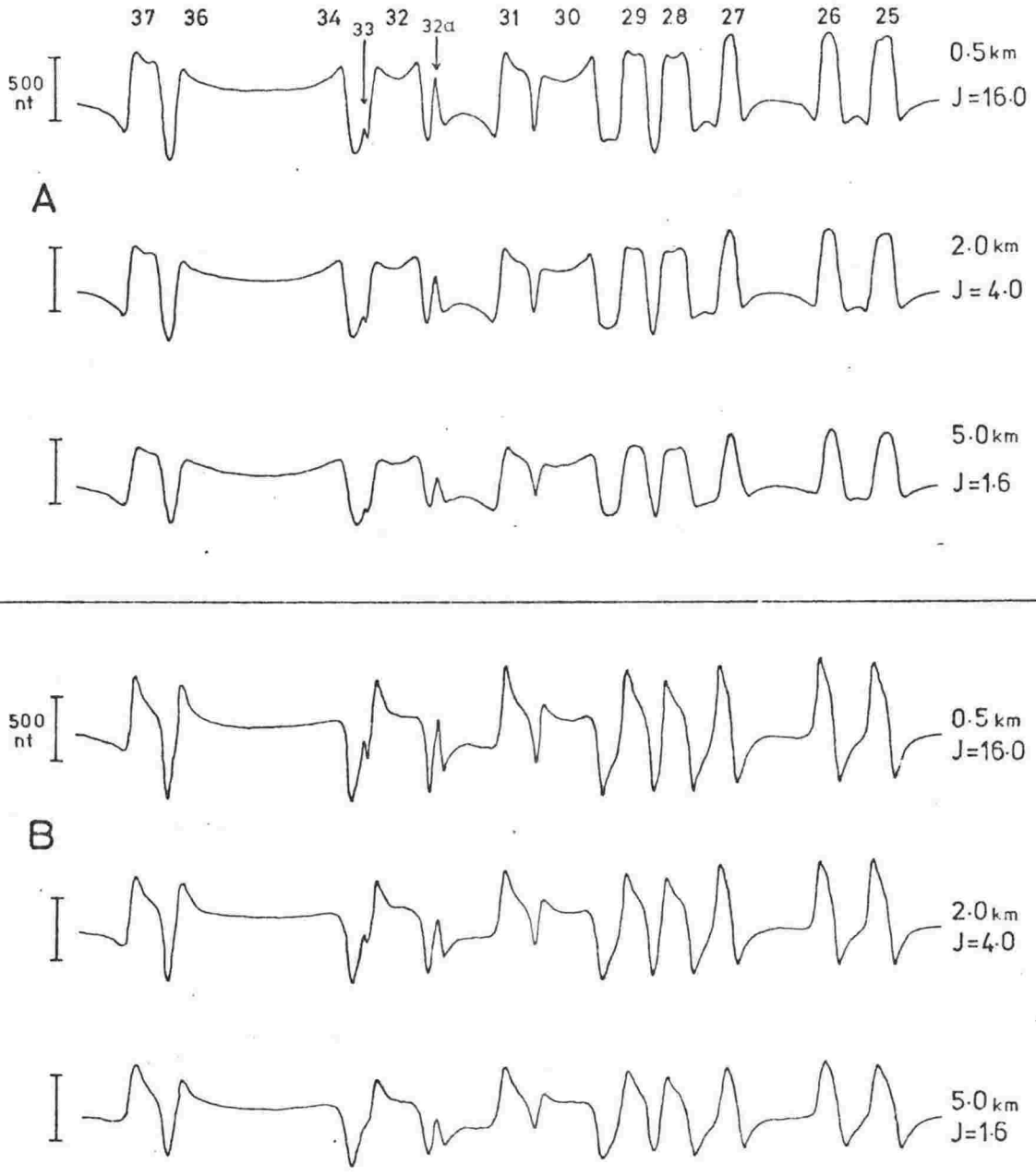


Fig. 6.10 Profiles for varying thickness of source layer as labelled; top of the layer at 5.0 km. Magnetization J in units of $10^{-3}$ emu/cm$^3$. Set A for remanent and present field inclination of $90^{o}$. Set B for in situ formation ($I = 70^{o}$).

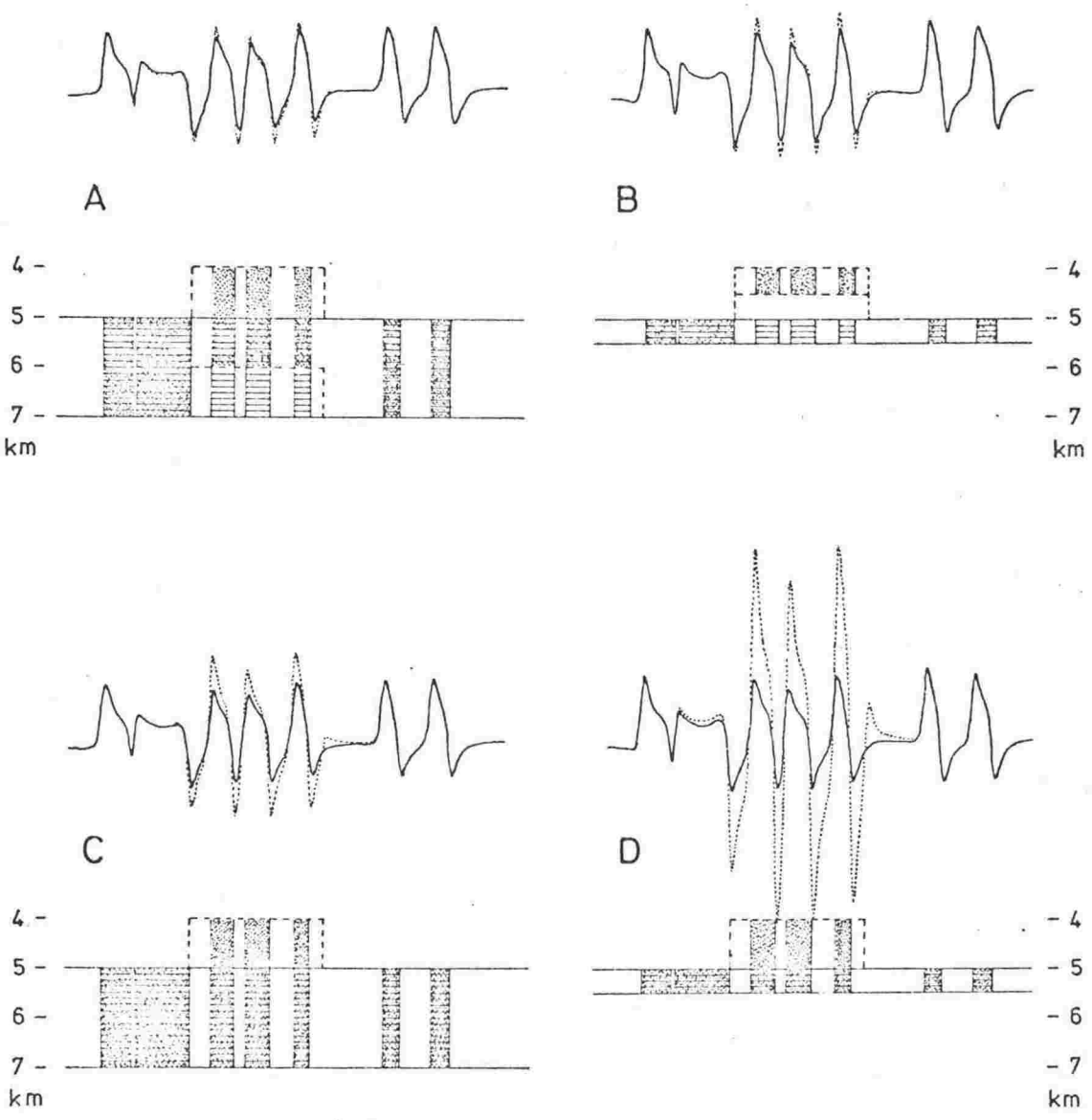


Fig. 6.11 Model profiles for the Tairoa fracture zone topography. Dotted profiles for the dotted block configurations, solid profiles for ruled configurations.

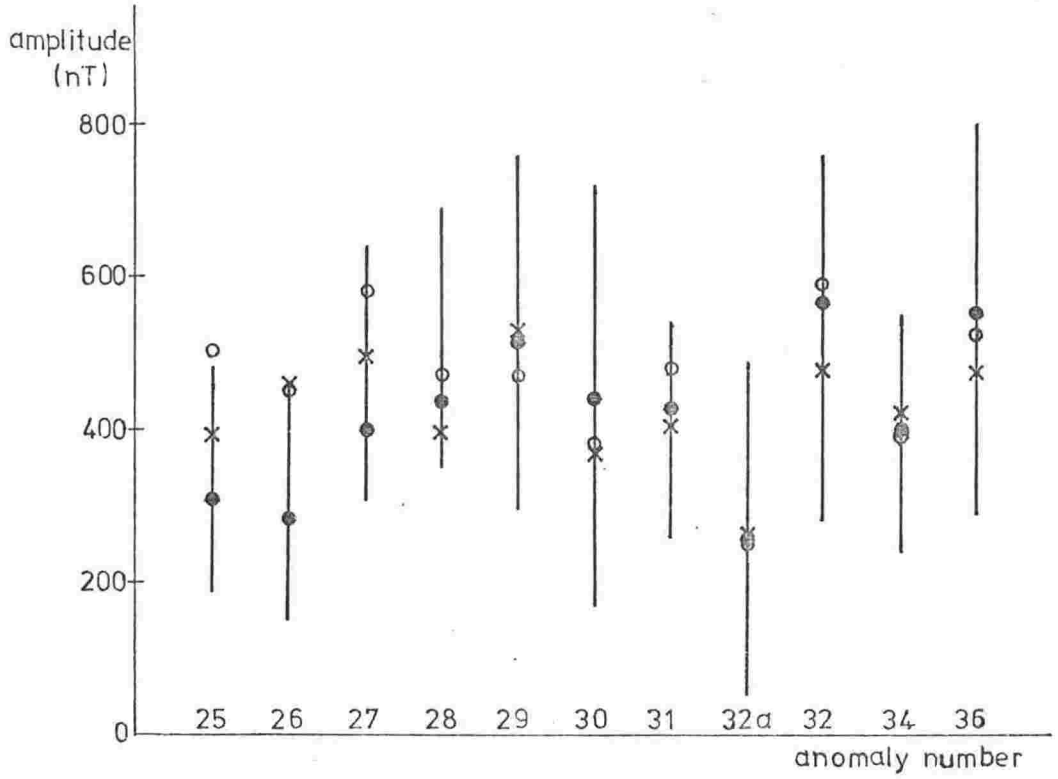


Fig. 6.12 Amplitudes of numbered anomalies. Closed circles, the southwest Pacific basin means, bars indicating the range. Open circles, NPAC profile. Crosses, model profile for in situ formation.

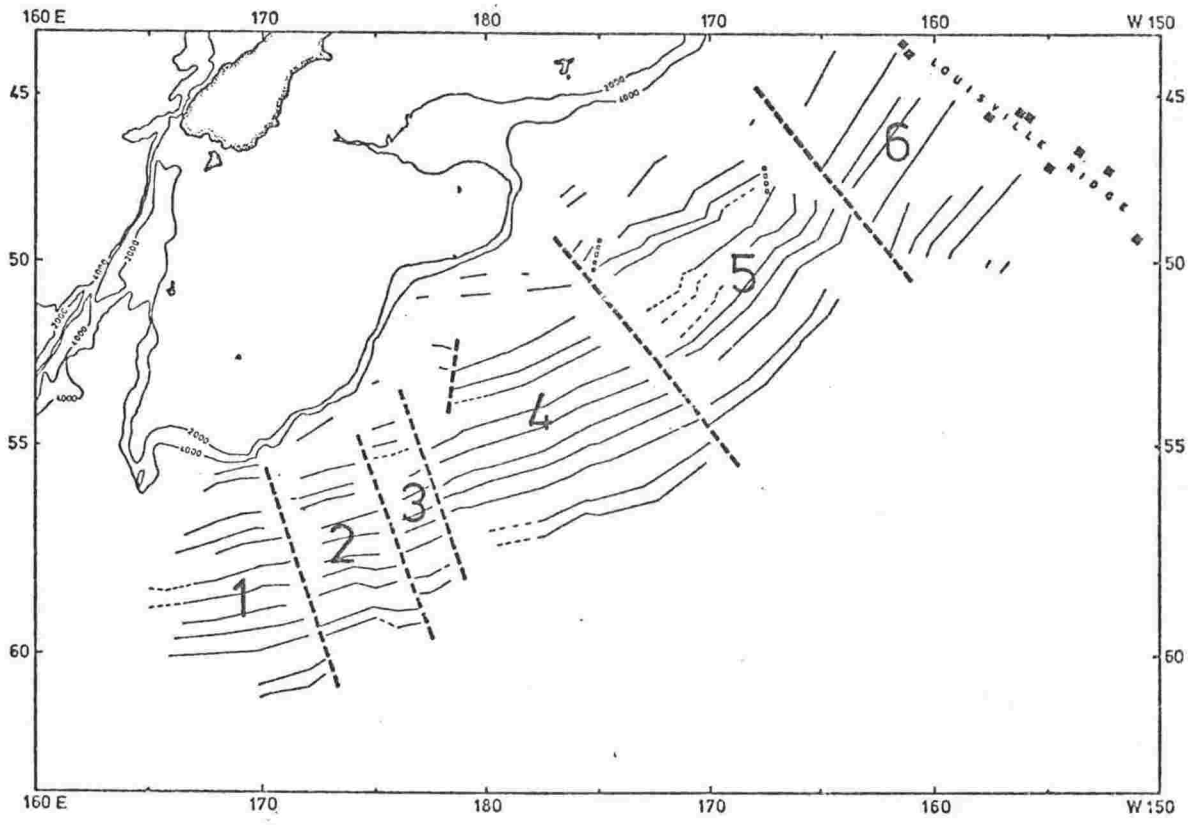


Fig. 6.13 Southwest Pacific basin anomaly lineations, with six zones delineated by major fracture zones indicated.

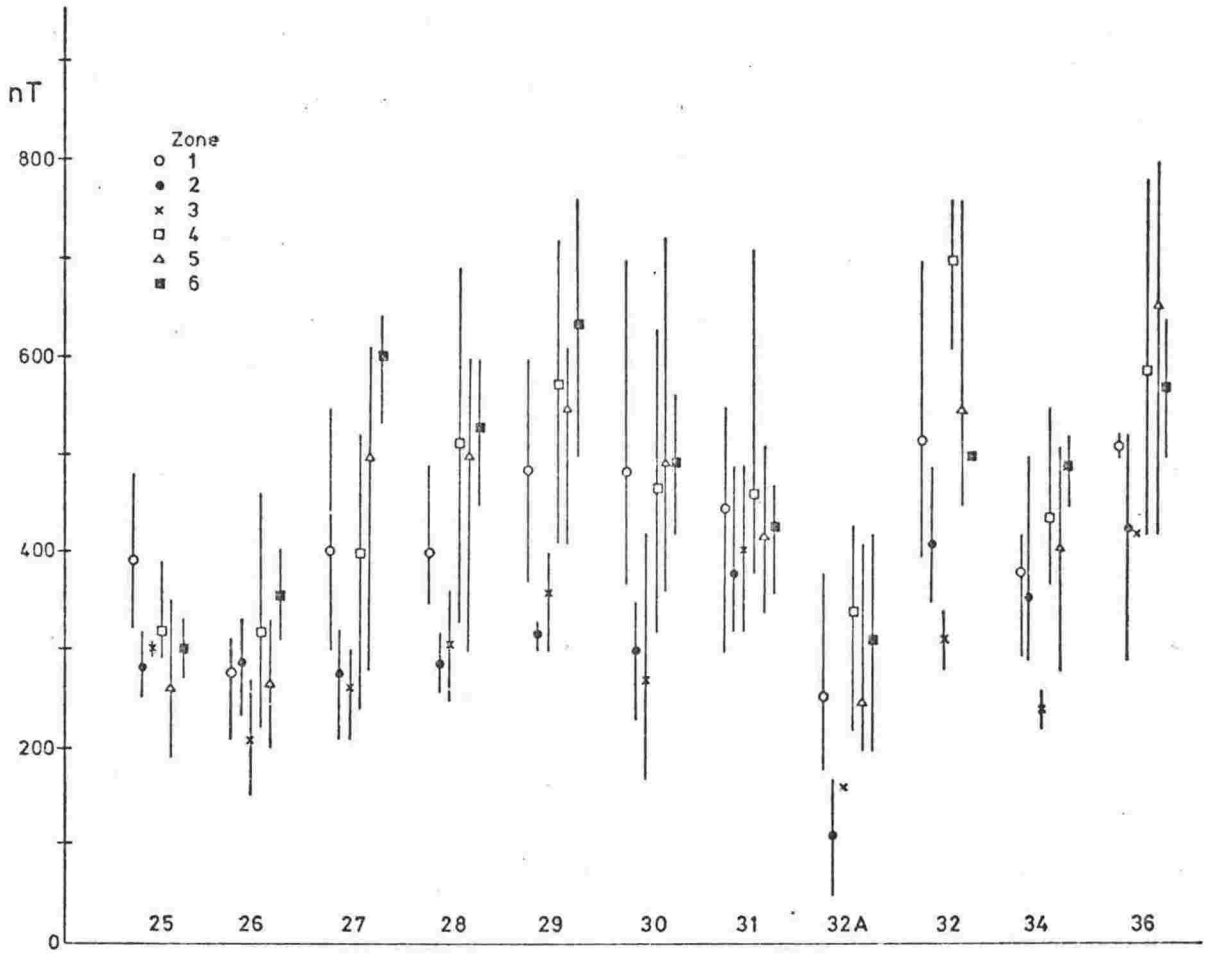


Fig. 6.14 Anomaly amplitudes for zones shown in Fig. 6.13. Bars indicate range, symbols show the means. Symbols without bars denote single values.

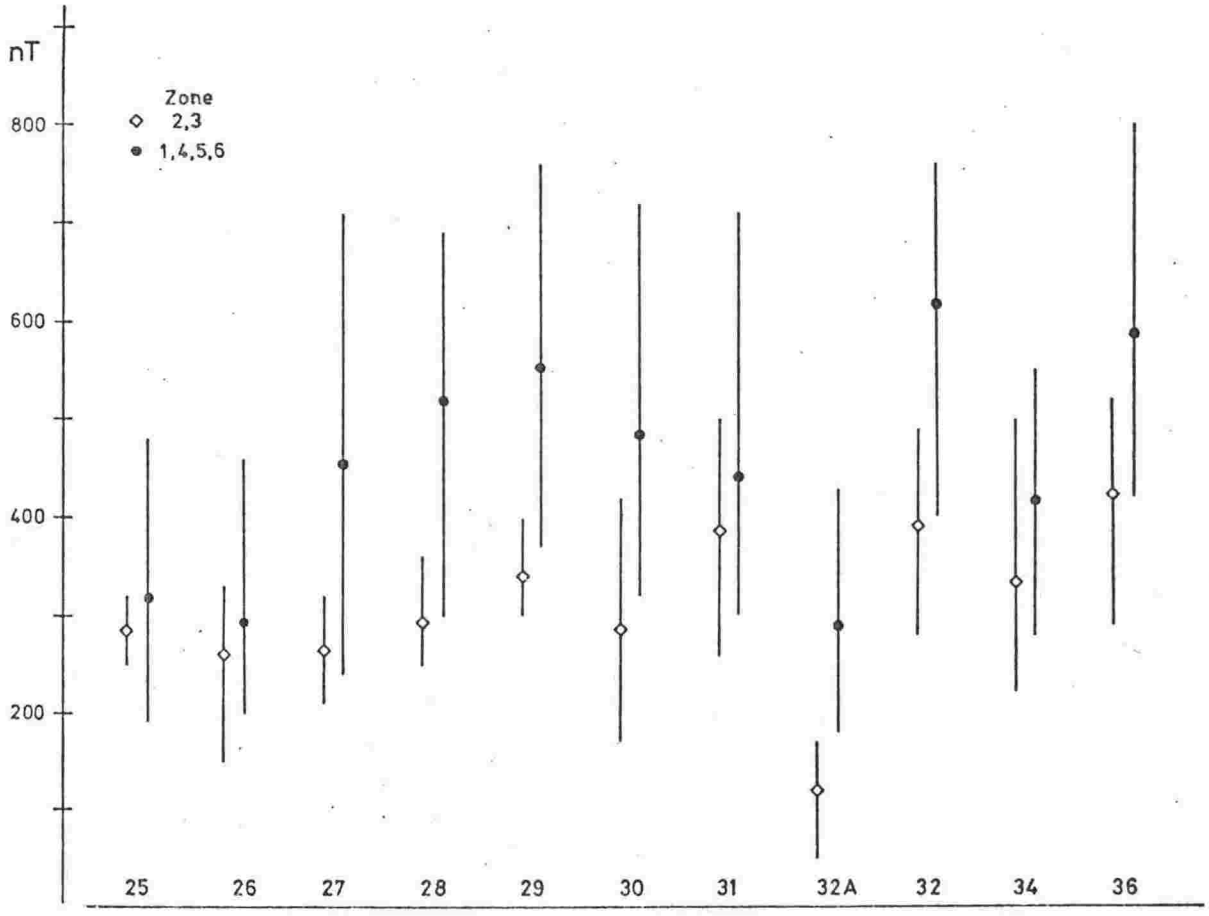


Fig. 6.15 Anomaly amplitudes of zones two and three compared with the other zones.

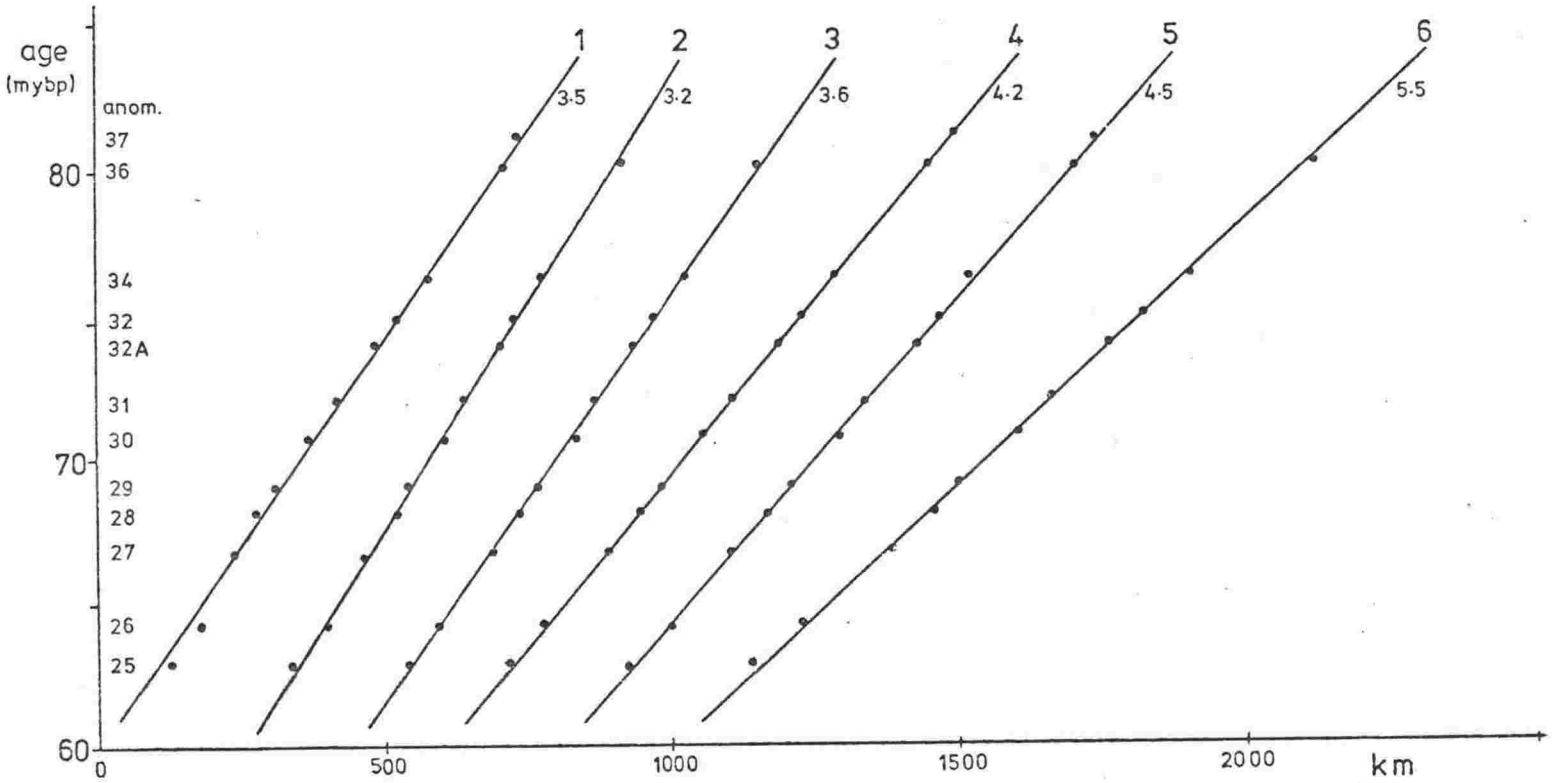


Fig. 6.16 Spreading rates in the zones shown in Fig. 6.13. Rates, in cm/y, labelled. For each zone the anomaly spacings are from a representative line perpendicular to the lineations. SPAC time scale.

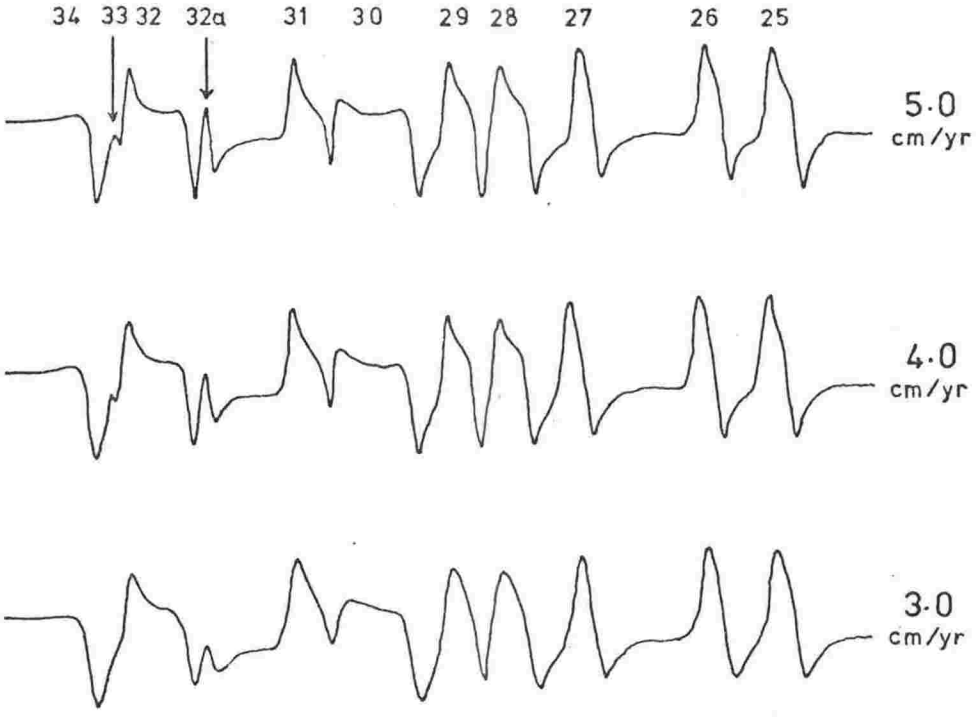


Fig. 6.17 Model profiles for different spreading rates. Model parameters for in situ formation.

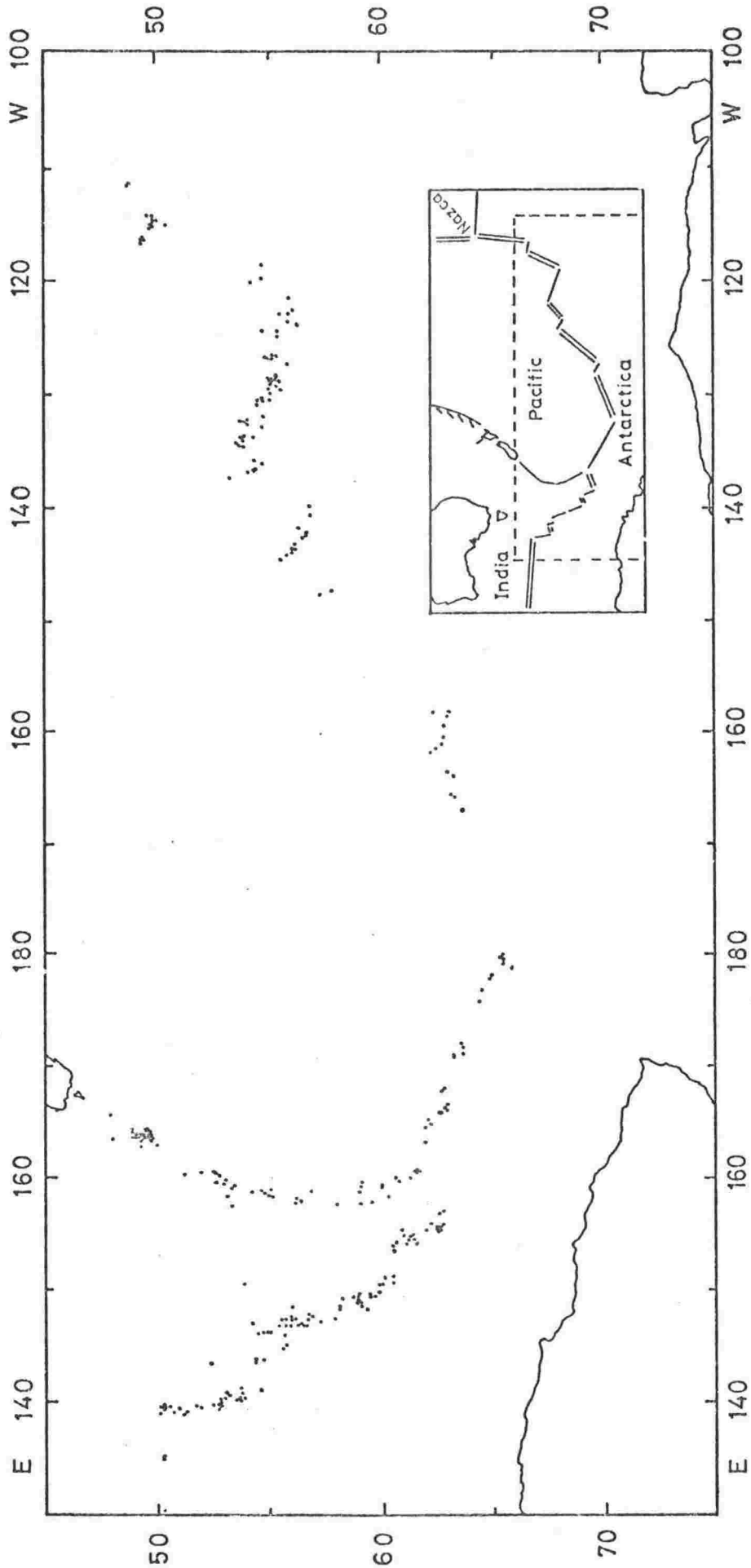


Fig. 7.1 Epicentres of earthquakes considered in the b value study.
USCGS epicentres Jan 1964-Dec 1972, south of 48°S only.

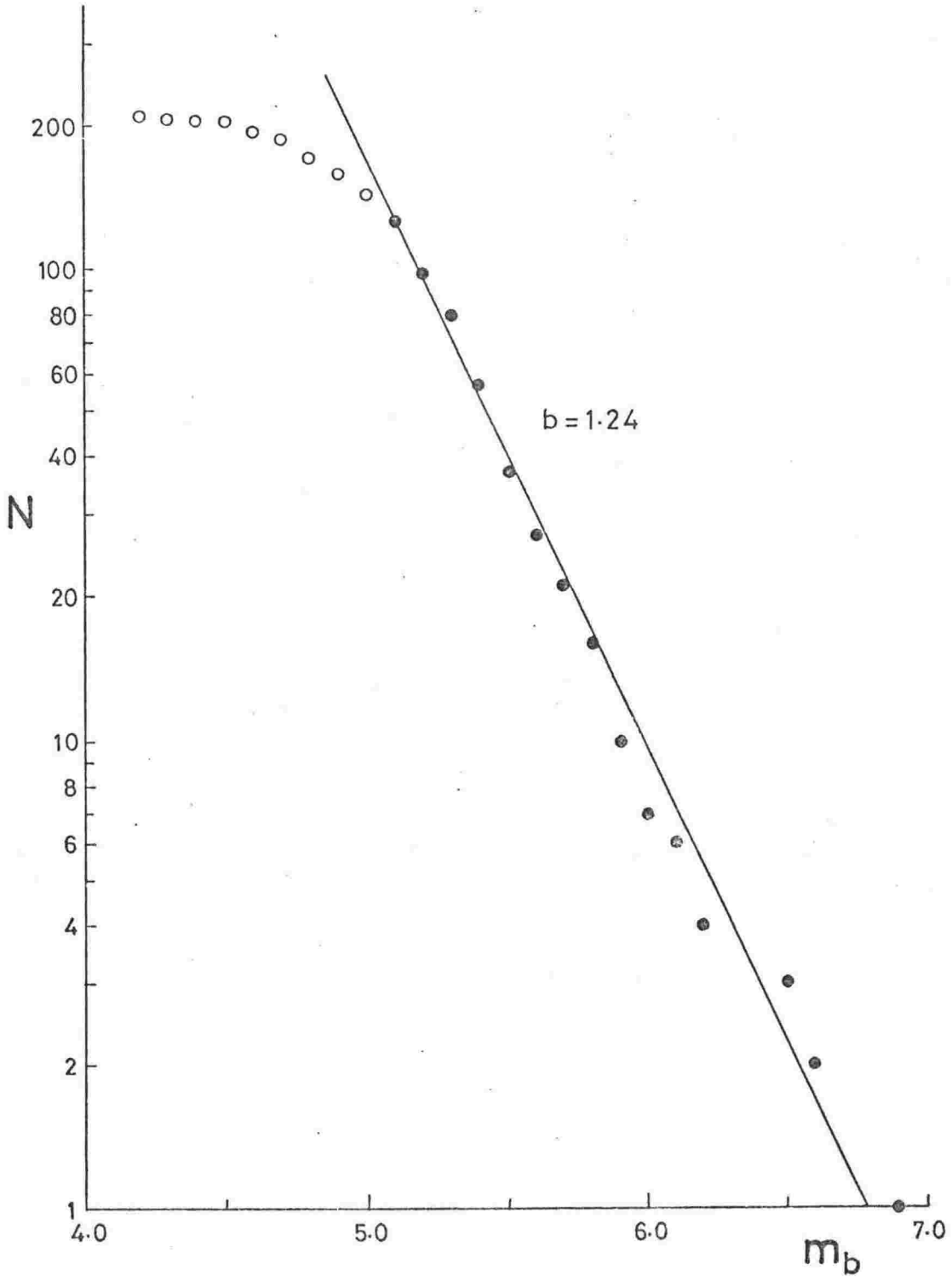


Fig. 7.2 Cumulative plot for the whole area. N is the number of earthquakes of magnitude M and greater. The line for b = 1.24 was calculated from magnitudes 5.1 and above, shown by solid symbols.

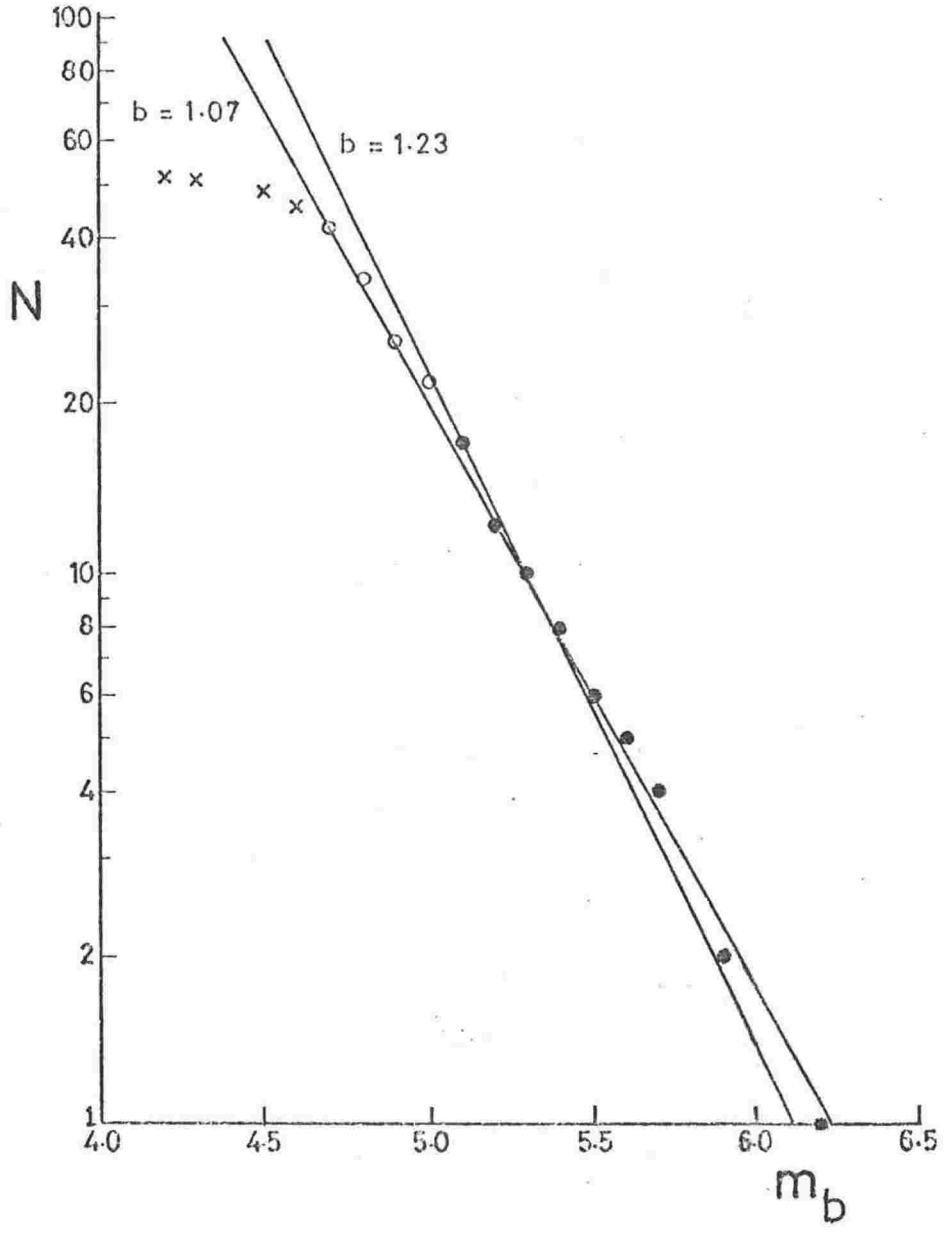


Fig. 7.3 Cumulative plot for the Eltanin fracture zone area. Line b = 1.23 from magnitudes 5.1 and above (closed circles). Line b = 1.07 from magnitudes 4.7 and above (open and closed circles).

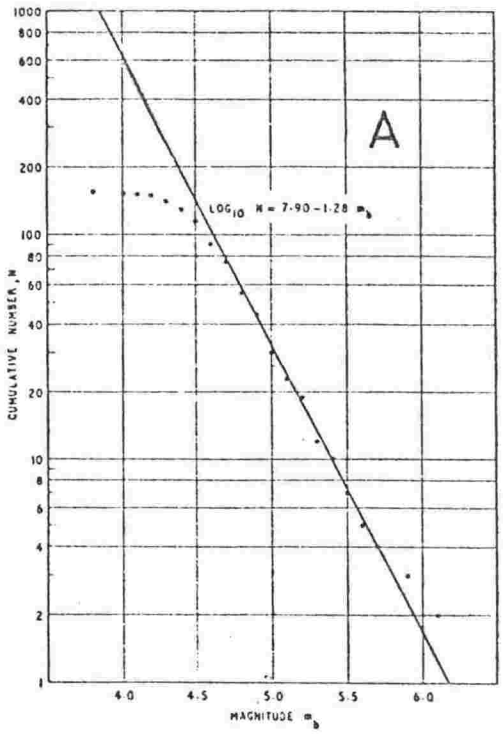


Fig. 2. Cumulative plot of 154 Mid-Atlantic ridge earthquakes for the period January 1963 to May 1967. $N$ is the number of events of magnitude $M$ and greater.

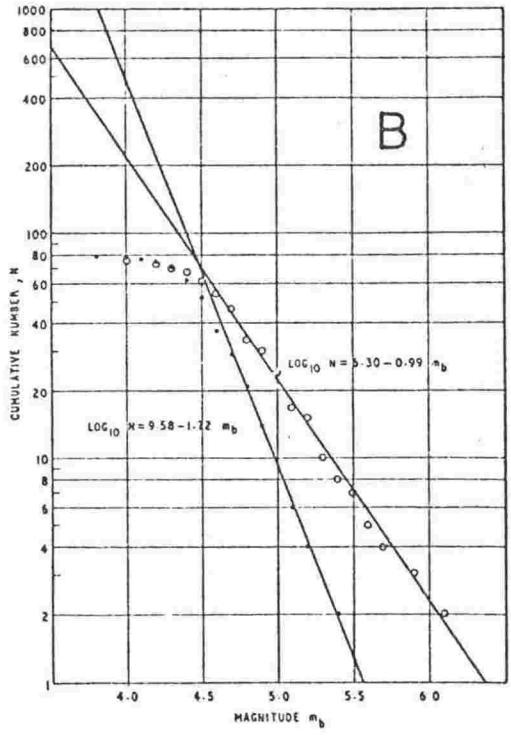


Fig. 3. Cumulative plots of the 154 earthquakes of fig. 2 distinguished as 79 rift zone events (solid circles) and 75 fracture zone events (open circles).

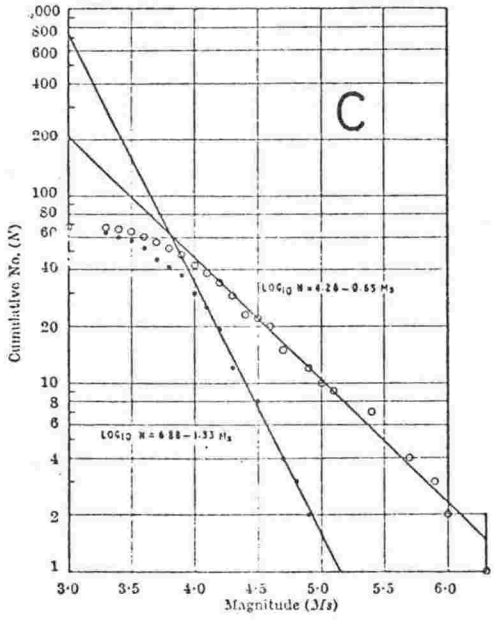


Fig. 2. Cumulative plot of sixty-four rift zone earthquakes (●) and sixty-eight fracture zone earthquakes (○) of the Mid-Atlantic ridge. $N$ is the number of events of surface wave magnitude $M_s$ and greater.

Fig. 7.4 Cumulative plots for the mid-Atlantic ridge system. A and B for body wave magnitudes, from Francis (1968a). C for surface wave magnitudes, from Francis (1968b).

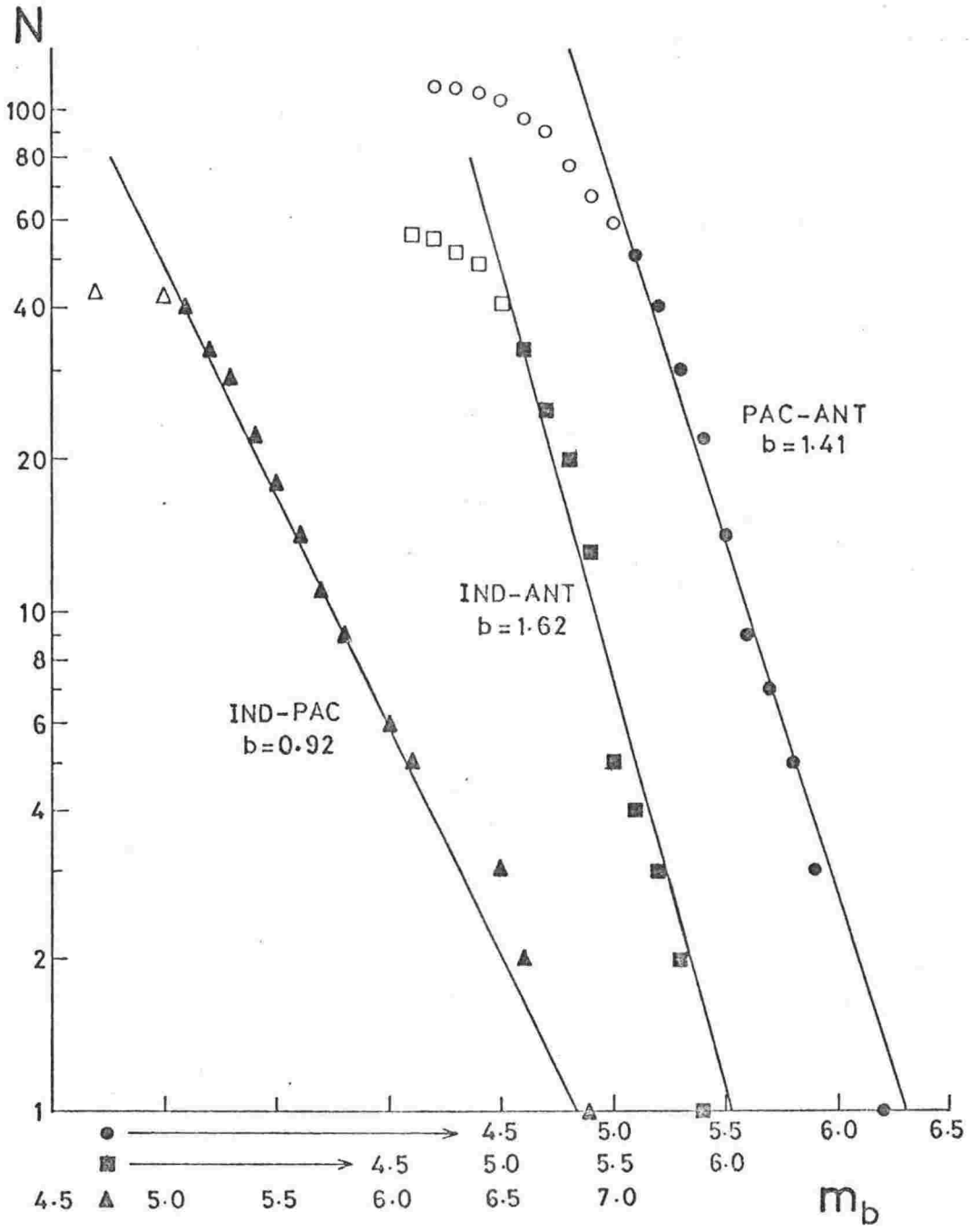


Fig. 7.5 Cumulative plots for the three plate boundaries in the southwest Pacific area. Lines from magnitudes 5.1 and above (solid symbols).

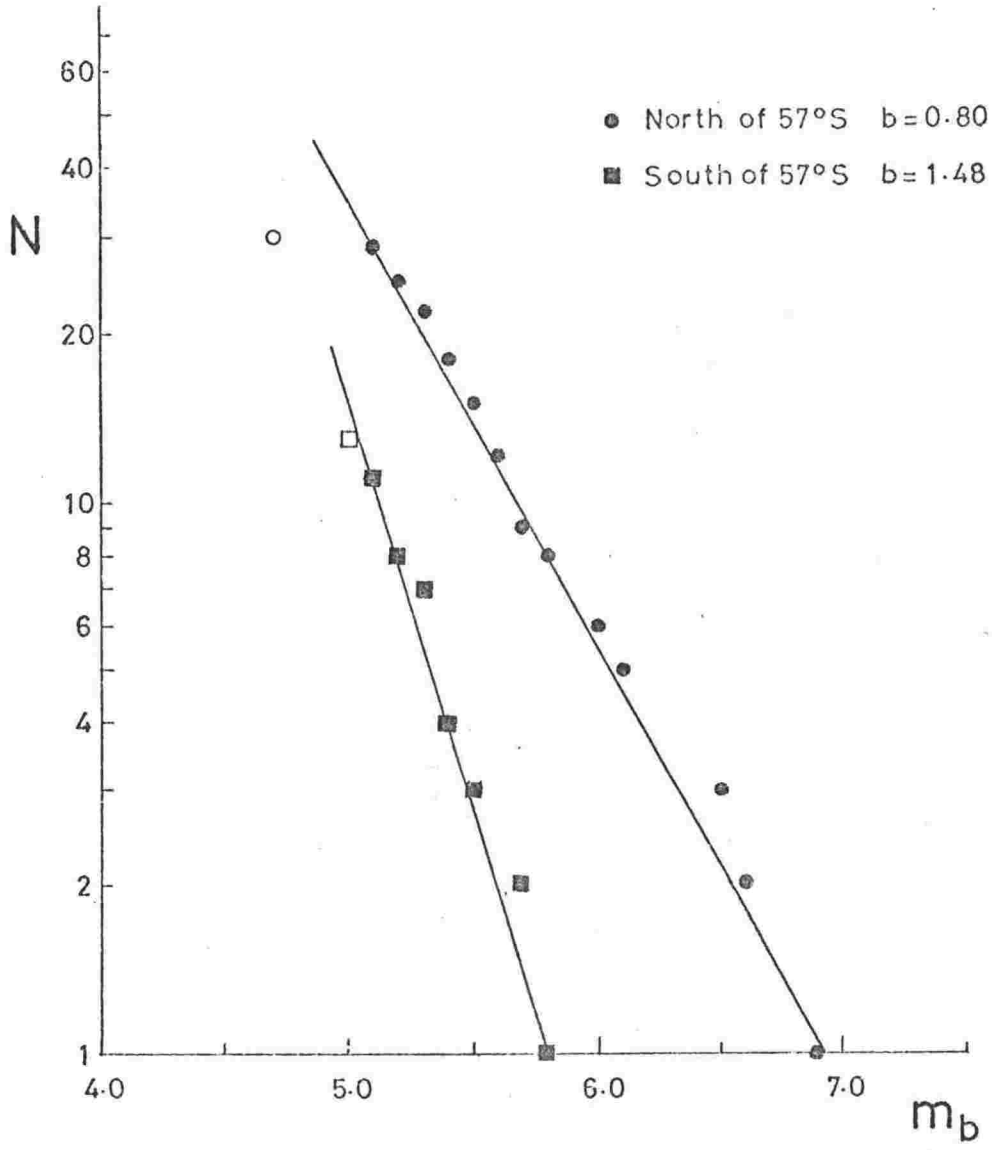


Fig. 7.6 Cumulative plots for the two parts of the Macquarie ridge complex. Lines from magnitudes 5.1 and above (solid symbols).

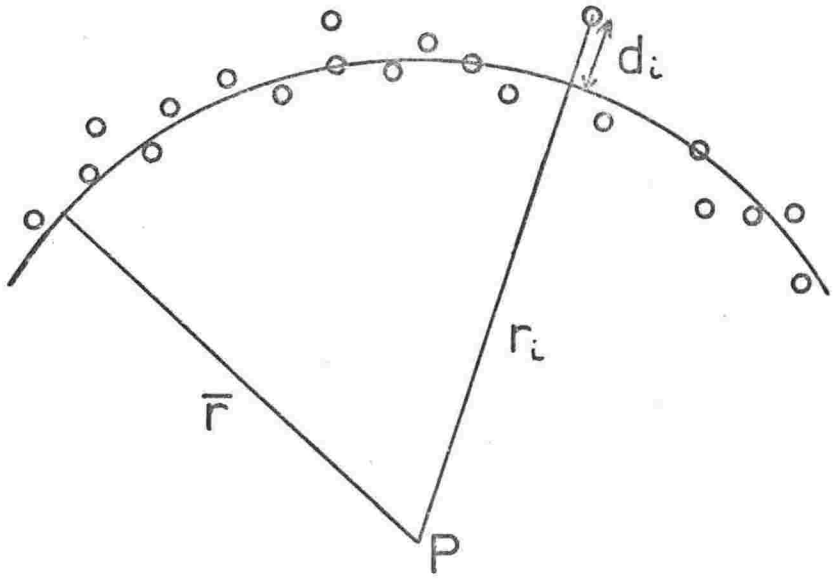


Fig. 8.1 Epicentral method notation. Seismic activity on a transform fault about the rotation pole P.

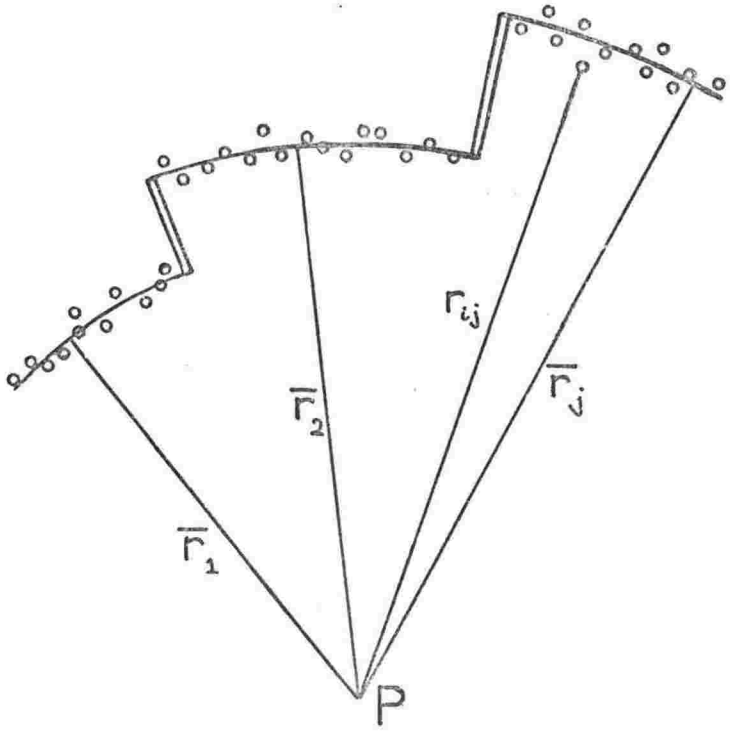


Fig. 8.2 Notation for several transform faults about P.

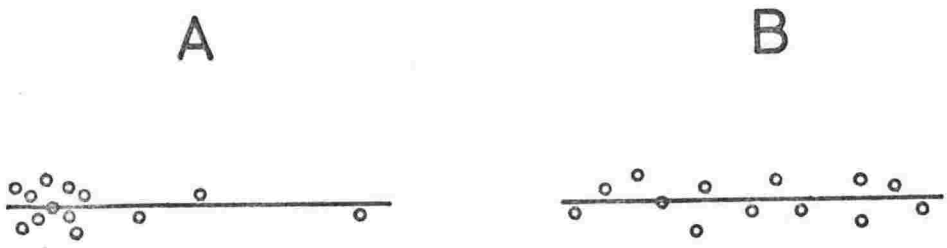


Fig. 8.3 Two distributions which have the same standard deviation and the same pole position.

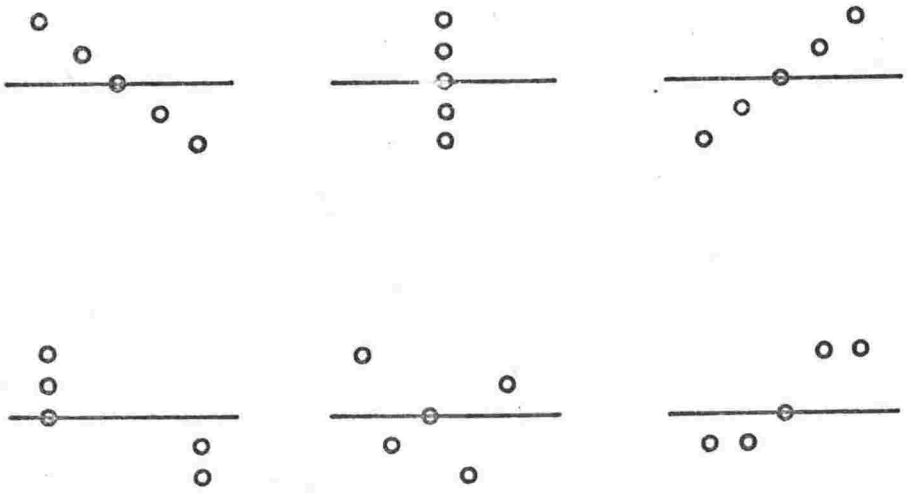

Fig. 8.4 Distributions which have the same standard deviation but different poles.

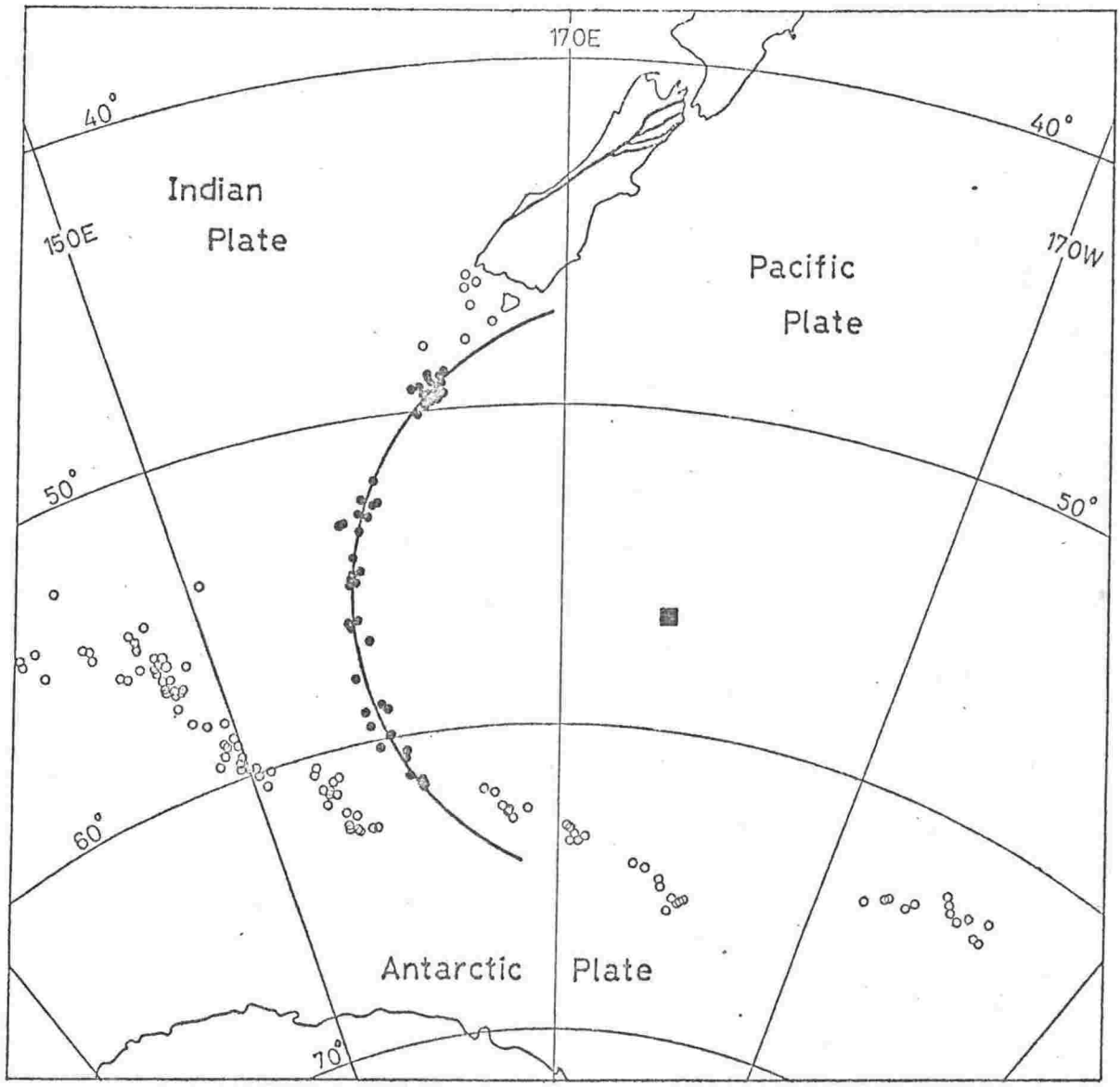


Fig. 8.5 USCGS epicentres south of 46°S, on a stereographic projection. Closed circles are the epicentres used for Indian-Pacific epicentral pole calculations. Arc is about the pole at 56°S, 176°E (square). Heavy lines in the South Island, New Zealand indicate the Alpine fault and its major branches.

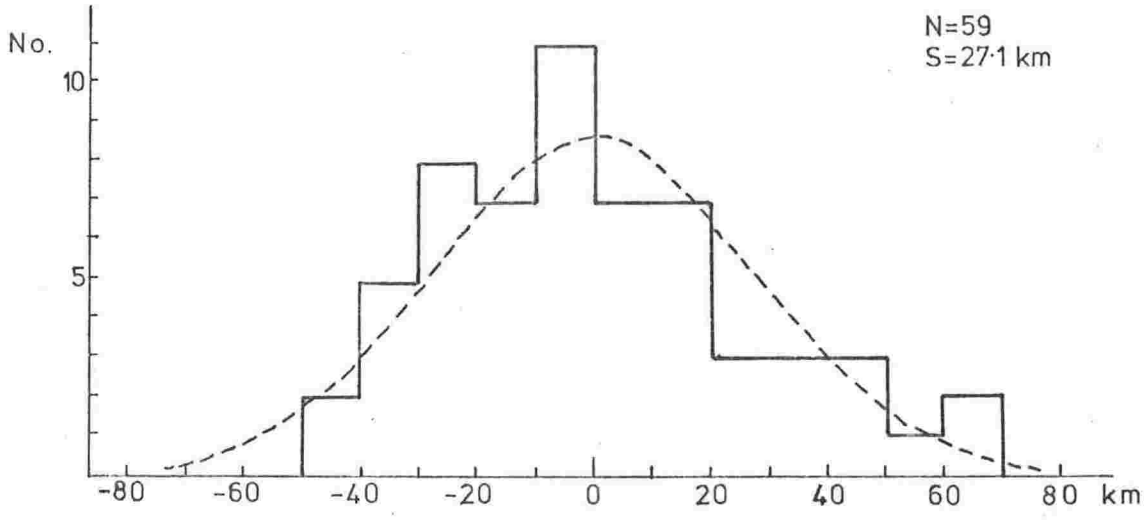


Fig. 8.6 Distribution of deviations from the arc of a pole at 56.0°S, 175.2°E. 59 USCGS epicentres. Dashed curve is normal distribution.

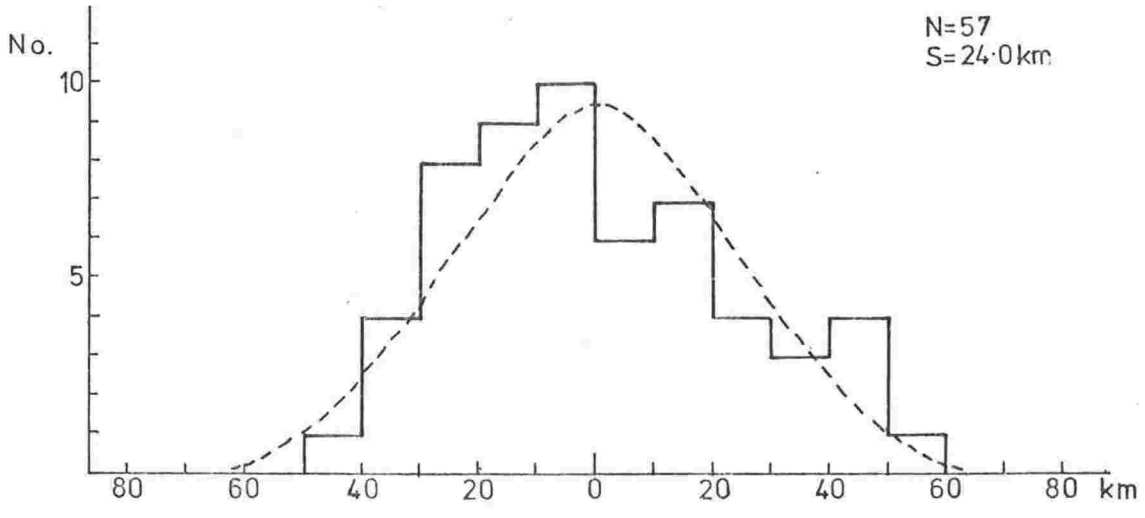


Fig. 8.7 Distribution of deviations from the arc of a pole at 56.0°S, 175.6°E. 57 USCGS epicentres.

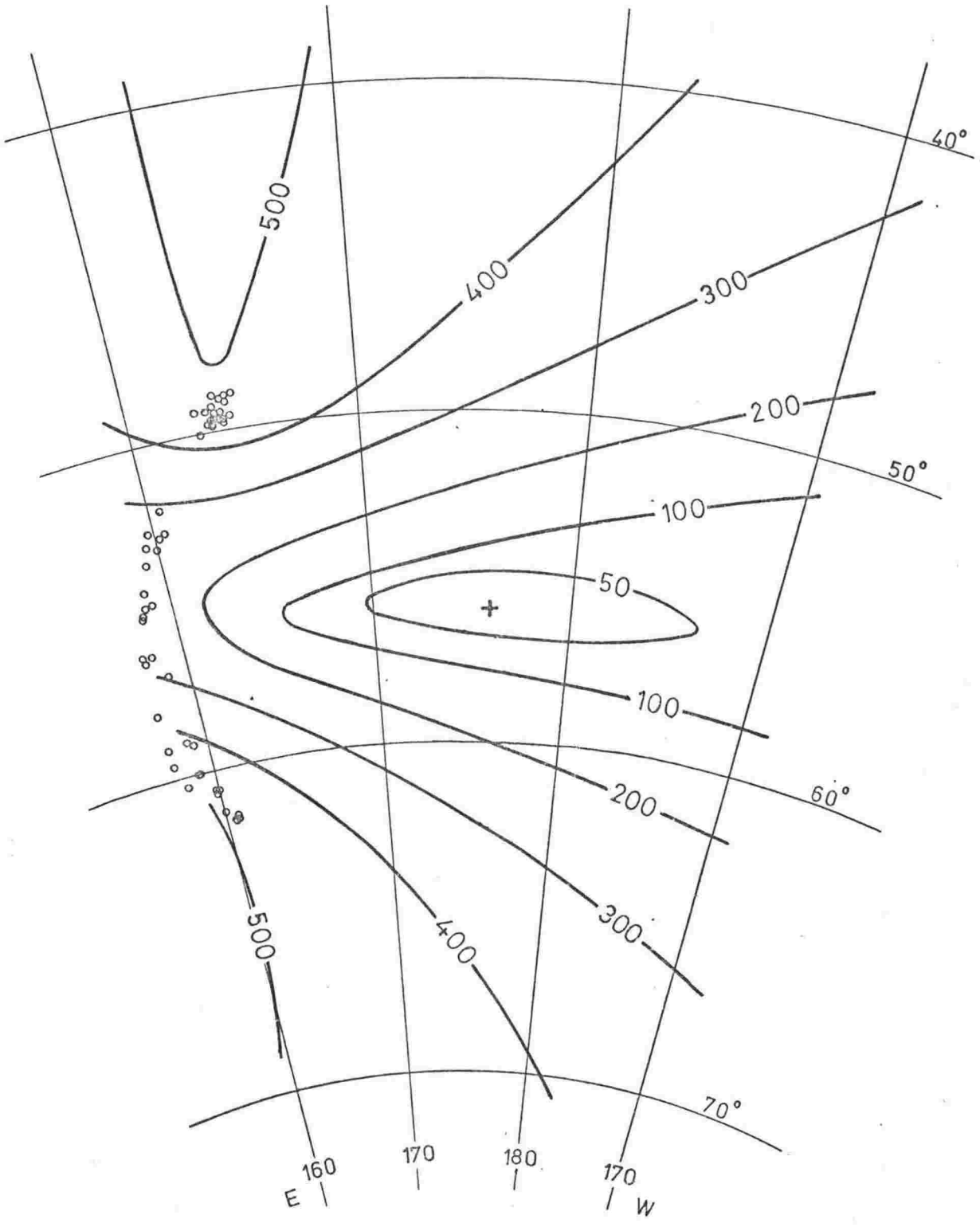


Fig. 8.8 Contours of epicentral standard deviation for Indian-Pacific pole from 57 USCGS epicentres (circles). Cross indicates pole, 56.0°S, 175.6°E. Contour units are km. Value at the pole, 24.0 km.

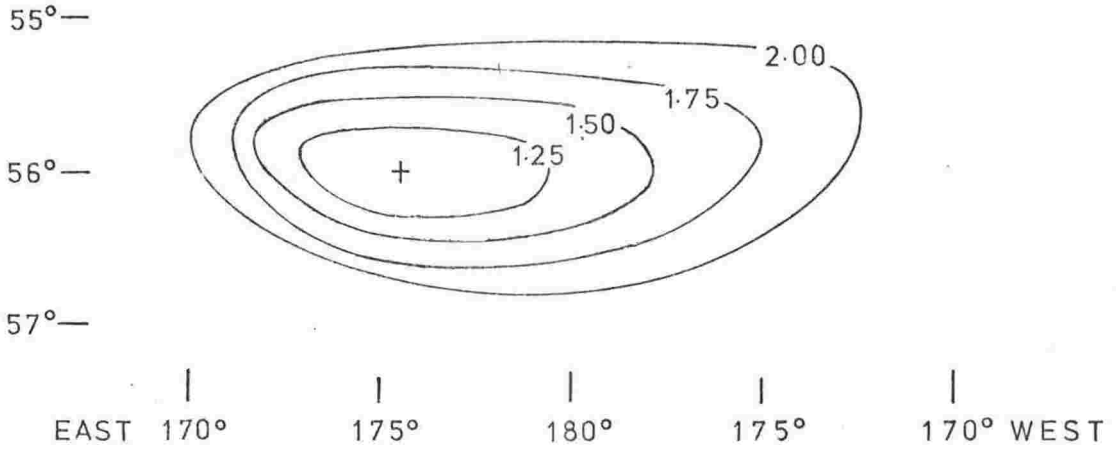


Fig. 8.9 Detailed contours for Indian-Pacific epicentral pole from 57 USCGS epicentres. Contours in units of the standard deviation at the pole (cross).

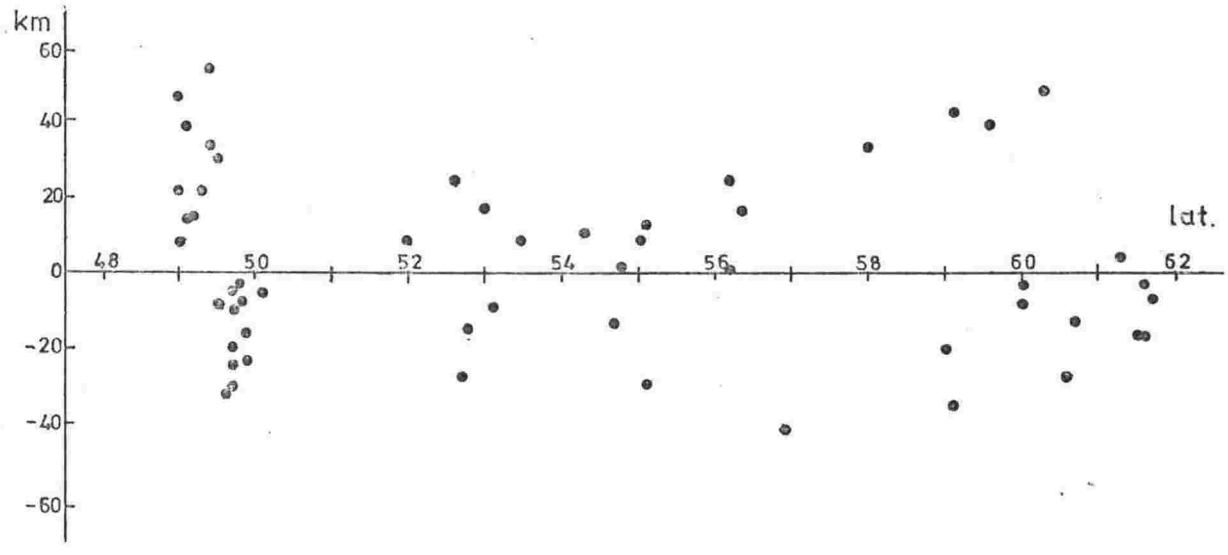


Fig. 8.10 Latitudinal distribution of USCGS deviations from the arc of a pole at 56.0°S, 175.6°E.

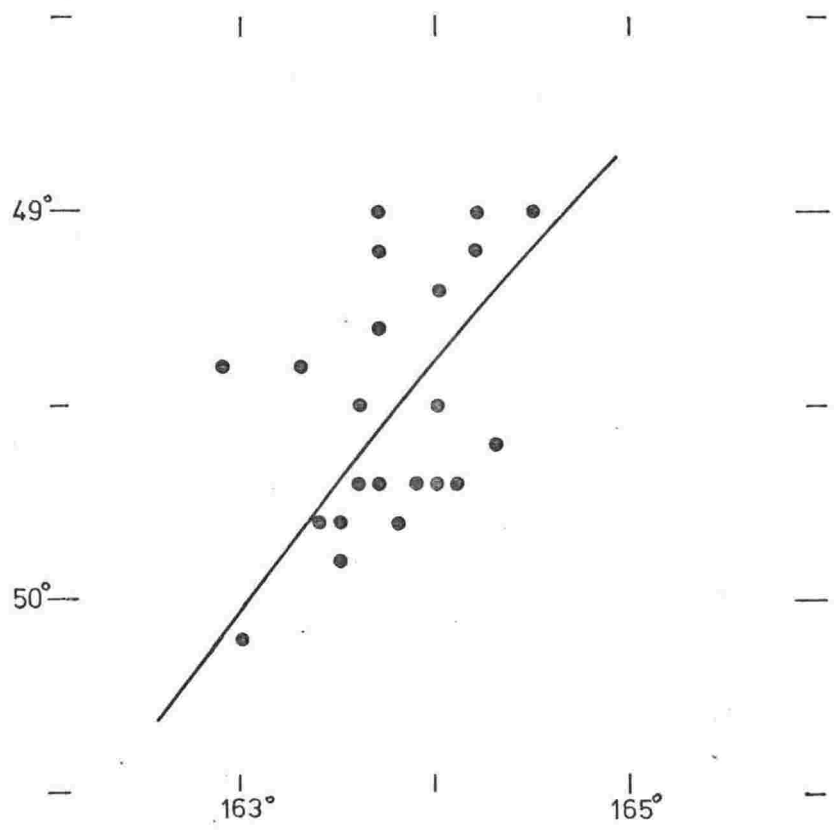


Fig. 8.11 USCGS distribution near 49°S. Heavy line is arc about pole at 56.0°S, 175.6°E.

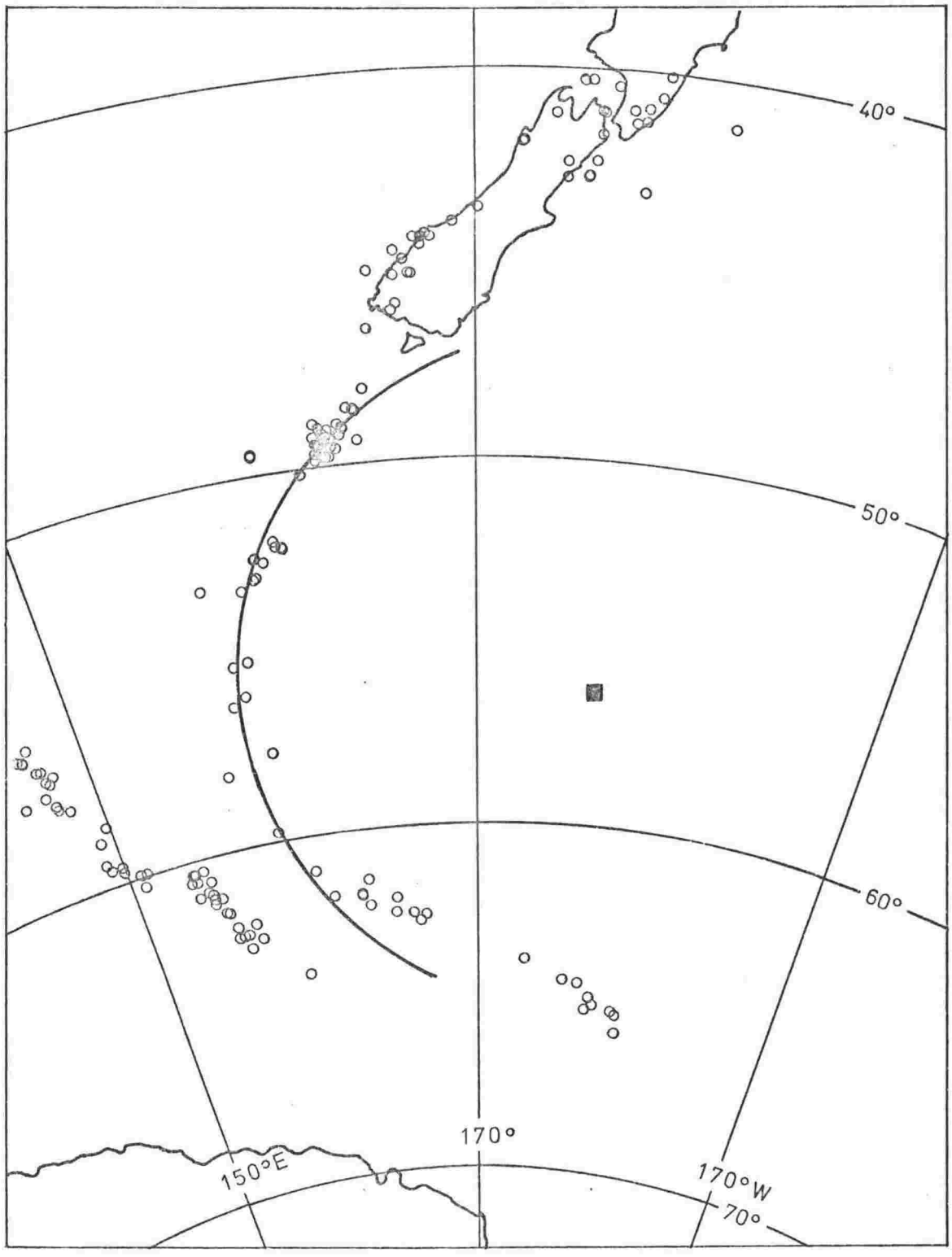


Fig. 8.12 Sykes' epicentres on stereographic projection. Arc is about the pole at 56°S, 176°E (square).

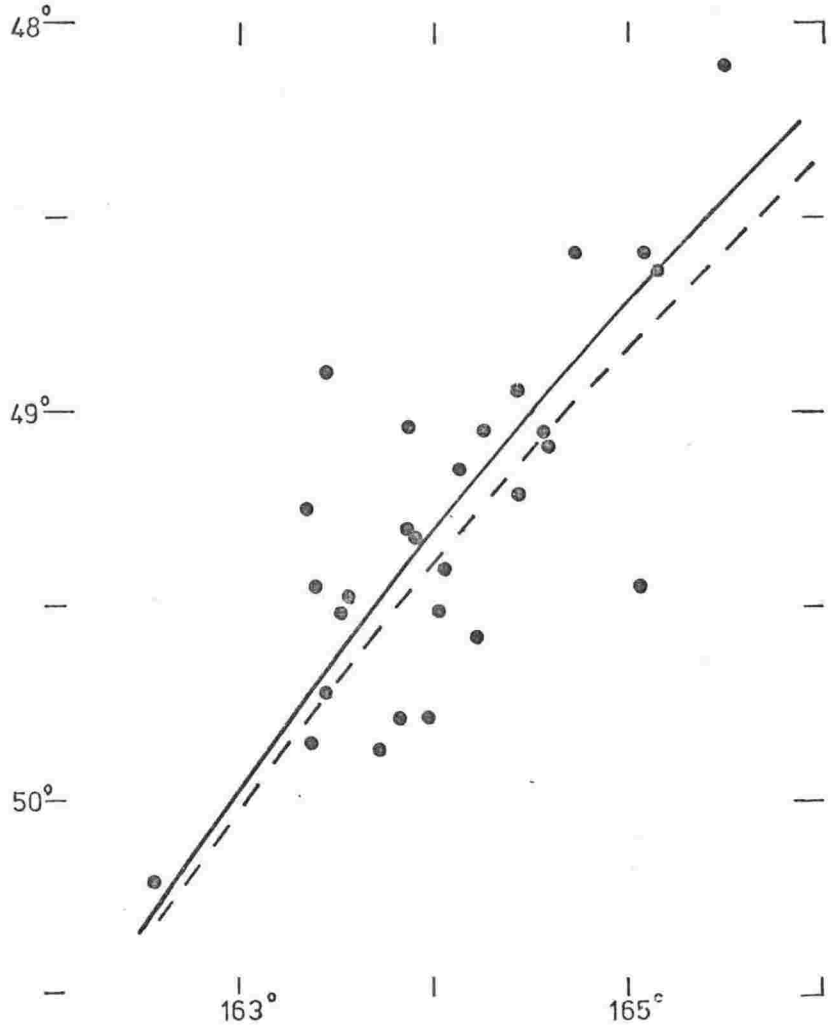


Fig. 8.13 Sykes' epicentres near 49°S. Heavy arc is about Sykes pole at 55.8°S, 176.4°E. Dotted arc is about USCGS pole at 56.0°S, 175.6°E.

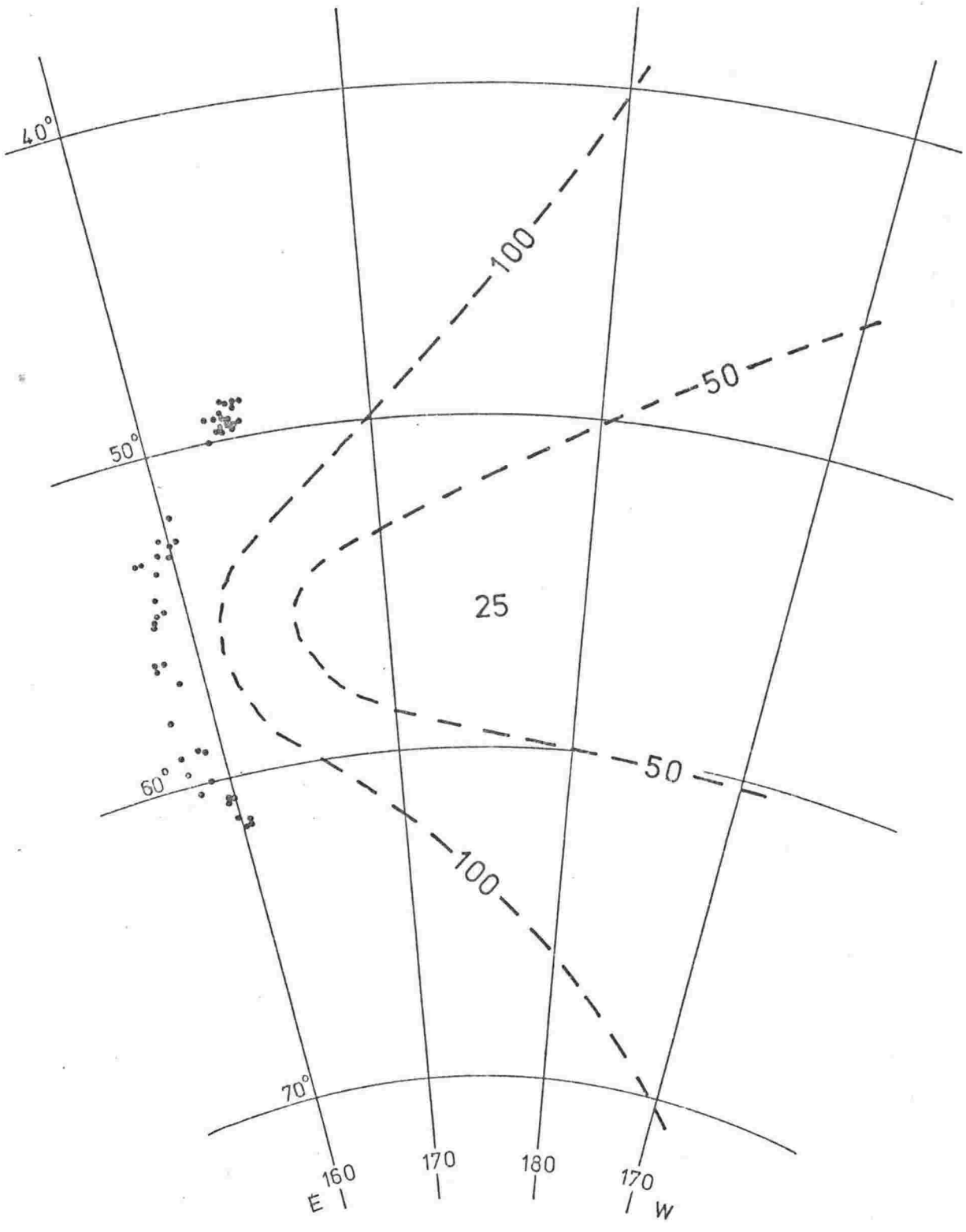


Fig. 8.14 Contours of epicentral standard deviation for the three zone USCGS data set. Compare with one zone contours of Fig. 8.8.

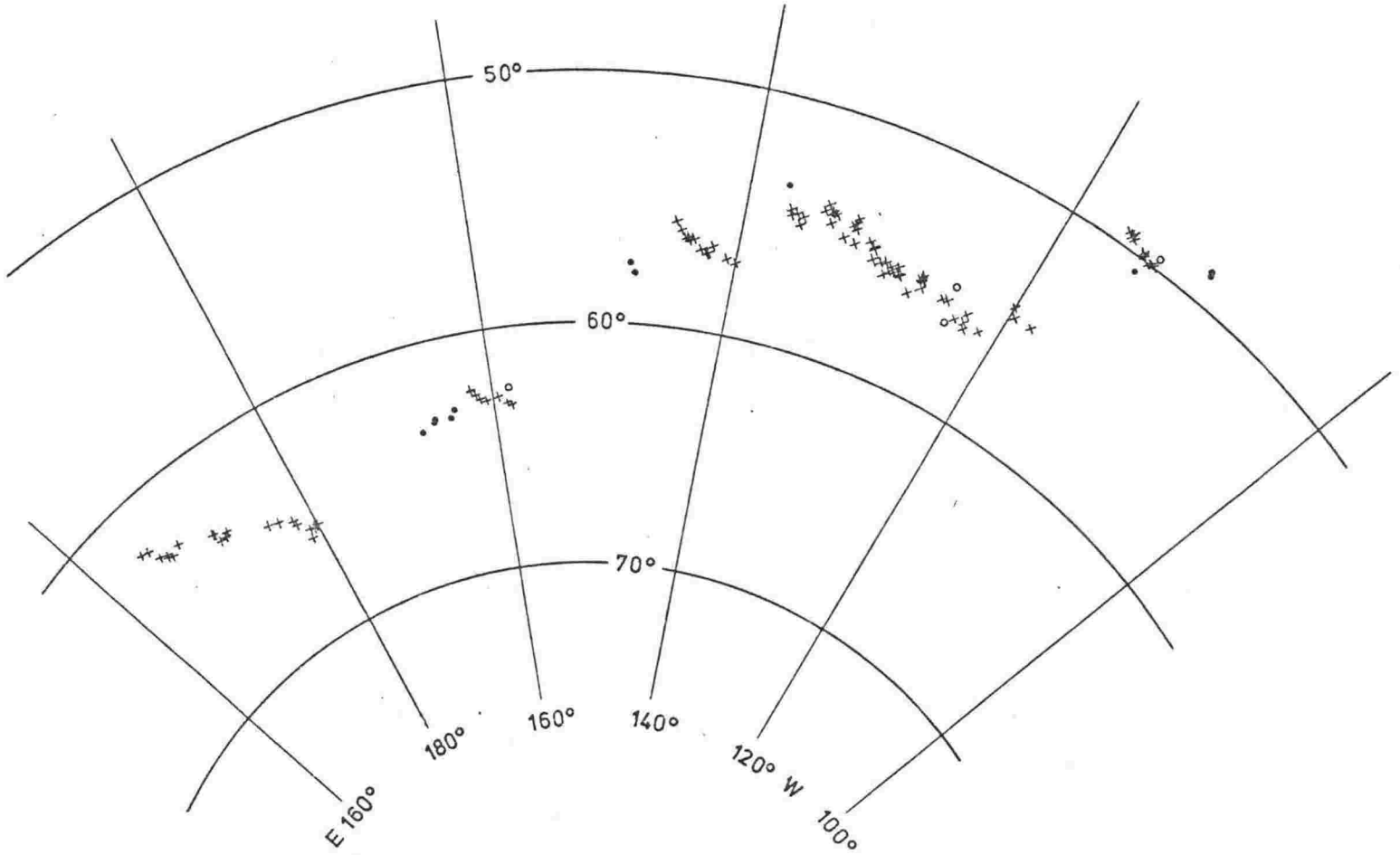


Fig. 8.15 Pacific-Antarctic boundary epicentres. Crosses - used for epicentral pole. Open circles - rejected because of large deviations. Closed circles - not considered. USCGS locations Jan. 1964 - March 1972. Stereographic projection.

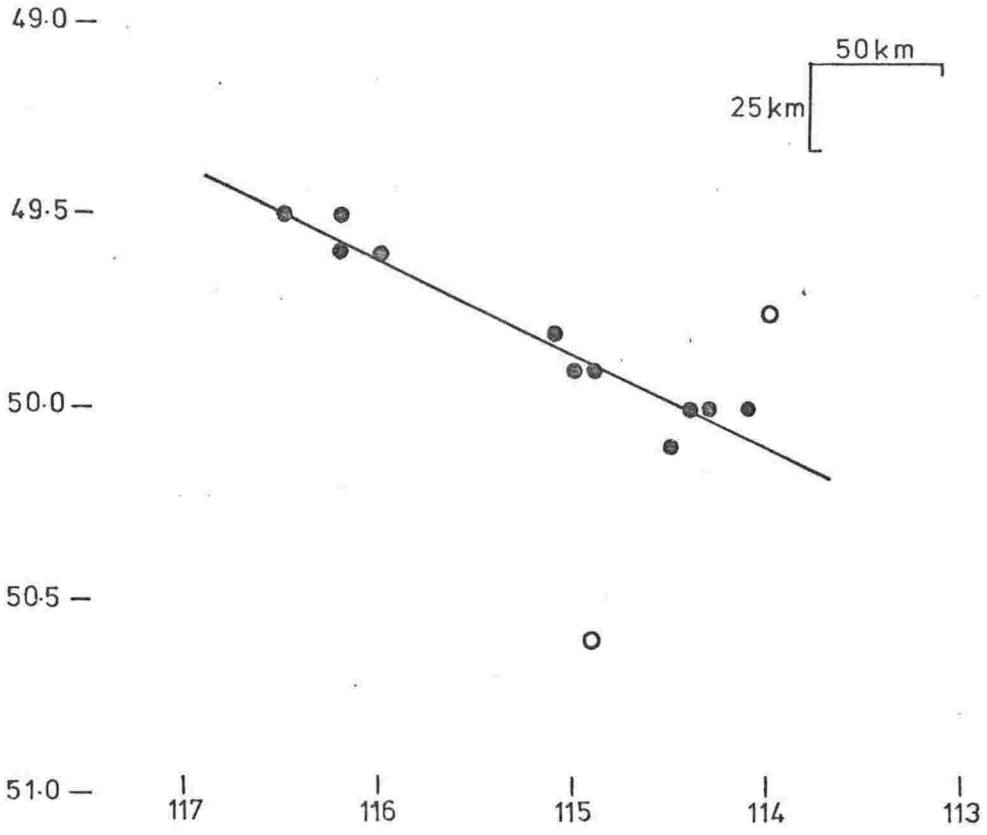


Fig. 8.16 Epicentre distribution at 115°W. Closed circles used for epicentral pole, open circles not considered. Arc is about the ten zone epicentral pole at 71°S, 122°E. An arc about the eight zone pole at 76°S, 144°E, is indistinguishable from the ten zone arc.

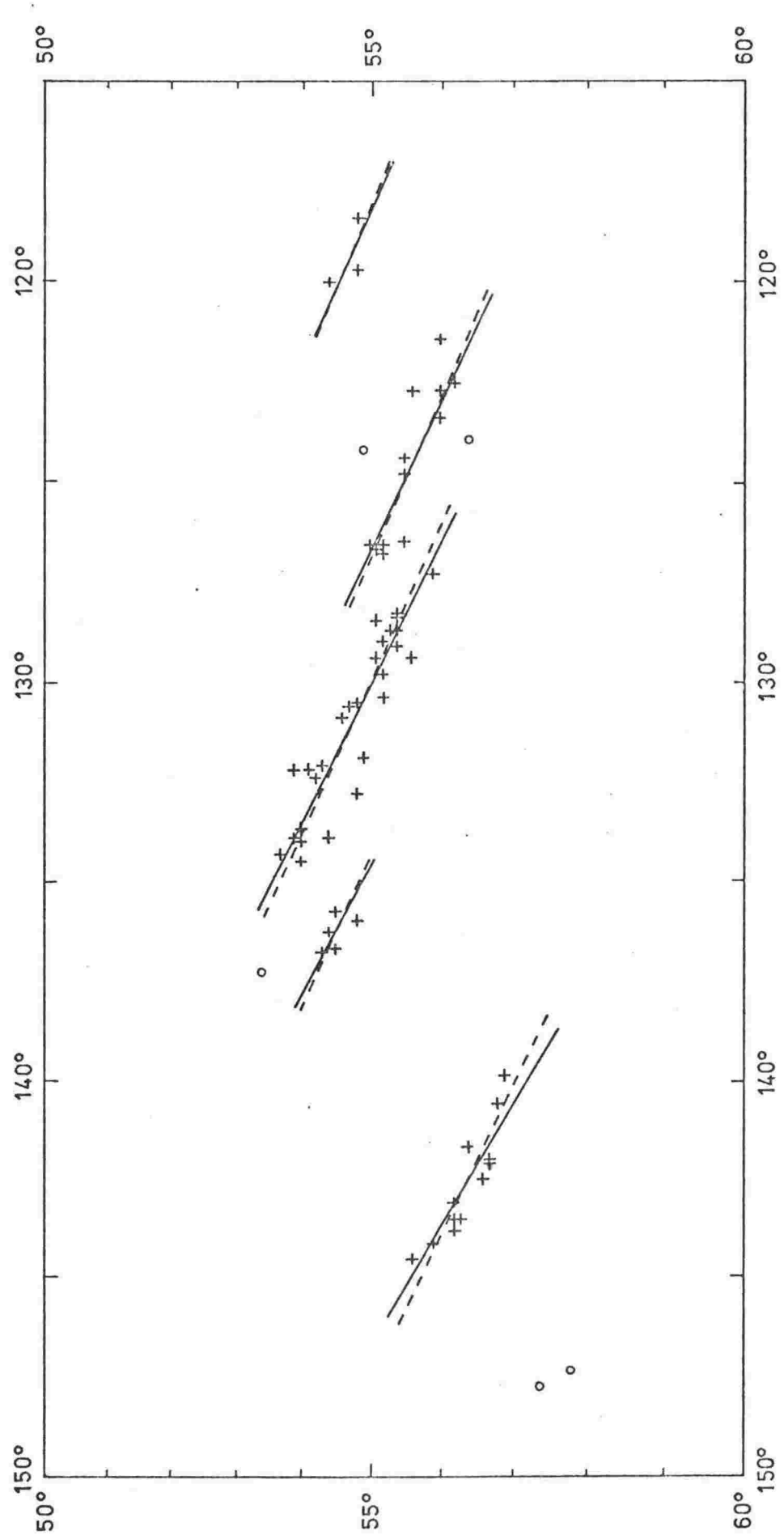


Fig. 8.17 Epicentre distributions 118°W to 150°W. Crosses used for epicentral poles, open circles not considered. Solid arcs about the ten zone pole at 71°S, 122°E, dashed arcs about the eight zone pole at 76°S, 144°E.

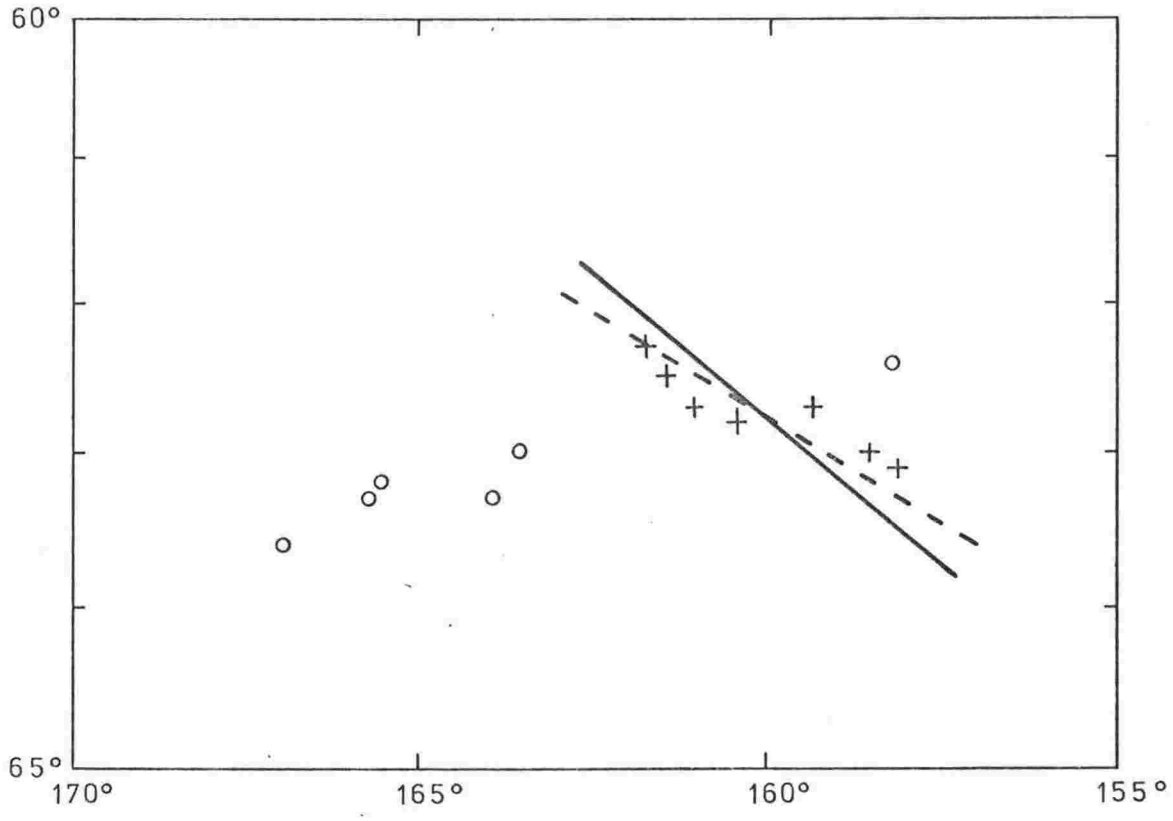


Fig. 8.18 Epicentre distribution at 160°W. Crosses used for epicentral poles, open circles not considered. Solid arc about the ten zone pole at 71°S, 122°E, dashed arc about the eight zone pole at 76°S, 144°E.

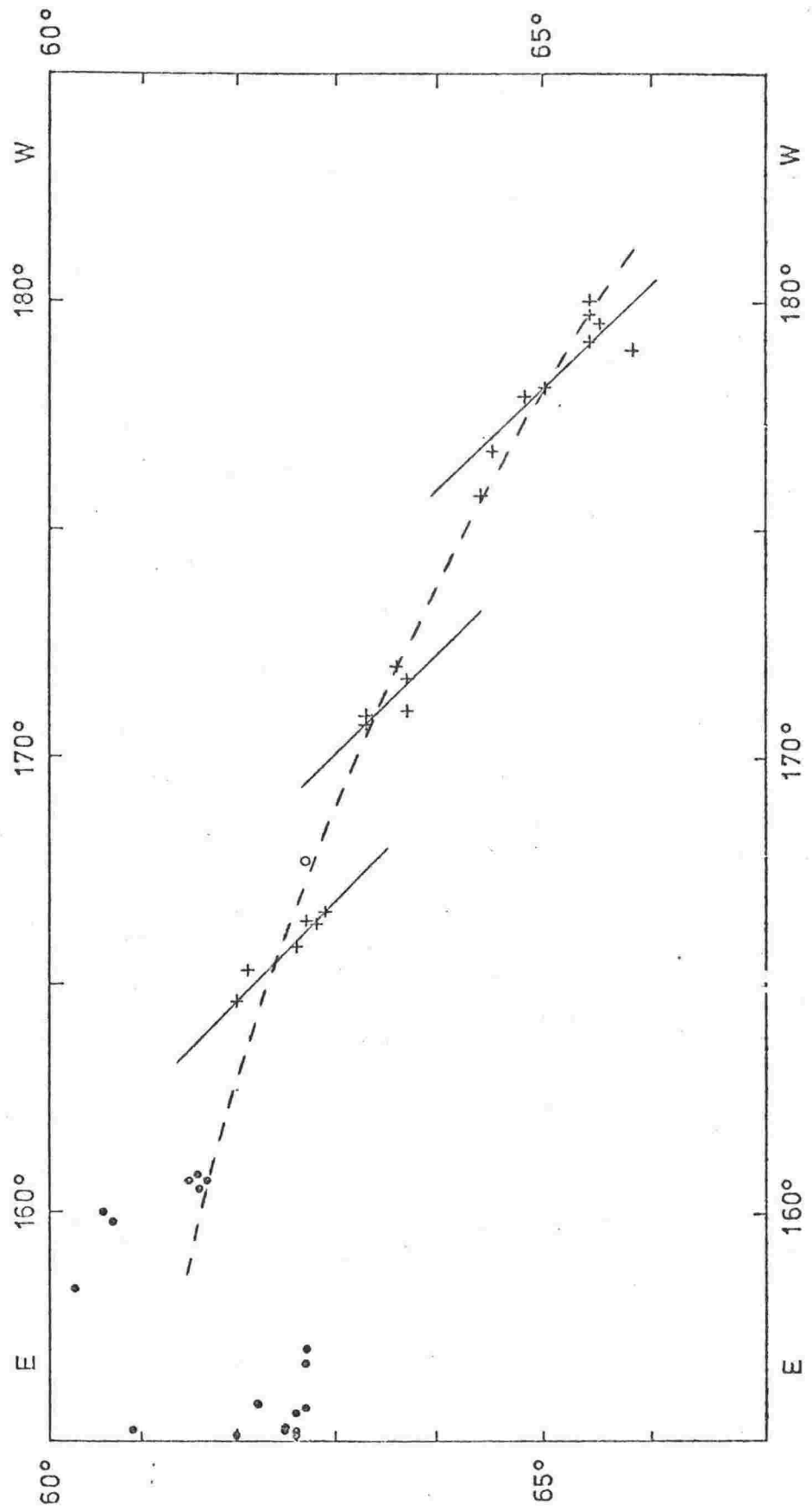


Fig. 8.19 Pacific-Antarctic fracture zone. Crosses used for ten zone pole. Crosses and open circle for eight zone pole. Closed circles are epicentres on the Indian-Antarctic and Indian-Pacific boundaries. Solid arcs about the ten zone pole at 71°S, 122°E; dashed arc about the eight zone pole at 76°S, 144°E.

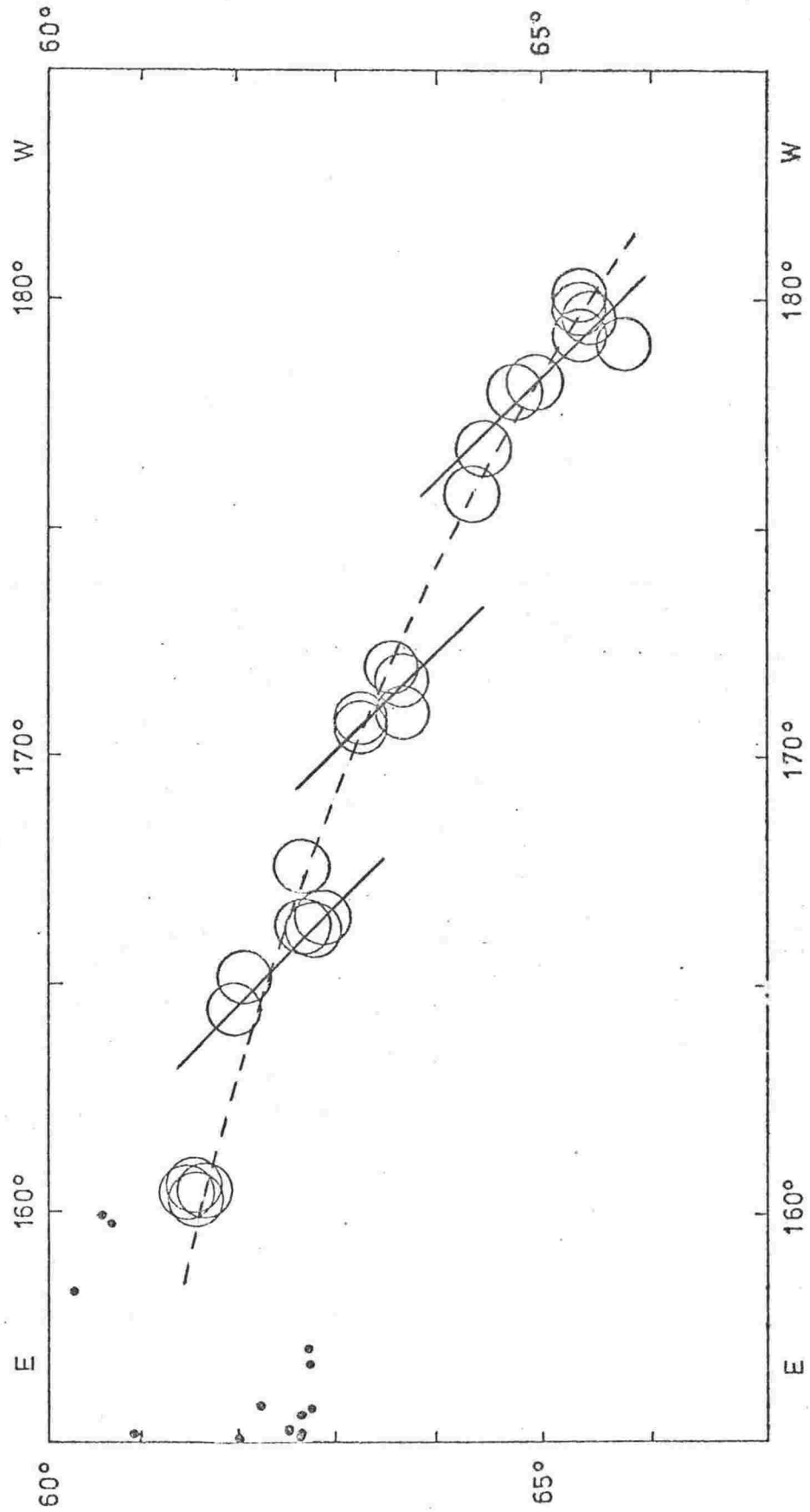


Fig. 8.20 Pacific-Antarctic fracture zone with circles of radius 25 km for the epicentres. The four circles at 160°E were not considered for the epicentral method. Solid arcs about the ten zone pole at 71°S, 122°E; dashed arc about the eight zone pole at 76°S, 144°E.

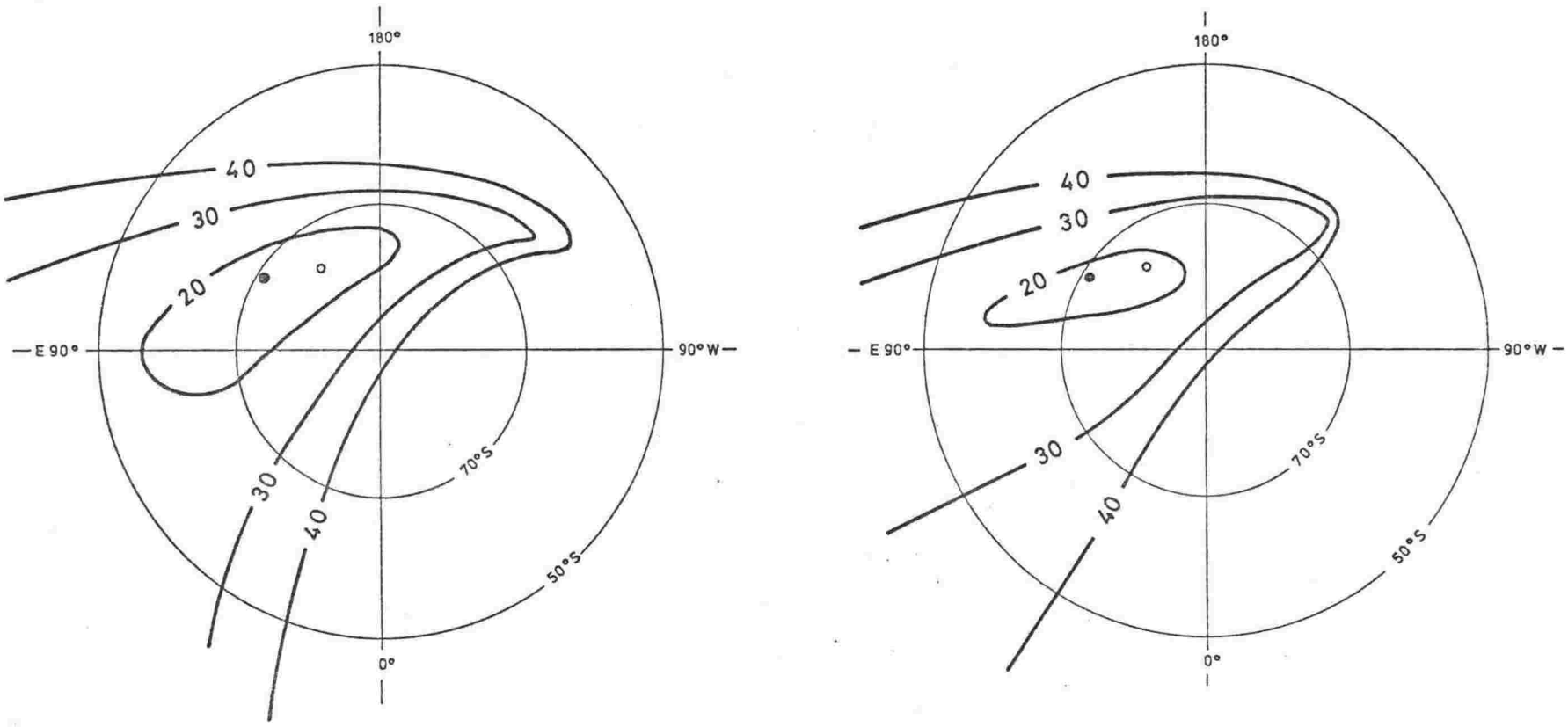


10 zones Pole (●) 71°S, 122°E S=14·9 km

8 zones Pole (○) 76°S, 144°E S=15·5 km

Fig. 8.21 Contours of epicentral standard deviation for the Pacific-Antarctic pole. Contour units are km. Equal area projections.

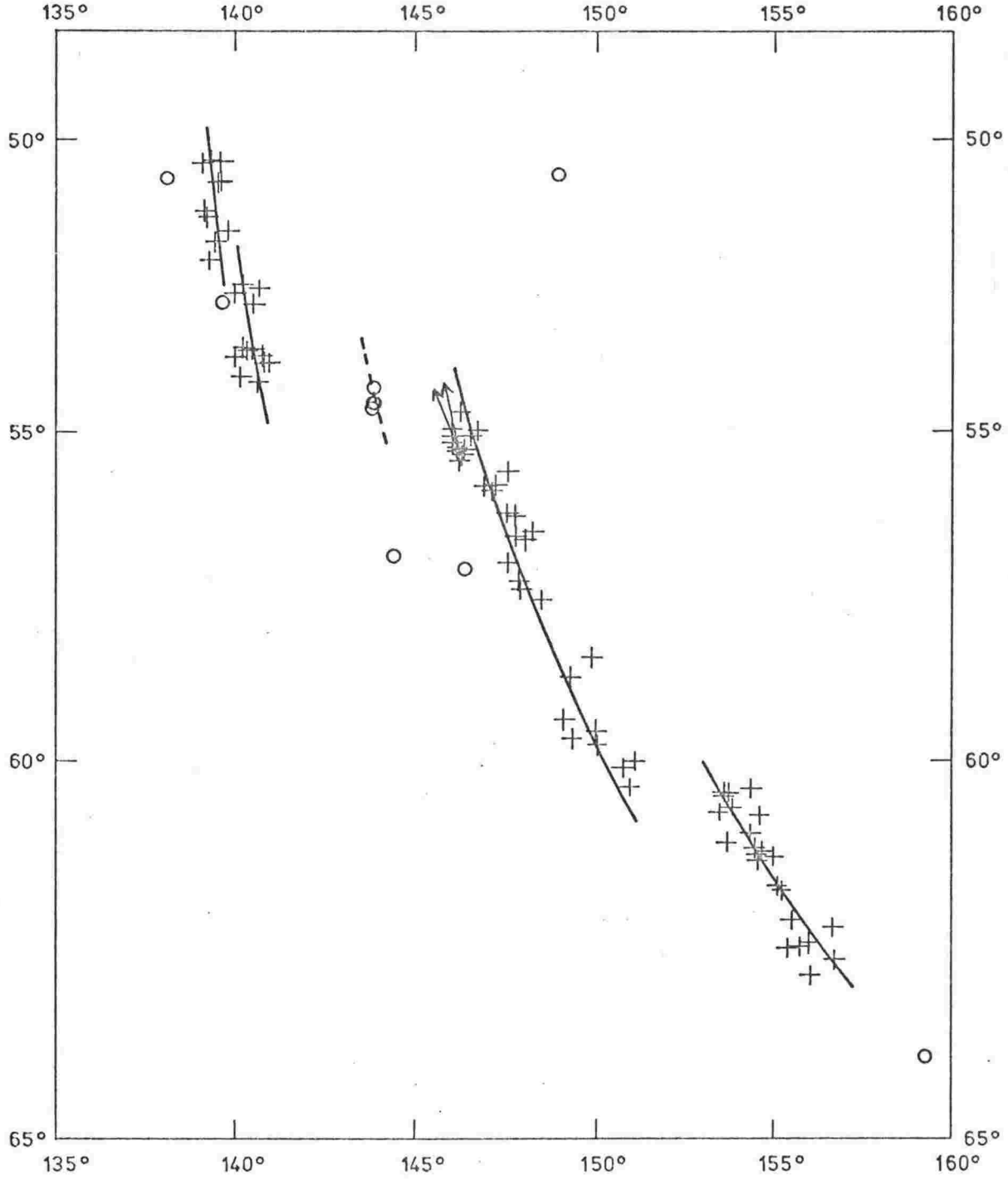


Fig. 8.22 Indian-Antarctic boundary east of 135°E. Crosses: epicentres used for epicentral method, circles: not used. Arcs are about pole at 30°S, 166°W. Arrows indicate the slip vectors deduced from focal mechanism studies of two earthquakes at 55.3°S.

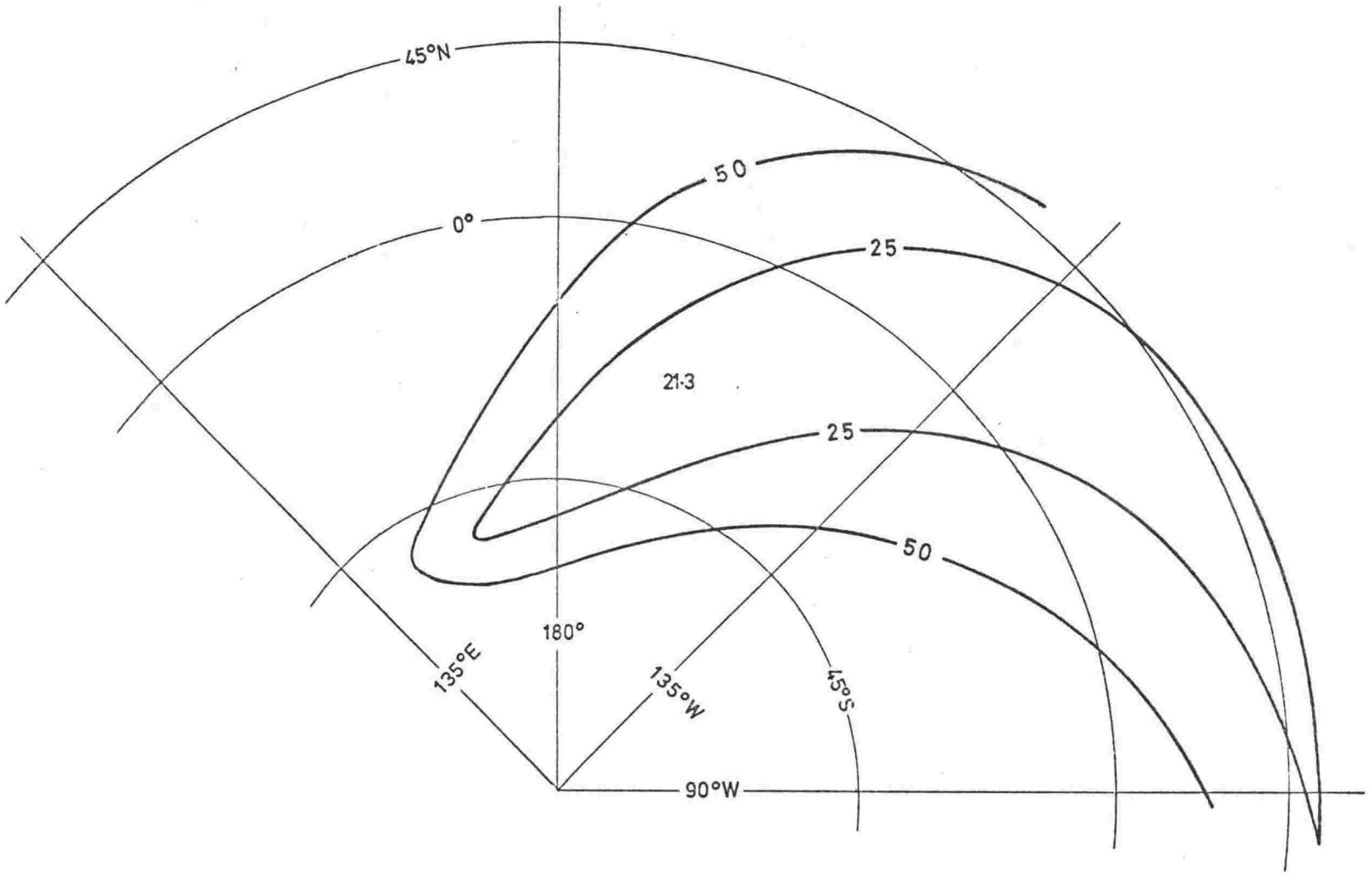


Fig. 8.23 Contours of epicentral standard deviation for the Indian-Antarctic pole, from data east of 135°E. Contour units are km, and pole (26°S, 163°W) is at the decimal point of the number indicating value at pole. Equal area projection.

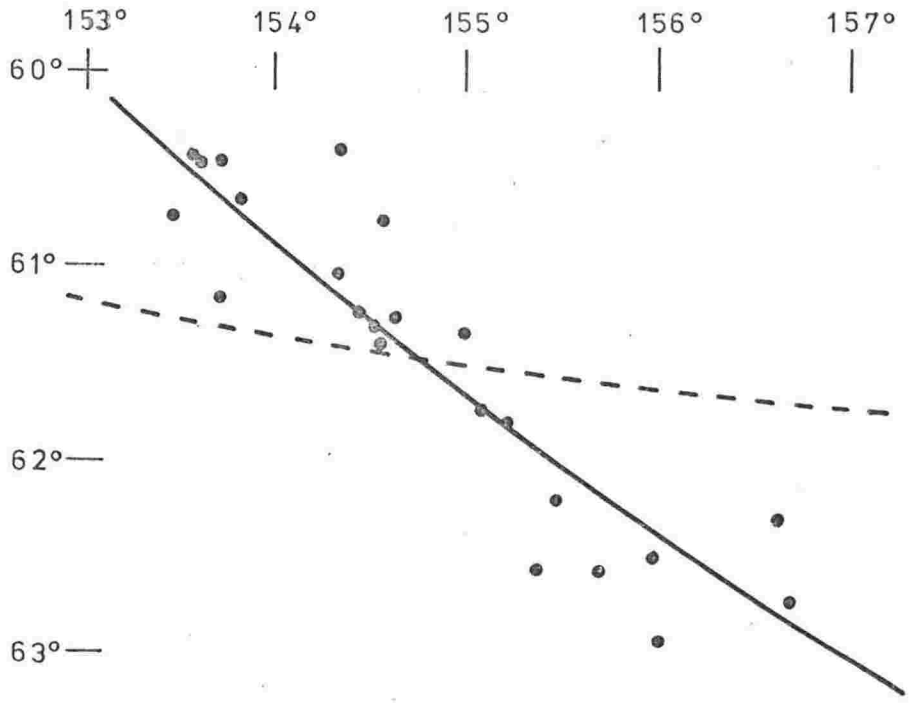


Fig. 8.24 Balleny fracture zone epicentres. Solid line is arc about epicentral pole 30°S, 166°W. Dashed arc is about "false" minimum at 50°S, 160°E.

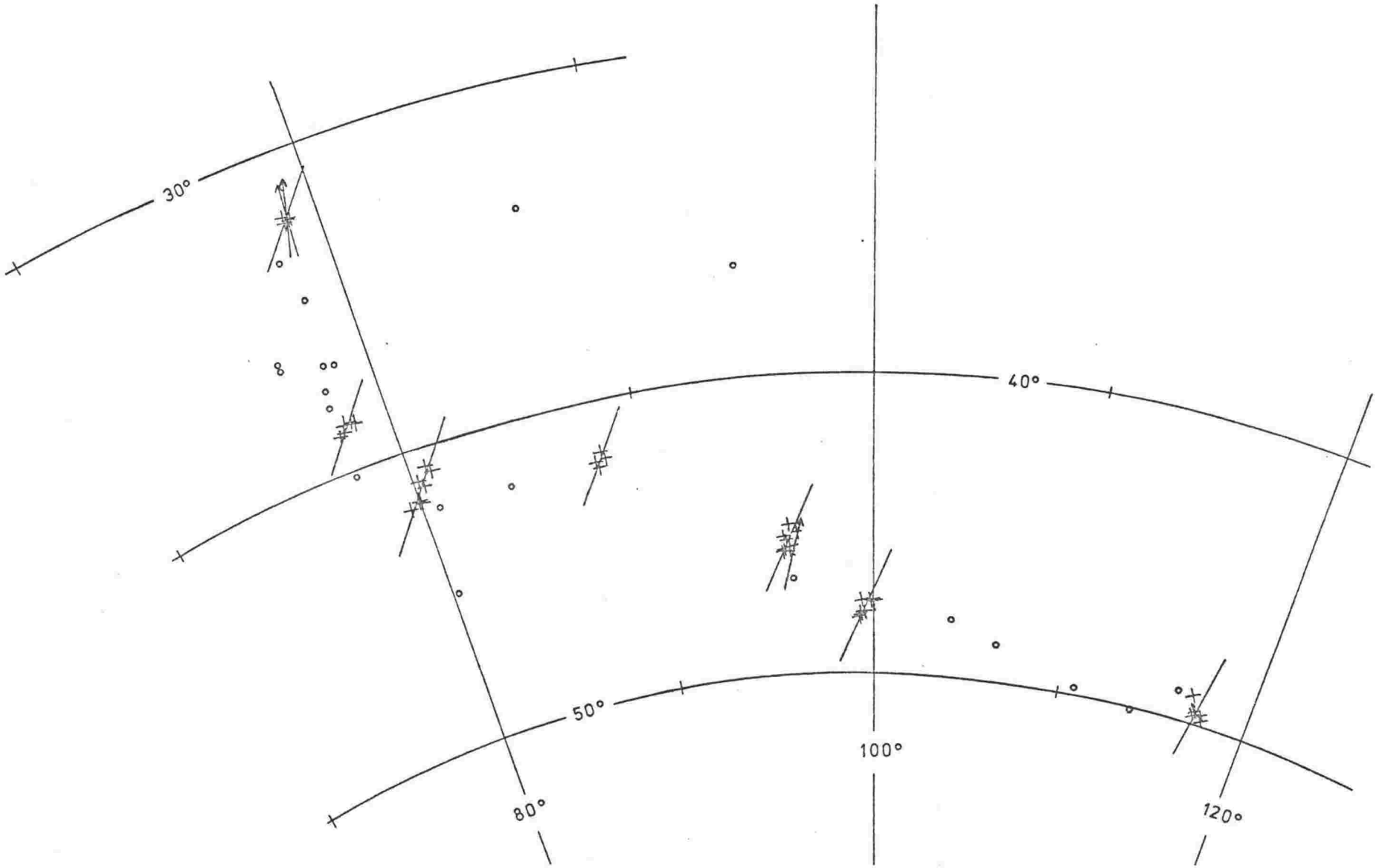


Fig. 8.25 Indian-Antarctic boundary west of 120°E. Crosses: epicentres used for epicentral method, circles: not used. Arcs about pole at 30°S, 166°W. Arrows indicate the slip vectors deduced from focal mechanism studies.

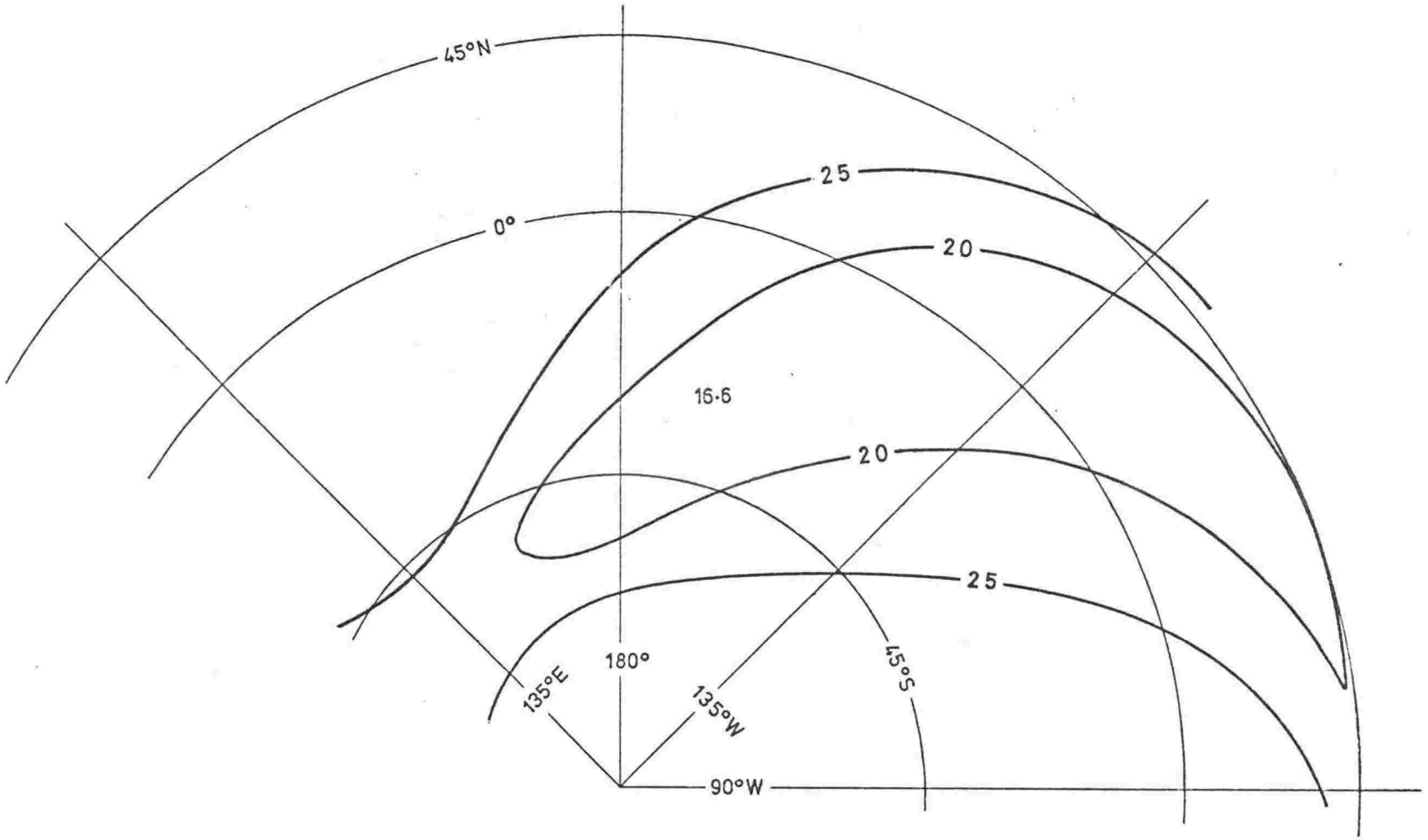


Fig. 8.26 Contours of epicentral standard deviation for the Indian-Antarctic pole, from data for whole boundary. Contour units are km, and the pole (30°S, 166°W) is at the decimal point of the number indicating value at pole. Equal area projection.

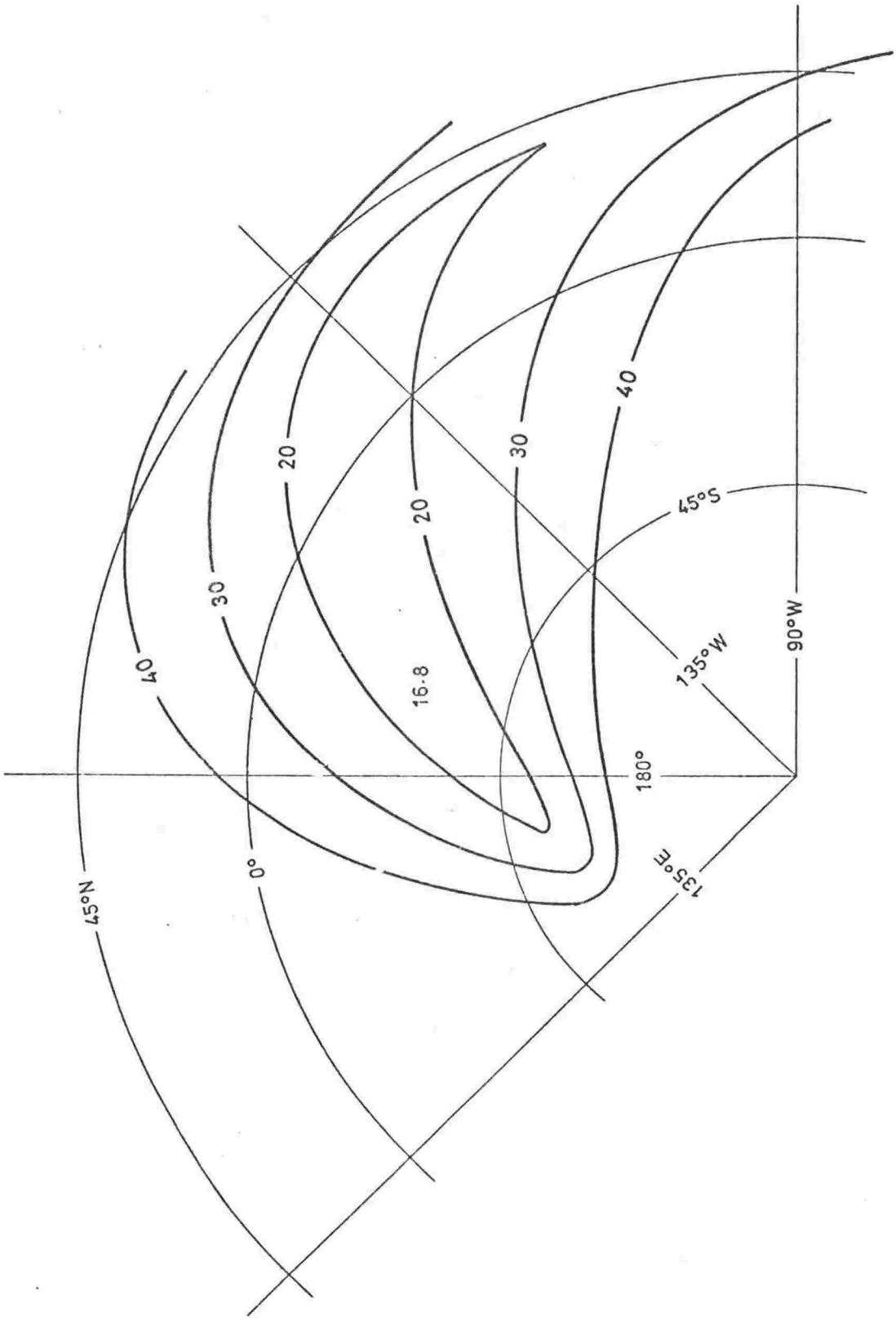


Fig. 8.27 Contours for the Indian-Antarctic pole when equal weighting of each fracture zone is used. Same data as Fig. 8.26, i.e. whole boundary, 9 zones.

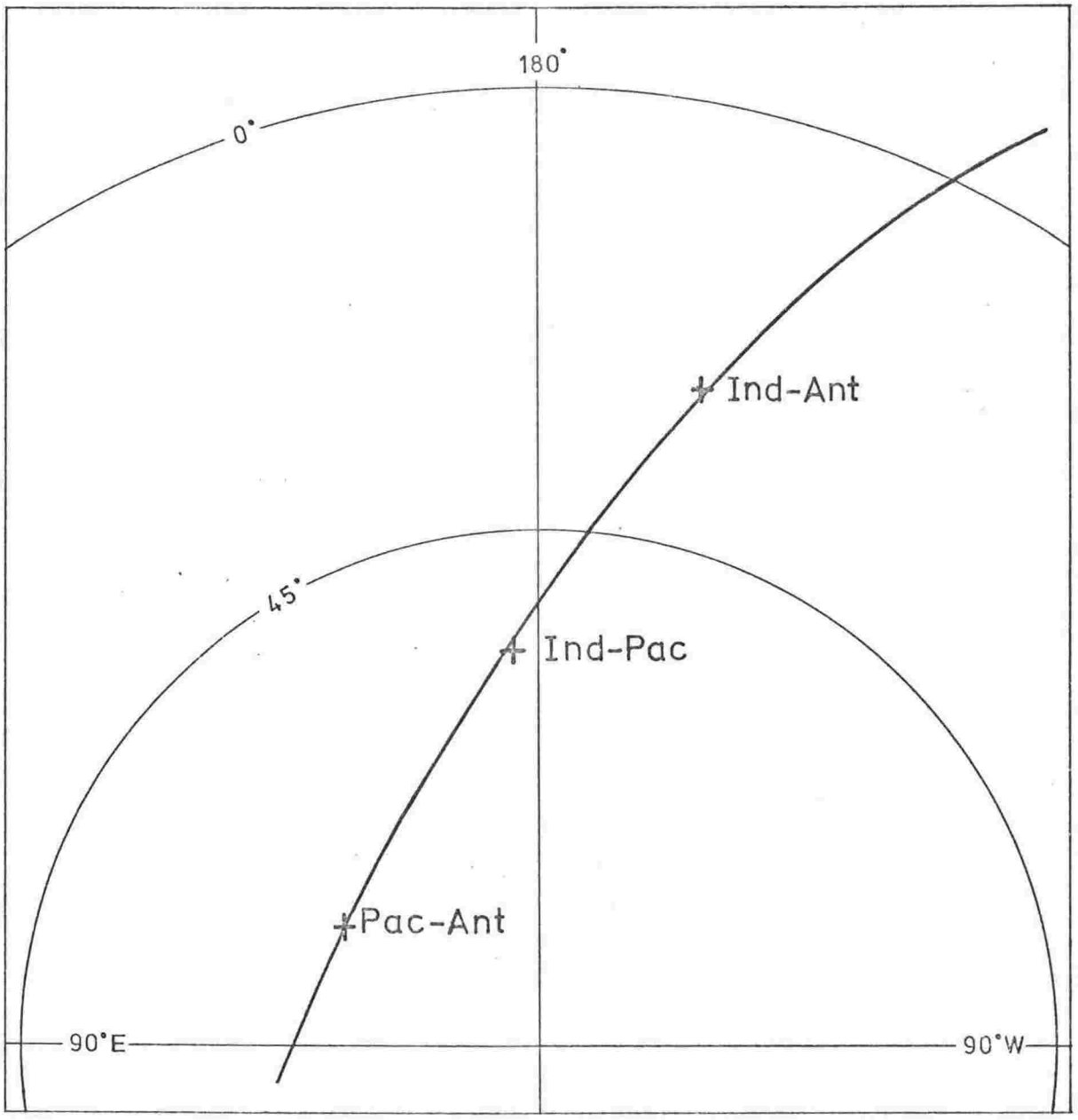


Fig. 8.28 The epicentral poles and the best fitting great circle through them. Equal area projection.

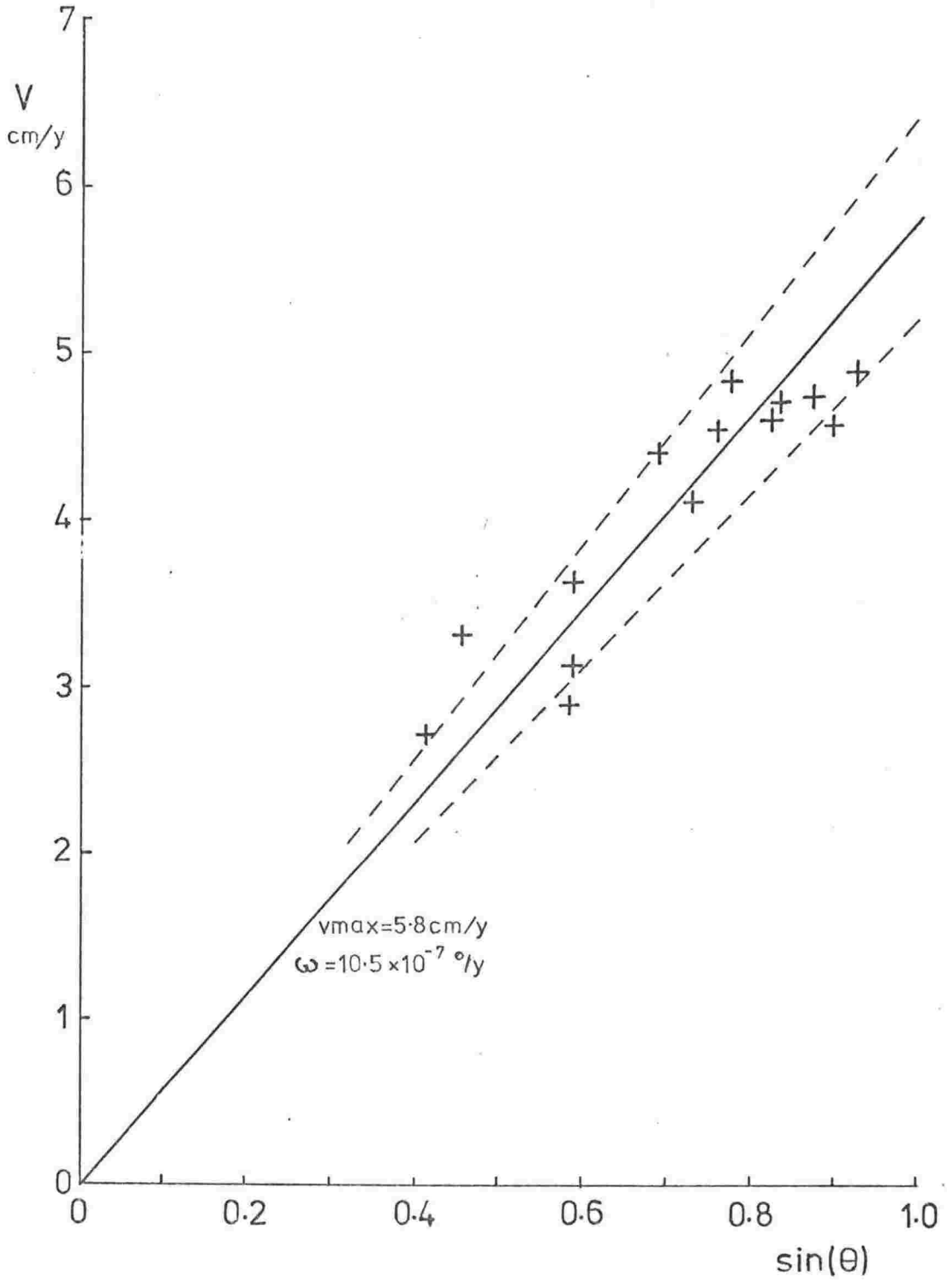


Fig. 8.29 Pacific-Antarctic boundary spreading rates, as a function of arc distance $\theta$ from the epicentral pole 71°S, 122°E. Rates are half spreading rates, calculated from the distance between anomaly 2 (1.79 mybp) on opposite sides of the Pacific-Antarctic ridge. Distances measured from profiles crossing the ridge, and projected parallel to direction of motion predicted from the pole position. Dashed lines are for vmax = 5.8 ± 10%. Data from Herron (1971, Fig. 3) and this study.

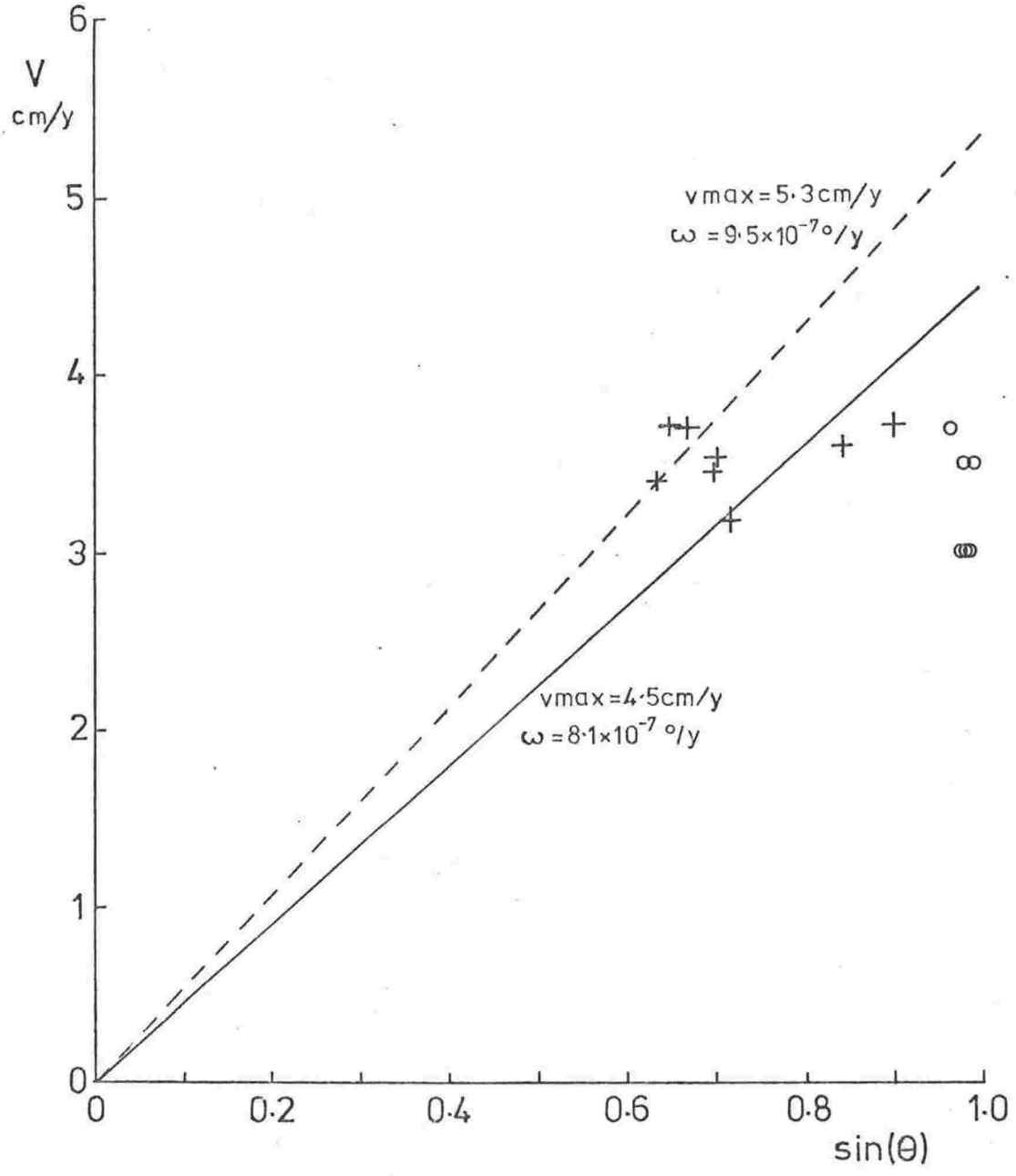


Fig. 8.30 Indian-Antarctic boundary spreading rates, as a function of arc distance $\theta$ from the epicentral pole 30°S, 166°W. Crosses are based on anomaly 2, data from Weissel and Hayes (1972, Fig. 2). Circles are based on anomaly 5, data from McKenzie and Sclater (1971, Table 2).

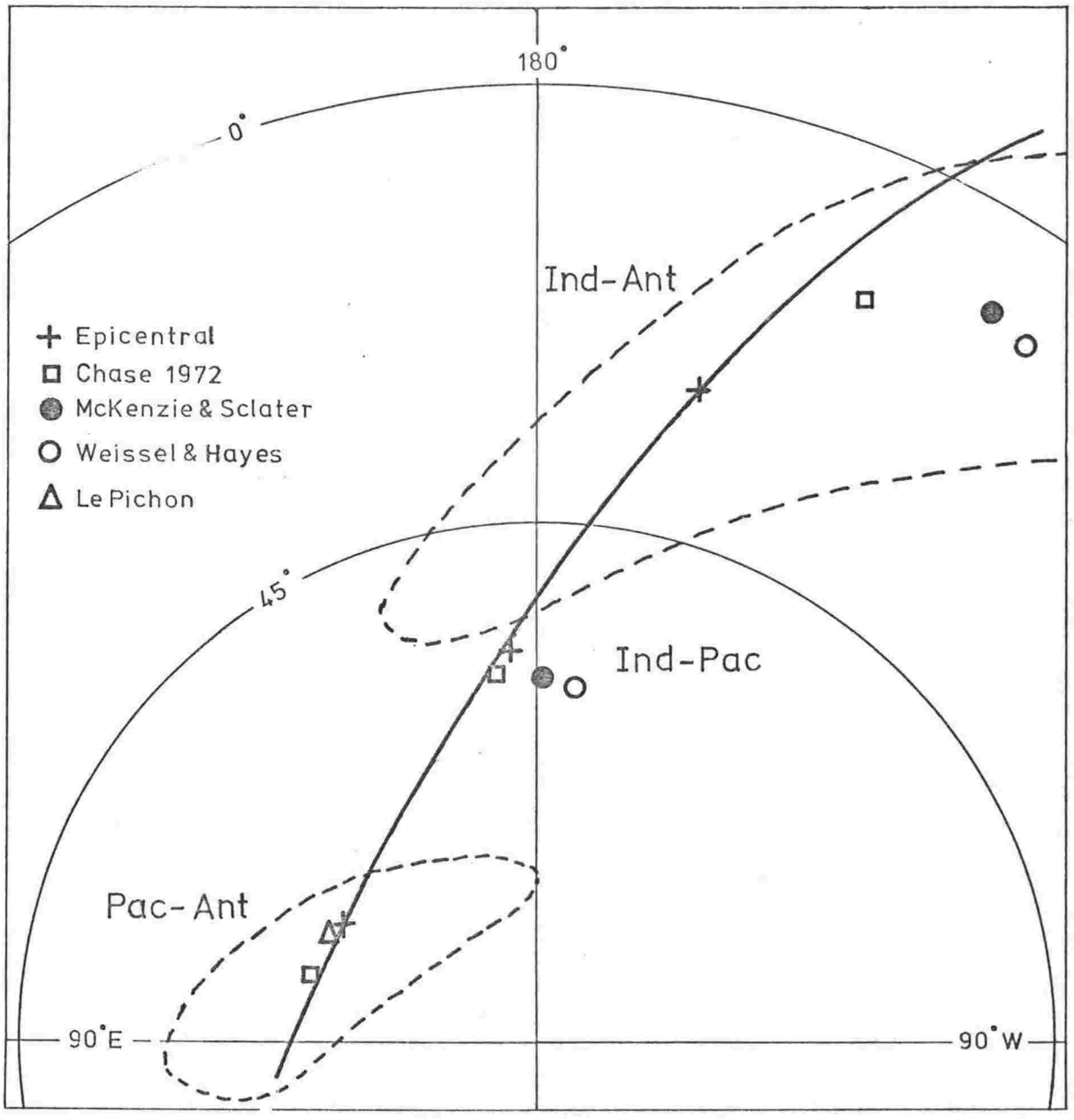


Fig. 8.31 The epicentral poles and other poles. Dashed lines indicate the confidence areas of the Pacific-Antarctic and Indian-Antarctic epicentral poles. The area for the Indian-Pacific pole is too small to show. Heavy arc is great circle through epicentral poles. Equal area projection.

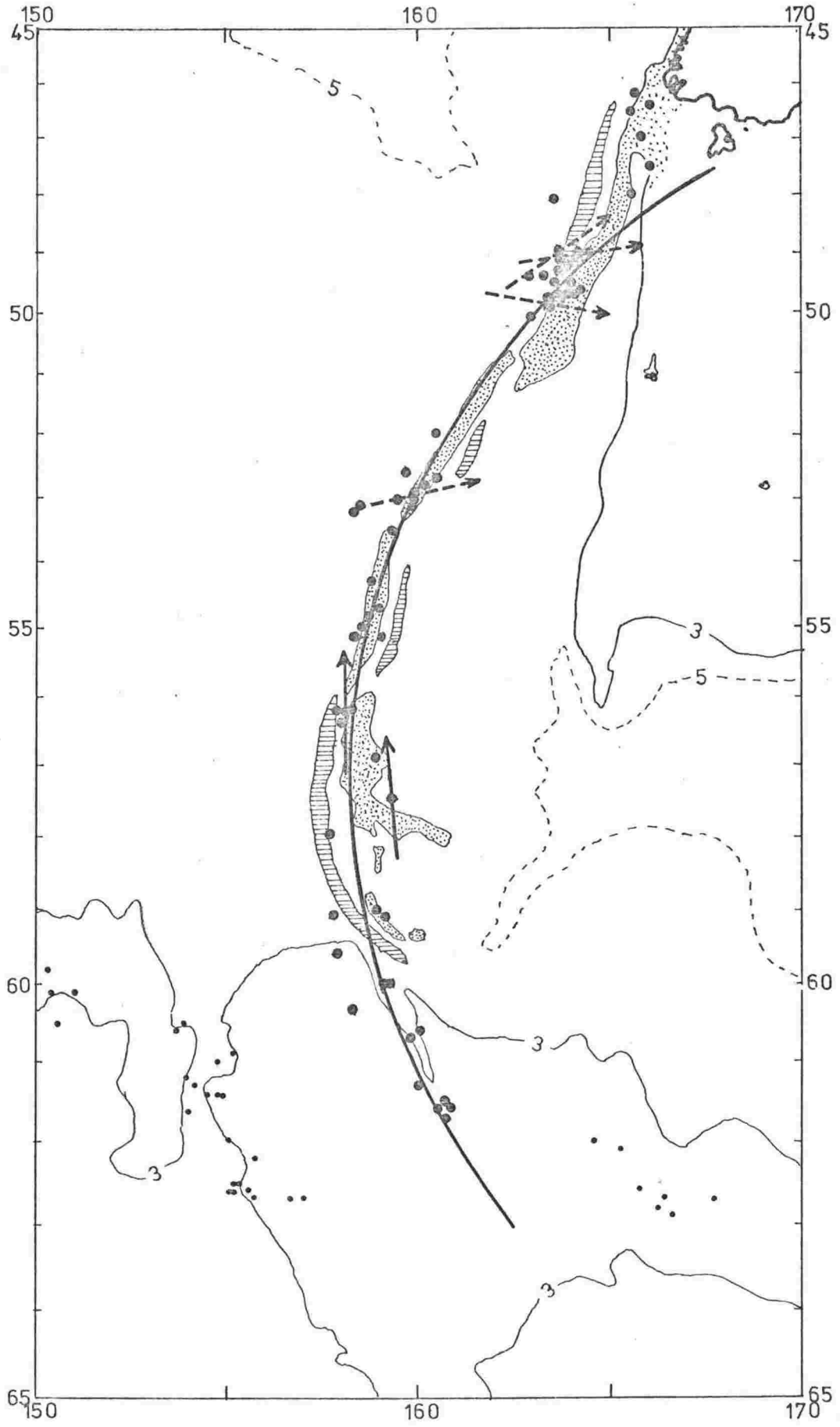


Fig. 8.32 The Macquarie ridge complex. Arc is about the epicentral pole 56°S, 176°E. Epicentres are USCGS locations 1964 - Mar 1972. Slip vectors deduced from focal mechanism studies are indicated by arrows centred on the relevant epicentres. Dashed arrows - thrust motion; solid arrows - strike-slip. Stippled areas of complex are shallower than 3 km, hatched areas deeper than 5 km.

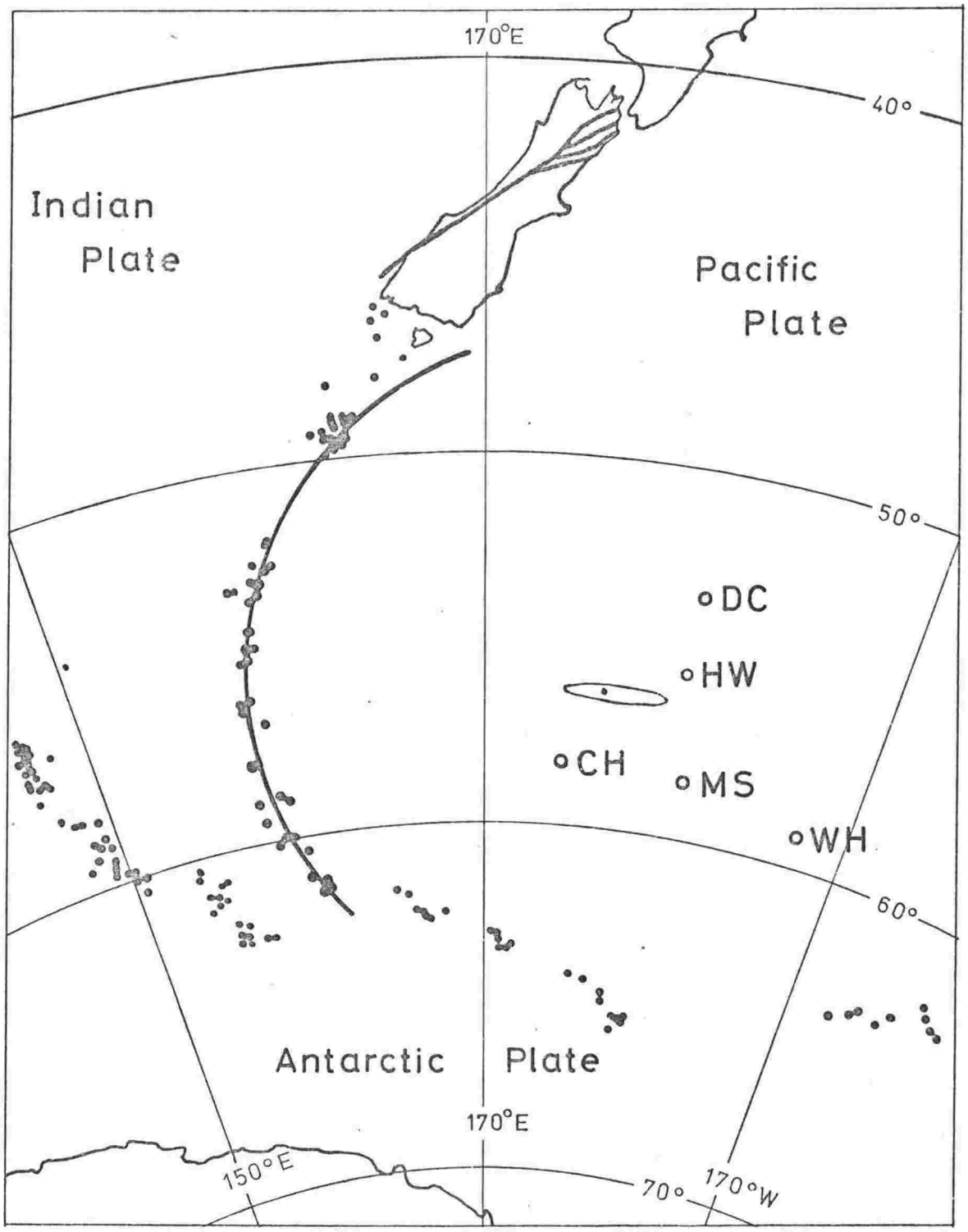


Fig. 8.33 Indian-Pacific pole positions. The oval is the epicentral pole confidence area. Other poles as follows. DC : Christoffel (1971), model 2. HW : Wellman (1973a). MS : McKenzie and Sclater (1971). WH : Weissel and Hayes (1972). CH : Chase (1972). Heavy arc is about the epicentral pole. Lines in the South Island, New Zealand are the Alpine fault and its major branches.

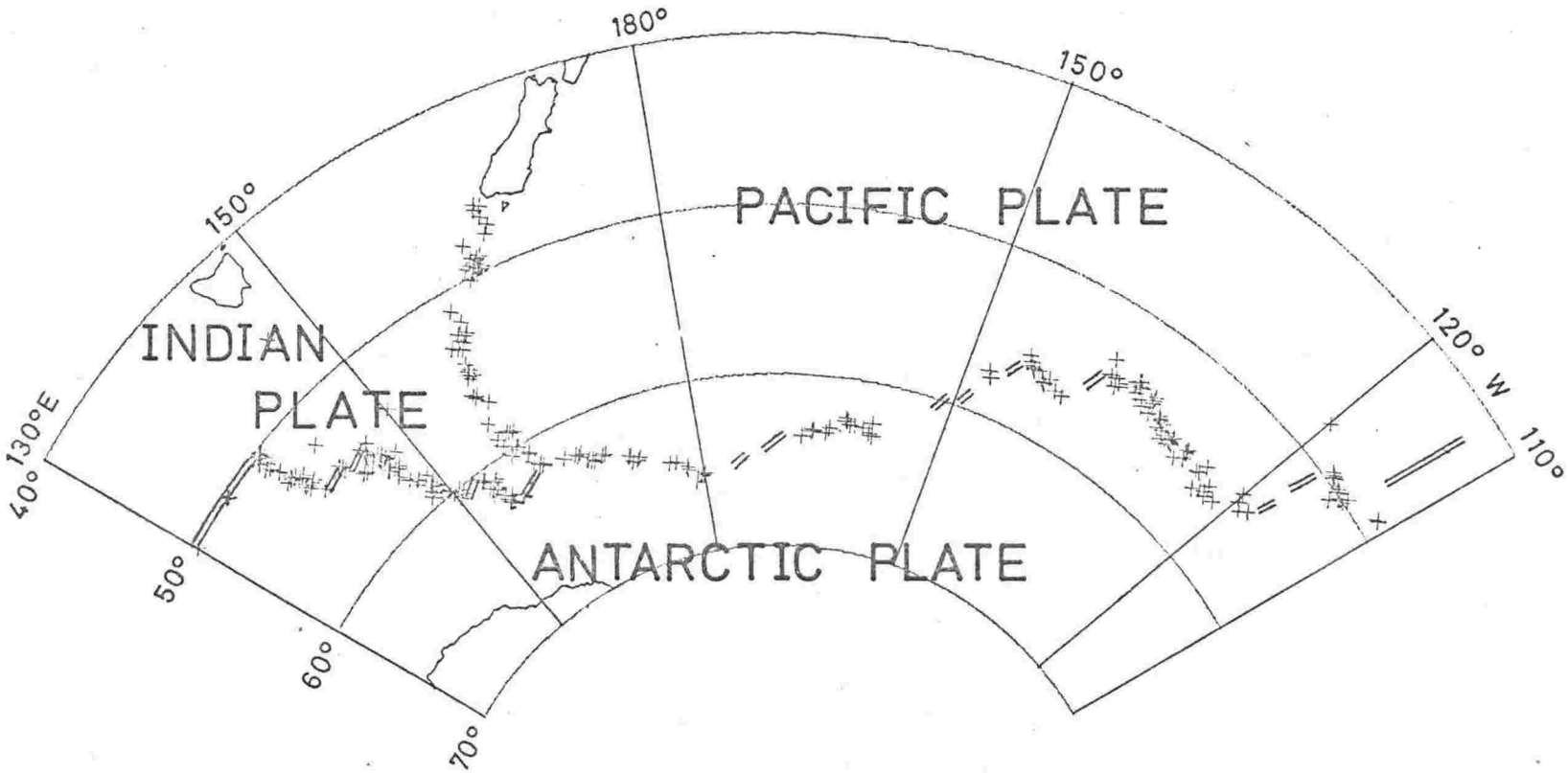


Fig. 9.1 The plates in the southwest Pacific area. Plate boundaries are indicated by epicentres (crosses), and known axes of spreading ridges (double lines). Epicentres are from the USCGS for 1964 - 1972. Epicentres which delineate the Indian-Pacific boundary through New Zealand are not shown.

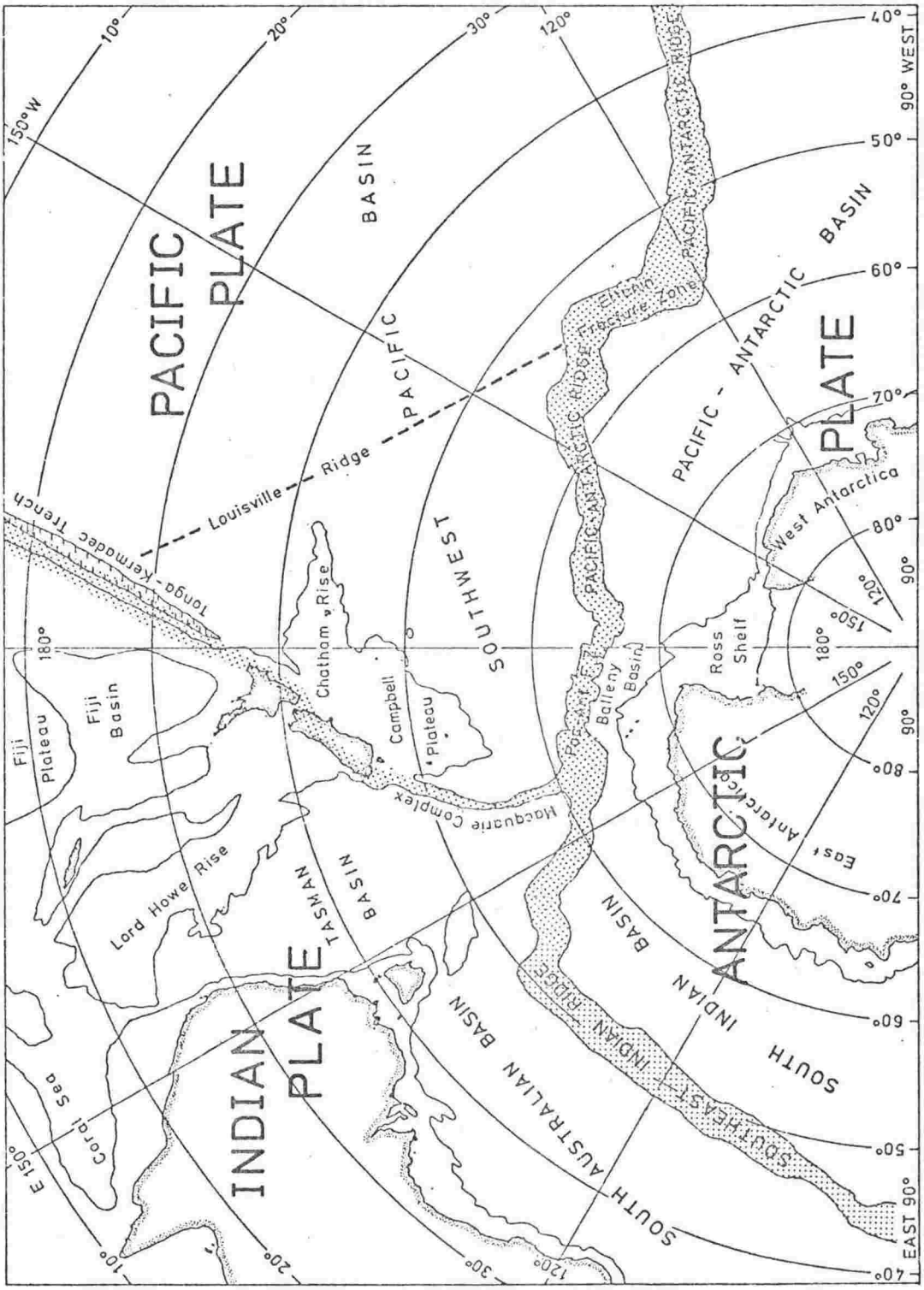


Fig. 9.2 Plate boundaries and morphology in the southwest Pacific area. Major morphologic features are outlined by the 3 km contour; and 6 km for the Tonga-Kermadec trench. Plate boundaries are indicated by the stippled areas.

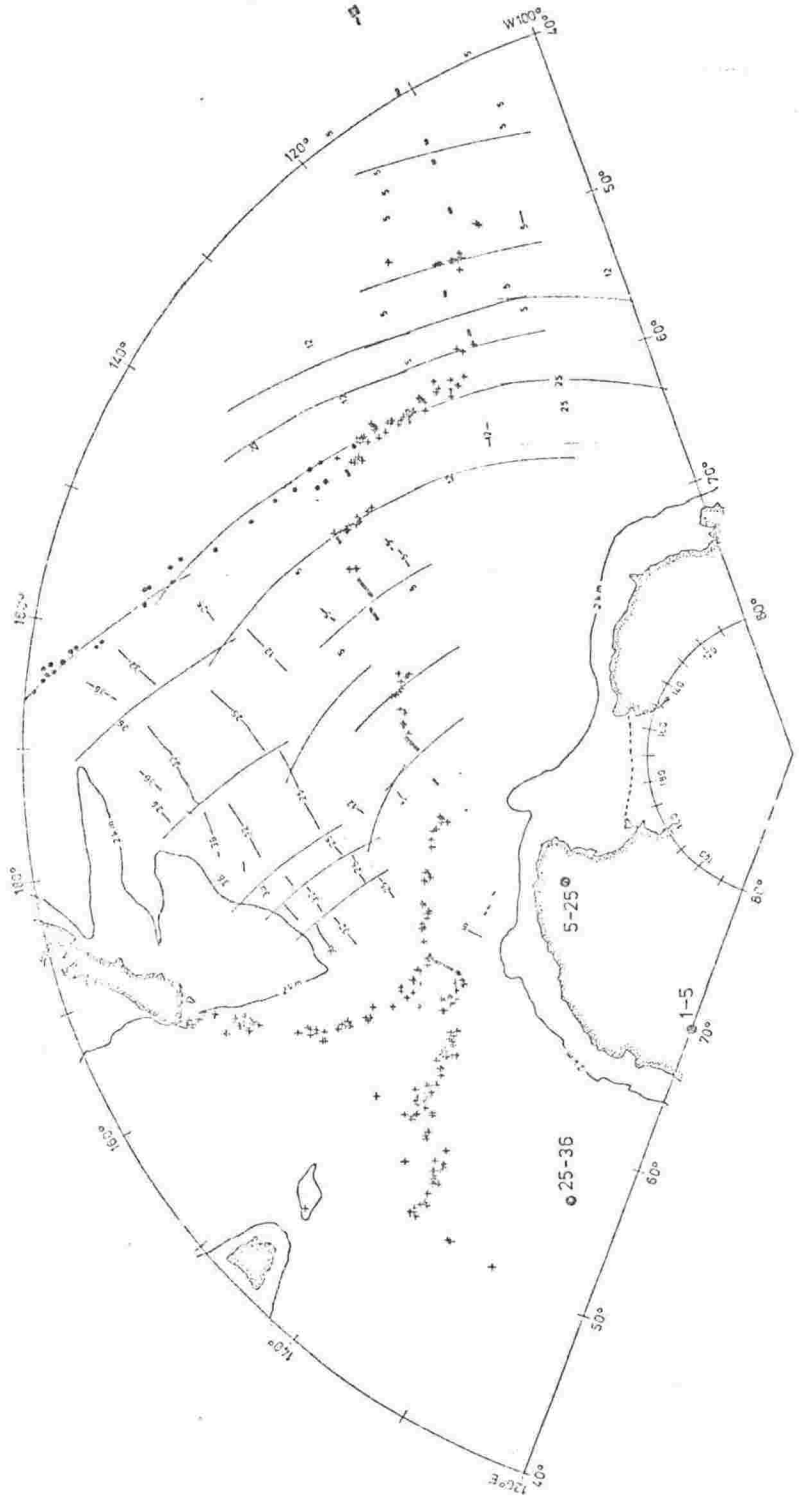


Fig. 9.3 Reduced copy. See pocket for full size diagram.

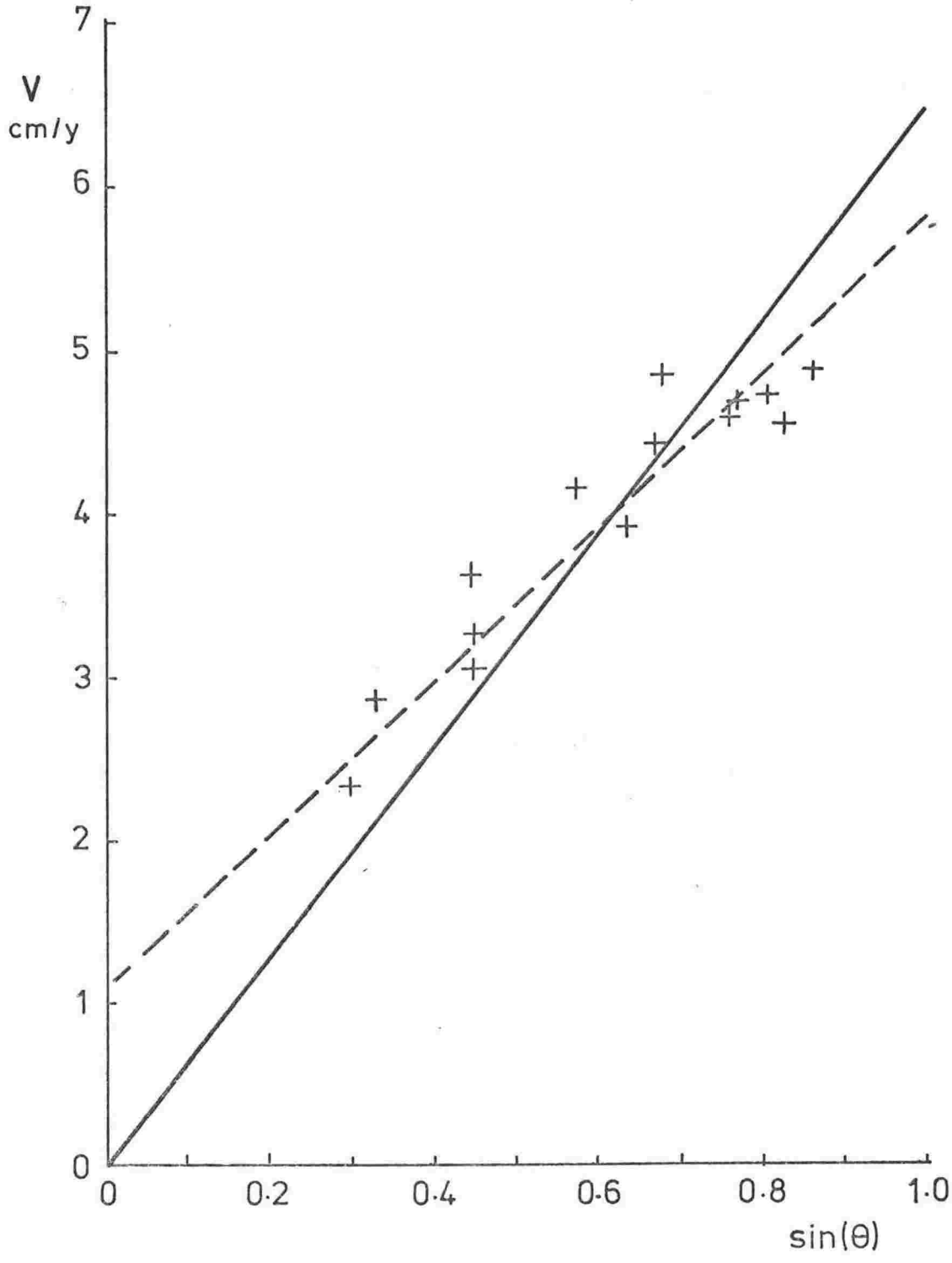


Fig. 9.4 Pacific-Antarctic boundary spreading rates as a function of arc distance θ from a pole at 76°S, 144°E. Rates are half spreading rates, calculated from the distance between anomaly 2 (1.79 mybp) on opposite sides of the Pacific-Antarctic ridge. Distances measured from profiles crossing the ridge, and projected parallel to the direction of motion predicted from the pole position. If the pole position was "correct" the data should fit the straight line through the origin. Dashed line is a visually estimated straight line through the data; but note that a best fitting line should not be exactly straight unless through the origin.

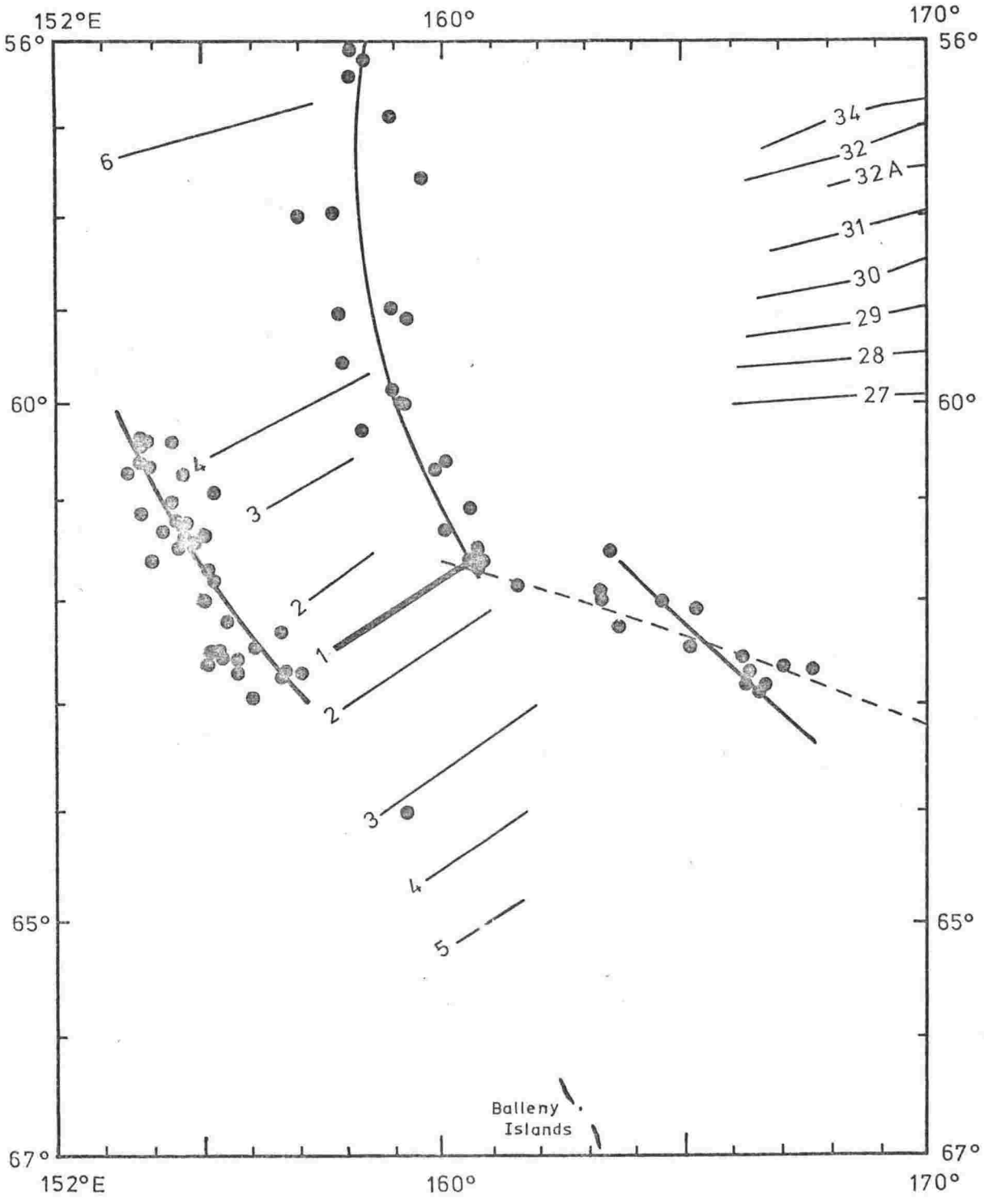


Fig. 9.5 The Indian-Antarctic-Pacific triple junction area. Anomaly lineations are shown numbered; anomaly 1 is the axis of the southeast Indian ridge. Arcs through the epicentres (dots) are the arcs defined by the epicentral method. The dashed line is about the "alternative" Pacific-Antarctic epicentral pole at 76°S, 144°E. Note: The epicentres shown are for 1950 - 1972, from Sykes and the USCGS. The Pacific-Antarctic and Indian-Pacific epicentral arcs were defined from only USCGS epicentres 1964 - 1972, and the Indian-Antarctic arc (the Balleny fracture zone) from only Sykes' epicentres 1950 - 1966.

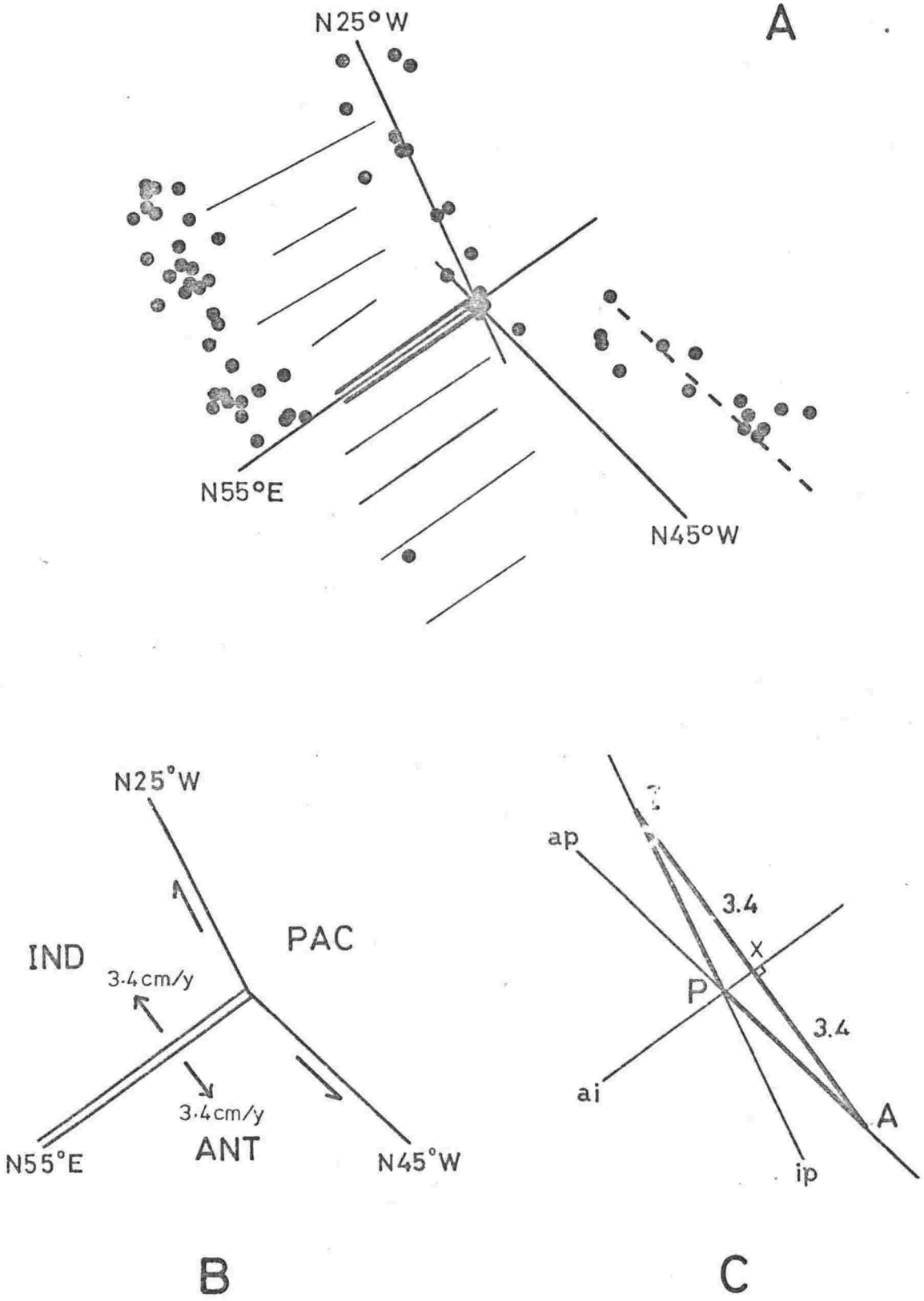


Fig. 9.6 The triple junction : structure and velocity diagrams. A : The anomaly lineations and epicentres of the area, with the assumed trends at the junction shown. B : The assumed physical configuration of the junction. C : The velocity space configuration.

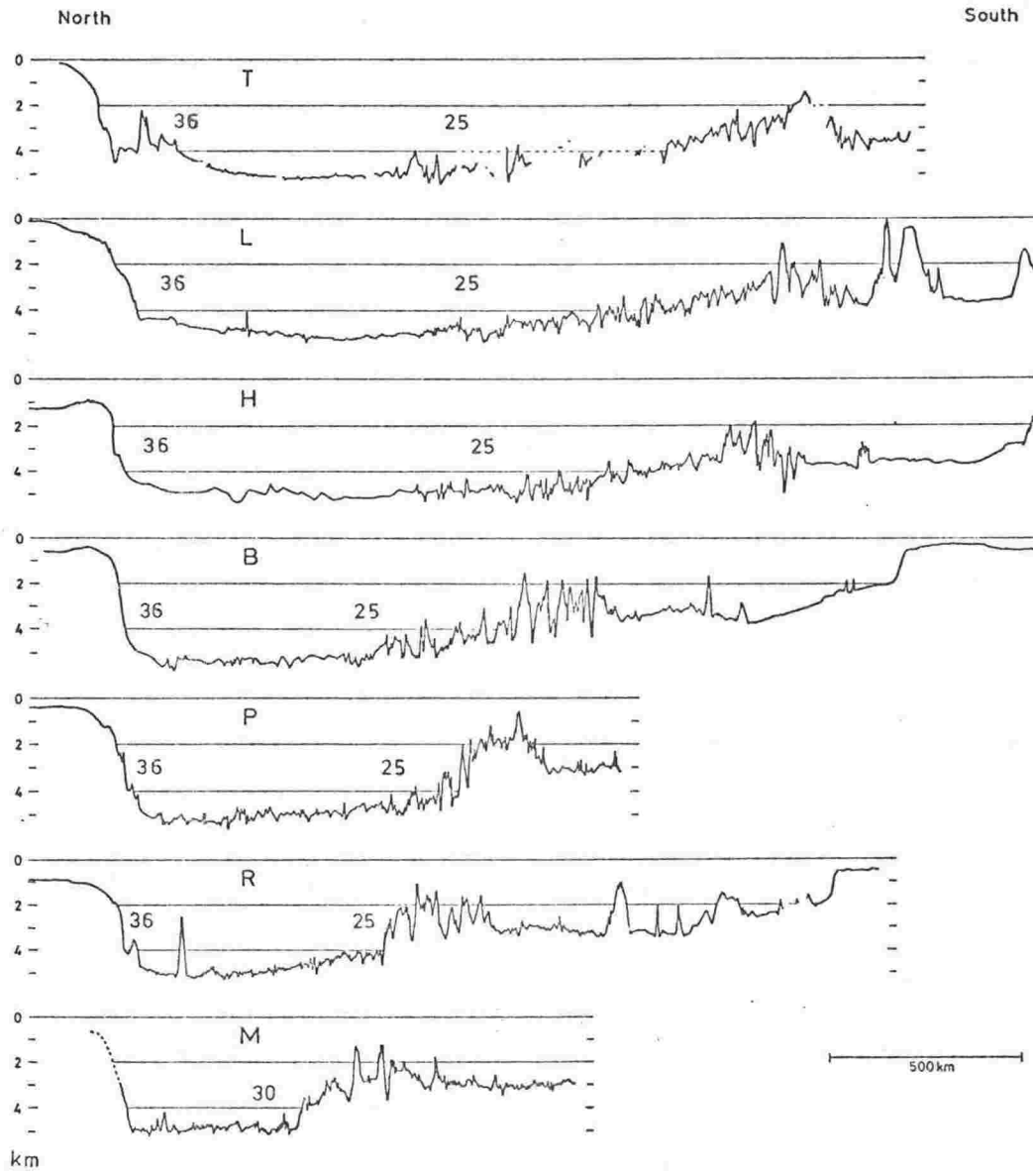


Fig. 9.7 Representative bathymetric profiles between 178°W and 165°E. Profiles are approximately north-south; eastern most one at the top. They are aligned approximately on the Campbell plateau margin, except for profile T which at the north passes over part of the Bollons seamount then up the eastern edge of the Campbell plateau. Numbers indicate the positions of anomalies 25 and 36 observed on or near each profile. On profile M only anomalies 30 and 31 are identifiable, and no identifiable anomalies are seen west of this profile.

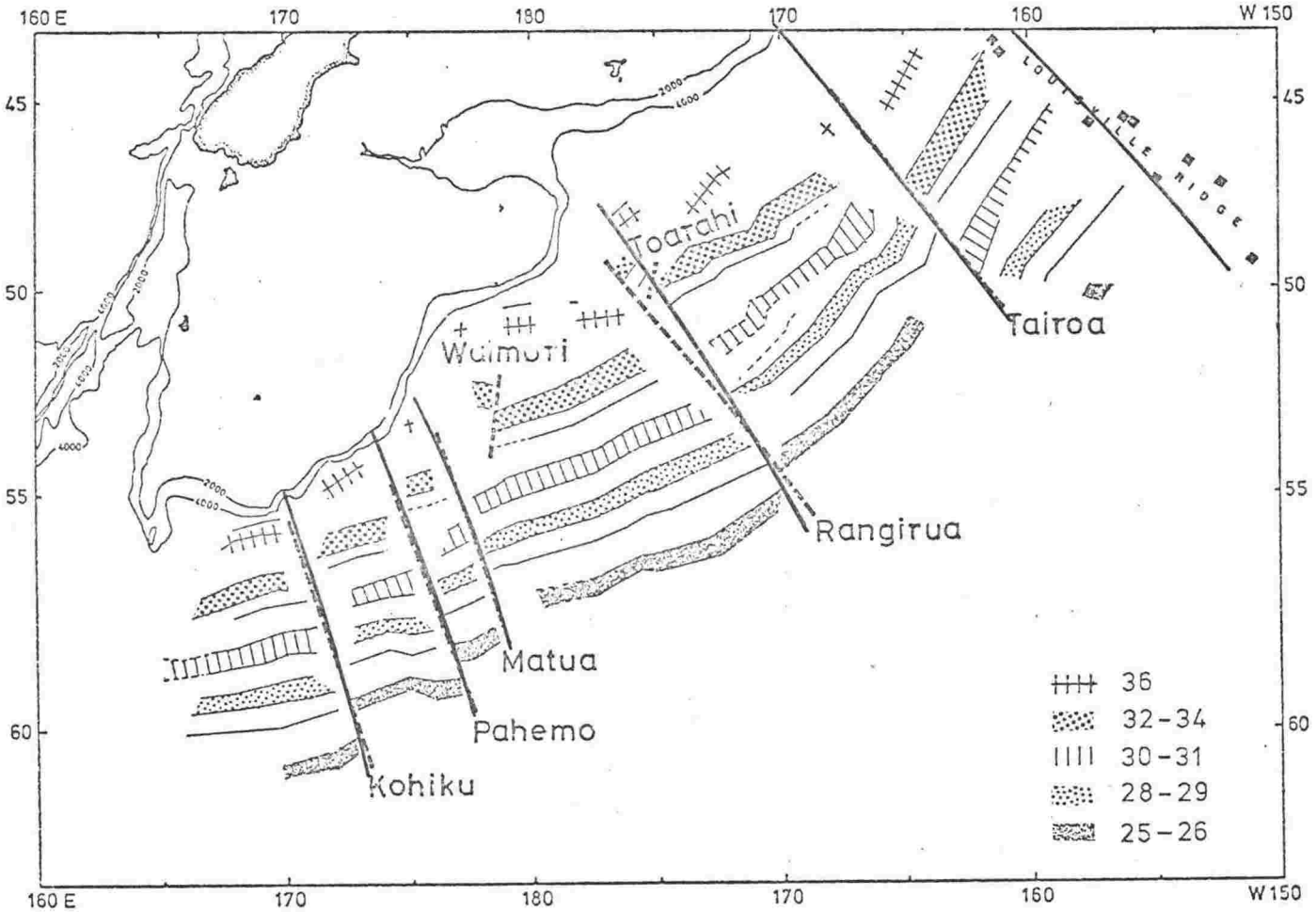


Fig. 9.8 Anomaly trends and fracture zones in the southwest Pacific basin. A copy of Fig. 4.8, with arcs (solid lines) about the Cretaceous pole superimposed on some of the fracture zones.

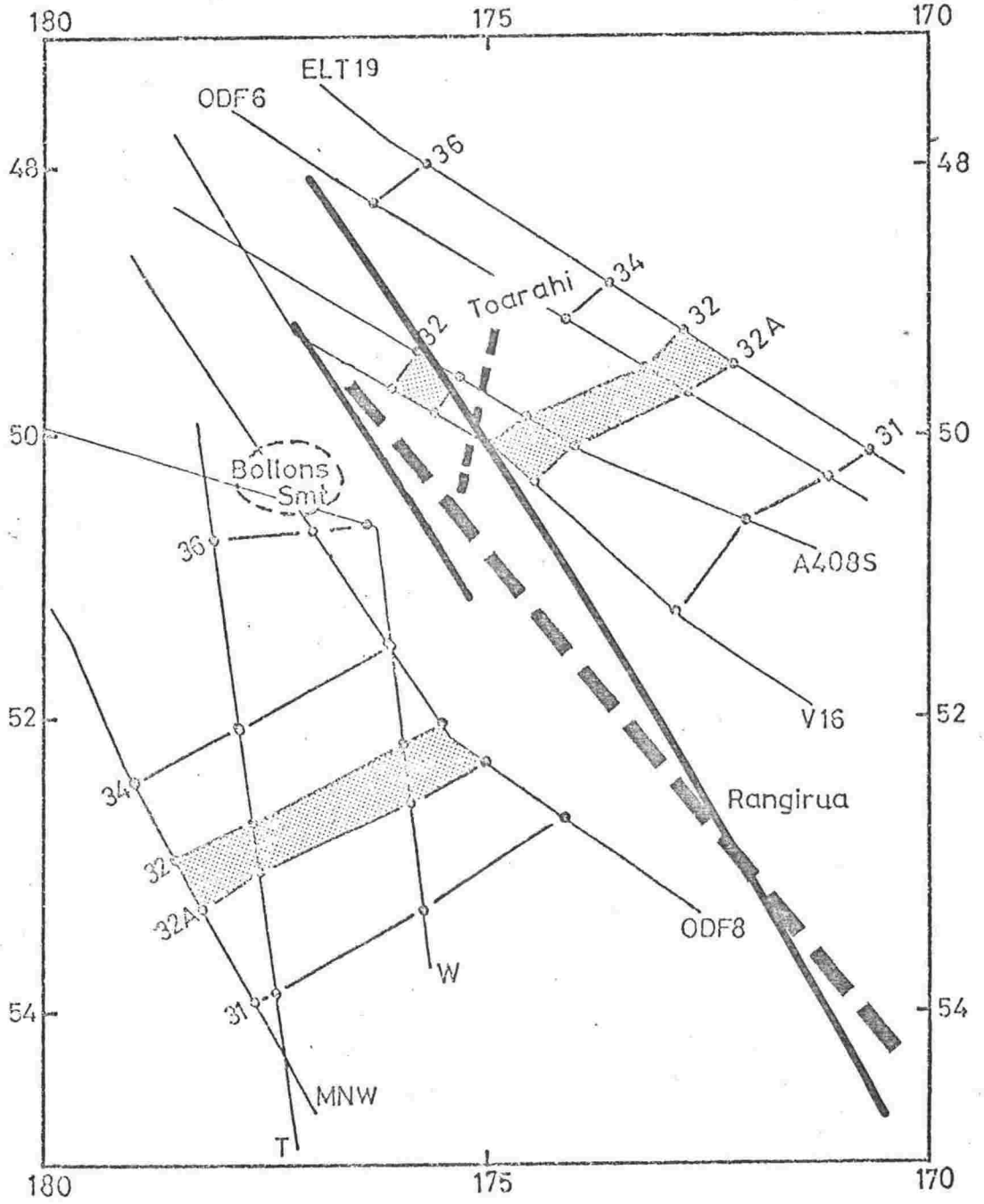


Fig. 9.9 The area of the Toarahi and Rangirua fracture zones. A copy of Fig. 4.12, with arcs (heavy solid lines) about the Cretaceous pole added. The long line is a detail of that shown in Fig. 9.8. Dashed lines indicate the original interpretation of the Toarahi and Rangirua fracture zones.

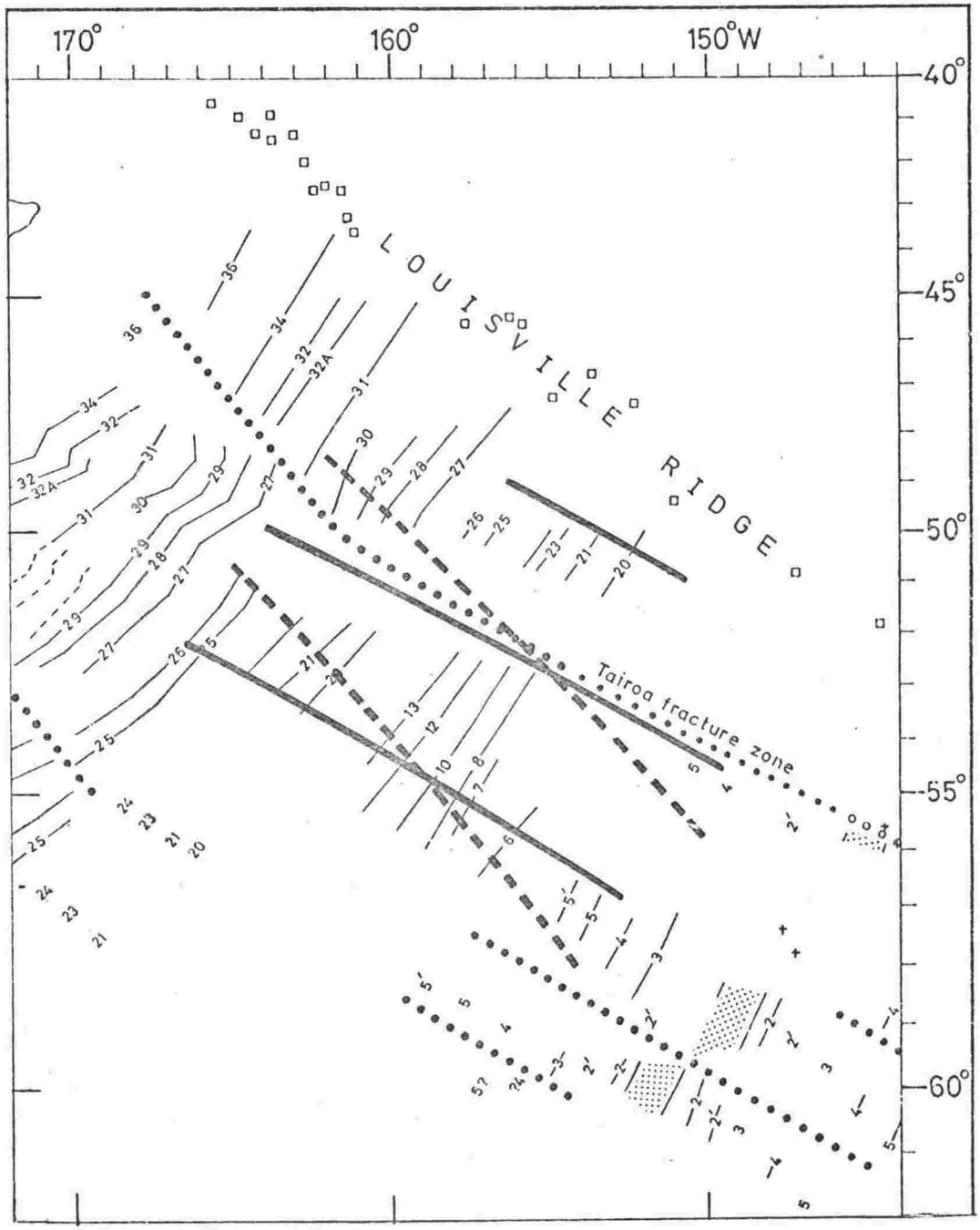


Fig. 9.10 Anomaly lineations and arcs about poles for anomalies 5 to 25. Heavy lines are about the adopted pole 72°S, 160°E. Dashed lines are about 64°S, 160°E.

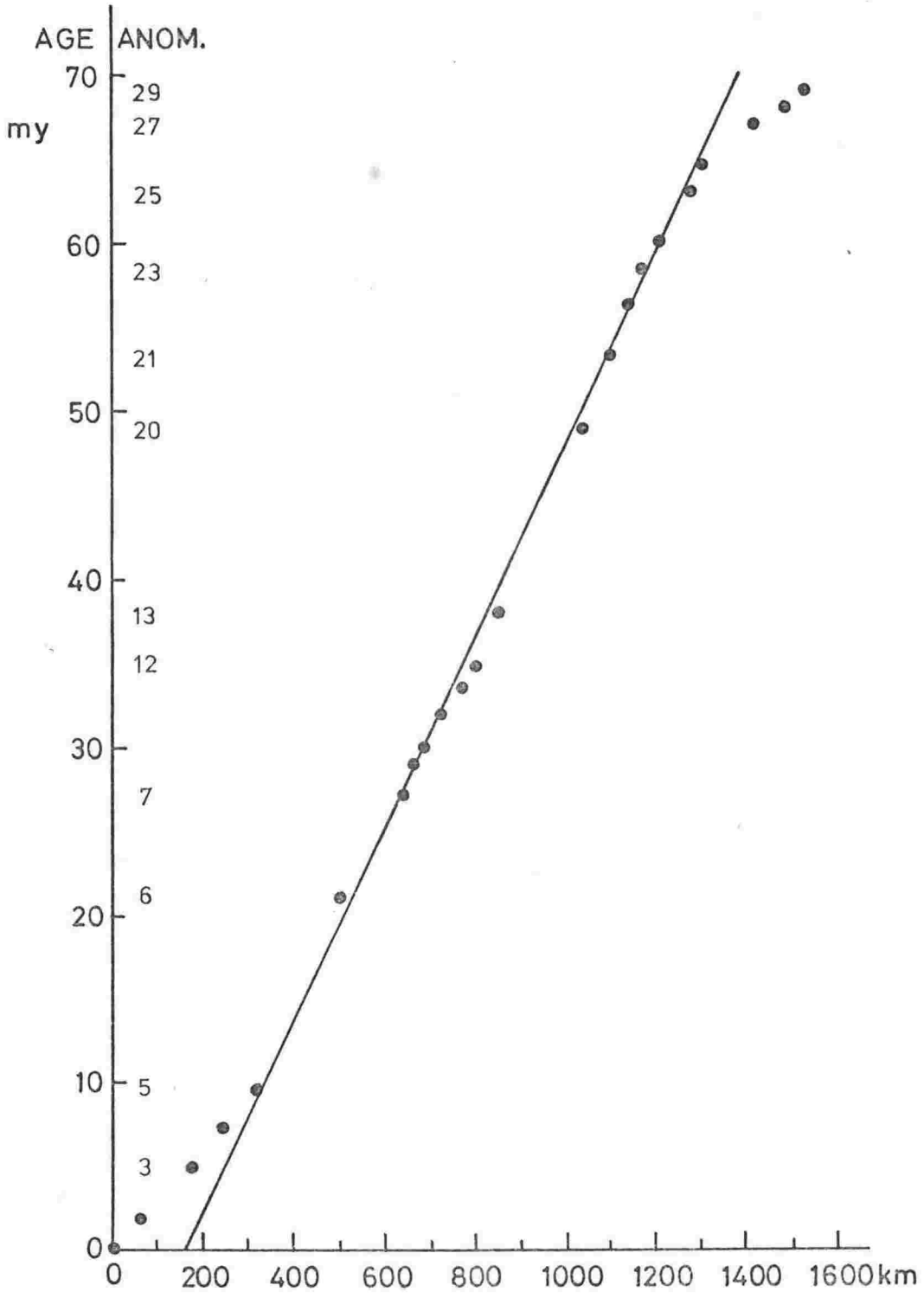


Fig. 9.11 Seafloor age versus distance from the axis, for a profile perpendicular to the anomaly lineations west of the Tairoa fracture zone (Fig. 9.10). The line through the points is for a spreading rate of 1.7 cm/y. This rate is calculated from a pole at 72°S, 160°E and a rotation of 22° for the interval 10 to 63 mybp.

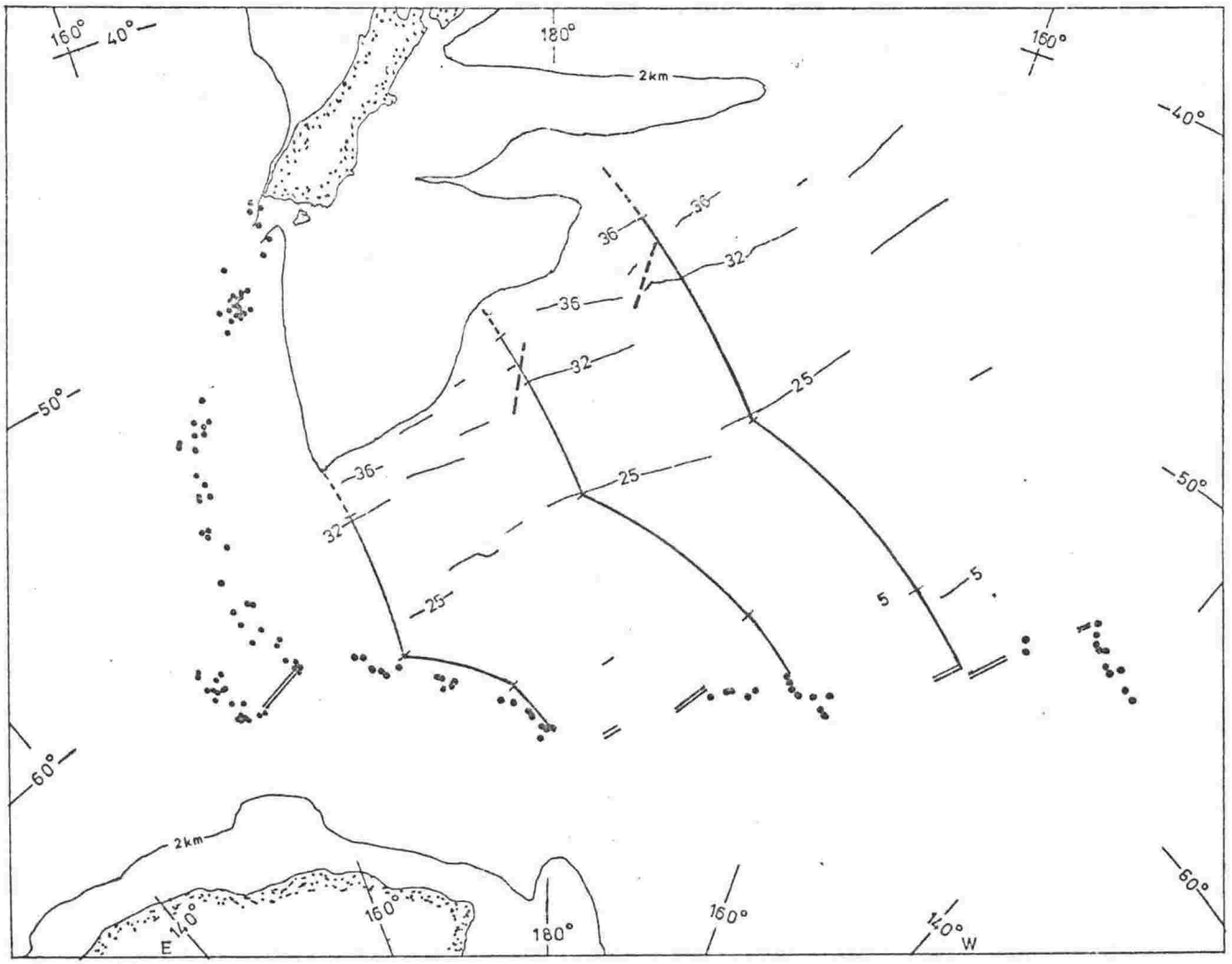


Fig. 9.12 Three representative sets of arcs in the southwest part of the Pacific plate. Each line starts from a point at the Pacific-Antarctic boundary and consists of an arc about each of the poles in Table 9.2 with the rotation angles stated there. Stereographic projection.

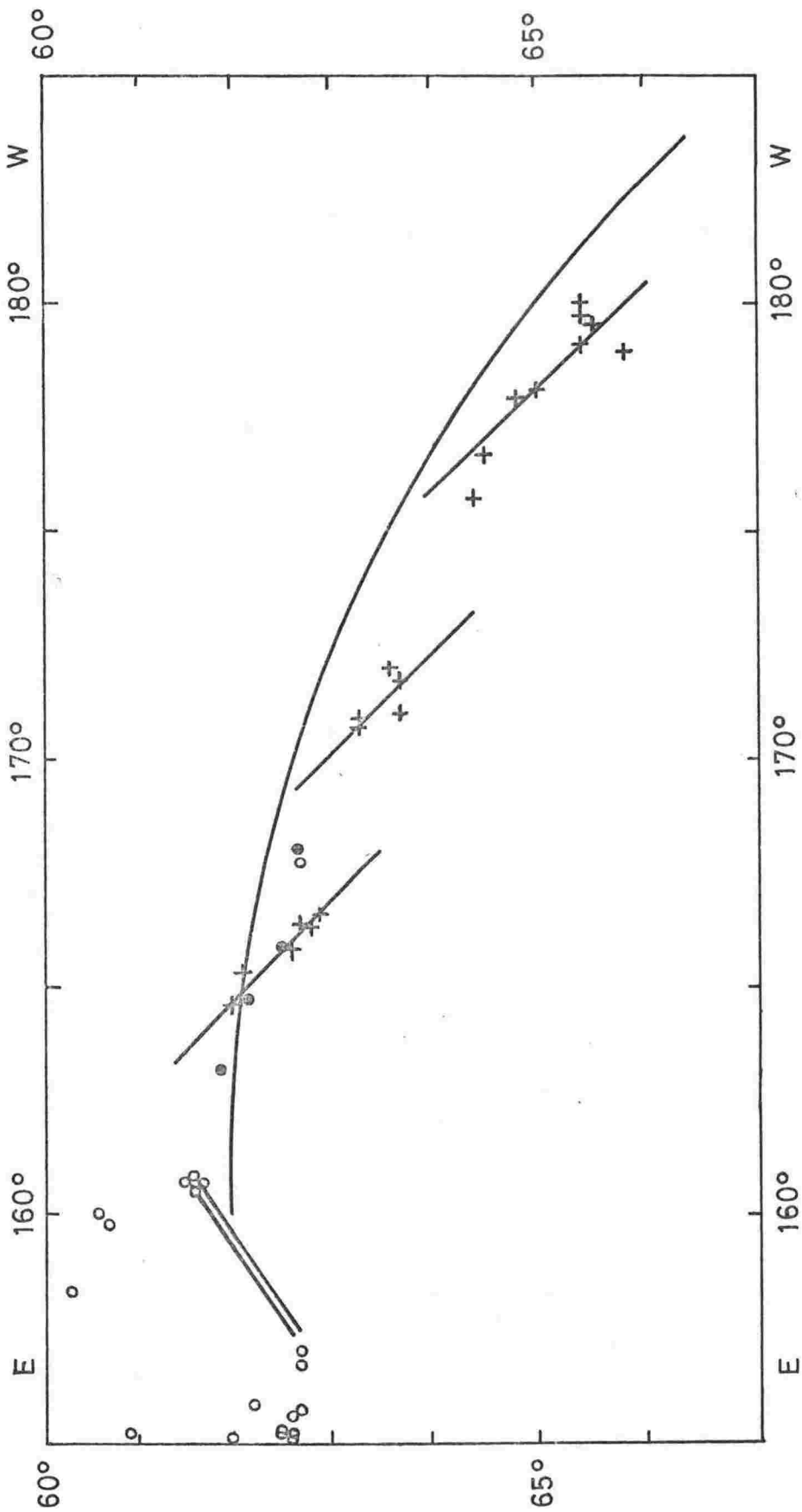


Fig. 9.13 The Pacific-Antarctic fracture zone area. The short arcs are those defined by the epicentral method, and are about 71°S, 122°E. The long arc is an arc 10° distant from the 10 - 63 mybp pole at 72°S, 160°E. Crosses are USCGS epicentres used for the epicentral method, open circles are epicentres that were not used. Closed circles are epicentres March 1972 - December 1972 that were not available when the epicentral calculations were done.

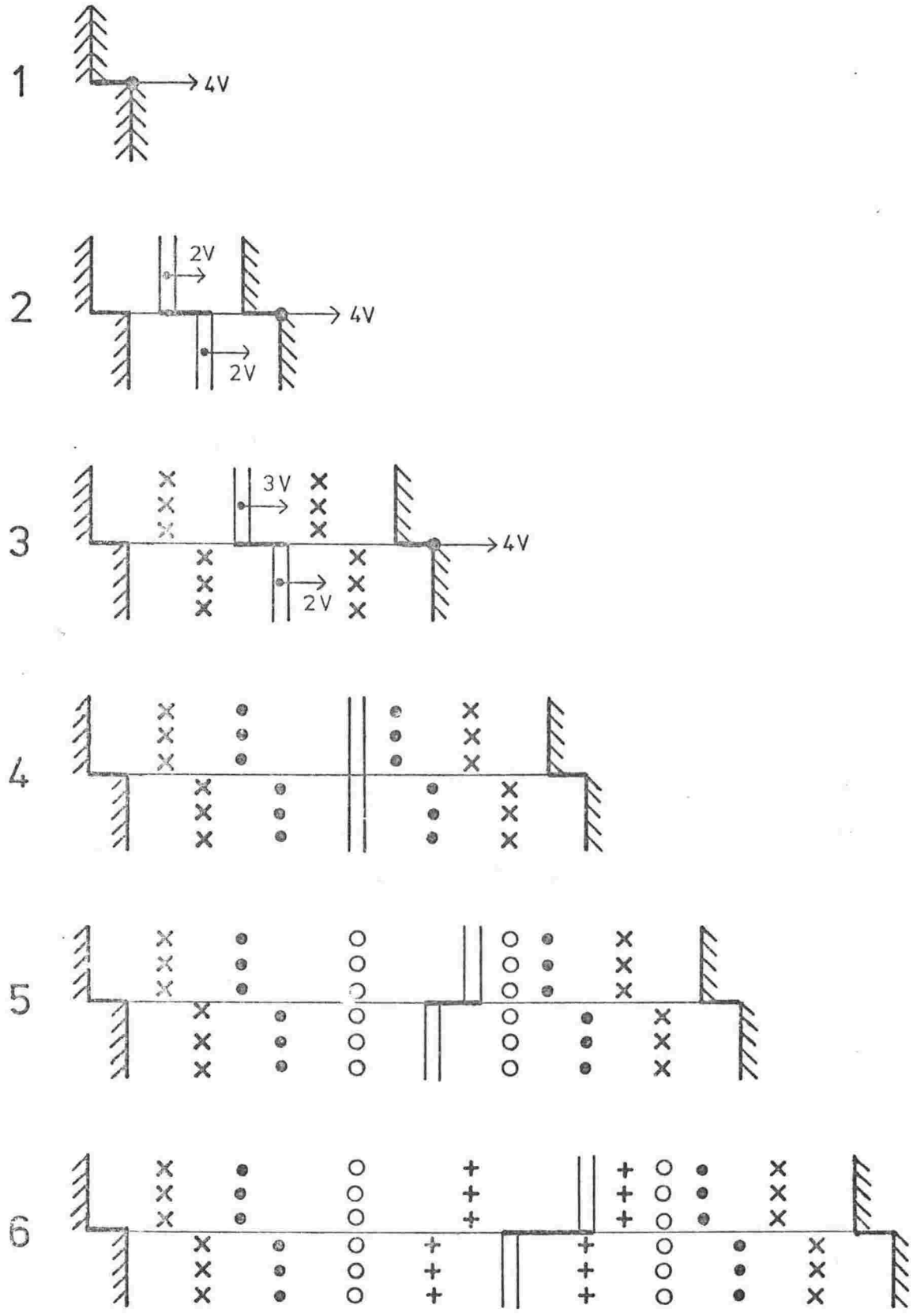


Fig. 9.14 A model for changing a sinistral offset into a dextral offset. Movement of two plates is shown for five equal time intervals. The plates are separating at a relative velocity of 4V throughout. Left plate is shown fixed but it needn't be. Double lines are the positions of the spreading axes, and velocities on the ridge are the velocity of the ridge relative to the left plate. Velocity of upper ridge changes at time 3 but stays at 3V thereafter. Lower ridge moves at 2V throughout.


Fig. 9.15 Hypothetical fracture zones for the movement of New Zealand from Antarctica as given by data in Table 9.3. The arcs were drawn starting from positions close to anomaly 36 in the southwest Pacific basin. Generalized 2 km contours are shown. Note: The arcs are not flow paths for New Zealand.

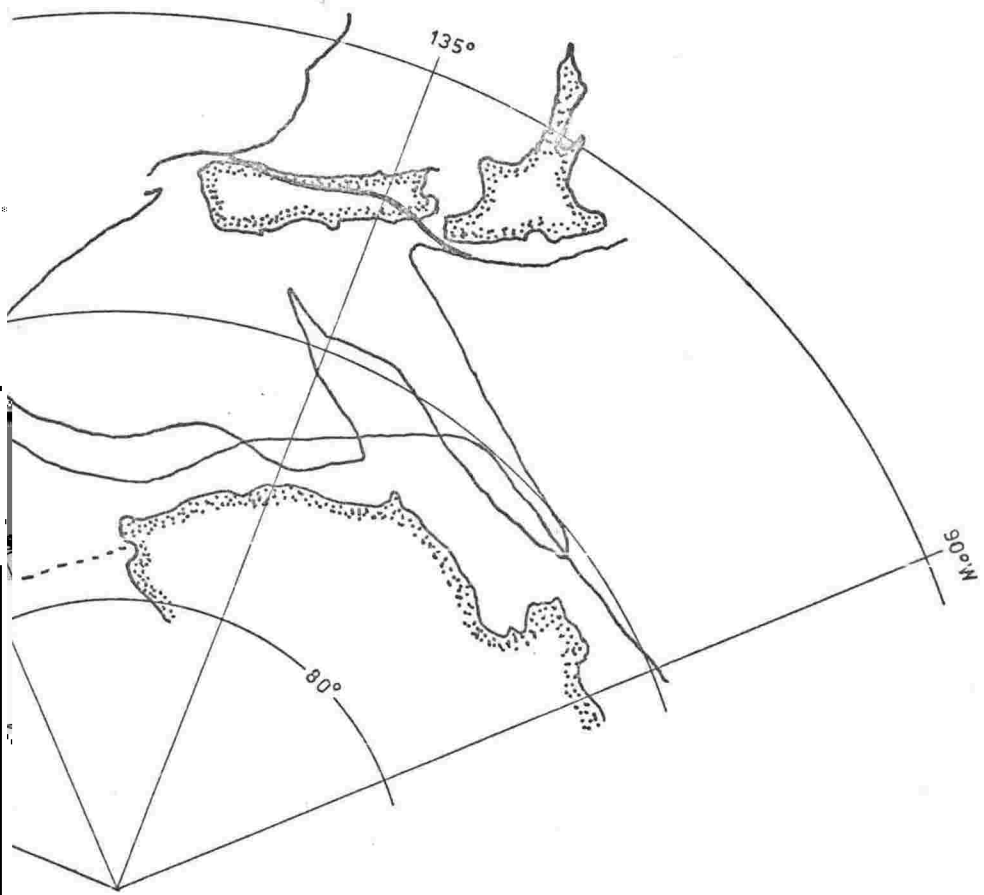


ealand relative to Antarctica at 80 mybp, as determined by the
ric contours indicate the likely edges of the continental areas.

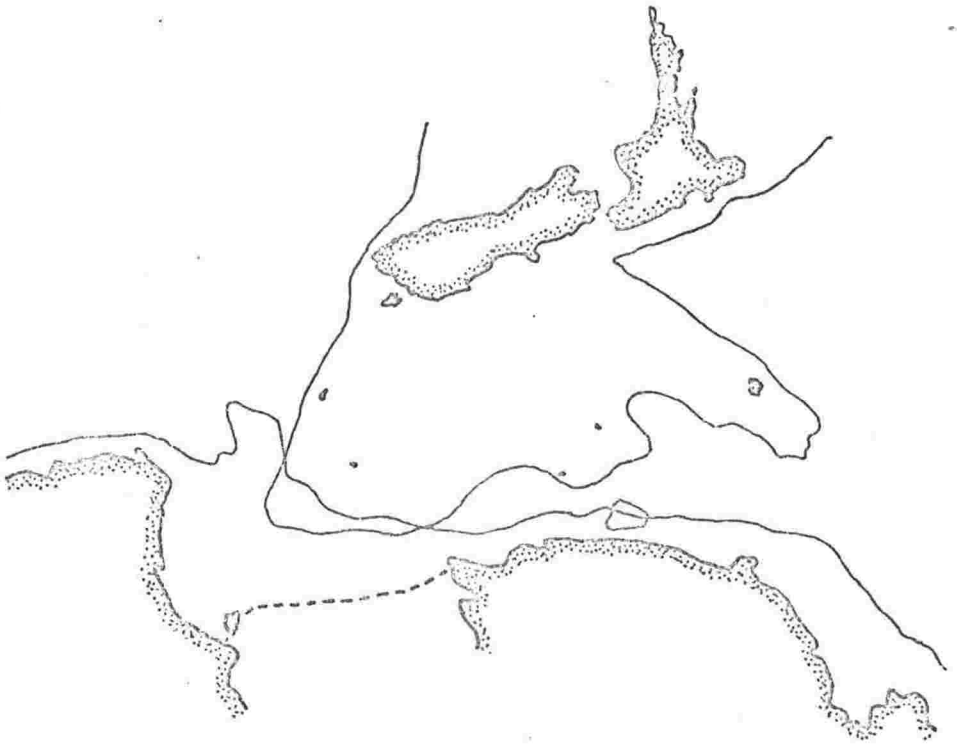

Poles and angles of rotation for spreading between Antarctica and New Zealand.

| Anomaly Span | Time Span m. y. | Pole Location | Angle of Rotation Degrees |
|---|---|---|---|
| 1– 5 | 0–10 | 70° S, 118° E | 10.8 |
| 5–25 | 10–63 | 64° S, 160° E | 41 |
| 25–36 | 63–84 | 0° S, 120° W | 14 |

Fig. 9.17 New Zealand-Antarctica reconstruction, from Christoffel and R.K.H. Falconer (1973). Antarctica was rotated back to New Zealand using the poles and angles listed in the table.

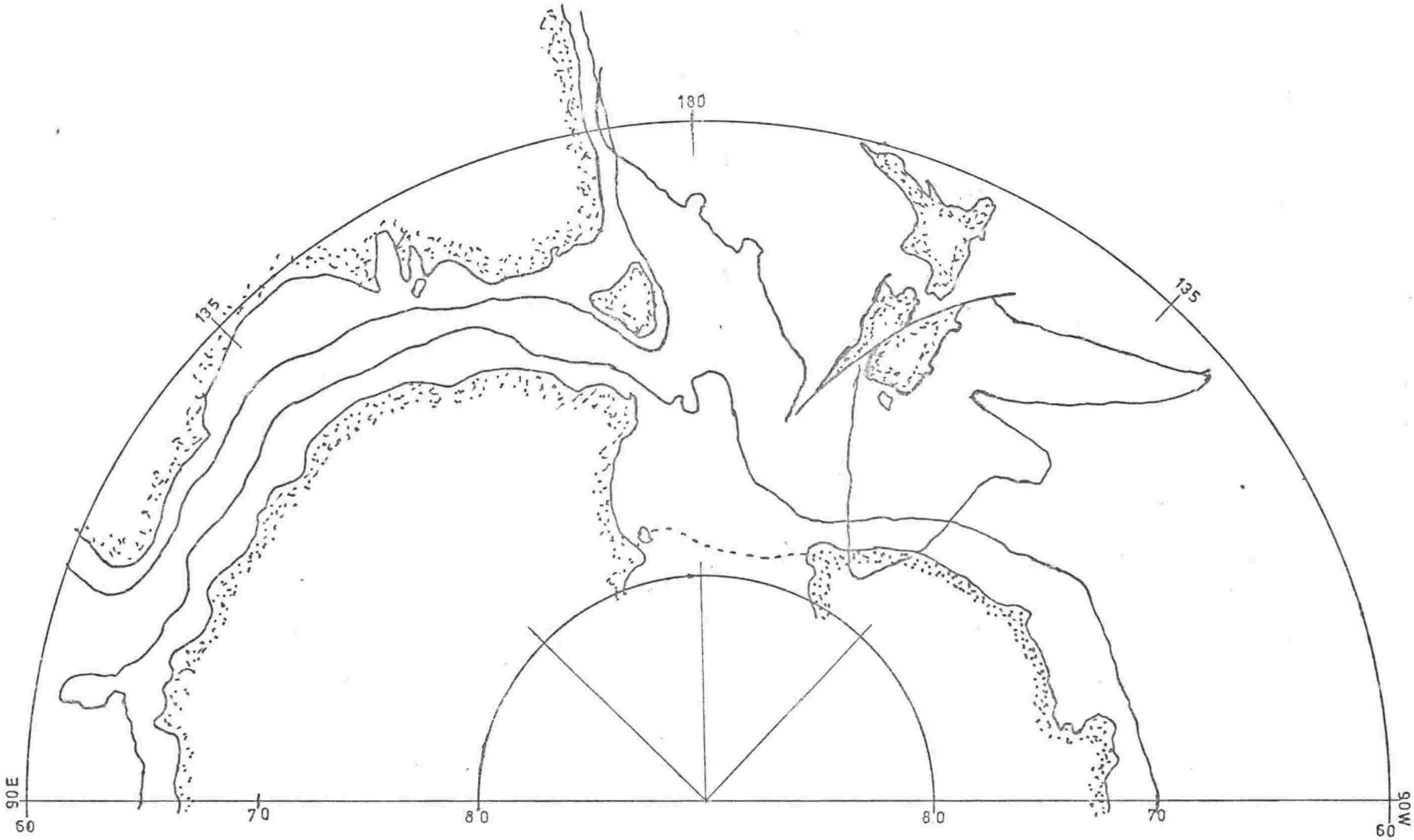


Fig. 9.18 Reconstruction of New Zealand, Antarctica, and Australia, sketched from Hayes and Ringis (1973, Fig. 7). The bathymetric contour is 1000 fm which is similar to the 2 km contour shown in other diagrams.

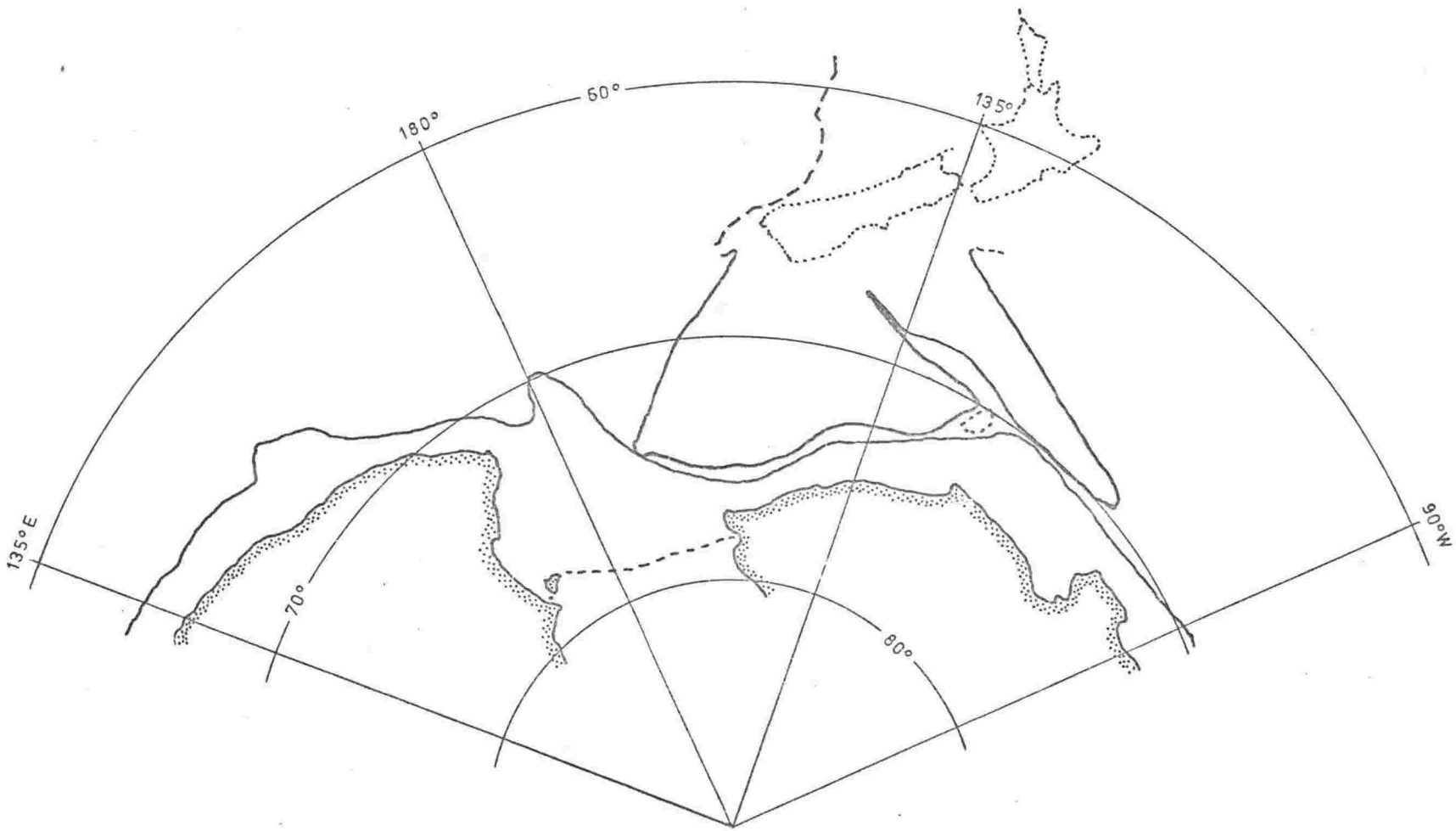


Fig. 9.19 An alternative reconstruction of New Zealand and Antarctica based on no overlap of the Campbell plateau onto Antarctica. The Bounty trough has been closed up. Subaerial New Zealand is shown in its present relationship to the Campbell plateau.

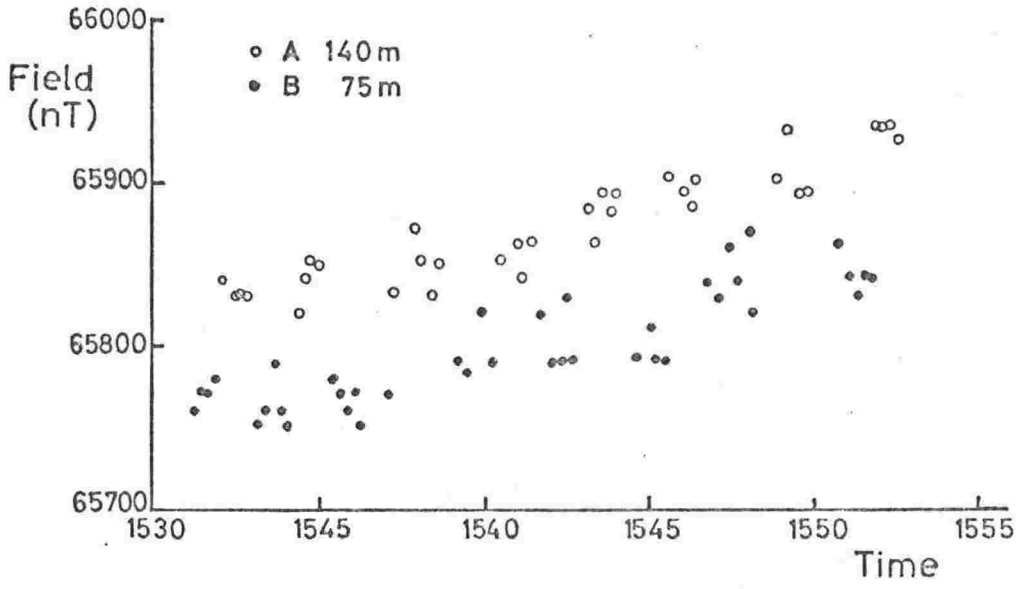


Fig. 3B.1 Total field readings with sensors A and B at fixed distances.

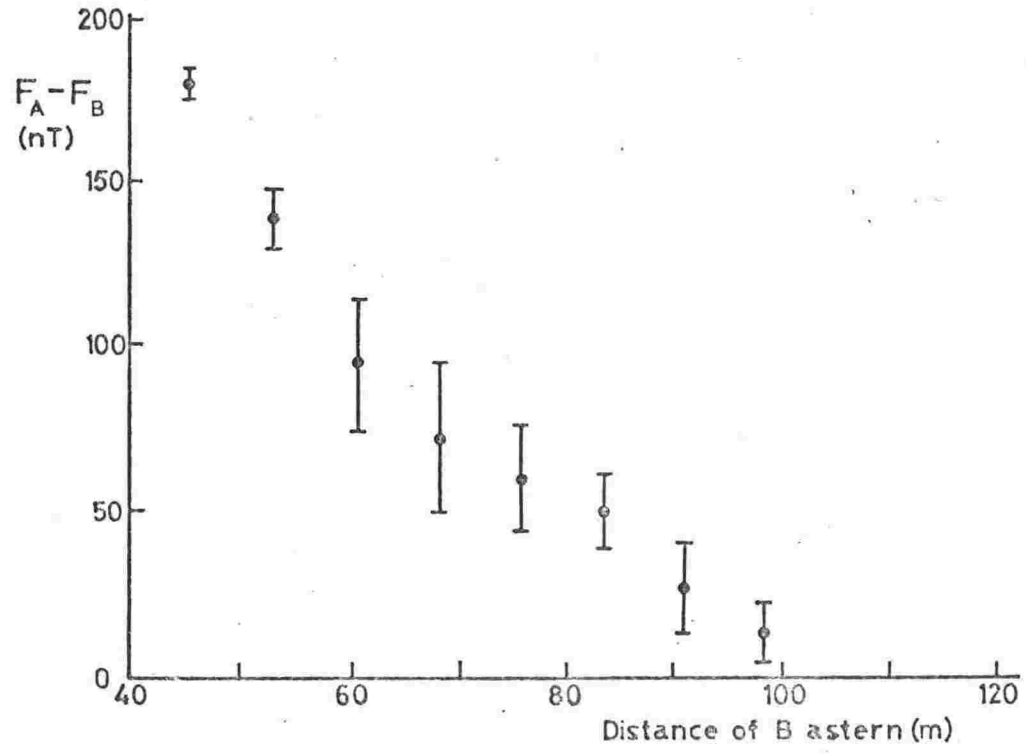


Fig. 3B.2 Variation with distance of field difference between sensors A and B. Sensor A held at 140 m.

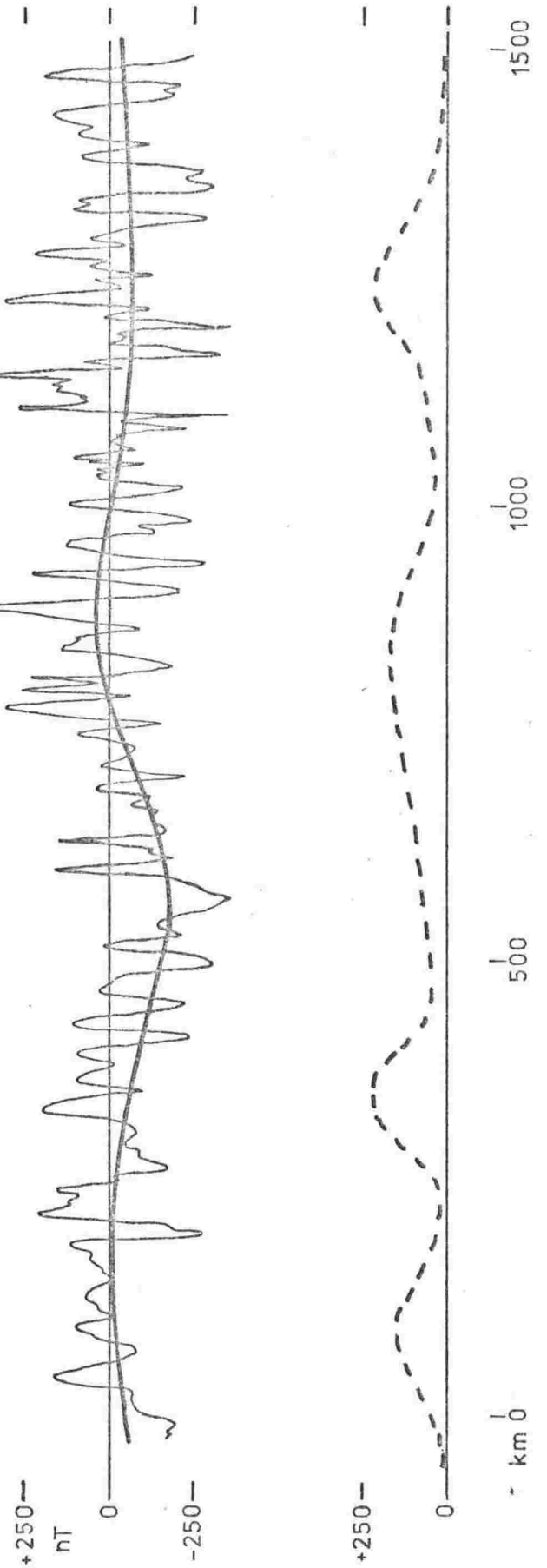


Fig. 3C.1 Upper: Magnetic anomaly profile B produced with IGRF regional field, heavy line a visual zero level line. Lower: The regional anomalies for profile B given by Ross (1966, Figs. 33, 34).

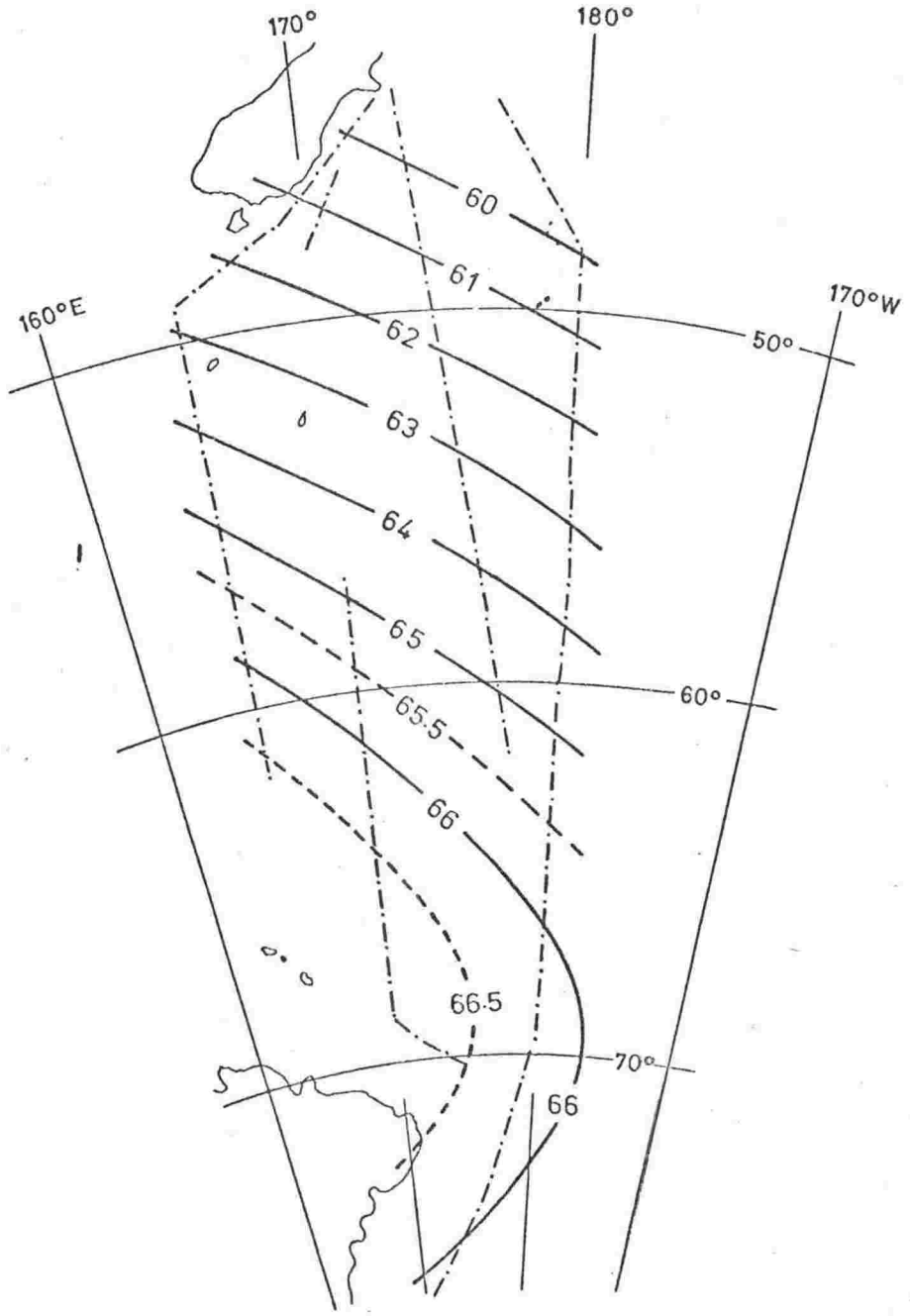


Fig. 3D.1 Total field map for 1966.0. Compiled from data obtained during Dec 1965-Feb 1966 along the tracks shown dashed and dotted. Contour units: thousands of nanotesla.

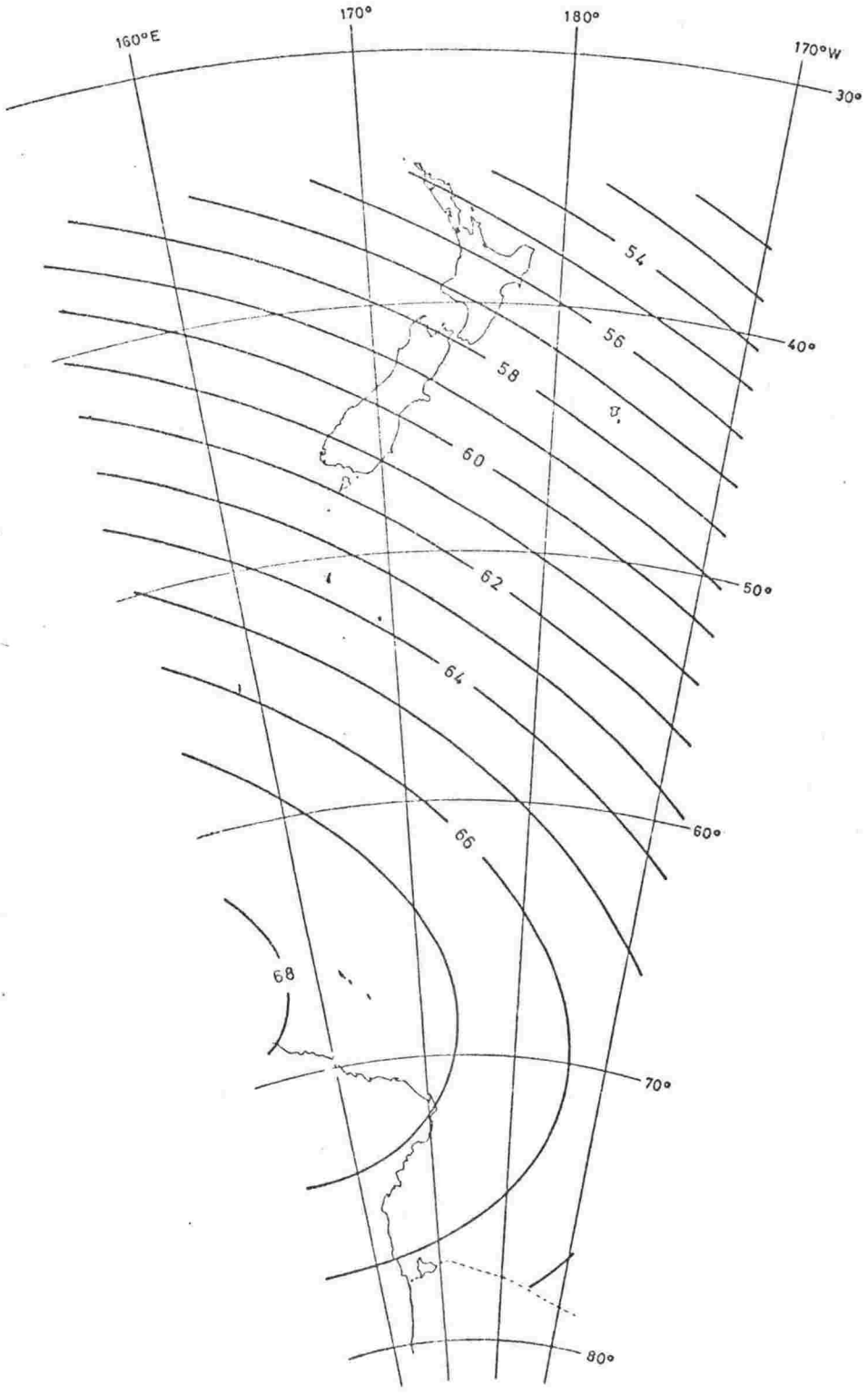


Fig. 3D.2 Total field for 1967.0, calculated from spherical harmonic coefficient set GSFC 12/66 (Cain et al., 1967). Contour units: thousands of nanotesla.

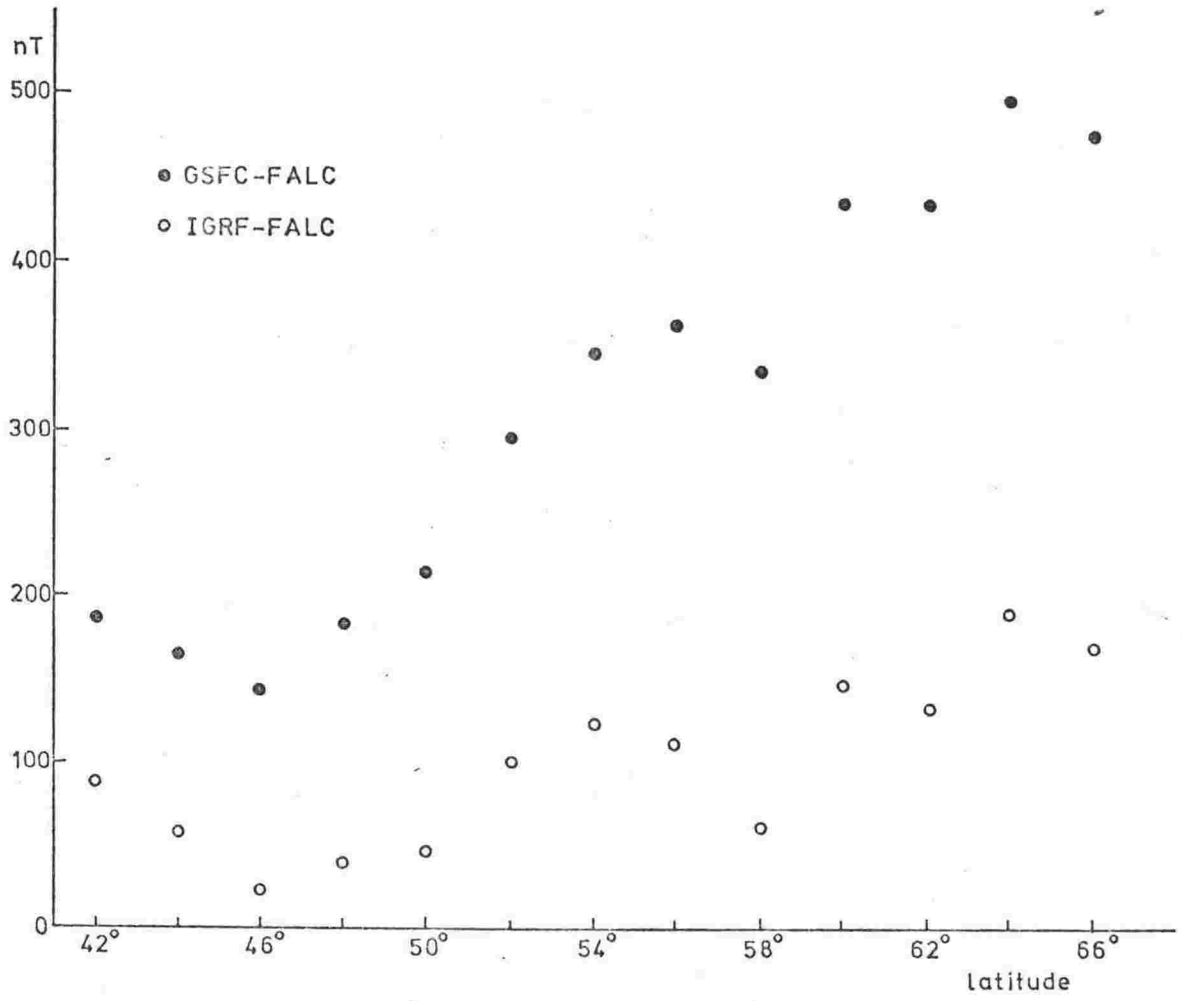


Fig. 3D.3 Comparison on longitude 172°E of the GSFC and IGRF fields with the 1967.0 field determined from the data (FALC).

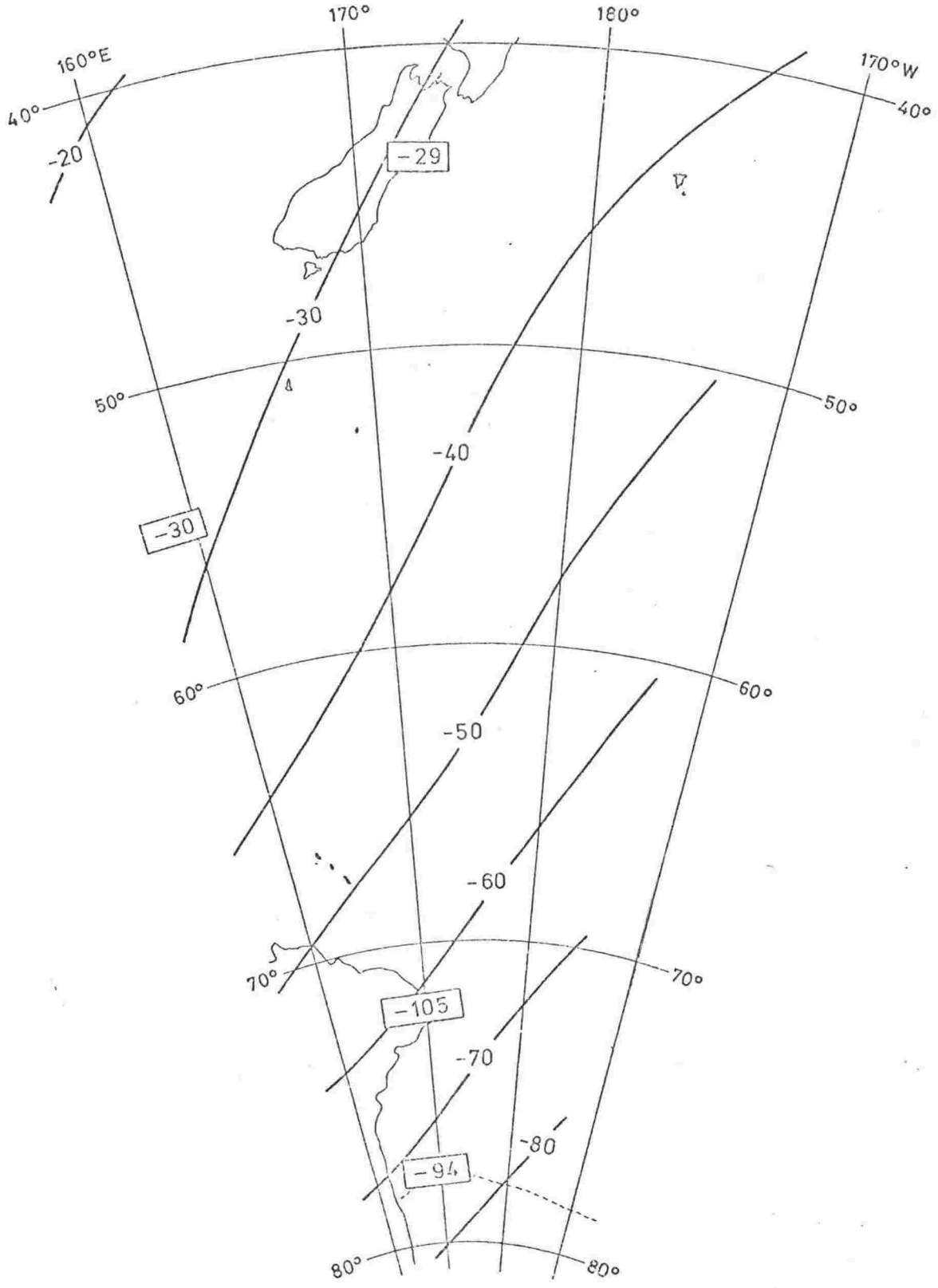


Fig. 3D.4 Secular variation: contours from the IGRF, numbers in squares from base stations. Units: nT/yr.

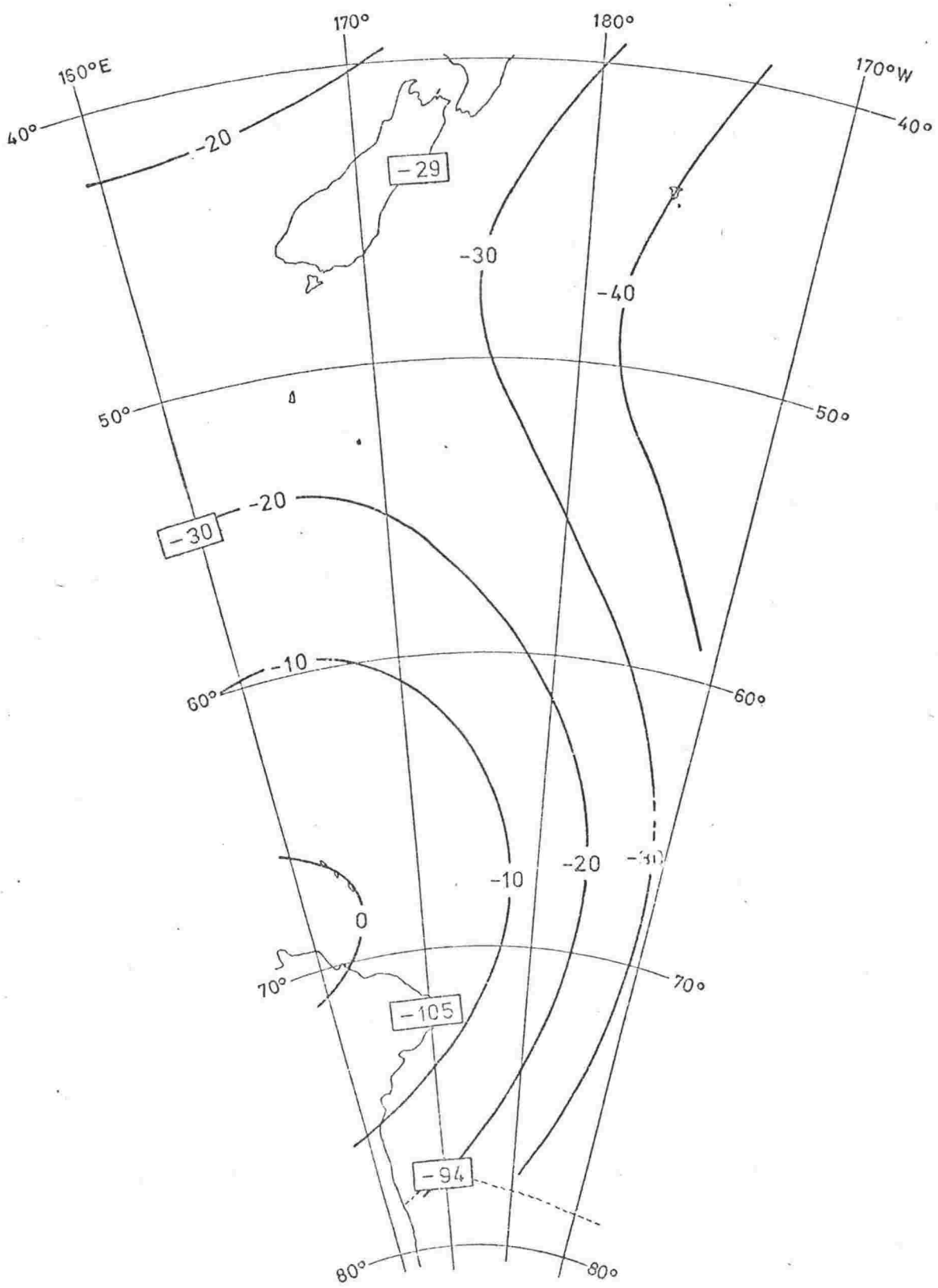


Fig. 3D.5 Secular variation: contours from the GSFC, numbers in squares from base stations. Units: nT/yr.

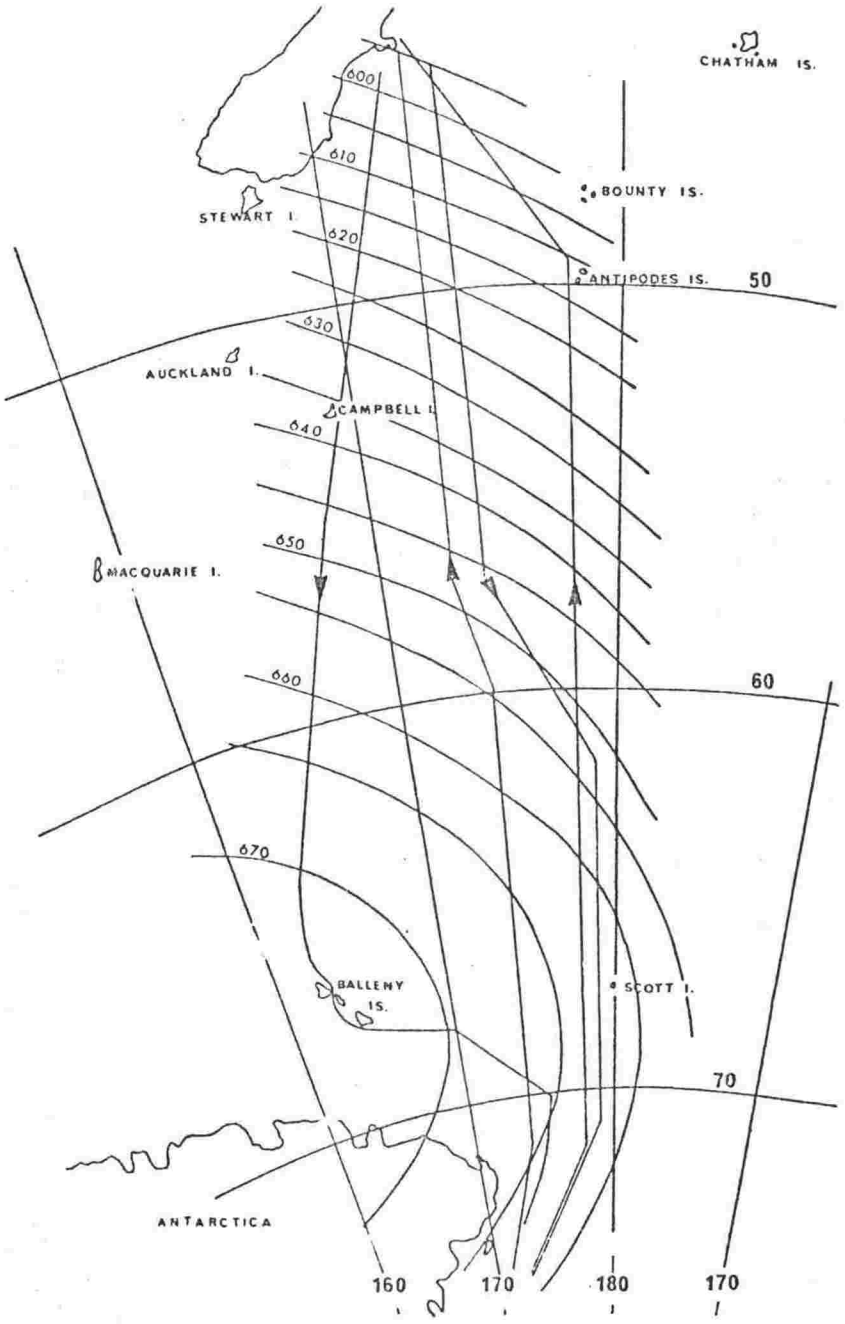


Fig. 3D.6 Total field for 1964.5 from Ross (1966, Fig. 32). Compiled from data obtained during Dec 1963-Jan 1965 along the tracks shown. Contour units: thousands of nanotesla.

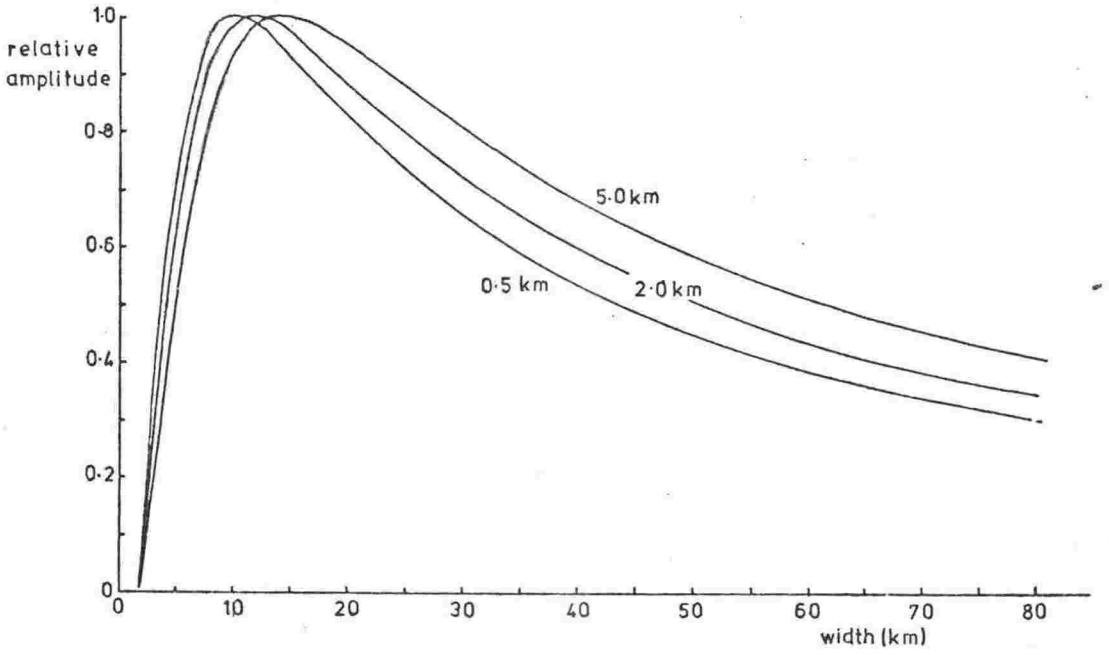


Fig. 6B.1 Variation with block width of the amplitude over a single block. Curves for three block thicknesses as shown. Top of the block at 5.0 km.

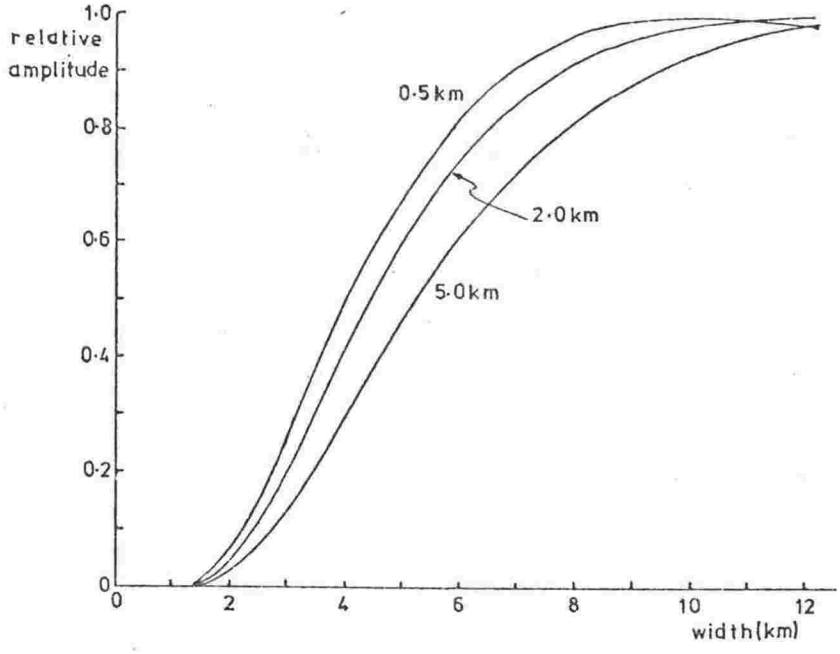


Fig. 6B.2 Detail of Fig. 6B.1.

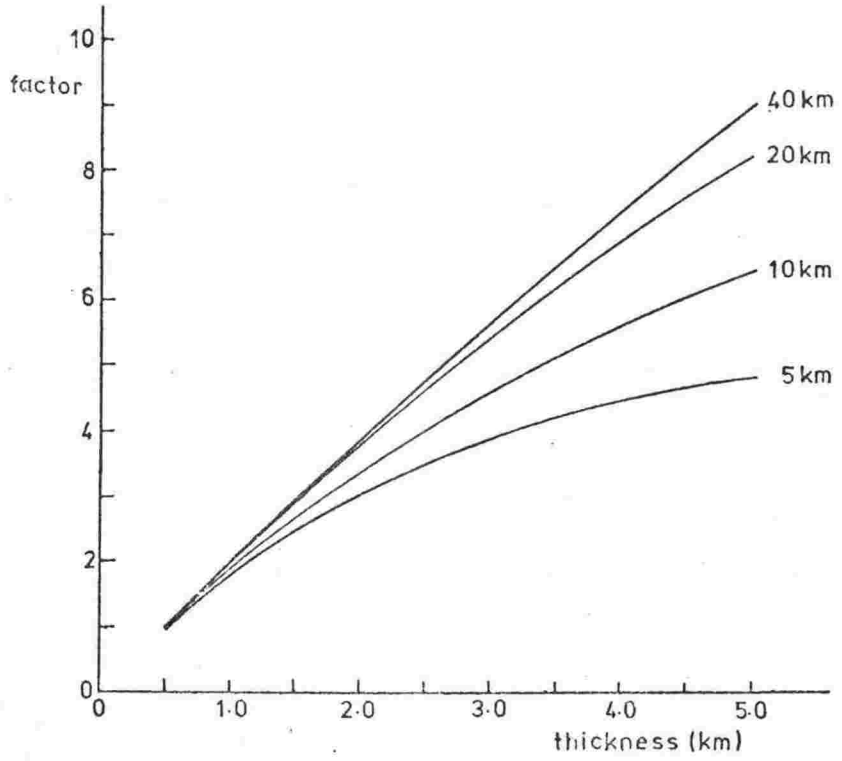


Fig. 6B.3 Variation with block thickness of the factor by which the magnetization appropriate for 0.5 km thick block has to be divided to give the same amplitude when a thicker block is used. Curves for blocks of widths as labelled.

(*Reprinted from Nature Physical Science, Vol. 243, No. 128, pp. 97–99, June 11, 1973*)

# Indian–Pacific Rotation Pole determined from Earthquake Epicentres

THE boundary between the Indian and Pacific plates[1] in the south-west Pacific is defined by the zone of seismic activity that extends along the Tonga–Kermadec Trench, through New Zealand, and along the Macquarie Ridge Complex[2] to the Indian–Antarctic–Pacific triple junction[3,4]. Neither spreading axes nor active transform faults have been identified on this boundary[2,5,6] so it is difficult to determine the Indian–Pacific pole of rotation from the boundary itself. I present here a new determination of the pole position, based entirely on the location of earthquakes on the Macquarie Complex.

When plotted on a stereographic projection (Fig. 1) all the earthquakes on the Macquarie Complex south of about 49° S lie close to the arc of a circle. In a stereographic projection a circle on the map represents a circle on the Earth. In plate tectonics a circle about the pole of rotation of two plates defines the locus of a possible fracture zone. Thus if the earthquakes on the Macquarie Complex are considered to be on a circular arc they define one continuous fracture zone separating the Indian and Pacific plates. The centre of the arc specifies the position of the Indian–Pacific rotational pole. This is at 55.8° S, 174.7° E, and is here referred to as the epicentral pole. The position is tightly constrained, as any shift of the pole by more than 50 km gives a noticeably poorer fit of the epicentres to a single arc. The scatter about the arc could be a consequence of the spreading out of tectonic activity within the boundary and of inaccuracies in determining the epicentre locations. The standard deviation of the distances of the epicentres from the arc is 26.5 km. Their locations are not likely to be determined more accurately than this.

The epicentral pole position is significantly different from other published pole positions (Table 1). These differences may be a result of different initial assumptions rather than uncertainties in pole determinations. Pole 3 is based on the assumption that the Indian–Pacific boundary is a single continuous transform fault from the triple junction to the southern end of the Kermadec Trench. All the other poles are calculated from summation of rotation vectors. Pole 2 is given only for reference because Le Pichon[7,8] has pointed out that it is subject to large errors. Poles 4–9 are calculated from various Indian–Antarctic and Pacific–Antarctic poles. Pole 10 is based on the simultaneous calculation of the relative

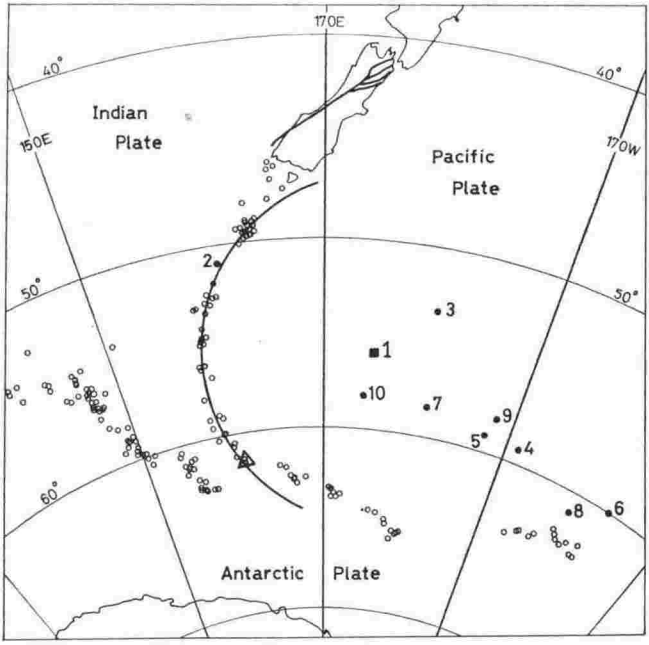


**Fig. 1** Earthquake epicentres and Indian–Pacific rotation poles. Epicentres (○) are for the period January 1963 through March 1972, and only south of 46° S. They were compiled from USCGS monthly listings. Pole positions are numbered as in Table 1. The heavy arc is the arc about the epicentral pole (■). The triangle indicates the Indian–Antarctic–Pacific triple junction. Heavy lines in the South Island of New Zealand are the Alpine Fault and its principal branches. Polar stereographic projection.

**Table 1** Indian–Pacific Rotation Poles

| Model No. | Source and source model No. | Latitude (S) | Longitude | Rate $10^{-7}$ deg $yr^{-1}$ |
|---|---|---|---|---|
| 1 | This communication | 55.8 | 174.7 E | 13.0 |
| 2 | Le Pichon[7,8] | 51.1 | 161.1 E | 12.4 |
| 3 | Christoffel[9] 2 | 53 | 180 | 18.3 * |
| 4 | Christoffel[9] 1 | 58 | 169 W | 18.3 |
| 5 | Weissel, Hayes[3] 1 | 59.0 | 173.0 W | 13.6 |
| 6 | Weissel, Hayes[3] 2 | 60.0 | 157.0 W | 13.6 |
| 7 | McKenzie, Sclater[10] | 58.2 | 179.5 W | 13.4 |
| 8 | Hayes, Talwani[2] 8 † | 61.0 | 161.1 W | 13.2 |
| 9 | Chase[11] 1971 | 58 | 172 W | 11.1 |
| 10 | Chase[12] S005ALL | 58 | 174 E | 12.9 |

* Original published rate (20.8) is an error (D. A. Christoffel, personal communication).

† Other model numbers refer to poles included in this table.

motions of eight plates and includes data from three focal mechanism studies on the Indian–Pacific boundary[12].

A useful way to assess the validity of the epicentral pole is to examine what it predicts along the plate boundary. The basic assumption of the method implies pure strike-slip motion along all the Macquarie Complex south of about 49° S. The epicentres do not give the sense of motion but other work[2,9] indicates that it is dextral. The fact that the Macquarie Complex consists of substantial ridges and troughs[2] could be taken as an indication that it is not a simple fault boundary. But the topographical structure may result from movement in time of the position of the rotation pole. The pole is close to the boundary so any shift could cause large changes in motion along the boundary. This could lead to the development of the major structural features.

There are reliable focal mechanism solutions for five earthquakes associated with the Macquarie Complex[6,13,14]. One (at 56° S) indicates strike-slip motion. The fault plane selected by Banghar and Sykes[14] is almost east–west. But the alternative plane striking N 04° E agrees within one degree with the direction predicted by the epicentral pole, and gives dextral motion. The other four solutions (between 49° S and 52° S) indicate predominantly east–west thrusting. This is not necessarily incompatible with regional strike-slip motion because focal mechanisms indicate only local motion. Any structure oblique to the boundary may lead to local motion which is different from the regional one.

North of about 49° S the epicentres diverge from the single arc, so the boundary cannot extend as a continuous strike-slip fault into New Zealand. In South Island the boundary is generally assumed to be associated with the Alpine Fault, which goes offshore from Fiordland. The vector of motion predicted for the area between 49° S and Fiordland implies a component of compression. If some of this compression is taken up by underthrusting the intermediate depth earthquakes observed in Fiordland are explained. They are not easily explained by poles 3–9 which predict almost pure strike-slip.

Poles 3–9 also predict almost pure strike-slip motion along the central Alpine Fault. The epicentral pole vector, however, strikes 25° east of the fault. The component of motion normal to the fault explains the observed uplift and thrust of the eastern side. In the northern part of the South Island the Alpine Fault branches into several fault traces[15]. The strikes of these faults where they break off from the main trace are within 5° of the strike of epicentral pole vector. After short distances, however, they seem to reorientate to a more northward trend. The structure of the area may be a consequence of the present motion being oblique to pre-existing structural trends.

The calculated directions of relative motion change from

east–west at the northern end of the South Island to 15° north of west at the northern end of the Tonga Trench. The directions agree with those given by focal mechanism studies[6] and are compatible with the under-thrusting indicated by the distribution of earthquakes[16].

The epicentral data do not provide a determination of the rate of rotation. But pole 10, which is closest to the epicentral pole, predicts similar directions of motion along the boundary. It has a rotation rate of $12.9 \times 10^{-7}$ deg yr$^{-1}$. Most of the other poles have higher rates. If a rate of $13 \times 10^{-7}$ deg yr$^{-1}$ is assumed the epicentral pole predicts 2.3 cm yr$^{-1}$ dextral strike-slip for the Macquarie Complex. At Fiordland the rate is 3.1 cm yr$^{-1}$ and it increases to 3.6 cm yr$^{-1}$ at the northern end of South Island. The component parallel to the central Alpine Fault at 170° E would be 2.8 cm yr$^{-1}$, which is less than the range 3.3–7.9 cm yr$^{-1}$ predicted by poles 3–9.

The epicentral pole is essentially an instantaneous pole, and pole 10 has elements of an instantaneous solution because it includes data from many earthquake focal mechanism studies. The other poles are largely based on magnetic anomalies formed during the past 10 m.y., and thus are average poles. Their positions relative to the epicentral pole suggest that the Indian–Pacific pole has moved westwards with time.

R. K. H. Falconer

*Physics Department,*
*Victoria University of Wellington,*
*Wellington, New Zealand*

Received April 9, 1973.

[1] Morgan, W. J., *J. Geophys. Res.*, **73**, 1959 (1968).
[2] Hayes, D. E., and Talwani, M., *Antarctic Oceanology II: The Australian-New Zealand Sector*, *Antarctic Res. Ser.*, **19**, 211 (1972).
[3] Weissel, J. K., and Hayes, D. E., *Antarctic Oceanology II: The Australian-New Zealand Sector*, *Antarctic Res. Ser.*, **19**, 165 (1972).
[4] Falconer, R. K. H., *Earth Planet. Sci. Lett.*, **17**, 151 (1972).
[5] Christoffel, D. A., and Falconer, R. F., *Proc. Intern. Symp. Oceanography. S. Pac.* (in the press).
[6] Johnson, T., and Molnar, P., *J. Geophys. Res.*, 77, 5000 (1972).
[7] Le Pichon, X., *J. Geophys. Res.*, **73**, 3661 (1968).
[8] Le Pichon, X., *J. Geophys. Res.*, **75**, 2793 (1970).
[9] Christoffel, D. A., *Recent Crustal Movements*, *Roy. Soc. NZ Bull.*, **9**, 25 (1971).
[10] McKenzie, D. P., and Sclater, J. G., *Geophys. J. Roy. Astron. Soc.*, **25**, 437 (1971).
[11] Chase, C. G., *Geol. Soc. Amer. Bull.*, **82**, 3087 (1971).
[12] Chase, C. G., *Geophys. J. Roy. Astron. Soc.*, **29**, 117 (1972).
[13] Sykes, L. R., *J. Geophys. Res.*, **72**, 2131 (1967).
[14] Banghar, A. R., and Sykes, L. R., *J. Geophys. Res.*, **74**, 632 (1969).
[15] NZ Geol. Survey, *South Island: Geological Map of New Zealand*, 1 : 1,000,000 (1972).
[16] Isacks, B., Oliver, J., and Sykes, L. R., *J. Geophys. Res.*, **73**, 5855 (1968).

Printed in Great Britain by Flarepath Printers Ltd., St. Albans, Herts.

EARTH AND PLANETARY SCIENCE LETTERS 17 (1972) 151–158. NORTH-HOLLAND PUBLISHING COMPANY



# THE INDIAN-ANTARCTIC-PACIFIC TRIPLE JUNCTION

R. K. H. FALCONER
*Physics Department, Victoria University of Wellington, Wellington, New Zealand*

Received 7 August 1972
Revised version received 18 September 1972

Bathymetric, magnetic and epicentral data have been analysed and show that the Indian, Antarctic and Pacific plates intersect in a ridge-fault-fault triple junction at 61°30'S, 161°E. The Indian-Antarctic boundary is an active spreading ridge, striking N55°E, with a half spreading rate of 3.4 cm/yr. The Pacific-Antarctic boundary strikes N75°W from longitude 180° to the triple junction. It is an extensively fractured area with the fractures probably striking N45°W. The Indian-Pacific boundary is a fracture zone which strikes N25°W from the triple junction to the southern end of the Hjort Trench. The trench is probably a continuation of the fracture zone. The observed configuration is in agreement with predictions based on plate tectonics, and would give a stable junction.

## 1. Introduction

The concept of plate tectonics [1, 2] supposes that the Earth's crust can be considered a mosaic of large rigid plates. The boundaries of the plates are of three basic types.

(1) Ridges, where new crustal material emerges.

(2) Trenches or fold belts, where material is respectively either absorbed or compressed.

(3) Fault boundaries, along which plates slip.

Three plates may meet at one point, called a triple junction [3]. The intersecting plate boundaries can be of any type and this leads to the classification of triple junctions in terms of the intersecting boundaries. For example, the intersection of a ridge and two faults gives a ridge-fault-fault junction.

The structure in an area where three plate boundaries meet is likely to be complex and therefore it may not be valid to give a precise position for a triple junction. However, if the nature of the three boundaries in the vicinity of the triple junction is determined the type of junction can be specified. The extrapolated region of intersection of the boundaries could then be taken as the triple junction, even if the boundaries are not precisely determined right at the position.

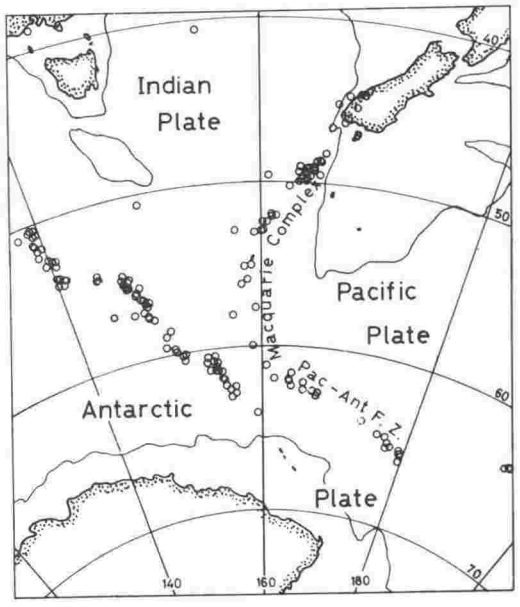


Fig. 1. The area in which the Indian, Antarctic, and Pacific plates intersect. The earthquake epicentres, shown by open circles, indicate the plate boundaries.

One of the present major triple junctions is formed at the intersection of three of the largest plates; the Indian, Antarctic and Pacific plates (fig. 1). Le Pichon [4] placed this junction in the region of 60°S, 160°E; while Sykes [5] placed it near 62°S, 160°E. The precise form and position of the junction was not known because the nature of the three plate boundaries in the area was not clear. On the basis of computed vector motions McKenzie and Sclater [6] conclude that the junction is of the ridge-ridge-fault type*.

Recent geophysical surveys south of 60°S, between 155°E and 165°E, now provide enough data to identify the form and location of the plate boundaries. These data will be presented so that a direct estimate may be made of the type and position of the triple junction. The regions containing each of the three boundaries will be considered in turn.

## 2. Data sources

The magnetic data presented are from the following sources. Tracks labelled NZ are from HMNZS Endeavour cruises, Victoria University of Wellington; EL, from USNS Eltanin cruises, Lamont-Doherty Geological Observatory; AR, from Aries II cruise, Scripps Institute of Oceanography; A708 from Project Magnet aeromagnetic survey, U. S. Naval Oceanography Office; DF, from Operation Deep Freeze, U. S. Navy Hydrographic Office [7]. The satellite navigation system was used on Eltanin cruises and the Aries II expedition. Conventional celestial and dead reckoning navigation was used for the remaining tracks.

Bathymetric data are primarily from N. Z. Oceanographic Institute 1:1 000 000 charts of the area [8]. There are considerably more tracks for bathymetry than magnetics and although the topography is rough in some parts, the charts should fairly well describe the area. The bathymetric profiles shown are from the sources of the magnetic profiles.

The earthquake epicentres used are from Sykes [5], for the period 1950 to 1966. Sykes also gives some epicentres for prior to 1950 but as they are not so well determined, they are not used.

* Note added in proof: There is a misprint in McKenzie and Sclater [6], p. 494 (McKenzie, pers. comm.). In fact they meant that the junction is of the ridge-fault-fault type. Their suggestion thus agrees with the conclusion of this paper.

## 3. Indian-Antarctic boundary

The boundary between the Indian Antarctic plates near the triple junction has not previously been clearly defined, although it is usually assumed to be of the ridge type [4, 5].

The profiles of fig. 2 clearly show the magnetic anomalies associated with an active spreading ridge. The axis is determined from several tracks (fig. 3) and anomaly lineations are identified on both sides of the ridge. The bathymetry also indicates a regular ridge, the axis of which coincides with the magnetic axis (profile EL27, fig. 4). The lineations of anomalies (fig. 3), including several unnumbered ones not shown, are closely parallel to the axis, which strikes N55°E. The Aries track ARc south of 63°40′S in fact consists of four close tracks (two profiles are shown in fig. 2), and correlations show that even over short distances individual anomalies strike N55°E.

The spreading rate has been calculated from the satellite navigation controlled tracks which cross the ridge axis. Least squares fits were made of anomaly distance against age. The time scale assumed was that of Talwani et al. [10] and only anomalies out to number 3 (4.6 my) were considered. The mean rate north of the ridge is 3.40 ± 0.14 cm/yr, the rate south is 3.37 ± 0.17 cm/yr. There is thus no significant difference between the spreading rate north and south of the ridge. A determination based on anomaly number 2 (1.9 my), which is clearly defined in several places both north and south of the axis (fig. 2) gives 3.37 ± 0.08 cm/yr.

The western end of the ridge is terminated by a fracture zone [5] striking approximately N30°W. This feature is clearly identified from the epicentres (fig. 3). The bathymetry contours also suggest that the ridge is offset about 320 km in a dextral sense. As a noticeable bathymetric step the fracture zone continues south to the Balleny Islands. These islands and nearby submarine banks strike N35°W, and are presumably associated with the fracture zone. The name Balleny Fracture Zone is suggested for this prominent fracture.

The complete lack of epicentres on the Indian-Antarctic Ridge in this area (fig. 3) is in marked contrast to the high activity on the Balleny Fracture zone. Active spreading ridges can also be identified further to the west on the Indian-Antarctic boundary [13,

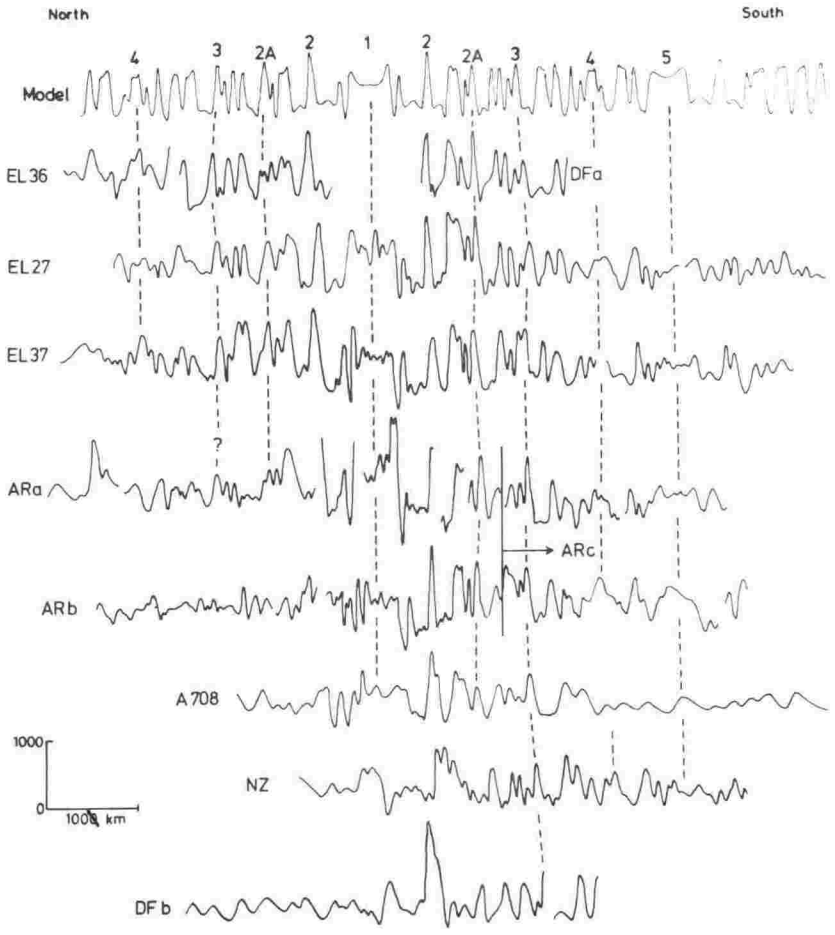


Fig. 2. Magnetic anomaly profiles projected perpendicular to the Indian-Antarctic Ridge. Anomalies numbered after [9]. Model based on the time scale of Talwani et al. [10] and a half spreading rate of 3.4 cm/yr.

14]. They are in aseismic sections, which are offset by epicentre lineations [5]. The tendency in this, and in other areas [15, 16], for earthquakes to be primarily on the fracture zones rather than on the ridges may be useful for distinguishing ridges from faults at complex boundaries.

The closest determination of the triple junction position would probably be given by the eastern termination of the Indian-Antarctic spreading axis. The epicentres (fig. 3) suggest that this may be near 161°E. However, the magnetic and bathymetric data provide a more precise location.

The magnetic anomalies characteristic of recent spreading cannot be recognised on profile NZ (fig. 2) closer to the axis than anomaly 2A on the south side of the ridge. Profiles A708 and ARb both show the characteristic anomalies over the southern flank of the ridge but they are not seen north of the axial anomaly. The bathymetry of profile ARb (fig. 4) shows a marked change, coincident with the loss of the characteristic anomalies. The smooth bathymetry typical of the spreading ridge (profile EL27) is not observed north of the ridge crest.

The loss of magnetic lineations, change of bathymetric character, and the earthquake epicentres all indicate that the Indian-Antarctic Ridge terminates just east of the axial magnetic anomaly observed on track ARb, i. e. close to 61°30′S, 161°E.

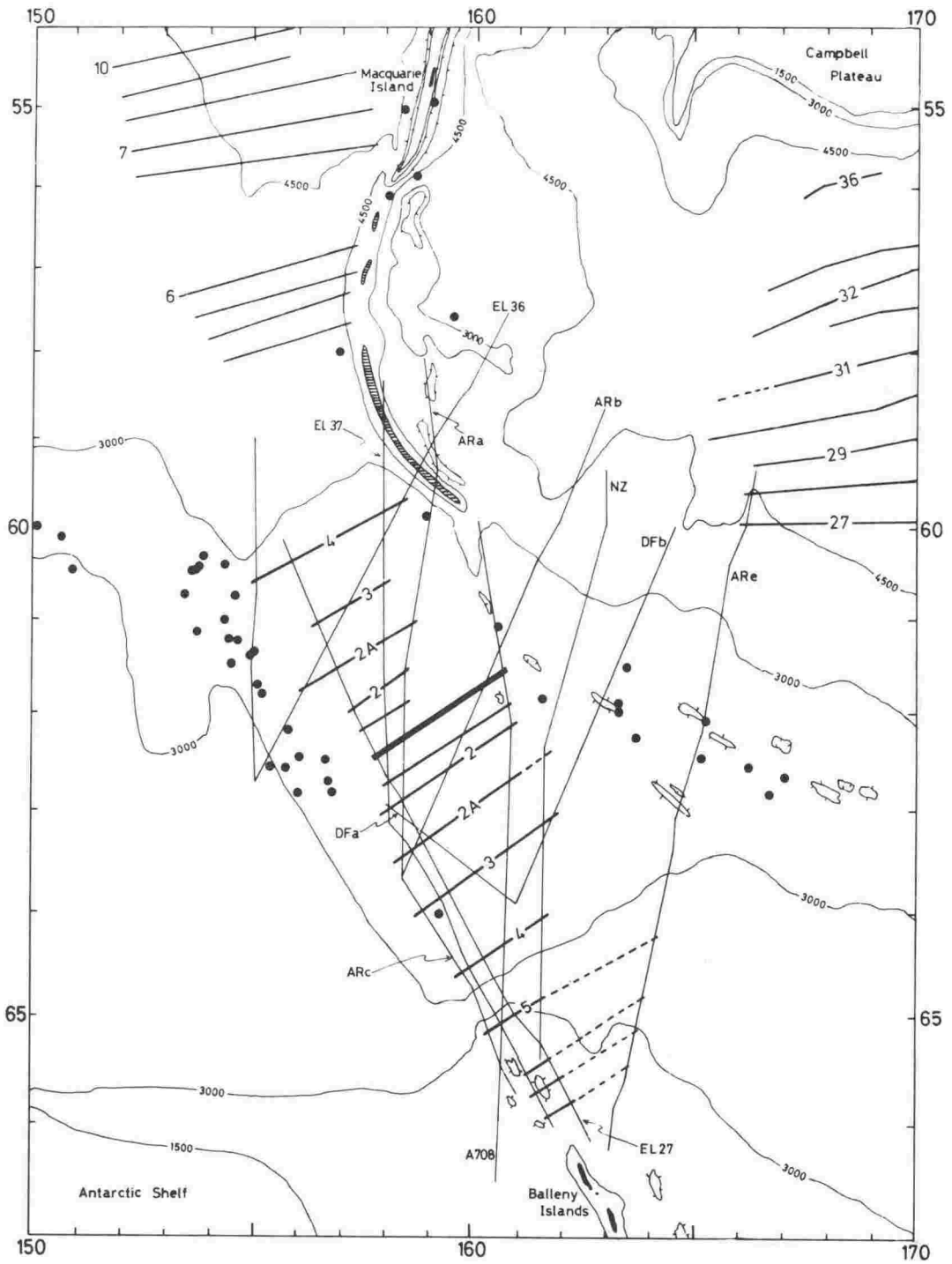


Fig. 3. The region surrounding the Indian-Antarctic-Pacific triple junction. Magnetic anomaly trends shown where identifiable; those north of 60° S from [11] for east of 160° E, from [12] for west of 160° E. Epicentres shown by solid circles. Bathymetry in metres; hatched area, deeper than 6000m, delineates the Hjort Trench.

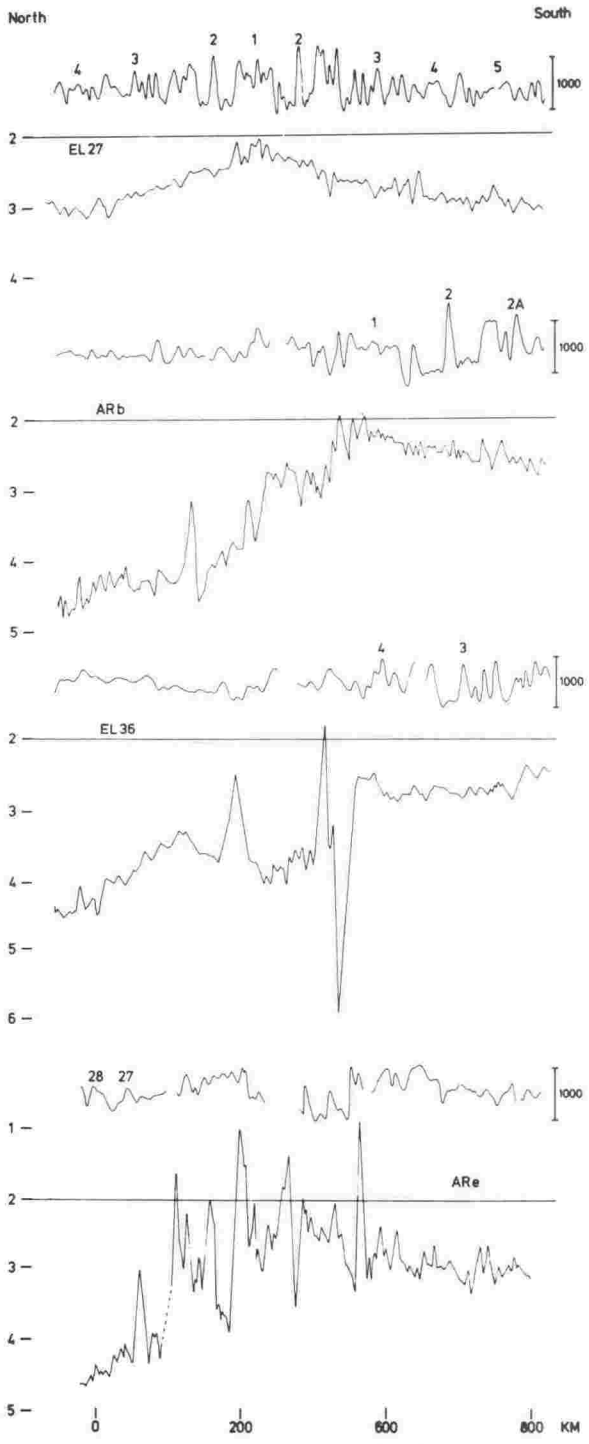


Fig. 4. Profiles from tracks across the plate boundaries. For each track the upper profile is magnetic anomalies in gamma, and the lower profile is bathymetry in km.

## 4. Pacific-Antarctic boundary

The boundary of the Pacific and Antarctic plates in the triple junction area has been considered a ridge [17]. However, Christoffel and Falconer [11] show that it is probably a substantial fracture zone. This zone, which they name the Pacific-Antarctic Fracture Zone, extends from 161°E to 180°. It is characterised by seismic activity, rough topography, and disturbed magnetics.

Profile ARe (fig. 4), shows topography typical of the zone [17]. The roughness is distinctly different from the regular ridge features observed both east of 180°, on the Albatross Cordillera [11, 16], and west of 161°E, on the Indian-Antarctic Ridge. The whole feature is asymmetrical, the Southwest Pacific Basin to the north being 2 km deeper than the Balleny Basin to the south.

Seventeen magnetic profiles [11] between 180° and 162°E show short wavelength, high amplitude anomalies, but no clear indication of sea floor spreading. The seismic activity [5] is in contrast to the Indian-Antarctic Ridge and Albatross Cordillera. The epicentres are scattered but coincide with the disturbed magnetics and bathymetry.

The whole structure has the characteristics of a major fracture zone but the width of the disturbed area makes it difficult to precisely define the boundary. The general strike is N75°W but Christoffel and Falconer [18] suggest that it could be considered a series of smaller fractures N45°W. The fracture zone as a whole, which defines the Pacific-Antarctic boundary, intersects the Indian-Antarctic Ridge at 61°30′S, 161°E.

## 5. Indian-Pacific boundary

The Indian-Pacific boundary south of New Zealand is generally considered to be associated with the Macquarie Ridge [4]. However, its precise nature is complex and elements of all three types of plate boundary; ridge, trench, and fault, may be present [19, 20]. The name Macquarie Ridge Complex has been suggested for the boundary [19].

The most prominent morphological feature of the southern part of the complex is the arcuate Hjort Trench (fig. 3). Magnetic lineations can be traced from the east right to the trench [12] and the bathymetric

transition is very abrupt (profile EL36 fig. 4). East of the trench the topography associated with the Macquarie Ridge is more subdued than further north [20]. No magnetic lineations have been identified between the trench and the well-mapped Cretaceous anomalies east of 165°E [11, 12].

The word 'trench' normally implies a consuming plate boundary. However, deep 'trenches' have elsewhere also been associated with fracture zone [21]. Sleep and Biehler [22] suggest that such deeps may form when spreading material binds to an effectively fixed boundary. The seafloor west of the Hjort Trench is less than 25 my old [12]. The age east of the trench is not known but the basement is at least 1km deeper [23], which suggest [6, 24] that it is older than west of the trench. Thus the Pacific plate could act as a fixed boundary for spreading from the Indian-Antarctic Ridge, and the Hjort Trench is not a trench but is a major fracture zone.

As a prominent feature the trench terminates near 59°30′S, 159°30′E. However, several tracks south of there show deep narrow troughs. The deeps lie on a line striking S25°E from the end of the trench. This line would intersect the Indian-Antarctic Ridge at 61° 30′S, 161°E. Profile ARb (fig.4) crosses the line just north of the ridge axis. The observed topography is what might be expected across the Indian-Pacific boundary if the Pacific plate is old and therefore [6, 24] deep near the boundary, and the boundary is a fault.

The low seismicity of the southern Macquarie Ridge Complex [5] does not provide much information on the boundary. However most of the activity is on or slightly west of the fracture zone defined by the bathymetric and magnetic data.

## 6. Discussion

The boundaries of the Indian, Antarctic, and Pacific plates established above intersect at 61°30′S, 161° E forming a ridge-fault-fault triple junction. If the strike of the Pacific-Antarctic Fracture Zone at the junction is N45°W then the configuration is as shown in fig. 5(a). If the geometry of this configuration does not alter in time, the junction is said to be stable [3]. The stability can be determined by vector addition of the relative plate motions at the junction (fig. 5(b)).

The motion of the Indian and Antarctic plates would be parallel to the Balleny Fracture Zone. The

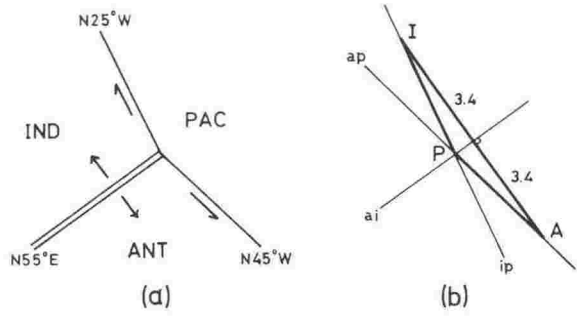


Fig. 5. (a) The physical configuration of the triple junction. (b) The velocity space configuration, following the notation of McKenzie and Morgan [3], spreading rate in cm/yr.

Indian-Antarctic Ridge is perpendicular to the fracture zone so the spreading rate determined for the ridge should give the separation rate of the Indian and Antarctic plates. Since the ridge is spreading symmetrically, the condition for stability of the triple junction is that the line of the ridge bisects the angle between the two fault boundaries. The configuration shown in fig. 5(a) does satisfy this condition; hence the triple junction would be stable.

Since the ridge spreading is symmetrical the rate of motion would be the same on both the fault boundaries. The spreading rate and the angles between the boundaries are known, hence the slipping rate on the faults can be found. It is given by AP or IP in the velocity triangle (fig. 5(b)) and is 3.5 cm/yr. Relative to Antarctica, the triple junction is moving to the northwest at 3.5 cm/yr, however the junction is stationary with respect to the Pacific plate. The active length of the Indian-Antarctic ridge is shortening at 0.6 cm /yr.

The velocity vectors given above have been deduced from data only in the triple junction area. However several authors have determined the poles of rotation rates for the plates involved, and this enables one to calculate the velocity vectors at the triple junction. Table 1 gives the motions determined by both means. Since the rotation poles were determined with data from areas other than the triple junction, the two methods are essentially independent.

The agreement is in general good, the greatest differences being on the fault boundaries, which are difficult to determine precisely. It is interesting to note that an Indian-Pacific fault striking due north, and a Pacific-Antarctic fault striking N75°W would be close to a stable junction configuration.

Table 1
Observed and calculated motions on the plate boundaries.

| | | | |
|---|---|---|---|
| India-Antarctica | | | |
| | This paper | WH | MS |
| Ridge strike | N55°E | N61°E | N60°E |
| Half spreading rate cm/yr | 3.4 | 3.4 | 3.1 |
| India-Pacific | | | |
| | This paper | CH | WH |
| Fracture zone strike | N25°W | N27°W | 000° |
| Slipping rate cm/yr | 3.5 | 3.6 | 3.4 |
| Pacific-Antarctica | | | |
| | This paper | XL | CH |
| Fracture zone strike | N45°W | N45°W | N75°W |
| Slipping rate cm/yr | 3.5 | 3.9 | 4.1 |

WH: Weissel and Hayes, given in [20]; MS: McKenzie and Sclater [6]; CH: Christoffel [25]; XL: Le Pichon [4].

The fact that the junction is now a stable ridge-fault-fault junction, does not mean that it was always so in the past [3]. More detailed surveys in the area would provide data that might reveal whether it has evolved from some other form.

## Acknowledgements

For providing unpublished data I am grateful to H. P. Stockard, U. S. Naval Oceanographic Office, for Project Magnet data; S. M. Smith, Scripps Institute of Oceanography, for Aries data; Lamont-Doherty Geological Observatory for Eltanin data; and D.E. Hurley, N. Z. Oceanographic Institute for bathymetric data. The U. S. National Science Foundation and Lamont-Doherty Geological Observatory provided the opportunity to participate in Eltanin cruises 27 and 37. The New Zealand University Grants Committee provided a grant for the purchase of a plotter. Discussions with D. A. Christoffel, Feriel Falconer, D. C. Krause, J. W. Brodie and D. E. Hurley were helpful. D. A. Christoffel and Feriel Falconer also read the manuscript.

## References

[1] D. P. McKenzie and R. L. Parker, The North Pacific: An example of tectonics on a sphere, Nature 216 (1967) 1276.
[2] W. J. Morgan, Rises trenches great faults and crustal blocks, J. Geophys. Res. 73 (1968) 1959.
[3] D. P. McKenzie and W. J. Morgan, Evolution of triple junctions, Nature 222 (1969) 125.
[4] X. Le Pichon, Sea floor spreading and continental drift, J. Geophys. Res. 73 (1968) 3661.
[5] L. R. Sykes, Seismicity of the Indian Ocean and a possible nascent island arc between Ceylon and Australia, J. Geophys. Res. 75 (1970) 5041.
[6] D. McKenzie and J. G. Sclater, The evolution of the Indian Ocean since the late Cretaceous, Geophys. J. 25 (1971) 437.
[7] U. S. Navy Hydrographic Office, Operation Deep Freeze 61, 1960–61, Marine Geophysical Investigations, Technical Report 105 (1962).
[8] E. W. Dawson, Balleny Bathymetry, N.Z.O.I., Oceanic Series, 1:1 000 000 (1970).
D. E. Hurley and D. C. Krause, Hjort Bathymetry, N. Z. O. I., Oceanic Series, 1:1 000 000, in prep.
D. E. Hurley and D. C. Krause, Emerald Bathymetry, N. Z. O. I., Oceanic Series, 1:1 000 000, in prep.
[9] W. C. Pitman, E. M. Herron and J. R. Heirtzler, Magnetic anomalies in the Pacific and seafloor spreading, J. Geophys. Res. 73 (1968) 2069.
[10] M. Talwani, C. C. Windisch and M. G. Langseth, Reykjanes Ridge crest: A detailed geophysical study, J. Geophys. Res. 76 (1971) 473.
[11] D. A. Christoffel and R. K. H. Falconer, Marine magnetic measurements in the southwest Pacific Ocean and the identification of new tectonic features, in: Antarctic Oceanology II, Antarctic Research Ser. 19 (American Geophysical Union, in press).
[12] D. A. Christoffel and R. F. Falconer, Magnetic measurements in the Macquarie Ridge region, Proc. Internat. Symp. on the Oceanography of the South Pacific, in press.
[13] R. Schlich and Ph. Patriat, Profils magnétiques sur la dorsale médio-océanique 'Indo-Pacifique', Ann Geophys. 23 (1967) 629.

[14] X. Le Pichon and J. R. Heirtzler, Magnetic anomalies in the Indian Ocean and seafloor spreading, J. Geophys. Res. 73 (1968) 2101.

[15] M. Barazangi and J. Dorman, World Seismicity Maps compiled from ESSA Coast and Geodetic Survey Epicentre Data 1961–1967, Bull. Seism. Soc. Am. (1969) 369.

[16] E. M. Herron, Crustal plates and sea floor spreading in the Southeastern Pacific, in: Antarctic Oceanology I, Antarctic Research Ser. 15, ed. J. L. Reid (American Geophysical Union, 1971) 229.

[17] D. I. Ross, Magnetic and bathymetric measurements across the Pacific-Antarctic Ridge south of New Zealand, N. Z. J. Geol. Geophys. 10 (1967) 1452.

[18] D. A. Christoffel and R. K. H. Falconer, Changes in the direction of sea floor spreading in the Southwest Pacific, Proc. Internat. Symp. of the Oceanography of the South Pacific, in press.

[19] D. E. Hayes, M. Talwani and D. A. Christoffel, The Macquarie Ridge Complex, in: Antarctic Geology and Geophysics, ed. R. J. Adie (Universitets Forlaget, Oslo, 1972), in press.

[20] D. E. Hayes and M. Talwani, A geophysical investigation of the Macquarie Ridge Complex, in: Antarctic Oceanology II, Antarctic Research Ser. 19 (American Geophysical Union, in press).

[21] B. C. Heezen, E. T. Bunce, J. B. Hersey and M. Tharp, Chain and Romanche Fracture Zones, Deep-Sea Res. 11 (1964) 11.
B. C. Heezen and J. E. Nafe, Vema Trench: Western Indian Ocean, Deep Sea Res. 11 (1964) 79.

[22] N. H. Sleep and S. Biehler, Topography and tectonics at the intersections of fracture zones with central rifts, J. Geophys. Res. 78 (1970) 2748.

[23] R. Houtz, J. Ewing and R. Embley, Profiler data from the Macquarie Ridge area, in: Antarctic Oceanology I, Antarctic Research Ser. 15, ed. J. L. Reid (American Geophysical Union, 1971) 239.

[24] J. C. Sclater and J. Francheteau, The implications of terrestrial heat flow observations on current tectonic and geochemical models of the crust and upper mantle of the earth, Geophys. J. 20 (1970) 509.

[25] D. A. Christoffel, Motion of the New Zealand Alpine Fault deduced from the pattern of sea floor spreading, in: Recent Crustal Movements, Roy. Soc. N.Z. Bull. 9 (I. U. G. S. ser B (2) U. M. P. 33), B. W. Collins and R. Fraser, eds. (1971) 25.

*Reprinted from*
ANTARCTIC RESEARCH SERIES, VOL. 19
**Antarctic Oceanology II: *The Australian—New Zealand Sector***
*Edited by* Dennis E. Hayes
AMERICAN GEOPHYSICAL UNION
Washington, D. C. 20036


# MARINE MAGNETIC MEASUREMENTS IN THE SOUTHWEST PACIFIC OCEAN AND THE IDENTIFICATION OF NEW TECTONIC FEATURES

D. A. CHRISTOFFEL*
*Lamont-Doherty Geological Observatory of Columbia University, Palisades, New York 10964*

R. K. H. FALCONER
*Physics Department, Victoria University of Wellington, Wellington, New Zealand*

*Abstract.* Analysis of 41 magnetic profiles in the southwest Pacific has enabled the pattern of magnetic anomaly correlations in the area to be clarified and extended. The time scale for sea floor spreading recognizable by characteristic magnetic anomalies has been increased from 76 to 81 m.y. We deduce that West Antarctica and New Zealand rifted just prior to 81 m.y. ago. Distinct periods of sea floor spreading can be identified with different poles of rotation for the motion between the Pacific and antarctic plates. South of New Zealand, the Albatross cordillera becomes a fracture zone at least 1200 km long, and we propose to name this section the Pacific-Antarctic fracture zone. A revised pole of 82°S, 120°E is suggested for the present Pacific-antarctic pole of rotation.

The pattern of magnetic lineations in the southwest Pacific Ocean was first demonstrated from two magnetic profiles by *Christoffel* [1961]. These profiles and those of *Christoffel and Ross* [1965] for just south of the Campbell plateau assisted in establishing the correlation of magnetic anomalies across the abyssal plain regions of the main oceans [*Vine*, 1966]. The global pattern of sea floor spreading and the relative poles of rotation between the Pacific and adjoining plates assigned by *Le Pichon* [1968] were shown by *Christoffel and Ross* [1970] to be not entirely compatible with the pattern of magnetic anomalies between the Campbell plateau and the shelf of the antarctic continent. The Pacific-antarctic pole of rotation of 70°S, 118°E assigned by Le Pichon does not correspond with the trend of the magnetic anomalies immediately south of the Campbell plateau. South of the Campbell plateau, poor correlation has been found between magnetic anomalies younger than number 20 on the classification of *Heirtzler et al.* [1968].

The most comprehensive analysis of magnetic and bathymetric data in the southwest Pacific Ocean has been presented by *Pitman et al.* [1968]. *Herron* [1971] has interpreted magnetic and bathymetric data in the southeastern Pacific as far west as 150°W. Much attention has recently been given to the Macquarie ridge by *Hayes et al.* [1972], *Houtz et al.* [1971], and *Christoffel* [1971].

We have obtained numerous magnetic and bathymetric measurements between New Zealand and Antarctica with our operations from the New Zealand antarctic supply ship, HMNZS *Endeavour*. We present here bathymetric and magnetic data, both from our own measurements and from previously published data, for the region between 150°W and 165°E that extends from the Campbell plateau in the north to south of the Pacific-Antarctic ridge. These data can be used to solve some of the questions raised in the interpretation of the plate tectonics of this and other regions.

## DATA REDUCTION

### *Data Sources*

For the region south of the Campbell plateau, most of the magnetic data have been obtained with our shipborne proton magnetometer towed from the *Endeavour* [*Christoffel and Ross*, 1965]. Those 18 tracks are identified in this paper by single letters. Portions of the tracks from the USNS *Eltanin* cruises 19, 23, 25, and 27 have been used [*Heirtzler et al.*, 1969; *Hayes et al.*, 1969] and are identified in the

* Now at Victoria University of Wellington, Wellington, New Zealand.

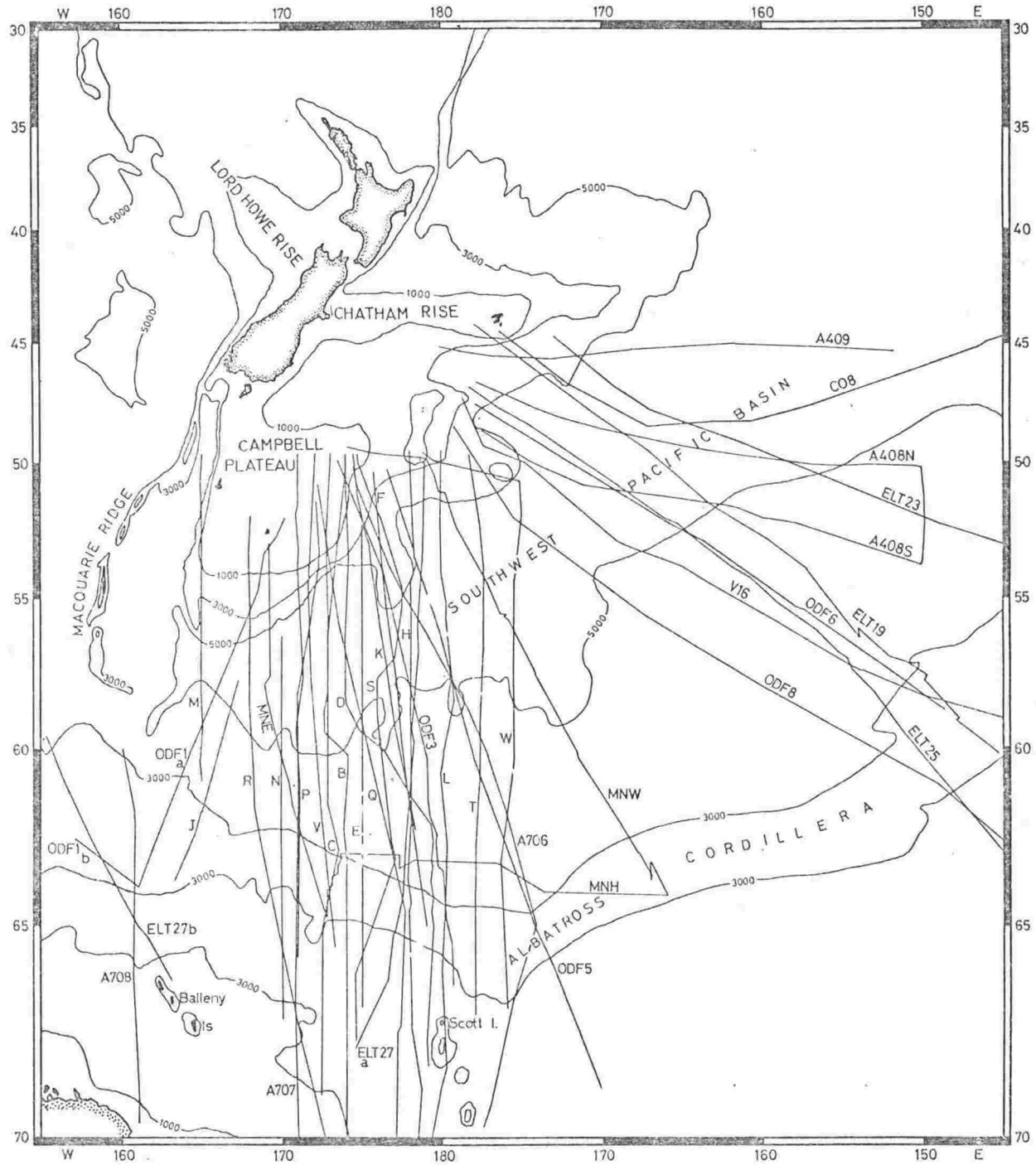


Fig. 1. Tracks used in the present study. The following abbreviations have been used: E, *Endeavour;* ELT, *Eltanin;* MN, Monsoon Expedition (RV *Argo*); ODF, Operation Deep Freeze (USNS *Staten Island* and *Burton Island*); A, aeromagnetic profiles from Project Magnet; V, *Vema;* CO, *Conrad.* Bathymetry contours are in meters.

following text and figures by ELT and the cruise number. Navigation, bathymetric, and magnetic measurements from the Operation Deep Freeze tracks 3, 5, 6, and 8 of the *Staten Island* and one track of the *Burton Island* have been obtained from the *U.S. Navy Hydrographic Office* [1962] and the *U.S. Naval Oceanographic Office* [1965]. These measurements are labeled ODF. Aeromagnetic profiles from Project

Magnet are identified by the letter A and the flight number. Portions of *Vema* cruise 16 are identified by V16, and portions of *Robert D. Conrad* cruise 8 are identified by CO8. Tracks from the Monsoon Cruise of the RV *Argo* from Scripps Institute of Oceanography are labeled MN.

*Navigation*

Most navigation was by conventional celestial and dead reckoning methods. The more accurate satellite navigation was available for *Eltanin* cruises 23, 25, and 27. Position errors for conventional navigation could be up to 75 km. Data from intersecting tracks show that average position errors are less than 25 km. Trends or offsets in anomaly patterns are considered established only to the latter limit unless several tracks delineate the feature.

*Magnetic Data Reduction*

The magnetic anomaly profiles were produced by subtracting from the recorded total field measurements a regional magnetic field calculated from the international geomagnetic reference field (IGRF) coefficients [*Fabiano and Peddie*, 1969]. The IGRF coefficients may require some revision since the anomaly profiles in this area had mean values differing considerably from zero. Most of the anomaly trends with wave lengths greater than 200 km were removed by this method. The only additional adjustment to any profile was the shifting of the zero reference line; the shift was equivalent to the removal of very long wave length components. No corrections were made for temporal variations. For the *Endeavour* cruises, the magnetic K indices and magnetic variograph recordings from Scott Base, Antarctica (77°51'S, 166°45'E), and Amberley, New Zealand (43°10'S, 172°45'E), have been checked over the cruise periods. No substantial magnetic storms occurred during the periods of measurement.

Anomalies are numbered according to the system of *Pitman et al.* [1968]. We have added the identification 32A for a characteristic positive anomaly just preceding anomaly 32.

## DATA ANALYSIS

Figure 1 shows the tracks for which magnetic data are presented. Also shown are bathymetry contours that were compiled from *Laurence* [1967], *U.S. Naval Oceanographic Office* [1969], *Udintsev et al.* [1964], and the New Zealand Oceanographic Institute (unpublished data, 1971). Figure 2 shows five bathymetric and magnetic profiles that we consider to be representative of the area. These profiles illustrate several features the identification of which simplifies the analysis.

The ELT25 magnetic profile exhibits symmetry about the ridge center (the Albatross cordillera) and contains an almost complete sequence of magnetic reversals. The corresponding bathymetric profile also shows general symmetry and is typical of bathymetry found over the East Pacific rise.

Profile ODF5 is similar to profile ELT25 in that symmetry about a spreading center is observed out to anomaly 5. The sequence of anomalies from 25 to 32 is also clearly seen, but, although this section is of similar length to that in ELT25, this section is closer to the ridge axis and the anomaly sequence 5–25 is not wholly clear.

The magnetic profile H shows the anomaly group 25–32, again with similar length to the previous profiles. No symmetrical center is obvious on either the magnetic or the bathymetric profile. High amplitude, short wave length anomalies are observed where the topography is most broken.

Profile B still shows the anomalies 25–32 but shows them closer to the 'ridge.' The section of disturbed bathymetry is rougher and broader than that to the east.

The ELT27b magnetic profile clearly shows symmetry, and the anomaly sequence agrees closely with that of the currently spreading ridges [*Vine*, 1966]. The bathymetry is also symmetrical. This profile indicates an area of active sea floor spreading similar to that observed much farther to the east along the ELT25 track.

These representative profiles illustrate the uniformity and persistence of the older magnetic anomalies throughout most of the area, the presence of active spreading in both the east and the west, and a region of disturbed bathymetry and magnetic signatures in between. In the light of these general observations, we shall divide the area into three regions and discuss them separately.

*Region 1*

This region includes the area containing magnetic anomalies numbered 25 and upward. The sequence of anomalies numbered from 25 to 32 is dated by *Heirtzler et al.* [1968] as covering the time span of 63–76 m.y. The sequence is identifiable on almost every track in this area.

Figure 3 shows the positions of these anomalies together with assumed trends and offsets. All the profiles

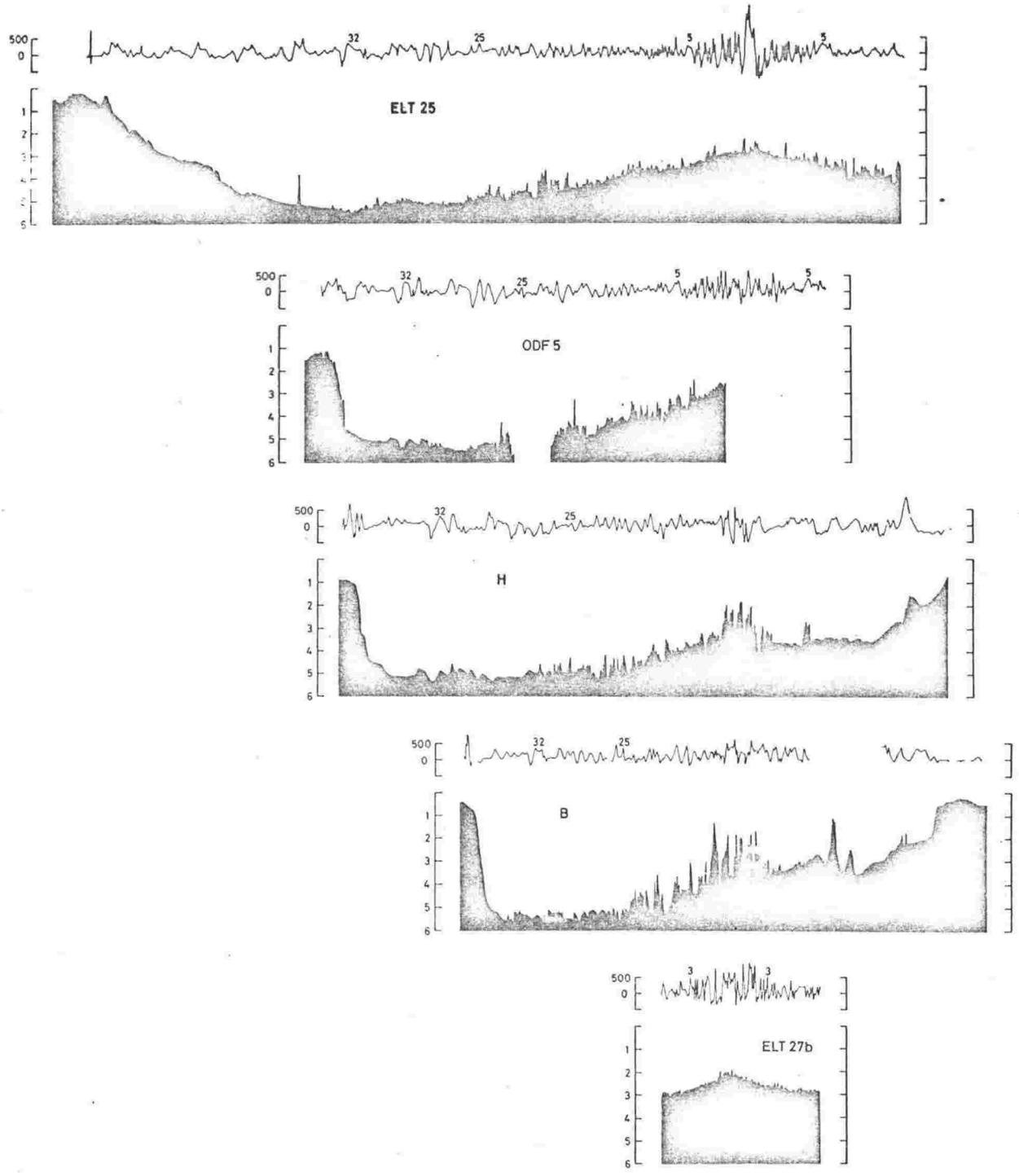


Fig. 2. Magnetic and bathymetric profiles for five tracks across the Southwest Pacific basin showing characteristic features discussed in the text. The upper trace in each pair of profiles shows the magnetic anomaly and scale in gammas; the lower trace in each pair of profiles shows the bathymetry scale in kilometers.

on which this figure is based are shown in Figures 4 and 5. The azimuths of the tracks vary considerably, and the profiles have been projected to produce roughly the same length of the sequence. For this reason, the positional relationships of the anomalies should be taken only from Figure 3.

A profile from the North Pacific (labeled NPAC) is included in Figures 4 and 5. This profile from *Raff*

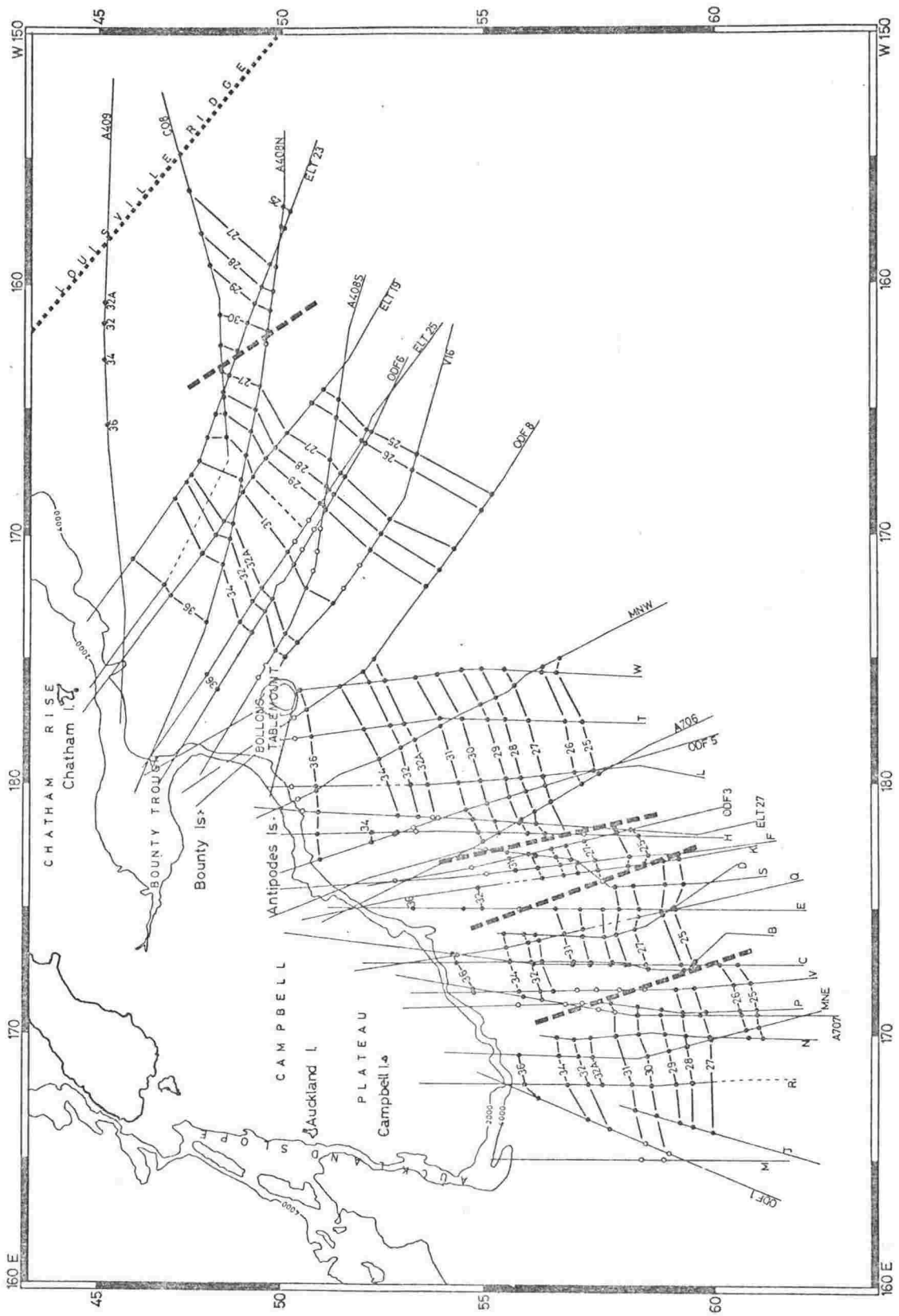


Fig. 3. Inferred correlation of magnetic anomalies in region 1 (anomalies 25–36). Fracture zones are shown as broken lines.

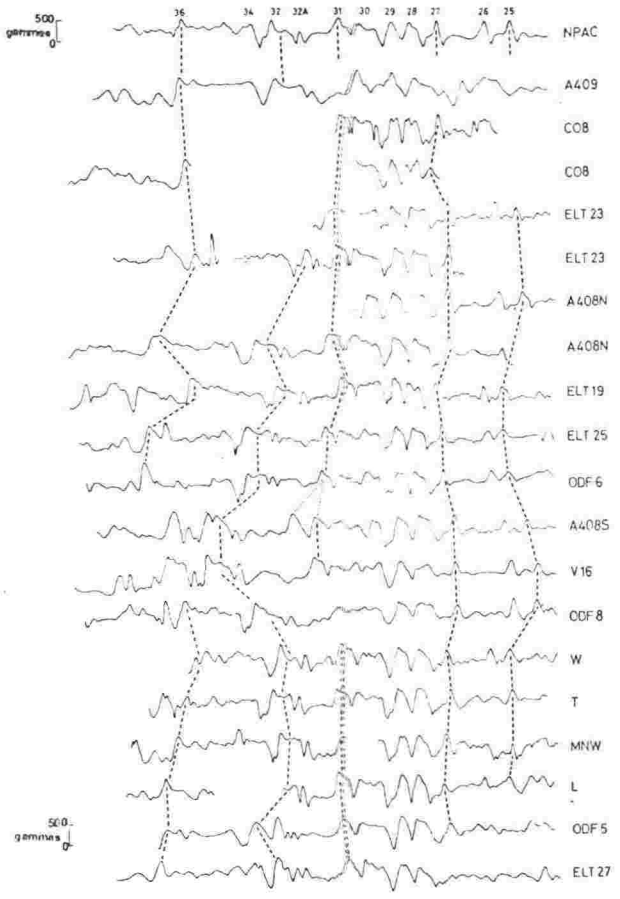


Fig. 4. Magnetic anomaly profiles from the northeastern portion of region 1. Profiles are aligned on anomaly series 27–31. Correlations of selected anomalies between tracks are shown as broken lines.

[1966] has previously been used out to anomaly 32 to establish the geomagnetic time scale [*Heirtzler et al.*, 1968]. An extension of this time scale is indicated by the fairly regular occurrence of a broad positive anomaly beyond anomaly 32. This broad anomaly, labeled by the numbers 34 and 36, is seen clearly on profiles A409, A408N, ODF8, and MNW. The anomaly can also be identified on some North Pacific profiles [*Raff*, 1966, Figure 2, tracks A, B, Q, R, and S]. By assuming the sea floor spreading rate for the section 32–36 to be the same as that immediately prior to anomaly 32, the age of anomaly 36 is approximately 81 m.y. Anomalies older than this age cannot be firmly correlated in this area.

Details of the anomaly pattern are discussed below. In general, the discussion proceeds from east to west in Figure 3. The profiles in Figures 4 and 5 are arranged with the most easterly profiles at the top.

In profile A409 along 45°S, the identification of anomalies 32A–36 is tentative but reasonable. The anomalies to the east of 32A are not very similar to those observed to the south. *Hayes and Ewing* [1971] have identified an apparently continuous aseismic ridge (the Louisville ridge) indicated in the upper right-hand corner in Figure 3. If their suggestion that this ridge is a westerly extension of the Eltanin fracture zone is correct, the sea floor to the east of the ridge could be quite different from that to the west. This suggestion would explain the irregular anomalies observed on A409 and at the eastern end of CO8.

In Figure 4, profiles CO8, ELT23, and A408N are each split into two, although the tracks are straight and continuous. We see that anomalies 27–30 are duplicated. Figure 3 shows that this duplication indicates an offset in the anomaly pattern of about 340 km

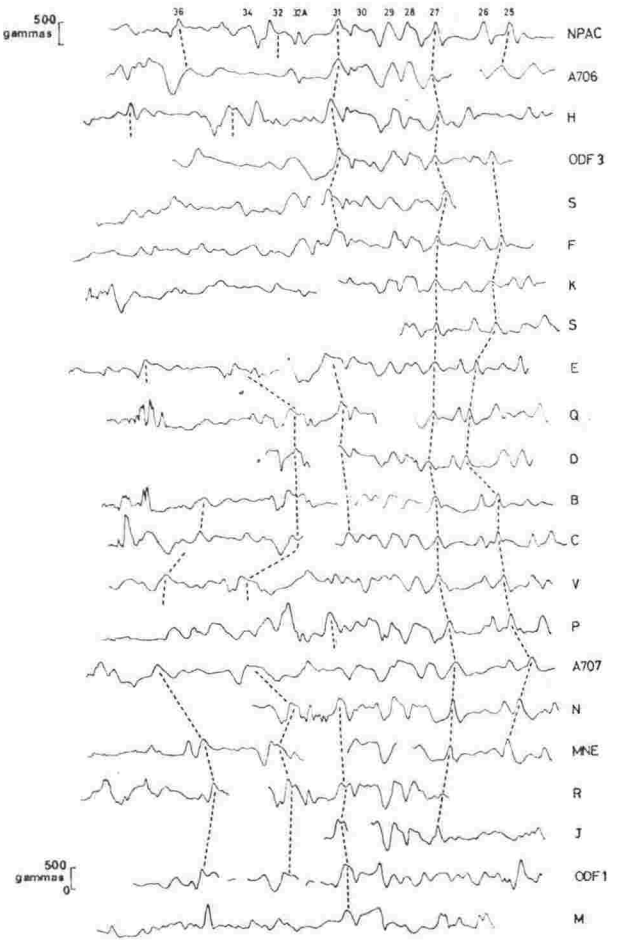


Fig. 5. Magnetic anomaly profiles from the southwestern portion of region 1.

in a dextral sense. The strike of the presumed fracture zone is probably between due north and 30° west of north. The strikes of the anomalies in this area lie between 30° and 40° east of north. Thus the fracture zone is not at right angles to the anomaly trend. *Pitman et al.* [1968, Figure 2] show that where ELT23 crosses the offset there is a blocklike bathymetric feature. The top of the block is about 220 km wide and is 1200 meters higher than the surrounding flat sea floor. Note that the western set of anomalies 27–29 are directly over this block but are not in any way irregular.

West of the fracture zone, the pattern is clear except for a disturbance between anomalies 29 and 31 at 170°W. Profiles ELT25, ODF6, A4085, and V16 indicate a broadening of anomaly 30. On ELT25, this broadening corresponds to a very slight bathymetric hump.

The anomaly pattern between 175°W and 180° is quite regular with a trend of N 70°E. This area has not been linked with that to the east for the following reasons:

1. Profiles ODF6 and V16 both show an apparent duplication of anomalies 32A and 32 and do not have anomalies 34–36.
2. The group of anomalies 32A and 32 is displaced 200 km northward with respect to the similar anomalies west of 175°W.
3. Profile ODF8 shows no anomaly 30 or 31.
4. The trend of anomalies 25–29 west of 175°W is different from that to the east. However, the eastern trend, N 30°E, is critically determined by track ODF8.

These points suggest that between 170°W and 175°W there is either a marked change of trend or one or more offsets. The data are insufficient to resolve these alternatives.

Between 175°E and 180°, *Christoffel and Ross* [1970] have mapped a fracture zone with a variable sinistral offset tending to zero at 60°S. The addition of more data in this study indicates that this area is more complex. On most profiles, anomalies 25–31 are relatively clear (e.g., A706, ODF3, E). However, the area north of anomaly 31 is best considered unclear (e.g., profiles S, F, K). At 178°E, profiles ODF5 and H indicate a dextral offset of anomalies 32A–34, but this offset cannot be identified either to the north in anomaly 36 or to the south. It is thus a localized feature. Farther west, the Endeavour fracture zone of *Christoffel and Ross* [1970] consists of two separate fractures, each with a sinistral offset and each striking normal to the anomaly trend. The displacement across each fracture zone is difficult to determine because the offsets are clear only over short lengths. The displacement across the fracture at approximately 179°E is about 45 km. The fracture at 177°E indicates a displacement of 55 km. When the fractures are considered together, the total displacement is comparable to that given by *Christoffel and Ross* [1970].

West of 175°E, the pattern is relatively clear. The complete sequence 25–36 is identifiable from several profiles, e.g., B, C, A707, MNE. A sinistral offset occurs between 173°E and 172°E. The offset of anomaly 25 is about 80 km, but the offset of anomaly 32 is only 45 km. This difference is not conclusive because profiles P and A707 are disturbed north of anomaly 30 and profile V is disturbed north of anomaly 28. Thus, possibly, the offset along this fracture decreases to the north.

West of 166°E, the pattern is confused. Anomalies 30 and 31 are tentatively identified on ODF1 and M, but the other anomalies of the sequence are not obvious. Unpublished *Eltanin* data recorded farther to the west also suggest that the regular anomaly pattern does not extend beyond about 165°E.

The anomaly sequence 25–32 shows that between 150°E and 165°W the sea floor of the Southwest Pacific basin is basically uniform in structure, although numerous offsets do occur. From Figure 3 we notice that west of 180°, anomaly 36 is close to the continental slope. The offsets on the fracture zones are such that the anomalies are successively displaced southward to the west and thus maintain a uniform distance from the steep continental slope.

East of 175°W, the continental slope is not so steep, but the anomalies still appear to maintain a constant distance from the New Zealand continent. The dextral offset on the major fault at 163°W is consistent with the eastward trend of the continent north of 45°S.

Around 50°S, 180°, the bathymetry is not well known, but a prominent bathymetric feature, the Bollons tablemount [*Lawrence*, 1967], is usually charted. The V16 track shows no sign of this feature, but it is seen on track T. The feature has thus been plotted smaller and farther to the south than is usually shown. The fact that anomaly 36, which occurs just south of this feature, is elsewhere close to the continent suggests that the Bollons tablemount may be a continental fragment. The presence of a continental fragment may explain why the magnetic

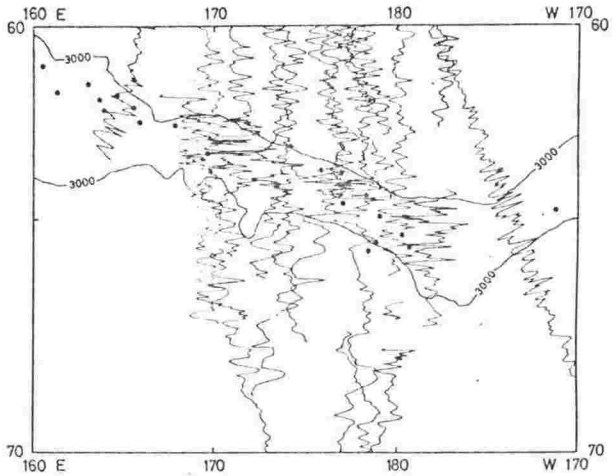


Fig. 6. Magnetic anomaly profiles over the Pacific-Antarctic ridge (region 2). Earthquake epicenters from *Barazangi and Dorman* [1969] and the 3000-meter bathymetric contour are shown.

trends are disturbed in the area. Anomaly 32 just to the east of the tablemount would be related to the continental slope well to the northwest.

The recognizable pattern of anomalies terminates to the west along 165°E; this longitude is in line with the Auckland slope that forms the western boundary of the Campbell plateau. This location further suggests that the anomalies are closely related to the continent bounding them to the north.

*Region 2*

The profiles in Figure 2 show that active sea floor spreading occurs east of 175°W and west of 160°E. Irregular high amplitude magnetic anomalies are observed on sections of profiles between those longitudes. Figure 6 shows that the irregular anomalies occur on many profiles and that they define a linear feature striking N 75°W. This feature coincides with an irregular bathymetric feature [*Ross*, 1967] and is associated with numerous earthquake epicenters [*Barazangi and Dorman*, 1969]. All the profiles west of 150°E that cross either the spreading ridge or the linear feature are shown in Figure 7. They have been plotted so as to align the prominent central anomaly of each profile and have been arranged in order of longitude with the most eastern profiles at the top.

If we consider the evidence for recent sea floor spreading to be the typical prominent squarish central anomaly and the characteristic anomaly sequence on both sides or even on only one side [*Vine*, 1966], then sea floor spreading is clear on only a few profiles. These profiles are ODF8, MNW, MNH, and

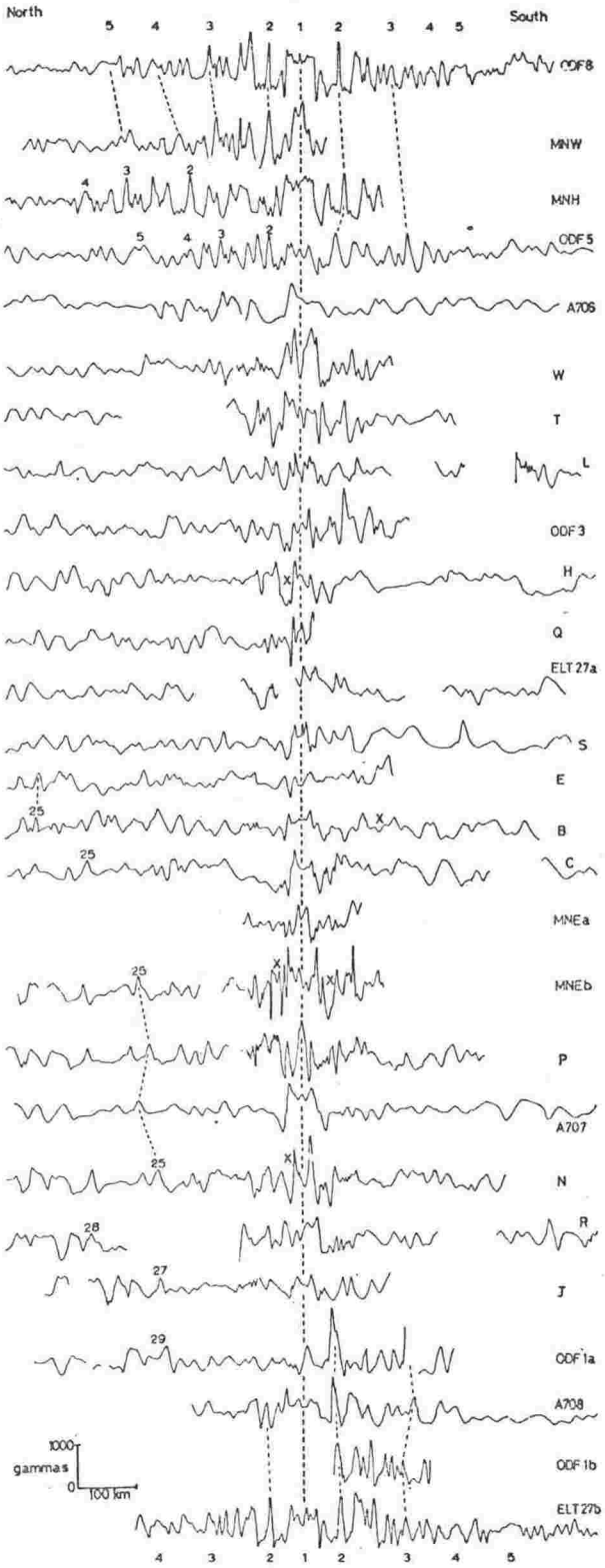


Fig. 7. Magnetic profiles across the Pacific-Antarctic ridge. Profiles are aligned on the 'central' anomaly. Other possible centers of symmetry are marked by an ×. The easternmost track is at the top.

ODF5, (all east of 180°) and ELT27b, ODF1b, and A708 (all west of 161°E). Profile ODF1a indicates part of the normal sequence on the south side. The central anomaly with the peak on either side associated with the Jaramillo event can be suggested for several other profiles but can be considered clear only on T and MNEb. Limited symmetry is visible in W, ODF3, H, B, C, P, and N. In profiles H, B, MNEb, and N, possible alternative centers of symmetry are recognized. These centers are marked with an × in Figure 7.

The alignment of profiles prejudices the visual identification of the prominent anomalies, symmetry centers, and identified sequences. Tests with 50 first year university students suggest that perception of such features depends largely on the scale in which profiles are drawn, similar amplitudes for symmetric anomalies, lack of data gaps, prealignment, and the availability of tracing paper. Numerical methods being developed by R. K. H. Falconer show signs of being able to overcome the visual problems.

*Ross* [1967], using five bathymetric profiles and seven magnetic profiles between 163°E and 180°, has shown that the high amplitude magnetic anomalies are associated with the crest of a rough ridge. More recent data confirm that this ridge is much rougher than the sections to the east and west on which active spreading is observed (Figure 8). The ridge is also noticeably asymmetric. The Balleny basin immediately south of the crest is flat-floored with a mean depth of 3 km. There is virtually no transition zone between the ridge and this basin. North of the ridge crest, rough flanks extend to the Southwest Pacific basin at a depth of 5 km. This depth is 2 km deeper than the Balleny basin.

Magnetic data are incomplete on most profiles in the Balleny basin because pack ice is often encountered there. However, the data are sufficient to show that anomaly wave lengths are longer than those observed across the ridge flanks to the north. No clear anomaly correlations have been established. Calculations of the depths to anomaly sources by *Ross* [1967] gave a mean anomaly depth that was less than 1 km deeper than the sea floor. Seismic profile records from *Houtz et al.* [1971] and more unpublished *Eltanin* data also show that the sediment thickness in the Balleny basin is less than 1 km. The bathymetric asymmetry is therefore not due to sediment in the Balleny basin.

For the period 1961–1967, *Barazangi and Dorman* [1969] list 19 earthquake epicenters for this area between 160°E and 180°. All are on or close to the linear feature defined by the bathymetry and magnetics. For the 20° of longitude from 180° to 160°W, only three epicenters are given. Data from many sections of the mid-ocean ridge suggest that most of the activity is on fracture zones that offset the ridge crest [*Sykes*, 1970].

The magnetic, bathymetric, and epicentral data all suggest that the prominent feature striking N 75°W between 180° and 160°E is a major fracture zone. We propose to call this feature the Pacific-Antarctic fracture zone.

In Figure 6, we see that the disturbed magnetic zone, presumably the result of fracturing, is about 70 km wide. This width also corresponds to the width of the ridge shown by the bathymetry. The epicenters of *Barazangi and Dorman* [1969] and *Sykes* [1970] for this region are scattered from a line to distances greater than the stated accuracy of determination. All these results show the Pacific-Antarctic fracture zone to be a broad feature. The short sections of symmetry on some magnetic profiles suggest that the fracture zone may consist of a series of en echelon fractures.

The western end of the fracture zone is not well defined but the actively spreading ridge clearly identified from profiles ELT27b, ODF1b, A708 (Figure 7) and the unpublished *Eltanin* data strikes N 55°E and would intersect the fracture zone at about 61°S, 162°E. The form of the Macquarie ridge in this area is not accurately known, but in general the form appears to be a fracture zone rather than a ridge [*Christoffel*, 1971; *Hayes et al.*, 1972]. The Pacific, Indian, and antarctic plates therefore meet in a triple junction that is of the ridge–fault–fault type [*McKenzie and Morgan*, 1969]. This junction is at 61°S, 162°E.

A change in the bathymetry trend of approximately 90° occurs at 65°S between 180° and 175°W, the epicenter lineation terminates at 65°S, 177°W, and sea floor spreading is clearly identifiable on profile ODF5 at 175°W. These three observations suggest that the Pacific-Antarctic fracture zone terminates in the east at 65°S between 180° and 175°W. The zone is thus approximately 1100 km long.

The strike of the ridge (Albatross cordillera) east of the fracture zone is difficult to determine because spreading is clearly seen on only MNW, MNH, and ODF5. Profile MNH is important because it is the only one running predominantly east-west. Anomalies 4–2 are clear but are displaced considerably from a spreading center to the east that is identified by the

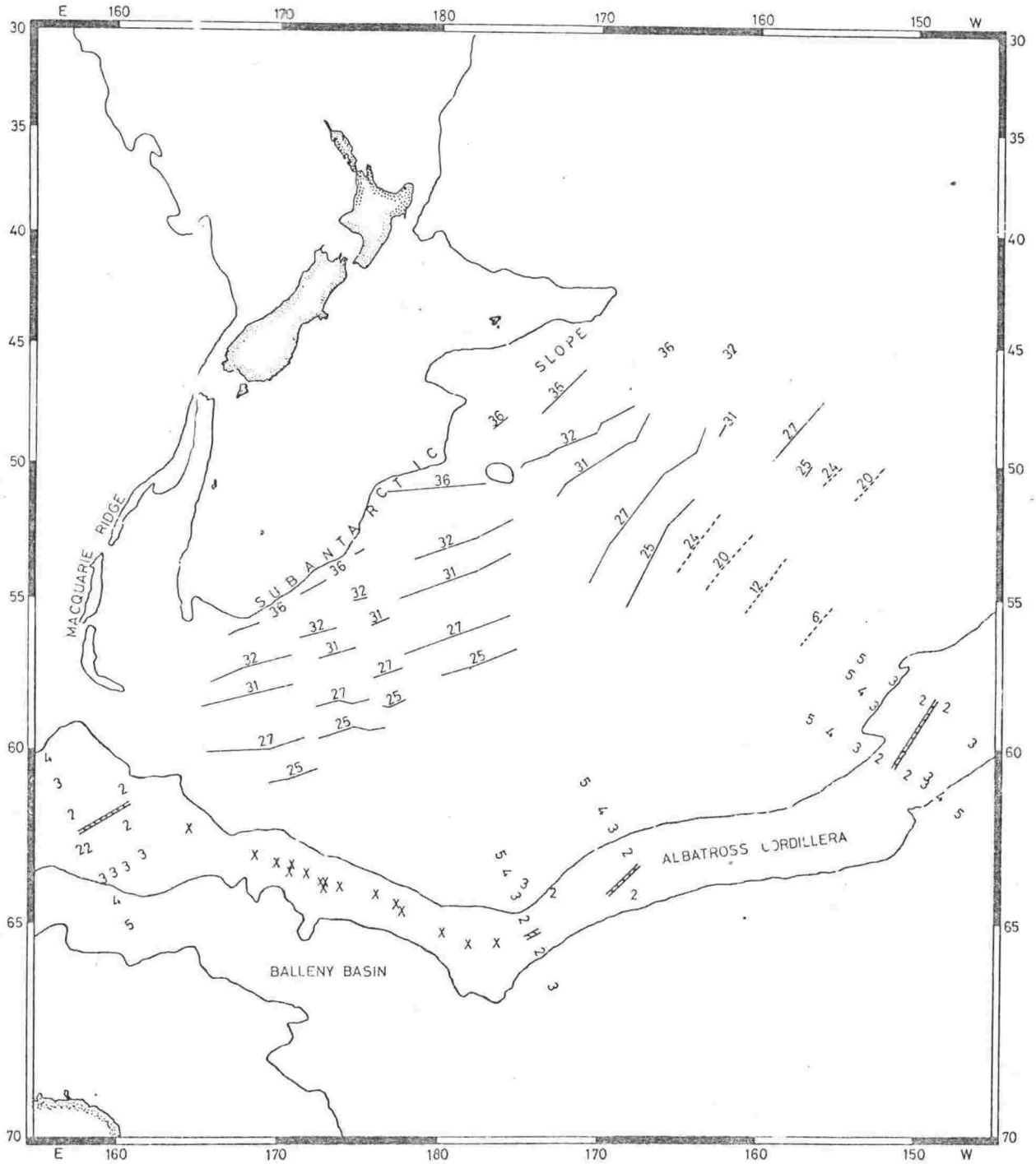


Fig. 8. Correlations of magnetic anomaly profiles in the three regions. Anomalies are numbered in the *Heirtzler et al.* [1968] convention. Along Pacific-Antarctic fracture zone, ×'s mark the positions of the 'central' anomaly.

central anomaly and characteristic anomalies east of it on the same profile. The general trend of the ridge is N 60°E, but probably in this area the ridge consists of short offset sections that may strike N 45°E. These ridge sections may not be normal to the direction of spreading, which should be parallel to the Pacific-Antarctic fracture zone. These sections are shown diagrammatically in Figure 8. Similar short

ridge sections are observed farther east over much of the Albatross cordillera [*Herron*, 1971].

*Region 3*

The area between the well-identified anomalies 25–36 and the ridge and fracture zone to the south is difficult to interpret (Figure 8). East of 170°W, bathymetry profiles show relatively smooth ridge flanks that merge into the Southwest Pacific basin. *Heirtzler et al.* [1968] have shown that magnetic anomalies along some sections of ODF6, ELT19, and ELT23 can be correlated with profiles from elsewhere in the world. However, throughout the area east of 170°W, the anomalies over the flanks between the numbers 5 and 25 have amplitudes less than half of those older than 25. The wave lengths are also generally shorter. The general appearance of the profiles is one of noise rather than the more distinctive patterns of both the older anomalies and the crest region. Detailed correlations are possible only when tracks are close, and even then correlations are not unambiguous. Identified anomalies are shown in Figure 8, but the trends indicated throughout this flank region east of 170°W should be considered tentative only.

To the west of 170°W, the data coverage is better, but the interpretation is no clearer. Bathymetry profiles show that the flanks of the Pacific-Antarctic fracture zone are rougher than the more conventional ridge flanks to the east of 170°W. Also, a sharper bathymetric boundary occurs between the flanks and the basin [*Christoffel and Ross*, 1965]. Neither the magnetic anomaly amplitudes nor the wave lengths differ greatly from those in the regions to the north or south. In this respect, they contrast with the anomalies to the east of 170°W.

Correlations between the tracks could be suggested, but these correlations would be so ambiguous that they would be of little real value. The rougher bathymetry presumably is a disturbing factor, but the area appears complex. Tracks with orientations other than north-south and closer track spacings are needed if correlations are to be identified.

## CONCLUSIONS

We can now extend our interpretation of the southwest Pacific Ocean in terms of plate tectonics beyond that of *Christoffel and Ross* [1970]. Figure 9 shows the main features that we intend to discuss.

On the basis of a consistent magnetic anomaly pattern south and east of the Campbell plateau, we feel justified in extending the *Heirtzler et al.* [1968] anomaly sequence from 32 to 36. Anomaly 36, calculated at 81 m.y., closely follows the 3500-meter contour at the base of the subantarctic slope. Our data extend just beyond the Albatross cordillera and allow us to recognize only one-half the magnetic anomaly pattern. However, we feel confident in predicting the mirror pattern to exist in the Southeast Pacific basin. We therefore conclude that the New Zealand continent rifted from the region of West Antarctica just prior to 81 m.y. ago. The Louisville ridge possibly formed an eastern boundary with a South American plate in a manner similar to the present-day Chile rise [*Herron and Hayes*, 1969].

At the time of anomaly 25 (i.e., 62 m.y. ago), a change in the spreading occurred. Recognition of younger anomalies becomes progressively less clear so that, west of 170°W, anomalies between 25 and 5 are unrecognized. The most probable reason for this can be seen from Figures 8 and 9. The mean strike of each of the fracture zones between anomalies 25 and 36 south of the subantarctic slope is reasonably well established from our measurements. The present strike of the Pacific-Antarctic fracture zone is also well determined, and we also assume that the strikes of the other fracture zones across this southern section of the Albatross cordillera will be determined by the same pole of relative motion. Between anomalies 25 and 5, a change in strike of over 15° has to be accommodated. From Figures 8 and 9, we see that the triangular region bounded by longitudes 170°E and 170°W is particularly affected. Considerable fracturing would be expected and is borne out by the disturbed topography. Probably only short segments of coherent spreading ridges will be present, these short segments requiring comprehensive magnetic and bathymetric surveys to establish any reasonable correlation of anomalies.

Although the measurements of *Christoffel and Ross* [1970] can be interpreted as showing a continual transition of the spreading direction, the rate of change must have considerably increased more recently than anomaly 20. The traces of the old transform faults south of the subantarctic slope have sinistral displacements. The present ones along the Albatross cordillera between 150°W and 175°W obviously have dextral displacement. We are unable to trace the old fracture zones to the south beyond anomaly 25, but there may be a pattern of continual transition of strike similar to that reported in the North Pacific Ocean by *Menard and Atwater* [1968]. If so,

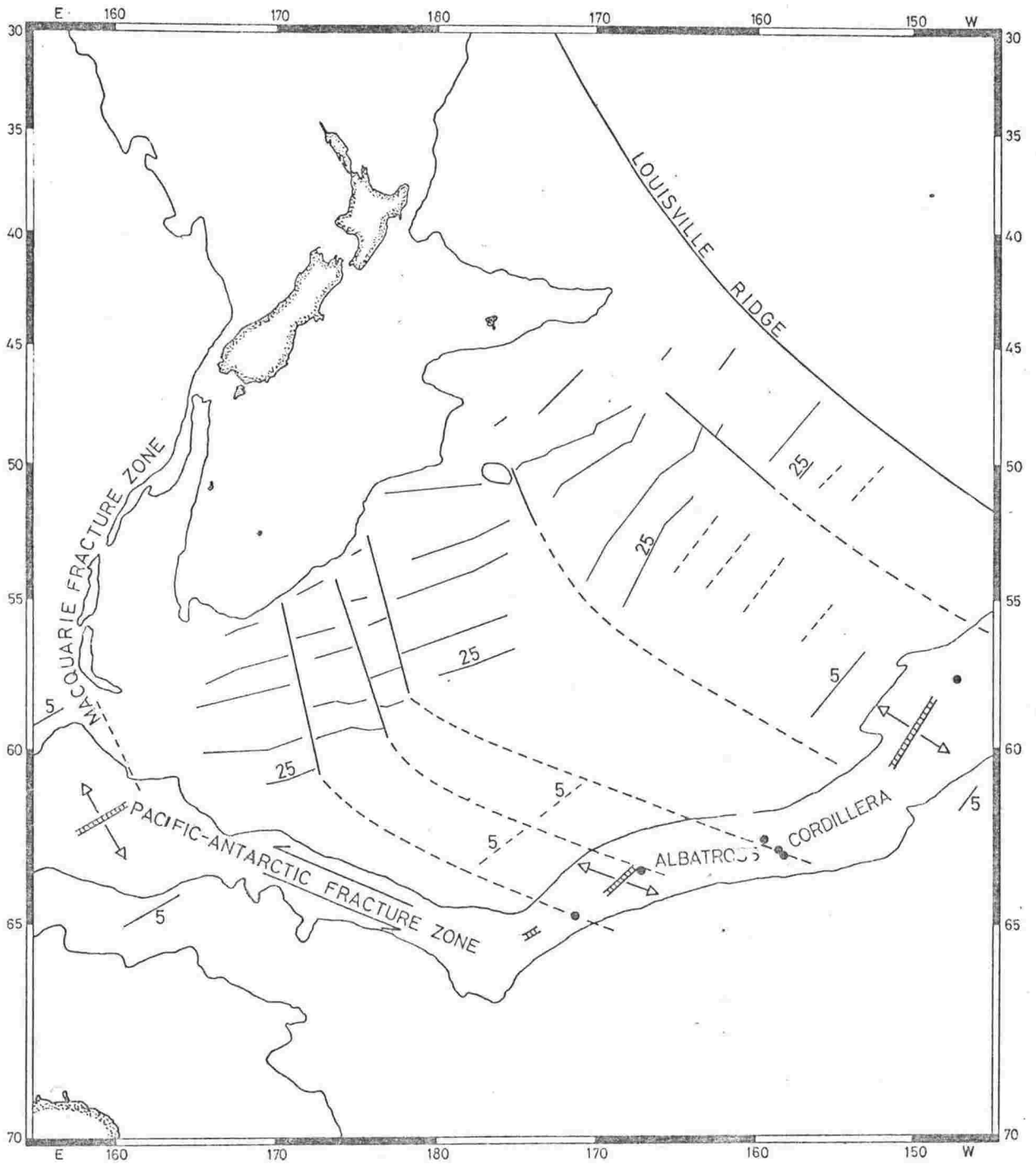


Fig. 9. Model of sea floor spreading in the southwestern Pacific. Solid lines mark established fracture zones; broken lines show inferred trends. Arrows indicate directions of motion. Closed circles on the Albatross cordillera are epicenters from *Barazangi and Dorman* [1969].

the fracture zones could continue in a manner shown by the broken line extensions in Figure 9.

Since anomaly 5 (i.e., 10 m.y. ago), the pattern of spreading seems to have persisted about the same relative pole of rotation until the present. We can identify a major fracture zone, which we propose to call the Pacific-Antarctic fracture zone, that extends at least 1200 km from approximately 65°S, 175°W

to 61°S, 162°E. This fracture zone corresponds to a pole of relative motion for the Pacific and antarctic plates at 82°S, 120°E rather than to the *Le Pichon* [1968], pole at 70°S, 118°E.

*Acknowledgments.* We gratefully acknowledge the cooperation from the Royal New Zealand Navy and the officers and men of HMNZS *Endeavour* for making our antarctic operations possible. We thank H. P. Stockard, U.S. Naval Oceanographic Office, for supplying us with microfilm copies of the Project Magnet records. Mrs. Feriel Falconer gave valuable assistance in data reduction and interpretation and in the drawing of some of the diagrams. D. A. Christoffel is indebted to Walter B. Pitman III, to the National Science Foundation grants GA-1415 and GV-23334, and to the Office of Naval Research grant N00014-67-A-0108-0004 for making possible a period of leave at Lamont-Doherty Geological Observatory, where the aeromagnetic and much of the shipborne data reduction was carried out.

Contribution 1779, Lamont-Doherty Geological Observatory.

## REFERENCES

Barazangi, M., and J. Dorman, World seismicity maps compiled from ESSA coast and geodetic survey epicenter data, 1961–1967, *Bull. Seismol. Soc. Amer., 59*(1), 369–380, 1969.

Christoffel, D. A., Total magnetic field measurements between New Zealand and Antarctica, *Nature, 190*, 776–778, 1961.

Christoffel, D. A., Motion of the New Zealand Alpine fault deduced from the pattern of sea floor spreading, in *Recent Crustal Movements*, edited by B. W. Collins and R. Fraser, *Roy. Soc. N. Z. Bull., 9*, 25–30, 1971.

Christoffel, D. A., and D. I. Ross, Magnetic anomalies south of the New Zealand plateau, *J. Geophys. Res., 70*(12), 2857–2861, 1965.

Christoffel, D. A., and D. I. Ross, A fracture zone in the south west Pacific basin south of New Zealand and its implications for sea-floor spreading, *Earth Planet. Sci. Lett., 8*, 125–130, 1970.

Fabiano, E. B., and N. W. Peddie, Grid values of total magnetic intensity, I.G.R.F. 1965, *Tech. Rep. C & GS 38*, Environ. Sci. Serv. Admin., Rockville, Md., 1969.

Hayes, D. E., and M. Ewing, The Louisville ridge–A possible extension of the Eltanin fracture zone, in *Antarctic Oceanology I, Antarctic Res. Ser.*, vol. 15, edited J. L. Reid, pp. 223–228, AGU, Washington, D. C., 1971.

Hayes, D. E., J. R. Heirtzler, E. M. Herron, and W. C. Pitman III, Preliminary report of volume 21, USNS *Eltanin* cruises 22–27, January 1966–February 1967, part A, Navigation, part B, Bathymetric and geomagnetic measurements, *Tech. Rep. 2-CU-2-69*, Lamont-Doherty Geol. Observ. of Columbia Univ., Palisades, N. Y., 1969.

Hayes, D. E., M. Talwani, and D. A. Christoffel, Macquarie ridge complex, in *Antarctic Geology and Geophysics*, edited by R. J. Adie, Universitets forlaget, Oslo, in press, 1972.

Heirtzler, J. R., G. O. Dickson, E. M. Herron, W. C. Pitman III, and X. LePichon, Marine magnetic anomalies, geomagnetic field reversals, and motions of the ocean floor and continents, *J. Geophys. Res., 73*(6), 2119–2136, 1968.

Heirtzler, J. R., D. E. Hayes, E. M. Herron, and Walter C. Pitman III, Preliminary report of volume 20 USNS *Eltanin* cruises 16–21 January 1965–January 1966, part A, Navigation, part B, Bathymetric and geomagnetic measurements, *Tech. Rep. 3-CU-3-69*, Lamont-Doherty Geol. Observ. of Columbia Univ., Palisades, N. Y., 1969.

Herron, E. M., Crustal plates and sea-floor spreading in the southeastern Pacific, in *Antarctic Oceanology I, Antarctic Res. Ser.*, vol. 15, edited J. L. Reid, pp. 229–237, AGU, Washington, D. C., 1971.

Herron, E. M., and D. E. Hayes, A geophysical study of the Chile ridge, *Earth Planet. Sci. Lett., 6*, 77–83, 1969.

Houtz, R., J. Ewing, and R. Embley, Profiler data from the Macquarie ridge area, in *Antarctic Oceanology I, Antarctic Res. Ser.*, vol. 15, edited J. L. Reid, pp. 239–245, AGU, Washington, D. C., 1971.

Lawrence, P., New Zealand region, Bathymetry, scale 1: 6,000,000, Miscellaneous Series, 15, N. Z. Oceanogr. Inst., Wellington, 1967.

Le Pichon, X., Sea-floor spreading and continental drift, *J. Geophys. Res., 73*(12), 3661–3697, 1968.

McKenzie, D. P., and W. J. Morgan, Evolution of triple junctions, *Nature, 224*, 125–133, 1969.

Menard, H. W., and T. Atwater, Changes in direction of sea-floor spreading, *Nature, 219*, 463–467, 1968.

Pitman, W. C., III, E. M. Herron, and J. R. Heirtzler, Magnetic anomalies in the Pacific and sea floor spreading, *J. Geophys. Res., 73*(6), 2069–2085, 1968.

Raff, A. D., Boundaries of an area of very long magnetic anomalies in the northwest Pacific, *J. Geophys. Res., 71*(10), 2631–2636, 1966.

Ross, D. I., Magnetic and bathymetric measurements across the Pacific-Antarctic ridge south of New Zealand, *N. Z. J. Geol. Geophys., 10*(6), 1452–1465, 1967.

Sykes, L. R., Seismicity of the Indian Ocean and a possible nascent island arc between Ceylon and Australia, *J. Geophys. Res., 75*(26), 5041–5055, 1970.

Udintsev, G. B., et al., New bathymetric map of the Pacific Ocean, *Oceanolog. Res., 9*, pp. 66–101, Inst. of Oceanolog., Acad. of Sci. of the USSR, Moscow, 1964.

U.S. Navy Hydrographic Office, Operation Deep Freeze 61, 1960–1961, Marine geophysical investigations, *Tech. Rep. 105*, Washington, D. C., 1962.

U.S. Naval Oceanographic Office, Operation Deep Freeze 62, 1961–1961, Marine geophysical investigations, *Tech. Rep. 118*, Washington, D. C., 1965.

U.S. Naval Oceanographic Office, New Zealand to Cape Adare, *H.O. 6710*, Washington, D. C., 1969.

Vine, F. J., Spreading of the ocean floor; New evidence, *Science, 154*, 1405–1415, 1966.

# Changes in the Direction of Sea Floor Spreading in the South-west Pacific

D. A. CHRISTOFFEL AND R. K. H. FALCONER
Physics Department, Victoria University of Wellington, Wellington, New Zealand

**Abstract**

A study of magnetic anomaly and bathymetric data extending from the Subantarctic slope to the Albatross Cordillera—Pacific Antarctic fracture zone gives evidence for at least three separate episodes of sea-floor spreading.

During the Upper Cretaceous (84–63 m.y.) relative spreading between New Zealand and Antarctica occurred about a pole north-east of the region at 0°, 120° W. During the Lower and Middle Tertiary (63–10 m.y.) the pole was possibly near the southern end of the (present) Macquarie Ridge 64° S, 160° E. Spreading for the Upper Tertiary has probably taken place about the pole determined by Le Pichon (70° S, 118° E).

Rotating of Antarctica back to New Zealand about these three poles gives a plausible reconstruction of the original fit between these two continents.

## INTRODUCTION

Correlations of marine magnetic anomalies south of the Campbell Plateau have established the existence of five substantial fracture zones (Christoffel and Ross, 1970; Christoffel and Falconer, 1972). The fracture zones appear as offsets of the Cretaceous magnetic anomalies 25–36. (63 m.y. to 82 m.y. on the time scale of Falconer (1973)). Fracture zones about the present Pacific-Antarctic pole of rotation at 70° S, 118° E, calculated by Le Pichon (1968), differ by 45–50° from the strikes of the Cretaceous transform fracture zones (fig. 1). The difference indicates that substantial changes in relative plate motions have occurred since the Cretaceous.

The anomalies 5–25 (10–63 m.y.) can be identified on magnetic profiles east of 175° W in the region 50° to 60° S. However, west of 175° W these anomalies cannot be recognised and there is a lack of correlation of anomalies between tracks south of 60° S. (Christoffel and Ross, 1965; Christoffel and Falconer, 1972). Because the anomalies 5–25 are not seen in this particular region Christoffel (1969) proposed that a pole of rotation for these anomalies lay at 64° S, 160° E.

The aim of this work is to examine the magnetic and bathymetric data south of the Campbell Plateau and find the best fit poles of rotation for the South-west Pacific. Following Christoffel and Falconer (1972), the region is divided into three sections which are defined by well-marked bathymetric and magnetic anomaly discontinuities. An attempt is then made to find a pole of rotation which best fits the data for each section.

*Oceanography of the South Pacific 1972, comp. R. Fraser. New Zealand National Commission for UNESCO, Wellington: 1973.*

## REGION 1: CRETACEOUS SPREADING

This region includes the magnetic anomalies 25–36 and covers the time 63 to 84 m.y. The five well-defined fracture zones are shown in fig. 1. In addition the Louisville Ridge (Hayes and Ewing, 1971) strikes across the north-east corner of the area forming the eastern boundary of the anomaly sequence. Its strike is sufficiently similar to the other fractures to allow the assumption that they were all formed about a common pole of rotation. Hayes and Ewing (1971) determined a pole at 5° N, 120° W for the mean strike of the full extent of the Louisville Ridge from the Pacific-Antarctic ridge to the Tonga-Kermadec Trench.

In fig. 1 fracture zones drawn about a pole at 0°, 120° W are superimposed on the fracture zones determined from the anomaly pattern. The strikes of the synthetic fracture zones agree to within 5° with those observed. This agreement is within the accuracy of the determinations. For comparison, fracture zones about the Le Pichon Pacific-Antarctic pole at 70° S, 118° E are also shown. The strikes of these fractures differ by up to 50° from the observed fractures. Spreading rates in the area are between 4.1 cm/yr and 3.6 cm/yr but do not vary in a regular manner. Christoffel and Ross (1970), and Christoffel and Falconer (1972), have shown that displacements across some of the fracture zones south of the Campbell Plateau are not constant. The variations may be due to adjustments in spreading rate after spreading commenced from an irregular shaped boundary (the Subantarctic slope). To obtain good estimates of the rate of spreading the other half of the pattern (in the Bellingshausen Basin) would need to be considered. Data for that area were not available. Based on the observed spreading rates a reasonable estimate of the half spreading angle for the Cretaceous pattern is 7°.

## REGION 2: RECENT SPREADING

This region is centred on the Albatross Cordillera and the Pacific-Antarctic Fracture Zone.

The Le Pichon (1968) pole at 70° S, 118° E, for the motion between the Pacific and Antarctic plates is generally regarded as well determined. However, Morgan (1968) and Le Pichon (1968) point out that the pole position is very dependent on the strikes of fracture zones west of 160° W. These are not well known. The pole position has important implications for the interpretation of the Pacific-Antarctic Fracture Zone between longitudes 160° E and 175° W.

Christoffel and Falconer (1972) have shown that

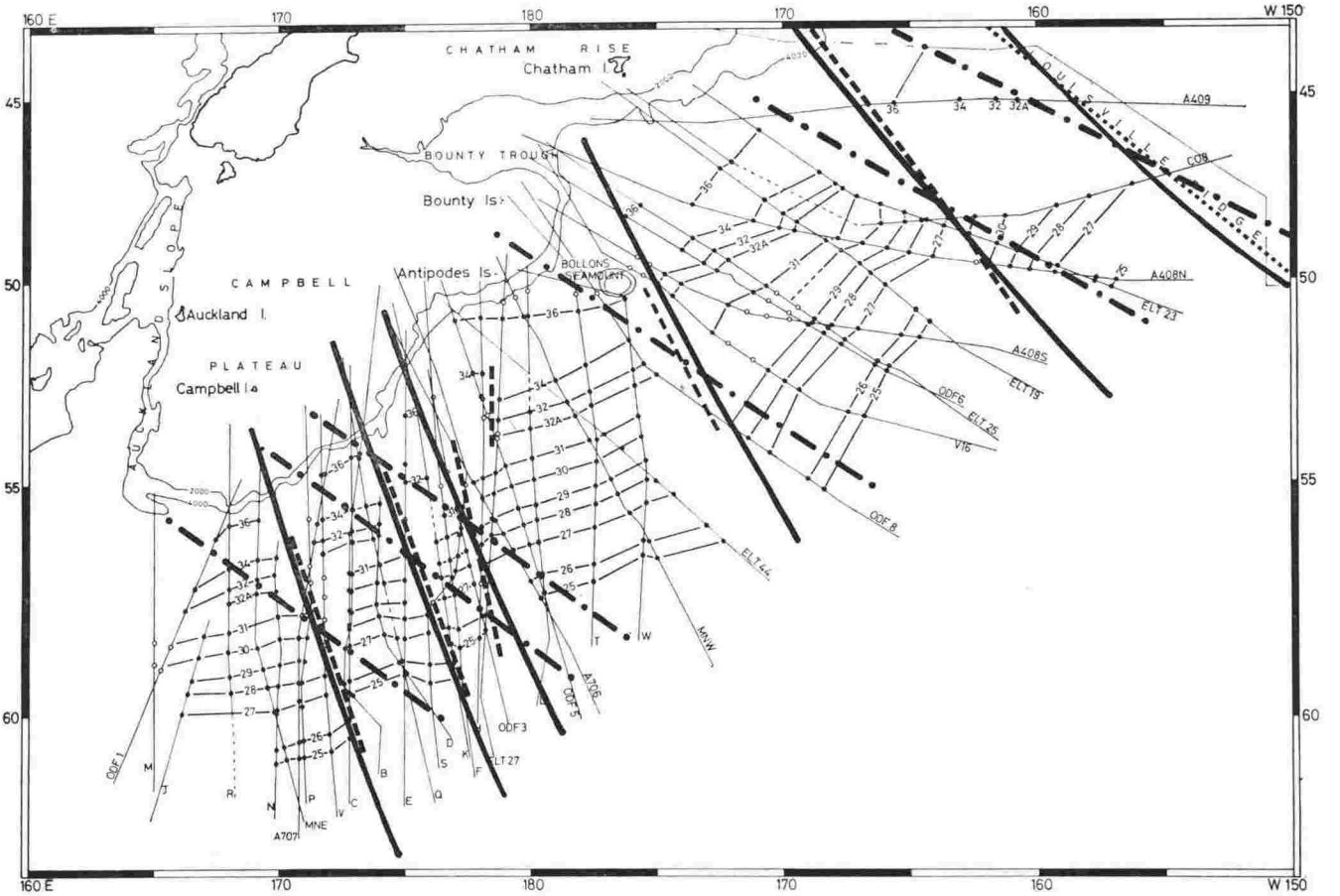


FIG. 1. Marine magnetic anomaly correlations and fracture zones for the Cretaceous anomalies, after Christoffel and Falconer (1972). Dashed lines are fractures established from the data. Heavy solid lines are fractures generated about a pole of rotation at 0°, 120° W. Dash and dot lines are fractures generated about the pole of Le Pichon (1968) at 70° S, 118° E.

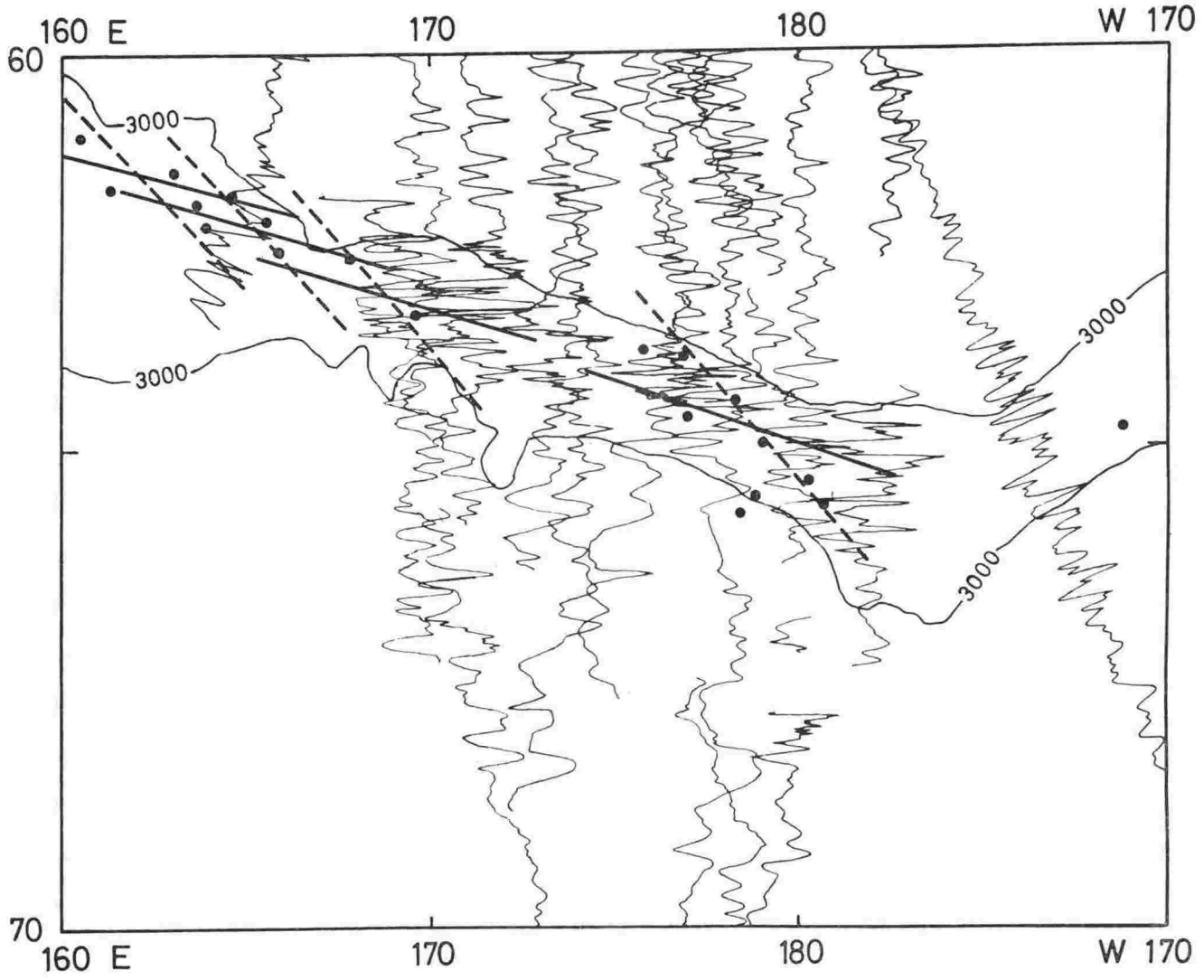


FIG. 2. Magnetic anomaly profiles across the Pacific-Antarctic Fracture Zone (from Christoffel and Falconer, 1972). Earthquake epicentres from Barazangi and Dorman (1969). Dashed lines, fractures about a pole at 70° S, 118° E; full lines, fractures about a pole at 82° S, 120° E.

although there are high amplitude short wavelength magnetic anomalies between 161° E and 175° W (fig. 2) the characteristic anomalies 1–5 cannot be recognised. The first profile east of 180° along which recent spreading can definitely be identified is that of ODF 5 (fig. 3). This track crosses the ridge at 65° S, 172° W, just east of where the ridge turns abruptly north-east. Westward of the bend the high amplitude anomalies and rough bathymetry are more characteristic of a fracture zone. The fractured nature of the ridge is apparent on profiles H and B (fig. 3) which are typical of crossings between 175° W and 161° E. The interpretation of this section as a fracture zone is confirmed by the high seismic activity (fig. 2), in marked contrast to the ridges to the east and west.

The bathymetric, magnetic, and seismic data indicate that the Pacific-Antarctic Fracture Zone is broad and so may be a series of *en echelon* fractures. The difficulty lies in determining the strikes of these fractures. If fractures are generated about the Le Pichon pole they strike across the general bathymetric axis at angles of around 25°, (figs 2 and 4). The five fractures shown in fig 4 fit the Sykes (1970) epicentres rather well. These epicentres are more accurately determined than those of Barazangi and Dorman (1969) but cover only the area west of 180°. Since the epicentres are slightly scattered and there are not more than five per fracture the reliability of the correspondence is low.

An equally plausible fit of the epicentres to fracture zones is to consider that the epicentres lie on fracture zones striking approximately N 75° W. A pole of rotation at 82° S, 120° E gives fractures with the correct strike, as shown in figs 2 and 4.

The pole at 82° S, 120° E with the same angular rotation rate as Le Pichon is compatible with spreading rates and fractures to the east across the Albatross Cordillera (Christoffel, 1969). Thus with the existing data it is difficult to choose between the two poles suggested. Mainly on the epicentre lineations the Le Pichon pole will be adopted here. However the other pole is not ruled out.

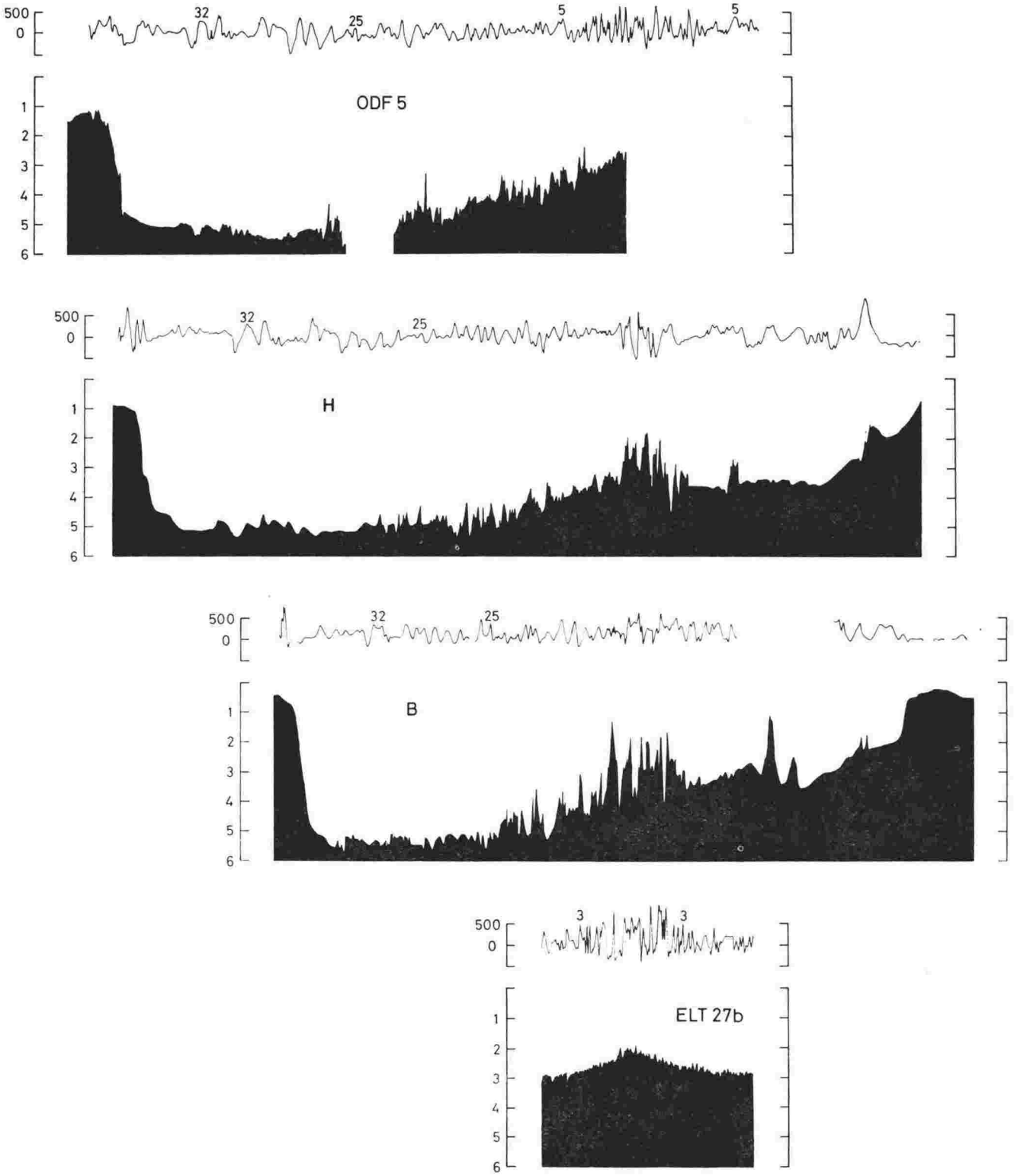


FIG. 3. Bathymetric and magnetic anomaly profiles across the Albatross Cordillera (ODF5), Pacific-Antarctic Fracture Zone (H and B), and Indian-Antarctic Ridge (ELT 27 b). Scales: Magnetic anomalies, gamma; bathymetry, km.

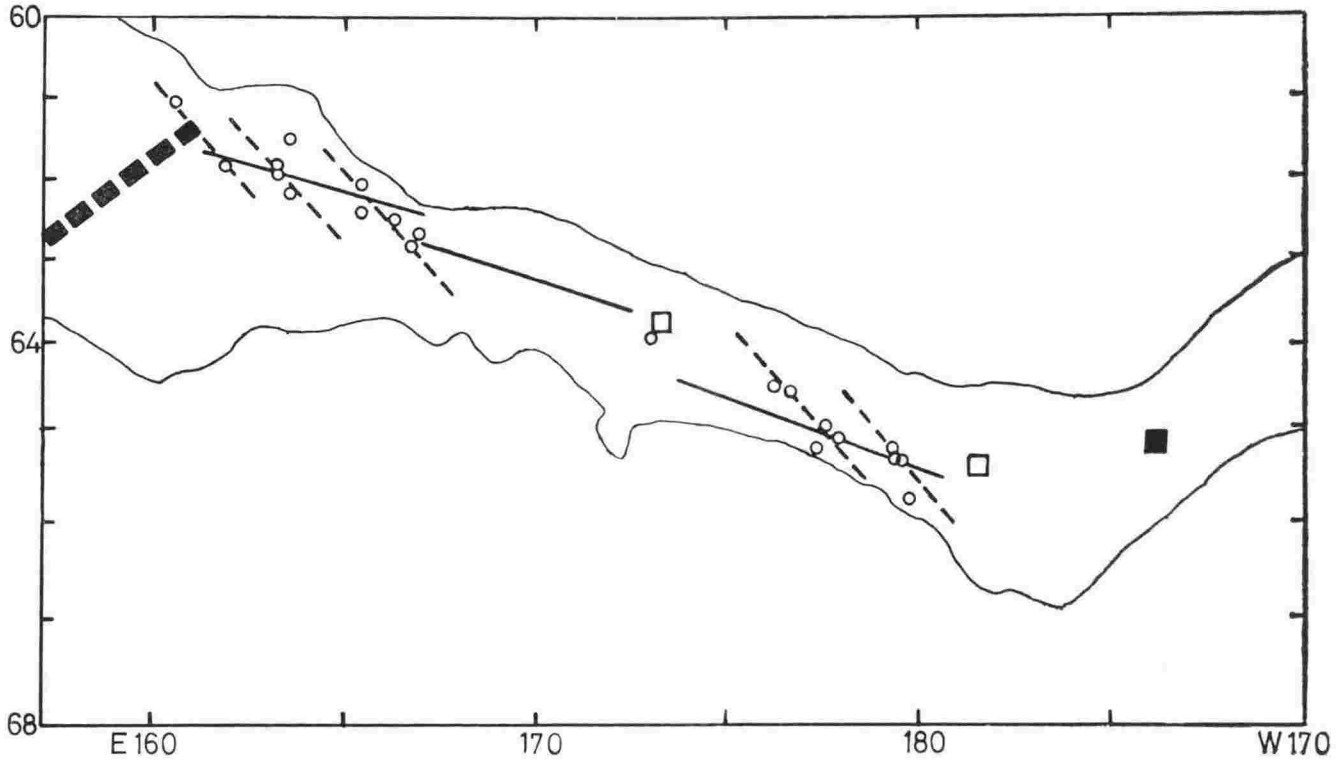


FIG. 4. The Pacific-Antarctic Fracture Zone. Epicentres from Sykes (1970) shown by circles. Fracture zones as in fig. 2. Heavy dashed line, the Indian-Antarctic Ridge from Falconer (1972). Other spreading centres shown by squares; open—tentative, closed—definite.

## REGION 3: LOWER AND MIDDLE TERTIARY SPREADING

Anomalies 5–25 represent the period from approximately 10 to 63 my. One way of explaining the inability to identify this anomaly sequence westward of 175° W is to assume that the spreading rate was low. Since the anomalies are identified further to the east it suggests that the pole of rotation may be south of the Campbell Plateau. Following Christoffel (1969) a pole at 64° S, 160° E is taken. Fracture zones about this pole, drawn through the continuations of the Cretaceous fracture zones are shown in fig. 5. For this pole the half angle of rotation from four determinations of spreading rate is 20.8° ± 1.7° (table 1).

TABLE 1

Determination of mean half spreading angle for region 3, about a pole at 64° S, 160° E.

| Position | Angular Spreading Degree Lat. | Half-spreading Angle Degree |
|---|---|---|
| 51° S 152° W | 9° | 19.2 |
| 56° S 160° W | 8° | 22.2 |
| 59° S 174° W | 4.5° | 19.7 |
| 60.5° S 178° E | 3.5° | 22.0 |
| Mean half spreading angle | | 20.8 ± 1.3 |

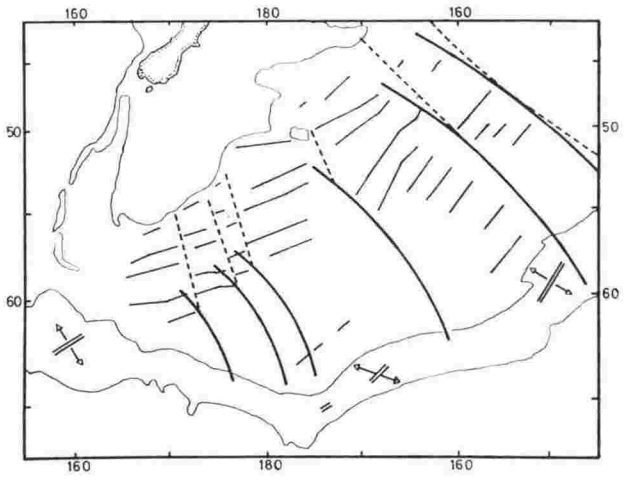


FIG. 5. Fracture zones generated about a pole of rotation at 64° S, 160° E for the region containing anomalies 5–25. Double line, spreading centre; single line, anomaly trends; dashed lines the observed Cretaceous fracture zones.

## COMPOSITE PICTURE

Putting together the spreading pattern given by the three separate poles of rotation (table 2) and assuming continuous extensions of the Cretaceous fracture zones the traces shown in fig. 6 are obtained. There is no reason for these fractures to be continuous and data are insufficient to trace them all the way. Nevertheless several of the fractures extend to presently active seismic areas on the ridge. Offsets in the ridge at 150° W (Herron, 1971) coincide with the intersection of one of the major fracture zones, and offsets in anomalies near 170° W are observed where a fracture zone is predicted.

TABLE 2
Poles and angles of rotation for spreading between Antarctica and New Zealand.

| Anomaly Span | Time Span m. y. | Pole Location | Angle of Rotation Degrees |
|---|---|---|---|
| 1– 5 | 0–10 | 70° S, 118° E | 10.8 |
| 5–25 | 10–63 | 64° S, 160° E | 41 |
| 25–36 | 63–84 | 0° S, 120° W | 14 |

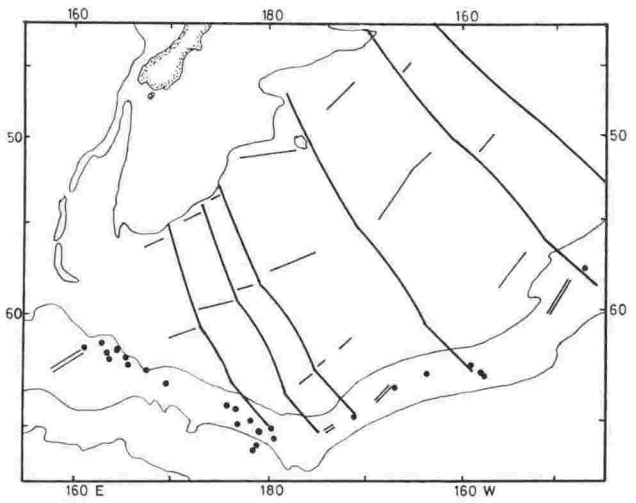


FIG. 6. Composite fracture zones generated about the three poles of rotation of table 2. Anomalies 5, 25, and 36 shown. Epicentres from Barazangi and Dorman (1969). Double line, spreading centre.

## DISCUSSION

There is no doubt that changes in spreading have occurred in the South-west Pacific since the Cretaceous. The analysis presented here in terms of three poles is adequate although somewhat arbitrary. Continuous changes in the pole positions rather than discrete changes are more probable.

The change in spreading at anomalies 24–25 is rather abrupt and could well be related to the cessation of spreading in the Tasman Sea at this time (Hayes and Ringis, 1973). It could also be related to world-wide effects associated with the Cretaceous-Tertiary boundary.

The initiation of spreading between Australia and Antarctica at approximately the time of anomaly 18 (45 m.y.) presumably would have some effect, especially in the western part of the region considered. This may explain why our poles do not give as good a reconstruction of that area as the area further east. The shift of the pole from 64° S 160° E to a pole between 70 and 80° S, near 120° E could be gradual. However some world-wide change at anomaly 5 (10 m.y.) is often suggested: e.g., Herron (1971), Morgan (1968), Menard and Atwater (1968).

The accuracy with which the poles of rotation and spreading rates can be determined is limited both by the small extent of the region over which the anomalies are found and also because data exist for only half of the spreading pattern. Many of the observed changes and apparent inconsistencies in spreading rate could be explained by asymmetrical spreading. The angles of rotation given in table 2 are also limited in accuracy for this reason.

A stringent test of the poles and rotation angles is to rotate Antarctica and New Zealand back about these poles of table 2. The reconstruction is shown in fig. 7. It is seen that the Subantarctic Slope on the

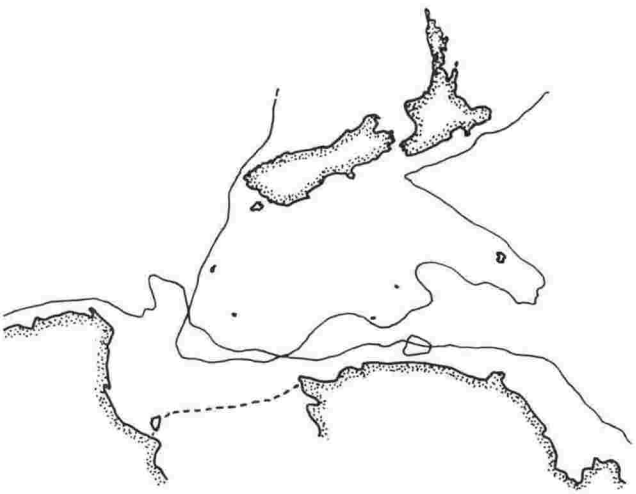

FIG. 7. Antarctica rotated back about the poles and angles of table 2.

edge of the Campbell Plateau fits reasonably well along the coastline of Western Antarctica but there is some overlap in the Ross Sea area. Either asymmetrical spreading or some relative motion between east and west Antarctica since the Cretaceous could account for this overlap. However bearing in mind that the poles are likely to be mean poles of rotation, this fit is better than could be expected.

Since the region is limited in extent, the only way to improve the precision of the determinations is to analyse data south of the Albatross Cordillera in the Pacific-Antarctic Basin, and to accurately survey the fracture zones extending southward from the Campbell Plateau.

## ACKNOWLEDGMENTS

The University Grants Committee provided funds for the purchase of a plotter.

## REFERENCES

BARAZANGI, M.; DORMAN, J. 1969: World seismicity maps compiled from ESSA, Coast and Geodetic Survey, epicenter data, 1961–67. *Bull. Geol. Soc. Am. 59*: 369–80.

CHRISTOFFEL, D. A. 1969: Sea floor spreading in the south-west Pacific and cenozoic drifting pattern of southern continents. *Trans. Am. Geophys. Union 5*: 185 (Abstract).

CHRISTOFFEL, D. A.; FALCONER, R. K. H. 1972: Marine magnetic measurements in the south-west Pacific Ocean and the identification of new tectonic features. *in* Antarctic Oceanology II: the Australian - New Zealand Sector, ed. D. E. Hayes. American Geophysical Union, *Antarctic Research Series 19*: 197–209.

CHRISTOFFEL, D. A.; ROSS D. I. 1965: Magnetic anomalies south of the New Zealand Plateau. *J. Geophys. Res., 70*: 2857–61.

——— 1970: A fracture zone in the south-west Pacific basin south of New Zealand and its implications for sea floor spreading. *Earth Planet. Science Lett. 8*: 125–30.

FALCONER, R. K. H. 1973: Numerical studies of Cretaceous magnetic anomalies in the south-west Pacific ocean. *in* Oceanography of the South Pacific 1972, comp. R. Fraser. New Zealand National Commission for UNESCO, Wellington.

HAYES, D. E.; EWING, M. 1971: The Louisville Ridge—a possible extension of the Eltanin Fracture zone. *in* Antarctic Oceanology I, ed. J. L. Reid. American Geophysical Union, *Antarctic Research Series 15:* 223–8.

HAYES, D. E.; RINGIS, J. 1973: The early opening of the central Tasman Sea. *In* Oceanography of the South Pacific 1972, comp. R. Fraser. New Zealand National Commission for UNESCO, Wellington.

HERRON, E. M. 1971: Crustal plates and sea floor spreading in the south-eastern Pacific. *In* Antarctic Oceanology I. American Geophysical Union. *Antarctic Research Ser., 15*: 229–237.

LE PICHON, X. 1968: Sea floor spreading and continental drift. *J. Geophys. Res. 73*: 3661–97.

MENARD, H. W.; ATWATER, T. 1968: Changes in the direction of sea floor spreading. *Nature, Lond. 219*: 463–7.

MORGAN, W. J. 1968: Rises, trenches, great faults, and crustal blocks. *J. Geophys. Res. 73*: 1959–82.

SYKES L. R. 1970: Seismicity of the Indian Ocean and a possible nascent island are between Ceylon and Australia. *J. Geophys. Res., 75*: 5041–55.

# Numerical Studies of Cretaceous Magnetic Anomalies in the South-west Pacific Ocean

R. K. H. FALCONER

Physics Department, Victoria University of Wellington, Wellington, New Zealand

**Abstract**

Numerical correlation of magnetic anomaly profiles is investigated using the product moment correlation coefficient.

Application of this method to an area of well-mapped magnetic anomalies indicates that consistent correlations can be obtained numerically. Fracture zones are confirmed and numerical results used in the interpretation of a small complex area. An extended geomagnetic time scale, back to 83 mybp, is given.

Numerical correlations between a model profile based on the time scale, south Pacific profiles and the north Pacific type profile confirm the assignment of the anomaly sequence in the South-west Pacific to Upper Cretaceous age.

## INTRODUCTION

Marine magnetic anomalies are used extensively in the study of the evolution of oceanic areas. Correlation of anomalies between closely spaced tracks has revealed the structure of particular areas (Mason and Raff, 1961; Talwani *et al*, 1971). Comparisons between widely spaced areas (Pitman and Heirtzler, 1966) have contributed to the concept of plate tectonics (Morgan, 1968; Le Pichon, 1968) which reveals the structure of much of the earth's crust.

The identification of magnetic anomaly patterns depends on correlation of anomalies between tracks. Satisfactory correlation is possible only when distinctive sequences are identifiable in the profiles. It is difficult to assess the uniqueness of a particular sequence and to determine the reliability of correlations. Up to the present, numerical correlation has rarely been used (Fuller, 1964; Luyendyk *et al.*, 1968; Loncarevic and Parker 1971). Visual correlations are adequate but are influenced by personal factors such as the scale of plotted profiles and preconceived ideas. Even when different investigators agree on a particular correlation they cannot easily compare their judgments. In an attempt to overcome some of these human limitations, numerical techniques are applied. To judge of the usefulness of such numerical methods, they are applied here to an area which has already been well studied (Christoffel and Falconer, 1972) using conventional methods.

## THEORY

Consider two magnetic anomaly profiles which when digitised at N equidistant points give two series x(i) and y(i). A good measure of the similarity of two profiles is the covariance coefficient vr given by

$$vr = \frac{1}{N} \sum_{i=1}^{N} [x(i)-mx].[y(i)-my] \qquad (1)$$

where mx and my are the means of series x(i) and y(i) respectively.

In comparing profiles in which the anomalies are similar but have different mean amplitudes, the amplitude variation is not very important. It is reasonable therefore to normalise each series to the same amplitude. This gives the Pearson product moment correlation coefficient r.

$$r = \frac{\sum_{i=1}^{N} [x(i)-mx].[y(i)-my]}{\left[\sum_{i=1}^{N} [x(i)-mx]^2.[y(i)-my]^2\right]^{\frac{1}{2}}} \qquad (2)$$

*Oceanography of the South Pacific 1972, comp. R. Fraser. New Zealand National Commission for UNESCO, Wellington: 1973.*

r will vary between + 1 for perfect correspondence of the series and — 1 for negative correspondence. r = 0 represents complete non-correlation. For convenience, values given in this paper are 100.r, i.e., 100 for perfect correlation.

If one profile is longer than another it is possible to calculate the correlation coefficient r for several different alignment positions of the profiles. If r is plotted as a function r(d) of distance, this is equivalent to sweeping profile x along profile y. A maximum in r(d) will indicate an alignment position at which the correlation is best.

To statistically compare different correlations it is necessary to know the confidence limits on r. The Fisher (1970) z-transformation method cannot be used automatically, since when profiles are digitised at close intervals each point is not independent of points adjacent to it, and hence the assumption that all N values of the series are independent is not correct. Awe (1964) has given methods for determining the effective number of independent points, Ne, but these methods apply only to particular types of data. The assumption, based on sampling theory (Jenkins and Watts, 1968), of two independent points per maximum could be used, but it is difficult to standardise the method of counting maxima. Considering only prominent maxima should give the minimum value of Ne. This would give the maximum range for confidence intervals on r.

## REGIONAL CORRELATIONS

Christoffel and Falconer (1972) showed that there is a clearly identifiable sequence of anomalies in the South-west Pacific (fig. 1) corresponding to the period 63 to 82 mybp, i.e., Upper Cretaceous age (Berggren, 1969). Six widely spaced profiles typical of the sequence are shown in fig. 2.

Correlations between the profiles are visually good. They should therefore provide a good test of the numerical method. Fifteen different comparisons are possible, giving a range for r of 47 to 18, with a mean of 33.

The correlations appear to be quite low, but the hypothesis that two profiles are uncorrelated can be statistically tested. Taking Ne = 30 and 5% significance levels, the hypothesis would not be rejected for 8 of the 15 correlations. It is clear that low correlations can result from profiles which are in fact visually similar.

One possible explanation for this is horizontal scale variations. Profiles B and R1 (fig. 3), are obviously similar and have a correlation value of 42. However, a change of only 3% in the length of R1 increases the

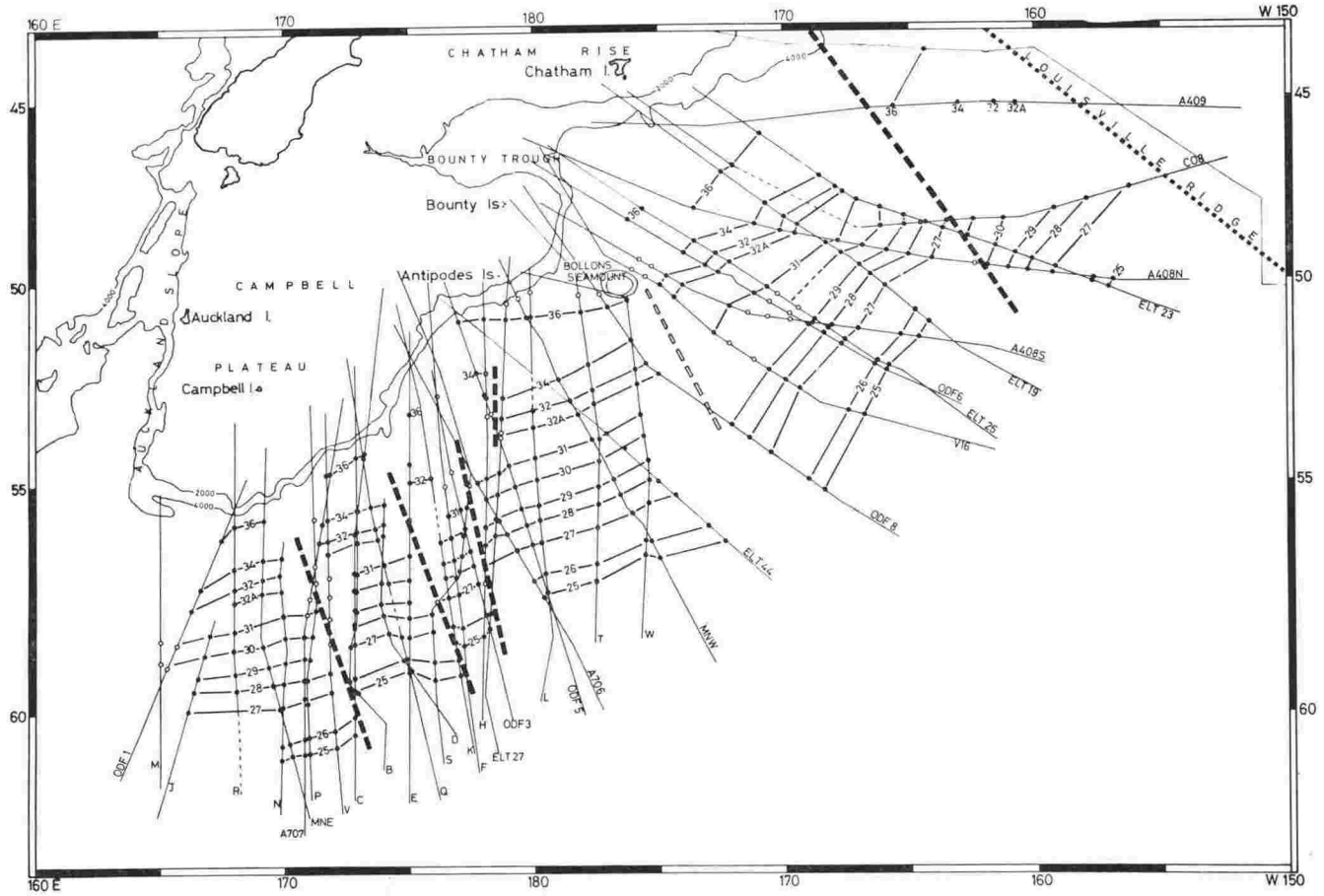


FIG. 1. Cretaceous magnetic anomaly correlations; based on Christoffel and Falconer (1972, fig. 3). Fracture zones shown dashed. Anomalies numbered after Le Pichon *et al.* (1968) and Christoffel and Falconer (1972).

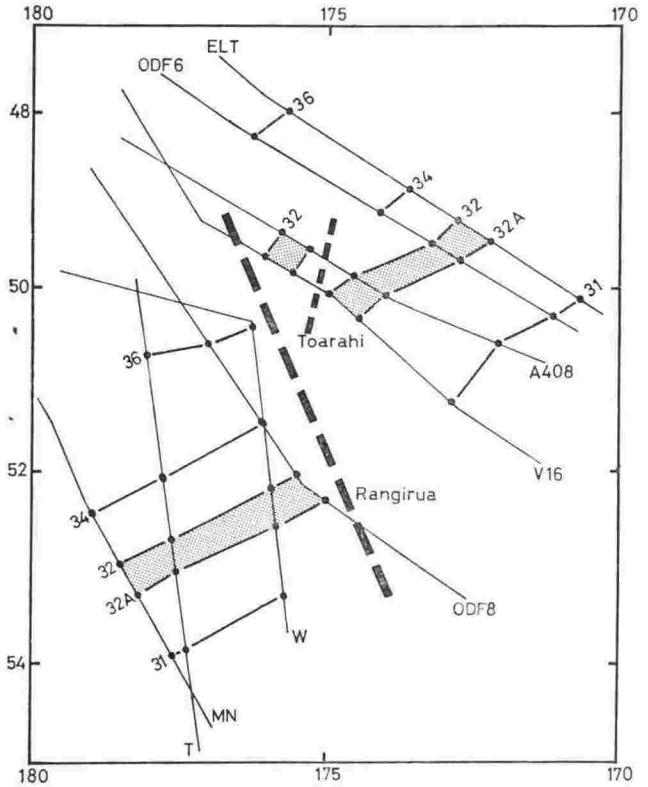


FIG. 5. Anomaly correlations and fracture zones in the small area near the Bollons seamount.

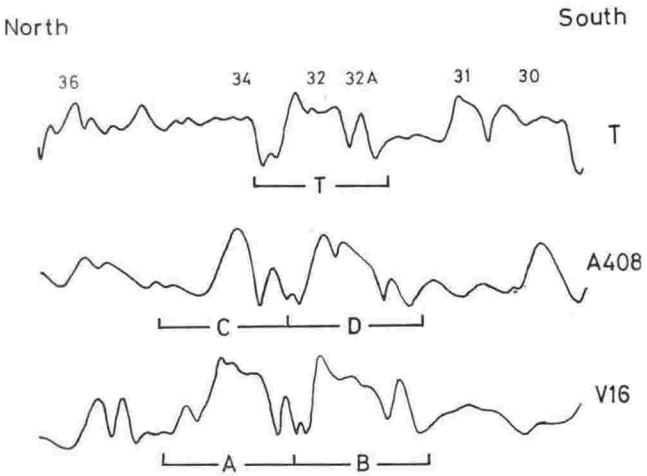


FIG. 6. Magnetic anomaly profiles used in the numerical tests applied to the area of fig. 5.

near the Bollons seamount (Fig. 1) provides a good test area. Christoffel and Falconer (1972) recorded the structure as complex and did not map any definite fractures. However, partially on the basis of the numerical results, an unusual configuration of two fracture zones (the Toarahi and Rangirua fracture zones) is here suggested (Fig. 5).

The Toarahi fracture zone is identified on tracks V16 and A408. Sweeping the section A + B of V16 (Fig. 6) along A408 gives a maximum correlation of 65. The position of maximum agrees with the best visual correlation. Correlations of 64 for A on C, and 85 for B on D also confirm the anomaly trends between V16 and A408 shown in fig. 5. The visual similarity of sections A and B in V16 further suggests a fracture between them. Correlation of 74 for A on B confirms this, and correlation of 69 for C on D further indicates that the fracture crosses between C and D.

The Rangirua fracture zone is confirmed by sweeping a section of profile T (fig. 6) along V16 and A408. Correlations of 82 and 58 for T on A and C respectively, and 71 and 82 for B and D respectively, support the identification of anomalies 32A and 32 shown in fig. 5.

The numerical tests applied in this area use only short sections of profiles and hence the statistical uncertainties are greater. Section C is the one section which is visually dissimilar from the others and correlations involving it always give values lower than those for other sections. This indicates that the numerical correlations will give consistent values which can be used to aid interpretation.

## TIME SCALE

The identification of anomaly trends allows an assessment of the structure of an area. However, discussion of the tectonic history requires additional information. The anomalies must be assigned an age, either absolute or relative. This involves comparison with a type profile such as the composite north Pacific Ocean profile NPAC (Vine, 1966), to which ages have been assigned.

The good correlations within the South-west Pacific anomalies allows one to establish a South Pacific type profile, SPAC (fig. 7). The high correlation value (89) of SPAC with the north Pacific type profile NPAC clearly shows that the anomalies in the South-west Pacific are of the same age as those of the north Pacific profile.

Vine (1966) gives the ages for anomalies 25 and 32 as 59 and 72 mybp respectively. Heirtzler *et al.* (1968) date them as 63 and 75 mybp respectively. Heirtzler *et al.* (1968) have tabulated the ages of the boundaries of a series of normally and reversely magnetised blocks which could produce the observed anomaly pattern.

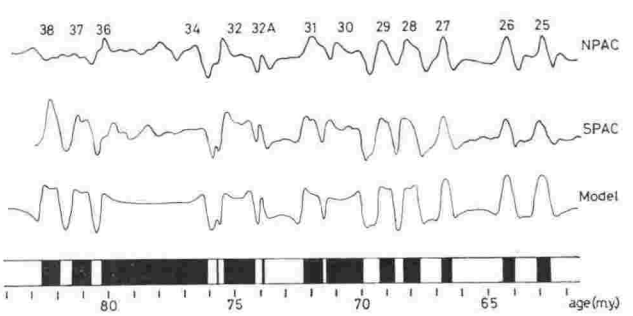


FIG. 7. North Pacific type profile NPAC. South Pacific type profile SPAC. Model profile calculated from the model blocks based on SPAC.

correlation to 64. Such differences in length of the same anomaly sequence on different profiles can be due either to variations in the orientation of the profiles with respect to the anomaly trends, or to differences in sea floor spreading rates at the location of the profiles. Visual correlation is not significantly affected by the variations, provided that profiles are drawn approximately the same length. However, the numerical method appears to be critically affected. It is easy to vary the scale of a profile numerically and recalculate the correlation, but the problem is more serious if the scale varies along a profile.

Low correlations can also be caused by a missing section in one profile. The effect is illustrated by profiles

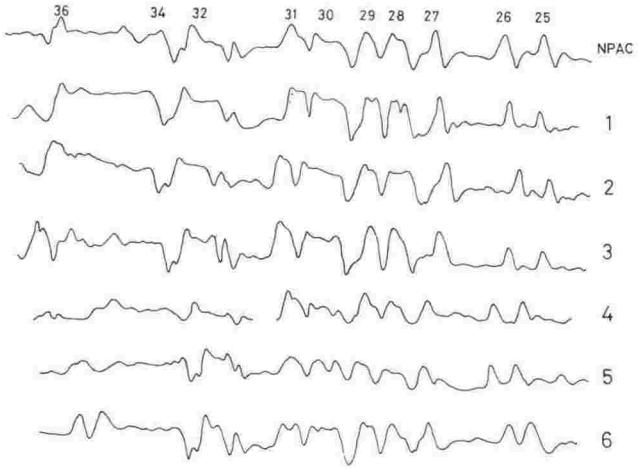


FIG. 2. Typical magnetic anomaly profiles of the Cretaceous sequence. NPAC from the north Pacific (Vine 1966), 1–6 from the area shown in fig. 1.

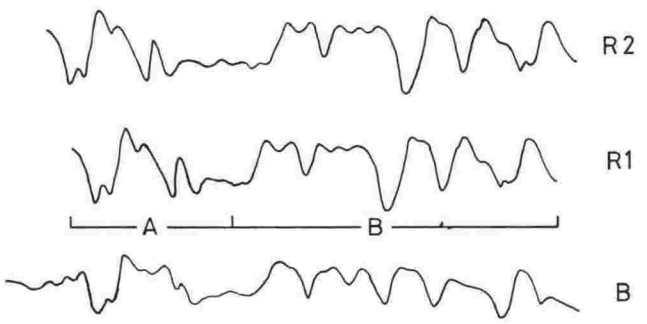


FIG. 3. Profiles which illustrate amplitude differences and missing sections.

R1 and R2 (Fig. 3). They have a correlation of 54 but are identical except for the insertion of a short artificial section between anomalies 31 and 32. Missing or extra sections in profiles are common if a track crosses a fracture zone.

The problems caused by missing sections or scale changes within profiles can be partially overcome by breaking one profile into shorter sections, then sweeping the short sections along the other profile, e.g., sections A and B of profile R1 (Fig. 3) both give $r = 100$ at the appropriate places on R2. Obviously the sections cannot be too short, since the statistical reliability of the correlation decreases with N.

Profiles B and R1 illustrate the need to normalise the profiles. The average amplitude of B is 350 gamma while that of R1 is 500 gamma. Use of the covariance coefficient [equation (1)] instead of the correlation coefficient [equation (2)] would be misleading in such cases.

## FRACTURE ZONES

The identification of a fracture zone normally requires several profiles for anomaly trends to be mapped, and the fracture position inferred from the offset of the anomalies. However, if the same anomalies occur twice in one profile, a fracture, although not its strike or offset, can be inferred from that profile alone. The large fracture zone at 165° W (Fig. 1), here named the Tairoa fracture zone, was initially identified from the ELT 23 profile only (Pitman *et al*, 1968). Fig. 4 shows the profile, on which the duplication of anomalies 27 to 31 is clear.

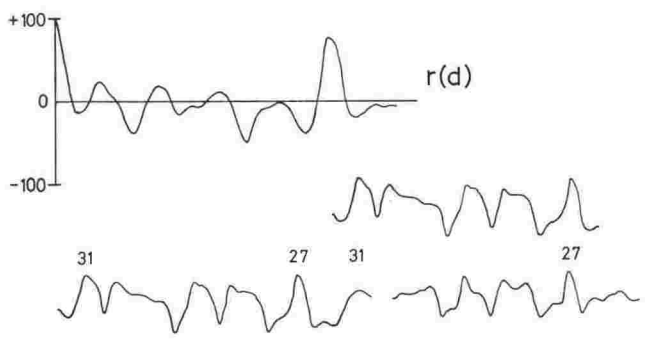


FIG. 4. ELT 23 profile across the Tairoa fracture zone, with the left hand 32–27 section above it in the best alignment position determined by the correlation coefficients r(d).

The numerical verification of the fracture is accomplished by sweeping one set of the anomalies along the full profile. The plot of r(d) peaks ($r = 79$) at one position, which corresponds to the position of best visual correlation. The $r = 100$ peak is as expected at alignment of the short section with itself.

This profile illustrates the problem of data gaps in correlation analyses. A correlation value of 79 was calculated with the data gap replaced by a straight line between the known values. Replacing the gap with values equal to the mean of the complete profile gives a correlation value of 69. Neither method is satisfactory, since each effectively inserts an anomaly structure which may not be present. A possible alternative is the omission of any data gap terms from the summations in the calculation of r.

Data gaps present a similar problem in visual correlation, and are a source of considerable personal bias. The extent of the gap is an important factor for both visual and numerical methods.

The numerical method is probably most useful when there is ambiguity in the visual correlations. An area

TABLE 1. Geomagnetic Time Scale Based on profile SPAC

| Anomaly | R–N | N–R |
|---|---|---|
| 25 | 62.75 | 63.28 |
| 26 | 64.14 | 64.62 |
| 27 | 66.65 | 67.10 |
| 28 | 67.75 | 68.45 |
| 29 | 68.75 | 69.40 |
| 30 | 70.00 | 71.50 |
| 31 | 71.60 | 72.40 |
| 32A | 73.95 | 74.05 |
| 32 | 74.30 | 75.60 |
| 33 | 75.80 | 75.85 |
| 34–36 | 76.20 | 80.40 |
| 37 | 80.75 | 81.55 |
| 38 | 82.00 | 82.75 |

The identification of anomalies beyond number 32 (Christoffel and Falconer, 1972) allows an extension of the reversal time scale. A scale is given (table 1), based on the SPAC profile and the Heirtzler *et al.* (1968) dates of anomalies 25 to 27. The similarity of SPAC to NPAC and to other north Pacific profiles (Peter *et al.*, 1971; Raff, 1966) suggests that the scale can be applied elsewhere.

Correlation between different areas of the world is often carried out by comparing profiles with a model profile calculated from a time scale (Pitman and Heirtzler, 1966). The correlation between SPAC and the model based on it is 94. Such a high value indicates that in general a simple model of normal and reversed blocks with the appropriate time scale will be adequate to describe the observed anomalies.

## CONCLUSIONS

Numerical calculations using the correlation coefficient r can be usefully applied to the correlation of magnetic anomaly profiles. This method overcomes the problem of which scales are best for visual correlation and avoids the problems of preconceived ideas. Long profiles can present difficulties because of variations within the profiles. Short sections give good results, but determination of an adequate length of profile to give statistically meaningful results is difficult. Visual methods involve the problem of establishing an adequately unique section of profile, but more comparisons of visual and numerical results may indicate the necessary criteria. Definite methods for handling data gaps may also be developed. The reliability of models can be rigorously checked by numerical correlation because one profile is controlled. This will permit good comparison between areas in which the same structure gives different anomaly shapes.

The product moment correlation coefficient r is not the only coefficient which may be used for correlation studies. Further studies are planned to investigate the usefulness of first moment correlation (Gibson, 1950), goodness of fit (Francheteau *et al.*, 1969) and other coefficients (Harrison, 1971).

Numerical coefficients are unlikely to supersede visual comparisons especially as most data need scrutinising before numerical methods can be usefully applied. However, numerical values provide quantitative comparisons, uninfluenced by any personal bias. Final interpretation will always be a personal matter but numerical coefficients at least provide a precise means of communication for discussions of the correlations.

## ACKNOWLEDGMENTS

Discussions with D. A. Christoffel and Feriel Falconer were very useful. Computing facilities were provided by Applied Mathematics Division, Department of Scientific and Industrial Research.

## REFERENCES

AWE, O. 1964: Errors in correlation between time series. *J. Atmos. Terr. Physics. 26:* 1239–1255.

BERGGREN, W. A. 1969: Cenozoic Chronostratigraphy, Planktonic Foraminiferal Zonation and the Radiometric Time Scale. *Nature, Lond. 224:* 1072–1075.

CHRISTOFFEL, D. A.; FALCONER, R. K. H. 1972: Marine magnetic measurements in the south-west Pacific Ocean and the identification of new tectonic features. *in* Antarctic Oceanology II: the Australian - New Zealand Sector. ed. D. E. Hayes. American Geophysical Union, *Antarctic Research Series 19:* 197-209.

FISHER, R. A. 1970: Statistical Methods for Research Workers: Oliver and Boyd, Edinburgh.

FRANCHETEAU, J.; SCLATER, J. G.; CRAIG, H. 1969: Magnetisation of a recently discovered seamount in the central Pacific. *Geophysics 34:* 645–651.

FULLER, M. D. 1964: Expression of east-west fractures in magnetic surveys in parts of U.S.A. *Geophysics 29:* 602–622.

GIBSON, G. D. 1950: A rapid method for ascertaining serial lag correlations. *Biometrika. 37:* 288–307.

HARRISON, C. G. A. 1971: A Seamount with a non magnetic top. *Geophysics 30:* 349–357.

HEIRTZLER, J. R.; DICKSON, G. O.; PITMAN, W. C. III; HERRON, E.; LE PICHON, X. 1968: Marine magnetic anomalies, geomagnetic field reversals, and motions of the ocean floor and continents. *J. Geophys. Res. 73:* 5855–5899.

JENKINS, G. M., WATTS, D. G. 1968: *Spectral Analysis and its Applications:* Holden Day.

LE PICHON, X. 1968. Sea floor spreading and continental drift. *J. Geophys. Res. 73:* 3661–3697.

LONCAREVIC, B. D.; PARKER, R. L. 1971. The Mid-Atlantic Ridge near 45° N. XVII Magnetic anomalies and ocean floor spreading. *Can. J. Earth Sci. 8:* 883–896.

LUYENDYK, B. P.; MUDIE, J. D.; HARRISON, C. G. A. 1968: Lineations of magnetic anomalies in the north east Pacific observed near the ocean floor. *J. Geophys. Res. 73:* 5951–5957.

MASON, R. G.; RAFF A. D. 1961: Magnetic survey off the west coast of North America, 32° N to 42° N latitude. *Bull. Geol. Soc. Am. 72:* 1259–1265.

MORGAN, W. J. 1968: Rises, trenches, great faults, and crustal blocks. *J. Geophys. Res. 73:* 1959–1982.

PETER, G.; ERICKSON, B. H.; GRIM, P. J. 1971: Magnetic structure of the Aleutian trench and Northeast Pacific Basin. *In* The Sea, Vol. 4, ed. A. E. MAXWELL: Wiley Interscience.

PITMAN, W. C. III; HERRON, E. M.; HEIRTZLER, J. R. 1968: Magnetic anomalies in the Pacific and sea floor spreading. *J. Geophys. Res. 73:* 2069–2085.

PITMAN, W. C. III; HEIRTZLER, J. R. 1966: Magnetic anomalies over the Pacific-Antarctic Ridge. *Science, 154:* 1164–1171.

RAFF, A. D. 1966: Boundaries of an area of very long magnetic anomalies in the north-east Pacific. *J. Geophys. Res. 71:* 2631–2636.

TALWANI, M.; WINDISCH, C. C.; LANGSETH, M. G. 1971: Reykjanes Ridge Crest: A detailed geophysical study. *J. Geophys. Res. 76:* 473–517.

VINE, F. J. 1966: Spreading of the ocean floor: new evidence. *Science 154:* 1405–1415.

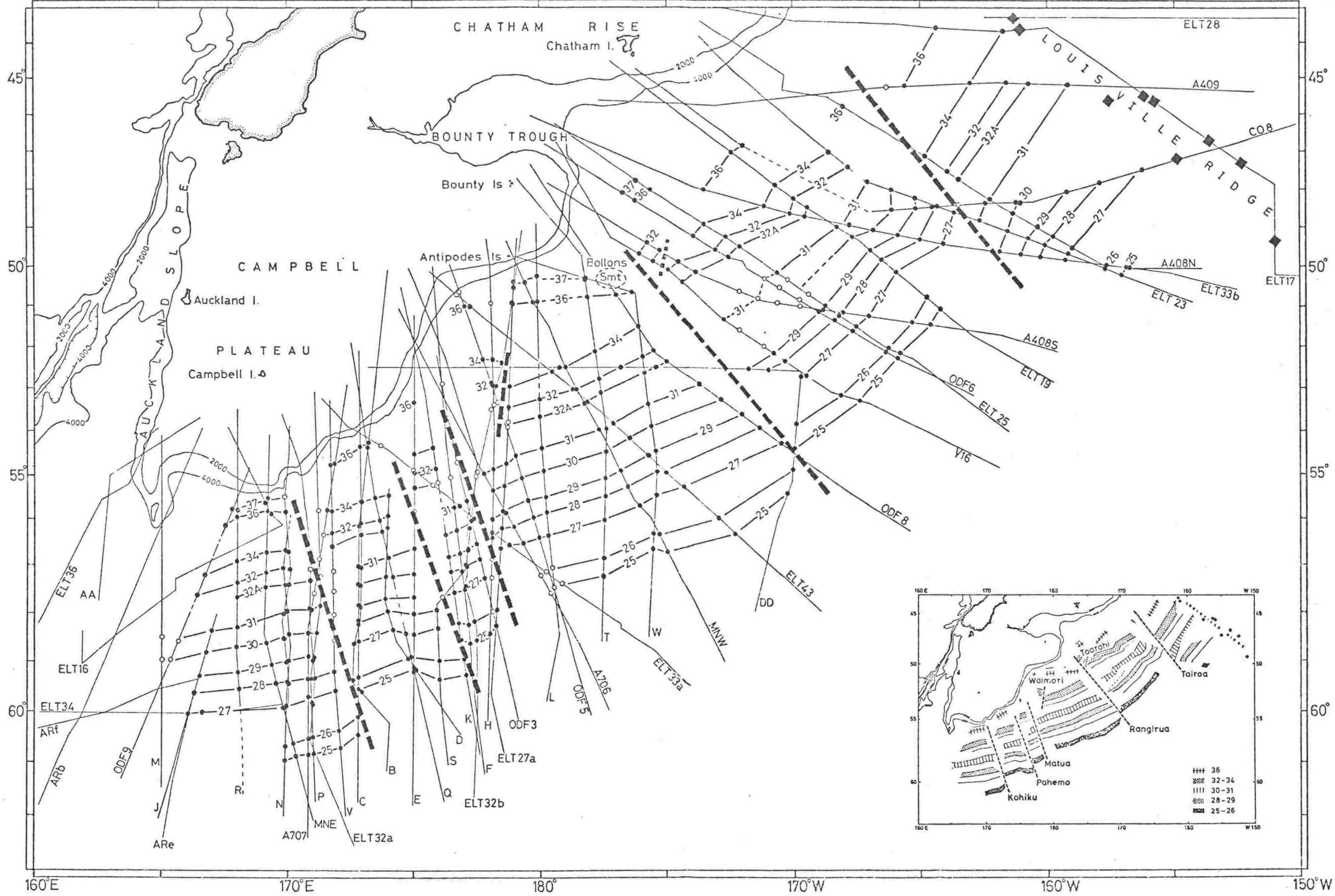


FIG. 4.3 MAGNETIC ANOMALIES IN THE SOUTHWEST PACIFIC BASIN.

Tracks for which magnetic data were available are shown. Closed circles are definite identifications of anomalies within the numbering system used. Open circles are either tentative identifications or prominent anomalies not assignable to the numbered sequence. Fracture zones inferred from offsets of the anomalies are shown by dashed lines. Squares are positions of the Louisville ridge, from Hayes and Ewing (1971) and this study. Inset shows the names given to the fracture zones.

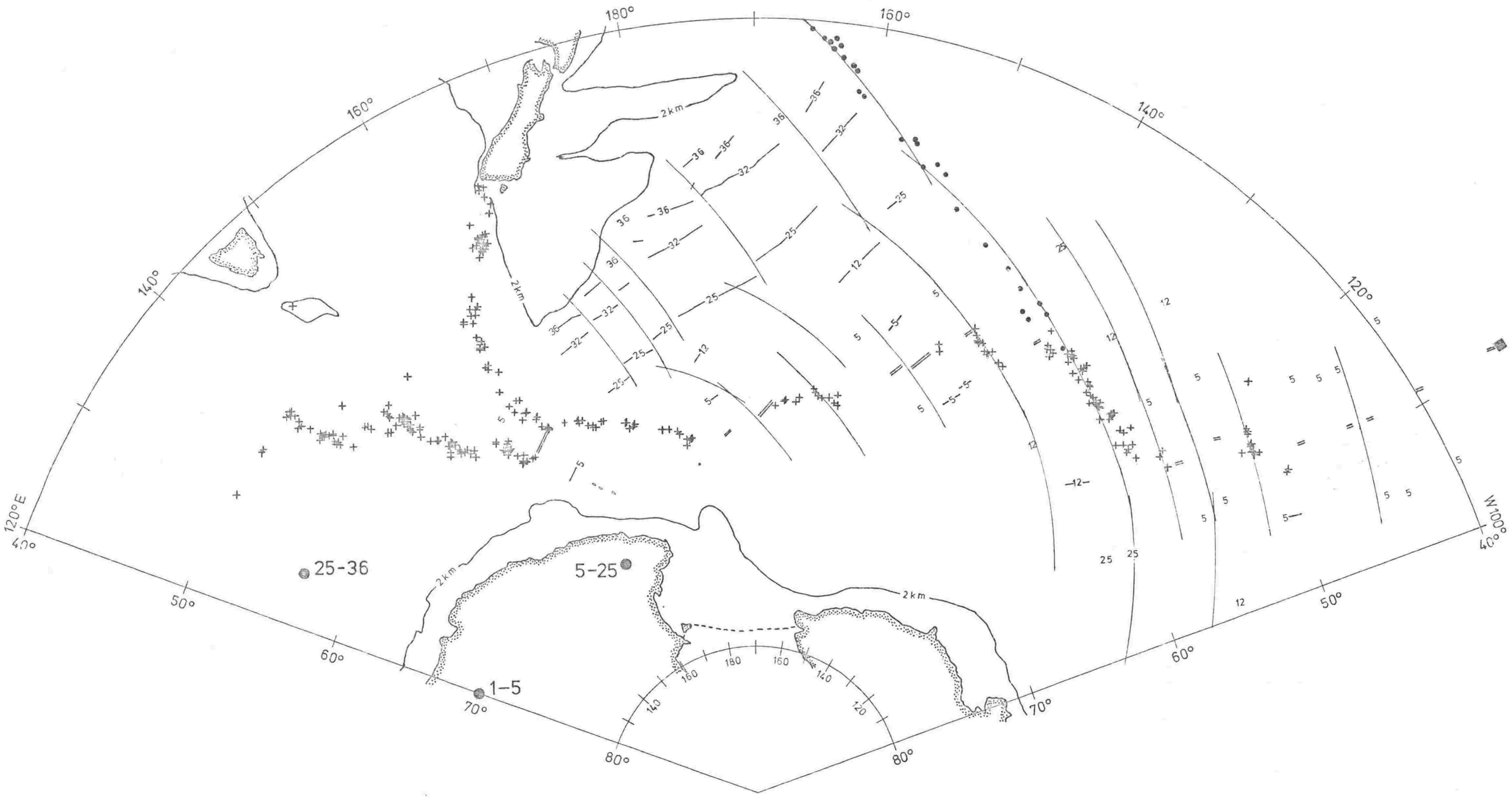


FIG. 9.3 THE SOUTHWEST PACIFIC AREA: MAGNETIC ANOMALIES, EPICENTRES, AND ARCS ABOUT POLES OF ROTATION.

Stereographic projection. Double lines indicate positions of magnetic anomaly number 1, i.e. the axial anomaly. Other representative anomalies are shown by single numbers for single identifications, and by lines where lineations are well established. Crosses are USCGS epicentres for 1964 - 1972. Large filled circles indicate the positions of the rotation pole of the southwest part of the Pacific plate, for the anomaly intervals as labelled. Representative arcs about these poles are shown at and north of the ridge axis. Three arcs south of the ridge for the interval 5 - 25 are also shown, drawn about the relevant Antarctic pole. Note: The arcs are not drawn only where there are fracture zones. Small closed circles are positions of the Louisville ridge. The square indicates the eastern end of the Pacific-Antarctic boundary, i.e. the Pacific-Antarctic-Nazca triple junction. Generalized 2 km bathymetric contour shown only for the continental areas. Magnetic data either side of the southeast Indian ridge are shown only near the triple junction.